Modulating inflammation for host defence and wound healing in the intestinal tract

By:

Jou Ann Lee

A thesis submitted in partial fulfilment of the requirements for the degree of

Doctor of Philosophy

The University of Sheffield

Faculty of Medicine, Dentistry and Health

Registration Number: 150254814

Submission Date: October 2020

Abstract

Over a million surgical procedures are carried out each year within the United Kingdom. Three quarters of these involve the gastrointestinal tract (GIT), and many require colonic resections with an anastomosis to re-join the ends of the remaining bowel to restore GIT continuity. While most anastomoses heal uneventfully, in up to 26% of patients, healing fails and an anastomotic leak (AL) develops, possibly resulting in death. Although it is well-established that prolonged inflammation plays a role in failure of healing, because of the hidden, and therefore less accessible, location of the intestine, substitution with buccal mucosa, lung or other epithelial surfaces have often been used as proxies to investigate this phenomenon. But these do not fully replicate the complexity of the intact intestinal environment. This thesis further develops the zebrafish as a model organism for this purpose, by establishing an intestinal injury model, a fluorescent gut line, and characterising intestinal colonisation with *E. faecalis*, a clinically relevant bacteria not usually found in zebrafish. The zebrafish is also validated as a model to study the action of specific modulators of inflammation resolution. The individual action profiles of these compounds on cells of the innate immune system, as well as the tissue-specific variation, their mechanism of action and their temporal effects are elucidated using fluorescently labelled neutrophils and macrophages and RNA sequencing. This thesis then introduces to the UK a validated mouse model of intestinal injury and healing, identifying a possible agent for enhanced intestinal wound healing. In conclusion, this work investigates the ways inflammation, genetics, and the microbiome, may work together in influencing the outcome of injury and healing in the intestinal tract.

(272/300 words)

Declaration

I, Jou Ann Lee, confirm that the Thesis is my own work. I am aware of the University's Guidance on the Use of Unfair Means (www.sheffield.ac.uk/ssid/unfair-means). This work has not been previously been presented for an award at this, or any other, university.

Publications arising from this work

Lee JA, Chico TJA, Renshaw SA. 'The triune of intestinal microbiome, genetics and inflammatory status and its impact on the healing of lower gastrointestinal anastomoses.' *FEBS J* 2018 Apr;285(7):1212-1225. doi: 10.1111/febs.14346. Epub 2017 Dec 22.

Loynes CA, **Lee JA**, Robertson AL, Steel MJG, Ellett F, Feng Y, Levy B, Whyte MKB, Renshaw SA. 'PGE_2 production at sites of tissue injury promotes an anti-inflammatory neutrophil phenotype and determines the outcome of inflammation resolution in vivo.' *Sci Adv* 2018 Sep 5;4(9):eaar8320. doi: 10.1126/sciadv.aar8320. eCollection 2018 Sep.

Statement of contribution and copyright permission

The following published manuscript has been incorporated as part of the thesis:

Title: "The triune of intestinal microbiome, genetics and inflammatory status and its impact on the healing of lower gastrointestinal anastomoses"

Publication status: Published in *FEBS J.* 2018 Apr;285(7):1212-1225
DOI: 10.1111/febs.14346

Authors: J. Lee, T. Chico, S. Renshaw.

Author contributions:

J. Lee: conceived ideas and concepts, performed literature review, constructed figures, wrote first draft of manuscript

S. Renshaw & T. Chico: Reviewed manuscript

Author signatures:

Jou A. Lee Date:15/03/2020

Stephen A. Renshaw Date:16/03/2020

Timothy J. A. Chico Date 24/03/2020

Acknowledgements

I would like to specially thank:

The Wellcome Trust for providing the funding and support that enabled me to carry out this work.

My supervisors Prof Alison Gartland and Dr Lynne Prince.

The excellent staff at the Animal Unit at Sheffield Hallam Hospital, the Electron Microscopy Unit, the Wolfson Light Microscopy Facility, and the Aquarium Unit.

And the many individuals who gave their time and effort to share with me their expertise, knowledge, experience, and use of their specialised equipment: a heart-felt ‘Thank You!’ to you all!

List of Abbreviations

AA	Arachidonic acid
ADA	Adenine deaminase
ADP	Adenosine diphosphate
AL	Anastomotic leak
ALP	Alkaline phosphatase
ATL	Aspirin triggered lipoxin or 15-epi-lipoxin
ATP	Adenosine triphosphate
A.U.	Arbitrary units
BHI	Brain Heart Infusion
BSA	Bovine serum albumin
bp	Base pairs
Cm	Chloramphenicol
CFU	Colony Forming Units
COX	Cyclooxygenase
DIG	Digoxigenin
DHA	Docosahexaenoic acid
DMSO	Dimethyl sulphoxide
DNA	Deoxyribonucleic acid
DNase	Deoxyribonuclease
dNTP	Deoxyribonucleoside-5'-triphosphate
dpf	Days post-fertilisation
DSS	Dextran Sodium Sulfate
DTT	Dithiothreitol
Ery	Erythromycin
EPA	Eicosapentaenoic acid
FA	Fatty acid
FPR2	Formyl Peptide receptor 2
FLIPr	FPR-like Inhibitory Protein
g	Gram

g	Gravity (relative centrifugal force)
GF	Germ-free
GFP	Green fluorescent protein
GIT	Gastrointestinal tract
HCl	Hydrochloric acid
HP	Hydroxyproline
hpf	Hours post fertilisation
hpi	Hours post injury or infection
iAP	Intestinal Alkaline Phosphatase
IBD	Inflammatory Bowel Disease
IL	Interleukin
IV	Intravascular
Kan	Kanamycin
L	Litre
LMW	Low molecular weight
LXA4	Lipoxin A4
LMP	Low melting point
LOX	Lipoxygenase
LPS	Lipopolysaccharide
M	Molar
MΩ	Mega Ohm
mg	Milligram
min	Minute
mL	Millilitre
mm	Millimetre
mM	Millimolar
Mcl-1	Myeloid cell leukaemia-1
MPO	Myeloperoxidase
NET	Neutrophil Extracellular Trap
NGS	Next Generation Sequencing
OCT	Optimal Cutting Temperature Compound

OD_{600}	Optical density measured at 600 nm
PBS	Phosphate buffered saline
PCR	Polymerase chain reaction
PD	Protectin
PFA	Paraformaldehyde
PNK	Polynucleotide Kinase
RNA	Ribonucleic acid
RNase	Ribonuclease
rpm	Revolutions per minute
RvD2	Resolvin D2
RvE1	Resolvin E1
SDS	Sodium dodecyl sulphate
SDS-PAGE	Sodium dodecyl sulphate polyacrylamide gel electrophoresis
SNP	Single Nucleotide Polymorphism
SPM	Specialised pro-resolving lipid mediator
TAE	Tris-acetate EDTA
TBST	Tris buffered saline Tween
TE	Tris-EDTA (buffer)
TEMED	N,N,N'N'-tetramethyl-ethylenediamine
Tet	Tetracycline
TNBS	2,4,6-Trinitrobenzenesulfonic acid
Tris	Tris (hydroxymethyl) aminomethane
TSA	Tyramide signal amplification
TdT	terminal deoxynucleotidyl transferase
VEGF	Vascular endothelial growth factor
µg	Microgram
µL	Microlitre
µm	Micrometre
µM	Micromolar
Φ	Phage

Contents

Abstract 2
Declaration 3
Publications arising from this work 3
Statement of contribution and copyright permission 4
Acknowledgements 5
List of Abbreviations 6
Contents 9
List of Figures 19
List of Tables 25
Chapter 1: Introduction 26
1.1 The importance of anastomotic leaks and the scope of the problem 26
1.2 The importance of inflammation to wound healing 27
1.3 Manipulating inflammation to promote wound healing 32
1.4 The role of lipid mediators (SPMs) in inflammation 36
1.5 Influence of microbial milieu on wound healing 39
1.1 The possible role of protein modulators in inflammation 42
1.2 The role of differential genetic expression 44
1.3 Rationale for animal models 46
1.4 Thesis aims and working hypothesis 47
Chapter 2: Methods & Materials 49
2.1 Reagents 49
2.2 Recipes for buffers 49
2.2.1 iAP buffer 49
2.2.2 Phosphate buffered saline (PBS) 49
2.2.3 Tris-Glycine SDS Sample Buffer 50
2.2.4 Tris-Glycine SDS Running Buffer 50
2.2.5 Zymogram Renaturing Buffer 50
2.2.6 Zymogram Developing Buffer 50
2.2.7 Coomassie Blue stain 51
2.2.8 SDS-PAGE loading buffer (5X) 51

2.2.9 TBST (20X) 51
2.2.10 Western Blot Transfer Buffer 51
2.2.11 Western Blot blocking buffer 52
2.2.12 TAE (50x) 52
2.2.13 TE buffer 52
2.2.14 EBT buffer 52
2.2.15 RNA fragmentation buffer 52
2.2.16 RNA fragmentation stop buffer 52
2.2.17 4%(w/v) paraformaldehyde (PFA) solution 52
2.2.18 Lysis buffer 52
2.3 Recipes for histological stains 53
2.3.1 Picrosirius red 53
2.3.2 Acidified Water 53
2.3.3 Alkaline water (Blue-ing solution) 53
2.3.4 Eosin Y stock solution 53
2.3.5 Eosin Y working solution 53
2.4 Culture media 54
2.4.1 Brain Heart Infusion (BHI) 54
2.4.2 BHI Agar 54
2.4.3 Milk Agar 54
2.4.4 Luria Bertani (LB) broth (Lennox) 54
2.4.5 LB Agar 54
2.4.6 LK media 54
2.4.7 LK agar 55
2.4.8 Antibiotics 55
2.4.9 Phage buffer 55
2.4.10 Sabouraud Dextrose Agar 56
2.4.11 Carboxymethylcellulose (CMC) 56
2.4.12 Zebrafish embryo media (E3) 56
2.5 Molecular biology techniques 56
2.5.1 RNA extraction from zebrafish larvae 56

2.5.2 Preparation of cDNA via reverse transcription PCR 57
2.5.3 Determining DNA or RNA concentration 57
2.5.4 Gel electrophoresis 57
2.5.5 Gel extraction of DNA 58
2.5.6 Purification of PCR products 58
2.5.7 DNA sequencing 58
2.5.8 RNA over-expression 58
2.5.9 Receptor cloning 58
2.5.10 Plasmid purification 60
2.5.11 Restriction endonuclease digestion 60
2.5.12 T4 DNA ligation 60
2.5.13 Electro competent EL250 cells 61
2.5.14 Transformation of EL250 or Top10 cells 61
2.5.15 BAC library selection 61
2.5.16 Double digest and examination of *Col1a2-eGFP* 61
2.5.17 Creation of a target construct for *Col1a2-eGFP* 62
2.5.18 Amplification of target construct 62
2.5.19 Targeting construct into EL250 cells 63
2.5.20 Removal of kanamycin marker 63
2.5.21 iTol2-Kan target construct amplification 63
2.5.22 Targeting of iTol2-Kan into the Chloramphenicol resistant site 64
2.5.23 Preparation of Tol-2 transposase mRNA for co-injection 65
2.6 Tomographic RNA sequencing (TomoSeq) 65
2.6.1 TomoSeq sample freezing and sectioning 65
2.6.2 TomoSeq RNA extraction 65
2.6.3 TomoSeq reverse transcription and *in vitro* transcription of RNA 66
2.6.4 TomoSeq library preparation 68
2.6.5 TomoSeq sequencing 70
2.6.6 Analysis of TomoSeq 70
2.7 Histochemical analysis 71
2.7.1 Alcian blue staining for goblet cell quantification 71

2.7.2 *In Situ* Alkaline phosphatase staining for endogenous expression 71
2.7.3 Acridine orange staining for cell death within the zebrafish larval intestine 71
2.8 Bacteriological techniques 72
2.8.1 Bacterial strains 72
2.8.2 Bacterial growth conditions 72
2.8.3 Transduction of *S. aureus* SA113 using bacteriophage 74
2.8.4 Direct cell counts (CFU mL^{-1}) and Spectrophotometric measurement (OD_{600}) ... 74
2.9 Zebrafish in vivo techniques 76
2.9.1 Zebrafish husbandry 76
2.9.2 Transgenic Fish Lines 76
2.9.3 Tailfin injury neutrophil assay of zebrafish larvae 78
2.9.4 Intravascular microinjections of zebrafish larvae 78
2.9.5 RNA and DNA microinjection at the 1-cell stage zebrafish embryo 80
2.9.6 Microgavage of zebrafish larvae 80
2.9.7 Tailfin regeneration assay 80
2.9.8 Neutrophil reverse migration assay in zebrafish larvae 81
2.9.9 TSA/TUNEL neutrophil apoptosis assay 83
2.9.10 Whole mount *In Situ* hybridisation 83
2.9.11 Mechanical Model of Bowel injury model in zebrafish larvae 85
2.9.12 Laser Model of Bowel injury model in zebrafish larvae 85
2.9.13 Inflammation assay for bowel injury in zebrafish larvae 85
2.9.14 Intravenous bacteraemia survival assay in zebrafish larvae 85
2.9.15 CFU quantification of *E. faecalis* in individual zebrafish larvae 86
2.9.16 Picrosirius red staining of whole mount or frozen sections 86
2.10 Imaging of zebrafish larvae 87
2.10.1 Time-lapse imaging of live larvae 87
2.10.2 Transmission Electron Microscopy 89
2.10.3 Light Sheet Microscopy 89
2.11 Mouse *in vivo* and *ex vivo* techniques 89
2.11.1 Mouse husbandry 89
2.11.2 Statistical design and sample size calculations 90

2.11.3 Faecal mass measurements 90
2.11.4 Activity measurement 91
2.11.5 Operative technique 91
2.11.6 Clinical assessment of mice post-operatively 91
2.11.7 Harvesting of specimens and sample preparation 94
2.11.8 Anastomotic bursting pressure 94
2.11.9 Stool culture for bacterial, fungal, cellulase and proteolytic activity 94
2.11.10 Frozen sectioning for histology 95
2.11.11 Haematoxylin and eosin staining of frozen sections 95
2.11.12 Picrosirius staining of frozen sections of intestine and skin 95
2.11.13 Wright-Giemsa staining of frozen sections 95
2.11.14 Hydroxyproline assay 95
2.12 Protein Analysis 96
2.12.1 Bradford protein assay 96
2.12.2 SDS-PAGE 96
2.12.3 Western blotting 97
2.13 Zymogram 98
2.13.1 Protein preparation for mass spectrometry 98
2.13.2 Protein mass spectrometry 99
2.14 Statistical analysis 99

Chapter 3: Specialised Pro-resolving Mediators (SPMs) in zebrafish models of inflammation 101
3.1 Introduction to SPMs and eicosanoids in zebrafish 101
3.2 Results 102
3.2.1 The standard neutrophil response to tailfin amputation 102
3.2.2 Inhibition of 15-LOX delayed inflammation resolution both early and late in the inflammatory cycle 104
3.2.3 Inhibition of 5-LOX accelerated inflammation resolution when given late, but delayed inflammation resolution when given early 106
3.2.4 Inhibition of 12-LOX did not affect inflammation resolution when given early, but delayed inflammation resolution when given late 106

3.2.5 LXA4 and RvE1, but not RvD2, accelerated neutrophilic resolution in tailfin transection 108

3.2.6 Only LXA4, and not RvD2 or RvE1, increased neutrophil apoptosis at 3 hours post treatment, but not at 6, 9 or 12 hours post treatment 111

3.2.7 Histochemical quantification of neutrophils matched live trends 113

3.2.8 All three SPMs increased reverse migration of neutrophils in different ways ... 115

3.2.9 LXA4 and RvE1, but not RvD2, increased NFκB reporter expression in tailfin injury 118

3.2.10 RvE1, but not LXA4 or RvD2, increased the rate of tailfin regeneration 118

3.2.11 LXA4 and RvD2 increased macrophage numbers and RvE1 accelerated arrival of macrophages in tailfin injury 121

3.2.12 LXA4, but not RvD2 or RvE1, improved survival in systemic *Staphylococcus aureus* infection 123

3.2.13 RvD2 and RvE1, but not LXA4, increased survival in systemic *Enterococcus faecalis* infection 123

3.2.14 Development of GIT injury model 126

3.2.15 LXA4 reduced, RvD2 did not affect, and RvE1 increased neutrophil numbers in a GIT injury 129

3.2.16 All three SPMs reduced peak macrophage numbers attending to an intestinal wound 132

3.3 Discussion and further work 135

3.4 Summary of important findings 139

Chapter 4: Investigation of SPM receptors in larvae and development of a spatial RNA analysis (TomoSeq) of zebrafish tailfin injury 140

4.1 Receptor expression and spatial RNA analysis in zebrafish 140

4.2 Results 141

4.2.1 *gpr18, cmklr1* and *fpr1* receptor RNA are expressed in zebrafish embryos from 1dpf 141

4.2.2 Over-expression of *fpr1, gpr18* and *cmklr1* did not reduce neutrophil numbers at 6hpi 143

4.2.3 Over-expression of *gpr18*, but not *fpr1* or *cmklr1*, increased neutrophil numbers at 12hpi 145

4.2.4 Over-expression of *fpr1*, *gpr18* and *cmklr1* did not affect neutrophil numbers at 24hpi.....147
4.2.5 Over-expression of *gpr18*, but not *fpr1* or *cmklr1*, increased tailfin regeneration..... 149
4.2.6 Endogenous *cmklr1* expression, but not *fpr1* or *gpr18*, was increased at the site of tailfin injury from 6hpi onwards.....151
4.2.7 Setup of Tomographic RNA sequencing (TomoSeq) 159
4.2.8 Preliminary validation of the TomoSeq results 161
4.2.9 Expression patterns of genes known to play a role in inflammation or have anatomical specificity recapitulated known patterns.....168
4.2.10 Top genes expressed in uninjured controls compared with injured larvae 171
4.2.11 Differential genes were up- and down- regulated in Go enrichment analysis 172
4.2.12 Growth and differentiation genes were up-regulated in controls and stimulus response genes in injured.....177
4.2.13 Functional enrichment analysis showed differential expression of cellular component genes.....181
4.3 Discussion and further work 183
4.4 Summary of important findings.....186

Chapter 5: *Enterococcus faecalis* intestinal colonisation in the zebrafish and its effect on inflammation 187
5.1 The importance of organ specificity, colonisation and *E. faecalis* in inflammation.... 187
5.2 Results.....188
5.2.1 Following microgavage, *E. faecalis* persisted in an anatomically distinct region of the zebrafish GIT.....188
5.2.2 The *E. faecalis* OG1RF-Δ*epaX* mutant had impaired colonisation of the zebrafish intestinal tract 189
5.2.3 The parental background strain of the Δ*EpaX* mutant did not affect colonisation potential 193
5.2.4 Persisting *E. faecalis* did not induce an increase in physiological inflammatory markers.....196
5.2.5 *E. faecalis* colonisation increased NFκB expression along the GIT 199

5.2.6 *E. faecalis* in an uninjured GIT did not incite a cellular inflammatory response 199
5.2.7 In contrast to *E. faecalis*, *S. aureus* SA113 incited a neutrophil response in the uninjured intestine 202
5.2.8 Colonisation with *E. faecalis* reduced the number of macrophages patrolling the intestinal region 202
5.2.9 Generation of a new transgenic zebrafish *TgBAC(Cldn15la:Col1a2-eGFP)* 205
5.2.10 Collagen was expressed within the basement membrane only from 15dpf onwards when infolding of the intestinal tract begins 207
5.2.11 Colonising *E. faecalis* was closely association with the intestinal villi 211
5.2.12 Colonising *E. faecalis* were viable and not invading intracellularly 213
5.2.13 In the presence of an acute intestinal injury, *E. faecalis* increased neutrophil infiltration 216
5.2.14 RvE1 and RvD2, but not LXA4 reduced peak neutrophil numbers at an intestinal injury in the presence of *E. faecalis* 218
5.2.15 SPMs differentially affected peak macrophage numbers attending an intestinal wound in the presence of *E. faecalis* 221
5.3 Discussion and future work 224
5.4 Summary of important findings 227

Chapter 6: Investigation of the mechanism of action of intestinal alkaline phosphatase (iAP) in the zebrafish 228
6.1 Introduction to iAP and its importance in immunology 228
6.2 Results 229
6.2.1 Persisting *E. faecalis* increased localised expression of iAP 229
6.2.2 iAP expression was up-regulated following distal intestinal injury 232
6.2.3 iAP decreased neutrophil numbers attending to an intestinal wound site, even in the presence of *E. faecalis* 234
6.2.4 iAP decreased macrophage numbers attending to an intestinal injury 237
6.2.5 iAP reduced neutrophil recruitment and accelerated inflammation resolution in a sterile tailfin injury 239
6.2.6 iAP increased the rate of arrival of macrophages but decreased peak macrophage numbers in a sterile tailfin injury 239

6.2.7 iAP did not increase rate of tailfin regeneration at 24hpi 243

6.2.8 iAP did not improve survival in severe *S. aureus* bacteraemia.....243

6.2.9 iAP effects on neutrophil recruitment were abrogated when either a generic adenosine receptor antagonist, or adenosine deaminase, were administered.....245

6.2.10 iAP exerted its neutrophilic anti-inflammatory effects via adenosine A2b receptors, but not A1 or A2a receptors 247

6.2.11 iAP reduced NFκB expression following tailfin injury 249

6.3 Discussion and further work 251

6.4 Summary of important findings.....254

Chapter 7: Intestinal alkaline phosphatase and intestinal wound healing in the mouse..... 255

7.1 The clinical burden of wound healing and the relevance of iAP.....255

7.2 Results.....256

7.2.1 Voluntary ingestion of Nutella as a mode of treatment delivery was feasible 256

7.2.2 A proximal colonic anastomosis was the choice for investigation.....259

7.2.3 iAP did not significantly alter the post-operative activity index of mice in the standard model 259

7.2.4 iAP significantly accelerated the return of normal bowel function post-operatively in the standard model.....264

7.2.5 iAP significantly increased post-operative weight gain in a standard model 266

7.2.6 iAP significantly increased anastomotic bursting pressure (ABP) on day three in the standard model.....268

7.2.7 iAP increased anastomotic hydroxyproline content on day three in the standard model.....268

7.2.8 iAP did not affect hydroxyproline content in the skin wound in the standard model.....272

7.2.9 iAP did not significantly alter spleen weights in the standard model.....272

7.2.10 iAP did not affect the diversity of faecal bacteria in the standard model 276

7.2.11 iAP did not affect the diversity of faecal fungi in the standard model 276

7.2.12 iAP did not affect faecal cellulolytic activity in the standard model 279

7.2.13 iAP did not affect faecal proteolytic activity in the standard model 279

7.2.14 iAP did not affect anastomotic MMP2 or MMP9 activity in the standard model..... 282
7.2.15 iAP did not affect skin MMP2 or MMP9 activity in the standard model..... 282
7.2.16 iAP significantly increased the activity of anastomotic DISP on day seven in the standard model..... 285
7.2.17 No ALs occurred in the iAP group in the leaking model..... 287
7.2.18 iAP significantly increased the activity index in the leaking model 289
7.2.19 iAP accelerated the return of normal bowel movements in the leaking model..... 289
7.2.20 iAP accelerated post-operative weight gain in the leaking model 291
7.2.21 iAP significantly increased ABP on day three in the leaking model 291
7.2.22 iAP significantly increased anastomotic hydroxyproline content on day three in the leaking model 291
7.2.23 iAP did not affect spleen weights in the leaking model..... 295
7.2.24 iAP did not affect diversity of faecal bacteria in the leaking model 295
7.2.25 iAP did not affect diversity of faecal fungi in the leaking model 298
7.2.26 iAP did not affect faecal cellulolytic activity in the leaking model 298
7.2.27 iAP decreased faecal proteolytic activity on day three in the leaking model.. 301
7.2.28 iAP did not affect anastomotic MMP2 or MMP9 activity in the leaking model..... 304
7.2.29 iAP did not affect skin MMP2 or MMP 9 activity in the leaking model..... 304
7.2.30 iAP did not increase DISP activity in the leaking model 304
7.3 Discussion and future work..... 308
7.4 Summary of important findings..... 312

Chapter 8: Conclusion and future work..... 313
References 318
Appendix 1: TomoSeq numbered primer sequences 360

List of Figures

Figure 1-1: The three overlapping stages of wound healing. 35
Figure 1-2: Simplified pathways of synthesis of SPMs. 37
Figure 1-3: The inflammatory response in an organ, such as the intestinal tract, that may be modulated by SPMs. 37
Figure 1-4: The tri-faceted approach to anastomotic healing. 48
Figure 2-1: Plasmid maps for zebrafish receptors cloned using the ZERO blunt TOPO II cloning kit. 59
Figure 2-2: Successful bacteriophage transduction. 75
Figure 2-3: Pelleted colonies following growth to exponential phase of selected fluorescent colonies. 75
Figure 2-4: Region of interest at the site of tailfin injury. 79
Figure 2-5: Intravascular microinjection site in 2dpf zebrafish larvae. 79
Figure 2-6: Reverse migration assay. 82
Figure 2-7: TSA/TUNEL assay. 84
Figure 2-8: Example snapshot of neutrophil tracking in from intestinal injury using Volocity 6.3. 88
Figure 2-9: Stool collected over 24 hours. 93
Figure 2-10: A normal anastomosis. 93
Figure 3-1: Time course of neutrophil response to tailfin transection. 103
Figure 3-2: Neutrophil counts at the region of tailfin injury, following treatment with the 15-LOX inhibitor (PD146176) or vehicle control. 105
Figure 3-3: Neutrophil counts at the region of tailfin injury, following treatment with the 5-LOX inhibitor (MK886) or vehicle control. 107
Figure 3-4: Neutrophil counts at the region of tailfin injury, following treatment with the 12-LOX inhibitor (ML355) or vehicle control. 107
Figure 3-5: Neutrophil counts at the site of tailfin injury, following treatment with SPM (LXA4, RvD2, or RvE1) or vehicle control. 109
Figure 3-6: Neutrophil counts at 12hpi the site of tailfin injury, following delayed treatment (5.5hpi) with SPM (LXA4, RvD2, or RvE1) or vehicle control. 110
Figure 3-7: TSA/TUNEL staining performed at 3, 6, 9 and 12 hours post treatment with SPM or vehicle control. 112
Figure 3-8: Biochemical neutrophil quantification with TSA in the region of tailfin injury. 114
Figure 3-9: Number of reverse migrating neutrophils over time at the region of tailfin injury. 116

Figure 3-10: Movement characteristics of reverse migrated neutrophils in the presence of SPMs. 117
Figure 3-11: Expression of NFκB in the region of injury in tailfin transection with SPM treatment. 119
Figure 3-12: Tailfin regeneration with SPM treatment. 120
Figure 3-13: Macrophage counts at tailfin ROI in 2dpf *Tg(mpeg1:NLS-Clover)sh436*. 122
Figure 3-14: Effect of SPMs on survival in systemic infection with *S. aureus*. 124
Figure 3-15: Effects of SPM on survival in systemic infection with *E. faecalis*..... 125
Figure 3-16: Laser injury to the GIT. 127
Figure 3-17: Neutrophil responses with laser or mechanical intestinal injury. 128
Figure 3-18: Neutrophil counts at the site of intestinal injury with SPM treatment. 130
Figure 3-19: Effect of SPMs on movement characteristics of neutrophils attending to an intestinal wound site. 131
Figure 3-20: Macrophage counts at the site of intestinal injury. 133
Figure 3-21: Effect of SPMs on movement characteristics of macrophages attending to an intestinal wound. 134
Figure 4-1: Reverse-transcription PCR for expression of SPM receptors in zebrafish embryos and larvae. 142
Figure 4-2: Neutrophil counts at 6hpi following over-expression of each receptor using RNA injection at one cell stage. 144
Figure 4-3: Neutrophil counts at 12hpi following over-expression of each receptor using RNA injection at one cell stage. 146
Figure 4-4: Neutrophil counts at 24hpi following over-expression of each receptor using RNA injection at one cell stage. 148
Figure 4-5: Receptor mRNA over-expression and tailfin regeneration..... 150
Figure 4-6: *fpr1*wholemount *in situ* hybridisation (WISH). 152
Figure 4-7: *cmklr1* WISH at 2 and 4hpi..... 153
Figure 4-8: *cmklr1* WISH at 6 and 8hpi..... 154
Figure 4-9: *cmklr1* WISH at 10 and 12hpi..... 155
Figure 4-10: *gpr18* WISH at 1 and 2hpi..... 156
Figure 4-11: *gpr18* WISH at 4 and 6hpi..... 157
Figure 4-12: *gpr18* WISH at 8 and 12hpi..... 158
Figure 4-13: Representative images showing a 2dpf zebrafish larvae of *TgBAC(mpx:GFP)i114* and position of frozen sectioning..... 160

Figure 4-14: First uninjured control larva. 162
Figure 4-15: Second uninjured control larva. 163
Figure 4-16: Third uninjured control larva. 164
Figure 4-17: First injured larva. 165
Figure 4-18: Second injured larva. 166
Figure 4-19: Third injured larva. 167
Figure 4-20: Expression of *cyr61l1*, an acute phase protein, along the zebrafish tailfin. 169
Figure 4-21: Expression patterns across all the zebrafish for *alox12, cldn15la,* and *alpi.1*. 170
Figure 4-22: Biological processes linked to enriched analysis in GOrilla in uninjured larvae. 173
Figure 4-23: Biological processes linked to enriched analysis in GOrilla in injured larvae. 174
Figure 4-24: Heatmap of up-regulated control genes. 178
Figure 4-25: Heatmap of up-regulated injured genes 179
Figure 4-26: Gene overlap between samples plotted with FunRich. 180
Figure 4-27: Cellular component analysis of functional enrichment analysis using FunRich. 182
Figure 5-1: Intestinal colonisation by *E. faecalis* in 4dpf zebrafish larvae. 190
Figure 5-2: *E. faecalis* colonisation of zebrafish intestinal tract. 191
Figure 5-3: Location of *epaX* mutations. 191
Figure 5-4: *EpaX* is required for *E. faecalis* colonisation of the zebrafish intestine. 192
Figure 5-5: Growth curves over 9 hours for OG1RF WT and *OPDV* Δ*EpaX* mutants. 194
Figure 5-6: The effect of *E. faecalis* mutations on intestinal colonisation. 195
Figure 5-7: Physiological inflammatory markers were not increased in *E. faecalis* colonisation. 197
Figure 5-8: Acridine orange staining for cell death as a marker of intestinal inflammation. 198
Figure 5-9: NFκB was up-regulated upon colonisation with *E. faecalis*. 200
Figure 5-10: Neutrophilic responses in region 2&3 of the zebrafish intestinal tract to PBS, *E. faecalis* or DSS 0.5% (w/v). 201
Figure 5-11: Neutrophilic response to SA113 microgavage in the zebrafish larval GIT. 203
Figure 5-12: Macrophage response to *E. faecalis* colonisation in the uninjured intestine. 204
Figure 5-13: Generation of *TgBAC(Cldn15la:Col1a2-eGFP)sh546*. 206
Figure 5-14: Picrosirius staining in 7-12dpf zebrafish. 208
Figure 5-15: Picrosirius staining in 13-22dpf zebrafish. 209
Figure 5-16: Picrosirius staining of 25-27dpf zebrafish. 210
Figure 5-17: Live imaging of *TgBAC(Cldn15la:Col1a2-eGFP)*. 212
Figure 5-18: TEM images of transverse sections of *E. faecalis* colonised 5dpf zebrafish. 214
Figure 5-19: TEM images of transverse sections of *E. faecalis* colonised 5dpf zebrafish. 215

Figure 5-20: Neutrophil responses to an acute intestinal injury in the presence of *E. faecalis* colonisation.....217
Figure 5-21: Neutrophil responses to an acute intestinal injury in the presence of *E. faecalis* colonisation with treatment with SPM treatment. 219
Figure 5-22:Parameters of neutrophil movement around an intestinal injury in the presence of *E. faecalis* with or without SPM treatment. 220
Figure 5-23: Macrophage responses to an acute intestinal injury in the presence of *E. faecalis* colonisation with treatment with SPM treatment. 222
Figure 5-24: Parameters of macrophage movement around an intestinal injury in the presence of *E. faecalis* with or without SPM treatment. 223
Figure 6-1: Ventral view of 5.2dpf zebrafish larvae demonstrating *in situ* expression of endogenous alkaline phosphatase.....230
Figure 6-2: Staining of endogenous ALP using NBT/BCIP. 231
Figure 6-3: Increase in ALP expression in proximal gut 6hpi. 233
Figure 6-4: Neutrophil numbers in the region of intestinal injury following microgavage with vehicle control or iAP, with or without *E. faecalis*. 235
Figure 6-5: Parameters of neutrophil movement after intestinal injury in uncolonised or E. faecalis colonised *TgBAC(mpx:GFP)i114*. 236
Figure 6-6: Effects of iAP on macrophage response to intestinal wound. 238
Figure 6-7: Immediate iAP treatment following sterile tailfin injury. 240
Figure 6-8: Delayed (5.5hpi) iAP treatment following sterile tailfin injury. 241
Figure 6-9: Effects of iAP on macrophage response to a sterile tailfin injury. 242
Figure 6-10: Effect of iAP on tailfin regeneration.....244
Figure 6-11: Effects of iAP on survival in a severe *S. aureus* bacteraemia. 244
Figure 6-12: Anti-inflammatory effects of iAP were abolished by caffeine, a non-selective adenosine receptor inhibitor, as well as adenosine deaminase. 246
Figure 6-13: Specific adenosine receptor inhibition in sterile tailfin injury in 2dpf *TgBAC(mpx:GFP)i114* larvae. 248
Figure 6-14: NFκB expression following tailfin injury and treatment with iAP or vehicle control. 250
Figure 7-1: Mouse taste test. 258
Figure 7-2: Colonic anastomosis in a male mouse.....260
Figure 7-3: Mice approximately 6 hours post-operative. 261
Figure 7-4: Tracking analysis of mouse movement. 263

Figure 7-5: Twenty four hour stool collection and weights in the standard anastomosis model. ...265
Figure 7-6: Percentage body weight on each post-operative day in the standard anastomosis model. 267
Figure 7-7: Anastomotic bursting pressure (ABP) in the standard anastomosis model. 269
Figure 7-8: Anastomotic hydroxyproline content in the standard anastomosis on the third and seventh post-operative days. 270
Figure 7-9: Picrosirius staining to investigate collagen architecture in the healed anastomosis. ...271
Figure 7-10: Hydroxyproline content in healing skin laparotomy wound in the standard anastomosis model. 273
Figure 7-11: Picrosirius red staining of laparotomy skin wound.....274
Figure 7-12: Spleen weights in the standard anastomosis model. 275
Figure 7-13: Bacterial morphologies isolated from stool in the region of the anastomosis in the standard model. 277
Figure 7-14: Fungi cultured from stool in the region of the anastomosis. 278
Figure 7-15: Cellulolytic activity in stool from the region of the anastomosis in the standard model. 280
Figure 7-16: Proteolytic activity in the stool from the region of the anastomosis in the standard model. 281
Figure 7-17: MMP2 and MMP 9 in the anastomosis on post-operative day three and day seven in the standard model. 283
Figure 7-18: MMP2 and MMP9 activity within the skin wound in the standard anastomosis model. 284
Figure 7-19: An anastomotic serine protease, later identified as DISP, on days three and seven. .286
Figure 7-20: Anastomotic leaks in the leaking model. 288
Figure 7-21: Leaking model activity index. 290
Figure 7-22: Measurement of 24hour Stool weight (grams) in the leaking model. 290
Figure 7-23: Percentage body weight against time for the leaking model. 292
Figure 7-24: Anastomotic bursting pressure in the leaking anastomosis model on the third and seventh post-operative days. 293
Figure 7-25: Hydroxyproline content in the anastomoses of the leaking model on the third and seventh post-operative days. 294
Figure 7-26: Spleen weights on post-operative day three and seven in the leaking model. 296
Figure 7-27: Growth of faecal bacteria from the region of the anastomosis in the leaking model on the third and seventh post-operative day. 297

Figure 7-28: Fungal growth morphology cultivated from stool taken from the region of the anastomosis in the leaking model on post-operative days three and seven. 299
Figure 7-29: Cellulolytic activity assessed using digestion of CMC agar plates on the third and seventh post-operative day in the leaking model. 300
Figure 7-30: Proteolytic activity in the faecal matter from the anastomotic region on the third and seventh post-operative day in the leaking model. 302
Figure 7-31: Frozen sections of the anastomotic region stained with haematoxylin and eosin (H&E) and Wright Giemsa (WG) on day three in the leaking model. 303
Figure 7-32: MMP2 and MMP9 expression at the anastomosis on day three and seven in the leaking model. 305
Figure 7-33: Evaluation of MMP2 and MMP9 expression in the skin laparotomy wound on day three and seven in the leaking anastomosis model. 306
Figure 7-34: Distal intestinal serine protease (DISP) on day three and seven of the leaking model. 307

List of Tables

Table 1-1: Exemplar interventions for prevention of ALs and their relationship to the inflammatory process. 29
Table 2-1: Antibiotic solutions and concentrations 55
Table 2-2:Bacterial strains. 73
Table 2-3: List of transgenic fish lines 77
Table 2-4: Sample size calculation. 90
Table 2-5: Wellness score 92
Table 2-6: Murine Sepsis Score 92
Table 4-1: Top ten expressed genes in all three larvae in the injured and uninjured groups. 171
Table 4-2: Go enrichment of conserved control genes 175
Table 4-3: Go enrichment of conserved injured genes 176
Table 7-1: Top five mass spectrometry matches according to iBAQ score 286

Chapter 1: Introduction

1.1 The importance of anastomotic leaks and the scope of the problem

Treatments for haemorrhoids have been described since the 12th and 13th century BC, but direct surgical intervention in other parts of the bowel was actively avoided in ancient times, being performed infrequently even in acute injuries, and almost always ending dismally (Warusavitarne and Phillips, 2007). Whilst cutaneous breaches alone, even surgically induced ones, are often trivial and chronic wounds tolerated for years, incisions involving the gastrointestinal tract (GIT) are complex, and the consequences of failure to heal in this region often rapidly life-threatening. It was only in 1783 that Dubois performed the first recorded operation on uninjured bowel in the form of a colostomy for anorectal malformation in a baby, who tragically survived only ten days (Yesildag, Muñiz and Buyukunal, 2010). Another forty years would pass before the first segmental colonic excision was survived in 1823, but followed soon after by a successful anorectal excision in 1826 (Graney and Graney, 1980). Since then, the numbers of GIT operations have grown exponentially. In the UK alone, between 2005-2014, lower GIT resections alone increased by almost a thousand cases per annum, to a total of over 29,000 resections in 2014 (Eurostats, 2017). This rising number comes as no surprise due to increasing public awareness of bowel cancer symptomatology, combined with screening programmes performed in an ageing population. Reassuringly, improvements in survival have been substantial compared to that first foray into GIT surgery in the 18th century, but one complication continues to haunt the surgeon, and indeed, the surviving patient: the anastomotic leak (AL).

Many resections now involve an anastomosis to re-join the ends of the remaining bowel, thus restoring GIT continuity. While most heal uneventfully, in up to 26% of patients (Schiff *et al.*, 2016) healing fails and an AL develops despite the best technical efforts. When an anastomotic leak occurs, intestinal contents leak into the peritoneal cavity. Intestinal contents contain multiple microorganisms and either digestive enzymes or frank faeces, depending on the location of the anastomosis within the GIT. This can result in a range of complications such as abscesses, erosion of surrounding tissues causing abnormal connections (fistulae), generalised infection of the peritoneum (peritonitis) with an accompanying systemic inflammatory response, and even multi-

organ failure and death. Because of the serious consequences of failure of healing, decades have been dedicated to optimising operative techniques such as accurate apposition of tissues with submucosal suturing to evert the mucosal layer for a leak-free join, careful preservation of the vascular arcades to the ends of the anastomosis with visible perfusion, and maintenance of a sterile operating field. When these failed to eliminate leaks, further fine-tuning extended to the peri-operative period with careful control of blood pressure and albumin levels, in addition to advances in surgical technology culminating in increasingly sophisticated staplers, and increasingly varied adjuncts such as fibrin glue and nickel-titanium compression rings (Tabola *et al.*, 2017). But none of these have proven infallible. For decades, surgeons have puzzled over this conundrum and searched for additional surgical or patient risk factors, such as smoking, male sex, anastomoses close to the anal verge, high arterial ligation or pre-operative radiotherapy (Kingham and Pachter, 2009; Trencheva *et al.*, 2012; Lee and Mishra, 2014; Byrne *et al.*, 2015). Indeed, many risk stratification strategies have emerged but again, none consistently predict or explain this often-catastrophic complication (Karliczek *et al.*, 2009; Erb, Hyman and Osler, 2014; Wu, Freek and Lange, 2014). Strikingly, despite increasing sophistication in surgical and anaesthetic techniques and equipment, the rate of anastomotic leaks has not decreased over the last few decades (Shogan *et al.*, 2013).

So what do we know so far about the reasons anastomoses leak? Literature directly related to molecular aspects of anastomotic healing is less extensive than would have been ideal, perhaps because of the technical challenges in creating an intestinal wound and subsequently directly observing healing in an internal organ in a clinically relevant manner, but observational studies generally support a central role for inflammation in affecting wound healing.

1.2 **The importance of inflammation to wound healing**

One of the defining observations in early medicine was that inflammation accompanies injury. First described by Celsus in 1AD (Rather, 1971), the cardinal features of inflammation, to different magnitudes, inevitably follow invasive surgical procedures. Many of the basic tenets of good surgical practice such as meticulously gentle tissue handling, preserving a good blood supply, debridement of non-viable tissue, and asepsis, may have their molecular basis in minimising the magnitude of inflammation that occurs. Whilst there is certainly no place for

gross departure from these principles, how important are they in preventing AL and how might they relate to cellular and molecular aspects of inflammation? Although these principles might seem like irrefutable and fundamental knowledge, many pharmacological potentiates based upon these principles have been reviewed over the years, and the results of these studies were often equivocal or even contradictory (a selection summarised in Table 1-1). However, interpretation of these experimental results is more complex than would seem at first glance, and differing conclusions not always simply due to different models or experimental setups.

Let us examine, as an example, the importance of a good blood supply to the ends of the bowel forming the anastomosis. It almost defies common sense that anything could be more important than this. And yet experimental evidence is conflicting. Early experiments in dogs with intentional vascular occlusion causing 5 cm of visible devascularisation of the anastomotic region showed that in the sterile bowel, maintained by intraluminal antibiotic treatment, anastomoses healed despite this ischaemia (Cohn and Rives, 1956). More recent examples in rodents with segmental colonic ischaemia at the sites of anastomoses suggested a lack of difference in levels of tissue hypoxia between healed or non-healed anastomoses (Shakhsheer *et al.*, 2017). However, in other studies using more severe arterial occlusion, positive effects with hyperbaric oxygen therapy (HBOT) have been demonstrated in healing, and negative effects with systemic hypoxia (Attard *et al.*, 2005; Boersema *et al.*, 2016). But even if we suppose that the conflicting results arose because the submucosal plexus of the intestine is more robust in animals, thus inadequately recapitulating human physiology, clinical reports also conflict. In humans, while reduced microperfusion of the rectal stump has indeed been linked to ALs in some studies (Vignali *et al.*, 2000), other studies show no histological differences in microvascular density between AL and healed specimens (Schouten *et al.*, 2014).

Table 1-1: Exemplar interventions for prevention of ALs and their relationship to the inflammatory process. This list includes some of the options that have been investigated, how they might ultimately impact upon the inflammatory pathways, and their often divergent conclusions.

Intervention investigated	Relationship to the inflammatory process	References	Conclusion
Ischaemia prevention	PHD/HIF pathways (see text)	(Cohn and Rives, 1956)	Ischaemia did not cause AL in a sterile bowel in dogs
		(Shakhsheer *et al.*, 2017)	No difference in tissue hypoxia levels in mice
		(Schouten *et al.*, 2014)	No differences in microvessel density in human histology specimens
		(Pommergaard *et al.*, 2015)	Impaired blood supply impairs healing in mice
		(Attard *et al.*, 2005)	Systemic hypoxia impairs healing in rats
		(Boersema *et al.*, 2016)	HBOT improves anastomotic healing in rats
Electro-magnetic field therapy (EMF)	Electromagnetic field therapy can down regulate inflammatory cytokines (IL6, IL1 COX2) and up regulate IL10 (Ongaro *et al.*, 2012; Pesce *et al.*, 2013)	(Mente *et al.*, 1996)	Improved mechanical strength and hydroxyproline content with EMF in rats
		(Nursal *et al.*, 2006)	No difference in rats
Amniotic membrane	Amniotic membranes have integral immuno modulatory properties to avoid rejection of foetus	(Barski *et al.*, 2017)	Increased inflammation and adhesion, does not prevent AL in rats
		(Moslemi *et al.*, 2016)	Prevents AL and reduced adhesions in rats
Fibrin glue/sealants	Mechanical barrier reducing peri-anastomotic inflammation	(Pantelis *et al.*, 2010)	Positive effect with fibrin glue in healing in mice
		(Senol *et al.*, 2013)	Improved hydroxyproline content with fibrin glue in rats
		(Nordentoft *et al.*, 2015)	A review showing lack of effect of fibrin glue
		(Slieker *et al.*, 2013)	No effect of six different sealants in mice
Sildenafil	Decreased neutrophil infiltration/decreased cytokine (see text)	(Cakir *et al.*, 2015)	Improved collagen maturity in rats
		(Irkorucu and Comert, 2009)	No effect on anastomotic integrity in rats

This confusion surrounding the hierarchical importance of blood supply however, has not slowed efforts to improve intraoperative visualisation of perfusion, with innovations such as scanning laser Doppler flowmetry (Boyle *et al.*, 2000) and fluorescent indocyanine green (ICG) being introduced in recent years. But again, for example with ICG, there is still a lack of randomised controlled trials evidencing a significantly reduced AL rate (Degett, Andersen and Gögenur, 2016). Although non-randomised studies have indicated no leaks in the anastomoses that were immediately revised based upon intraoperative ICG fluorescence, it is unknown if these would ultimately have leaked without revision as ethical concerns prohibit such studies in humans (Jafari *et al.*, 2015).

Perhaps some of the difficulties in obtaining a clear-cut conclusion are because the hypoxia-inflammation axis is more complex within the bowel, compared to other mucosal surfaces like the lung. The bowel is unique in that highly vascularised intestinal structures are in proximity to a physiologically hypoxic lumen especially within the lower GIT (Zheng, Kelly and Colgan, 2015). Studies in humans suggest the existence of a counter current flow within small intestinal villi which allows this permissive hypoxia (Hallback *et al.*, 1978), although there is absence of evidence for this in other mammals such as the rat (Bohlen and Lash, 1995), and the picture is complicated by fluctuations in blood flow from post-prandial hyperaemia. But within the colon, where post-prandial hyperaemia has not been demonstrated, the steep hypoxic gradient appears to be maintained by subsets of facultative anaerobes residing close to the mucosa (Albenberg *et al.*, 2014). In line with this gradient, the GIT is well adapted to tolerate hypoxia and intestinal epithelial cells express the three hypoxia-inducible factor (HIF) α subunits and the constitutive HIF-1β subunit that completes the heterodimer, as well as their inhibitors, the three prolyl hydroxylases (PHDs) and factor-inhibiting HIF1 (FIH1) (Cummins and Crean, 2016). Under basal conditions of physiologic hypoxia, HIF-1α is stabilised and, as a transcription factor, serves to perform enhanced barrier integrity functions in the gut by increasing expression of a multitude of genes such as those coding for mucin (Louis *et al.*, 2006) and antibacterial peptide production (Glover, Lee and Colgan, 2016). As oxygen becomes plentiful, PHDs hydroxylate the inducible α subunit and target it for degradation. So central is the role of HIF1 in maintenance of mucosal homeostasis that inhibitors of PHDs are being trialled clinically as treatment for the chronic inflammatory states of Crohn's Disease and Ulcerative Colitis

(Robinson *et al.*, 2008; Marks *et al.*, 2017), suggesting that higher oxygen tensions are not necessarily always beneficial in healing of this anatomical region.

The early stages of inflammation involve an influx of innate immune cells, neutrophils followed by macrophages, which patrol the inflamed area removing debris and invading pathogens. Neutrophils are primarily glycolytic (Borregaard and Herlin, 1982) and therefore able to function without detriment in environments of low oxygen tension. However, neutrophils also increase hypoxia in inflammatory environments as they consume many more times the amount of oxygen than other cells, when generating an antimicrobial oxidative burst (Colgan and Taylor, 2010). Whilst it might be imagined that hyperbaric oxygen therapy (HBOT) in the animal experiments above acts solely by reversing this hypoxia, the picture is more complex. HBOT, in fact, also acts in an independently anti-inflammatory manner within the intestine, and has been shown to directly block interleukin-1β (IL-1β) and increase HIF-1α mRNA (Novak *et al.*, 2016). This is possibly through stabilisation of HIF-1α via formation of oxygen radicals, but exact mechanisms are as yet unclear (Novak *et al.*, 2016). A similar example of the complexity of mechanism of action is with sildenafil, a vasodilator beneficial in anastomotic healing ostensibly by increasing blood flow and thus oxygenation (Ayten *et al.*, 2008), but which again has independent anti-inflammatory properties by decreasing TNF-α and interleukin-6 (IL-6) in human studies (Vlachopoulos *et al.*, 2015). The importance of inflammation is also often also under-emphasised in related areas that may indirectly impact upon healing. One example is that of post-operative ileus, where normal GIT motility fails to return in a timely manner. The sympathetic neural response to intrusion of the peritoneal cavity and handling of bowel causes a reactive hypomotility of the GIT, which usually fades quickly upon abdominal closure, but prolonged ileus can occur, has been shown to be associated with increased IL-6 and leukocyte infiltration of the bowel (Kalff *et al.*, 1999; The *et al.*, 2007), and has a positive correlation with rates of AL (Moghadamyeghaneh *et al.*, 2016). Here again evidence shows that inhibiting the inflammatory axis improves ileus (Schwarz *et al.*, 2001; Raju *et al.*, 2015), with clinical studies comparing laparoscopic with open surgery confirming a relationship between decreased inflammation, as evidenced by lower CRP levels post-laparoscopy, with lower ileus and AL rates (Mungo *et al.*, 2017). So how might improving inflammation improve wound healing?

1.3 **Manipulating inflammation to promote wound healing**

Wound healing can be divided into three overlapping phases (Figure 1-1A). Any breach in epithelial or mucosal layer of an organism, even in the absence of immediate ingress of microorganisms, generates an initial inflammatory response which is characterised by the influx of inflammatory cells. Neutrophils are the first cells to be mobilised to the site, and play an important role in controlling pathogens and to a certain extent, debris. Although removal of debris is not traditionally thought to be one of the main roles of neutrophils, in guinea pig wound models, the number of erythrocytes in neutrophil-depleted, macrophage-normal, wounds were six times that of normal wounds (Simpson and Ross, 1972). It was speculated that neutrophils could release a haemolytic substance that aided in clearance of erythrocytes. Intriguingly, there was no evidence of impaired cutaneous wound healing despite this, whereas a long history of surgical observation (Guo and DiPietro, 2010) suggests that haematoma formation would impede healing, especially within the bowel. This is because coagulated blood would represent an enriched medium for bacterial proliferation. Certainly in mice with Haemophilia B, wound healing is delayed with an abundance of erythrocytes seen within the wound (Hoffman *et al.*, 2015), although it is difficult to tease out the role of thrombin deficiency from that of erythrocyte accumulation affecting wound healing in those experiments.

The second phase of wound healing is a granulation stage, marked by resolution of the acute inflammation, and initiation of the laying down of extracellular matrix, contraction of myofibroblasts, and proliferation of cells at the wound edge. This is then followed closely by, or occurs concurrently with, the final phase which includes the remodelling of the wound, including the formation of more collagen, to restore tissues to their former homeostatic state (Clarke, 1988). Resolution of the initial inflammation stage appears to be a pre-requisite for proper procession toward complete wound healing. The persistence of high numbers of activated neutrophils leads to chronic inflammation which disrupts the normal flow of healing (Figure 1-1B) due to the continued release of factors such as elastase and gelatinase that prevent laying down of normal extracellular matrix (Jiang *et al.*, 2016). Although any one of these overlapping phases of healing could go wrong, in all cases of the emerging chronic wound, there exist imbalances between pro-inflammatory and pro-resolution mediators resulting in chronic inflammation (Pierce, 2001). The alluring prospect of a therapeutic agent that could halt the

chronicity of inflammation and drive the healing process to completion (Figure 1-1C) is a current area of active research. Already it has been shown that in diabetic mice models with chronic wounds, neutrophil depletion using anti-mouse antibodies increased the rate of healing by 50% (Dovi, He and Dipietro, 2003).

But going even further, perhaps healing could be accelerated, even in the absence of pathology, by a therapeutic anti-inflammatory agent thus enhancing the organisms natural processes (Figure 1-1D). Or could the inflammation phase be skipped altogether? There is controversial evidence about whether inflammation is required for the wound healing process. Early work on wound healing using the CXCR2-knockout mouse (Devalaraja *et al.*, 2000), suggested that neutrophils were essential to initiate healing. CXCR2 is a chemokine that is essential for neutrophil recruitment to a wound. But CXCR2 is also present on keratinocytes and removing this might influence their behaviour during the granulation phase in ways that could not be accounted for in that model. Evidence against the requirement for neutrophils are in models of neutrophil-depleted mice (Dovi, He and Dipietro, 2003), where not only was wound healing was accelerated but healing occurred with less scarring. It should be pointed out however that in this model, 15% of neutrophils still remained and a sterile wounding technique was used. Nonetheless, other studies using *pu.1*-null mice that do not have functioning neutrophils or macrophages (Martin *et al.*, 2003), have also demonstrated improved wound healing that occurs without scarring in this group. Again, it should be noted that these experiments were done in neonatal mice, and foetal skin is fundamentally different to adult skin, where scar-less healing could be an intrinsic property of the foetal fibroblast rather than purely a consequence of lack of inflammatory cells (Leavitt *et al.*, 2016).

Indeed, although it has been demonstrated that having any histological evidence of chronic inflammation, for example in patients with inflammatory bowel disease (IBD), at the joined ends of an anastomosis conferred an odds ratio of 2.7 in developing an AL (Telem *et al.*, 2010), completely eliminating inflammation *per se* does not seem to be a panacea because, paradoxically, anti-inflammatory drugs have met with unexpected failure in preventing ALs. Instead, non-steroidal anti-inflammatory drugs were associated with an increase in AL (Holte *et al.*, 2009; Bakker *et al.*, 2015). This may be because, while COX-1 is constitutively expressed

by intestinal epithelial cells, COX-2 expression is induced by the presence of inflammatory mediators. Recent studies in mice have identified COX-2 dependent production of PGE_2 as essential for neovascularisation and subsequent intestinal healing, with disruption of this pathway increasing ALs (Reisinger *et al.*, 2017), but other inflammatory mediators such as IL-6 have also been shown to be essential during the initial injury phase to promote epithelial reconstitutition within the intestine (Kuhn *et al.*, 2014).

Interestingly, in the Reisinger experiments, administration of PGE_2 alone did not fully rescue the COX-2 knockout AL phenotype (Reisinger *et al.*, 2017). As the authors suggested, this could have been due to dosage, since mice appear to have a high sensitivity to the loss of even one functional allele of the parent gene (Manieri *et al.*, 2012). But perhaps it could also be due to COX-2 inhibition blocking M2 macrophage differentiation (Na *et al.*, 2015; X. Wang *et al.*, 2017) and thus disrupting the closely intertwined production pathways of specialised pro-resolving mediators (SPMs) such as lipoxins and resolvins (Norris, Libreros and Serhan, 2019). SPMs are the end products of the eicosanoid pathways (Capra *et al.*, 2015), and they have a role in limiting acute inflammation or even reversing chronic inflammation. SPMs are synthesised from three different fatty acid (FA) precursors: arachidonic acid (AA), docosahexaenoic acid (DHA) and eicosapentaenoic acid (EPA). Their synthesis requires three different lipoxygenase (LOX) enzymes in the human, often concatenated in action, but these pathways are significantly simplified in Figure 1-2 for clarity. In the most simplified version of these pathways, each essential FA gives rise to a different series of SPMs. Synthesised from AA are the Lipoxins A4 (LXA4) and B; from EPA, the Resolvins (Rv) E1-3; and from DHA, RvD1-6, Protectin 1 (PD1), and Maresin (Mar) 1-3.

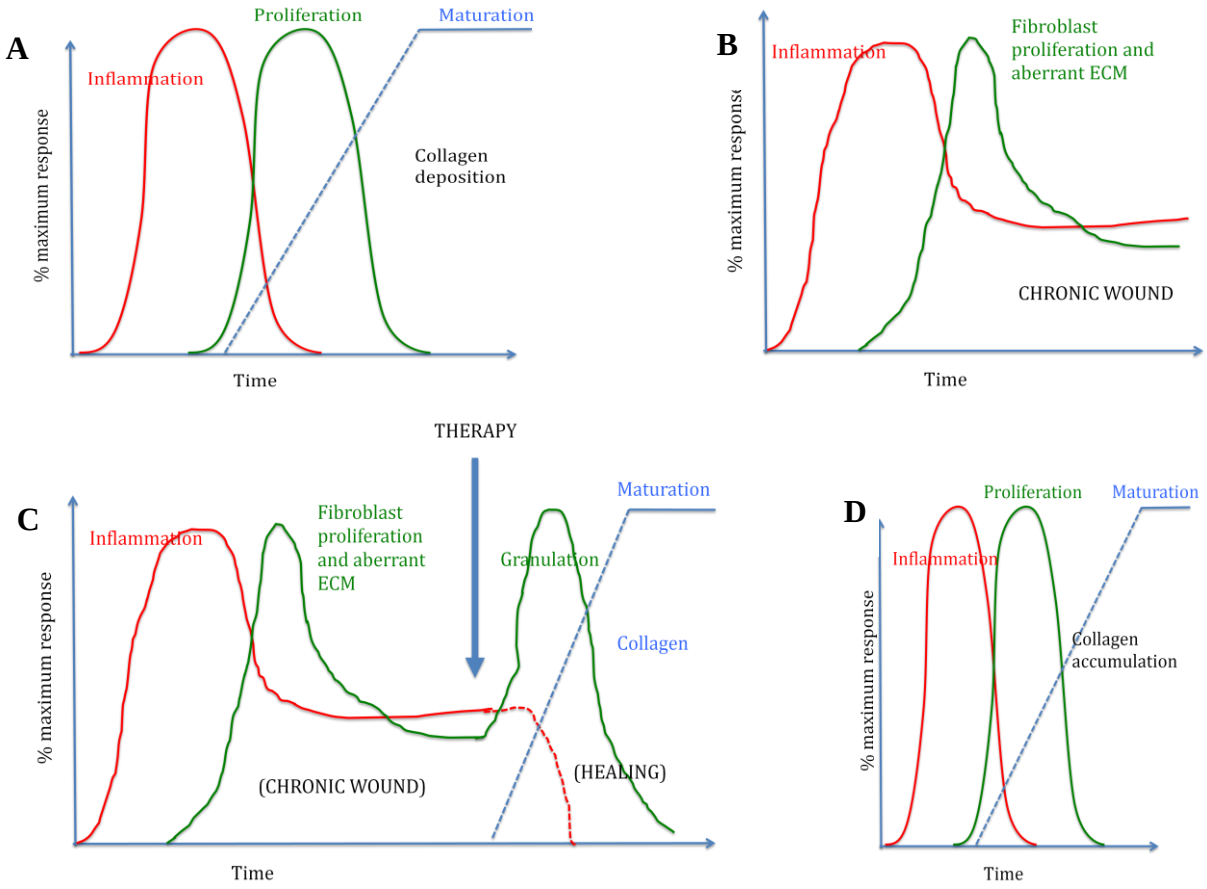

Figure 1-1: The three overlapping stages of wound healing. A. Normal wound healing (Clarke, 1988). **B**. Wound healing disrupted in chronic inflammation. **C**. Therapeutic intervention to allow rescue of wound healing in cases of chronic inflammation. **D**. Accelerated wound healing with shortened inflammatory stage.

1.4 **The role of lipid mediators (SPMs) in inflammation**

SPMs have been shown to actively drive resolution of inflammation (Souza and Norling, 2015), but each SPM may play subtly different roles in this process. LXA4, being one of the first SPMs to be synthesised, appears to be instrumental in initiating the resolution process by inhibiting recruitment of neutrophils, whereas RvE1 is able to shorten the entire inflammatory process (Bannenberg *et al.*, 2005). There are various phases in the inflammatory process (Figure 1-3) in which SPMs may exert their effects. Very soon after an injury or a microbial insult to the tissues, the inflammatory response begins with chemotactic signals that recruit more neutrophils. These signals can be attenuated by SPMs, for example, RvE1 acts as a partial LTB4 (a potent chemo-attractant) receptor antagonist (Arita *et al.*, 2007), effectively muting the signal for neutrophil recruitment. On mucosal surfaces, a similar chemotactic gradient is observed that draws neutrophils via a transepithelial route to mount a defensive response on the mucosal surface. There is some evidence that the mass migration of neutrophils via this route disrupts the tight junction barriers and precedes the development of ulceration in IBD. In these cases, LXA4 appears to down regulate transepithelial migration by decreasing TNFα and IL8, both strong chemo attractants (Gronert *et al.*, 1998).

But traversing tight junctions is not the only way neutrophils can cause detrimental effects. Neutrophils kill invading bacteria in several ways: by internalising them and then fusion of the phagosome with intracellular granules killing bacteria by both oxidative and non-oxidative mechanisms, by discharging these granules directly into the extracellular region (Kang et al., 2001), or by neutrophil extracellular traps (NETs) (Brinkmann et al., 2004). Because neutrophil degranulation and NETs concentrate a high level of toxic substances locally, prolonged activity from the persistently high neutrophil numbers in tissues with chronic inflammation (Kolaczkowska and Kubes, 2013) could lead to significant tissue damage and compromised wound healing. SPMs can downgrade the persistence of neutrophils by enhancing non-inflammatory attrition of neutrophils at the injury site. These non-inflammatory processes include neutrophil apoptosis (El Kebir and Filep, 2010), reverse migration (Hamza et al., 2014; Ellett et al., 2015), or removal into the luminal space (Brazil et al., 2010).

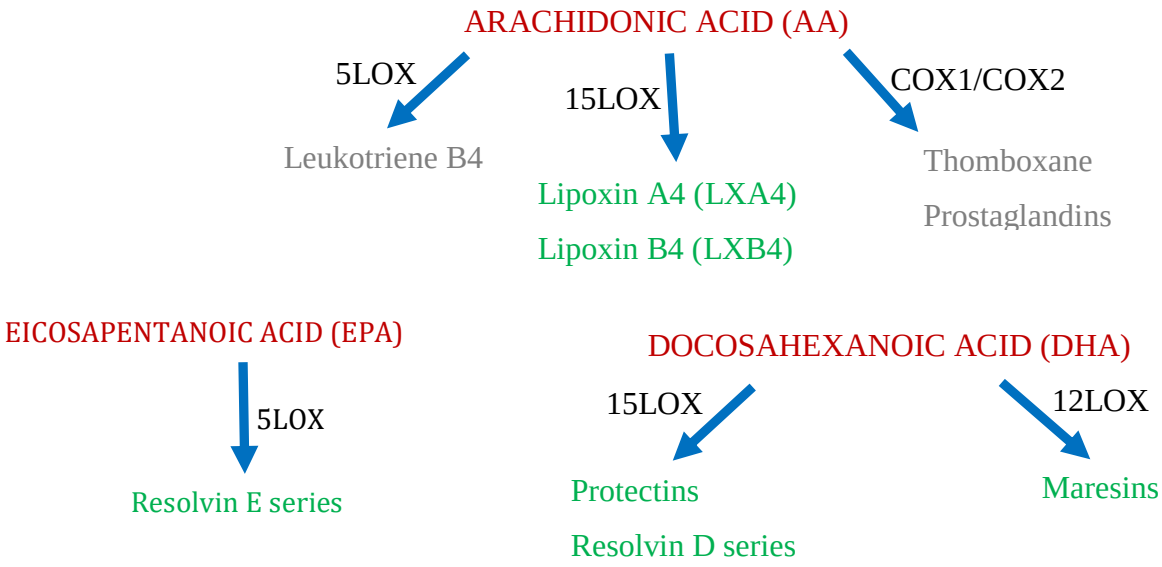

Figure 1-2: Simplified pathways of synthesis of SPMs. SPMs (shown in green) or related eicosanoids (in grey) are synthesised from essential fatty acids (in red) via different lipoxygenase enzymes (LOX) shown in black. (Fredman and Serhan, 2011)

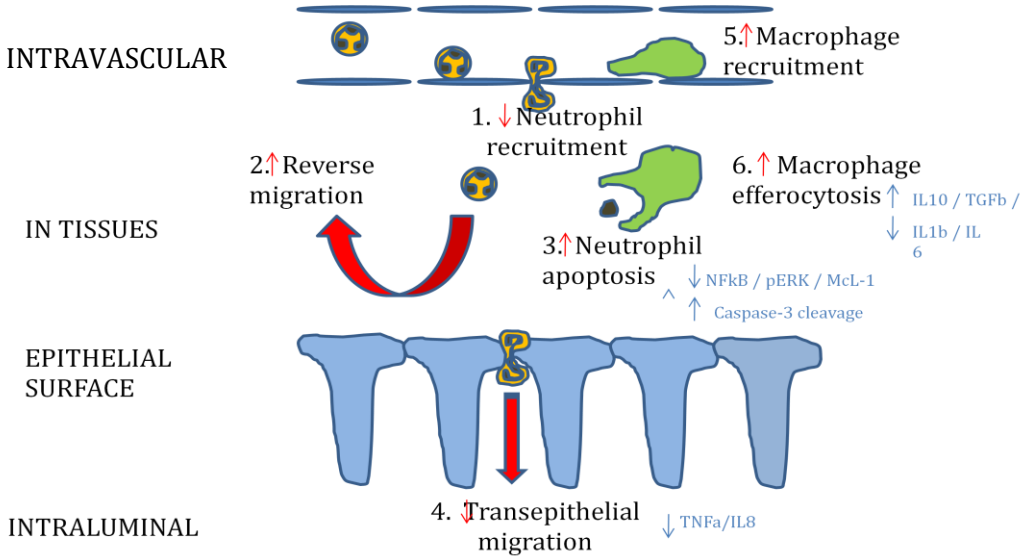

Figure 1-3: The inflammatory response in an organ, such as the intestinal tract, that may be modulated by SPMs. (1). Inflammation begins with recruitment of neutrophils in response to an injury or microbial insult. The recruited neutrophils migrate into tissues, and the resolution of inflammation involves removal of neutrophils via reverse migration (2), apoptosis (3), or loss into the intestinal lumen (4). Clearance of apoptotic neutrophils requires macrophages (5) which in turn secrete pro-resolution cytokines (6). SPM modulation (in blue) result in overall increase or decrease of each phase (red arrows).

Evidence for enhanced neutrophil apoptosis appears to be SPM-specific. While RvE1 enhances neutrophil apoptosis via down regulation of myeloid cell leukaemia-1 (Mcl-1, a member of the pro-survival family of molecules) (El Kebir, Gjorstrup and Filep, 2012), while 15-epi-lipoxin, an aspirin triggered lipoxin (ATL), enhances caspase-3 dependent apoptosis (El Kebir *et al.*, 2009). Apoptotic neutrophils are removed by macrophages, and SPMs have also been shown to influence the subsequent influx and behaviour of macrophages. LXA4, ATL and RvD1 increase efferocytosis in macrophages in a dose-dependent manner (Godson *et al.*, 2000), and promote the release of anti-inflammatory chemokines such as IL10 and TGF-β whilst at the same time decreasing pro-inflammatory chemokines like IL1β and IL6 (Titos *et al.*, 2011). Neutrophils that do not undergo apoptosis can move away from the site of injury and these neutrophils are said to have reverse migrated. Reverse migration of neutrophils in response to LXA4 has thus far only been demonstrated in microfluidic cell channel systems (Hamza *et al.*, 2014). Finally, neutrophils that have already undergone transepithelial migration to be attached to the mucosal surface can be removed by loss into the lumen. Persistence of neutrophils on the surface of epithelial cells has been linked to crypt abscesses and chronic inflammation in IBD, and RvE1 has been shown to stimulate expression of the CD55 receptor (Campbell *et al.*, 2007), an anti-adhesion molecule expressed on the apical surface of epithelial cells, thus promoting loss into luminal space and active inflammation resolution.

But efforts at reducing neutrophil numbers can result in the negative consequence of also reducing immunity to potential pathogens (De Bosscher, Vanden Berghe and Haegeman, 2000). There are indications that in infection with *Streptococcus pneumoniae*, supplementation of LXA4 too early in the phase of infection worsened survival of rats (Sordi *et al.*, 2013), while in other separate studies, supplementing LXA4 promoted proliferation of *Mycobacterium tuberculosis* (Tobin *et al.*, 2010). On the other hand, various studies have suggested that SPMs are, in fact, broadly beneficial in infections. RvD1, RvD5 and PD1 all enhanced the potency of antibiotics in *Escherichia coli* and *Staphylococcus aureus* pouch infections (Chiang *et al.*, 2012), although this was not due to a direct effect on microorganisms, but an enhancement of the host ability to engulf and perform intracellular killing of these bacteria. In other models of infection, RvE1 and ATL both reduced the severity of *E. coli* pneumonia (El Kebir *et al.*, 2009; Seki *et al.*, 2011). Microbial defence is particularly important in the heavily colonised intestine,

but here again, a simple cause and effect conclusion is not easily reached. In the example of HBOT, not only are anti-inflammatory pathways activated, but the increased pressure of oxygen perturbs the hypoxic gradient of the intestine and alters the composition of up to 29 species of bacteria within the rodent intestine (Albenberg *et al.*, 2014). This has the potential for wide-ranging consequences on wound healing, since the inflammatory responses are not only primed by the intestinal microbiome, but in addition, the functional responses of mature intestinal lymphoid cells can be rapidly changed by altered microbial composition (Gury-benari *et al.*, 2016). A study comparing the inflammatory responses of germ-free (GF) and conventional mice to LPS and ischaemic injury showed that GF mice had a significantly increased lipoxin-induced production of IL10 and a dampened inflammatory response (Souza *et al.*, 2004). In addition, in post-operative ileus, a condition associated with increased inflammation, it was shown over half a century ago that improvement occurred with administration of antibiotics (Polacek and Close, 1963). So could the simple complete eradication of microbiota alone ameliorate ALs?

1.5 **Influence of microbial milieu on wound healing**

The field of microbiomics has rapidly expanded in recent years with sequencing techniques that allow identification of non-culturable bacteria (Kim *et al.*, 2017). The identification of this vast community of microbiota quickly led to demonstration of the consequences of intestinal microbiota in diseases once thought to be far removed and distinct from the gut, such as hypertension (Bryan, Tribble and Angelov, 2017) and Parkinson's Disease (Hill-burns *et al.*, 2017). But as interactions between distant systems are increasingly uncovered, interest in the relevance of gut microbiota closer to home, within the GIT itself, has also had a revival with excellent reviews suggesting an important role for microbiota in wound healing in surgery and GIT cancers (Krezalek *et al.*, 2016; Bachmann *et al.*, 2017; Kinross *et al.*, 2017; Schardey *et al.*, 2017). Intestinal antisepsis is not a new concept in GIT surgery, particularly in the lower GIT, which harbours the highest concentration of bacteria within the human body under conditions of health. Antibiotics were used in colorectal surgery as early as 1938, and since the work of Poth, Cohn and Cohen (Poth, 1982; Schardey *et al.*, 2017), it is now widely accepted that intestinal microbes play important roles in ALs.

We know that although the core milieu of microbiota within the GIT persists stably in an individual (Jalanka-Tuovinen *et al.*, 2011), it is still changeable and alters over time with age (Claesson *et al.*, 2011), and within hours to dietary and lifestyle changes such as exercise, smoking (Allais *et al.*, 2016; Campbell *et al.*, 2016; Singh *et al.*, 2017) and indeed surgery. Experiments in rats demonstrated a 500-fold increase in *Enterococcus* and 200-fold increase in *Escherichia*, in conjunction with a 20-fold decrease in *Ruminococcaceae, Clostridia* and *Prevotellaceae* (Shogan *et al.*, 2014) following a surgical procedure. A similar change was demonstrated in human patients undergoing a colectomy, again with an increase in *Enterobacteriaceae, Enterococcus, Staphylococcus,* and *Pseudomonas* (an aerobe), and a decreased in obligate anaerobes like *Bifidobacterium* (Ohigashi *et al.*, 2013).

These changes are of particular interest since *Enterococcus faecalis* is potentially directly responsible for ALs by degrading collagen through expression of gelatinase E (Shogan *et al.*, 2015). Emerging evidence also suggests that prior radiotherapy, as is commonly used for some rectal cancers, may cause mutations in bacteria such as *Pseudomonas* that increase bacterial virulence. In a rat model of rectal surgery, pre-treatment with radiotherapy in the presence of *Pseudomonas* significantly increased ALs due to a mutation increasing pyocyanin and collagenase activity (Olivas *et al.*, 2012). This was in clear contrast to the complete lack of ALs in rats who underwent radiotherapy and an anastomosis but were free of *Pseudomonas*. These appear to be compelling pieces of evidence that eradication of microbiota may hold the key to ameliorating ALs; so much so that a recent summary of clinical trials to date (Schardey *et al.*, 2017) concluded that routine bowel preparation with non-absorbable antibiotics should be recommended. But could it be that the resultant significant changes in intestinal microbiota, as would be the case even for narrow spectrum antibiotics, may cause more harm than good both in the short and long term? It is indisputable that prolonged and repeated courses of antibiotics and polypharmacy influence the long-term diversity of the microbiome (Silverman, Konnikova and Gerber, 2017; Ticinesi *et al.*, 2017), but even a single pulse of broad spectrum antibiotics in mice appear to cause long term microbiome changes (Ruiz *et al.*, 2017) which ultimately have the potential to negatively impact later physical health (such as growth, diabetes and obesity), mental health (Bercik, Collins and Verdu, 2012; Livanos *et al.*, 2016; Guida *et al.*, 2017) and even mortality (Jackson *et al.*, 2016; Ticinesi *et al.*, 2017).

It is, in fact, quite impossible to eradicate intestinal microbiota in its entirety, because it would be necessary to ensure that the chosen antibiotic would be able to reach and eradicate both autochthonous (resident) microbes and not just allochthonous (luminal transient) microbes throughout the length of the GIT. Even then, such an action would be undesirable since the risk remains that dormant spores of *Clostridium difficile*, insensitive to antibiotics, might reactivate causing serious disease (Theriot *et al.*, 2014). Furthermore, in all discussions of antimicrobials, it is of vital importance to remember that it is not only bacteria that make up the intestinal biomes. Fungal, archaeal, and viral entities also co-exist (Ogilvie and Jones, 2015; Carding, Davis and Hoyles, 2017), and their roles have yet to be fully explored in the pathogenesis of a multitude of conditions. It was only a few years ago that a study demonstrated an increased fungal load in the chronically inflamed intestines of Crohn's patients (Liguori *et al.*, 2016) even though fungi have been identified in the GIT for over a century (Anderson, 1917). Over the past decade, experiments in rodents have identified a rich mycobiome that exists alongside the microbiome, and which similarly influences health and disease. Mice lacking the innate immune receptor Dectin-1, which is also a fungal signalling receptor, are highly susceptible to severe colitis, paralleling observations in humans (Iliev *et al.*, 2012), suggesting that fungal presence may add some benefit to the overall homeostasis of the GIT.

Although yet to be demonstrated specifically in anastomotic wounds, evidence also exists that fungal pathogenicity increases with antibacterial therapy, and are implicated in necrotic or non-healing wounds (Kalan *et al.*, 2016a). Interestingly, within the intact gut of the worm, *Candida albicans* and *E. faecalis* show a symbiotic relationship, each concurrently reducing the pathogenicity of the other. In the absence of *E. faecalis*, *C. albicans* showed an increased hyphal morphogenesis, a key virulence factor (Garsin and Lorenz, 2013). This type of relationship is not limited to the GIT. Even in the skin, co-colonisation of pathogenic *S. aureus* with the commensal, *Corynebacterium striatum*, caused a down regulation of *Staphylococcal* haemolysin activity and a shift toward commensalism (Ramsey *et al.*, 2016). And in the urinary tract, escherichelin production by *Enterobacteriaceae* cause an inhibition of growth of *Pseudomonas* by competitive inhibition of iron transport (Ohlemacher *et al.*, 2017). These examples should serve to promote caution in advocating blanket antimicrobials for the removal of any one

species of bacteria shown to be responsible for ALs within the highly regulated environment of an animal facility, since the results may not be quite as straightforward in real-world human cases.

But quite apart from that, evidence is accumulating that the presence of the microbiome may be beneficial, and even necessary, for optimal wound healing, in addition to its other whole-organism effects. *In vitro* studies have shown that *Akkermansia muciniphila* and *Bacteroides fragilis* significantly improved gut epithelial integrity, and furthermore survive normoxic conditions despite being anaerobes (Reunanen *et al.*, 2015), an important consideration since exposure to environmental oxygen during a surgical resection temporarily increases oxygen tension within the lower GIT and diminishes obligate anaerobes. These bacterial effects have been replicated *in vivo* in mice with encouraging results showing accelerated mucosal re-epithelialisation (Pull *et al.*, 2005; Alam *et al.*, 2016). Conversely, a lag in skin wound healing in GF guinea pigs has been noted from experiments in the 1960s (Tipton and Dingman, 1966), with similar findings of a lower tensile strength of intestinal anastomoses in GF mice (Okada, 1994; Okada *et al.*, 1999).

1.6 **The possible role of protein modulators in inflammation**

This positive effect of certain bacteria on wound healing could be due to the fact that the intestinal microbiota is directly implicated in the proper development of the immune system. The presence of intestinal commensals is vital in the development of gut-associated lymphoid tissues, secretory IgA, and Th17 cells, a subset of T-helper cells important in inflammation (Mazmanian *et al.*, 2005). But, as mentioned previously, the importance of microbiota does not end in development. Throughout life, the microbiome continues to exert a tonic effect on the inflammatory response, for example, with the gut commensal *Faecalibacterium prausnitzii* orchestrating anti-inflammatory effects by inducing secretion of IL10 and reducing IL12 and IFNγ (Sokol *et al.*, 2008). Even a single factor, Polysaccharide A from *Bacteroides fragilis*, is able to induce production of IL10 and confer protection from experimental colitis in animal models (Mazmanian, Round and Kasper, 2008).

But more than that, in response to microbes, the intestinal epithelial cells secrete a range of antimicrobial peptides (AMPs) such as defensins in the small intestine, and cathelicidins in the large intestine (Muniz, Knosp and Yeretssian, 2012). AMPs have been associated with improved wound healing across the species, even in invertebrates (Mizoguchi, 2012; Dupont *et al.*, 2014; Mangoni, McDermott and Zasloff, 2016). But other secreted peptides within the intestine also contribute to microbial homeostasis, for example intestinal alkaline phosphatase (iAP) can detoxify LPS (Bates *et al.*, 2006) and preserve a benign environment. iAP is an enzyme that has been evolutionarily conserved and is most known for its action on LPS. Multiple studies have shown that LPS is cleaved by iAP thus contributing to a reduction in inflammation stimulated by LPS (Bates *et al.*, 2007), and that LPS by itself, without the presence of bacteria is able to stimulate expression of iAP. iAP is found in the intestine in three forms, attached to the apical membrane , cleaved from the membrane and secreted into the lumen, and secreted in vesicles from the apical cells (Alpers, Eliakim and DeSchryver-Kecskemeti, 1990; Nakano *et al.*, 2009; Shifrin *et al.*, 2012). Decreased expression of iAP has been noted in children with chronic intestinal inflammation (Tuin *et al.*, 2009a), and the utility of this protein has been demonstrated in mice, where chemically-induced colitis is improved by administration of iAP (Ramasamy *et al.*, 2011). Perhaps then it is the manipulation of these proteins that could be the answer rather than direct microbial manipulation? This is particularly so since direct microbiome manipulation is more difficult to achieve than would be imagined, and results are often variable. Take for example two diseases associated with microbial imbalance, *C. difficile* colitis, and Ulcerative colitis (UC). In *C. difficile* infections, where the presence of a single offending microorganism prevails, faecal microbiota transplantation (FMT) is able to achieve remission in 96% (Rohlke and Stollman, 2012). However, when the same FMT is used in UC, which is thought to result from an imbalance of a range of microorganisms rather than a single offender, remission rates are between 30-70% (Sunkara *et al.*, 2018). So whilst there is evidence that the microbiome is malleable by exogenous therapeutic agents, substantial inter-disease and inter-individual variation exists. Evidence is emerging that genetic variation may be one of the key factors in controlling both the differing inflammatory responses to the same microbial stimulus (Li *et al.*, 2016), as well as the stable personal microbiome composition, since even in cattle, host genetics affects gut microbiota composition, which in turn affects growth and health (Fan *et al.*, 2019).

1.7 **The role of differential genetic expression**

The physiological inflammatory response to injury and infection, unperturbed by external therapeutic intervention, has to be carefully controlled to avoid disease states. Classical eicosanoids, docosanoids, as well as the newer bioactive lipid mediators have a dynamic expression that is dependent on many factors such as time, tissue specificity and cell-cell interactions (Dennis and Norris, 2015), but also on an individual's genetic makeup. Over the past decade, the role of genetics in lipid pathway expressions in human disease has been investigated in some detail (Cha and DuBois, 2007). Although the primary end-point in many of these studies was cancer, they remain relevant because of implications for the role of inflammation, which has been shown to have both a cell-autonomous and non-cell-autonomous function in promotion of carcinogenesis (Clevers, 2004). Epidemiological studies show that up to 20% of cancers are the direct result of chronic inflammation (Grivennikov, Greten and Karin, 2010), and over the past century, tumour initiation, maintenance and progression has been proven to have clear molecular (Dvorak, 1986; Arwert, Hoste and Watt, 2012) as well as microbial (Francescone, Hou and Grivennikov, 2014) similarities with the non-healing wound. Therefore polymorphisms in pathways found to be important in cancer prevention or development are also likely to be important in prevention of ALs.

Take for example, the pathways of polyunsaturated fatty acids (PUFAs). Humans are unable to convert ω-6 PUFAs into ω-3 PUFAs and therefore the availability of each in the diet corresponds to its abundance within the body thus facilitating epidemiological studies. Cohort studies with manipulation of the exogenous supply of each (ω-6 in excess being pro-inflammatory and ω-3 anti-inflammatory) have been performed, which were then correlated to cancer risk. Results of these early studies have been contradictory and overall failed to definitively associate a reduction in sporadic forms of cancer with increased ω-3 PUFA consumption. These equivocal results can partly be explained by newly discovered single nucleotide polymorphisms (SNPs) within the COX genes, such that only those with a pro-inflammatory COX-1 variant derived benefit from ω-3 PUFA supplementation (Poole *et al.*, 2007). The converse is also true, albeit shown in a distinct Chinese population, with pro-inflammatory COX-2 polymorphisms conferring elevated risk when combined with increasing

ω-6 PUFA consumption (Koh *et al.*, 2004). Similarly, clinical studies have shown that individuals express different levels of SPMs, and can be categorised into pro-inflammatory or pro-resolving human groups (Pillai *et al.*, 2012), with a direct correlation with eventual outcome in critical illness. But genetic background is not limited to the effects on the inflammatory pathways, and it is now emerging that genetic makeup also plays an important role in personal selection of a stable microbial community within the GIT, because while short-term upheavals in composition might follow intervention, or long-term reduction in diversity follow the administration of antibiotics, the core microbiome remains somewhat similar overall, with higher concordance in monozygotic versus dizygotic twins (Goodrich *et al.*, 2014; Davenport, 2016; Hall, Tolonen and Xavier, 2017). This may be one explanation for the conflicting results of the efficacy of probiotic usage through the years (Zmora *et al.*, 2018), and perhaps why attempts to modulate microbiome composition with faecal transplantation in IBD have met with low success rates (Lopez and Grinspan, 2016).

But is there a hierarchical relationship between inflammation, the microbial milieu and genetic background? At present there is insufficient information to make a definitive conclusion of any single one taking precedence over the others, but it is probable that manipulation of one aspect, without consideration of the others, is unlikely to result in a consistently positive outcome in clinical scenarios. Certainly, it has been shown that attempts to personalise medicine based on genetic makeup alone has been unsuccessful in the past, with failed efforts at achieving optimum platelet control with clopidogrel, a pro-drug requiring enzymatic conversion, by controlling for polymorphisms in relevant enzymes (CYP2C19) or transporter molecules (ABCB1) (Lampa *et al.*, 2013) alone. It therefore seems probable that in order for successful translation to clinical practice in a region as complex as the intestine, a tri-faceted approach to intestinal wound healing needs to be adopted (**Figure 1-4**), involving careful evaluation of each aspect in the context of the others. Our understanding of the role of individual expression profiles of inflammatory response elements to outcomes of disease and wound healing is still in its infancy, and the genetic possibilities are huge, not simply in base pair variations, but also in epigenetic and even in protein translation variations, as demonstrated by the huge phenotypic spread of the human race despite a very narrow range of actual differences in raw genetic material (Batzer and Jorde, 2007). Although direct genetic manipulation, even with CRISPR

technology (Lander, 2015), is far from being routine clinical practice, a greater understanding of the expression of important modulators may aid the ability to manipulate the microbial milieu and inflammatory response.

1.8 **Rationale for animal models**

To this end, the possibility of studying the RNA expression profiles of the inflammatory response is one of the primary reasons this thesis utilises animal models. The entire genome of *Danio rerio* has been sequenced (Howe *et al.*, 2013), thus allowing identification and comparison of expression patterns, but in addition, the small size of the zebrafish larvae allows determination of the spatial pattern of expression using newly developed RNA tomography techniques. This is particularly valuable since the zebrafish has become an indispensable organism in the investigation of inflammatory physiology and pathology, and anti-inflammatory drug screening (Wang *et al.*, 2014). Using established fluorescently labelled transgenic lines for neutrophils (Renshaw *et al.*, 2006) and macrophages (Ellett *et al.*, 2011) it is also possible to follow in real time the ebb and flow of these cells during the inflammatory process. While studies of neutrophil directionality and speed done in rats involved artificial chambers and channels (Kurihara *et al.*, 2013) which may have unforeseen effects on the neutrophils, following these cells *in vivo* in the live organisms overcomes these deficiencies. The zebrafish has the advantage of optical transparency, allowing time-lapse imaging following wounding, and has been used successfully in fin injury investigations (de Oliveira, Rosowski and Huttenlocher, 2016) as well as infection models (Davis *et al.*, 2002; Bradford *et al.*, 2017). But, wound healing differs between mucosal surfaces and skin, with a different profile of cytokines and interleukins being produced, a different degree of bacterial challenges, a quicker pace of healing in the former (Szpaderska, Zuckerman and Dipietro, 2003), a difference in the shear stresses encountered, and, in skin, a consistent occurrence of scarring (Thornton and Barbul, 1997). Therefore currently, it is insufficient to substitute *in vitro* replicas or another epithelial or mucosal surface for that of the intestine in examining factors that might affect wound healing. Inflammation studies specific to the intestinal tract is less well developed in teleosts, and certainly, there exist anatomical differences between the species, such as the absence of a stomach, crypts, Paneth cells and a submucosa in the zebrafish (Wallace *et al.*, 2005). But despite the differences, there is conservation of gut and immune genes across species, and

zebrafish models have already been instrumental in discovering novel aspects of intestinal immunity, as it was in the zebrafish larvae that the role of intestinal alkaline phosphatase in detoxifying LPS was first demonstrated (Bates *et al.*, 2007). But while the zebrafish is able to assist in untangling molecular and genetic aspects of many diseases, the differences in the digestive tract remain, not least because of the mainly aerobic, rather than anaerobic luminal conditions common to mammals. Thus, although it remains a useful model for initial investigations, and worthy of further development, validation of potential therapeutic agents require a higher mammal, and the mouse anastomotic model, although not used in the UK prior to this time, has been shown to be a robust model and is used for this reason. Although rats are more commonly used due to their larger size and therefore ease of operating, rats are naturally very resilient to intestinal operations and mouse models of a leaking anastomosis appear to be more successful (Pommergaard, 2014). A leaking anastomosis model would simulate an environment suitable for bacterial overgrowth and virulence, and provide evidence that rescue of this situation is possible, in an analogous manner to rescue of healing of a chronic wound.

1.9 **Thesis aims and working hypothesis**

Thus, the aim of this thesis is to perform a wide-based exploration of the impact of different protein and lipid anti-inflammatory agents on modulation of the inflammatory response to an acute injury or microbial insult, and if modulating the inflammatory response to an injury, whether in a sterile or complex environment such as the intestine, would result in a corresponding modulation of wound healing. The specific hypothesis tested are:

1. That zebrafish would be a sensitive and comparable model to interrogate the modulatory actions of SPMs on neutrophils and macrophages
2. That the zebrafish express the relevant receptors for SPMs and that the zebrafish can be used to spatially explore the inflammatory response to injury
3. That the zebrafish model can be colonised by *E. faecalis* and the colonisation modulates the inflammatory response to SPM and injury
4. That iAP exerts an anti- inflammatory response independent of LPS
5. That iAP can enhance healing in a mouse intestinal injury

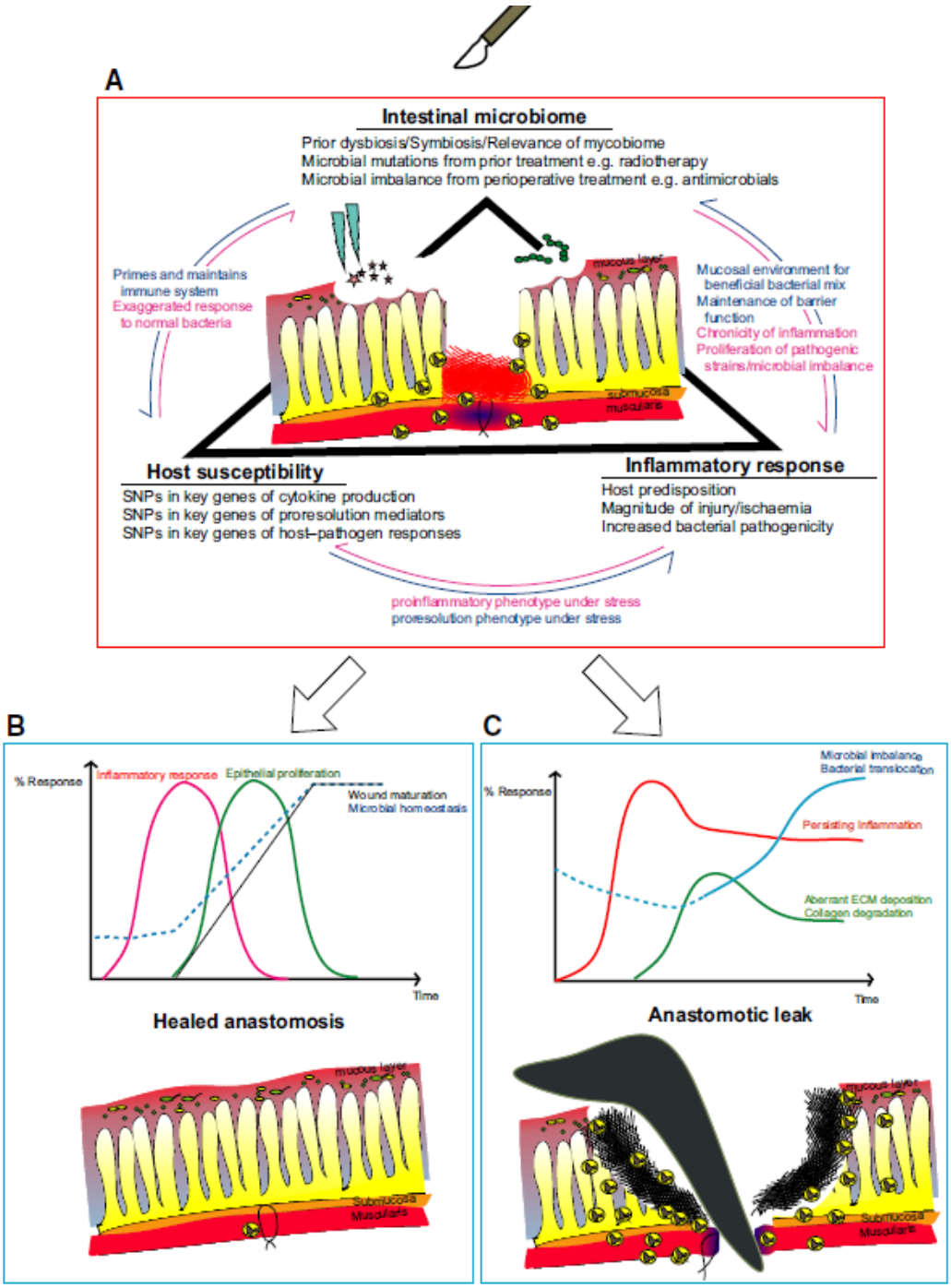

Figure 1-4: The tri-faceted approach to anastomotic healing. A. Surgical resection and anastomosis of the bowel where wound healing is influenced by three interdependent factors: host genetic susceptibility, inflammatory response, and the existing intestinal microbiome. The interaction of these three factors leads either to (**B**) healing of anastomosis with epithelial restitution, resolved inflammatory responses, restored mucous barriers and microbial homeostasis; or to (**C**) failed healing leading to an anastomotic breakdown, leakage of intestinal contents, bacterial translocation and systemic sequela. Reproduced under the terms of the Creative Commons Attribution License http://creativecommons.org/licenses/by/4.0/ (Lee, Chico and Renshaw, 2018).

Chapter 2: Methods & Materials

2.1 **Reagents**

PD146176, MK886 and ML355, Calf intestinal alkaline phosphatase (iAP), adenosine deaminase, caffeine, DPCPX and ZM241385, LB tablets (Lennox), tetracycline, erythromycin, kanamycin were obtained from Sigma Aldrich (Dorset, UK). MRS1754 was obtained from Abcam (Cambridge, UK). LXA4 (Calbiochem, San Diego, US), Mar1, RvD2 and RvE1 were obtained from Cayman Chemicals (Ann Arbor, MI). MMP2, MMP9 were purchased from R&D Systems (Abingdon, UK). All other chemicals were of laboratory grade or HPLC grade depending on use, obtained from Fisher Scientific (Loughborough, UK), Sigma Aldrich (Dorset, UK), and enzymes and kits were obtained from New England Biolabs (Herts, UK), Qiagen (Germantown, US) or Illumina (Eindhoven, Netherlands). OCT was obtained from VWR Chemicals (Leicestershire, UK).

2.2 **Recipes for buffers**

Unless stated otherwise, all chemicals were dissolved in ultrapure H_2O (18.2 MΩ·cm at 25°C) and solutions were either autoclaved for 20 min at 121°C, 103 kilopascal, or filter sterilised through a sterile Millex® GV Filter Unit 0.22 µm Durapore PVDF membrane (Merck Millipore, Dorset, UK) under aseptic conditions.

2.2.1 **iAP buffer**

Tris-HCl pH8.2	10 mM
KCl	50 mM
$MgCl_2$	1 mM
$ZnCl_2$	0.1 mM
Glycerol	50% (v/v)

2.2.2 **Phosphate buffered saline (PBS)**

NaCl	8 g/L
Na_2HPO_4	1.4 g/L

KCl	0.2 g/L
KH_2PO_4	0.2 g/L

The pH was adjusted to 7.4 with NaOH.

2.2.3 **Tris-Glycine SDS Sample Buffer**

Tris HCl	63 mM
Glycerol	10% (v/v)
SDS	2%
Bromophenol Blue	0.0025%

Each time, 10mL of 2X Tris-Glycine SDS Sample Buffer was prepared by mixing:

Tris-HCl 0.5 M (pH 6.8)	2.5 mL
Glycerol	2 mL
SDS 10%	4 mL
Bromophenol Blue 0.1%	0.5 mL

2.2.4 **Tris-Glycine SDS Running Buffer**

Tris pH8.3	25 mM
Glycine	192 mM
SDS	0.1%

Each time, 10X Tris-Glycine SDS Running Buffer was prepared by dissolving:

Tris Base	29 g/L
Glycine	144 g/L
SDS	10 g/L

2.2.5 **Zymogram Renaturing Buffer**

Triton® X-100	2.7% (w/v) in H_20

2.2.6 **Zymogram Developing Buffer**

Tris base	50 mM
HCl	40 mM
NaCl	200 mM

$CaCl_2$	5 mM
Brij 35	0.02% (w/v)

Each time, 10X Zymogram Developing Buffer was prepared by dissolving:

Tris Base	60.4 g/L
6N HCl	66 mL
NaCl	117 g/L
$CaCl_2.2H_2O$	7.4 g/L
Brij 35	2.0 g/L

2.2.7 **Coomassie Blue stain**

Coomassie Blue G-250	0.1% (w/v)
Methanol	50% (v/v)
Acetic acid glacial	10% (v/v)

2.2.8 **SDS-PAGE loading buffer (5X)**

Tris-HCl pH6.8	250 mM
SDS	10% (w/v)
Bromophenol blue	0.5% (w/v)
Glycerol	50% (v/v)
DTT	0.5 M

2.2.9 **TBST (20X)**

Tris	48.4 g/L
NaCl	20 g/L
Tween-20	2% (v/v)

The pH was adjusted to 7.6 with 6N HCl solution.

2.2.10 **Western Blot Transfer Buffer**

Tris Base	2.4 g/L
Glycine	11.26 g/L
Methanol	20% (v/v)

2.2.11 **Western Blot blocking buffer**

BSA	3% in 1X TBST

2.2.12 **TAE (50x)**

Tris	242 g/L
Glacial acetic acid	5.7% (v/v)
Na_2EDTA pH 8.0	0.05 M

2.2.13 **TE buffer**

Tris	10 mM
EDTA	1 mM

The pH was adjusted to 8.0.

2.2.14 **EBT buffer**

Tris-HCl pH 8.0	10 mM
Tween 20	0.05%

2.2.15 **RNA fragmentation buffer**

Tris-acetate pH8.1	200 mM
KOAc	500 mM
MgOAc	150 mM

2.2.16 **RNA fragmentation stop buffer**

0.5M EDTA pH8

2.2.17 **4%(w/v) paraformaldehyde (PFA) solution**

4 g of paraformaldehyde in 100 mL of PBS. The PFA solution was stored up to 3 months at 4^oC.

2.2.18 **Lysis buffer**

1M Tris-HCl	1.25 mL

2M NaCl	2.5 mL
10% (v/v) IGEPAL	5 mL
MQ H2O	41.25 mL

The solution was sterile-filtered and stored at 4˚C and confirmed to be clear before use.

2.3 **Recipes for histological stains**

Gram's iodine, safranin, crystal violet and Wright-Giemsa stains were purchased ready to use from Sigma-Aldrich.

2.3.1 **Picrosirius red**

Direct Red 80	0.5 g
Picric Acid (Saturated)	500 mL

2.3.2 **Acidified Water**

Glacial acetic acid	5 mL
Distilled water	995 mL

2.3.3 **Alkaline water (Blue-ing solution)**

28% Ammonium hydroxide	1 mL
MQ H_2O	999 mL

2.3.4 **Eosin Y stock solution**

Eosin Y	2.0 g
MQ H_2O	40 mL
95% Ethanol	160 mL

2.3.5 **Eosin Y working solution**

Eosin Y stock	200 mL
80% ethanol	600 mL
Glacial acetic acid	4 mL

2.4 **Culture media**

Culture media were made up in ultrapure water and autoclaved at 121°C, 103 kilopascal for 20 minutes (min) prior to use.

2.4.1 **Brain Heart Infusion (BHI)**

BHI (Oxoid)	37 g/L

2.4.2 **BHI Agar**

BHI (Oxoid)	37 g/L
Bacteriological agar No. 1	1.5% (w/v)

2.4.3 **Milk Agar**

BHI (Oxoid)	37 g/L
Skimmed milk	15% (v/v)
Bacteriological agar No.1	1.5% (w/v)

2.4.4 **Luria Bertani (LB) broth (Lennox)**

Tryptone	10 g/L
Yeast Extract	5 g/L
NaCl	5 g/L

2.4.5 **LB Agar**

Tryptone	10 g/L
Yeast Extract	5 g/L
NaCl	5 g/L
Bacteriological Agar	1.5%

2.4.6 **LK media**

Tryptone (Oxoid)	10 g/L
Yeast extract (Oxoid)	5 g/L
KCI	7 g/L

2.4.7 **LK agar**

Tryptone (Oxoid)	10 g/L
Yeast extract (Oxoid)	5 g/L
KCI	7 g/L
Bacteriological agar	1.5 % (w/v)

2.4.8 **Antibiotics**

Antibiotics used are listed in Table 2-1. Stock solutions were filter sterilised (0.22 µm) and stored at -20˚C until use. When used for agar plate preparation, agar was cooled to 55˚C just prior to addition of antibiotics.

Table 2-1: Antibiotic solutions and concentrations

Antibiotic	**Stock Concentration (mg/mL)**	**Diluent**	***E. coli* working concentration (µg/mL)**	***E. faecalis* working concentration (µg/mL)**	***S. aureus* working concentration (µg/mL)**
Ampicillin	100	dH_2O	100	-	-
Chloramphenicol	10	100% v/v ethanol	12.5	10	10
Kanamycin	50	dH2O	50	-	50
Tetracycline	5	100% v/v ethanol	-	5	5
Erythromycin	5	100% v/v ethanol	-	30	30

2.4.9 **Phage buffer**

$MgSO_4$	1 mM
$CaCl_2$	4 mM
Tris-HCl pH 7.8	50 mM

NaCl	0.6% (w/v)
Gelatine	0.1% (w/v)

2.4.10 **Sabouraud Dextrose Agar**

Bacteriological agar	1.5% (w/v)
Dextrose	40 g/L
Mycological peptone	10 g/L

2.4.11 **Carboxymethylcellulose (CMC)**

Bacteriological agar	1.5% (w/v)
$NaNO_3$	0.2% (w/v)
K_2HPO_4	0.1% (w/v)
$MgSO_4$	0.05% (w/v)
KCl	0.05% (w/v)
CMC sodium salt	0.2% (w/v)
Peptone	0.02% (w/v)

2.4.12 **Zebrafish embryo media (E3)**

NaCl	5 mM
KCl	0.17 mM
$CaCl_2$	0.33 mM
$MgSO_4$	0.33 mM
Methylene blue	0.00005%

2.5 **Molecular biology techniques**

2.5.1 **RNA extraction from zebrafish larvae**

Zebrafish larvae, either tailfin injured or uninjured, at the designated hpf were anaesthetised and then snap frozen in pure ethanol and dry ice at a density of 20 fish/Eppendorf. Five hundred µL of TRIzol® (Sigma Aldrich) was added to each Eppendorf. The larvae were homogenised using a pipette and incubated for 5 min at room temperature in a QIAshredder (Qiagen), before being centrifuged at room temperature at full speed. The contents were then transferred to a new 1.5

mL Eppendorf and 100 µL chloroform added. Each tube was shaken vigorously by hand and incubated at room temperature for 3 min. Separation of the liquid layers was aided by further full speed centrifuging for 5 min. The aqueous layer was then removed to a new 1.5 mL Eppendorf and incubated with 250 µL isopropanol overnight to allow precipitation of RNA. The precipitation was completed by a microfuge centrifuge full speed spin at 4°C for 30 min, followed by washing with 75% ethanol. RNA was re-suspended in 20 µL DEPC H2O and stored at -80°C.

2.5.2 **Preparation of cDNA via reverse transcription PCR**

2 µg of RNA prepared in Section 2.5.1 was used to prepare cDNA. Reverse transcription was performed using SuperScript II (Invitrogen, Massachusetts, USA) following manufacturer's protocol. PCR was then performed using Q5-HF DNA Polymerase (NEB, Hertz, UK) in a T100™ Thermal Cycler (Bio-Rad), using a Tm of 58˚C, 28 cycles, and the following primers:

fpr1 (Gene ID: ENSDARG00000042984) : 5'-ATGAGCTACAACGACCCAGT-3', 5'-TTA TACCTCTGCATCAGAGAAGG-3',

gpr18 (Gene ID: ENSDARG00000062009): 5'-ATGGACCATAGCACAACTTTG-3', 5'-TCA GATCATGGCA CTGGTCA-3',

cmklr1 (Gene ID: ENSDARG00000090890): 5'ATGGATTTACTAGACTTAACATAT GATTAC-3', 5'CAGATATGAGTGGAAGCCC-3'.

2.5.3 **Determining DNA or RNA concentration**

The NanoDrop™ 1000 Spectrophotometer (Thermo Fisher Scientific) was used to obtain concentrations. Blank measurements were taken using the relevant solubiliser (EBT, TE or ultrapure H_2O) and measurements subsequently taken at 260 nm for nucleic acids. Careful attention was paid to the 260/280 nm absorbance ratio, ensuring this was approximately 1.8 for pure DNA and 2.0 for pure RNA (Wilfinger, Mackey and Chomczynski, 1997).

2.5.4 **Gel electrophoresis**

DNA or RNA was run on 1% (w/v) agarose gel with 0.5-1 µg/mL ethidium bromide in 1X TAE buffer. Blue 5X DNA loading dye (Bioline, London) was used, with 1Kbp or 100bp DNA ladders (Bioline, London) and gels resolved for 30 min at room temperature at 100-120V. A UV

transilluminator interfaced to a UVi Tec Digital camera and UVi Doc Gel documentation system was used to image the gel.

2.5.5 **Gel extraction of DNA**

The selected band of correct size was excised from the gel using a clean scalpel under low intensity UV transilluminator to minimize random mutations. DNA was extracted from the gel using the QIAGEN QIAquick Gel Extraction kit as per manufacturer's instructions.

2.5.6 **Purification of PCR products**

DNA products were purified using the QIAGEN QIAquick PCR Purification kit as per manufacturer's instructions.

2.5.7 **DNA sequencing**

PCR products were sequenced by the Core Genomic Facility at the University of Sheffield.

2.5.8 **Receptor cloning**

PCR products were confirmed to be of the correct size and then extracted from the gel using the QIAquick Gel Extraction Kit (Qiagen, Manchester, UK). These were then cloned using the ZERO blunt TOPO II cloning kit (Invitrogen, Massachusetts, USA) and a heat shock transformation protocol performed as per manufacturer's protocol with TOP10 competent cells (Thermo Fisher Scientific, Massachusetts, USA). Outgrowth was performed on LB plates containing 50 µg/mL kanamycin at 37˚C overnight. Colonies were then selected, and DNA extracted with the QIA Plasmid Mini Kit (Qiagen, Manchester, UK) and sent for sequencing to confirm the correct insert and its orientation. Sequencing allowed the correct orientation of the insets to be mapped, as shown in , and also for confirmation of fidelity of the inserted sequence. Once confirmation was obtained, 500 µL of the original culture of each correct colony was further cultured in 100 mL of LB with kanamycin at 37˚C with gentle agitation at 300 rpm for 16 hours. The cultures were then pelleted by centrifugation at 6000 x *g* for 15 mins at 4˚C, and prepared using the QIA Plasmid Midi Prep for RNA transcript over-expression or probe preparation.

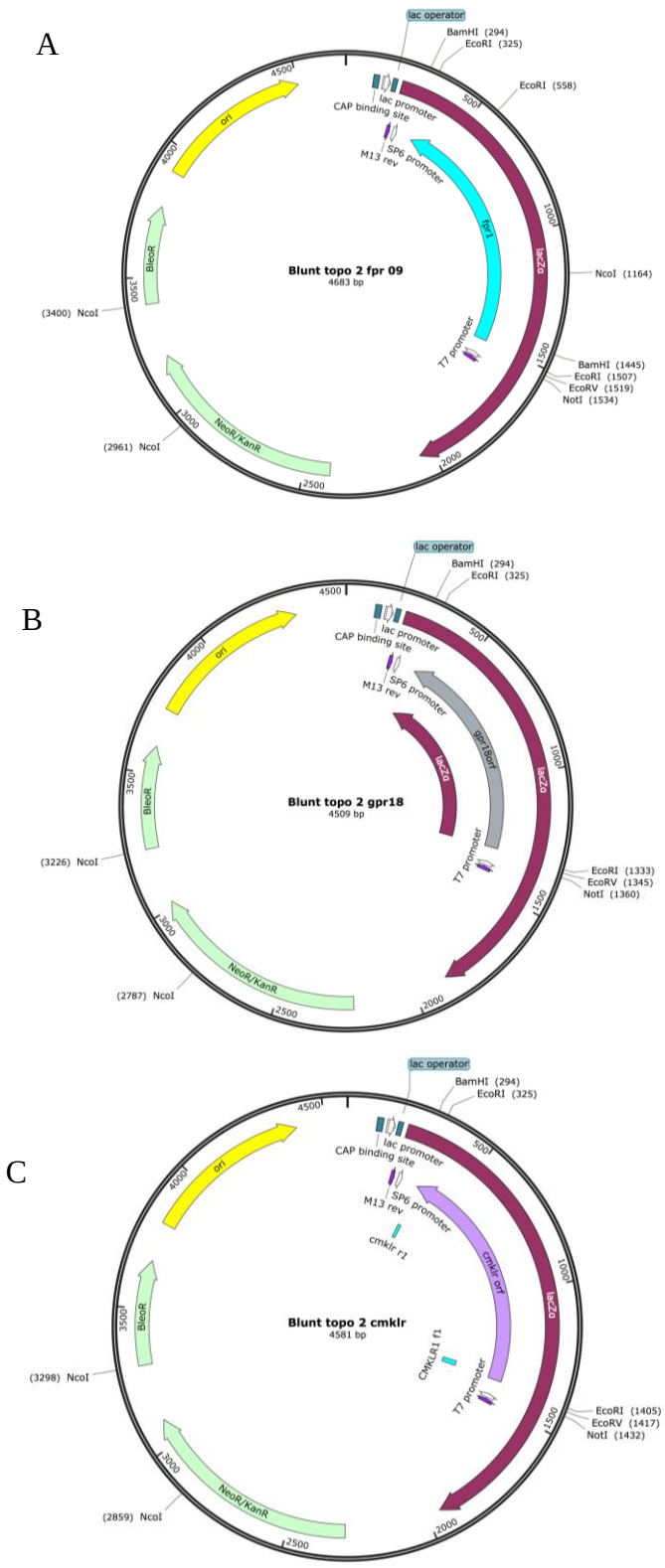

Figure 2-1: Plasmid maps for zebrafish receptors cloned using the ZERO blunt TOPO II cloning kit. A. *fpr1*, **B**. *gpr18*, **C.** *cmklr1*.

2.5.9 **RNA over-expression**

RNA transcripts were then prepared by linearising the previous Midiprep with the appropriate restriction enzyme (*gpr18* and *cmklr1*: Not1 (T7), BamH1 (SP6); *fpr1*: Not1(T7), HindIII(SP6)) and digested for 2 hours at 37˚C. The total reaction was purified using the Qiagen PCR purification kit (Qiagen, Manchester, UK) according to manufacturer's protocol. 0.5 µL of the purified product was then quantified on a 1% electrophoresis gel and finally 1 µg of total linearised product used for transcript production with the mMessage mMachine Transcription kit (Thermo Fisher Scientific) according to manufacturer's protocol. The resultant product was injected into zebrafish eggs at the one cell stage as previously described (Rosen, Sweeney and Mably, 2009) and embryos raised in the standard manner to 2dpf.

2.5.10 **Plasmid purification**

Plasmid purification was performed using a Nucleobond® Midiprep kit (Machery-Nagel, Germany) as per the manufacturer's instructions.

2.5.11 **Restriction endonuclease digestion**

Digestion of DNA (or purified plasmid) was performed using selected enzymes, in the appropriate buffers as recommended by the manufacturer. The reaction mixtures were incubated at the recommended temperatures (usually 25˚C or 37˚C) for between 1 h and 16 h. Products were run on a 2% gel to confirm a match to the predicted digestion for successful insert.

2.5.12 **T4 DNA ligation**

Insert and vector DNA were prepared for ligation reaction in a 20 µL volume:

Vector DNA	50 ng
Insert DNA	37.5 ng
T4 DNA ligase	1 µL
T4 DNA ligase buffer (10x)	2 µL
MQ H_2O	up to 20 µL

The reaction mix was incubated at 16˚C overnight. The ligation products were used to transform competent *E. coli* cells.

2.5.13 **Electro competent EL250 cells**

Fresh EL250 cells were prepared each time to maximize efficiency of electroporation. A single colony of EL250 cells were grown overnight in 2 mL of fresh LB media at 32˚C with agitation at 200 rpm. One mL of this culture was then inoculated into 50 mL of fresh LB culture agitated at 200 rpm for 4-5 hours at 32˚C. OD_{600} would be expected to be between 0.4-0.6. Cells were pelleted by centrifugation at 4˚C 300 x *g* for 15 min and washed a further four times with dH_2O. The final resuspension was in 500 µL ice-cold dH_2O. 50 µL of cells were used each time for electroporation.

2.5.14 **Transformation of EL250 or Top10 cells**

50 µL of cells was defrosted on ice. 4 µL of ligation reaction was added and electroporation was performed at 1.75 kVm 25 µF and 200 Ω using a GenePulser Xcell Electroporation system (Bio-Rad) in a pre-chilled electroporation cuvette (Bio-Rad). Cells were recovered in 400 µL fresh LB at 37˚C with agitation at 250 rpm. Cells were spread on LB plates and incubated at 37˚C until colonies appeared.

2.5.15 **BAC library selection**

BAC clones were picked by selecting those overlapping the start site of *Cldn15la* which has been shown to be expressed within the gut at 72 hours (Alvers *et al.*, 2014). The library clone (CHORI-211) was streaked onto LB agar containing chloramphenicol (12.5 µg/mL) and grown overnight at 37˚C.

2.5.16 **Double digest and examination of *Col1a2-eGFP***

*Sma*I and *Bst*II were used simultaneously to generate sticky ends to enable re-ligation of *Col1a2-eGFP* into the target construct. Integrity of *Col1a2-eGFP* was checked at multiple points by sequential PCR and sequencing using the following:

Coll F2: 5’- CCTGCTGGAGTTCGTGACC-3’

Coll R2: 5’-CATCAAACCCATAGGTCCAGG-3’

Coll F3: 5’-CTGGTTTCCCTGGCCCTAGAG-3’

Coll R3: 5’-ACCAGAATCTCCCTTCACTCCAAC-3’

Coll F4: 5’-TGGTGTGAAGGGAGAGCGTC-3’

Coll R4: 5’-CCAGGCTCTCCCTTGTTTCC-3’

Coll F5: 5’-TGGTCTGGCTGGTGAGAAGG-3’

Coll R5: 5’-AGACCACGGTCACCTCTG-3’

Coll F6: 5’-GCTGGTCCTCCTGGATCTC-3’

Coll R6: 5’-GCCTGGTCAGCTCTGTAC-3’

2.5.17 **Creation of a target construct for *Col1a2-eGFP***

A target construct containing tBS-GFP (truncated BlueScript) with kanamycin resistance and overlapping arms was constructed to overlap the BAC and designed to contain a Kozak sequence (Kozak, 1986; Grzegorski *et al.*, 2014). The 74mer primers were as follows:

Forward: 5’- GGACACCTATACAGATTCTTCCCTTGAATTTTGGATTTCTGAG GGCAAACATGCTCAGCTTTGTGGATACCCGG-3’

Reverse: 3’- TGGGTCGGCTAGTTTGTGTACTTCATAGGGCAGTGGAGATTACGAC ATCTCTATAGACGTCTTAAGCGGGAACT-5’

2.5.18 **Amplification of target construct**

A 300 µL large PCR reaction was prepared as follows:

Midi prep of tBS-GFP frt-kan-frt	5 µL
Q5 reaction buffer	60 µL
dNTPs 10mM	6 µL
Forward primer 10uM	30 µL
Reverse primer 10uM	30 µL
Q5 HF	3 µL
RNase free H_2O	166 µL

The reaction mixture was run in the thermocycler using the following program:

98 ˚C 1 min

25 cycles of: 98 ˚C 10 s

55 ˚C 10 s

72 ˚C 90 s

72 ˚C 10 min

5 µL Dpn1 was added to the PCR product and the mixture incubated at 37˚C for one hour. The product was then purified as per Section 2.5.10 and eluted in 10 µL of EBT. 0.5 µL of this purified product was run on a 1% gel to quantify using 1, 2 and 5 µL of the 1 kb Hyperladder (Bioline). 300 ng of product was used for targeting.

2.5.19 **Targeting construct into EL250 cells**

25 ng of the purified and prepared BAC DNA was added to 40 µL EL250 cells. Electroporation was performed as per Section 2.5.14 and cells recovered in 1 mL SOC in a sterile culture tube and shaken at 32˚C for 2.5 hours at 250 rpm. Successful targeting was confirmed by growth on chloramphenicol containing plates at 32˚C overnight. A single colony was then grown in 1mL LB broth with chloramphenicol with shaking at 32˚C overnight. 0.4 mL of this culture was then grown to OD_{600} of 0.5 in 20 mL of LB and 10 mL of this used for targeting. This was transferred to a 250 mL conical flask warmed to 42˚C with shaking for 15 min, transferred precipitously onto ice and then spun down at 4˚C at maximum speed for 30 s to pellet the cells. Cells were washed in ice cold water twice and finally resuspended in 50 µL ice cold water. The construct was added and electroporation was performed at 1.8kV. Cells were recovered for 90 min with shaking at 32˚C and then plated onto antibiotic containing LB plates and grown overnight at 32˚C. Successful targeting of the construct would cause a gain in kanamycin resistance therefore simultaneous plating onto kanamycin, chloramphenicol and ampicillin plates allowed selection of a colony demonstrating only ampicillin sensitivity.

2.5.20 **Removal of kanamycin marker**

A successful colony from above was grown overnight as described in Section 2.5.19 and after growth to exponential phase, the entire culture was incubated with 0.1% L-arabinose (Santa-Cruz) for 1 hour at 32˚C with shaking. 100 µL of treated culture was recovered in 900 µL LB broth again for 1 hour at 32˚C and plated for overnight growth. Successful colonies now demonstrate kanamycin and ampicillin sensitivity but chloramphenicol resistance.

2.5.21 **iTol2-Kan target construct amplification**

The following primer sequences were used for iTol2 amplification:

Reverse: GTAGAAACTGCCGGAAATCGTCGTGGTATTCACTCCAGAGCGATGAAAAC ATTATGATCCTCTAGATCAGATCT

Forward: TGGGATAGTGTTCACCCTTGTTACACCGTTTTCCATGAGCAAACTGAAACC CCTGCTCGAGCCGGGCCCAAGTG

The following shorter primers were used to check construct amplification only

Reverse: CACTCCAGAGCGATGAAAAC

Forward: TTCCATGAGCAAACTGAAAC

Using the ultramer primers PCR amplification was performed using the following mixture:

iTol2-Kan plasmid	5 µL
Forward primer	10 µL
Reverse primer	10 µL
Q5 10X reaction buffer	40 µL
Q5 HF enzyme	2 µL
10mM dNTP	4 µL
H_2O	129 µL

And the following thermo cycler program:

98˚C 2 min

30 cycles of: 98˚C 20 s

55˚C 30 s

72˚C 2 min

72˚C 10 min

The product was then separated on a 1% gel and the 1.4kb band extracted and purified.

2.5.22 **Targeting of iTol2-Kan into the Chloramphenicol resistant site**

A successful colony from Section 2.5.19 was cultured overnight at 32˚C with shaking. This was then further cultured in 40 mL to exponential phase. 300 ng of the iTol2-Kan construct from Section 2.5.21 was then targeted into the kanamycin resistant site and successful generation of KanR AmpS CmS colonies tested as per Section 2.5.19-2.5.20.

2.5.23 **Preparation of Tol-2 transposase mRNA for co-injection**

The restriction enzyme Not1 was used to linearise 20 µg of a Midiprep of the iTol2 construct. A reaction mixture of 200 µL would be cut to completion by 2 hours at 37˚C. This was PCR purified and eluted in 30 µL EBT, and synthesis of capped RNA performed using the mMessage mMachine kit as per manufacturer's instructions. The RNA pellet was extracted using the standard phenol:chloroform protocol and the final product eluted in 20 µL nuclease-free water and stored at -80˚C until use. For co-injection with the Tol2 plasmid DNA prepared above, a concentration of approximately 20 ng/µL was used.

2.6 **Tomographic RNA sequencing (TomoSeq)**

2.6.1 **TomoSeq sample freezing and sectioning**

Under RNA-free conditions the live, anaesthetised zebrafish were transferred into cryomoulds using a glass pipette. Excess fluid was removed and the larvae rapidly covered with OCT. Under a dissection microscopy, the zebrafish was positioned with Affi-Gel ® Blue (Sigma) to indicate start and end of sectioning. The entire block was then snap frozen on dry ice. Samples were stored at -80˚C until ready for use. Sectioning was performed on a Bright OTF5000 cryostat. Prior to sectioning, the cryotome was cleaned with 70% ethanol and a clean new blade was used each time to avoid RNA cross-contamination of specimens. 96 Lo-Bind Eppendorfs of 1.5mL were frozen at -80˚C for an hour prior to sectioning and kept on dry ice throughout sectioning. 9 µm thickness was used for 70 slices from the tail end, and 25 µm for 26 slices from the cloaca. Sections were transferred to individual Eppendorfs, avoiding any thawing of the sections.

2.6.2 **TomoSeq RNA extraction**

Prior to RNA extraction, care was taken to ensure surfaces were free of RNase by liberal application of RNaseZap™ (Sigma). Each slice of tissue in OCT of the 96 Eppendorfs was dissolved in 0.5 mL of TRIzol reaction with 0. 5 µL GlycoBlue (Sigma Aldrich, Dorset, UK) and 2 µL ERCC spike-in (Ambion, Texas, USA) diluted to 1:500000. Extraction was performed in groups of 24 tubes to ensure thawing to room temperature did not occur in the absence of TRIzol and thus avoid loss of RNA. After addition of the mixture, tubes were closed tightly and shaken vigorously for 15 s, and then incubated at room temperature for 5 min. 100 µL chloroform was then added to each of the 96 tubes, and again shaken vigorously for 15 s and

incubated at room temperature for 5 min. Tubes were centrifuged at 12000 x *g* for 15 min at 4°C. The colourless aqueous phase was transferred to 96 new individually labelled LoBind Eppendorfs, carefully avoiding the interface layer. 250 µL isopropanol to the aqueous phase and tubes shaken vigorously for 15 s. Incubation was done at -20˚C overnight to maximise yield. The next day, tubes were centrifuged in batches of 24, at 12000 x *g* for 10 min at 4°C. A small blue pellet visible in each of the 96 tubes indirectly confirmed the presence of RNA. If any tubes were missing the blue dot, the sample was discarded and a fresh sample cryosectioned. The supernatant was discarded and the RNA pellet washed with 500 µL 75% ethanol, centrifuged at 7500 x *g* for 5 min at 4°C, and the air dried at room temperature until completely dry.

2.6.3 **TomoSeq reverse transcription and *in vitro* transcription of RNA**

This was performed using the Ambion MessageAmpII kit but with modifications to the manufacturer's instructions in order to make this compatible with the 96 sample tomography and subsequent library creation. First, each of the 96 tubes was resuspended in 1.2 µL of bar-coded primer (5 ng/µL) (primer #1 to section #1 etc.) on ice. Getting this step absolutely correct was of paramount importance so that tomography could be accurately mapped after sequencing. Numbered primers were used as listed in Appendix 1: TomoSeq numbered primer sequences.

First strand synthesis was then performed by adding the following to each of the 96 samples:

First strand buffer	0.2 µL
dNTP	0.4 µL
RNase Inhibitor	0.1 µL
ArrayScript	0.1 µL

Samples were incubated in a thermo cycler at 42°C for 2 hours.

Second strand synthesis was then performed on ice by adding the following to each of the 96 samples:

Nuclease free water	6.3 µL
Second strand buffer	1 µL
dNTP	0.4 µL
DNA Polymerase	0.2 µL
RNaseH	0.1 µL

Samples were incubated in a thermo cycler at 16°C for 2 hours.

The cDNA obtained was cleaned using the kit as per manufacturer's instructions. Eight samples were pooled into one and twice the volume of cDNA binding buffer added into a cDNA cleanup column. This was spun at 10000 x *g* for 1 minute at room temperature and the flow through discarded. This was repeated until all 96 samples had been run through the same cleanup column. Then 500 µL of wash buffer was inserted in the column, spun at 10000g and the flow through discarded. The column was dried by spinning for an additional minute and then transferred to a clean tube. 10 µL water at 55°C was added to the centre of the column membrane and the column incubated for 2 min at room temperature. cDNA was then eluted by spinning for 1.5 min at 10000 x *g*. Elution was repeated a second time for a total volume of 20 µL which was stored at -20˚C.

In vitro transcription was then performed by using the following mixture:

cDNA	6.4 µL
T7 buffer	1.6 µL
T7 enzyme	1.6 µL
A	1.6 µL
G	1.6 µL
C	1.6 µL
U	1.6 µL

The sample was incubated in a thermo cycler at 37°C for 13 h with lid at 70°C.

The resulting amplified RNA was then fragmented and cleaned as follows:

aRNA	16 µL
Fragmentation buffer	4 µL

This was incubated at 94°C for exactly 2.5 min and then the reaction was put immediately on ice and 2 µL of ice cold fragmentation stop buffer added. This step was of utmost importance as over fragmented RNA would be unsuitable to prepare a library. The fragmented sample was cleaned using the aRNA cleanup columns also from the Ambion kit, as per manufacturer's instructions. Briefly, the following mixture was prepared:

Nuclease free water	8 µL

aRNA binding buffer	105 µL
100% ethanol	75 µL

This was loaded onto an aRNA column, spun at 10000 x *g* for 1 min and flow-through discarded. The column was washed with 500 µL wash buffer and dried by a further spin at 10000 x *g* for one minute before being transferred to a clean collection tube. 15 µL of RNase free water at 55°C was added to the centre of the column membrane, incubated for 2 min, and then spun at 10000 x *g* for 1.5 min. This elution was repeated to give a final total of 30 µL. To confirm the fragmentation produced a peak at ~500bp, 1 µl was run on a Bioanalyzer RNA pico chip.

2.6.4 **TomoSeq library preparation**

The Illumina TruSeq small RNA kit was utilised to perform library preparation but with modifications as below.

Firstly, Antarctic Phosphatase treatment was performed using aRNA at 20 ng/µL:

aRNA	16 µL
10X phosphatase buffer	2 µL
Antarctic phosphatase	1 µL
RNaseOUT®	1 µL

The mixture was incubated in a thermocycler with the following settings:

37°C for 30 min

65°C for 5 min

4°C indefinite hold

Next, polynucleotide (PNK) treatment was done to add a phosphate group to the 5' end of the RNA to enhance efficiency of synthesis. This was performed by adding the following mixture:

Nuclease free water	17 µL
10X PNK buffer	5 µL
ATP 10mM	5 µL
RNaseOUT	1 µL
PNK	2 µL

Incubation was performed in thermocycler at 37°C for 60 min.

Cleanup of this product was performed with the RNeasy kit (Qiagen) as per manufacturer's instructions. Elution was then performed with 14 µL nuclease free water.

3' adapter ligation was then performed using the adapter supplied in the Illumina kit but diluted by a factor of 5. The following mixture was prepared using product from the Illumina kit, apart from the T4 truncated RNA Ligase 2 which was purchased separately from NEB, and incubated at 70°C for 2 min.

PNK treated aRNA	5 µL
Diluted 3' adapter	1 µL

Then the following mixture was added and incubated at 28°C for 1 h:

5X HM Ligation Buffer	2 µL
RNase Inhibitor	1 µL
T4 RNA Ligase 2, truncated	1 µL

1µL Stop Solution was then added, a further incubation of 15 min at 28°C was performed before 3 µL ice-cold nuclease-free water was added.

Reverse transcription was then performed by preparing the following mixture and incubating at 70°C for 2 min:

adapter-ligated RNA	6 µL
RNA RT Primer	1 µL

Followed by addition of:

First strand buffer	2 µL
12.5mM dNTP	0.5 µL
100mM DTT	1 µL
RNase Inhibitor	1 µL
SuperScript III RT	1 µL

The mixture was then incubated at 50°C for 1 h and then PCR amplification done by adding the following mixture:

Nuclease free water	8.5 µL
PCR mix	25 µL
RNA PCR Primer	2 µL
Indexed RNA Primer	2 µL

The mixture was then amplified with the following protocol:

30 s at 98°C

12 cycles of: 10 s at 98°C

30 s at 60°C

30 s at 72°C

10min at 72°C

The PCR product was then cleaned using 50 µL Agencourt AMPure XP Beads (Beckman Coulter) added to the 50 µL PCR reaction. Room temperature incubation for 15 min was performed prior to magnetic separation for 1 min. The supernatant was discarded and beads washed with 200 µL of freshly prepared 80% ethanol. Beads were air dried for 15 min before the process being repeated with 32.5 µL EBT. 30 µL of supernatant this time was transferred to a new tube and 39 µL beads used to repeat the cleanup process. The final libraries were eluted in 12.5 µL EBT and transferred to a new tube. 1 µL of this was used to assess library quality using a DNA HiSensitivity Qubit to confirm the size distribution around 400bp and not lower.

2.6.5 **TomoSeq sequencing**

The libraries were pooled using recommended Primers in the Illumina Small RNA indices kit, and quantified using a Qubit 4 Fluorometer (Invitrogen, Burlington, ON). The final pooled samples and loaded into a HiSeq Sequencer (Illumina, San Diego, CA, USA) at 4 nM with a 5% PhiX spike-in and sequenced using a 50bp paired-end standard protocols as recommended by the manufacturer, at a density of two samples per lane.

2.6.6 **Analysis of TomoSeq**

Data were analysed by utilizing high performance computing with Python programming to map libraries to the Genome Reference Consortium Zebrafish Build 10 (GRCz10) sequence. Normalisation to RNA spike in, plotting of graphs and heatmaps, significance calculation and identification of ranked genes were performed using code written in R software, FunRich software (Pathan *et al.*, 2015) or Web-based GO Analysis (Eden *et al.*, 2009).

2.7 **Histochemical analysis**

2.7.1 **Alcian blue staining for goblet cell quantification**

Larvae were fixed overnight in 4% PFA. Staining was performed as previously described (Chen *et al.*, 2012). Briefly, whole embryos were then rinsed in PBS, washed in acidified alcohol (3% acetic acid and 70% ethanol) and stained for 3.5 h in Alcian Blue dye (Sigma A5268) at room temperature. Larvae were then cleared in two washes of 100% methanol, and transferred to 2:1 benzyl benzoate:benzyl alcohol. Images were obtained using Nikon AZ100 microscope with an automated stage (Prior Scientific) interfaced with NIS-Elements Extended Depth of Focus software (Nikon). Quantification was performed using Image J.

2.7.2 ***In Situ*** **Alkaline phosphatase staining for endogenous expression**

Zebrafish larvae were fixed in 4% PFA overnight. Whole embryos were permeabilised with 100% acetone for 20 min at -20˚C and then stained with BCIP/NBT in groups of 20 fish each. Staining was observed in real time and stopped with 5 mM EDTA at the same moment of time in each group, as soon as intestinal staining was observed. Fish were then cleared in methanol and imaged in 80% glycerol using Nikon AZ100 microscope with an automated stage (Prior Scientific) interfaced with NIS-Elements Extended Depth of Focus software (Nikon). Blocking of intestinal isoform of alkaline phosphatase was done with 50 µM L-Phenylalanine, and non-intestinal isoforms with 50 µM Levamisole. Quantification of intensity was performed using Image J (FIJI, (Schindelin *et al.*, 2012)).

2.7.3 **Acridine orange staining for cell death within the zebrafish larval intestine**

Zebrafish larvae were either gavaged or immersed in treatment compounds or vehicle controls. A positive control of 50 mM glafenine immersion was used. 45 min before imaging, zebrafish larvae were transferred to clean 3 cm Petri dishes with a standard ten fish per dish, and immersion was performed for 30 min in 1 µM acridine orange in clear E3. Following this, three washes in clear E3 was done, and the larvae anaesthetised for imaging using the MCherry channel on a Nikon Eclipse TE2000-U microscope and 20X objective lens. NIS-Elements AR® was used for imaging and analysis. Quantification was performed using intensity over the ROI of the bowel.

2.8 **Bacteriological techniques**

2.8.1 **Bacterial strains**

Bacterial strains used are listed in Table 2-2.

2.8.2 **Bacterial growth conditions**

To obtain bacteria within the exponential growth phase for experimental work, a single colony was picked and cultured in 5 mL of BHI with 50 µg/mL tetracycline overnight at 37˚C with vigorous shaking at 250 rpm in a sterile culture tube. After 16 hours, 500 µL of the overnight growth was re-cultured in a conical flask without antibiotics, under the same conditions, to give an optical density (OD_{600}) of 0.5-0.8. The bacteria were then pelleted by centrifuging at 4˚C (or room temperature for *E. faecalis*), 4500 x *g* for 20 min. Bacterial cultures were resuspended to the desired concentration in sterile PBS before injection.

Table 2-2:Bacterial strains.

Strain	Description	Reference
S aureus SH1000	Functional *rsbU+* derivative of 8325-4	(Horsburgh *et al.*, 2002)
S aureus SJF4308	SH1000-pMV158-mCherry	(Boldock *et al.*, 2018)
S aureus SA113	Restriction-deficient mutant derived from strain NCTC 8325	ATCC®35556™
S aureus SA113-mCherry	SA113-pMV158-mCherry	This thesis
E. faecalis OG1RF	Plasmid-free, virulent laboratory strain isolated from the oral cavity	(Dunny, Brown and Clewell, 1978)
E. faecalis OPDV	Δ*oatA* Δ*pgdA* Δ*dltA* Δ*sigV*	(Smith *et al.*, 2019)
E. faecalis ΔEpaOX	*OPDV_11715*::*Tn2.13*	(Smith *et al.*, 2019)
E. faecalis OG1RF-*mCherry*	OG1RF- pMV158-mCherry	(Salamaga *et al.*, 2017)
E. faecalis ΔEpaX-mCherry	*OPDV_11714*::*Tn2.14*+ - pMV158-mCherry	Kind gift from Bartlomiej Salamaga (Mesnage Lab, University of Sheffield)
E. faecalis ΔEpaX-Comp- mCherry	*OPDV_11714*::*Tn2.14 + pTet OG1RF_11714* + - pMV158-mCherry	Kind gift from Bartlomiej Salamaga (Mesnage Lab, University of Sheffield)
E. faecalis ΔEpaX-Comp	*OPDV_11714*::*Tn2.14 + pTet OG1RF_11714*	(Smith *et al.*, 2019)
E. faecalis Δ2.5	*OPDV_11720*::*Tn2.5*	(Smith *et al.*, 2019)
E. faecalis Δ2.8	*OPDV_11720::Tn2.8*	(Smith *et al.*, 2019)
E. coli EL250	DH10B [λcl857 *(cro-bioA < > araC-*P_{BAD}*flpe]*	(Lee *et al.*, 2001)
E. coli TOP10	F^- *mcrA* Δ(*mrr-hsd*RMS-*mcr*BC) Φ80*lac*ZΔM15 Δ*lac*X74 *rec*A1 *ara*D139 Δ(*ara-leu*) 7697 *gal*U *gal*K *rps*L (Str^R) *end*A1 *nup*Gλ-	Invitrogen™

2.8.3 **Transduction of *S. aureus* SA113 using bacteriophage**

Stock bacteriophage Φ11 (Mani, Tobin and Jayaswal, 1993) was used for phage transduction for introduction of the fluorescent plasmid into strain SA113 *S. aureus*. First, the phage lysate was prepared by combining 200 µL of overnight *S. aureus* SH1000-mCherry with 5 mL BHI, 5mL phage buffer, and 100 µL of phage lysate stock. The mixture was incubated at 37˚C overnight until clear (Figure 2-2), and the filter-sterilised using 0.2 µm syringe filter and stored at 4˚C. 50 mL of fresh LK was inoculated with a single colony of *S. aureus* SA113 WT and then grown overnight at 37˚C 250 rpm. The culture was centrifuged at room temperature for 10 min at 5000 x *g*, and the pellet resuspended in 3mL fresh LK. The following were prepared in fresh culture tubes:

SA113 WT overnight growth	500 µL
Phage lysate from SH1000-mCherry	500 µL
LK media	1 mL
1M $CaCl_2$	10 µL

Control tubes were included without phage lysate. Tubes were incubated at 37˚C, static for 25 min then at 250 rpm for 15min. After this, 1 mL ice-cold 0.02 M sodium citrate was added to the mixture and tubes incubated on ice for 5 min. Cells were pelleted by centrifugation at 5000 x *g* for 10 min at 4˚C. The pellet was resuspended in 1 mL 0.02 M sodium citrate and incubated on ice for a further 60 min. 100 µL, 250 µL and 500 µL of resuspended cells were streaked on LK plates containing 0.05% (w/v) sodium citrate and incubated overnight at 37˚C. Colonies were re-streaked on BHI plates with tetracycline (50 µg/mL) to confirm plasmid transfer. Further confirmation of fluorescence was performed by viewing plates under fluorescence stereomicroscopy but often this was visible after spinning down the pellet (Figure 2-3).

2.8.4 **Direct cell counts (CFU mL^{-1}) and Spectrophotometric measurement (OD_{600})**

Viable colony numbers were determined directly. 10 µL samples of the bacteria suspended in sterile PBS were spotted onto BHI agar plates in triplicate. Colonies were counted averaged to obtain CFU/mL of bacterial culture. Measurements at 600 nm (OD_{600}) were taken using Beckman DU®520 Spectrophotometer and Semi-micro polystyrene cuvettes (Fisherbrand).

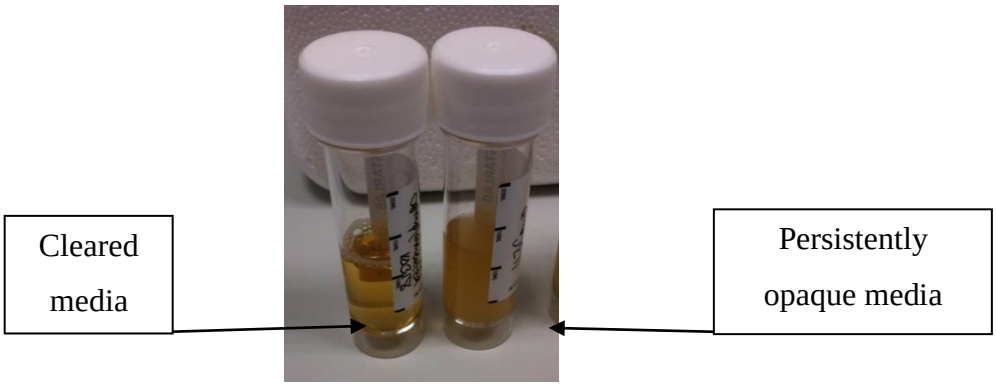

Figure 2-2: Successful bacteriophage transduction. This is first visually confirmed by clearing of media (left universal) compared with persisting opacity of control (right universal). Subsequent plating and overnight culture would confirm successful incorporation of mCherry fluorescent when colony fluorescence could be observed under fluorescence microscopy.

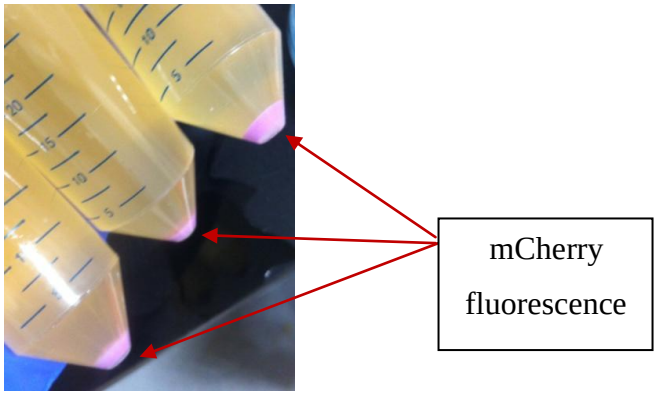

Figure 2-3: Pelleted colonies following growth to exponential phase of selected fluorescent colonies. Although confirmation of fluorescence colonies was always confirmed by microscopy prior to selection, successful transduction could also be seen by mCherry in the pellets after growth to exponential phase.

2.9 **Zebrafish in vivo techniques**

2.9.1 **Zebrafish husbandry**

Zebrafish were raised according to standard protocol (Avdesh *et al.*, 2012). The fish were maintained in tanks of 20-60 fish in a closed and continually recycling system. They were fed a diet of live *Artemia* the mornings and Zebrafeed® dry fish pellets (Sparos Ltd, Portugal) in the evenings. A 14/10 hour light - dark cycle at 28˚C was the standard condition used in the aquaria, as well as the embryo incubators. Fish were bred either by pairing or by inserting a box of marbles to stimulate egg production. Eggs were collected and washed and sorted into 10cm Petri dishes of 60 embryos each, incubated in either 30ml of sterile autoclaved E3 (Westerfield, 2007), or non-sterile E3 mixed with 10% tank water. At the end of each experiment, and before 5.2 days post-fertilisation (dpf), the larvae were culled by immersion in bleach, or fixed with 4% PFA. All procedures were carried out in strict accordance with the Home Office and the Animals (Scientific Procedures) Act, and for experiments using larvae beyond 5.2dpf, according to Project Licence Number P1A4A7A5E.

2.9.2 **Transgenic Fish Lines**

Transgenic fish lines used are listed in Table 2-3.

Table 2-3: List of transgenic fish lines

Transgenic or wildtype line	Description	Reference
Nacre	Lacking melanocytes as mutant for *mitfa* gene	(Lister *et al.*, 1999)
Casper	Doubly mutant for *roy* and *nacre*	(White *et al.*, 2008)
Wild-type TU	Tuebingen	(Haffter *et al.*, 1996)
TgBAC(mpx:GAL4-VP16)sh267;Tg(UAS:Kaede)i222	Neutrophil-specific photoconvertible RFP-GFP	(Dixon *et al.*, 2012)
Tg(6xHsa.NFκB:eGFP)sh235	NFκB - eGFP	Kind gift from Nikolay Ogryzko (University of Edinburgh)
TgBAC(mpx:GFP)i114	Neutrophil–specific GFP	(Renshaw *et al.*, 2006)
Tg(mpeg1:NLS-Clover)sh436	Macrophage-specific Clover	Kind gift from Nikolay Ogryzko (University of Edinburgh)
TgBAC(klf2a:GFP)	Endothelial specific *Klf2a*-H2B-GFP	(Heckel *et al.*, 2015)
TgBAC(Cldn15la:eGFP)sh545	eGFP expression driven by *Cldn15la* promoter	This study
TgBAC(Cldn15la:Col1a2-eGFP)sh546	*Collagen1a2*-eGFP fusion protein driven by *Cldn15la* intestine specific promoter	This study

2.9.3 **Tailfin injury neutrophil assay of zebrafish larvae**

Tailfin injury in zebrafish larvae at 2dpf was performed with Tricaine methane sulfonate (MS-322) at 0.167 mg/mL (Westerfield, 2007), using a sterile scalpel blade #27 (Swann-Morton, England). Immediately after injury, or at 5 hours post-injury (hpi), intravascular injection of treatment or vehicle control was performed under anaesthesia. The *Tg(mpx:GFP)i114* (Renshaw *et al.*, 2006) line with green fluorescently labelled neutrophils allowed manual quantification of neutrophil numbers within the region of injury (boxed area in Figure 2-4) under a fluorescence stereomicroscope (Leica MZ10F) at 6hpi for recruitment assays, 12hpi for resolution assays and 24hpi for delayed resolution assays.

2.9.4 **Intravascular microinjections of zebrafish larvae**

Intravascular microinjections were performed on zebrafish larvae at 2dpf into the duct of Cuvier at the point behind the potential cleithrum (Figure 2-5), as previously described (Benard *et al.*, 2012). Microinjections were performed using a Pneumatic PicoPump PV820 (World Precision Instruments) using a hold pressure of 5psi and eject pressure of 30psi, and a Leica MZ12.5 stereo microscope. Calibration of drop size was done using a Pyser-SGI graticule (100X0.1=10mm). Needles were pulled from TW100 borosilicate capillary tubes (World Precision Instruments) using a P97 Fleming/Brown micropipette puller (Sutter Instrument Co., Novato USA), loaded using sterile Eppendorf MicroLoader tips, and the needle end bevelled using a razor blade. Success of intravascular injection could be appraised immediately at time of procedure by observing flow of injected substances into the circulation.

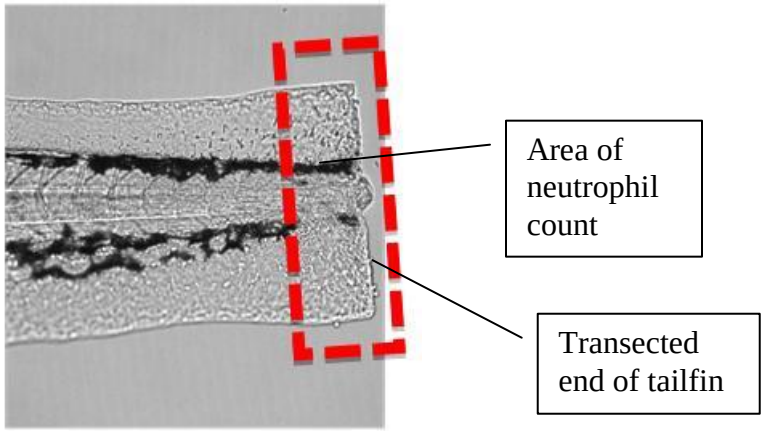

Figure 2-4: Region of interest at the site of tailfin injury. Neutrophils within the area boxed in red were caudal to the circulation end in a zebrafish and were counted as being within the region of injury.

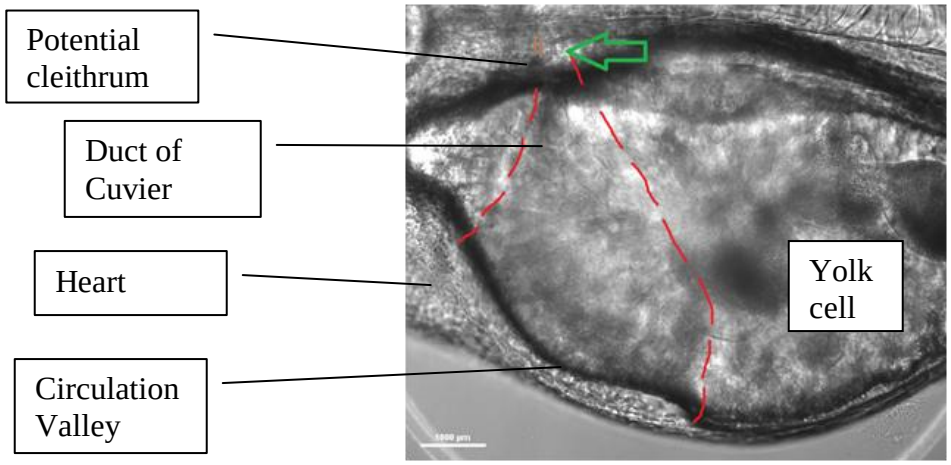

Figure 2-5: Intravascular microinjection site in 2dpf zebrafish larvae. Duct of Cuvier (marked in red) and circulation valley in 2dpf larvae. Point of injection marked with green arrow, behind the potential cleithrum.

2.9.5 **RNA and DNA microinjection at the 1-cell stage zebrafish embryo**

Zebrafish were pair-mated in individual tanks and dividers removed at the start of the light phase at 8am in the morning. After 15 min of undisturbed mating time, eggs were collected and rinsed with sterile E3. Under RNase free conditions, the eggs were organised using a sterile glass slide and an equal amount of purified an iTol2 BAC construct and iTol2 RNA was injected into the cell as previously described (Rosen, Sweeney and Mably, 2009). Yolk injections were preferred for RNA microinjections as these could be performed with rapidity, whereas cytoplasmic injections were used preferentially for DNA injections to increase efficiency. The maximum time from collection of eggs to completion of injections were timed to be less than 20 min, to ensure delivery was within the duration of the 1-cell stage of development (Pei and Burgess, 2019). Approximately 30 uninjected eggs from the same clutch are used as a control to monitor egg quality for each experiment.

2.9.6 **Microgavage of zebrafish larvae**

Microgavage was performed as previously described (Cocchiaro and Rawls, 2013). Briefly, this involved anaesthesia of 4dpf zebrafish larvae which were then supported on 2% agarose. A blunt ended microcapillary needle (Heat 380, Pull 225, Velocity 150, Time 225), attached to a Pneumatic PicoPump PV820 (World Precision Instruments) using a hold pressure of 5psi and eject pressure of 20psi, was guided under microscopy into the oropharynx, past the oesophageal sphincter and into the intestinal bulb of each larvae. Calibration of drop size was done using a Pyser-SGI graticule (100X0.1=10 mm). A volume of 4.6 nL was used for each zebrafish as this consistently caused minimal spillage occurred from either the anal pore or the oropharynx.

2.9.7 **Tailfin regeneration assay**

The zebrafish tailfin is unique in that it can regenerated itself within three days when injured, even in the adult fish (Azevedo *et al.*, 2011). Tailfin amputation was performed as described in Section 2.5. Intravascular treatment was given immediately following injury and the larvae were then imaged after one hour of recovery using a Nikon Eclipse TE2000-U microscope interfaced with NIS-Elements AR® software. This hour of recovery was important to ensure that initial measurements were obtained after wound contraction had resolved. Each larva was maintained in a separate well in a 24-well plate to allow direct comparison of growth in the same larvae. At

24hpi, the tailfin was imaged again in the same manner. Tailfin length was defined as the length of a line drawn along the longitudinal axis of the larvae from the end of the circulation loop to the edge of the wound at this point. Percentage increase in length was then calculated.

2.9.8 **Neutrophil reverse migration assay in zebrafish larvae**

The *TgBAC(mpx:GAL4-VP16)sh267;Tg(UAS:Kaede)i222* photo-convertible line and protocol was performed as previously published (Holmes *et al.*, 2012). Briefly, 2dpf zebrafish underwent tailfin amputation, and were treated at 4hpi with either intravascular injection of a vehicle control or SPM, and immediately mounted in 0.8% low melting point (LMP) agarose (Sigma) with 0.0167% Tricaine. At 5hpi, neutrophils in the area boxed in red (Figure 2-7) was photo converted using the Ultraview PhotoKinesis device (Perkin Elmer) 405 nm laser at 40% power and 120 cycles. Photo conversion was performed by alternating the groups to avoid introducing bias since the process could take up to an hour to complete. The mounted specimens were then time-lapsed every 5 min for the next 6 h using an inverted Olympus microscope with Yokagawa CXU spinning disk and Volocity®(Perkin Elmer) software for image capture and analysis. Neutrophils were said to have reverse migrated if they moved proximally to the area boxed in Figure 2-6.

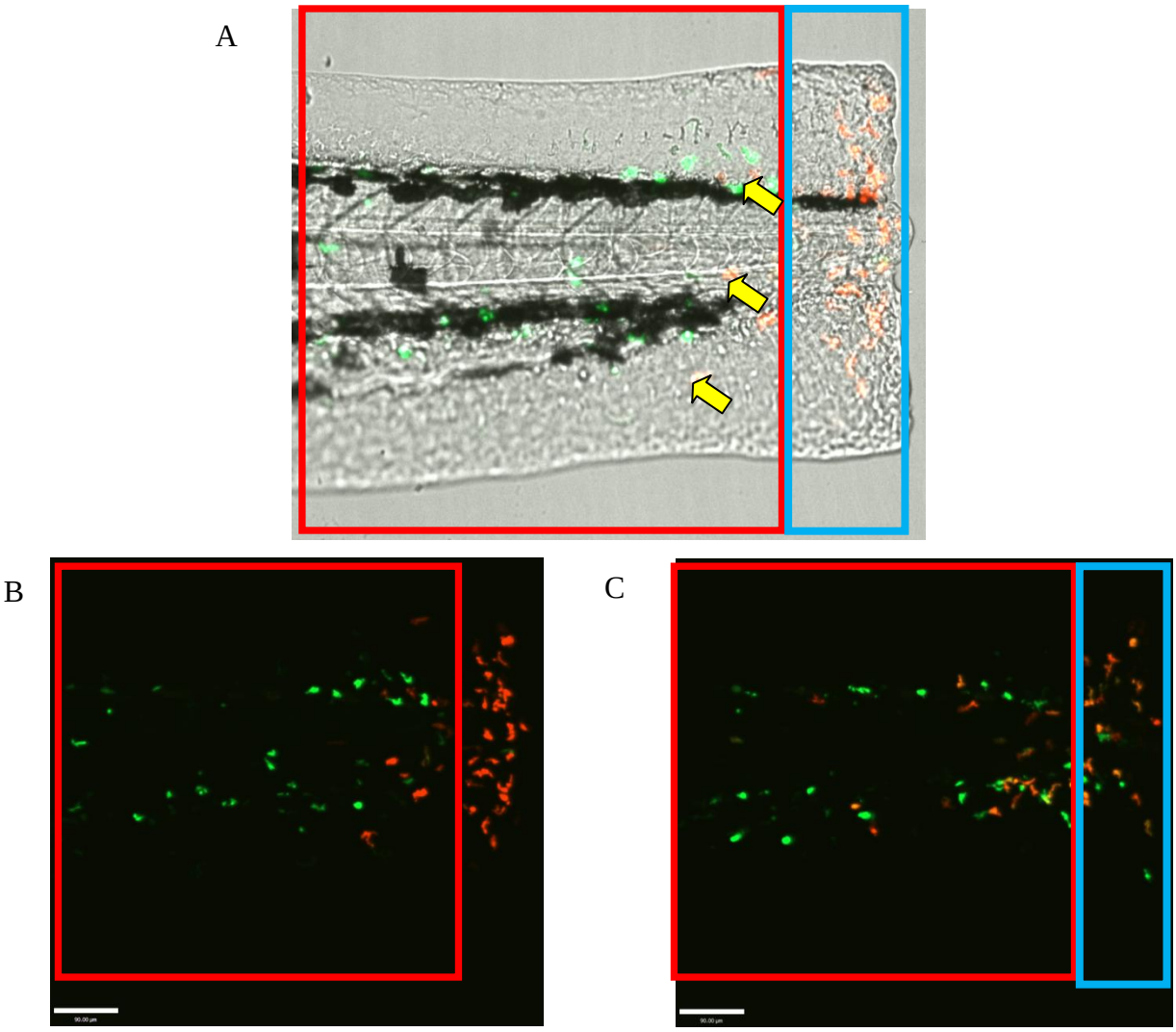

Figure 2-6: Reverse migration assay. The *TgBAC(mpx:GAL4-VP16)sh267;Tg(UAS:Kaede)i222* photo-convertible line was used, and 2dpf larvae underwent tailfin injury. **A**. Merged brightfield, GFP and mCherry channels demonstrating outline of tailfin injury. At the set time post-injury, neutrophils in the region of injury (ROI, blue box) were photo converted from green to red. Red neutrophils outside the region of injury (red box) were said to have reverse migrated from the wound site (examples marked with yellow arrows). **B**. GFP and mCherry fluorescent channels at 20X objective demonstrate reverse migrated neutrophils at 6.75hpi. **C**. Merged GFP and mCherry fluorescent channels at 20X objective demonstrating the same fish at 10hpi demonstrate a few new green neutrophils have migrated into ROI (blue box) after photo conversion at 5hpi, and more neutrophils have reverse migrated into the area boxed in red.

2.9.9 **TSA/TUNEL neutrophil apoptosis assay**

The number of neutrophils undergoing apoptosis at a given time point was assessed by staining with the ApopTag®Red In Situ Apoptosis Detection Kit (MerkMillipore, Massachusetts, USA) and Tyramide Signal Amplification (TSA)™ Plus Fluorescein System (PerkinElmer, Buckinghamshire, UK). Larvae underwent tailfin amputation as described and were fixed at a pre-determined time-points (3hpi, 6hpi, 9hpi and 12hpi). Staining was then performed as per manufacturer's instructions. Briefly, the first stain was done for 10 min at 28˚C with 1:50 TSA:Amplification diluents. Larvae then underwent digestion with 10 µg/mL Proteinase K for 75 min, and the second staining with ApopTag®Red performed. Imaging was done on an inverted Olympus microscope with Yokagawa CXU spinning disk and Volocity® (Perkin Elmer) software for image capture. To allow accurate analysis, Z-slices of 2 µm were captured throughout the tailfin and a 20X objective lens was used. Apoptotic neutrophils were identified by observing co-localisation of green (*mpx*) and red (DNA strand breaks) fluorescence within a single z slice (Figure 2-7).

2.9.10 **Whole mount *In Situ* hybridisation**

Sense (control) and antisense RNA probes were synthesised using the SP6/T7 DIG-RNA labelling kit (Sigma Aldrich, Dorset, UK) as per manufacturing protocol. Control and injured 2dpf larvae were anaesthetised and fixed in 4% PFA at the predetermined time-points post injury. The *in situ* hybridisation protocol used was as previously published (Thisse et al. 1993). Briefly, larvae were digested in 10µg/mL of Proteinase K for 35 min and incubated overnight at 70˚C with the probe (50% formamide, 50 µg/mL heparin, 500 µg/mL tRNA, 0.1% Tween 20, 3 mM NaCl, 300 µM sodium citrate, citric acid to pH6, and 1:200 RNA probe). Imaging was performed with a Nikon SMZ1500 extended focus microscope and images processed with NIS-Elements BR® version3.1.

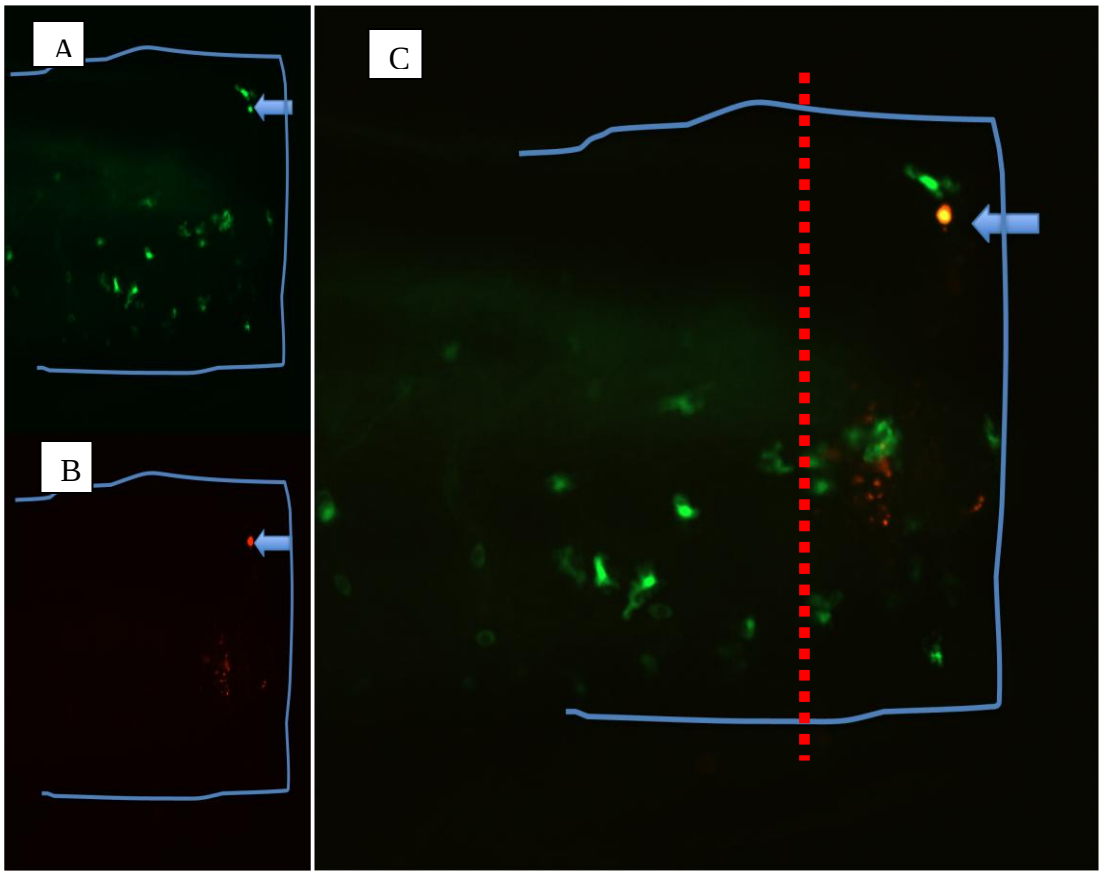

Figure 2-7: TSA/TUNEL assay. Representative images of an apoptotic neutrophil are shown. **A**. GFP channel showing labelled neutrophils, apoptotic neutrophil marked by blue arrow, note rounded small appearance. **B**. TxRed channel showing apoptotic bodies, blue arrow marking apoptotic neutrophil. **C**. Apoptotic neutrophil confirmed by co-localisation of both red and green within the same XY plane shows up as orange round body marked by blue arrow. Neutrophil and apoptotic body counts are all performed within area of injury distal to end of circulation marked by red dotted line. Outline of tailfin shown by blue line in all pictures.

2.9.11 **Mechanical Model of Bowel injury model in zebrafish larvae**

Bowel injury was performed under brief anaesthesia with MS-322. A microcapillary needle was microforged to 50 µm in diameter using a MF-900 Narishige Microforge, the tip bevelled and thoroughly rinsed in filtered water prior to use. The puncture injury was performed approximately 120 µm from the anal opening. Somite injury was performed at somite level in line with the cloacal opening.

2.9.12 **Laser Model of Bowel injury model in zebrafish larvae**

Zebrafish larvae at 4dpf were anaesthetised with Tricaine as previously described. Larvae were then mounted in groups of six on a number 0 glass slide using 1% LMP agarose with 0.0167% Tricaine. These cover slips were then affixed using high vacuum grease (Dow Corning®) to a 25 mm Petri dish with a predrilled 10 mm opening at its base to accommodate the fish. The Petri was filled with E3 to prevent drying out of the agarose and also to dissipate the laser heat. Lasering was performed using an Andor Micropoint Laser attached to an inverted Olympus microscope with Yokagawa CXU spinning disk and run with IQ software. A 40X oil immersion lens was used. The laser power was set at 77% which was the optimal power to cause an ablation injury in 100% of the larvae.

2.9.13 **Inflammation assay for bowel injury in zebrafish larvae**

The youngest age at which the zebrafish larvae could be used for gut specific analysis was at 4dpf as this was the time when the gut was reliably colonised with bacteria (Kanther and Rawls, 2010), and both the oral and anal orifices were fully open to the environment. Therefore this assay used 4dpf larvae. The larvae underwent microgavage of 5 nL of vehicle control or treatment and then immediately underwent mechanical bowel wounding described in Section 2.9.11. The larvae were then mounted in 0.8% LMP agarose and a time-lapse performed on an inverted Olympus microscope with Yokagawa CXU spinning disk interfaced with Volocity 6.3.

2.9.14 **Intravenous bacteraemia survival assay in zebrafish larvae**

Staphylococcus aureus or *Enterococcus faecalis* bacteraemia survival assays in zebrafish were performed as previously published (Prajsnar *et al.*, 2008) but modified so that only 2dpf zebrafish were used as prior to this neutrophils may not yet be fully developed and interpretation

of results would be difficult. Briefly this involved preparation of *S. aureus* or *E. faecalis* as described above. 2500CFU of the *S. aureus* (or 1500CFU of *E. faecalis*) was injected intravascularly into zebrafish larvae at 48hpi which had been pre-injected with either vehicle control or drug no more than 30 min post-infection. CFU counts were performed before the start of injections and immediately after the completion of injections to ensure that concentrations of bacteria injected were the intended CFU and constant throughout the experiment. Any experiment that was found to have great variation in CFU before and after injection was discarded. The zebrafish larvae were then maintained in individual wells in a 96 well plate to allow inspection 12 hourly from the time of infection. Groups were blinded prior to any injections and blinding kept throughout the survival study. The number found to be dead, defined as a cessation of heartbeat, at each inspection point was documented until 5.2dpf when the remaining zebrafish were culled.

2.9.15 **CFU quantification of *E. faecalis* in individual zebrafish larvae**

Larvae were euthanised with an overdose of MS-322, then rinsed three times in sterile filtered PBS to remove any possible extra-intestinal bacteria adherent to external surfaces of the larvae. Each fish was then manually homogenised using a motorised micro-pestle (Bel-Art ProCulture Micro-Tube Homogenizer System, SP Scienceware). Serial dilutions were spotted onto a BHI agar plate containing tetracycline to ensure selection of only the introduced bacteria containing the resistant plasmid, thus avoiding overestimation of colonies from spurious growth. Colonies were seen to be uniformly fluorescent using the mCherry filter under a stereo microscope and morphology matched those of clean colonies of *E. faecalis*.

2.9.16 **Picrosirius red staining of whole mount or frozen sections**

Wildtype zebrafish from 0dpf to 30dpf were killed according to Schedule 1 and preserved in 4% PFA. At least three from each dpf were stained with picrosirius directly or the GIT dissected out and stained with picrosirius directly, while a further three samples from each dpf were frozen in OCT and stored at -80˚C. Cryosections of 6 µm thickness were collected onto SuperFrost® Plus slides. Slides were then incubated in a Coplin jar containing picrosirius red for strictly one hour at room temperature. Slides were then rinsed twice in acidified water, dehydrated in incremental ethanol solutions, and cleared with xylene. Once dry, slides were cover-slipped with DPX.

Staining of whole mount or dissected GIT were performed in Eppendorfs and then mounted on slides with DPX in a similar manner. Visualisation was performed under a MZ12.5stereomicroscope (Leica) with polarising lenses, interfaced with a SPOT Insight Colour camera, and SPOT Advanced digital image capture software (Diagnostic Instruments).

2.10 **Imaging of zebrafish larvae**

2.10.1 **Time-lapse imaging of live larvae**

Zebrafish larvae were embedded in 0.8% low-melting-point agarose with Tricaine, in chambered wells and imaged using a Nikon Eclipse TE2000-U microscope, extended focus Nikon SMZ1500 microscopes, the Light sheet Leica TCS SP8 DLS, and the Ziess LSM880 AiryScan Confocal or an inverted Olympus microscope with Yokagawa CXU spinning disk. Analysis was performed using ImageJ, Perkin Elmer Volocity® 6.3, Zeiss Black, Zeiss Blue or NIS Elements AR® software. Tracking of individual neutrophils was possible using the embedded software capabilities of Volocity 6.3, with settings set to the Shortest Tracking path model and to ignore objects that were stationary to avoid a falsely inflated number of detected objects. An example tracking snapshot is shown below (Figure 2-8).

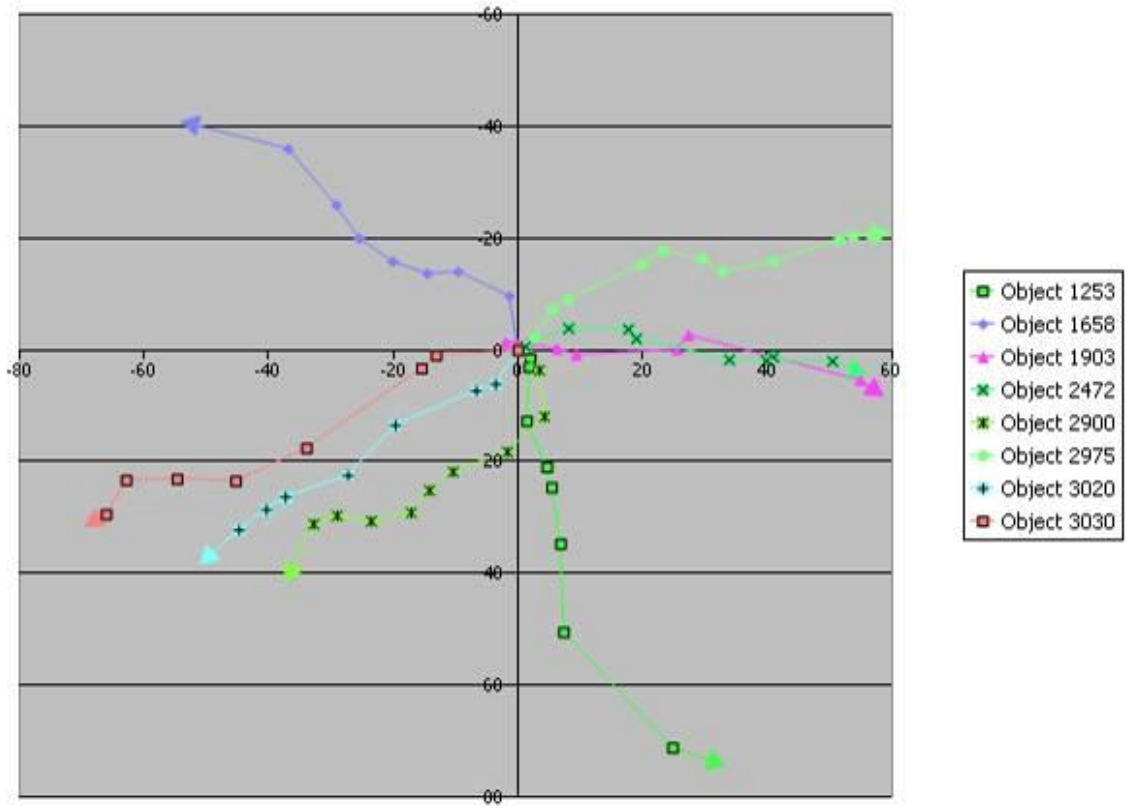

Figure 2-8: Example snapshot of neutrophil tracking in from intestinal injury using Volocity 6.3. Each line represents the path of a tracked object. The area of intestinal injury is seen centred as the point of intersection of the x and y axes, and labelled zero.

2.10.2 **Transmission Electron Microscopy**

Larvae were fixed in 2.5% gluteraldehyde and secondary fixation done with 2% osmium tetroxide for 1 h at room temperature and then dehydrated through a graded series of ethanol. Infiltration was performed with propylene oxide and Araldite resin, and then embedded in fresh Araldite resin at 60˚C for two days. Semi-thin sections were then cut on a Reichert Ultracut E ultramicrotome and confirmation of the correct segment performed with staining with 1% toluidine blue in 1% borax. Ultrathin sections of 90 nm were then cut on the same ultramicrotome and stained for 30 min with 3% uranyl acetate followed by Reynold's lead citrate for 5 min. A FEI Tecnai G2 Spirit Transmission Electron Microscope at an accelerating voltage of 80 kV was used to visualise each section and images taken using a Gatan digital camera. At least 30 sections of the relevant section of intestine from each of three separate larvae were examined.

2.10.3 **Light Sheet Microscopy**

Anaesthetised zebrafish larvae, or dissected intestinal tract of culled adult fish were mounted into glass capillaries in 0.8% LMP agarose in E3 together with 1:7000 dilution 0.5 µm fluorescent red latex beads (Sigma). These beads allow localization for 3D reconstruction using ImageJ. A Light Sheet Leica TCS SP8 DLS microscope with a 10X or 20X objective lens was used, and acquisition performed with Zen Black ® software.

2.11 **Mouse *in vivo* and *ex vivo* techniques**

2.11.1 **Mouse husbandry**

C57BL6/J male mice were purchased from Charles River Laboratories (Margate, UK) each time at 6 weeks of age. They were then housed singly on absorbent paper and allowed to acclimatise for seven days before the start of experiments. Mice were fed standard Teklad Global Rodent Diet (18% protein, 6% fat, moderate phytoestrogen, irradiated for sterility) with fresh water *ad libitum* and maintained at a standard temperature and humidity controlled facility in accordance with strict Home Office regulations. A 12 hour light-dark cycle was also maintained, and any work required during the dark cycle was carried out using a darkroom safelight (Paterson Photographic Equipment, West Midlands, UK). All procedures were carried out in strict

accordance with the Home Office and the Animals (Scientific Procedures) Act, Licence number P0E9E8941.

2.11.2 **Statistical design and sample size calculations**

This section was performed in collaboration with Amy Spencer and Pete Laud of the Sheffield University Biomedical Statistical Services Unit. Calculations were performed with the assumptions of a Student's t-test that the data would be normally distributed and that the variances in the two groups would be equal. The end-point of interest would be the improvement of healing as evidenced by an increase in hydroxyproline (HP) content of the anastomosis, as well as the time after surgery when this effect can be seen. Therefore comparison of data between control and treatment groups on post-operative day 3 and day 7 of two types of anastomoses, a simple anastomosis, and a leaky anastomosis would be performed. A significance level of 5%, and 80% power was used. A previously published experiment (Pantelis *et al.*, 2010) compared HP content at day 5 but in their study, only 5 mice per group were used so there were sparse data resulting in fairly approximate estimates of means and SD, especially given the different time-points. Nevertheless, these published data were used to calculate the sample sizes needed per group in Table 2-4. The middle value of 75 µg HP/g bowel was chosen as the end-point for experiments.

Table 2-4: Sample size calculation. Number per treatment group required to have 80% power to detect various differences in means at the 5% significance level assuming various SD. Calculations performed using online calculator available at http://www.sample-size.net/sample-size-means/

Difference in means (µgHP/g bowel)	SD (µgHP/g bowel)	
	76 (leaking model)	127 (standard model)
50	38	102
75	18	46
100	11	27

2.11.3 **Faecal mass measurements**

Mice were housed individually on absorbent paper rather than wood chips. These were changed daily at 7am, and all faecal matter collected into 3 cm sterile Petri dishes labelled specific for

each mouse (Figure 2-9). Faecal matter was air dried in the mouse room (controlled humidity and temperature) for 24 hours before weighing.

2.11.4 **Activity measurement**

Mice were acclimatised to being videotaped for 15 seconds each day during the daily cleaning of their individual cages for the week before the start of the experiment. Three days prior to the operative day, videotaping was performed for 15 seconds using a Canon IXUS 185 Digital Camera. Parameters of movement of each mouse was quantified using the AnimalTracker plugin in ImageJ as previously described (Gulyás *et al.*, 2016).

2.11.5 **Operative technique**

50X50 cm fenestrated 6X9 cm drapes were used to maintain sterility. All microsurgical instruments were autoclaved separately and a clean set used for each mouse. For the normal anastomotic group, mice were anaesthetised with isofluorane, skin antisepsis performed with 2% chlorhexidine in 70% alcohol and a mini-laparotomy performed. The caecum was positively identified and complete division of the intestine performed cleanly using scissors. Complete division was confirmed by visualizing a gap between both ends. Anastomosis was performed using 8/0 taper point polypropylene (LUXSutures, Luxembourg) interrupted sutures. Eight were used for the complete anastomosis producing a leak-free join shown in preliminary studies to be water-tight (Figure 2-10), and four were used for the leaking model. Closure was performed in two layers using 5/0 polyglycolic acid braided suture on a 3/8 reverse cutting (LUXSutures, Luxembourg), with a continuous muscle closure, and interrupted buried subcuticular. 50 µL 1% lidocaine was instilled between layers during closure. Mice were recovered in a enclosure warmed to 32˚C.

2.11.6 **Clinical assessment of mice post-operatively**

Weights were performed 12 hourly using an Ohaus portable scale CR621 (0.1 g precision). A Wellness Score (Komen *et al.*, 2009) was used to assess mice twice daily during weighing sessions. Scoring points are summarised in Table 2-5. As this scoring system was brief and quick to complete, should a mouse score low on the Wellness Score, a more detailed Murine Sepsis Score (Shrum *et al.*, 2014) was performed as summarised in Table 2-6.

Table 2-5: Wellness score

Parameter	Grading	Score
Activity	Normal / medium / low	2 / 1 / 0
Fur	Smooth / fluffy / erect	2 / 1 / 0
Eyes	Clean and open / clean and closed /dirty and closed	2 / 1 / 0
Able to stand straight	Yes / no	1 / 0
Posture	Normal / modestly curled / fully curled up	2 / 1 / 0
Position on feet	Normal / high	1 / 0
Solitary	Yes / no	0 / 1
Shivering	Yes / no	0 / 1

Table 2-6: Murine Sepsis Score

Parameter	Grading	Score
Appearance	Smooth / Patches piloerect / All piloerect / "Puffy" / Emaciated	0/1/2/3/4
Consciousness	Active / Hunched but active / Ambulant but slow / Movements only when provoked / Stationery when provoked	0/1/2/3/4
Activity	Normal / Not climbing / Occasional movement / Stationary / Tremor	0/1/2/3/4
Stimulus response	Auditory / Touch / Few steps to touch / Head movement to touch / unable to right itself if pushed over	0/1/2/3/4
Eyes	Open / Slightly closed / Up to Half closed / More than half closed / Closed	0/1/2/3/4
Respiration rate	Normal / Decreased not visually quantifiable / Moderately reduced by eye / 0.5s between breaths / 1s between breaths	0/1/2/3/4
Respiration quality	Normal / Periods of laboured / Laboured / Intermittent gasps / Gasping	0/1/2/3/4

Figure 2-9: Stool collected over 24 hours. The Petri dish contains a representative 24 hour stool collection from a normal C57BL6J male mouse at 6 weeks of age. Standardised air drying of the stool was performed for 24 hours prior to weighing.

A

B

Figure 2-10: A normal anastomosis. A. Completed normal (non-leaking) anastomosis technique demonstrated to be (**B**) water-tight using by infusing methylene blue intraluminally under pressure. This operative procedure was performed on a mouse already culled under Schedule 1, prior to the first live operation to confirm technical suitability of operative method.

2.11.7 **Harvesting of specimens and sample preparation**

On the 3rd or 7th post-operative day, or if the Wellness Score was below 6, mice were anaesthetized with isofluorane and cardiac puncture performed to exsanguinate the mice. The blood was stored on ice until culling was complete. This was then spun down immediately at 4˚C 17500 x *g* and the serum transferred to a clean Eppendorf and stored at -80˚C. Cervical dislocation was then performed after exsanguination. The abdominal cavity was then opened and the degree of adhesions, contamination, or abscess formation documented. Then anastomosis was then excised en-bloc together with any adhered organs for anastomotic bursting pressure. The spleen was harvested and its weight measured immediately.

2.11.8 **Anastomotic bursting pressure**

The proximal end was secured to a 16Fr metal straight gavage needle connected to saline in an Aladdin Programmable Syringe Pump AL1000-220 (World Precision Instruments, Hertz, UK) at a steady state of 1 mL/min. The pump was run before securing the distal end of the anastomosis to gently flush out any faecal matter within the lumen. When the effluent was clear, the pump was paused and the distal end secured to another 16Fr gavage needle connected to a Fisherbrand™ Traceable Manometer. The maximal pressure reading (mmHg) achieved before bursting was recorded. The anastomotic region was then dissected free and divided into three for enzymatic, histological and collagen assays.

2.11.9 **Stool culture for bacterial, fungal, cellulase and proteolytic activity**

Triplicates of 5 µL 1:10000 dilutions homogenised stool solutions (1 µg/µL) were spotted onto Sabouraud Dextrose, BHI, CMC and BHI-milk plates. Cellulase and proteolytic activity was measured semi-quantitatively by measuring diameter of clearing in CMC agar plates or after staining with Gram's iodine, using ImageJ, and categorising the degree of clearing of BHI-milk plates. All bacterial plates were cultured at 37˚C overnight and all fungal plates cultured at 28˚C for up to seven days. Fungal plates were imaged at 48 hours and again at 7 days. Imaging was performed using Epson Perfection V700 Photo Scanner interfaced with Silverfast Epson Perfection Software Version 3.1.1.

2.11.10 Frozen sectioning for histology

Sections of skin and anastomosis which had been fixed in 4% PFA were submerged in 15% to 30% sucrose gradient at 4˚C for 24 hours and then embedded separately in OCT in 5X7 mm moulds and snap frozen and stored at -80˚C until sectioning. Sectioning was performed as described in section 2.6.1 but at a thickness of 4µm. Sections were arranged onto SuperFrost ® Plus slides and stained immediately as below.

2.11.11 Haematoxylin and eosin staining of frozen sections

Slides were dipped into Coplin jars containing haematoxylin for 3 min. Slides were then rinsed in deionised water and then rinsed with blue-ing solution until adequate colour change was noted. Slides were rinsed with deionised water and dehydrated using graded alcohol solutions up to 95% ethanol. Slides were dipped into eosin for 60 s and then rinsed in absolute alcohol, dipped in xylene twice, and allowed to dry before fixing with DPX and cover-slipped. Imaging was performed using an Olympus BX51 microscope interfaced with an Olympus DP71 colour camera.

2.11.12 Picrosirius staining of frozen sections of intestine and skin

Picrosirius staining was performed as outlined in section 2.9.16. Imaging was performed using polarising lenses an Olympus BX51 microscope interfaced with an Olympus DP71 colour camera.

2.11.13 Wright-Giemsa staining of frozen sections

Slides were flooded with Wright-Giemsa stain for 5 min. This was then diluted 1:2 with PBS buffer and mixed by blowing gently on the slide. The diluted stain was left for 1minute. Slides were then rinsed twice with distilled water and air-dried. Clearing was done with xylene dipping and slides were cover-slipped with DPX mounting media. Imaging was performed using an Olympus BX51 microscope interfaced with an Olympus DP71 colour camera.

2.11.14 Hydroxyproline assay

Assay performed as previously described (Kivirikko and Liesmaa, 1959). Briefly, a third of the circumference of the anastomotic region was dissected free with sterile microsurgical

instruments. This was weighed and then placed immediately in 6N hydrochloric acid (Honeywell). Samples were frozen at -20˚C until collection was complete. Samples were then boiled at 110˚C for 18 hours in 2 mL O-ring tubes, and then freeze-dried to remove the hydrochloric acid. Samples were reconstituted in 250 µl ultrapure (18.2 MΩ·cm at 25°C) water. Dilute sodium hypobromite (Sigma) was prepared fresh each time and 500 µL added to each and allowed to oxidise for 5 min at room temperature before 250 µl of 6N HCl was added. 500 µl of 5% p-Dimethylaminobenzaldehyde in 1-propanolol was then added and the solution heated at 70˚C for 15 min before being cooled quickly in ice. A standard curve was obtained with each assay using relevant concentrations of hydroxyproline (Sigma). Absorbency of samples and standard were measured at 560 nm using a NanoDrop 3300 fluorospectrometer and operating software v.2.8.0. Values were then standardised by weight for comparison.

2.12 **Protein Analysis**

2.12.1 **Bradford protein assay**

A third of the circumference of the anastomotic ring was dissected out with sterile microsurgical instruments, weighed, and immediately immersed in ice cold lysis buffer (IGEPAL CA-630, NaCl, Tris-HCl pH adjusted 7.5) with an anti-protease cocktail (Aprotinin, leupeptin and benzamide). Homogenisation of samples was performed using zirconium ceramic beads (Thermo Fisher) at 6000 rpm for 30 s (repeated twice for skin samples) on a Precellys Evolution Homogeniser. Samples were then spun down for 3 min at 4˚C and 17200 x *g*. The supernatant was carefully removed to clean tubes. Quantification was performed using Bio-Rad Protein assay and Beckman DU®520 Spectrophotometer at 595 nm and Semi-micro PS cuvettes (Fisherbrand). Ascending concentrations of bovine serum albumin (BSA) were used to perform a standard curve with each run of assay. Each time, 15 min incubation at room temperature of completely mixed sample and dye was performed prior to measurement of absorbance. A blank sample contained all diluents but with 0 µg of BSA.

2.12.2 **SDS-PAGE**

Denaturing SDS-PAGE was performed according to modified Laemmli's method (He, 2011). A resolving gel was prepared as follows:

SDS-PAGE 10% (w/v) resolving gel:

dH2O	4 mL
1.5 M Tris-HCl pH 8.8	2.5 mL
10% (w/v) SDS	100 µL
30% (w/v) acrylamide/bis (37.5:1)	3.5 mL
10% (w/v) APS	100 µL
TEMED	20 µL

The mixture was mixed and immediately loaded into the glass casting plates (1.0 mm Mini-Protean, Bio-Rad). 100% isopropanol was layered onto the mixture to isolate it from air and ensure a flat surface. Isopropanol was then removed and a stacking gel prepared as follows:

SDS-PAGE 4% (w/v) stacking gel:

dH2O	3.6 mL
0.5 M Tris-HCl pH 6.8	0.75 mL
10% (w/v) SDS	50 µL
30% (w/v) acrylamide/bis (37.5:1)	0.65 mL
10% (w/v) APS	50 µL
TEMED	20 µL

The mixture was loaded on the top of the resolving gel and a 15 well comb inserted. The gel was either stored for less than a week at 4˚C or used immediately in a Bio-Rad tank. Samples were mixed with SDS-PAGE loading buffer, incubated at 96˚C for 5 min in a hot block and then briefly spun down at 13000 x *g* at room temperature and loaded into the wells. Separation was performed at 110V till the dye front was seen to reach the base of the plate.

2.12.3 **Western blotting**

Following SDS-PAGE, the gel was equilibrated in blotting buffer for 10 min to allow for expansion of the gel. Electroblotting onto Hybond ECL 0.2 µm pore-size nitrocellulose membrane (GE Healthcare) via cooled wet transfer was performed at 170V for 90 min. Blocking was performed at room temperature with gentle tilting for an hour. The membrane was then rinsed 10 min in TBST three times, again at room temperature. Incubation with 1:40000 primary mouse antibody to β-actin (Abcam) was performed overnight with gentle tilting at 4˚C. The next day, further rinsing in TBST was performed at room temperature before 60 min incubation in 1:40000 secondary rabbit anti-mouse HRP-conjugated antibodies (Abcam) with

gentle tilting. Three 20 minute rinses with TBST was then performed to remove all residual antibodies to ensure a clean background before using the ECL Western Blotting Substrate (Thermo Fisher Scientific) as per manufacturer's instructions. Imaging was performed using the Biorad Chemidoc MP Imaging system with ImageLab Software version 5.2.1. Densitometry was performed on images using ImageJ.

2.13 **Zymogram**

50 ng of skin samples and 100 ng of intestinal samples were loaded into each zymogram well and a concurrent Western Blot (Section 2.12.3) performed for normalization allowing a semi-quantitative zymogram analysis. In both cases calibration of protein size was performed using Novex® Sharp Pre-stained Protein Standard (ThermoFisher, Loughborough, UK). Zymograms were performed using 1.0 mm Invitrogen gels (10% gelatine) run at 125V, renatured, developed overnight at 37˚C for 16 hours with gentle agitation on an orbital shaker at 50 rpm. After rinsing with ultrapure water three times, the gels were then stained using Coomassie blue stain. Imaging was performed using a Biorad Chemidoc MP Imaging system with ImageLab Software version 5.2.1, and quantified using image J for densitometry calculation. Gels were then dried using the Novex DryEase® Mini-Gel Drying System (Thermofisher, Loughborough, UK) as per manufacturer's protocol, for long term storage.

2.13.1 **Protein preparation for mass spectrometry**

Bands were excised from the stained zymogram gel using a sterile technique over a transilluminator to avoid exogenous peptide contamination. Gel bands were diced into small pieces to maximize surface area and were destained using 50% (MS grade) acetonitrile in 50 mM ammonium bicarbonate and incubated at room temperature overnight with vigorous shaking. Once visual inspection confirmed that gel pieces were completely destained, the supernatant was discarded and gel pieces were sequentially dehydrated using increasing concentrations of acetonitrile in 10 min incubations. The final dehydration step of 100% acetonitrile was repeated and gel pieces were visually inspected to be opaque indicating adequate dehydration. Reduction of the cysteine residues of protein within the gel pieces was performed by adding 200 µL of 50 mM Tris(2-carboxyethylphosphine) for 20 min at 70˚C. Samples were cooled and then alkylation of the reduced cysteine residues was performed by

adding 200 µL of freshly prepared 50 mM iodoacetamide and incubating in the dark at room temperature for 30 min. The gel pieces were then washed in 500 µL of 100 mM ammonium bicarbonate for 10 min at room temperature, and again dehydrated with incremental concentrations of acetonitrile. After the final repeat of incubation with 100% acetonitrile, the tubes were left open to allow full evaporation of all liquid for 10 min at room temperature. Digestion was then performed with 1 ng/µL trypsin (Promega) in 100 mM ammonium bicarbonate. The digestion was allowed to proceed for 14 h at 37˚C. The next day, digestion was stopped with 100% acetonitrile at 37˚C for 15 min. Peptides were then extracted by incubation at room temperature with 0.5% formic acid alternating with 100% acetonitrile. The supernatant containing the peptides were then transferred to a clean Eppendorf and stored at -20˚C prior to running on the mass spectrometer.

2.13.2 **Protein mass spectrometry**

Mass spectrometric measurements were conducted with a MS-MS machine (Thermo Fisher) with IonSpray Orbitrap. Mass spectrometric needle voltage was set at 3.5kV, cone voltage at 75V and temperature at 225˚C. All samples were detected with a mass range of 100 to 1000m/z. Analysis was performed using the MaxQuant software (Cox and Mann, 2008).

2.14 **Statistical analysis**

All experiments performed were blinded until analysis was complete and included three independent repeats unless otherwise stated. Statistical analysis was performed using GraphPad Prism 8.3.0®. Graphs were drawn with SD or SEM as indicated. Survival curves were drawn using the Kaplan-Meier method and analysed by the log-rank (Mantel-Cox) test. Contingency graphs were plotted for comparison between two outcomes and chi-squared tests used. An unpaired t-test was used for analysis of two groups, repeated-measures two-way ANOVA or one-way ANOVA with Bonferroni or Sidak's correction for multiple comparison was used for analysis of more than two groups. All data was checked for normality using the D' Agostino-Pearson Omnibus K2 normality test, and non-parametric comparisons performed with the Mann-Whitney test, or Kruskal-Wallis with Dunn's multiple comparison correction. Linear regression was used to analyse differences in slopes or intersections of time-lapse data if no obvious curve to the data could be fitted. If time lapse data could be fitted to a curve model such

as Logistic growth, or Beta Growth and Decline, then non-linear (Poisson) regression was used and Ymax (peak numbers) or K (slope of curve) compared. The same analysis, either linear or non-linear, was used for comparison within groups. A *p*-value of <0.05 was considered significant. *$p<0.05$, **$p<0.01$, ***$p<0.001$, ****$p<0.0001$.

Chapter 3: Specialised Pro-resolving Mediators (SPMs) in zebrafish models of inflammation

3.1 Introduction to SPMs and eicosanoids in zebrafish

Inflammation resolution is now widely accepted as an active process in which the timely production of specialised pro-resolving mediators (SPMs) such as lipoxins, resolvins and protectins play an important role (Serhan, 2017). SPMs are the end products of the co-ordinated action of cyclooxygenases and 5-, 12-, and 15-lipoxygenases (LOXs), working in sequence on three classes of fatty acids: arachidonic acid (AA), docosahexaenoic acid (DHA) and eicosapentaenoic acid (EPA). The bioavailability of these precursors is an important limiting factor in the production of various lipid mediators. In human studies, changing the availability of precursors affects subsequent inflammatory processes, and this represents an area of growing importance for the development of new treatments to modulate chronic inflammatory conditions, infective responses, and even cancer (Paschoal *et al.*, 2013; Piazzi *et al.*, 2014; Newell *et al.*, 2017). Studies in zebrafish have contributed to the investigation of the role of SPMs in some of these areas, such as that of Lipoxin A4 (LXA4) in supra-physiologic concentrations in tuberculosis (Tobin *et al.*, 2012). In part, the popularity of this model organism is because zebrafish possess a rapid reproductive cycle, allow live *in vivo* observation of cells by virtue of its optical transparency, and maintain an ease of genetic manipulation particularly at larval stages. But teleosts do differ from terrestrial animals, not least in their environment, but also in diet and tissue composition, which is higher in fatty acids such as DHA and EPA (Rainuzzo, Reitan and Jorgensen, 1992). Although many studies utilise zebrafish larvae prior to the feeding stage, this developmental phase is also characterised by its high lipid content, particularly of DHA and AA resulting from absorption of the yolk sac, the fatty acid composition of which, in turn, is affected by the diet of the parent female fish (Weigand, 1996). As such, due to precursor variability, it remains a possibility that as a result SPMs may have differing effects on the innate immune system, specific to this organism. Despite this, the working hypothesis was that SPMs would have similar effects to mammalian models, and that the zebrafish at this developmental stage would be able to demonstrate subtleties that would be missed in more complex models. To investigate this, the effect of inhibition of each LOX

enzyme (15-LOX, 5-LOX and 12-LOX) was tested. This was further investigated with exogenous treatment with Lipoxin A4 (LXA4), Resolvin E1 (RvE1) and Resolvin D2 (RvD2) as representatives of the end product of each precursor fatty acid and LOX enzyme. *In vitro* and rodent studies suggest that the biological roles of the many SPMs appear to have considerable overlap in modulating neutrophilic inflammation resolution and infection control (Campbell *et al.*, 2007; Dona *et al.*, 2008; Kurihara *et al.*, 2013; Chiang *et al.*, 2015; Herrera *et al.*, 2015), and zebrafish models of inflammation were used to investigate these in turn.

3.2 **Results**

3.2.1 **The standard neutrophil response to tailfin amputation**

To examine the impact of LOX inhibitors and their related SPMs on neutrophil response, the fluorescently-labelled neutrophil line, *TgBAC(mpx:GFP)i114* (Renshaw *et al.*, 2006) was used, and neutrophils quantified in the region of tailfin injury in live larvae. The inflammatory response curves of wounds depend heavily on the extent of injury, having a quicker time of resolution with less severe wounding models (Harvie and Huttenlocher, 2015). Therefore it was of considerable importance to determine the inflammatory response curve for the tailfin wounding model shown in Figure 2-4, to obtain the optimal times of capturing peak recruitment and adequate resolution for the experiments.

In untreated and injured fish, neutrophil counts peaked at 6hpi and returned to low levels from 12hpi onwards (Figure 3-1). From this, the optimal timing to detect a difference in the number of neutrophils recruited to a wound site was shown to be at 6hpi, and at 12hpi neutrophil numbers would be sufficiently low to reliably differentiate a delay in inflammation resolution. At 24hpi any substantial delay in inflammation resolution as a result of treatment could be adequately demonstrated.

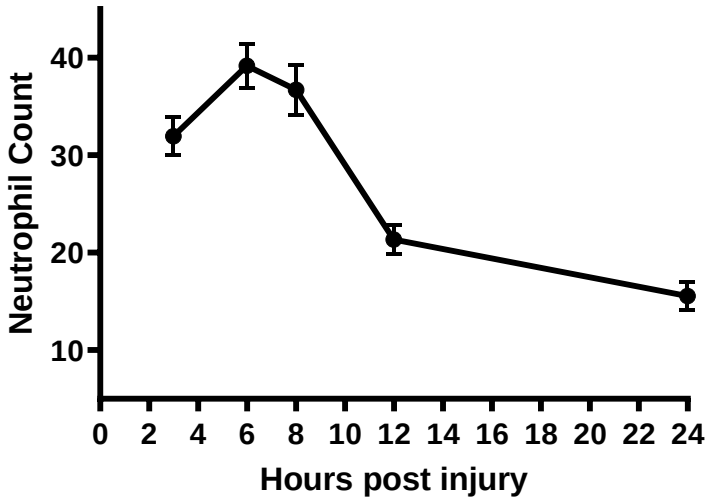

Figure 3-1: Time course of neutrophil response to tailfin transection. A 2dpf *TgBAC(mpx:GFP)i114* zebrafish underwent tailfin transection under sterile conditions. Fluorescent neutrophils were quantified in the region of injury using a Leica MZ10F epifluorescent stereomicroscope with live, anaesthetised but otherwise untreated zebrafish larvae at the corresponding times post-injury. Error bars show SEM, each point represents the average of N=17 in three independent repeats.

3.2.2 **Inhibition of 15-LOX delayed inflammation resolution both early and late in the inflammatory cycle**

Although the LOX enzymes have been identified in zebrafish, it is unknown whether the pathways are similar to humans. Inhibition of the LOX enzymes would be expected to delay inflammation resolution by reducing the production of the SPM end products. Using the *TgBAC(mpx:GFP)i114* line as above, with tailfin transection followed immediately, or at 5hpi, by intravascular (IV) administration of a 15-LOX inhibitor (PD146176), neutrophils were quantified at 24hpi to determine the overall effect on inflammation resolution. The treatment concentration of PD146176 (167 nM) was chosen based on the IC_{50} in rabbits of 540 nM (Bocan *et al.*, 1998) and also from dose response experiments performed as a preliminary step to these studies. As this was an intravascular systemic injection, final dosage estimated at the site of injury was calculated by dividing by 60 nL, the total blood volume in a 2dpf zebrafish larvae (Craig *et al.*, 2012). The vehicle control was DMSO, the diluent for PD146176. In zebrafish larvae, inhibiting 15-LOX after injury resulted in delayed inflammation resolution demonstrated by a persistently raised neutrophil count 24hpi. This was significant both when treatment was given immediately post-injury (Control mean +/- SEM: 14.24 +/- 0.90, PD146176: 18.21 +/- 1.07, p=0.061, t-test, Figure 3-2A) but also when given later in the inflammatory process, at 5hpi (Control mean +/- SEM: 12.67 +/- 0.54, PD146176: 16.22 +/- 0.69, p<0.0001, t-test, Figure 3-2B). This distinction is important since SPMs are thought to exert their effect early, within a few hours of inflammation initiation, in humans (Chiang and Serhan, 2017).

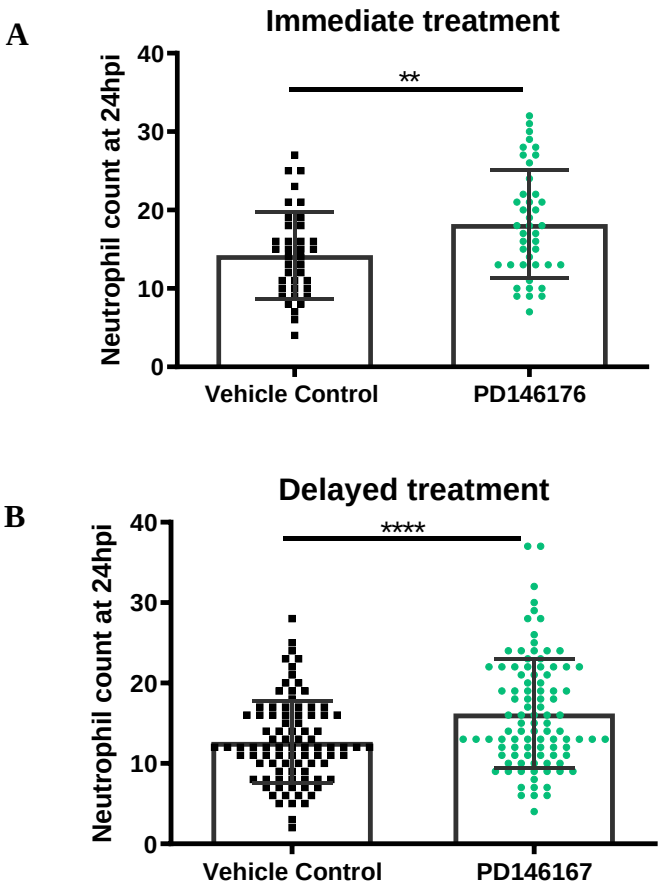

Figure 3-2: Neutrophil counts at the region of tailfin injury, following treatment with the 15-LOX inhibitor (PD146176) or vehicle control. A. Treatment was given immediately following injury and neutrophil counts in the ROI were performed at 24hpi. N=40/group in three independent repeats, comparison with t-test, $^{**}p<0.01$, error bars show SD. **B**. Treatment was given at 5hpi and neutrophil counts performed at 24hpi as before. N=90/group in six independent repeats (the number of repeats were increased due to the use of a new batch of drug), t-test, $^{****}p<0.0001$, error bars show SD.

3.2.3 **Inhibition of 5-LOX accelerated inflammation resolution when given late, but delayed inflammation resolution when given early**

5-LOX is thought to have a pro-inflammatory effect compared to the other LOX enzymes, in that over-expression of this LOX is thought to be harmful rather than helpful to inflammation resolution because of its concurrent ability to convert arachidonic acid to leukotrienes (Maier *et al.*, 2008; Guimarães *et al.*, 2018). However, in concert with other LOX enzymes, 5-LOX also plays a role in the production of SPMs, particularly the D- and E-series resolvins. A specific 5-LOX inhibitor, MK886, with an IC_{50} of 2.5 nM in human leukocytes (Datta, Biswal and Kehrer, 1999) was chosen, and a concentration close to this (16.7 nM), derived from preliminary dose response experiments, was used to investigate its effect in zebrafish larvae. The vehicle control was DMSO, the diluent for MK886. In zebrafish larvae, the response obtained was very much dependent upon the timing of treatment. When 5-LOX was inhibited immediately after injury, neutrophil numbers remaining at the wound site at 24hpi were increased (Control mean +/- SEM: 15.56 +/- 1.02, MK886: 20.51 +/- 1.20, p=0.0021, t-test, Figure 3-3A). However, the opposite was true when the 5-LOX inhibitor treatment was delayed until 5hpi, with neutrophil numbers at 24hpi now being significantly reduced (Control mean +/- SEM: 12.75 +/- 0.68, MK886: 10.14 +/- 0.66, p=0.0071, t-test, Figure 3-3B).

3.2.4 **Inhibition of 12-LOX did not affect inflammation resolution when given early, but delayed inflammation resolution when given late**

ML355 has been shown to be a specific 12-LOX inhibitor with an IC_{50} of 340 nM (Luci *et al.*, 2010). Used within this range at 167 nM, a concentration derived from preliminary dose response experiments, ML355 did not alter neutrophil counts at 24hpi when given immediately post-injury (Control mean +/- SEM: 12.10 +/- 0.83, ML355: 11.93 +/- 0.68, p=0.8746, t-test, Figure 3-4A). The vehicle control was DMSO, the diluent for ML355. However, when 12-LOX inhibition was performed at 5hpi, inflammation was prolonged (Control mean +/- SEM: 11.44 ++/- 0.77, ML355: 14.10 +/- 0.82, p=0.0209, t-test, Figure 3-4B).

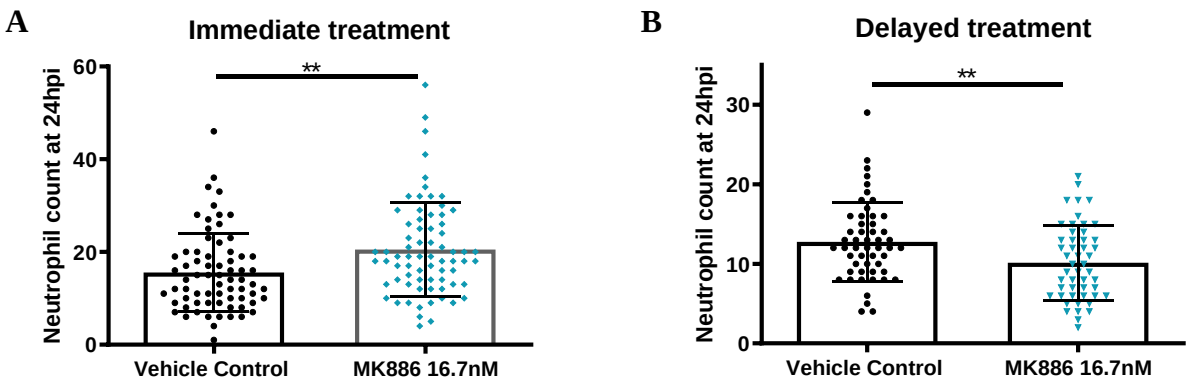

Figure 3-3: Neutrophil counts at the region of tailfin injury, following treatment with the 5-LOX inhibitor (MK886) or vehicle control. A. Treatment was given immediately post-injury and neutrophil counts at ROI performed at 24hpi. N=66/group in six independent repeats (repeats increased due to egg-laying problems limiting the number of larvae in each experiment), t-test, $**p<0.01$, error bars show SD. **B**. Treatment given 5hpi and neutrophil counts performed at 24hpi as before. N=68/group in six independent repeats (repeats increased for the same reason above), t-test, $**p<0.001$, error bars show SD.

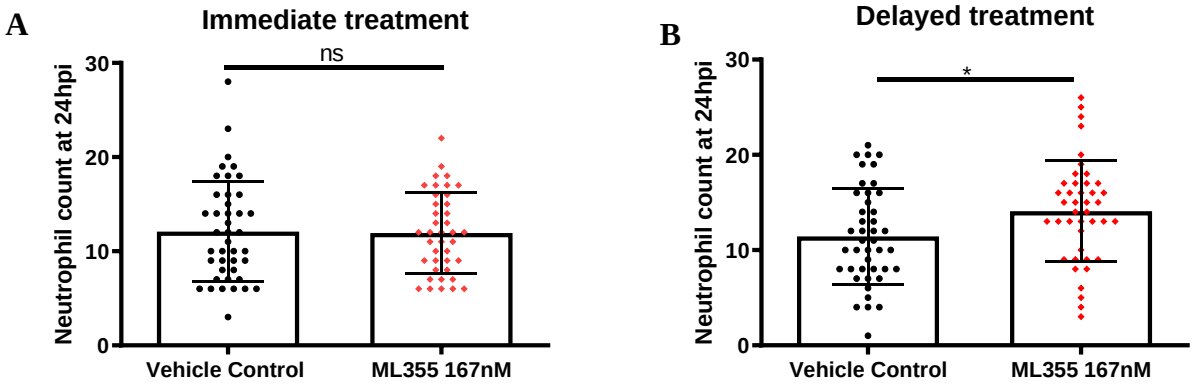

Figure 3-4: Neutrophil counts at the region of tailfin injury, following treatment with the 12-LOX inhibitor (ML355) or vehicle control. A. Treatment was given immediately post-injury and neutrophils quantified at 24hpi. N=42/group in three independent repeats, comparison with t-test, n=non-significant, error bars show SD. **B.** Treatment given 5hpi and neutrophil counts performed at 24hpi as before. N=42/group in three independent repeats, comparison with t-test, $*p<0.05$, error bars show SD.

3.2.5 **LXA4 and RvE1, but not RvD2, accelerated neutrophilic resolution in tailfin transection**

The LOX enzymes modulate more than just SPM production, they often work in concert with each other, and even have a direct role in apoptosis and ferroptosis (Li *et al.*, 2018). Therefore, to increase experimental specificity and simplify interpretation, a single end product of each LOX pathway was used. For 15-LOX, Lipoxin A4 (LXA4) was used; for 5-LOX, Resolvin E1 (RvE1); and for 12-LOX, Resolvin D2 (RvD2). Earlier time points were also used to allow separate conclusions to be drawn regarding the effects of each SPM firstly on neutrophil recruitment (quantification at 6hpi), and then on inflammation resolution (quantification at 12hpi). Counts at 24hpi were not used because SPMs are lipids that are easily oxidised, and previously shown to be rapidly and actively inactivated in mammals (Arita *et al.*, 2006) so its effects could be missed with delayed quantification. Using *TgBAC(mpx:GFP)i114* larvae with supplementation of 167 nM of LXA4 immediately following tailfin injury, neutrophil numbers were significantly reduced both at 6hpi (Control mean +/- SEM: 24.48 +/- 0.69, LXA4: 21.69 +/- 0.74, p=0.0063, t-test, Figure 3-5A) and also at 12hpi (Control mean +/- SEM: 21.57 +/- 0.80, LXA4: 18.21 +/- 0.74, p=0.0023, t-test, Figure 3-5B), in accordance with mammalian studies (Campbell *et al.*, 2007; Buckley, Gilroy and Serhan, 2014). In contrast, immediate treatment with RvD2 at 16nM increased recruited neutrophil numbers at 6hpi (Control mean +/- SEM: 25.60 +/- 1.18, RvD2: 30.49 +/- 1.10, p=0.0033, t-test, Figure 3-5C), but by 12hpi this difference was lost and overall inflammation resolution was not delayed (Control mean +/- SEM: 14.61 +/- 0.81, RvD2: 15.30 +/- 0.77, p=0.5384, Figure 3-5D). Immediate treatment with RvE1 (167 nM) did not affect neutrophil numbers at 6hpi (Control mean +/- SEM: 22.33 +/- 0.91, RvE1: 21.25 +/- 0.90, p=0.4502, t-test, Figure 3-5E), but significantly reduced numbers at 12hpi (Control mean +/- SEM: 19.11 +/- 1.02, RvE1: 14.79 +/- 0.84, p=0.0015, Figure 3-5F). SPMs are thought to be agents of inflammation resolution, and in effort to isolate the effect of SPMs solely on the resolution phase, treatment was given at 5.5hpi to minimise the effects, if any, on neutrophil recruitment. Surprisingly, none of the three SPMs, LXA4 (Control mean +/- SEM: 16.06 +/- .074, LXA4: 15.61 +/- 0.72, p=0.6664, t-test, Figure 3-6A), RvD2 (Control mean +/- SEM: 15.32 +/- 0.88, RvD2: 16.93 +/- 1.05, p=0.2425, Figure 3-6B) nor RvE1 (Control mean +/- SEM: 17.40 +/- 0.99, RvE1: 16.20 +/- 1.15, p=0.4289, Figure 3-6C) administered at or after 5.5hpi exerted any significant effect on inflammation resolution.

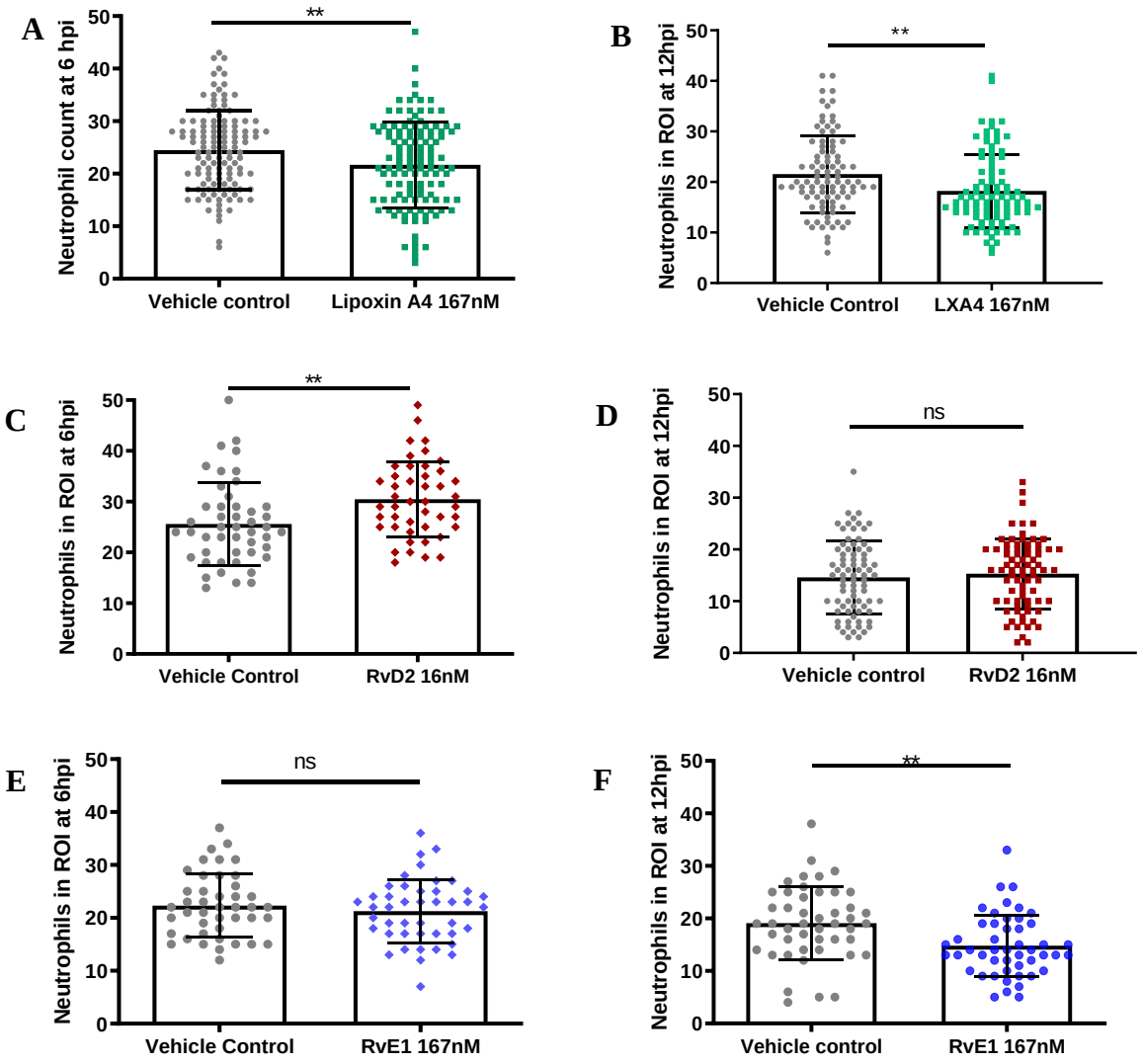

Figure 3-5: Neutrophil counts at the site of tailfin injury, following treatment with SPM (LXA4, RvD2, or RvE1) or vehicle control. 2dpf *TgBAC(mpx:GFP)*i114 underwent tailfin injury and immediate treatment, with neutrophils in the ROI quantified at either 6hpi or 12 hpi. **A.** Neutrophils quantified at 6hpi with LXA4 167 nM. N=120/group in six independent repeats. **B.** Neutrophils quantified at 12hpi with LXA4 167 nM. N=120/group in six independent repeats. **C.** Neutrophils quantified at 6hpi with RvD2 16 nM. N=45/group in three independent repeats. **D.** Neutrophils quantified at 12hpi with RvD2 16 nM. N=90/group in four independent repeats. **E.** Neutrophils quantified at 6hpi with RvE1 167 nM. N=45/group in three independent repeats. **F.** Neutrophils quantified at 12hpi with RvE1 167 nM. N=45/group in three independent repeats. In all graphs error bars show SD, comparison with t-test, ns=non-significant, $**p<0.01$.

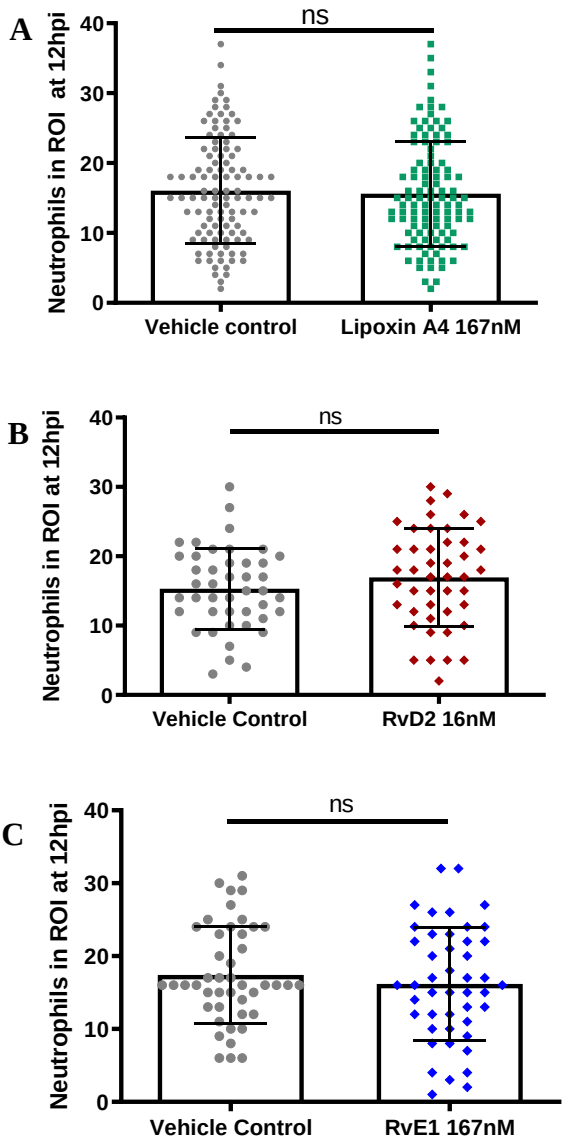

Figure 3-6: Neutrophil counts at 12hpi the site of tailfin injury, following delayed treatment (5.5hpi) with SPM (LXA4, RvD2, or RvE1) or vehicle control. 2dpf *TgBAC(mpx:GFP)*i114 underwent tailfin injury and delayed treatment, and neutrophils in the ROI quantified at 12 hpi. **A.** LXA4 167 nM. N=120/group in six independent repeats. **B**. RvD2 16 nM. N=45/group in three independent repeats. **C**. RvE1 167 nM. N=45/group in three independent repeats. In each graph: comparison with t-test, error bars show SD, ns=non-significant.

3.2.6 **Only LXA4, and not RvD2 or RvE1, increased neutrophil apoptosis at 3 hours post treatment, but not at 6, 9 or 12 hours post treatment**

Neutrophils are removed from sites of inflammation by apoptosis and subsequent efferocytosis by macrophages (El Kebir and Filep, 2010) or by reverse migration away from the site of injury (J. Wang *et al.*, 2017). To investigate if neutrophil apoptosis was increased by SPM treatment, TUNEL staining was performed at 3, 6, 9 and 12 hours post treatment. These times were chosen to optimise the possibility of detecting differences in rates of apoptosis that could contribute to the differences in neutrophil numbers. When LXA4 was given immediately post-injury and quantification performed at 3 hours post treatment an increase in neutrophil apoptosis was demonstrated (Control mean +/- SEM: 0.81% +/- 0.16. LXA4: 1.48% +/- 0.24, p=0.0342, Mann-Whitney test, Figure 3-7A), but no significant different in apoptosis was shown at 6 hours post treatment (Control mean +/- SEM: 2.18% +/- 0.27, LXA4: 1.91% +/- 0.23, p=0.5109, Figure 3-7D), 9 hours post treatment (Control mean +/- SEM: 0.98% +/- 0.25, p=0.9548, Figure 3-7G), or 12 hours post treatment (Control mean +/- SEM: 1.48% +/- 0.29, LXA4: 1.06% +/- 0.23, p=0.1732, Figure 3-7J). Similarly, when RvD2 was given immediately after injury, no significant differences in neutrophil apoptosis was seen at 3 hours post treatment (Control mean +/- SEM: 0.44% +/- 0.12, RvD2: 0.29% +/- 0.15, p=0.0941, Mann-Whitney test, Figure 3-7B), 6 hours post treatment (Control mean +/- SEM: 0.33% +/- 0.13, RvD2: 0.40% +/- 0.12, p=0.4092, Figure 3-7E), 9 hours post treatment (Control mean +/- SEM: 0.52% +/- 0.14, RvD2: 0.57% +/- 0.15, p=0.9097, Figure 3-7H) or 12 hours post treatment (Control mean +/- SEM: 0.73% +/- 0.19, RvD2: 0.57% +/- 0.15, p=0.9553, Figure 3-7K). For RvE1, as treatment effect was noted to be later at 12hpi, analysis of apoptosis was performed each time at 9hpi and 12hpi, with later treatment times in order to keep the intervals between treatment and analysis comparable to the other SPMs. Three hours post RvE1 treatment, no differences in neutrophil apoptosis was demonstrated (Control mean +/- SEM: 0.65% +/- 0.20, RvE1: 0.52% +/- 0.18, p=0.1615, Mann-Whitney test, Figure 3-7C), and this remained the case at 6 hours post treatment (Control mean +/- SEM: 0.56% +/- 0.22, RvE1: 0.72% +/- 0.23, p=0.8796, Figure 3-7F). As with the other SPMs, no differences in percentage apoptosis was demonstrated at either 9 hours post treatment with RvE1 (Control mean +/- SEM: 0.60% +/- 0.22, RvE1: 1.15% +/- 0.38, p=0.5219, Figure 3-7I) or at 12 hours post treatment (Control mean +/- SEM: 0.88% +/- 0.31, RvE1: 0.79% +/- 0.22, p=0.3939, Figure 3-7L).

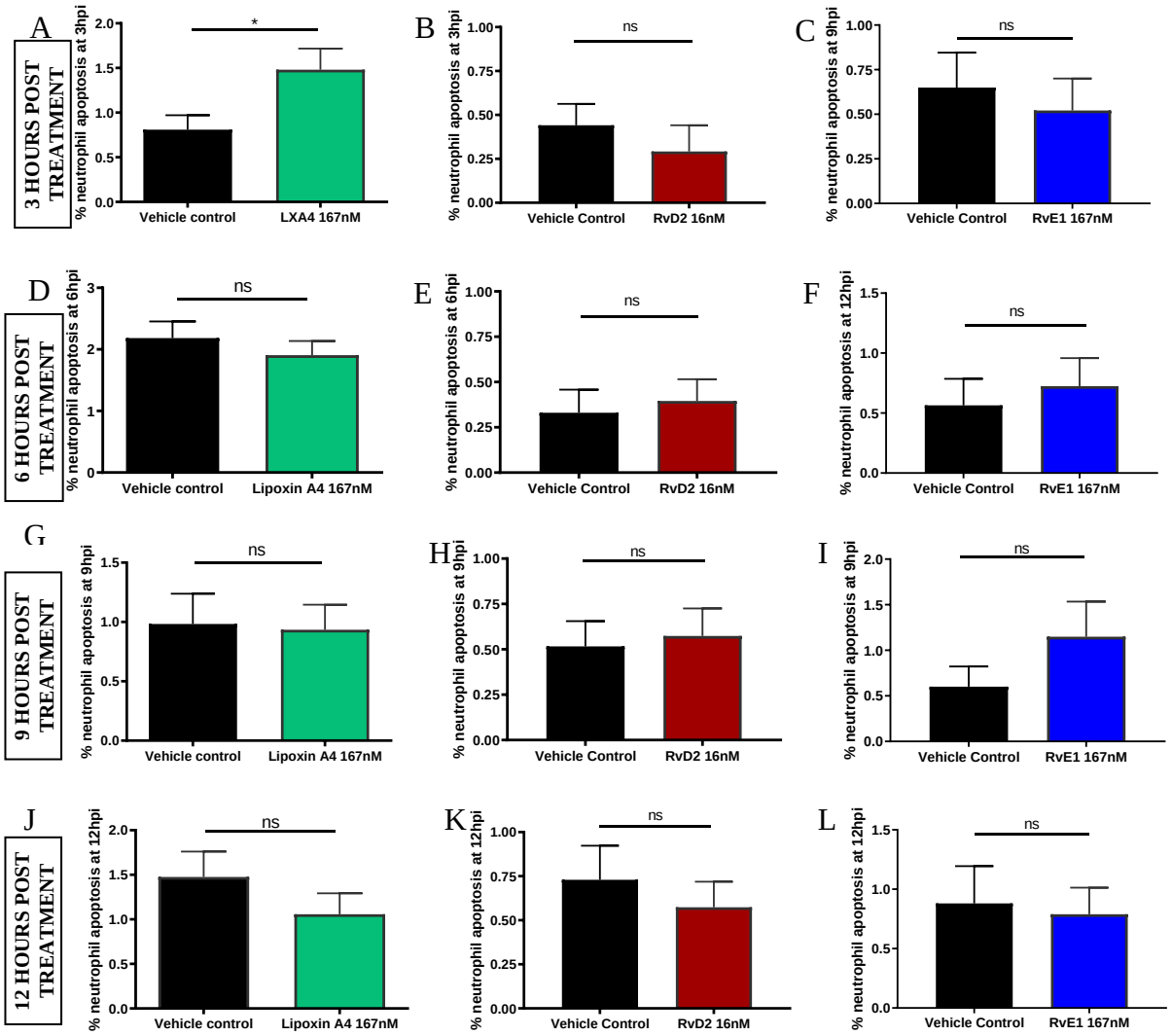

Figure 3-7: TSA/TUNEL staining performed at 3, 6, 9 and 12 hours post treatment with SPM or vehicle control. **A**. Immediate treatment with LXA4 or vehicle control and analysis at 3hpi. **B**. Immediate treatment with RvD2 and analysis at 3hpi. **C**. Treatment with RvE1 at 5hpi followed by analysis 3 hours post-treatment. **D**. Immediate treatment with LXA4 or vehicle control and analysis at 6hpi. **E**. Immediate treatment with RvD2 and analysis at 6hpi. **F**. Treatment with RvE1 at 5hpi followed by analysis 6 hours post-treatment. **G**. Immediate treatment with LXA4 and analysis at 9hpi. **H**. Immediate treatment with RvD2 and analysis at 9hpi. **I**. Immediate treatment with RvE1 and analysis at 9hpi. **J.** Immediate treatment with LXA4 and analysis at 12hpi. **K**. Immediate treatment with RvD2 and analysis at 12hpi. **L**. Immediate treatment with RvE1 and analysis at 12hpi. In all graphs % apoptosis calculated in each larvae by taking the average ratio of apoptotic neutrophils to the total number of neutrophils in the ROI, error bars show SEM, comparison with Mann-Whitney test, ns=non-significant, *p<0.05, N=120/group in two independent repeats.

3.2.7 **Histochemical quantification of neutrophils matched live trends**

The biochemical method of TSA staining, as part of the TUNEL staining, allowed confirmation of the reproducibility of the live *in vivo* neutrophil quantification obtained initially. Using this method confirmed that neither LXA4 (Control mean +/- SEM: 26.70 +/- 0.85, LXA4: 27.65 +/- 0.88, p=0.4342, t-test, Figure 3-8A) nor RvE1 treatment (Control mean +/- SEM: 20.64 +/- 1.02, RvE1: 19.56 +/- 0.85, p=0.4178, t-test, Figure 3-8C) showed any differences in neutrophil numbers at 3 hours post-treatment, but RvD2 showed a significant increase in neutrophil numbers at 3hpi (Control mean +/- SEM: 22.22 +/- 0.66, RvD2: 25.12 +/- 0.66, p=0.0021, t-test, Figure 3-8B). At 6 hours post-treatment, both LXA4 (Control mean +/- SEM: 34.92 +/- 0.96, LXA4: 31.02 +/- 0.91, p=0.0036, Figure 3-8D) and RvE1 (Control mean +/- SEM: 17.37 +/- 0.81, RvE1: 15.09 +/- 0.68, p=0.0324, Figure 3-8F) showed significant decreases in neutrophil numbers, while RvD2 (Control mean +/- SEM: 22.54 +/- 0.73, RvD2: 24.63 +/- 0.76, p=0.0485, Figure 3-8E) showed a continued increase in neutrophil numbers, matching live quantification. At 9 hours post treatment, none of the SPMs, LXA4 (Control mean +/- SEM: 23.19 +/- 0.89, LXA4: 22.95 +/- 0.72, p=0.8305, Figure 3-8G), RvD2 (Control mean +/- SEM: 24.23 +/- 0.90, RvD2: 25.28 +/- 0.82, p=0.3864, Figure 3-8H) or RvE1 (Control mean +/- SEM: 19.19 +/- 0.77, RvE1: 17.46 +/- 0.69, p=0.0951, Figure 3-8I), showed any differences in neutrophil numbers. And finally, at 12hpi, only RvE1 (Control mean +/- SEM: 13.70 +/- 0.52, RvE1: 10.82 +/- 0.41, p<0.0001, Figure 3-8L), but not LX4 (Control mean +/- SEM: 18.73 +/- 0.77, LXA4: 18.88 +/- 0.91, p=0.8977, Figure 3-8J) or RvD2 (Control mean +/- SEM: 22.70 +/- 0.68, RvD2: 23.80 +/- 0.75, p=0.2802, Figure 3-8K) reduced neutrophil numbers, again matching live quantification trends.

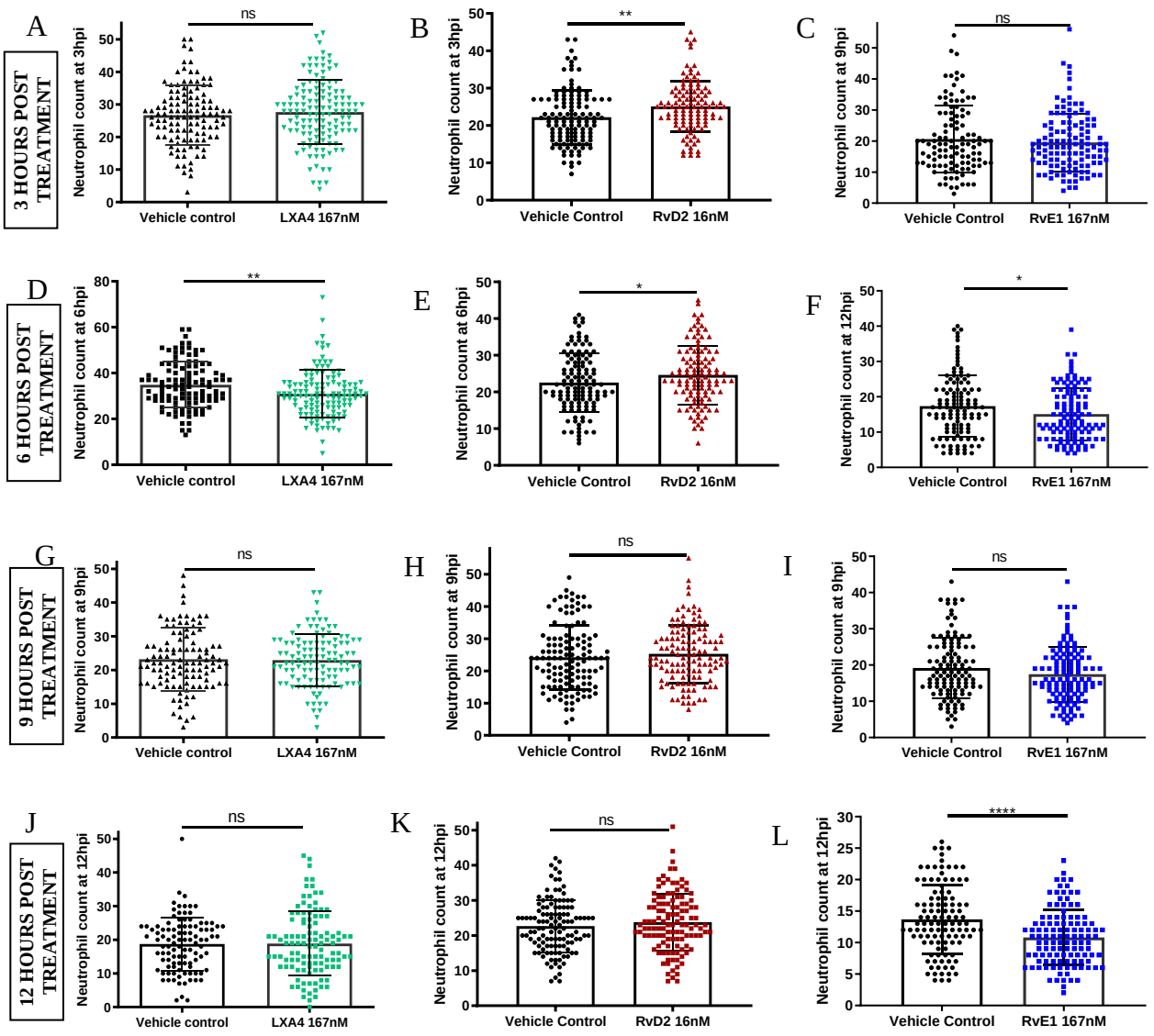

Figure 3-8: Biochemical neutrophil quantification with TSA in the region of tailfin injury. 2dpf wildtype (nacre) zebrafish larvae were fixed in PFA at each time point of analysis post-injury. **A**. Immediate LXA4 treatment with quantification 3 hpi. **B**. Immediate RvD2 treatment with quantification 3 hpi. **C.** RvE1 treatment was delayed to 5hpi (to keep the treatment interval) with quantification 3 hours later. **D.** Immediate LXA4 treatment with quantification 6hpi. **E**. Immediate RvD2 treatment with quantification 6hpi. **F**. RvE1 treatment at 5hpi with neutrophil quantification 6 hours later. **G**. Immediate LXA4 treatment with quantification 9hpi. **H**. Immediate RvD2 treatment with quantification 9hpi. **I.** Immediate RvE1 treatment with quantification 9hpi. **J.** Immediate LXA4 treatment with quantification 12hpi. **K**. Immediate RvD2 treatment with quantification 12hpi. L. Immediate RvE1 treatment with quantification 12hpi. For each: comparison with t-test, ns=non-significant, *p<0.05, **p<0.001, ****p<0.0001, error bars show SD, N=120/group in two independent repeats.

3.2.8 **All three SPMs increased reverse migration of neutrophils in different ways**

To investigate the effect of each SPM on reverse migration profile, tracked photo-converted neutrophils in the *TgBAC(mpx:GAL4-VP16)sh267;Tg(UAS:Kaede)i222* zebrafish line was used as previously described (Dixon *et al.*, 2012). The number of neutrophils reverse migrating at any one time point was plotted and the slopes of the curves compared using linear regression to give the rate of neutrophil reverse migration over time from 6hpi to 12hpi. The rate was decreased in LXA4 (p=0.0074, linear regression, Figure 3-9A), but the overall numbers of reverse migrating neutrophils at all times were consistently higher with LXA4 even though this did not reach significance (Overall control mean +/- SEM: 7.12 +/- 0.17, LXA4: 8.31 +/- 0.15, p=0.1771, multiple-measures two-way ANOVA). This is likely due to initiation of reverse migration earlier such that the acceleration phase was not captured during the time of imaging, and this would fit with the earlier findings of decreased neutrophils at 6hpi. Treatment with RvD2 increased the rate of reverse migration significantly (p<0.0001, linear regression, Figure 3-9B) and overall numbers reverse migrating were similar (Overall control mean +/- SEM: 6.47 +/- 0.10, RvD2: 5.40 +/- 0.17, p=0.3026, multiple-measures two-way ANOVA). Given the earlier findings of increased neutrophils at 6hpi but no overall delay in inflammation resolution at 12hpi, this could indicate a delayed initiation of reverse migration. Treatment with RvE1 unequivocally increased the rate of neutrophils reverse migrating (p=0.0009, linear regression, Figure 3-9C). It is likely the timing of imaging ideally captured the height of the effect of RvE1. None of the SPMs, LXA4 (Control mean +/- SEM: 0.039 +/- 0.001, LXA4: 0.040 +/- 0.001, p=0.3655, t-test, Figure 3-10A), RvD2 (Control mean +/- SEM: 0.031 +/- 0.001, RvD2: 0.030 +/- 0.002, p=0.6037, t-test), or RvE1 (Control mean +/- SEM: 0.040 +/- 0.001, RvE1: 0.041 +/- 0.001, p=0.2442, t-test) influenced the speed of reverse migrating neutrophils. Path length of reverse migrating neutrophils was also unchanged by LXA4 (Control mean +/- SEM: 180.7 +/- 4.12, LXA4: 181.5 +/- 4.53, p=0.8899, t-test, Figure 3-10B) and RvD2 (Control mean +/- SEM: 128.8 +/- 5.43, RvD2: 122.2 +/- 7.38, p=0.4761, t-test), but was increased with RvE1 (Control mean +/- SEM: 171.2 +/- 2.39, RvE1: 179.5 +/- 3.10, p=0.0371, t-test). Directness of neutrophil movement was increased by both LXA4 (Control mean +/- SEM: 0.287 +/- 0.004, LXA4: 0.299 +/- 0.003, p=0.0353, t-test, Figure 3-10C) and RvD2 (Control mean +/- SEM: 0.304 +/- 0.019, RvD2: 0.356 +/- 0.015, p=0.0353, t-test), but not RvE1 (Control mean +/- SEM: 0.278 +/- 0.004, RvE1: 0.275 +/- 0.004, p=0.6590, t-test).

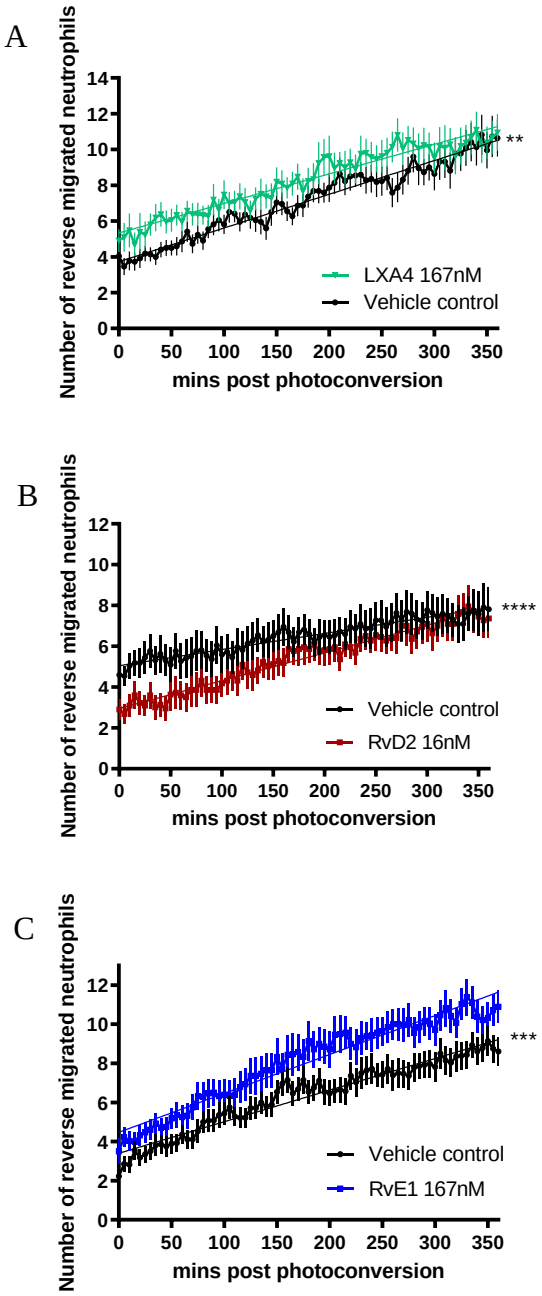

Figure 3-9: Number of reverse migrating neutrophils over time at the region of tailfin injury. Neutrophils at the injury site of 2dpf *TgBAC(mpx:GAL4-VP16)sh267;Tg(UAS:Kaede)i222* zebrafish larvae were photo converted at 5hpi and then tracked for 6 h using Yokagawa CXU spinning disk and Volocity®(Perkin Elmer) software. A. Treatment with LXA4 or vehicle control. B. Treatment with RvD2 or vehicle control. C. Treatment with RvE1 or vehicle control. For each graph: Linear regression to compare slopes of curves, error bars show SEM, $^{**}p<0.01$, $^{***}p<0.001$, $^{****}p<0.0001$, each point represents the average of N=18/ group in three independent repeats.

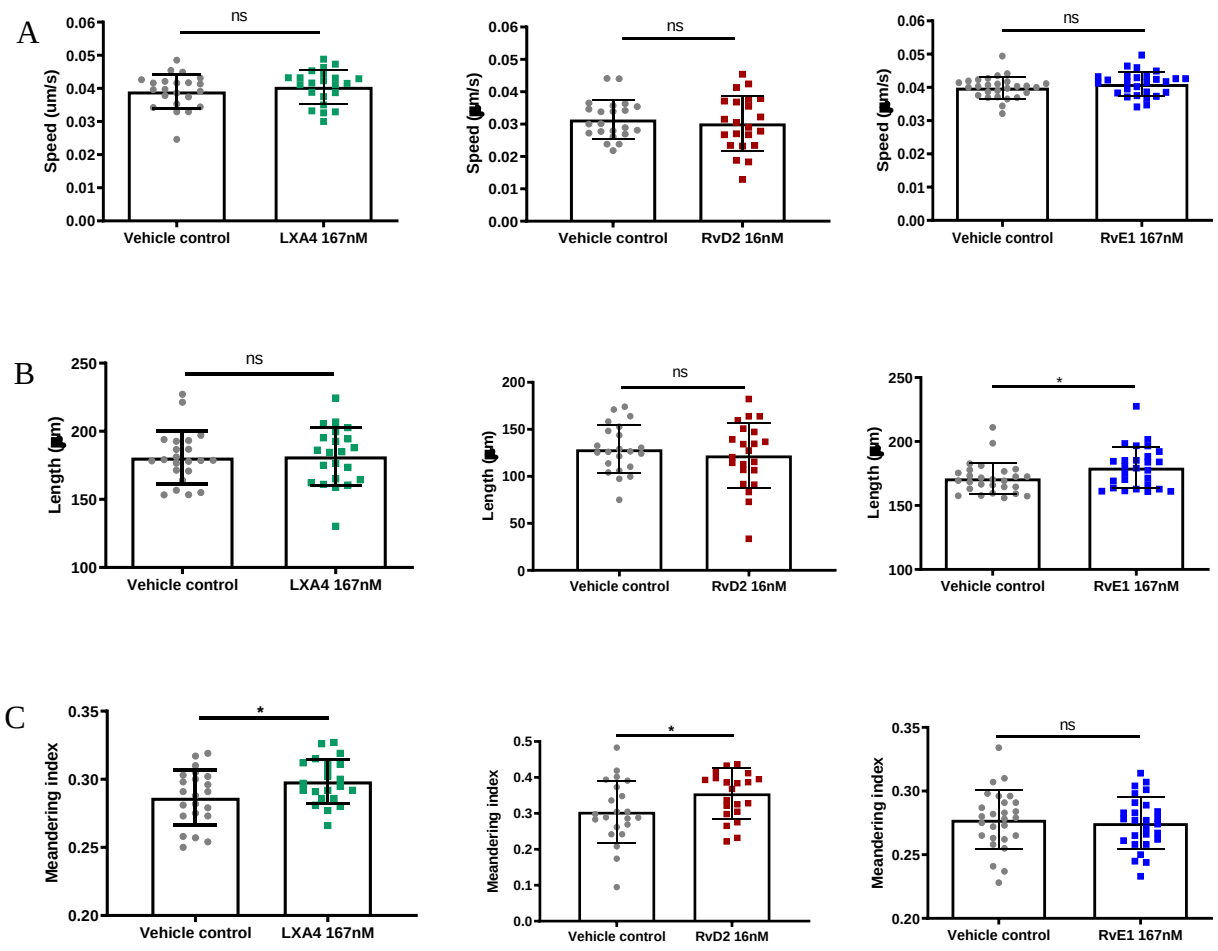

Figure 3-10: Movement characteristics of reverse migrated neutrophils in the presence of SPMs. Analysis was performed using Perkin Elmer Volocity® 6.3 on data obtained tracking photo converted reverse migrating neutrophils of *TgBAC(mpx:GAL4-VP16)sh267;Tg(UAS:Kaede)i222* zebrafish larvae. Comparison between the treatment vehicle control and the SPMs (LXA4, RvD2, and RvE1) were made for the following parameters of movement of reverse migrated neutrophils: **A**. Speed, **B**. Path length, and **C**. Meandering index (or directness of travel) where a number closer to 1 indicates a straighter path. In each graph, comparison was performed with a t-test, ns=non-significant, *$p<0.05$, error bars show SD, N=18/group in three independent repeats.

3.2.9 **LXA4 and RvE1, but not RvD2, increased NFκB reporter expression in tailfin injury**

NFκB has been previously shown to be central to the co-ordination of inflammatory pathways and is increased in certain inflammatory conditions (Baldwin, Hill and Carolina, 1996), with inhibition of NFκB accelerating neutrophil apoptosis (Castro-alcaraz *et al.*, 2018). However, its expression later in an inflammatory process can also enhance inflammation resolution (Kusano and Ferrari, 2015). Using the fluorescently labelled *Tg(6xHsa.NFKB:eGFP)sh235* reporter line (Kanther *et al.*, 2011) expression of NFκB, as demonstrated by the intensity of GFP, was monitored for twelve hours following tailfin injury, with or without SPM treatment. Although RvD2 (p=0.3308, linear regression, Figure 3-11B) did not alter NFκB reporter expression in this timeframe, both LXA4 (p=0.0013, linear regression, Figure 3-11A) and RvE1 (p<0.0001, linear regression, Figure 3-11C) induced an increase in reporter expression with curves diverging after approximately 5hpi.

3.2.10 **RvE1, but not LXA4 or RvD2, increased the rate of tailfin regeneration**

In addition to its well-documented inflammatory role, NFκB has been shown to play a role in regeneration in liver cells in rats (Zhao *et al.*, 2016), and cardiac (Karra *et al.*, 2015) and neural tissues in zebrafish (Kyritsis *et al.*, 2012). Increased expression of NFκB, together with the accelerated resolution of inflammation, could result in accelerated regeneration of the injured tailfin. To test this, 2dpf wildtype zebrafish were injured and percentage increase in length of the amputated tailfin calculated after 24 hours. Both LXA4 (Control mean +/- SEM: 25.32% +/- 2.84, LXA4: 24.26% +/- 2.23, p=0.7686, t-test, Figure 3-12A) and RvD2 treatment (Control mean +/- SEM: 43.25% +/- 5.11, RvD2: 33.96% +/- 3.55, p=0.1402, t-test, Figure 3-12B) did not enhance tailfin regrowth, but treatment with RvE1 significantly increased tailfin regeneration (Control mean +/- SEM: 15.77% +/- 3.54, RvE1: 31.10% +/- 3.30, p=0.0021, t-test, Figure 3-12C).

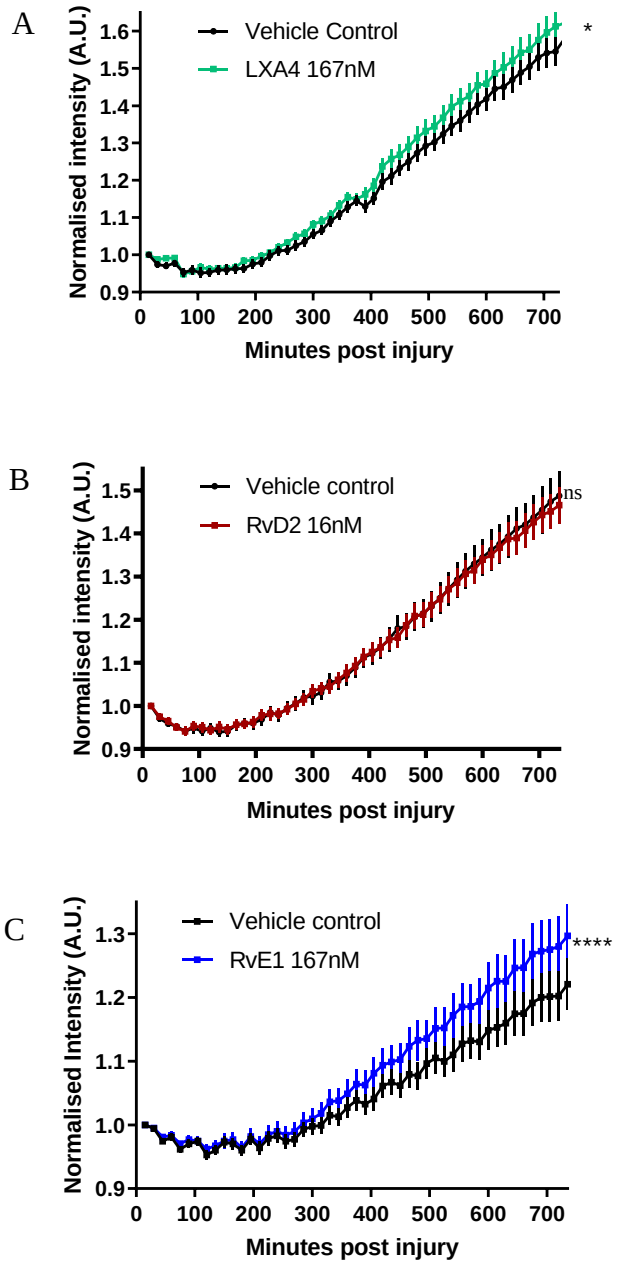

Figure 3-11: Expression of NFκB in the region of injury in tailfin transection with SPM treatment. With each SPM or vehicle control, treatment was given immediately following tailfin injury of 2dpf *Tg(6xHsa.NFκB:eGFP)sh235* and larvae embedded directly with 0.8%agarose and imaged on a Nikon Eclipse TE2000-U microscope without delay. GFP fluorescence was quantified and images analysed with NIS Elements AR® software by normalising to the first intensity after background subtraction. **A**. Treatment with LXA4 or vehicle control. **B.** Treatment with RvD2 or vehicle control. **C.** Treatment with RvE1 or vehicle control. For each graph: slope comparison with linear regression, ns=non-significant, *p<0.05, ****p<0.0001, error bars show SEM, N=21/group in three independent repeats.

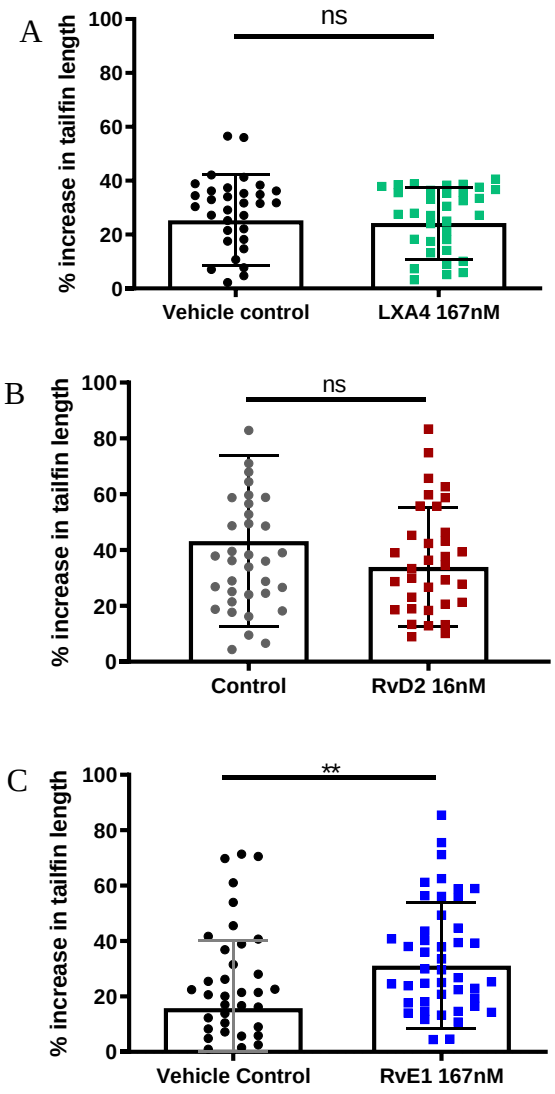

Figure 3-12: Tailfin regeneration with SPM treatment. Tailfin amputation was performed and an initial image obtained using a Nikon Eclipse TE2000-U microscope after an hour recovery to minimise errors from the normal initial wound shrinkage immediately post-injury. A second image was then obtained 24hpi. Measurements were made, blinded to treatment groups, from the end of circulation to the cut edge and the % increase in tailfin length calculated. **A**. Immediate treatment with LXA4. N=36/group in three independent repeats **B.** Immediate treatment with RvD2. N=36/group in three independent repeats **C.** Immediate treatment with RvE1. N=45/group in three independent repeats. In each graph:: comparison with t-test, ns=non-significant, $**p<0.01$.

3.2.11 **LXA4 and RvD2 increased macrophage numbers and RvE1 accelerated arrival of macrophages in tailfin injury**

Wound healing and regeneration depends on a more complex interplay between other cells of the innate response, such as macrophages, whose influx follows neutrophils in classical models of inflammation. All SPMs were shown earlier to increase neutrophil reverse migration, and this, together with the overall low level of neutrophil apoptosis seen is in concordance with published data suggesting that, in zebrafish, majority of neutrophils leave a sterile injury by reverse migration (de Oliveira, Rosowski and Huttenlocher, 2016). But neutrophil reverse migration has been shown to be dependent on macrophages in zebrafish (Tauzin *et al.*, 2014), therefore it was hypothesised that SPMs would increase macrophage numbers attending to an injury. To investigate this, the original tailfin transection model was used with a fluorescently-labelled macrophage line, *Tg(mpeg1:NLS-Clover)sh436*. Following tailfin injury with treatment at 0hpi, macrophage numbers were significantly increased in LXA4 (Control Ymax: 33.94, LXA4: 39.05, logistic growth model, $p<0.0001$, Poisson regression, Figure 3-13A) and RvD2 (Control Ymax: 20.38, RvD2: 24.14, logistic growth model, $p<0.0001$, Poisson regression, Figure 3-13B). For RvE1, the macrophage numbers were not increased but the curves diverged early with an accelerated arrival of macrophages in RvE1compared with controls (Control Ymax: 30.04, RvE1: 28.24, logistic growth model; Control curve slope: 0.0468, RvE1: 0.0917, $p<0.0001$, segmental regression slope comparison, Figure 3-13C). Specific characteristics of macrophage movement such as speed, path length, or directness of travel could not be assessed due to unavailability of tracking software with NIS Elements AR at the time of analysis.

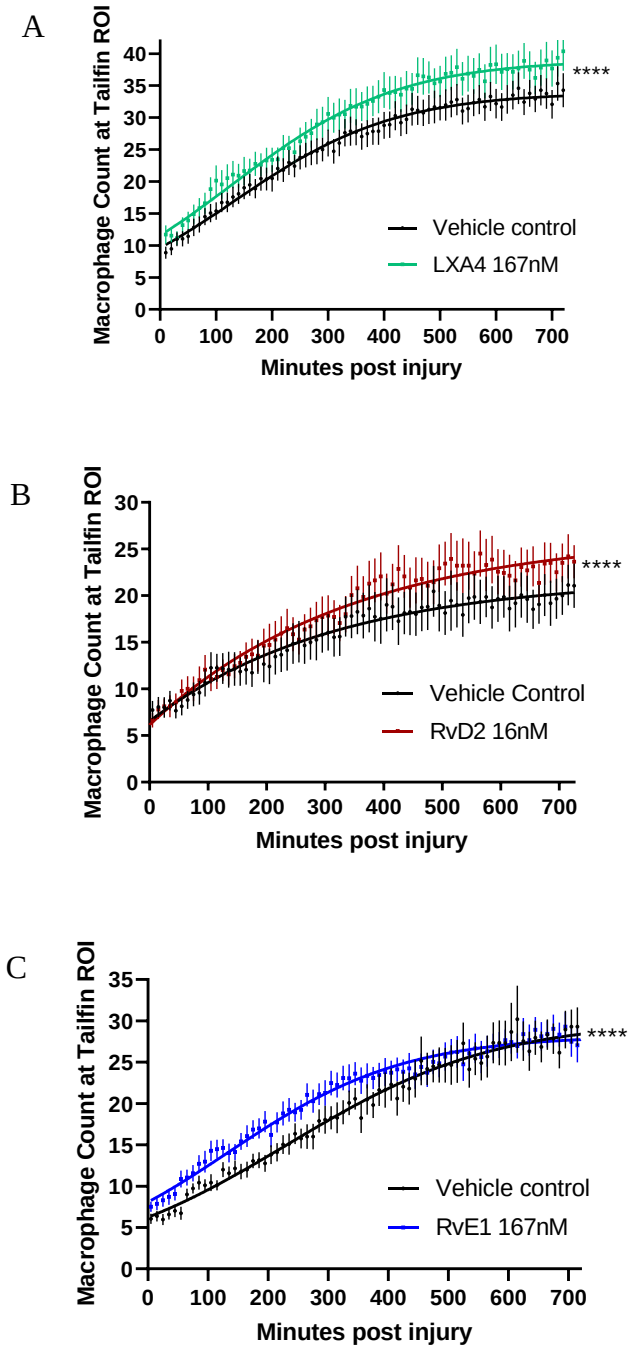

Figure 3-13: Macrophage counts at tailfin ROI in 2dpf *Tg(mpeg1:NLS-Clover)sh436*. Immediate treatment with SPM or vehicle control was performed following tailfin injury and larvae imaged over 12hpi on a Nikon Eclipse TE2000-U microscope interfaced with NIS Elements AR. **A.** LXA4 treatment or vehicle control. **B.** RvD2 treatment or vehicle control. **C.** RvE1 treatment or vehicle control. In all graphs: logistic growth curves fitted, comparison of curves performed with Poisson regression, ****$p<0.0001$, error bars show SEM, N=18/group in three independent repeats**.**

3.2.12 **LXA4, but not RvD2 or RvE1, improved survival in systemic *Staphylococcus aureus* infection**

An uncontrolled inflammatory response is an important cause of multi-organ failure and death in sepsis (Aziz *et al.*, 2013), and RvD2 has previously been shown to mitigate this response in mice (Chiang *et al.*, 2017), but thus far, this SPM effect has not yet been investigated in zebrafish. *S. aureus* is an ubiquitous commensal as well as pathogen in humans and many other species (Torraca *et al.*, 2014; Kernbauer *et al.*, 2015), and therefore was chosen as a suitable bacterium for initial investigation. An infection model has been described in zebrafish larvae, but larvae at 30hpf were used (Prajsnar *et al.*, 2008). At this stage of development, neutrophils are not sufficiently matured (Le Guyader *et al.*, 2008a) and therefore this younger age would not have been suitable to determine if the neutrophilic effects, seen here in earlier experiments, would exert differential results. Therefore, slightly older larvae (2dpf) were used and infected intravenously with 5000CFU of SH1000. This induced 50% mortality in untreated, infected zebrafish larvae, and showed that SPMs treatment in zebrafish resulted in different effects on survival. Treatment with LXA4 increased survival in *S. aureus* bacteraemia (p=0.0145, Mantel-Cox, Figure 3-14A), but RvD2 (p=0.9778, Mantel-Cox, Figure 3-14B) and RvE1 (p=0.9677, Mantel-Cox, Figure 3-14C) did not affect survival.

3.2.13 **RvD2 and RvE1, but not LXA4, increased survival in systemic *Enterococcus faecalis* infection**

Although *S. aureus* is commonly found on superficial epidermal surfaces, gastrointestinal abundance of *S. aureus* is less common (Lopez and Skaar, 2017), so *E. faecalis*, another bacteria also frequently implicated in systemic infection in humans, was used to test the impact of SPM treatment. Again, opposing effects with SPM treatment were found, with LXA4 treatment causing decreased survival in *E. faecalis* systemic infection (p<0.0001, Mantel-Cox, Figure 3-15A), whereas increased survival was found with treatment with RvD2 (p=0.0034, Mantel-Cox, Figure 3-15B) and RvE1 (p<0.0001, Mantel-Cox, Figure 3-15C).

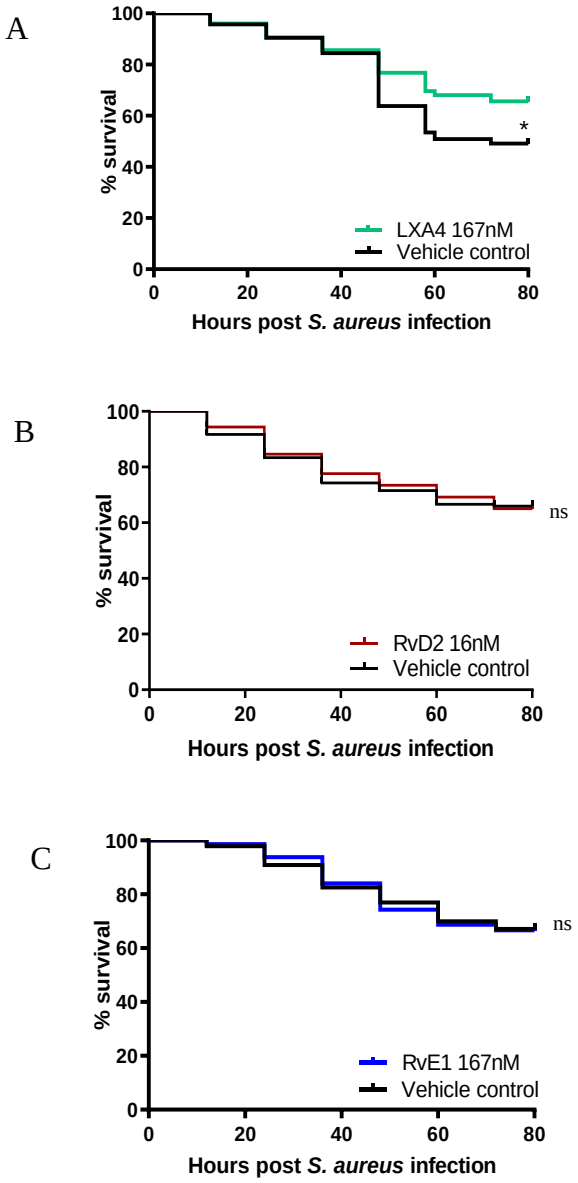

Figure 3-14: Effect of SPMs on survival in systemic infection with *S. aureus*. 2dpf wildtype zebrafish larvae were injected with 2500CFU SH1000 and treated with either SPM or vehicle control. Larval survival was tracked twice daily till 5.2dpf. **A.** Treatment with LXA4 or vehicle control. N=96/group in four independent repeats, extra due to new stock LXA4. **B.** Treatment with RvD2 or vehicle control. **C.** Treatment with RvE1 or vehicle control. In each graph, comparison with Mantel-Cox test, ns=non-significant, *$p<0.05$, N=72/group in three independent repeats.

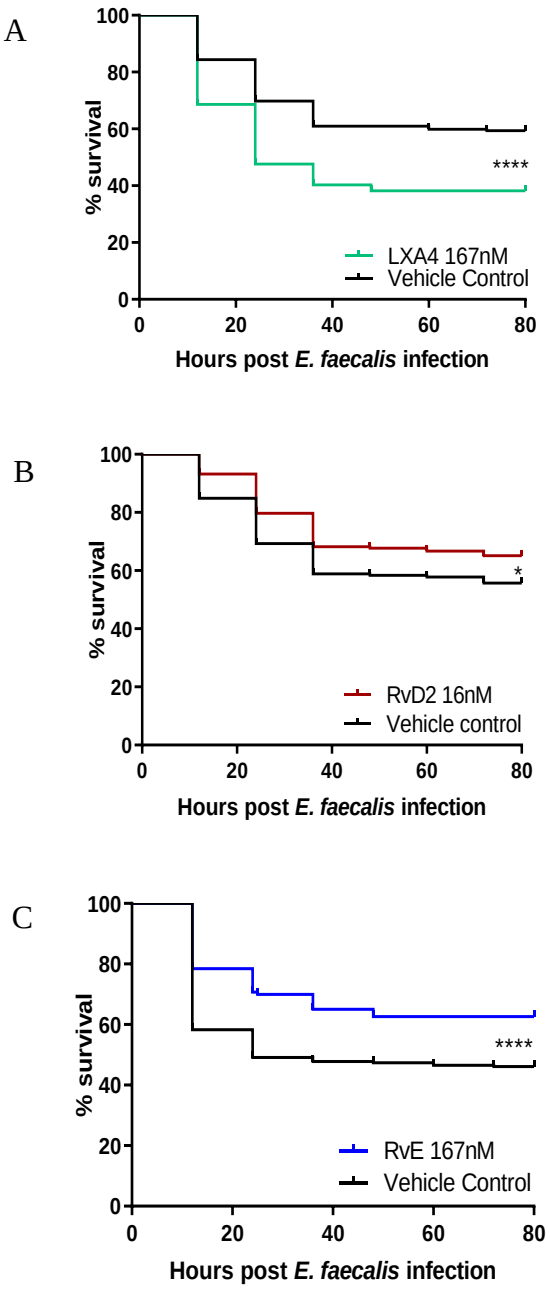

Figure 3-15: Effects of SPM on survival in systemic infection with *E. faecalis*. 2dpf wildtype zebrafish larvae were injected with 1500CFU OG1RF and treated with either SPM or vehicle control. Larval survival was tracked twice daily till 5.2dpf. **A.** Treatment with LXA4 or vehicle control. **B.** Treatment with RvD2 or vehicle control. **C.** Treatment with RvE1 or vehicle control. In each graph, comparison with Mantel-Cox test, *$p<0.05$, ****$p<0.0001$, N=72/group in three independent repeats.

3.2.14 **Development of GIT injury model**

Because of the differential effects of the SPMs with bacterial infections, investigation was extended to the GIT, an organ with a naturally heavy load of diverse microbiota. Real time investigation of inflammation within the GIT has always been challenging because of its hidden location. The zebrafish offers an opportunity to circumvent this difficulty because of its larval transparency. Only chemically induced bowel injury models using Dextran Sodium Sulfate (DSS) or 2,4,6- trinitrobenzenesulfonic acid (TNBS) (Oehlers *et al.*, 2012) have been described in teleosts. Therefore it was imperative to find a reproducible model of mechanical injury to study localised inflammation since chemical agents can have unintended effects on the intestinal microbiome, as well as possible systemic effects, thus complicating interpretation of results. Two different models of injury were investigated, a laser injury and a mechanical injury. For the laser injury, techniques used in drosophila (Chang and Keshishian, 1996) were adapted to allow tissue ablation in the zebrafish distal GIT. However, unlike drosophila, where an epithelial defect is often visible post-injury, the intestinal tract showed no lasting visible damage (Figure 3-16A), possibly due to its higher fluid content. Laser ablation was therefore visually confirmed by positively identifying a bubble of vaporised tissue (Figure 3-16B) which disappeared after 30-40 seconds. To be certain that definite tissue damage was being inflicted, the *Tg(klf2a:GFP)* (Heckel *et al.*, 2015) fish line was used. For reasons that are yet to be understood, although *klf2a* is a vascular marker (Lee *et al.*, 2006), this line also has a fluorescing anal region (Figure 3-16C). Post-ablative absence of fluorescence (Figure 3-16D) thus confirmed positive tissue destruction, which was consistent with the visible, though transient, bubble. Nonetheless, the neutrophil response to these laser injuries lacked vigour, as shown by the small initial difference in neutrophil counts in the ROI that was not sustained, returning to baseline by the end of the time-lapse (N=5 in a single experiment, Figure 3-17A-B). Given the large biological variation inherent in live experiments, this model would not have been a viable technique for larger scale studies. The possibility of a mechanical bowel injury was then explored. A puncture wound was found to be easily reproducible (Figure 3-17C) with a consistent inflammatory response. This model caused a significant and sustained increase in neutrophil numbers (Figure 3-17D), and was used henceforth for further investigation of the inflammatory response in the GIT.

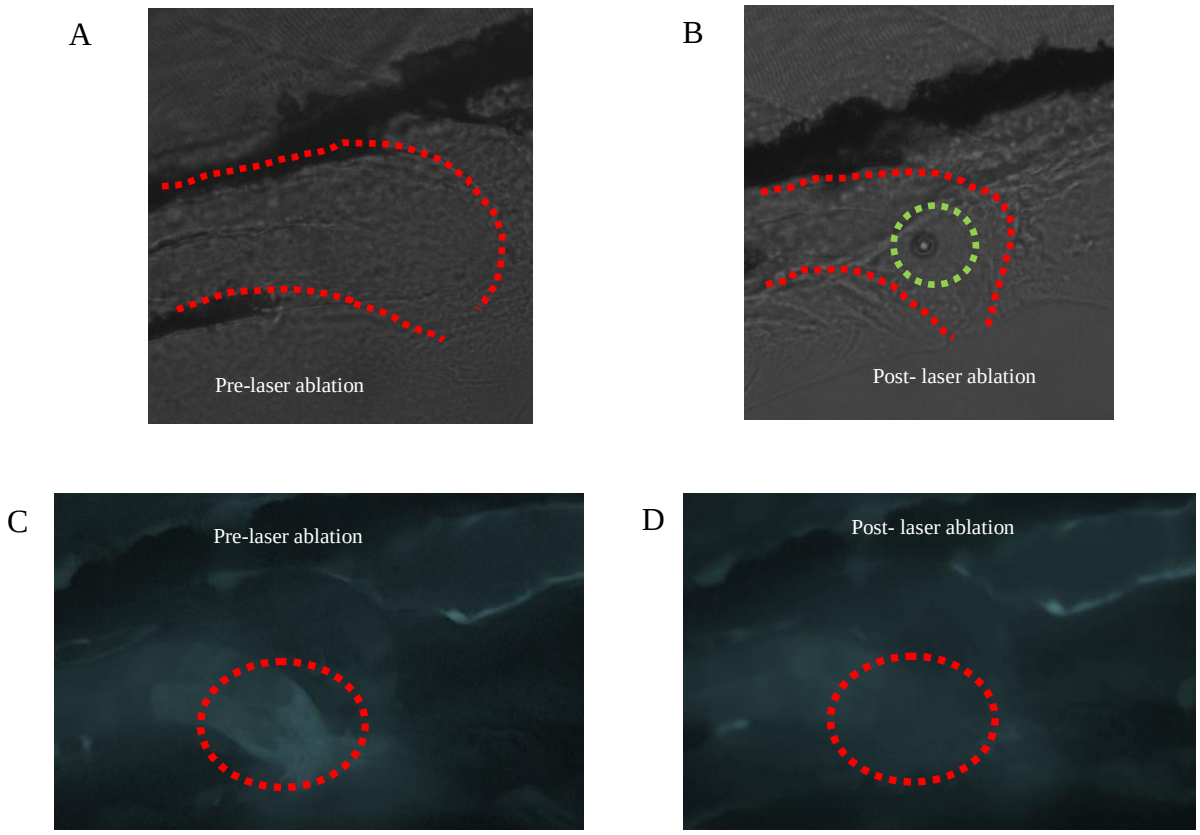

Figure 3-16: Laser injury to the GIT. A. Representative bright field image of anal pore in an uninjured 4dpf zebrafish larvae of *TgBAC(mpx:GFP)i114*, visualised using the 40X objective on the inverted Olympus microscope with Yokagawa CXU spinning disk. N=5/group in a single exploratory experiment. Normal contour of anal region outlined in red dotted lines of the zebrafish in standard position (head to left and tail to right of image). **B.** Transient bubble indicated by green circle, showing position of vaporised tissue, which disappeared after approximately 30 seconds. **C.** 4dpf *Tg(klf2a:GFP)*, showing the fluorescing anal region (red dotted circle) before laser ablation. **D.** Laser ablation was performed at 77% power using an Andor Micropoint Laser controlled with IQ software. Loss of fluorescence shown post laser-ablation (dotted red circle).

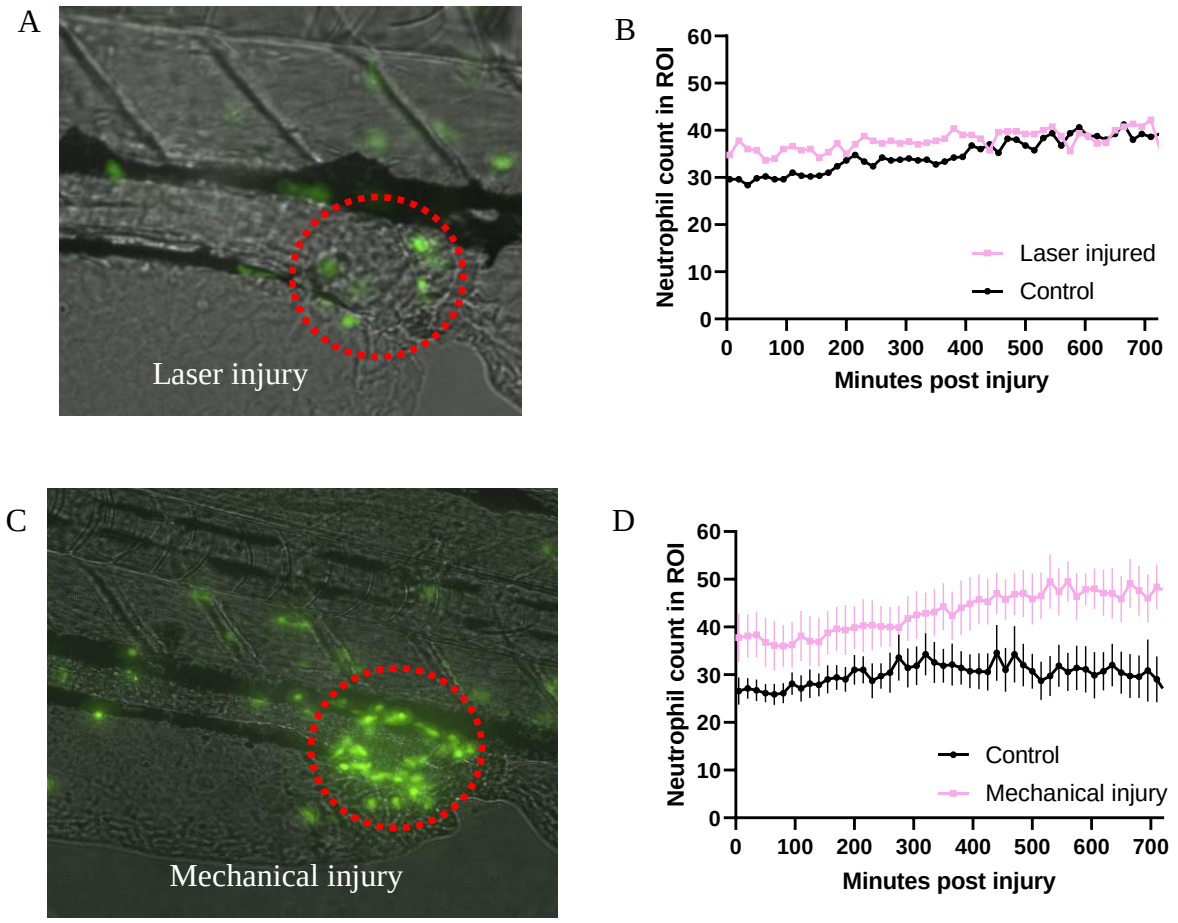

Figure 3-17: Neutrophil responses with laser or mechanical intestinal injury. *TgBAC(mpx:GFP)i114* 4dpf larvae were injured either with a laser or puncture wound in the GIT and imaged for 12hpi. **A.** Representative image of merged brightfield and GFP channels of the anal pore imaged at 20X on a Yokagawa CXU spinning disk, taken immediately post-injury, with the area of laser ablation shown by the red circle. Neutrophils are seen as green dots. **B.** Graph showing the neutrophil counts in a region 200X200 µm centred on the point of laser injury (ROI). N=5/group in a single experiment, error bars omitted for clarity. The controls were uninjured larvae imaged at the same region. No comparative statistics were performed as this was a single exploratory experiment. **C**. Representative image of merged brightfield and GFP channels of the anal pore taken at 20X on a Yokagawa CXU spinning disk, at 6hpi, with the area of injury surrounded by green neutrophils and circled in a red dotted line. **D.** Graph of neutrophil numbers in the same region as the laser injury, plotted over time. N=7/group in a single experiment, error bars show SEM. The controls were uninjured larvae imaged at the same region. No comparative statistics were performed as this was a single exploratory experiment.

3.2.15 LXA4 reduced, RvD2 did not affect, and RvE1 increased neutrophil numbers in a GIT injury

The initial neutrophil response to an injury and immediate intraluminal treatment with SPMs was investigated using the new model described above. The intraluminal mode of delivery of treatment was utilised for this model for two reasons, firstly, because SPMs are thought to be produced at the sites of inflammation and exert their effects mainly locally rather than systemically (Hasturk *et al.*, 2007; Dalli and Serhan, 2016), and secondly to limit the specificity of action to the GIT, rather than as a result of a systemic anti-inflammatory action. The duration of the GIT time-lapses also captured the start of neutrophil resolution and therefore the Beta Growth and Decline model was used to plot the curves. In the presence of an intestinal wound, intraluminal treatment with LXA4 decreased peak neutrophil numbers (Control Ymax: 28.00, LXA4: 24.81, $p<0.0001$, Poisson regression, Figure 3-18A). Treatment with RvD2 did not change peak neutrophil numbers compared to controls (Control Ymax: 27.75, RvD2: 27.72, $p=0.8902$, Poisson regression, Figure 3-18B). Treatment with RvE1 however, increased the peak number of neutrophils (Control Ymax: 26.18, RvE1: 27.53, $p<0.0001$, Poisson regression, Figure 3-18C). Movement characteristics of neutrophils attending the intestinal wound were assessed using Volocity ® 6.3, but none of the SPMs appeared to alter parameters of neutrophil movement in the GIT. Neutrophil speed was unaltered with LXA4 (Control mean +/- SEM: 0.027 +/- 0.002, LXA4: 0.026 +/- 0.001, $p=0.5629$, t-test, Figure 3-19A), RvD2 (Control mean +/- SEM: 0.040 +/- 0.0009, RvD2: 0.041 +/- 0.0008, $p=0.2980$) and RvE1 (Control mean +/- SEM: 0.035 +/- 0.001, RvE1: 0.037 +/- 0.002, $p=0.2372$). Similarly, neutrophil path length was unchanged in LXA4 (Control mean +/- SEM: 144.9 +/- 2.02, LXA4: 146.7 +/- 2.74, $p=0.6061$, t-test, Figure 3-19B), RvD2 (Control mean +/- SEM: 140.4 +/- 3.1, RvD2: 144.3 +/- 2.7, $p=0.3434$, t-test) and RvE1 (Control mean +/- SEM: 124.2 +/- 5.1, RvE1: 132.0 +/- 5.3, $p=0.2971$, t-test). Finally directness of travel, or meandering index, was also unaffected in LXA4 (Control mean +/- SEM: 0.31 +/- 0.005, LXA4: 0.31 +/- 0.007, $p=0.8453$, t-test, Figure 3-19C), RvD2 (Control mean +/- SEM: 0.29 +/- 0.004, RvD2: 0.30 +/- 0.006, $p=0.2458$, t-test) and RvE1 (Control mean +/- SEM: 0.28 +/- 0.005, RvE1: 0.27 +/- 0.007, $p=0.3574$, t-test).

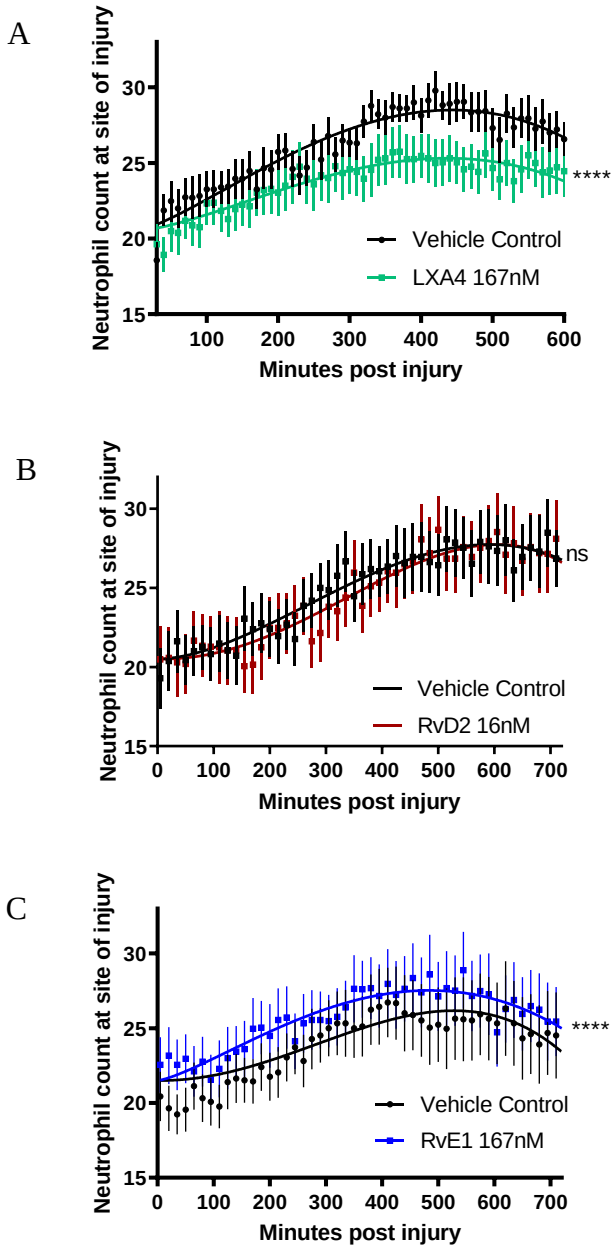

Figure 3-18: Neutrophil counts at the site of intestinal injury with SPM treatment. *TgBAC(mpx:GFP)i114* 4dpf larvae underwent a mechanical puncture injury to the distal GIT followed by microgavage of SPM or vehicle control. Imaging was performed on an inverted Olympus microscope with Yokagawa CXU spinning disk and Volocity® 6.3 (Perkin Elmer). **A**. Treatment with LXA4. N=21/group in three independent repeats. **B**. Treatment with RvD2. N=21/group in three independent repeats. **C**. Treatment with RvE1. N=24/group in three independent repeats. For each graph: Curve fitting with Beta Growth Decline model, comparison of Ymax with Poisson regression, ns=non-significant, ****$p<0.0001$, error bars show SEM.

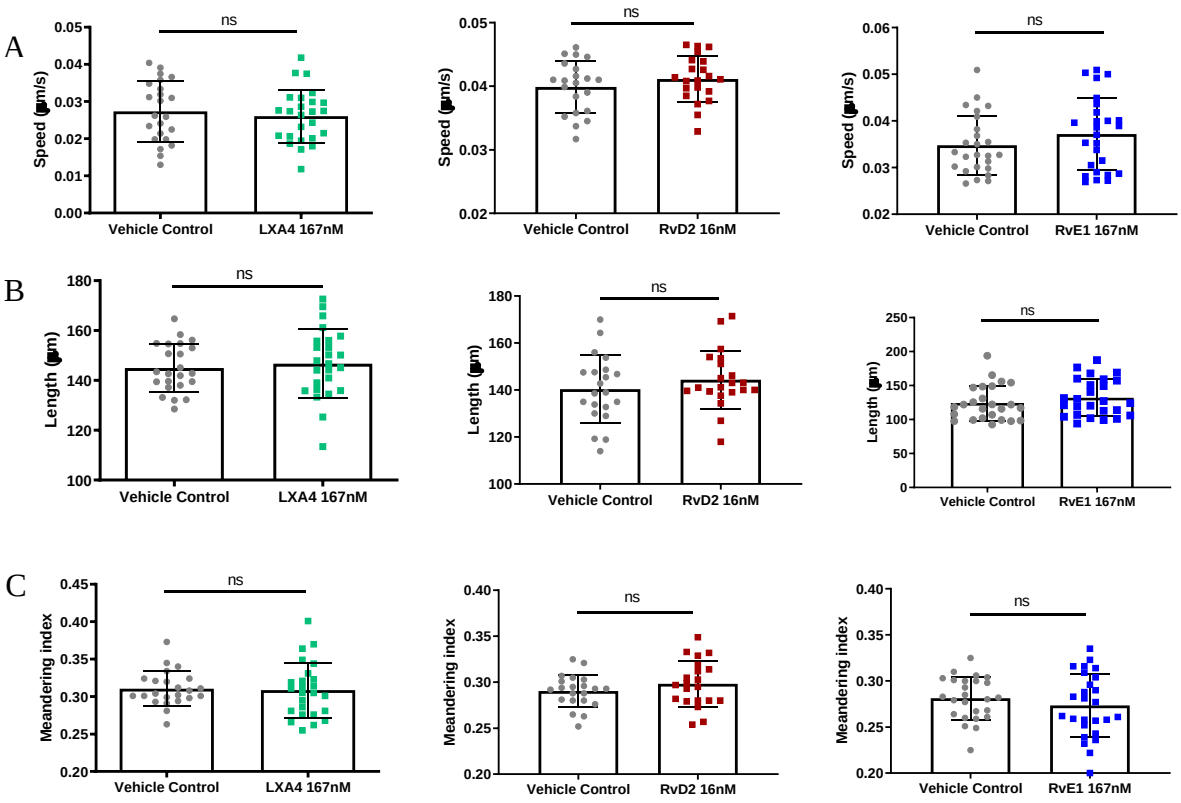

Figure 3-19: Effect of SPMs on movement characteristics of neutrophils attending to an intestinal wound site. Analysis was performed on neutrophils tracked in the time lapse of 4dpf *TgBAC(mpx:GFP)i114* with GIT injury and intraluminal SPM treatment, using Perkin Elmer Volocity® 6.3. Comparison between the treatment vehicle control and the SPMs (LXA4, RvD2, and RvE1) were made for the following parameters of movement of neutrophils in the intestinal region: **A**. Speed, **B**. Path length, and **C**. Meandering index (or directness of travel) where a number closer to 1 indicates a straighter path. Comparison with t-test, error bars show SD, ns=non-significant, N≥21/group in three independent repeats.

3.2.16 **All three SPMs reduced peak macrophage numbers attending to an intestinal wound**

Differences in innate immune responses in different organs would not be totally unexpected, partly because of the differences in colonising microbiota, but also because the intestinal tract is, to a certain extent, an immuno-privileged site, allowing bacterial, fungal and even viral entities to remain in close association with the mucosal surface without causing a robust defensive response (Murall, Abbate and Touzel, 2017). Therefore the macrophage response to localised intestinal injury and SPM treatment was also investigated using the *Tg(mpeg1:NLS-Clover)sh436* line. Peak macrophage numbers were reduced with LXA4 (Control Ymax: 34.75, LXA4 Ymax: 31.37, $p<0.0001$, Poisson regression, Figure 3-20A), RvD2 (Control Ymax: 37.03, RvD2 Ymax: 35.55, $p<0.0001$, Poisson regression, Figure 3-20B) and RvE1 (Control Ymax: 37.49, RvE1 Ymax: 35.55, $p<0.0001$, Poisson regression, Figure 3-20C). Movement characteristics of macrophages attending the intestinal wound assessed using Volocity ® 6.3 revealed that macrophage speed was unaffected by LXA4 (Control mean +/- SEM: 0.036 +/- 0.0007, LXA4: 0.037 +/- 0.0006, $p=0.2826$, t-test, Figure 3-21A), RvD2 (Control mean +/- SEM: 0.032 +/- 0.0007, RvD2: 0.033 +/- 0.0007, $p=0.7383$, t-test) and RvE1 (Control mean +/- SEM: 0.034 +/- 0.0006, RvE1: 0.033 +/- 0.0007, $p=0.5539$, t-test). Similarly, path length was unaffected by LXA4 (Control mean +/- SEM: 132.7 +/- 2.76, LXA4: 139.8 +/- 3.39, $p=0.1134$, t-test, Figure 3-21B), RvD2 (Control mean +/- SEM: 123.8 +/- 2.85, RvD2: 123.2 +/- 3.23, $p=0.8758$, t-test), and RvE1 (Control mean +/- SEM: 127.1 +/- 2.57, RvE1: 127.4 +/- 3.14, $p=0.9432$). Directness of travel was unaffected by LXA4 (Control mean +/- SEM: 0.33 +/- 0.008, LXA4: 0.33 +/- 0.010, $p=0.9147$, t-test, Figure 3-21C) and RvD2 (Control mean +/- SEM: 0.32 +/- 0.008, RvD2: 0.31 +/- 0.007, $p=0.4316$, t-test), but was reduced with RvE1 (Control mean +/- SEM: 0.33 +/- 0.005, RvE1: 0.31 +/- 0.005, $p=0.0303$, t-test, Figure 3-21C).

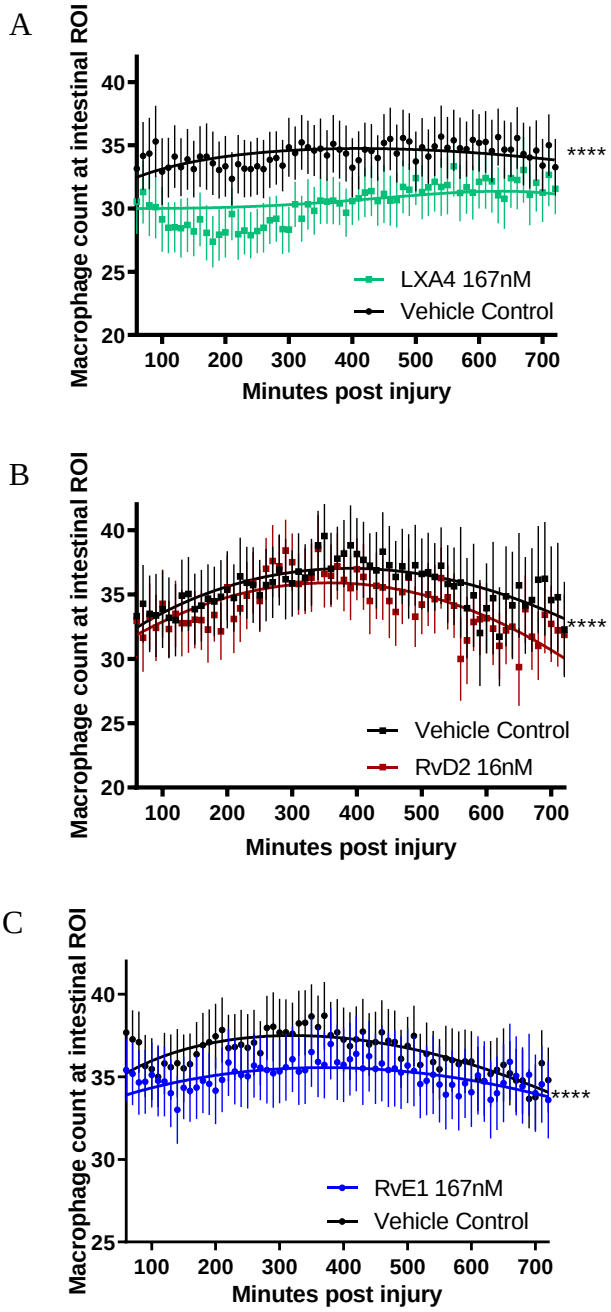

Figure 3-20: Macrophage counts at the site of intestinal injury. *Tg(mpeg1:NLS-Clover)sh436* 4dpf larvae underwent a mechanical puncture injury to the distal GIT followed by microgavage of SPM or vehicle control. Imaging was performed on an inverted Olympus microscope with Yokagawa CXU spinning disk and Volocity®(Perkin Elmer). **A.** LXA4. N=24/group in three independent repeats. **B.** RvD2. N=22/group in three independent repeats. **C.** RvE1. N=28/group in four independent repeats. In each graph: curves fitted with Beta Growth and Decline model, Comparison of Ymax with Poisson regression, ****$p<0.0001$, error bars show SEM.

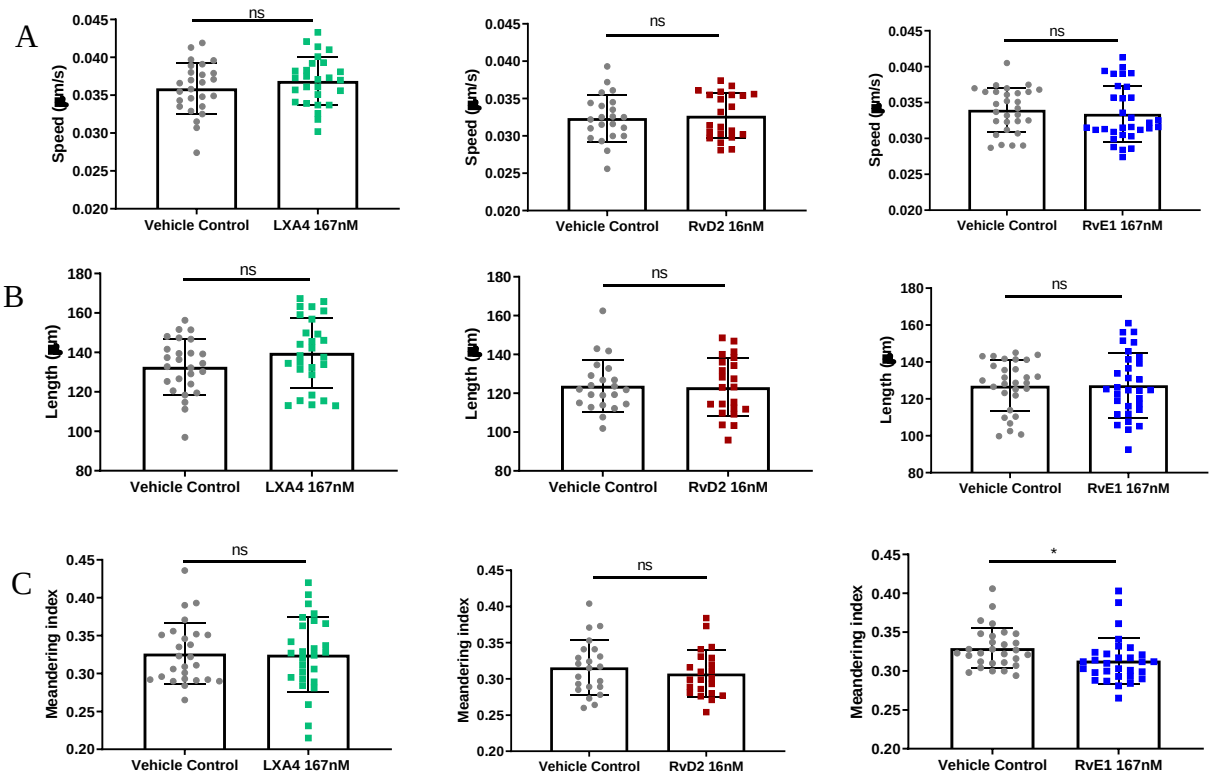

Figure 3-21: Effect of SPMs on movement characteristics of macrophages attending to an intestinal wound. Analysis was performed on macrophages tracked in the time lapse of 4dpf *Tg(mpeg1:NLS-Clover)sh436* larvae, using Perkin Elmer Volocity® 6.3. Comparison between the treatment vehicle control and the SPMs (LXA4, RvD2, and RvE1) were made for the following parameters of movement of reverse migrated neutrophils: **A**. Speed, **B**. Path length, and **C**. Meandering index (or directness of travel) where a number closer to 1 indicates a straighter path. In each graph: comparison with t-test, ns=non-significant, *$p<0.05$, N≥22/group in three independent repeats, error bars show SD.

3.3 **Discussion and further work**

Zebrafish express many of the eicosanoids found in its mammalian counterparts, and these have been detected in zebrafish tissue extracts as well as cell suspensions (Zarini *et al.*, 2014). Nevertheless the pathways of synthesis of these eicosanoids are yet to be fully described in zebrafish. For example, in the zebrafish, around 20 orthologues of the lipoxygenase genes exist, in comparison to the six functional human lipoxygenase genes, and the zebrafish orthologues have a low percentage of similarity of amino acid identity to the human enzymes (Kuhn *et al.*, 2018). Quite apart from the evolutionary differences that may exist in enzyme function, lipid pathways have also been shown to be highly malleable by dietary composition (Alvarez-Curto and Milligan, 2016; Lands, Bibus and Stark, 2016) and since teleosts have a diet, and resulting body composition, that is naturally high in the relevant precursor lipids, it was of importance to determine if, in fact, there were differences in the effects of specialised pro-resolving lipid mediators (SPMs) in this organism. This is an important fundamental aspect to establish, especially since the zebrafish is gaining popularity as a model organism to interrogate the innate immune system, due to its facility for *in vivo* real time imaging and genetic manipulation.

The lipoxygenase pathways for the production of SPMs are intertwined, with more than one LOX enzyme involved sequentially in the production of each end product SPM (Serhan, 2007), and with inhibition of a single LOX possibly shunting precursors down related pathways (Levy *et al.*, 2001). In addition, redundancies and complicated enzyme kinetics abound in these pathways (Aharony, 1986; Mestre *et al.*, 2001; Gilbert, 2020). Although inhibition of 15-LOX, upstream of LXA4, disrupted inflammation resolution when given at all times in the inflammatory process, inhibition of 5-LOX, upstream of RvE1, was anti-inflammatory when given late. This anti-inflammatory effect of 5-LOX inhibition seems to concur with human studies, and indeed 5-LOX has been quite widely implicated in disease, and inhibitors have been utilised with clinical benefit (Martel-Pelletier, 2003; Joshi and Praticò, 2015; Guimarães *et al.*, 2018). However, the persisting inflammation with early blockade of 5-LOX shown here has not been noted before. There is no easy explanation for this because although RvE1 is a product of 5-LOX, leukotriene B4 (LTB4) production is also thought to be an early event (Haeggström, 2018). One major caveat of using these inhibitors is that its specificity in inhibiting the zebrafish enzyme is unknown, especially given the high degree of amino acid conservation between the

various zebrafish isozymes, and the results obtained may simply be a reflection of this. In addition, the lipoxygenase enzymes appear to have a spectrum of bioactivity that is independent of their function in the synthesis of lipid mediators, such as being able to alter the transcription of enzymes via increasing intracellular peroxide, and modifying lipid-protein structures such as the cell membrane (Adel *et al.*, 2014; Kuhn, Banthiya and van Leyen, 2015; Kuhn *et al.*, 2018) further complicating the interpretation of these results. Therefore given these complexities, further investigation was confined to downstream SPM products of LOXs.

In prior mammalian and *in vitro* models, all SPMs invariably reduced neutrophil recruitment even in the presence of bacteria. In these zebrafish studies, similar results were obtained with LXA4 and RvE1. The reduction in neutrophil infiltration with LXA4 was consistent with published literature, and to be expected since LXA4 has been isolated previously in rainbow trout (Pettitt, Rowley and Secombes, 1989), and therefore likely to be functionally conserved in all teleosts. But in addition, the zebrafish tailfin model has shown that the temporal actions of these two SPMs (LXA4 and RvE1) vary within the inflammatory cycle, with LXA4 acting early, and RvE1 exerting its effects mainly in the later stages. The enhanced reverse migration of neutrophils appeared to be the predominant mechanism of action resulting in a reduction of neutrophil numbers, most evident with RvE1 treatment. This fits nicely with the role of RvE1 as a partial BLT1 receptor antagonist (Arita *et al.*, 2007). RvD2 has previously been shown to reduce the directness of travel toward a chemokine (Norling *et al.*, 2012; Chiang *et al.*, 2017) but the zebrafish model has shown that, in addition, SPMs also exerted the opposite effect, of increasing the directness of travel of neutrophils moving away from an inflammatory site. This alone is important as neutrophil migration has been known for some time to be defective in Crohn's patients (Segal and Loewi, 1976), and perhaps improving the directionality of neutrophils could mitigate some symptoms of this chronic inflammatory disease.

SPMs also decreased neutrophilic inflammation in zebrafish via another mechanism, demonstrated by LXA4 which increased apoptosis of neutrophils very early in inflammation, in concordance with previous *in vitro* studies (El Kebir *et al.*, 2009). A limitation of the TUNEL experiments was that they were performed at three-hour intervals and it remains a possibility

that significant increases in neutrophil apoptosis induced by the other SPMs could have been missed if it occurred at other times.

Ongoing inflammation often features heavily, not only in chronic diseases, but also in chronic wounds (Willenborg and Eming, 2018), and accelerating inflammation resolution could theoretically also accelerate wound healing. LXA4 has previously been shown to improve healing in corneal wounds (Gronert, 2005), but treatment with LXA4 did not appear to enhance tailfin regeneration in the zebrafish model. This could be because LXA4 has also been shown to inhibit the vascular endothelial growth factor (VEGF) (Baker *et al.*, 2009), and whilst angiogenesis is not central to the avascular corneal healing, it would be vital for healing or regeneration of other, more vascular body parts such as the tailfin. It is possible that a local application to the wound might have exerted a greater effect than IV treatment, however, the method of application was kept standardised across the experiments to enable comparability and to link observations in innate immune inflammatory responses with that of regeneration.

Other publications have shown that RvD2 and RvE1 increase regeneration in planaria (Serhan *et al.*, 2009). The tailfin regeneration studies shown here are the first higher vertebrate data, and concur in part with published data, as significantly increased tailfin regeneration was seen with RvE1 treatment. RvD2 however, did not increase zebrafish tailfin regeneration. There are several possible explanations for this. Firstly, the inflammatory modulation, evidenced by a reduction in neutrophil counts, was not seen with RvD2 as it was with the other SPMs in this zebrafish larval model. Secondly, DHA, the precursor for RvD2, appears to have a privileged role in the composition of the yolk and in developing larvae, with preferential maintenance of its levels at the expense of other lipids (Weigand, 1996), and previously published mass spectrometry studies did not detect the related RvD1 precursor in zebrafish larvae (Zarini *et al.*, 2014). Thus, it is possible that at this stage of zebrafish development, a fully functioning DHA/RvD pathway has yet to be established for phagocytes, although studies have shown RvD2 receptors to already be present within zebrafish thrombocytes (Nikhil, 2013). This is not to say, however, that the DHA lipid pathways should be discounted completely in this model. Quite the contrary, the need to consider innate immunity and coagulation concurrently has long

been advocated (Delvaeye and Conway, 2019), and this is certainly an area for further investigation in future.

The development of the bowel injury model was of potentially significant benefit, because the bowel is inherently different to the rest of the body. For example, we know that immune cells display a significant 'inflammatory anergy' toward bacteria in the GIT (Smythies *et al.*, 2005) enabling the mucosa to tolerate the immuno-stimulatory proximity of bacteria without mounting a response. Thus, organ specific investigations are of paramount importance. Two methods of simulating an intestinal injury were examined, a laser ablation and a mechanical puncture. Although some publications have suggested that laser ablation (Matrone *et al.*, 2013) allows a more consistent injury in regions such as the heart and the kidney, this was not the case with the zebrafish GIT. Differences in the peristaltic movements of the intestine, the contour of the zebrafish body at the region, or even the intraluminal liquid content meant that often the laser intensity was attenuated in an unpredictable manner. Mechanical injury, however, offered a more precise and reproducible neutrophil response. Using this model of intestinal injury, SPMs did indeed demonstrate a different response to injury within the GIT compared to the tailfin. In the GIT, only LXA4 significantly reduced neutrophil numbers. This correlates with the knowledge that not only is LXA4 secreted in the colonic mucosa in humans, in human pathologies of increased neutrophil infiltration and damage for example in ulcerative colitis, LXA4 is deficient (Mangino *et al.*, 2006). LXA4 and RvE1 reduced macrophage numbers attending to the wound, and this was opposite to the response seen in the tailfin injury. This demonstrated clearly the importance of organ specific investigation, even in one as inaccessible as the GIT, revealing the differential, and possibly directly opposing, effects of SPMs.

The effects of SPMs on systemic infections were then investigated in zebrafish larvae, especially since concerns remain that increased risk of infections may be directly attributed to the anti-inflammatory actions of SPMs (Fenton *et al.*, 2013). The survival curves for *S. aureus* and *E. faecalis* revealed further interesting areas for future studies, with LXA4 increasing *S. aureus* survival but decreasing *E. faecalis* survival, and the RvD2 and RvE1 only increasing *E. faecalis* survival. It is possible that the enhanced survival of *S. aureus* with LXA4 may be due to physical occupation of the *fpr* receptors by LXA4, thus blocking the efficacy of the bacteria

derived FPR-specific virulence factors (Prat *et al.*, 2009), rather than a direct immune system effect. But, in addition, further scrutiny of the survival curves reveal a later divergence, at approximately 48hpi in *S. aureus*, compared with 24hpi with *E. faecalis*. These results are important because they showed for the first time that not all SPMs improve survival in different infective models, and could in fact decrease survival in infection, highlighting additional subtleties that need further attention.

3.4 **Summary of important findings**

Zebrafish express many conserved enzymes in the eicosanoid pathways of inflammation. However, it was unknown if specialised pro-resolving lipid molecules (SPMs) exerted identical effects in teleosts to their mammalian counterparts, as teleosts have a proportionately higher tissue level of fatty acids. In humans, dietary modulations can affect lipid availability and subsequent stress responses. Using zebrafish models of inflammation, infection and regeneration, it was shown that despite theoretical differences in levels of precursor fatty acids, exogenous SPMs modulated the inflammatory response in approximately the same manner in teleosts as in mammals. LXA4 and RvE1, although not RvD2, recapitulated mammalian models in reducing neutrophilic inflammation, partly by apoptosis but mainly by increased reverse migration. Furthermore, a temporal difference was demonstrated in the action of LXA4 and RvE1, with the latter acting later in the inflammatory response. In addition, in this higher vertebrate model, RvE1 increased tailfin regeneration. Differential effects on survival in systemic infection were also demonstrated, as although LXA4 increased survival in *S. aureus* bacteraemia, and RvE1 and RvD2 similarly in *E. faecalis* bacteraemia, LXA4 decreased survival in *E. faecalis* bacteraemia. Thus, not only was the zebrafish model at this stage of development able to recapitulate many aspects of mammalian SPM biology, but in addition, was sensitive enough to demonstrate further subtleties in the individual actions of SPMs that may not have been apparent, or even detectable, in other models, and is therefore a relevant and important model for the *in vivo* study of eicosanoid biology.

Chapter 4: Investigation of SPM receptors in larvae and development of a spatial RNA analysis (TomoSeq) of zebrafish tailfin injury

4.1 Receptor expression and spatial RNA analysis in zebrafish

The zebrafish inflammatory responses showed many similarities in SPM modulation as their mammalian counterparts, and in addition, demonstrated superiority in further elucidating subtleties in differential actions of SPMs. However, given the early developmental stage of the larval model, it was important to investigate whether these differences could be attributed to a variation in constitutive receptor expression linked to larval age. Theorthologues for the RvD2 receptor (Chiang *et al.*, 2015), *gpr18*, and the RvE1 receptor (Arita *et al.*, 2007), *cmklr1*, are present in the zebrafish genome, but the homologue for the LXA4 receptor, *FPR2* in humans (Maderna *et al.*, 2010), has yet to be determined. But not only do SPMs exert their effects through specific receptors (Brink *et al.*, 2003), SPMs are rapidly inactivated through enzymatic catabolism in human tissues (Arita *et al.*, 2006). Therefore the possibility of manipulating receptor expression to influence the inflammatory response remains an attractive possibility for longer-lasting effects. This is additionally so given the genetic tractability of the zebrafish that could allow transient receptor RNA over-expression without permanent genomic manipulation enabling rapid observation of effects (Finckbeiner *et al.*, 2011), a manoeuvre that is more difficult in mammalian models. Given the positive responses obtained from exogenous SPM supplementation in earlier studies, it was hypothesised that zebrafish larvae would express the relevant SPM receptors even at an early developmental stage, and that over-expression of these receptors could result in a functional response similar to exogenous supplementation of SPMs.

Exogenous SPM supplementation and live quantification of the inflammatory response over time provides a snapshot of the temporal response to injury and its external malleability, but it is now understood that many signalling pathways, including those of eicosanoids, have inbuilt redundancies and overlapping functions (Mestre *et al.*, 2001), potentially complicating the interpretation of the responses to either exogenous supplementation or genetic manipulation. Therefore observation of an unmanipulated inflammatory response to an injury, together with its micro-environment, is of increasing importance, and could bring new mechanistic insights or discovery of molecules of interest. The value elucidating the spatial transcriptomic micro-

environment has already been demonstrated in prostate cancers (Berglund *et al.*, 2018) and lung tumours (de Bruin *et al.*, 2014), and has recently also been shown in the exploration of chronic disease pathology (Carlberg *et al.*, 2019). It was therefore hypothesised that by applying spatial transcriptomics to an acute wound in the zebrafish larva using whole body sequential sectioning, RNA extraction and Next-Generation Sequencing (NGS), an additional perspective of inflammation could be mined for unsuspected insights into the inflammatory and regenerative landscapes. This technique, Tomographic Sequencing (TomoSeq), was therefore developed and validated in the zebrafish tailfin transection model.

4.2 **Results**

4.2.1 ***gpr18, cmklr1*** **and** ***fpr1*** **receptor RNA are expressed in zebrafish embryos from 1dpf**

The LXA4 receptor has been characterised in the human but not in the zebrafish. Since LXA4 itself has been isolated in trout (Pettitt, Rowley and Secombes, 1989), a receptor for LXA4, similar to that in humans, was expected to be expressed in teleosts. However, blasting the zebrafish genome did not identify any highly similar genes to the human *FPR2*. A previous study of the human FPR2 had identified the 7th transmembrane segment (TM7) to be important for the specificity of FPR2 to LXA4 (Arita *et al.*, 2007), as is the case with the majority of G-protein coupled receptors (GPCRs) (Magalhaes, Dunn and Ferguson, 2012). Therefore this region was blasted against the zebrafish proteome, and returned a single hit of fpr1. In attempt to expand the possible candidates, the 3rd extracellular (EC3) region, also known for GPCR ligand binding (Rana and Baranski, 2010), was blasted agaist the zebrafish genome, but this again returned no hits. Therefore the zebrafish *fpr1* was used for further investigation as a possible receptor for LXA4, together with *gpr18,* the RvD2 receptor (Chiang *et al.*, 2015), and *cmklr1*, the RvE1 receptor (Arita *et al.*, 2007). First, endogenous expression of each receptor was determined on 1-5dpf. Reverse transcription-PCR of RNA extracted from zebrafish larvae at ages 1-5dpf, with an additional set at 2dpf 6hpi, was performed with each set of primers. Comparable expression of *fpr1* (Figure 4-1A), *gpr18* (Figure 4-1B), and *cmkrl1* (Figure 4-1C) was shown on all days of zebrafish development, including the 2dpf injured larvae.

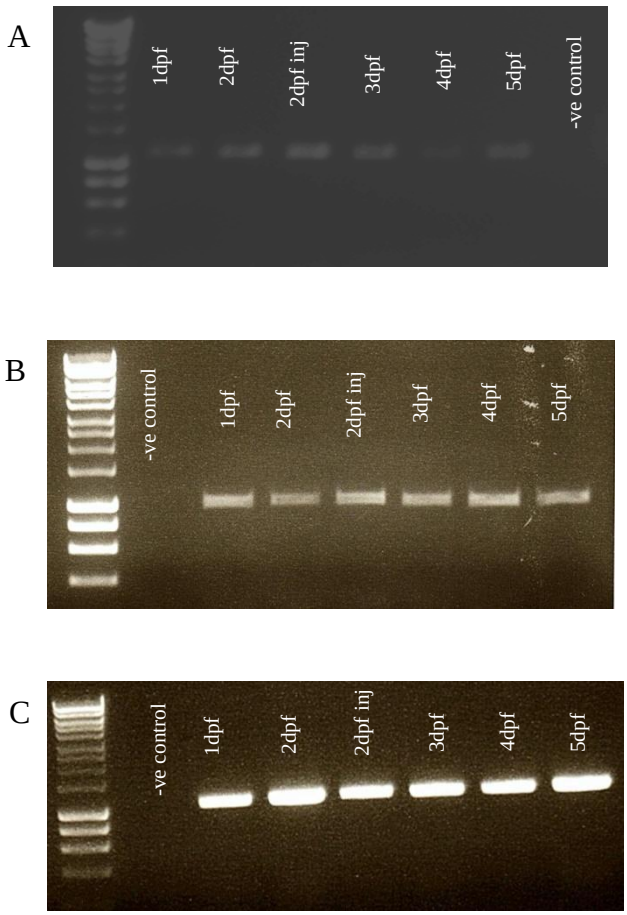

Figure 4-1: Reverse-transcription PCR for expression of SPM receptors in zebrafish embryos and larvae. RNA extracted from zebrafish on 1-5dpf, including an extra extraction at 6hpi in 2dpf larvae (labelled as 2dpf inj). **A**. *fpr1* (expected size 1164bp), **B.** *gpr18* (expected size 945bp), and **C**. *cmklr1* (expected size 1157bp). PCR reactions were repeated on three different RNA extractions, yielding similar results each time. 1kb DNA ladder shown on the left in each gel.

4.2.2 **Over-expression of *fpr1*, *gpr18* and *cmklr1* did not reduce neutrophil numbers at 6hpi**

Each receptor was cloned and then over-expressed by RNA injection at the one cell stage in *TgBAC(mpx:GFP)i114* larvae. Since this was a transient over-expression, quantifying success of protein expression would only indicate the success of that particular injection set and therefore could not be generalised to injections at other times. Normally, this would be overcome by tagging the protein of interest with a fluorescent marker, however this was actively avoided here to prevent any possible changes to receptor function post-translation. Instead, the receptor RNA was co-injected with a small amount of mCherry RNA. Fluorescence was tracked and an assumption was made that this indicated equally successful incorporation of both sets of RNA. No excess of phenotypic abnormalities in the developing larvae were detected at any point in all groups of RNA injected larvae. For the control groups, an equivalent amount of mCherry RNA was injected. At 2dpf, fluorescent larvae were selected, tailfin injury performed as previously described, and neutrophils quantified at 6hpi. At 6hpi, neutrophil numbers were not significantly altered by over-expression of the *fpr1* (Control mean +/- SEM: 29.20 +/- 0.95; *fpr1*: 26.29 +/- 0.77, p=0.0762, one-way ANOVA, Figure 4-2A), *gpr18* (Control +/- SEM: 24.95 +/- 0.80; *gpr18*: 24.91 +/- 0.98, p=0.9263, one-way ANOVA, Figure 4-2B) or *cmklr1* (Control mean +/- SEM: 27.14 +/- 0.70, *cmklr1*: 25.81 +/- 0.86, p=0.5936, one-way ANOVA, Figure 4-2C). Similarly, when the relevant SPM was supplemented in both groups, no additional benefits were seen with over-expression of *fpr1*(Control with LXA4 mean +/- SEM: 22.64 +/- 0.71; *fpr1* with LXA4: 22.06 +/- 0.96, p=0.9616, one-way ANOVA), *gpr18* (Control with RvD2 mean +/- SEM: 26.78 +/- 0.75; *gpr18* with RvD2: 26.04 +/- 0.84, p=0.9185, one-way ANOVA) or *cmklr1* (Control with RvE1 mean +/- SEM: 23.68 +/- 0.73; *cmklr1* with RvE1: 22.79 +/- 0.67, p=0.8281, one-way ANOVA). However, consistent with previous results, neutrophil counts at 6hpi were reduced with LXA4 treatment compared to untreated groups (Control *vs* Control with LXA4: p< 0.0001; and *fpr1 vs fpr1* with LXA4: p=0.0031, one-way ANOVA). This was also the case with RvE1 treatment reducing neutrophil numbers compared to untreated groups (Control *vs* Control with RvE1: p=0.0060, *cmklr1* vs *cmklr1* with RvE1: p=0.0230, one way ANOVA).

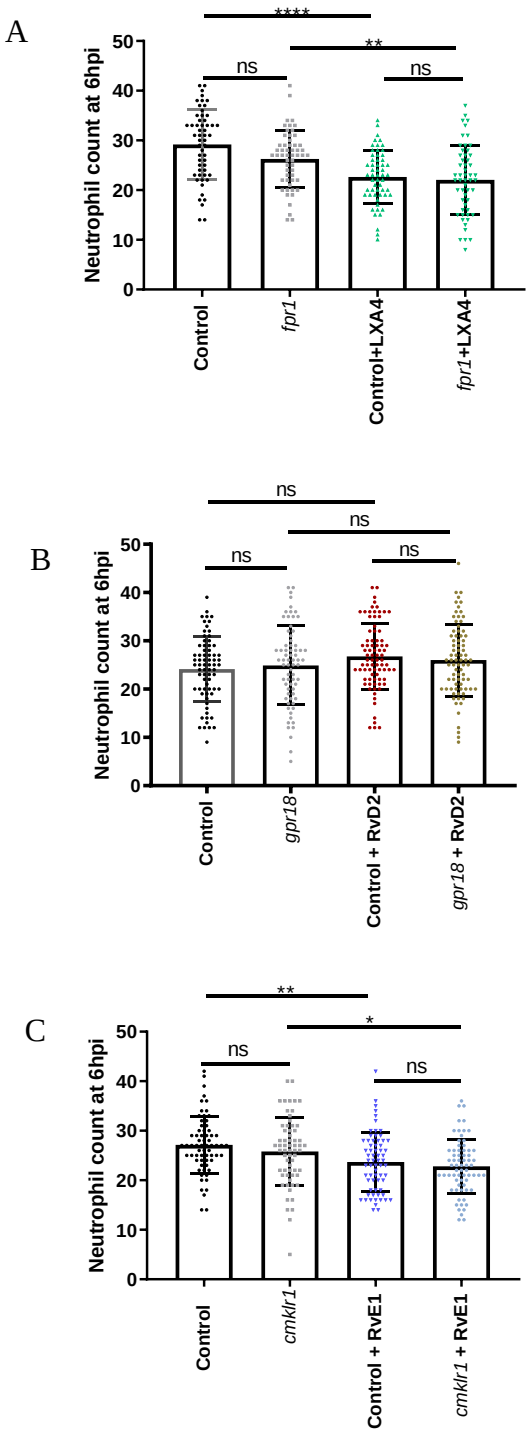

Figure 4-2: Neutrophil counts at 6hpi following over-expression of each receptor using RNA injection at one cell stage. A. *fpr1* over-expression with tailfin injury in 2dpf *TgBAC(mpx:GFP)i114* larvae, with or without LXA4. **B**. *gpr18* over-expression with or without RvD2. **C**. *cmklr1* over-expression with or without RvE1. In each case, N=60/group, ns= non-significant, *p<0.05, **p<0.01, ****p<0.0001, comparison with one-way ANOVA, error bars show SD.

4.2.3 **Over-expression of *gpr18*, but not *fpr1* or *cmklr1*, increased neutrophil numbers at 12hpi**

Similar experiments to the previous were performed, but this time, neutrophils were quantified at 12hpi. At 12hpi, over-expression of *fpr1* did not affect the number of neutrophils attending to a tailfin injury (Control mean +/- SEM: 20.30 +/- 0.87; *fpr1*: 19.31 +/- 0.64, p=0.7825, one-way ANOVA, Figure 4-3A). Supplementation of LXA4 reduced neutrophil numbers in both the control (Control mean +/- SEM: 20.30 +/- 0.87; Control with LXA4: 16.11 +/- 0.59, p=0.0005, one-way ANOVA) as well as *fpr1* over-expression (*fpr1* mean +/- SEM: 19.31 +/- 0.64, *fpr1* with LXA4: 16.06 +/- 0.83, p=0.0116, one-way ANOVA).

gpr18 over-expression alone however did result in an increase in neutrophil numbers at 12hpi (Control mean +/- SEM: 15.04 +/- 0.68, *gpr18*: 18.09 +/- 0.92, p=0.0264, one-way ANOVA, Figure 4-3B), but this response was not augmented or abrogated by exogenous RvD2 supplementation (Control with RvD2 mean +/- SEM: 18.09 +/- 0.66; *gpr18* with RvD2: 18.39 +/- 0.69, p=0.9900).

On its own, *cmklr1* over-expression did not accelerate neutrophilic resolution at 12hpi (Control mean +/- SEM: 18.83 +/- 0.57, *cmklr1*: 19.03 +/- 0.68, p=0.9954, one-way ANOVA, Figure 4-3C). However, additional RvE1 treatment enhanced the resolution effect compared to untreated controls (Control mean +/- SEM: 18.83 +/- 0.57, Control with RvE1: 15.55 +/- 0.61, p=0.0008, one-way ANOVA) and untreated *cmklr1* over-expression (*cmklr1*mean +/- SEM: 19.03 +/- 0.68, *cmklr1* with RvE1: 14.56 +/- 0.53, p<0.0001, one-way ANOVA).

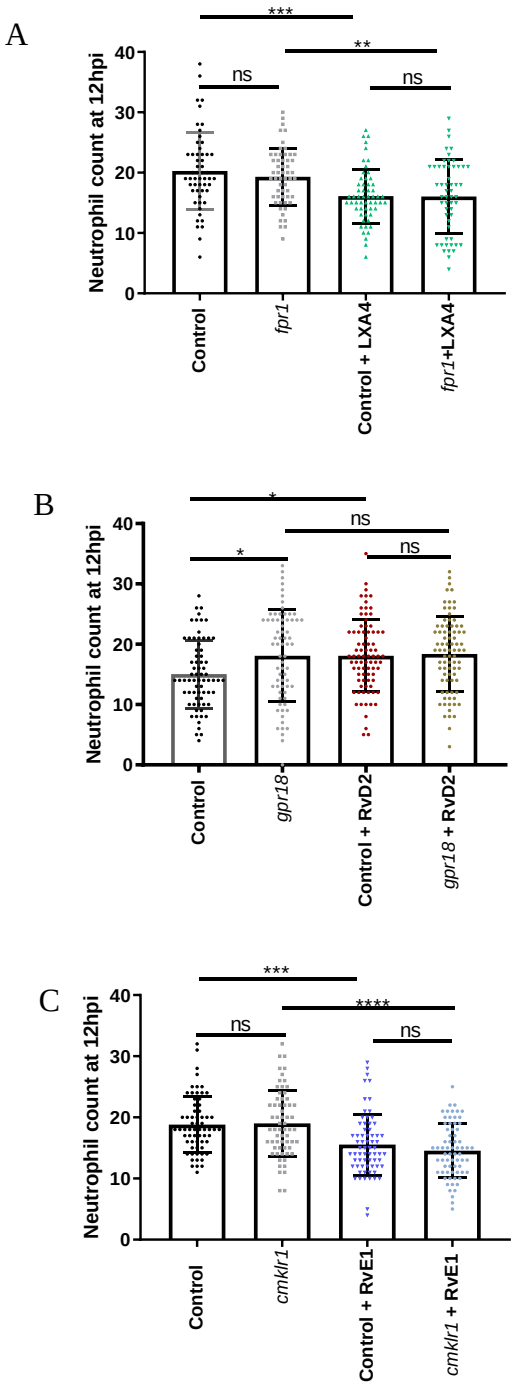

Figure 4-3: Neutrophil counts at 12hpi following over-expression of each receptor using RNA injection at one cell stage. A. *fpr1* over-expression with tailfin injury in 2dpf *TgBAC(mpx:GFP)i114* larvae, with or without LXA4 treatment. **B**. *gpr18* over-expression with or without RvD2 treatment. **C**. *cmklr1* over-expression with or without RvE1 treatment. In each case, N=60/group, ns=non-significant, **p*<0.05, ***p*<0.01, ****p*<0.001, *****p*<0.0001, one-way ANOVA, error bars show SD.

4.2.4 Over-expression of *fpr1*, *gpr18* and *cmklr1* did not affect neutrophil numbers at 24hpi

As a precaution to cover the possibility of delayed maturation or a delayed inflammatory response due to the protein over-expression, the experiment protocol was extended to include a neutrophil count at 24hpi. However, in keeping with the earlier results, none of the over-expressed receptors, *fpr1* (Control mean +/- SEM: 13.69 +/- 0.76, *fpr1*: 12.17 +/- 0.58, p=0.3355, one-way ANOVA, Figure 4-4A), *gpr18* (Control mean +/- SEM: 10.52 +/- 0.54, *gpr18*: 11.56 +/- 0.61, p=0.5647, one-way ANOVA, Figure 4-4B), or *cmklr1* (Control mean +/- SEM: 12.38 +/- 0.57, *cmklr1*: 11.70 +/- 0.53, p=0.8117, one-way ANOVA, Figure 4-4C) caused any changes in neutrophil numbers at 24hpi. This held true even with supplementation of LXA4 (Control with LXA4 mean +/- SEM: 10.91 +/- 0.54, *fpr1* with LXA4: 11.02 +/- 0.65, p=0.9994, one-way ANOVA), RvD2 (Control with RvD2 mean +/- SEM: 13.76 +/- 0.52, *gpr18* with RvD2: 12.42 +/- 0.52, p=0.2835, one-way ANOVA), and RvE1 (Control with RvE1 mean +/- SEM: 10.67 +/- 0.62, *cmklr1* with RvE1: 11.03 +/- 0.41, p=0.9632, one-way ANOVA).

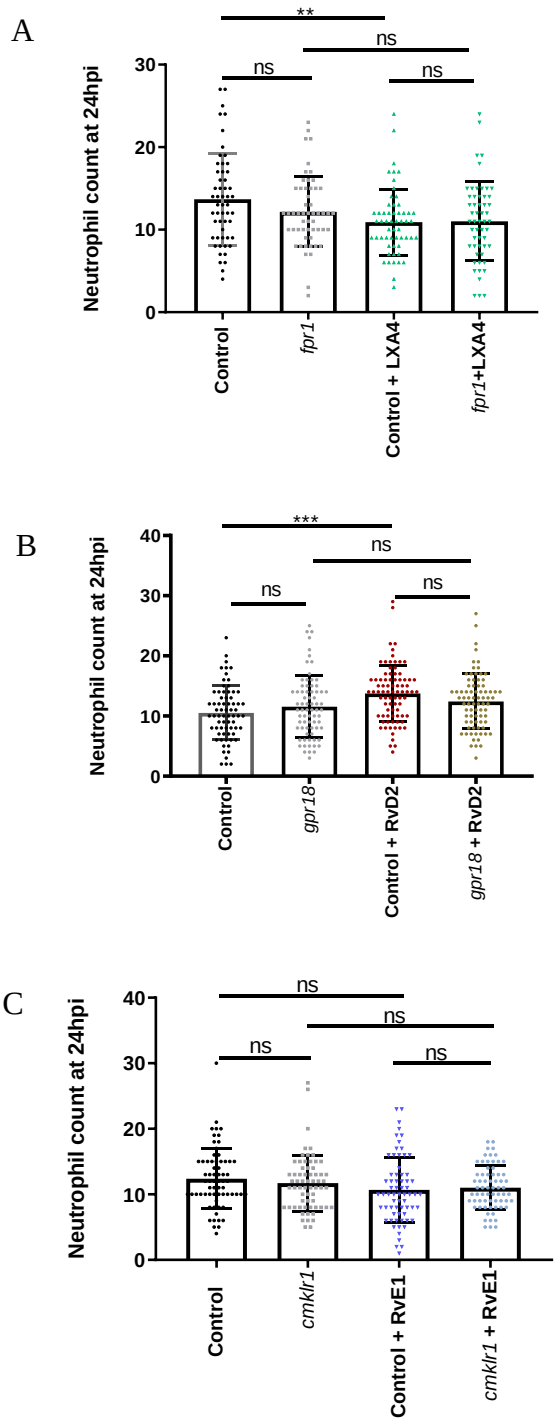

Figure 4-4: Neutrophil counts at 24hpi following over-expression of each receptor using RNA injection at one cell stage. A. *fpr1* over-expression with tailfin injury in 2dpf *TgBAC(mpx:GFP)i114* larvae, with or without LXA4 treatment. **B**. *gpr18* over-expression with or without RvD2 treatment. **C**. *cmklr1* over-expression with or without RvE1 treatment. In each case, N=60/group, ns=non-significant, ***p*<0.01, ****p*<0.001, one-way ANOVA, error bars show SD.

4.2.5 **Over-expression of *gpr18*, but not *fpr1* or *cmklr1*, increased tailfin regeneration**

Although neutrophil numbers were not influenced by over-expression of receptors alone (apart from the increase with *gpr18* at 12hpi), further investigation was undertaken to see if wound regeneration would be affected. Over-expression of *fpr1* did not increase tailfin regeneration (Control mean +/- SEM: 30.74% +/- 5.92, *fpr1*: 55.51% +/- 8.35, p=0.0942, Kruskal-Wallis with Dunn's correction, Figure 4-5A). This still did not reach significance with the exogenous addition of LXA4 to both groups (Control with LXA4 mean +/- SEM: 18.91% +/- 5.14; *fpr1* with LXA4: 32.52% +/- 4.50, p=0.0929, Kruskal-Wallis with Dunn's correction).

Over-expression of *gpr18* alone increased regeneration compared to controls (Control mean +/- SEM: 8.59% +/- 3.33, *gpr18*: 18.78% +/- 3.67, p=0.0341, Kruskal-Wallis with Dunn's correction, Figure 4-5B). Addition RvD2 to both groups negated this increase (Control with RvD2 mean +/- SEM: 16.38% +/- 5.07, *gpr18* with RvD2: 15.79% +/- 4.65, p>0.9999, Kruskal-Wallis with Dunn's correction).

Over-expression of *cmklr1* alone did not affect tailfin regeneration (Control mean +/- SEM: 28.62% +/- 6.97, *cmklr1*: 27.59% +/- 6.97, p>0.9999, Kruskal-Wallis with Dunn's correction, Figure 4-5C). The increase in tailfin regeneration when both groups were supplemented with RvE1 also did not reach significance (Control with RvE1 mean +/- SEM: 48.51% +/- 7.42, *cmklr1* with RvE1: 58.30% +/- 7.73, p>0.9999, Kruskal-Wallis with Dunn's correction). However, addition of RvE1 in the presence of *cmklr1* over-expression significantly increased regeneration compared to *cmklr1* over-expression alone (p=0.0057, Kruskal-Wallis with Dunn's correction).

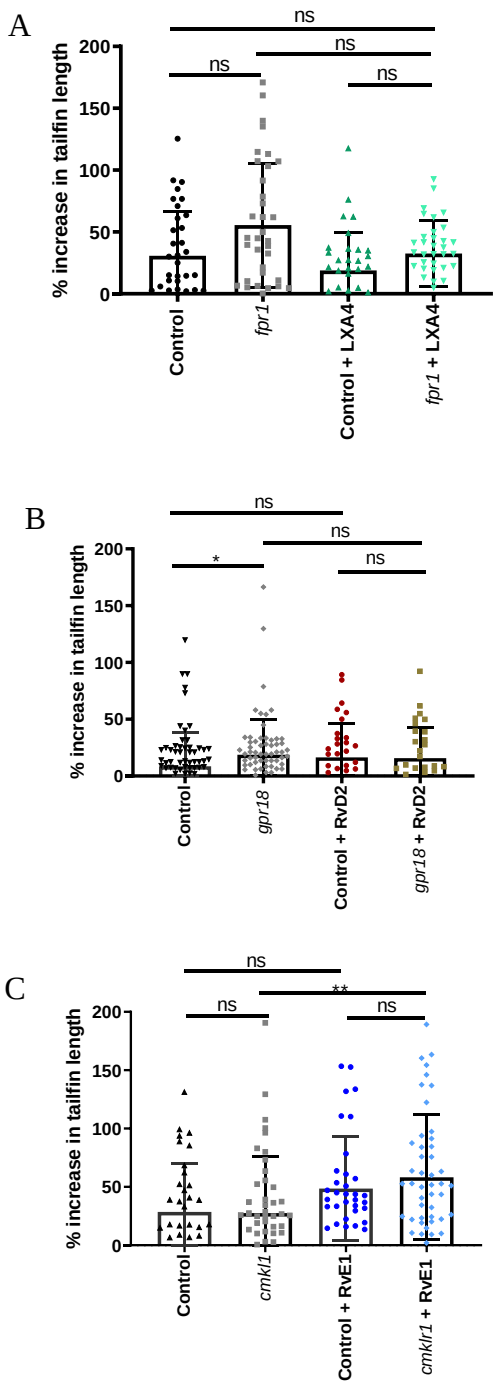

Figure 4-5: Receptor mRNA over-expression and tailfin regeneration. **A**. *fpr1* over-expression followed by tailfin injury at 2dpf in wildtype larvae, with or without LXA4 supplementation. % increase in tailfin length calculated at 24hpi. **B**. *gpr18* over-expression with or without RvD2 supplementation. **C**. *cmklr1* over-expression with or without RvE1 supplementation. In each: N=36/group in three independent repeats, comparison with Kruskal-Wallis with Dunn's multiple comparison correction, ns=non-significant, *$p < 0.05$, **$p < 0.01$, error bars show SD.

4.2.6 **Endogenous *cmklr1* expression, but not *fpr1* or *gpr18*, was increased at the site of tailfin injury from 6hpi onwards**

Native distribution of expression of these receptors was then investigated using one of the oldest techniques in zebrafish research, *in situ* hybridisation (Jowett, 1994), to discern if differences in spatial expression existed following tailfin injury. All three FPR receptors in humans are highly expressed in white blood cells (Migeotte, Communi and Parmentier, 2006), but in the zebrafish larvae, *fpr1* expression appeared to be limited to the renal tract, rather than in a cellular distribution. There were also no noticeable differences between control (regions indicated by arrows in Figure 4-6A) and injured (Figure 4-6B) groups. This staining however was absent in the sense control groups (Figure 4-6C), suggesting a degree of probe specificity. Nonetheless, most larvae in both control and injured groups showed similar staining at all time points (Figure 4-6D).

For *cmklr1*, expression appeared cellular, and distributed within the circulation, most obvious within the blood island overlying the yolk sac seen in both injured and control fish at 2 and 4 hours (Figure 4-7). From 6hpi there was increased expression shown in the region of tailfin amputation, and observed only in the injured group (Figure 4-8). This became more prominent at 8, 10 and 12 hours, again demonstrated only in injured fish (Figure 4-9). The absence of staining in the sense controls confirms probe specificity for this receptor (Figure 4-9).

gpr18, was seen to be expressed mainly within the caudal haematopoietic tissue (CHT) region, and no increase in expression was seen at the tailfin site of injury at 1 or 2 hours post injury (Figure 4-10), 4 or 6hpi (Figure 4-11), or 8 and 12hpi while the clarity of the sense control for *gpr18* showed that the probe expression was specific and therefore the lack of changes at the amputated site likely to be specific (Figure 4-12).

A

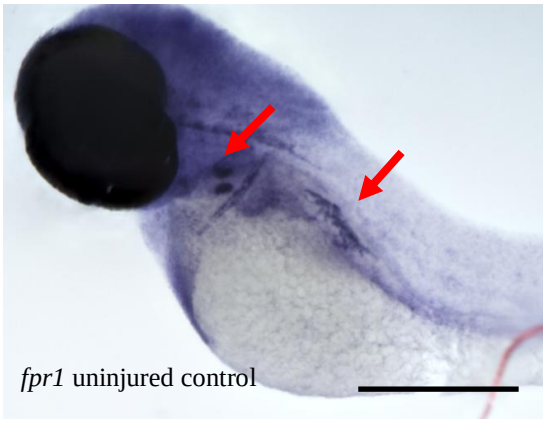

B

C

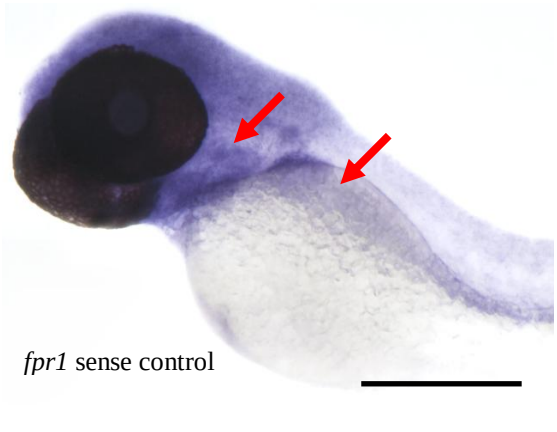

D

Fraction stained	Control	Injured
2hpi	35/40	36/40
4hpi	38/40	39/40
6hpi	36/40	40/40
8hpi	39/40	40/40
10hpi	40/40	40/40
12hpi	40/40	40/40
Sense controls 6hpi	0/30	0/30

Figure 4-6: *fpr1*wholemount *in situ* hybridisation (WISH). 2dpf nacre larvae were uninjured (control group) or injured, and fixed at 2hour intervals from the time of injury, up till 12hpi. Imaging was performed with a Nikon SMZ1500 extended focus microscope interfaced with NIS-Elements BR® version 3.1. **A**. Representative image of uninjured control (red arrows = renal tract). **B**. Representative image of injured larvae at 6hpi (red arrows = renal tract). N=40 at each time point in two independent repeats. **C**. Sense control (red arrows = renal tract). Scale bar = 250 µm. **D**. Table of the number of larva showing the staining patterns in the representative images (A&B) at each time point.

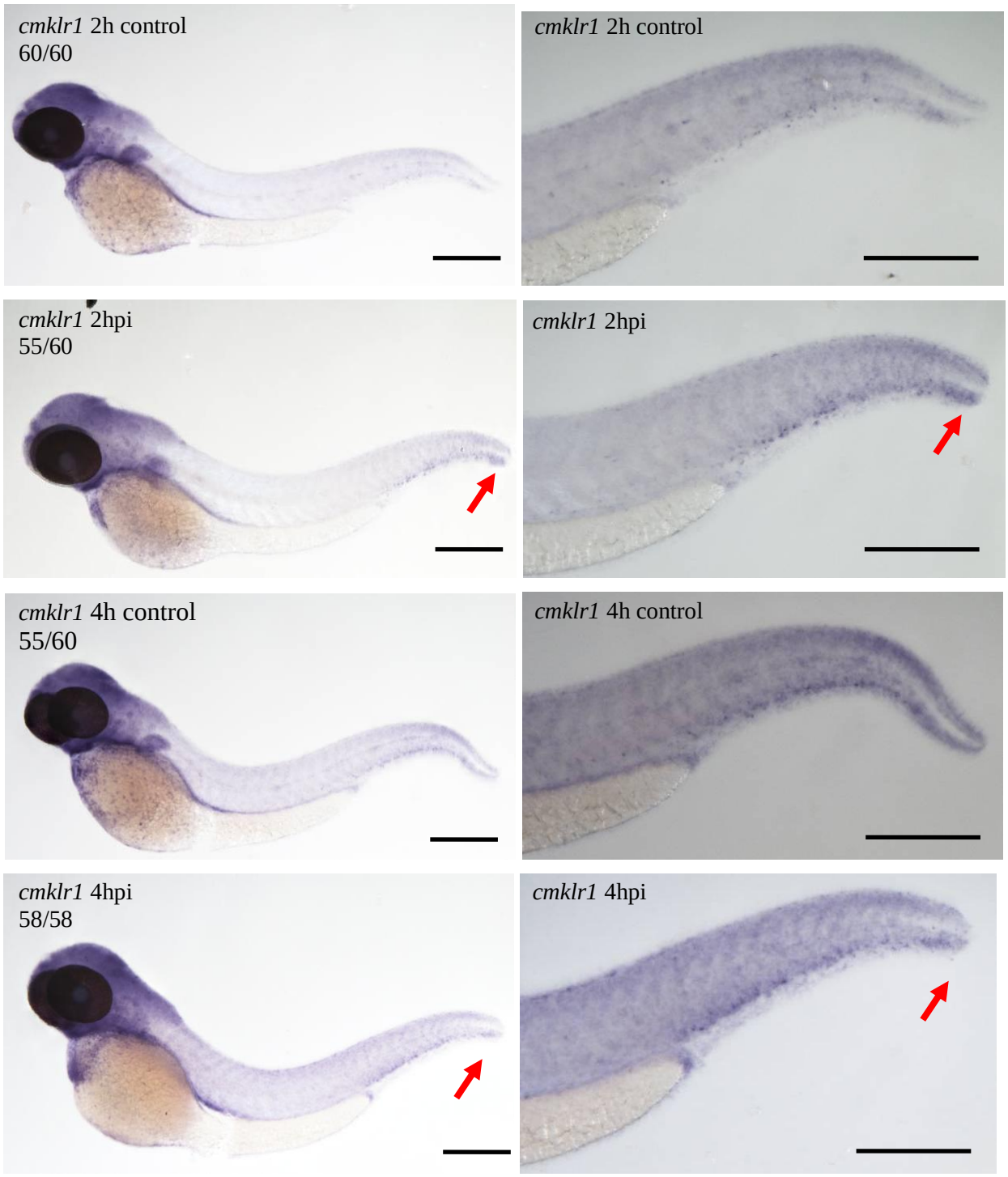

Figure 4-7: *cmklr1* WISH at 2 and 4hpi. Injured and control (uninjured) 2dpf nacre larvae were fixed at similar time periods at 2hpi and 4hpi. Representative images shown taken on Nikon Extended Focus SMZ stereomicroscope. Scale bar = 250 µm. The number of larvae that demonstrated the staining pattern shown at each time point is noted at the top left of each image. Two independent repeats performed to obtain total larval numbers.Area of tailfin injury indicated by red arrows.

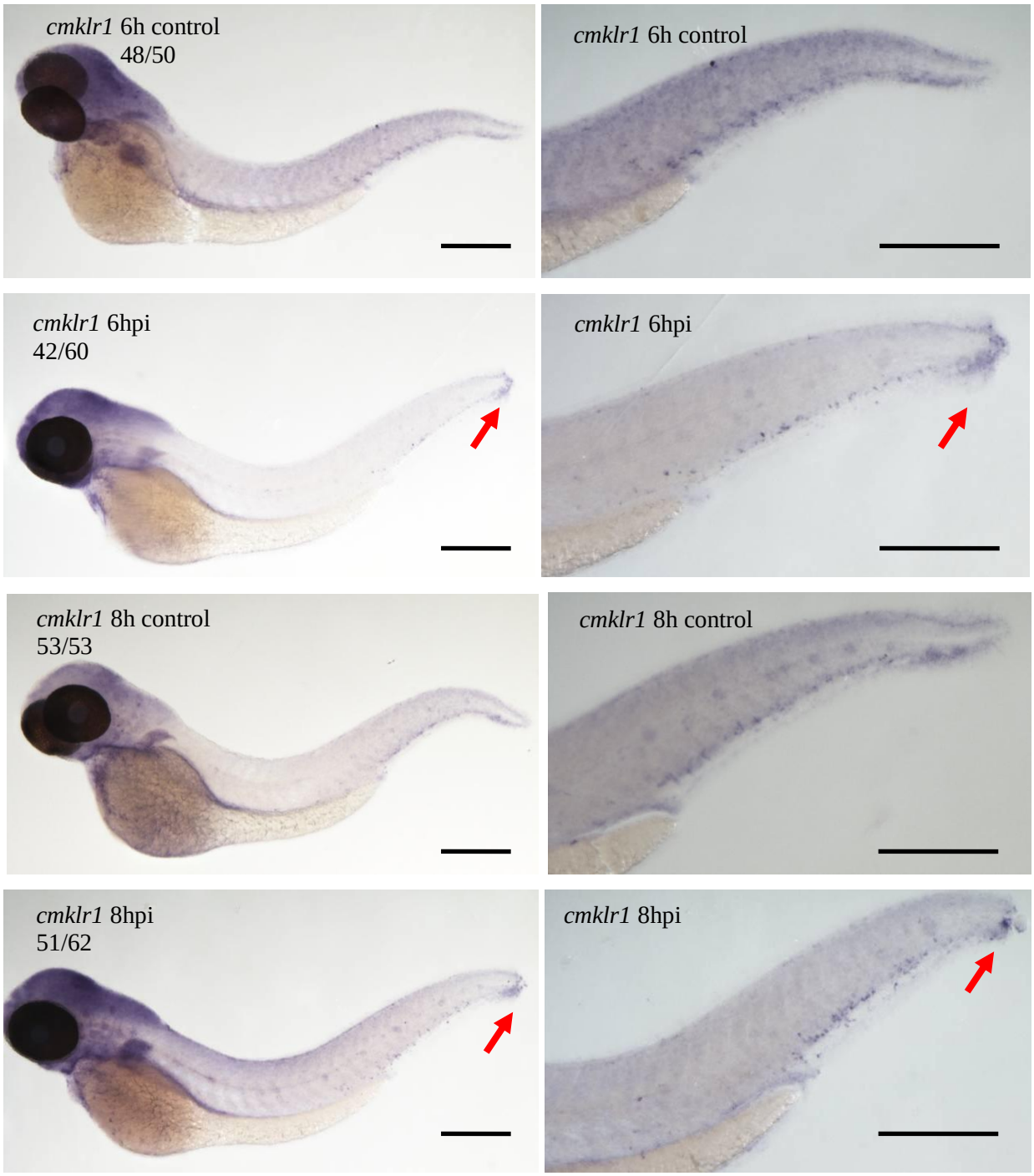

Figure 4-8: *cmklr1* WISH at 6 and 8hpi. Injured and control (uninjured) 2dpf nacre larvae were fixed at time points 6hpi and 8hpi. Representative images shown taken on Nikon Extended Focus SMZ stereomicroscope. Scale bar = 250 µm. The number of larvae that demonstrated the staining pattern shown at each time point is noted at the top left of each image. Two independent repeats performed to obtain total larval numbers. .Area of tailfin injury indicated by red arrows.

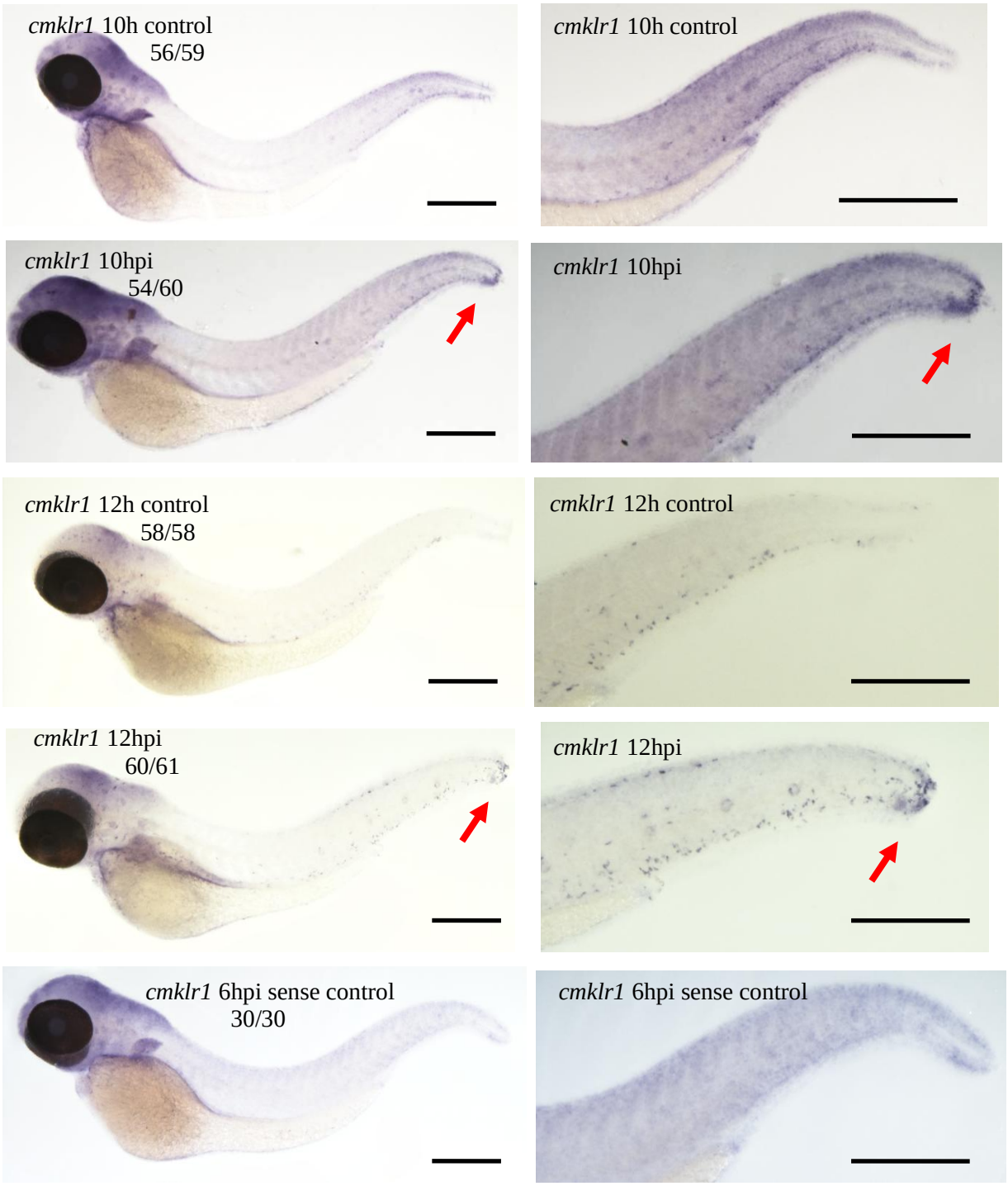

Figure 4-9: *cmklr1* WISH at 10 and 12hpi. Injured and control (uninjured) 2dpf nacre larvae were fixed at time points 10hpi and 12hpi. Representative images shown taken on Nikon Extended Focus SMZ stereomicroscope. Scale bar = 250 µm. The number of larvae that demonstrated the staining pattern shown at each time point is noted at the top left of each image. Two independent repeats performed to obtain total larval numbers. Area of tailfin injury indicated by red arrows.

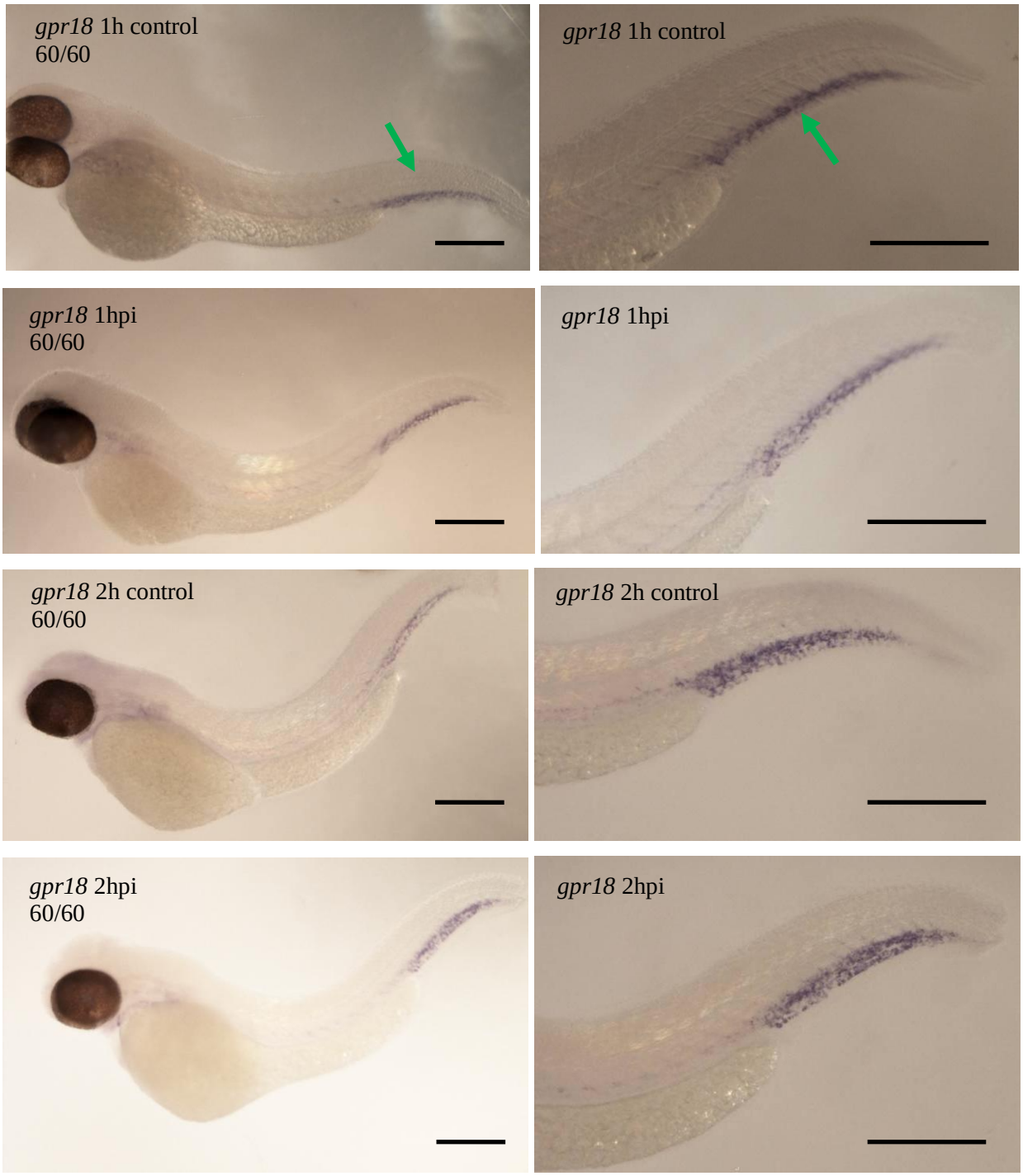

Figure 4-10: *gpr18* WISH at 1 and 2hpi. Injured and control (uninjured) 2dpf nacre larvae were fixed at time points 1hpi and 2hpi. Representative images shown taken on Nikon Extended Focus SMZ stereomicroscope. The CHT is indicated by the green arrow. Scale bar = 250µm. The number of larvae that demonstrated the staining pattern shown at each time point is noted at the top left of each image. Two independent repeats were performed to obtain total larval numbers.

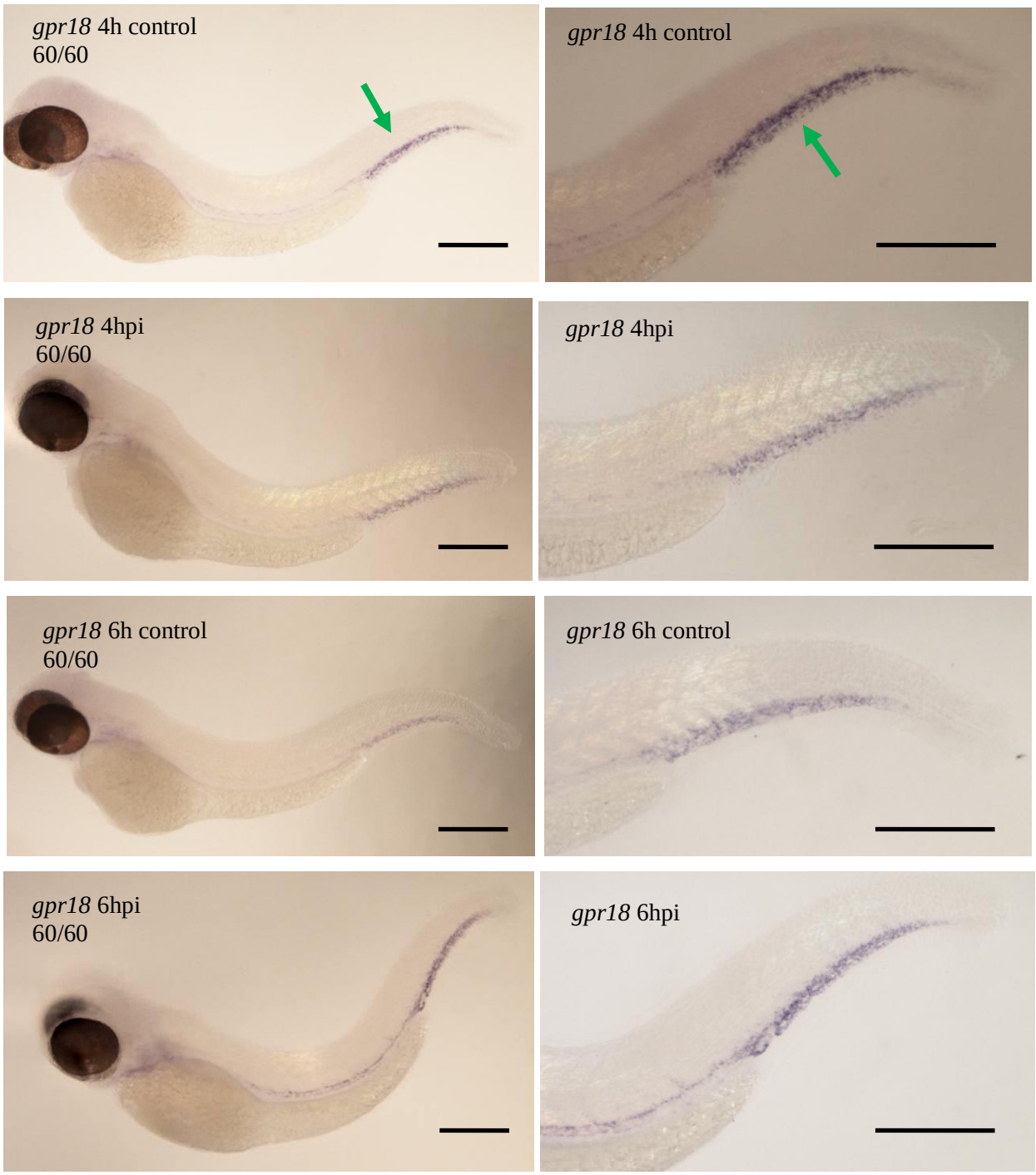

Figure 4-11: *gpr18* WISH at 4 and 6hpi. Injured and control (uninjured) 2dpf nacre larvae were fixed at time points 4hpi and 6hpi. Representative images shown taken on Nikon Extended Focus SMZ stereomicroscope. The CHT is indicated by the green arrow. Scale bar = 250µm. The number of larvae that demonstrated the staining pattern shown at each time point is noted at the top left of each image. Two independent repeats were performed to obtain total larval numbers.

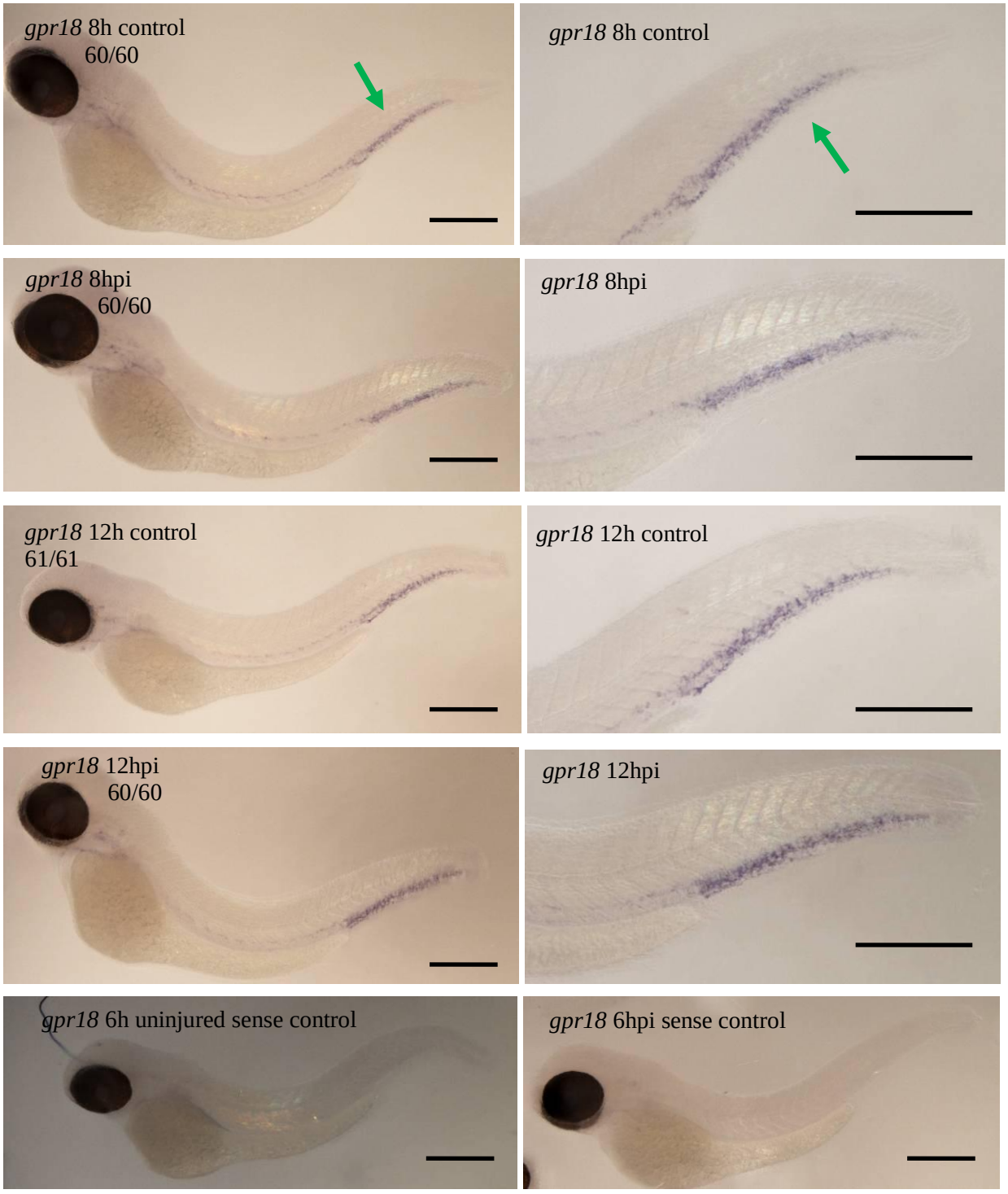

Figure 4-12: *gpr18* WISH at 8 and 12hpi. Injured and control (uninjured) 2dpf nacre larvae were fixed at time points 8hpi and 12hpi. Representative images shown taken on Nikon Extended Focus SMZ stereomicroscope. The CHT is indicated by the green arrow. Scale bar = 250 µm. The number of larvae that demonstrated the staining pattern shown at each time point is noted at the top left of each image. Two independent repeats were performed to obtain total larval numbers.

4.2.7 **Setup of Tomographic RNA sequencing (TomoSeq)**

Because of the inherent uncertainties of RNA over-expression, its limitation to early stages of development, and the increasing importance of the transcriptomics landscape, it was of interest to determine if endogenous inflammasome expression could be observed tomographically in the zebrafish. This method has been used previously in uninjured 1dpf zebrafish embryos (Junker *et al.*, 2014). However, given the much larger size of the 2dpf zebrafish, and the intention to capture spatial expression of the inflammasome, thinner slices would be required, and anatomical comparison would be paramount. In all samples, sequenced slices would begin at the start of the pigment line, which also corresponded with the line of tailfin amputation, with 70 slices each of 9 µm, totalling a distance of 630 µm. The following 25 slices would then start from the cloaca and extend cranially with each slice having a thickness of 25µm, giving a total distance of 625 µm (Figure 4-13). A minimum of two million 50 bp paired-end reads were generated from each larvae. A total of six larvae were sequenced, three controls and three injured, pooled across two lanes in two separate runs, with an even balance of controls and injured in each run to minimise technical bias. Reads were aligned using Ensembl Genome Reference Consortium Zebrafish Build 10 (GRCz10) sequence (Howe *et al.*, 2013).

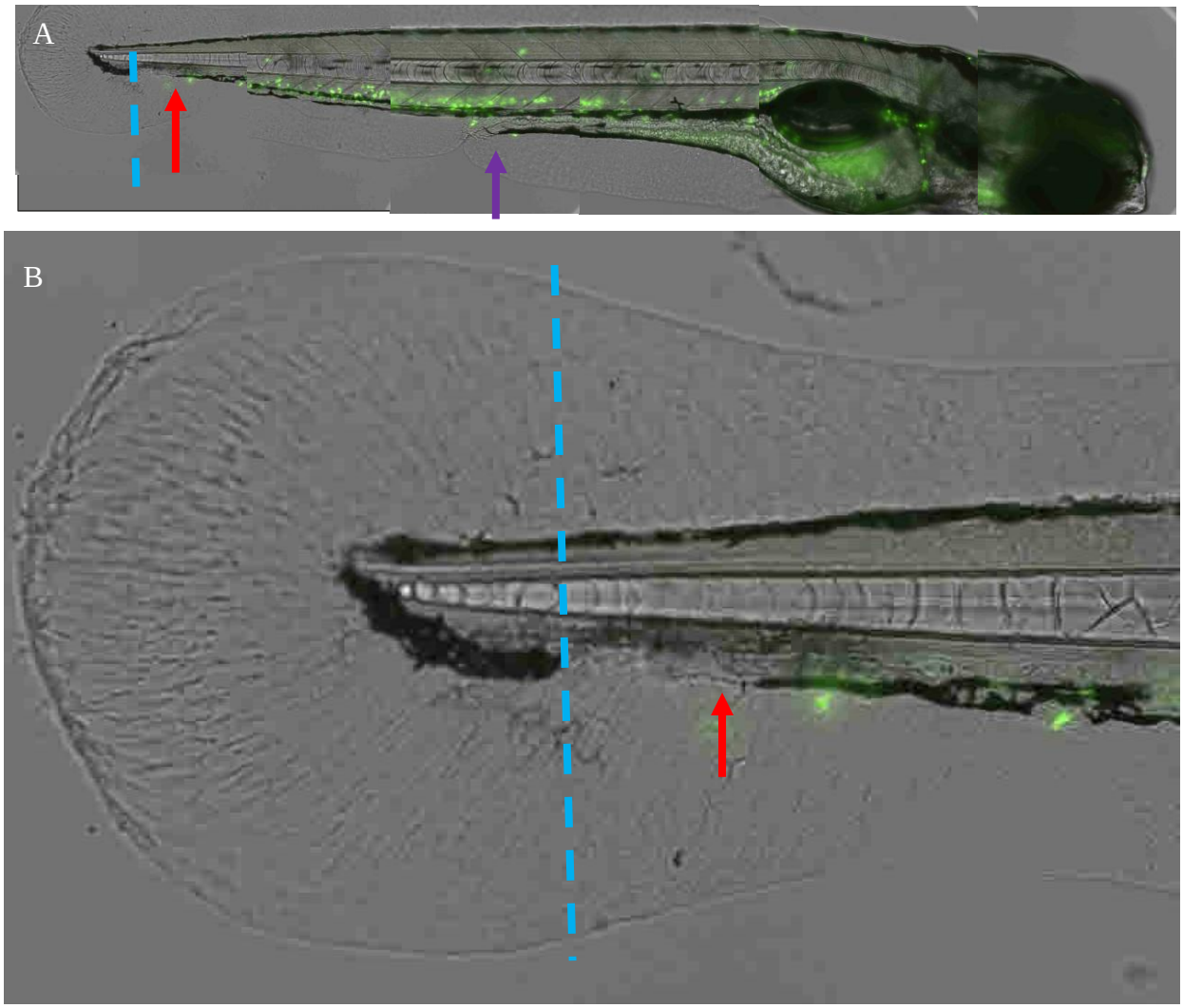

Figure 4-13: Representative images showing a 2dpf zebrafish larvae of *TgBAC(mpx:GFP)i114* and position of frozen sectioning. A. Merged brightfield and GFP fluorescent channels using a Nikon Eclipse TE2000-U microscope, and image stitched using NIS Elements AR®. Sectioning began at the break in the pigment line shown by the blue dotted line in the uninjured fish (this is also the region where injury is performed), with the 71st slice taken at the cloacal opening marked by the purple arrow. **B**. This enlarged image shows the circulation end more clearly, and is marked by the red arrow (similar to image A). The orientation of both images are opposite to that conventionally used to depict zebrafish, and has been intentionally flipped to allow easy association with the graphs subsequently plotted in this chapter.

4.2.8 **Preliminary validation of the TomoSeq results**

In order to compare RNA and GFP expression, images were taken at 6hpi of uninjured and injured *TgBAC(mpx:GFP)i114* 2dpf larvae, immediately prior to the samples being flash frozen in OCT as per methods in Section 2.6.1. Three replicates of an uninjured control, as well as an injured larva were obtained. In the first uninjured control, although *mpx* expression was low, it appeared to match GFP expression (Figure 4-14). Unfortunately, in the second control, the primers failed for slice 20, corresponding to the area of bright fluorescence (Figure 4-15) but although *mpx* expression did not appear to fully match the observed fluorescence seen on imaging of the third control (Figure 4-16), total expression remained low. This slight discrepancy could be for two reasons, either the neutrophils had moved in the time between imaging and freezing (samples were fresh frozen), or it is possible that *mpx* mRNA expression occurred at haematopoietic sites in the quiescent state (Shen *et al.*, 2013) and this expression could have been captured in the sectioned slices. Nonetheless, *mpx* expression in the all the injured fish appeared to correlate well with GFP expression (Figure 4-17 to Figure 4-19). Next, *mmp2* and *mmp9* profiles were assessed since inflammatory neutrophils in mice attending to an area of ischaemia express high levels of matrix metalloproteinases (MMP) (Daseke *et al.*, 2019). In the controls, levels of *mmp* expression were generally very low and no specific expression pattern could be seen. In the injured specimens however, levels of *mmp* expression were higher and high levels of *mmp9* correlated strongly with the wound edge, while *mmp2* appeared to have a similar pattern to *mpx*. Finally, given the thin slices, it was not always possible to determine by eye if tissue sectioning occurred at the very first slice with the injured larvae despite the guiding bead. Therefore, *col1a1a*, highly expressed in skin, was plotted to allow determination of the first slice of injured larvae that would contain tissue, and thus allow accurate comparison across injured specimens. Expression of *col1a1a* showed that for the first injured larvae, tissue sectioning started at slice 12 (Figure 4-17), for the second injured larvae slice 4 (Figure 4-18), and for the third, slice 24 (Figure 4-19). It was not possible to determine if all the uninjured larvae were sectioned at a similar point of tissue, partly because of the differing rates of growth between larvae even when reared under similar conditions, and partly because no suitable tissue markers are currently known. However, it was assumed that in the absence of inflammation, small differences in starting point would not influence overall comparison of readings in the absence of an inflammasome.

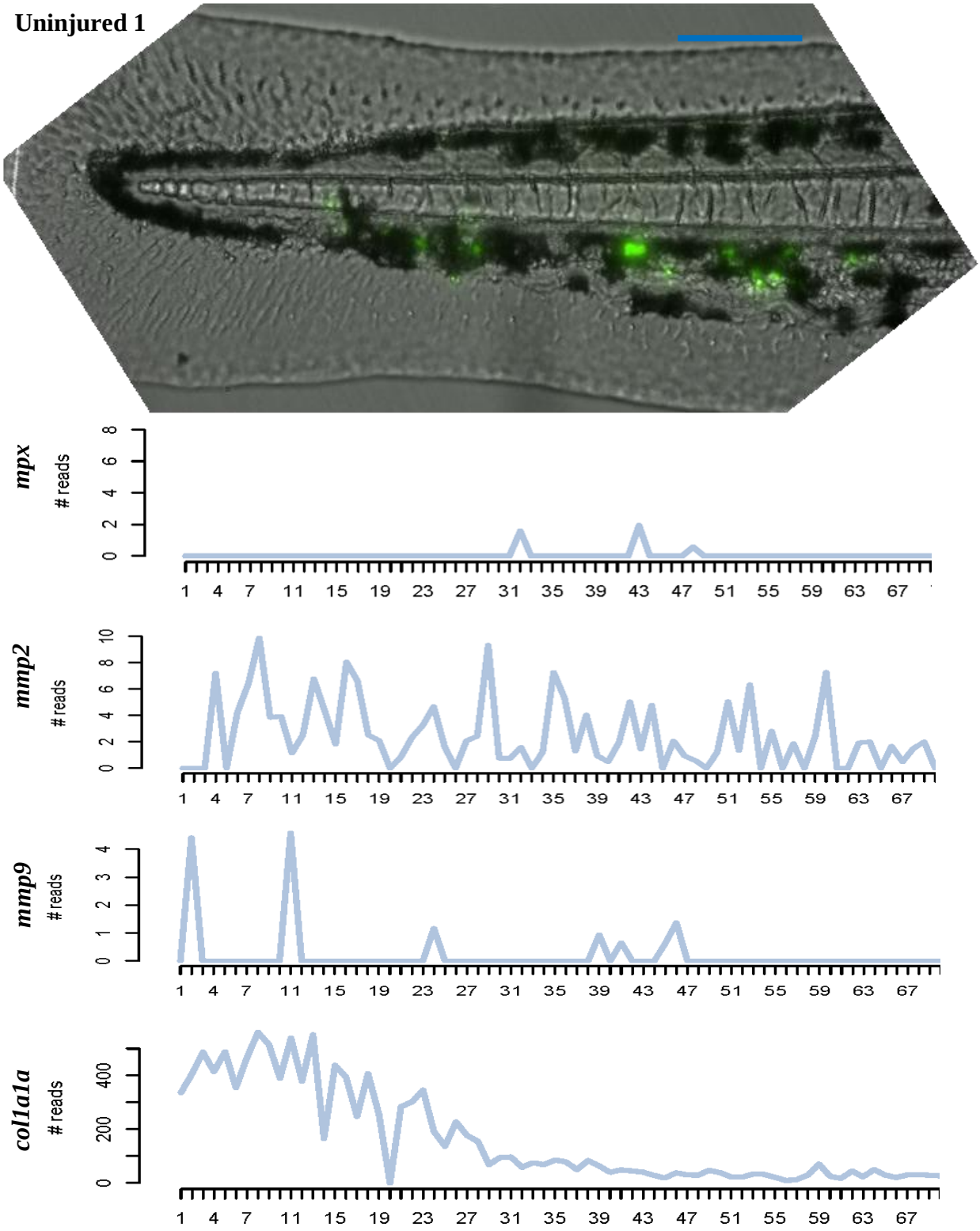

Figure 4-14: First uninjured control larva. Merged brightfield and GFP fluorescent channels using a Nikon Eclipse TE2000-U microscope Blue scale bar = 100 µm. Gene reads plotted according to TomoSeq slice (each of 9µm) and matched to image.

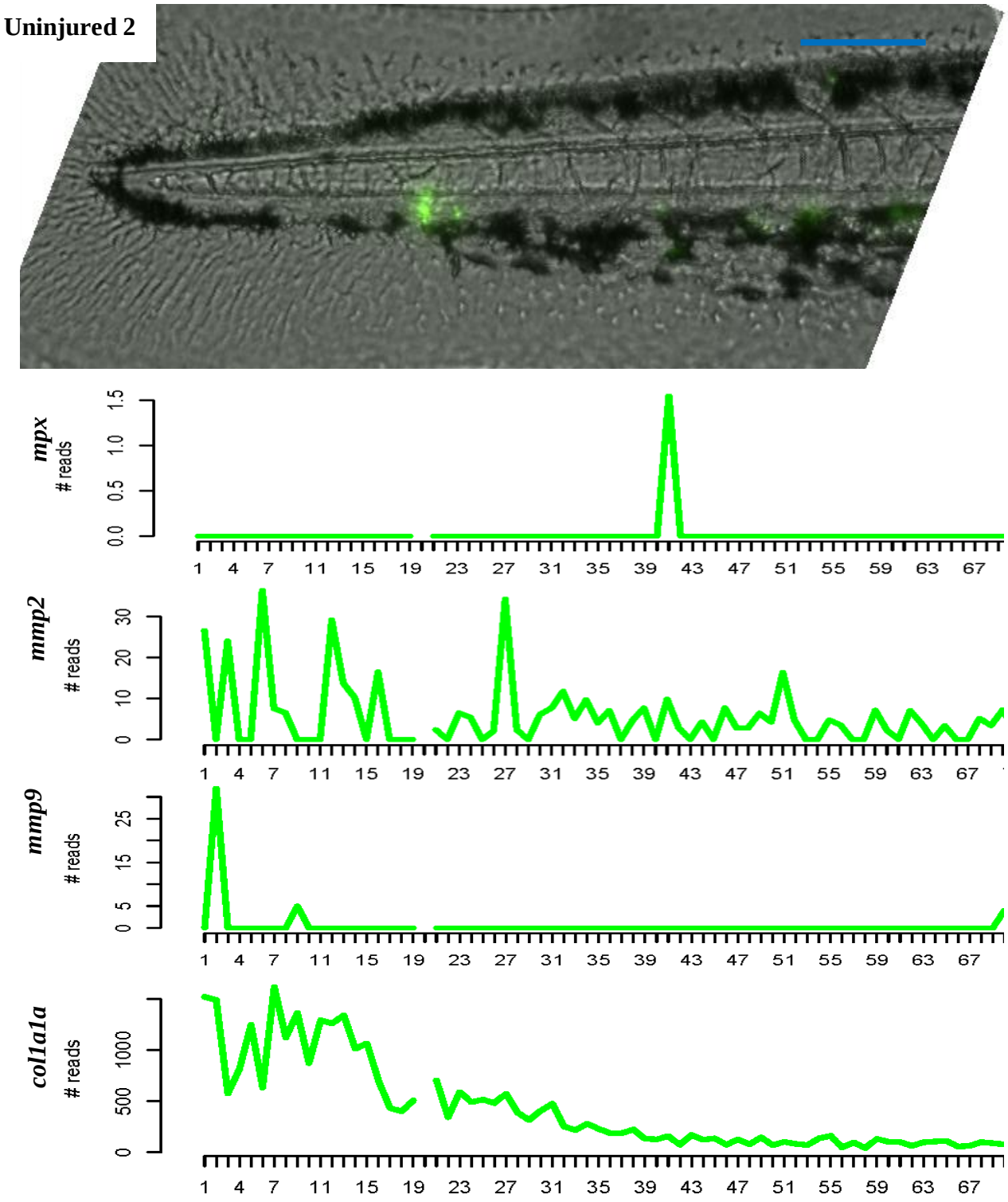

Figure 4-15: Second uninjured control larva. Merged brightfield and GFP fluorescent channels using a Nikon Eclipse TE2000-U microscope Blue scale bar = 100 µm. Gene reads plotted according to TomoSeq slice (each of 9µm) and matched to image. In this sample, primers for slice 20 failed to read and therefore was automatically excluded from the reads.

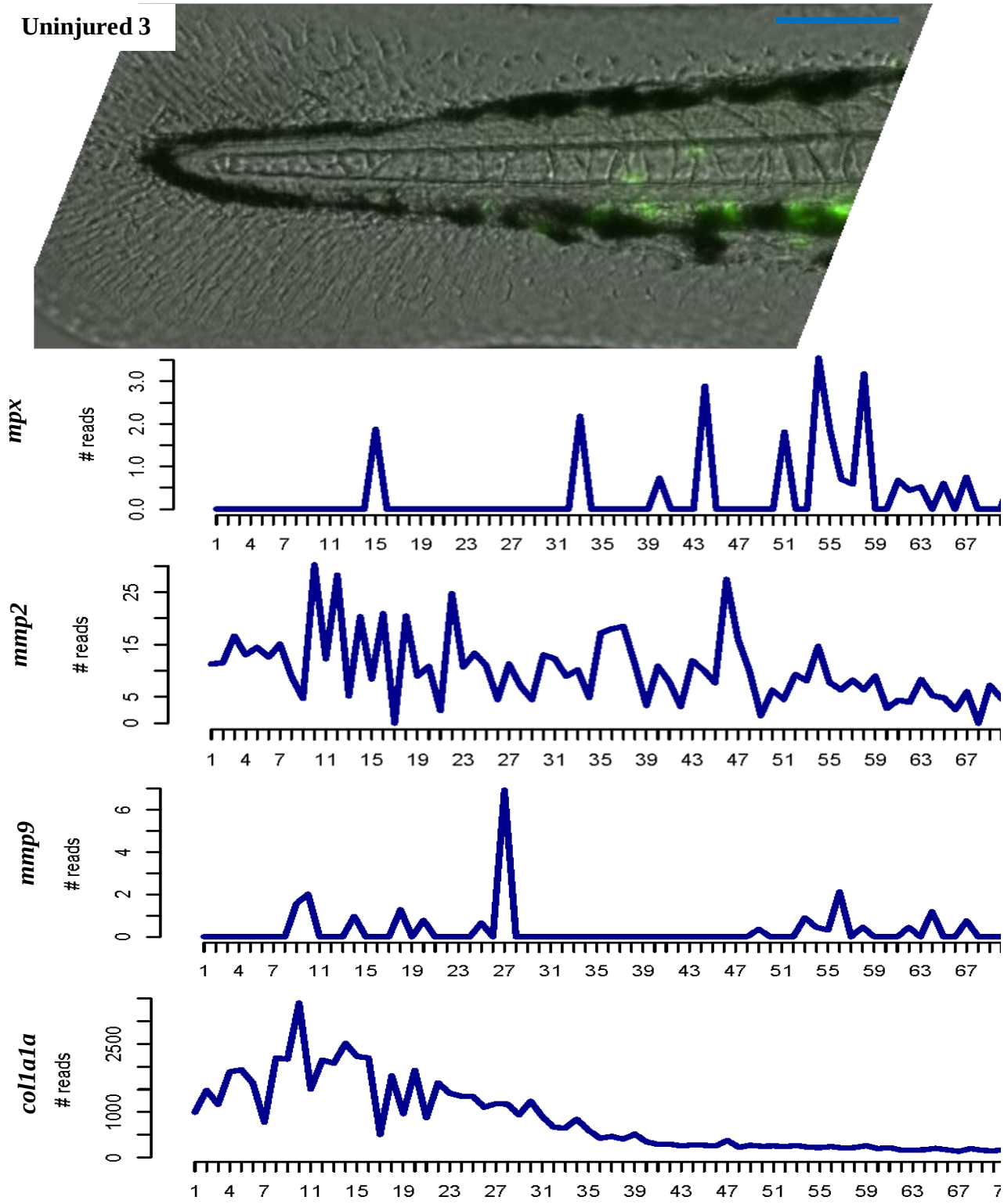

Figure 4-16: Third uninjured control larva. Merged brightfield and GFP fluorescent channels using a Nikon Eclipse TE2000-U microscope Blue scale bar = 100 µm. Gene reads plotted according to TomoSeq slice (each of 9µm) and matched to image.

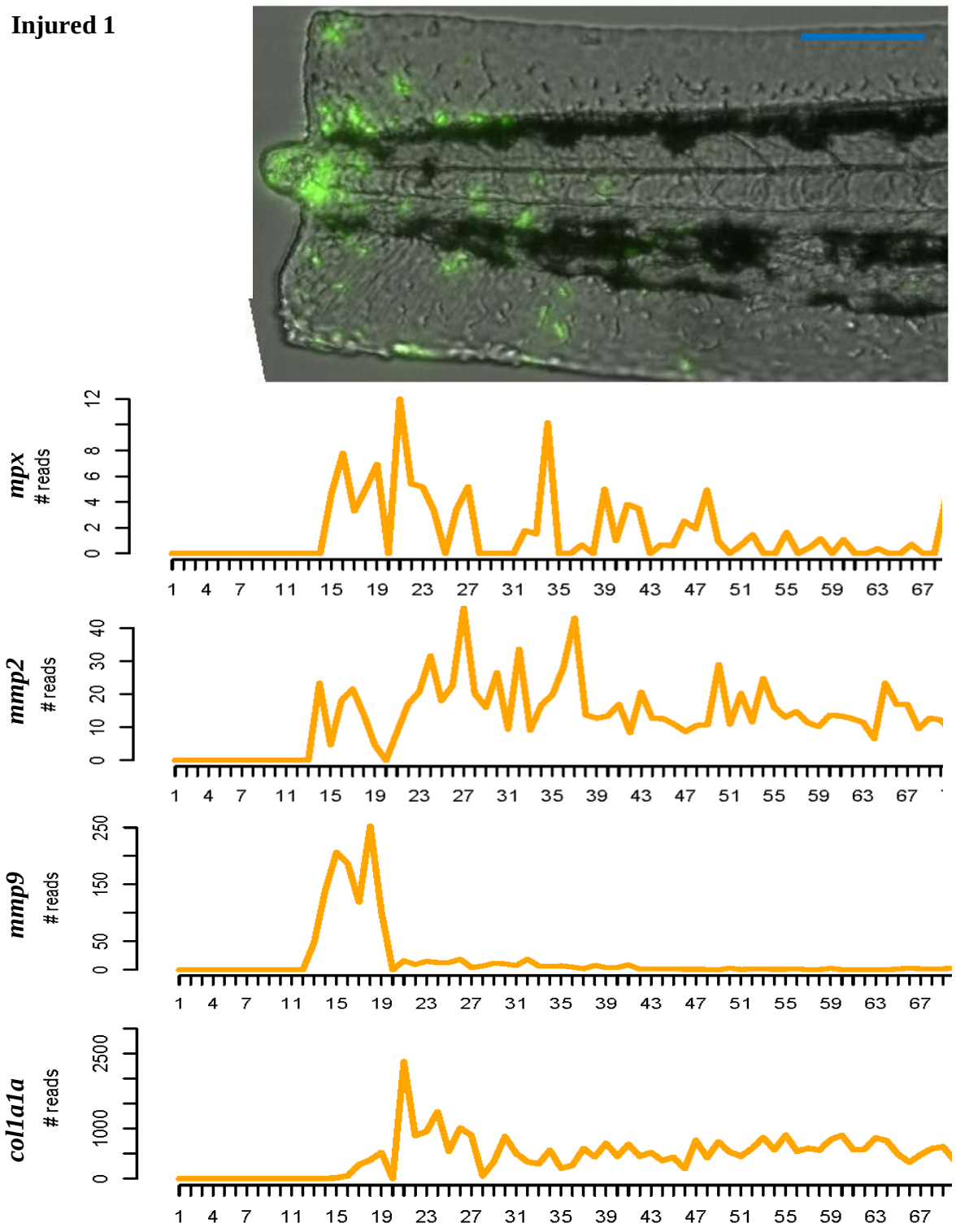

Figure 4-17: First injured larva. Merged brightfield and GFP fluorescent channels using a Nikon Eclipse TE2000-U microscope Blue scale bar = 100 µm. Gene reads plotted according to TomoSeq slice (each of 9µm) and matched to image.

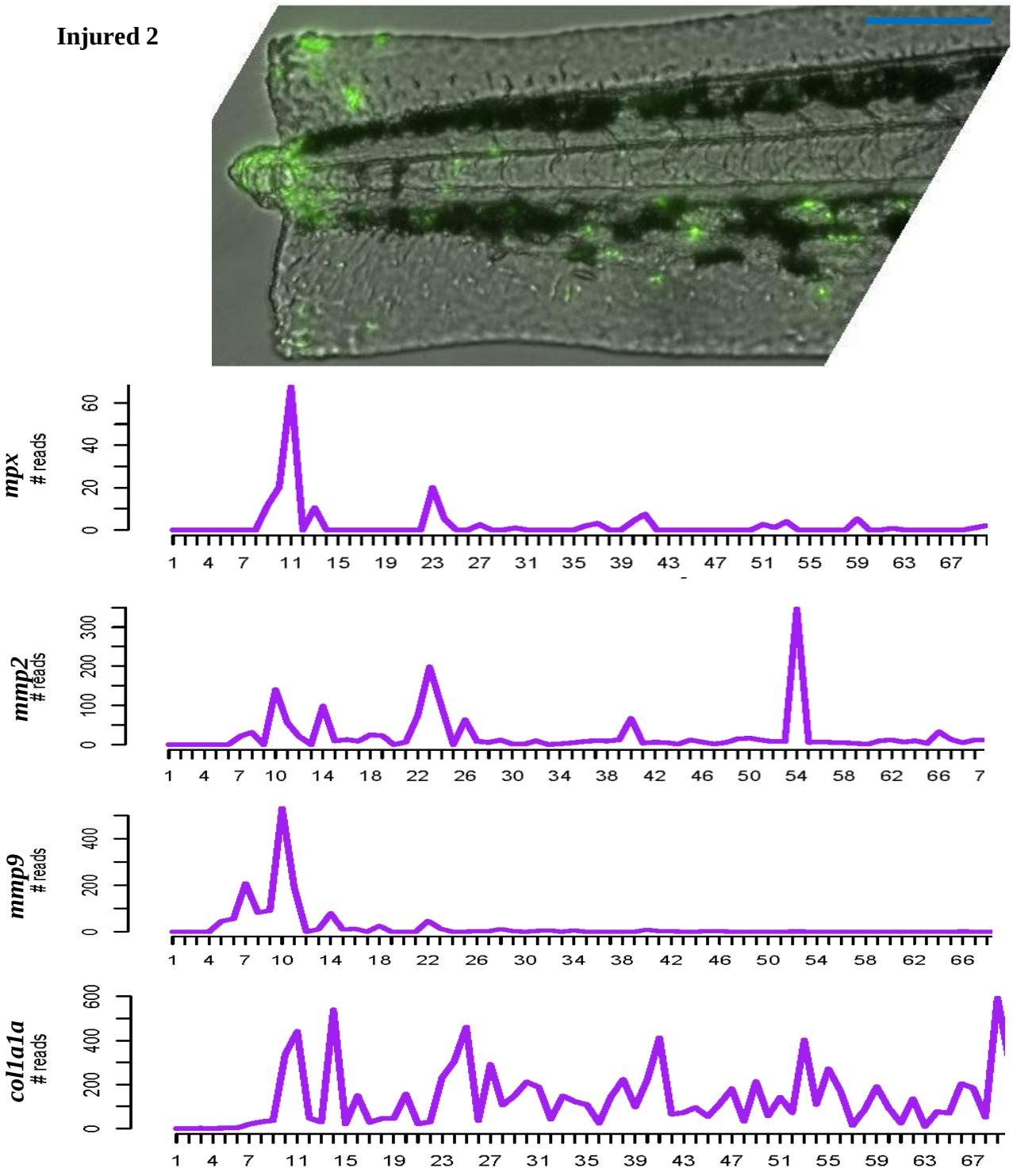

Figure 4-18: Second injured larva. Merged brightfield and GFP fluorescent channels using a Nikon Eclipse TE2000-U microscope Blue scale bar = 100 µm. Gene reads plotted according to TomoSeq slice (each of 9µm) and matched to image.

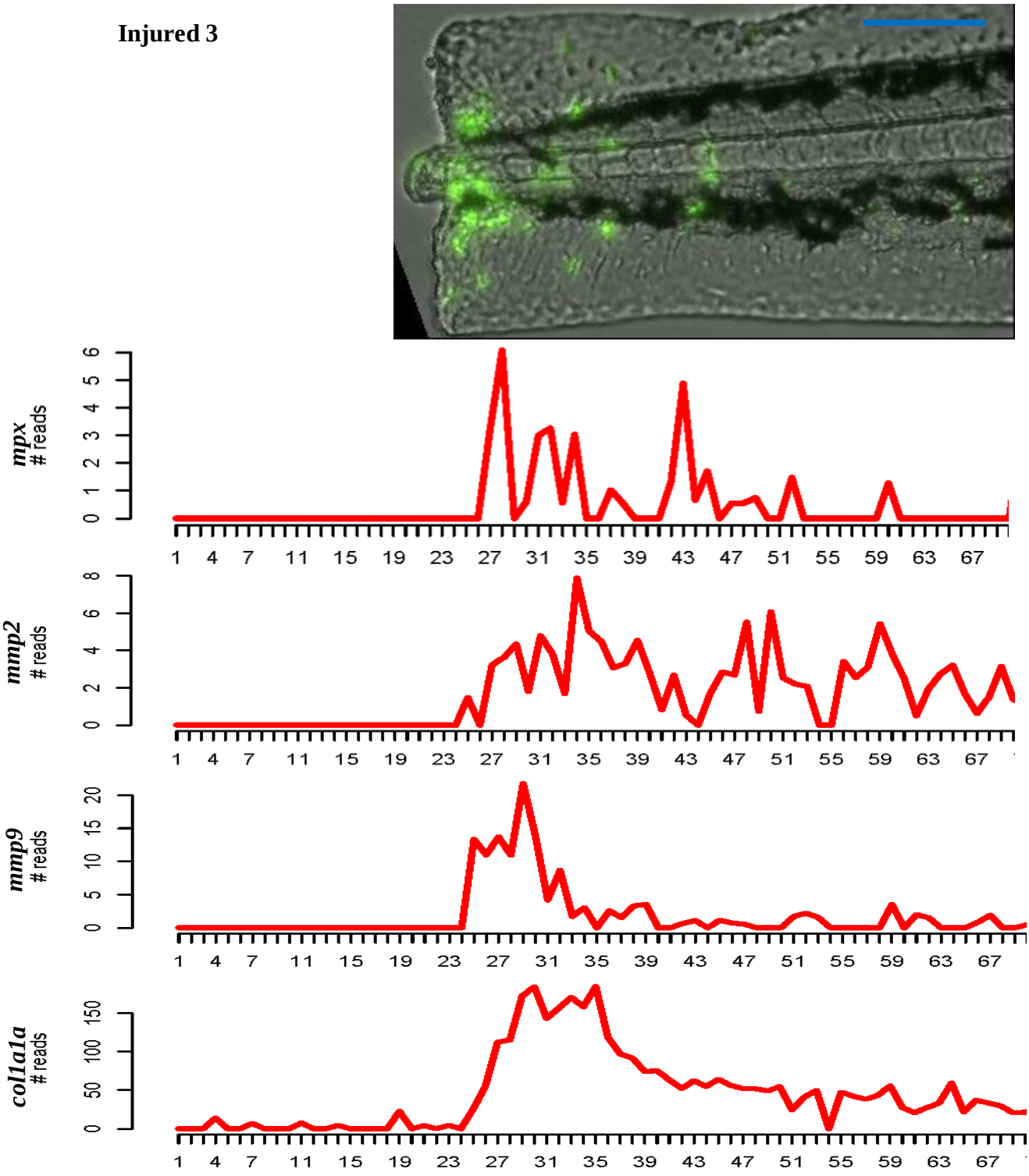

Figure 4-19: Third injured larva. Merged brightfield and GFP fluorescent channels using a Nikon Eclipse TE2000-U microscope Blue scale bar = 100 µm. Gene reads plotted according to TomoSeq slice (each of 9µm) and matched to image.

4.2.9 **Expression patterns of genes known to play a role in inflammation or have anatomical specificity recapitulated known patterns**

Probing the genes expressed within the injured segments revealed that a gene *cyr61l1* is highly expressed at the leading edge of the wound. This gene is highly conserved in mammals and teleosts, and under quiescent conditions has a low expression (Lau, 2011). This concurs with the results of the TomoSeq, in which the controls express only sporadic low level (<1) reads, mainly in the proximal body. However, in injured larvae, its synthesis is highly concentrated (>15) at the wound edge (Figure 4-20). As such, in future TomoSeq analyses comparing amputated tailfins, this gene would form a useful marker to delineate the wound edge, in addition to *col1a1a*, to allow accurate comparison of sections.

Investigation was then extended to the LOX enzymes. Generic constitutive expression of *alox12* was seen, without obvious difference between injured and uninjured fish (Figure 4-21B). This concurs with published data on *alox12* expression (Haas *et al.*, 2011).

Two final validation steps were performed. The first was with expression of *cldn15la*. This tight junction protein is known specifically to localise to the gills, GIT, kidneys and the gonads and is not found elsewhere (Sun *et al.*, 2015). In keeping with this, expression was only seen in slice 70 onwards (Figure 4-21B), coinciding with the cranially oriented sections from the cloacal region involving the intestinal region. Finally, expression of *alpi.1*, the intestinal-specific isoform of alkaline phosphatase was assessed. Surprisingly, constitutive expression of this gene, outside the intestine was seen in both injured and uninjured (Figure 4-21C). Although the zebrafish possesses other non-intestinal isoforms of alkaline phosphatase, these were not detected in this assay. This extra-intestinal expression of *alpi.1* has previously been seen in unpublished *in situ* hybridisation work (Thisse and Thisse, 2004) submitted directly to ZFIN, showing expression from the 1-4 somite stage onwards in the segmental plate, developing fin fold, and otic vesicles. The exact role played by this enzyme, and the importance of its expression in extra-intestinal regions during this time of development, has not yet been determined.

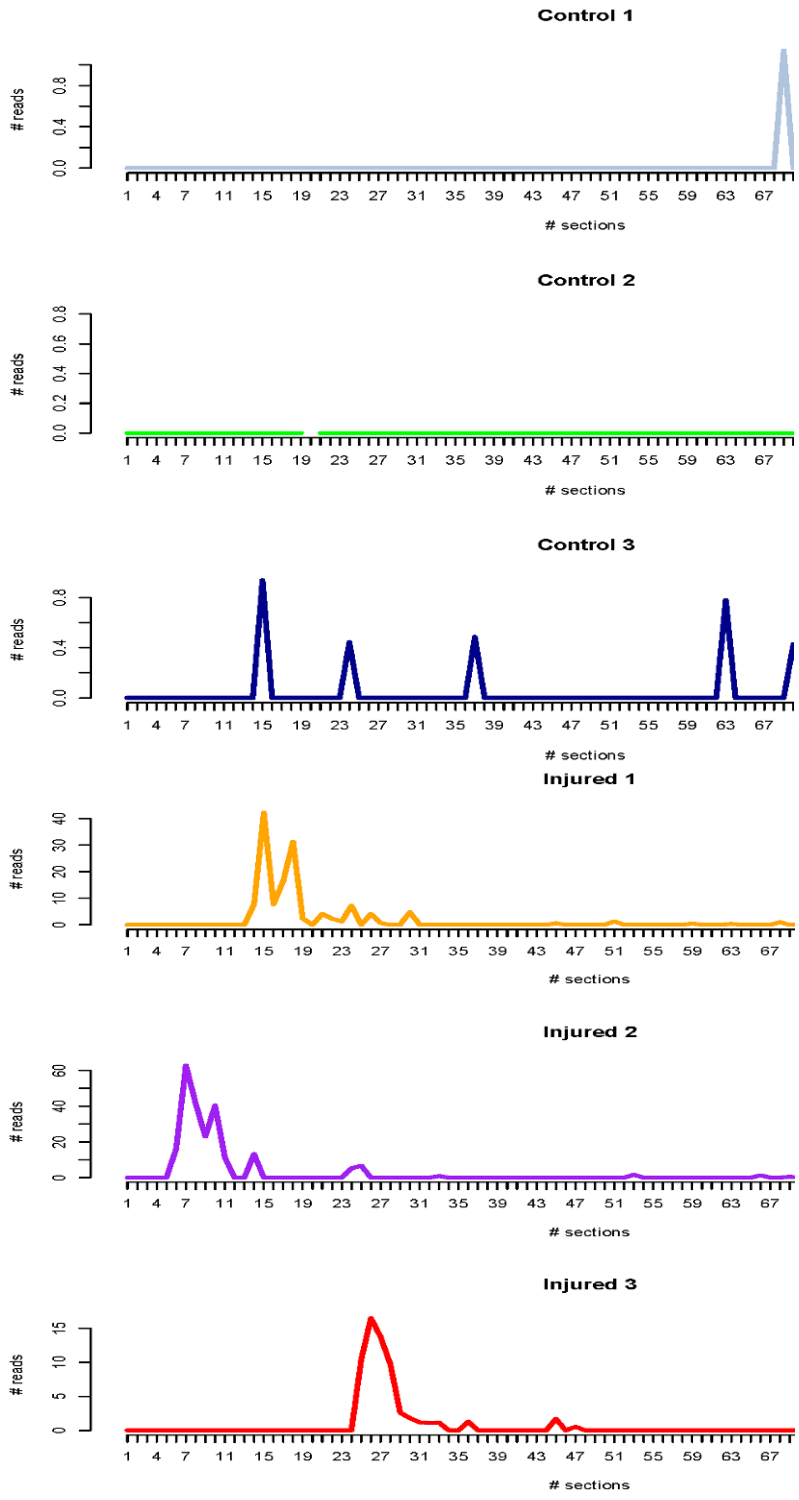

Figure 4-20: Expression of *cyr61l1*, an acute phase protein, along the zebrafish tailfin. Low level (<1) reads are seen in all three control fish. Expression is increased and coincides sharply with the demarcation of injury in the injured fish, section 13 in Injured 1, section 5 in Injured 2, and section 24 in Injured 3.

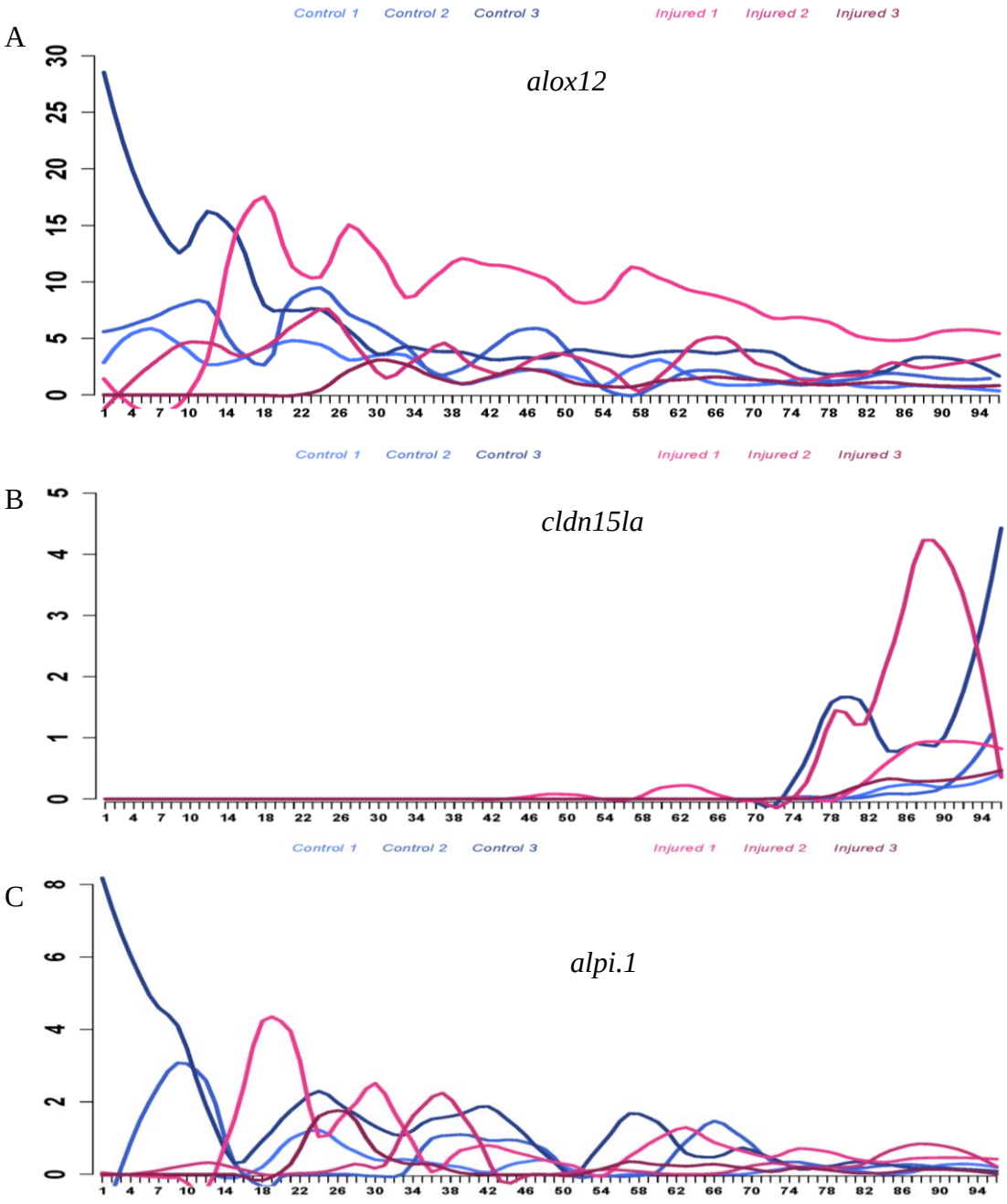

Figure 4-21: Expression patterns across all the zebrafish for *alox12*, *cldn15la*, and *alpi.1*. Plots were done on a single axis to allow comparison across all six specimens. **A**. *alox12* is expressed in both injured (lines with red hues) and uninjured (lines with blue hues). **B**. *cldn15la* is expressed exclusively in the GIT and gonads and expression is seen only after slice 70, where the GIT starts. **C**. *alpi.1* is expressed extra-intestinally, in a pattern not dissimilar to *alox12*.

4.2.10 **Top genes expressed in uninjured controls compared with injured larvae**

Using the starting points determined earlier for the injured larvae, data from each zebrafish were analysed individually to allow normalisation to spike-in RNA. Comparison was made of the region 100µm at the injured end compared to a segment of tailfin approximately 500µm cranial to this. The three datasets were then cross-analysed to select those genes listed in the top 100 which were expressed across all three samples. The top ten genes for the control and injured groups are shown in Table 4-1. Of the genes expressed in the uninjured group, all of them were involved in development. For example *and1*, *and2* and *and3* are vital in development of the fin-fold (König *et al.*, 2017). Indeed, *and1* has been shown to be required for tailfin development and fluorescent reporter lines (Lalonde *et al.*, 2016; Phan *et al.*, 2019, p. 1) show expression only starting at 2dpf. *lama5* and *frem2a* are also essential components of all basement membranes and vital for homeostasis and development (Sztal *et al.*, 2011), while *angptl7* is angiogenesis regulator (Niki, Katsu and Yokouchi, 2009), and *c1qtnf5* a neurogenesis regulator. Of the top genes shared by all three injured larvae, almost all are exclusively expressed only in the injured fish, and are involved in collagen metabolism (*mmp9, mmp13b*), and responses to biotic stimuli (*lect2l, cyr61l1, serpine1*).

Table 4-1: Top ten expressed genes in all three larvae in the injured and uninjured groups.

Top ten shared genes in uninjured larvae	Top ten shared genes in injured larvae	Top ten exclusively injured genes
lama5	*tgm2l*	*tgm2l*
angptl7	*serpine1*	*serpine1*
c1qtnf5	*FO704661.1*	*FO704661.1*
and2	*mmp9*	*lect2l*
col1a1a	*lect2l*	*csf2rb*
and1	*csf2rb*	*mmp13b*
and3	*mmp13b*	*pprc1*
frem2a	*pprc1*	*sall1b*
fgf24	*sall1b*	*cyr61l1*
qdpra	*cyr61l1*	*junba*

4.2.11 **Differential genes were up- and down- regulated in Go enrichment analysis**

Analysis was performed using GOrilla (http://cbl-gorilla.cs.technion.ac.il) (Eden *et al.*, 2009) to allow ranking of genes common to the control uninjured group, or to the injured group, against reference genes for ontological comparison. The control group of genes had significant enhancement in genes involved in appendage or fin differentiation and development (Figure 4-22, Table 4-2), while the injured group had an overall narrower selection of biological processes as seen in Figure 4-23 (Table 4-3), which was specific to the inflammatory response, as would be expected.

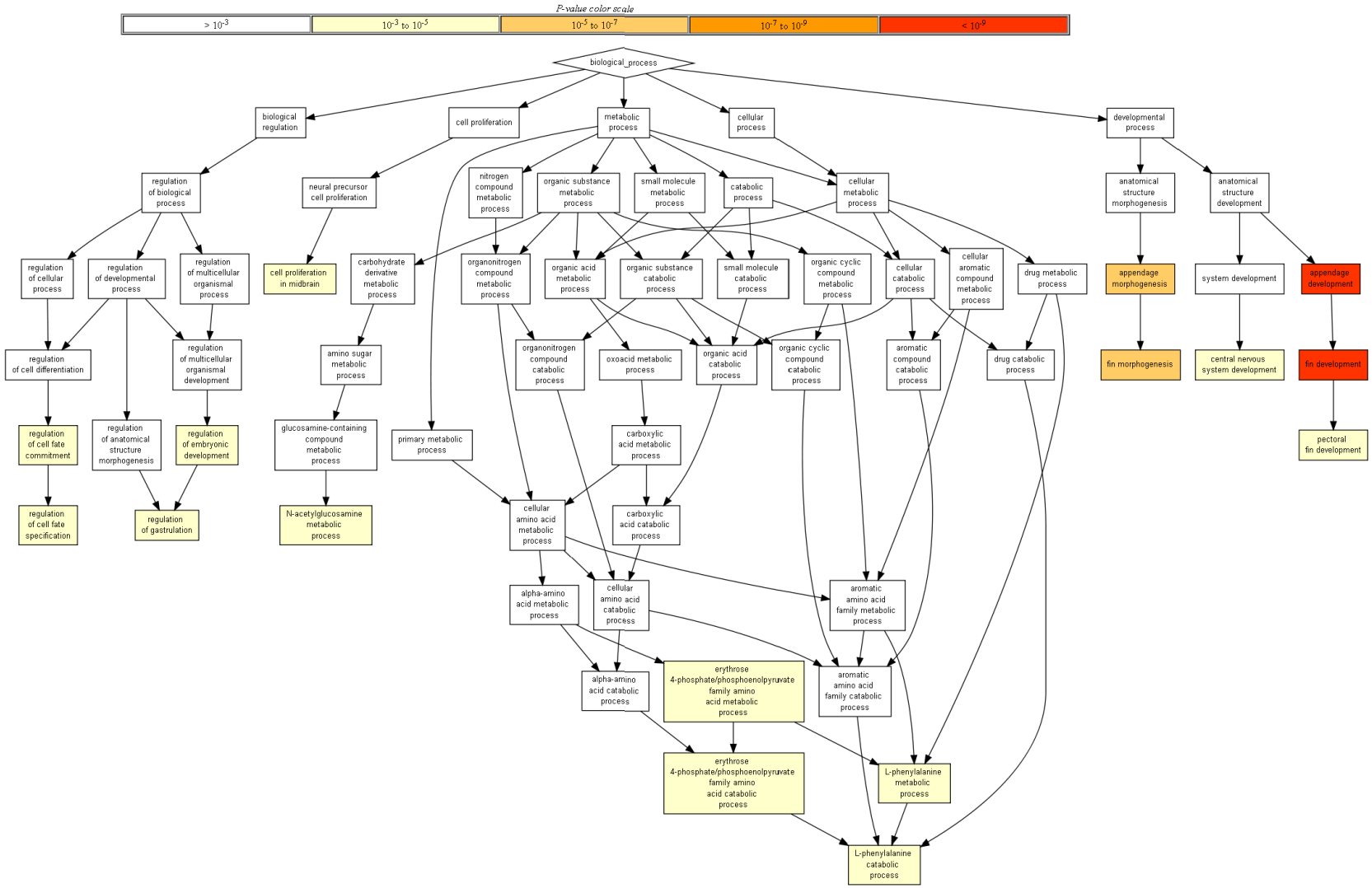

Figure 4-22: Biological processes linked to enriched analysis in GOrilla in uninjured larvae. The number of biological processes cover a large range, from metabolic processes to regulation of cell differentiation, but the highest expression were related to appendage, specifically fin, development, as would be expected for the region under investigation.

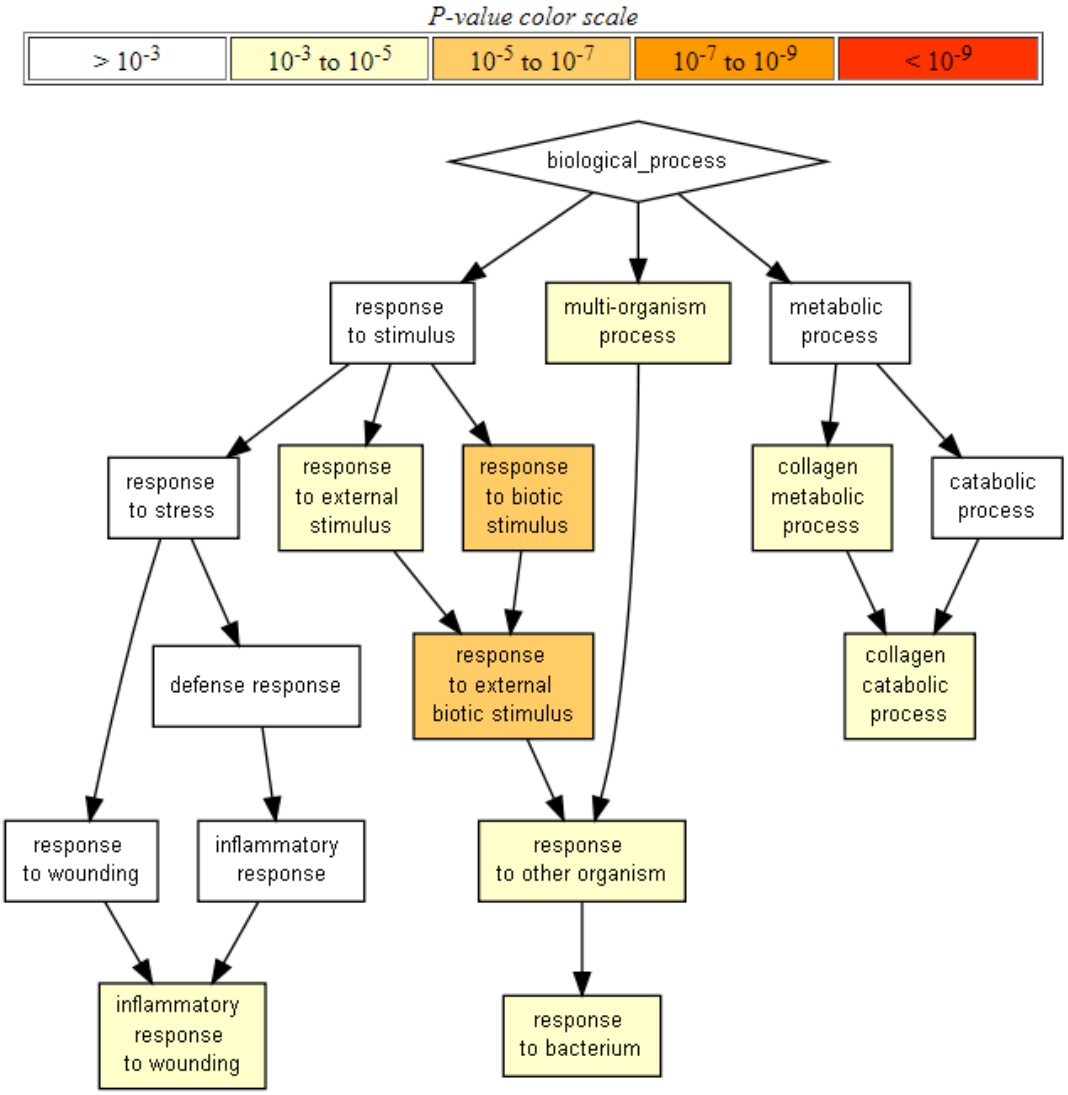

Figure 4-23: Biological processes linked to enriched analysis in GOrilla in injured larvae. The number of biological processes were streamlined to three main processes, the inflammatory response to wounding, response to bacterium ingress, and collagen catabolism.

Table 4-2: Go enrichment of conserved control genes

GO term	Description	P-value	FDR q-value	Enrichment (N, B, n,b)	Genes
GO:0033333	fin development	2.04E-10	1.60E-06	29.45 (10768, 45, 65, 8)	*plod1a* *frem2a* *and2* *col1a1a* *bhlha9* *fgf24* *and1* *lama5*
GO:0048736	appendage development	4.19E-10	1.64E-06	27.05 (10768, 49, 65, 8)	*plod1a* *frem2a* *and2* *col1a1a* *bhlha9* *fgf24* *and1* *lama5*
GO:0033334	fin morphogenesis	1.96E-07	5.11E-04	23.12 (10768, 43, 65, 6)	*plod1a* *frem2a* *col1a1a* *fgf24* *lama5*
GO:0035107	appendage morphogenesis	2.96E-07	5.81E-04	21.61 (10768, 46, 65, 6)	*plod1a* *frem2a* *col1a1a* *fgf24* *lama5*
GO:0007417	central nervous system development	5.33E-05	8.35E-02	12.18 (10768, 68, 65, 5)	*emx3* *ecrg4a* *zic2b* *zic2a* *vcana*
GO:0042659	regulation of cell fate specification	1.61E-04	2.10E-01	27.61 (10768, 18, 65, 3)	*eve1* *dusp6* *fgf24*
GO:0045995	regulation of embryonic development	4.02E-04	3.94E-01	11.42 (10768, 58, 65, 4)	*eve1* *dusp6* *fgf24* *lama5*
GO:0010470	regulation of gastrulation	5.54E-04	4.34E-01	18.41 (10768, 27, 65, 3)	*eve1* *dusp6* *fgf24*
GO:0006558	L-phenylalanine metabolic process	7.39E-04	4.83E-01	47.33 (10768, 7, 65, 2)	*qdpra* *pah*
GO:0006044	N-acetylglucosamine metabolic process	9.81E-04	4.81E-01	41.42 (10768, 8, 65, 2)	*renbp* *chst3a*

Table 4-3: Go enrichment of conserved injured genes

GO term	Description	P-value	FDR q-value	Enrichment (N, B, n,b)	Genes
GO:0043207	response to external biotic stimulus	4.79E-06	3.84E-02	10.29 (11533, 133, 59, 7)	*irg11* *mmp9* *irg1* *lect2l* *junba* *zgc:158446* *ncf1*
GO:0009607	response to biotic stimulus	5.29E-06	2.12E-02	10.14 (115333, 135, 59, 7)	*irg11* *mmp9* *irg1* *lect2l* *junba* *zgc:158446* *ncf1*
GO:0051707	response to other organism	1.96E-05	5.23E-02	10.66 (11533, 110, 59, 6)	*irg11* *mmp9* *irg1* *lect2l* *zgc:158446* *ncf1*
GO:0030574	collagen catabolic process	2.04E-05	4.08E-02	53.31 (115333, 11, 59, 3)	*mmp9* *mmp13b* *mmp13a*
GO:0009617	response to bacterium	2.08E-05	3.32E-02	14.81 (11533, 66, 59, 5)	*irg11* *mmp9* *irg1* *lect2l* *zgc:158446*
GO:0051704	multi-organism process	3.37E-05	4.49E-02	9.69 (11533, 121, 59, 6)	*irg11* *mmp9* *irg1* *lect2l* *zgc:158446* *ncf1*
GO:0009605	response to external stimulus	3.51E-05	4.01E-02	6.31 (115333, 248, 59, 8)	*irg11* *mmp9* *irg1* *lect2l* *junba* *zgc:158446* *ncf1* *lepb*
GO:0032963	collagen metabolic process	5.54E-05	5.54E-02	39.09 (11533, 15, 59, 3)	*mmp9* *mmp13a* *mmp13b*
GO:0090594	inflammatory response to wounding	5.31E-04	4.72E-01	55.85 (11533, 7, 59, 2)	*irg11* *mmp9*

4.2.12 **Growth and differentiation genes were up-regulated in controls and stimulus response genes in injured**

Although the examined RNA expression was spread across an area of injury, heatmaps of differentially expressed genes could also be generated from ranked genes in a similar manner to single cell RNA sequencing or microarrays. Overall, genes that were up regulated in control larvae were down-regulated in injured larvae (Figure 4-24). Many of these were identified earlier, such as *and1* and *col1a1*. There were a few that were not identified earlier, such as *twist3*, a gene lost in mammals through synfunctionalisation (Gitelman, 2007). Again this gene is involved in development and cell differentiation (Yeo *et al.*, 2009). One other highlighted gene is *im:7150988*, which encodes the Golgi-associated plant pathogenesis-related protein 1 (GAPR-1). This gene was previously found to be down-regulated in zebrafish mutants that have deformed tailfins due to disrupted Hippo pathway transcriptional co-activators (Kimelman *et al.*, 2017), and is thought to function as a serine protease (Serrano *et al.*, 2004).

Similarly, genes up regulated in injured samples were not highly expressed in uninjured controls (Figure 4-25), such as the lipoxygenases (LOX, non-specified) involved in the inflammatory response. However, it was observed that there was noticeable overlap between expression such as in Control3 and Injured3. Indeed, all the samples showed considerable overlap in the mapped genes when assessed overall (Figure 4-26A&B). An overlap would be expected since, this being a spatial tissue analysis, gene expression of normal tissue is seen. Nonetheless, there appeared to be more overlap between Control3 and the Injured group as a whole (Figure 4-26B). An appreciation of this was maintained during data interpretation, and there could be several reasons for this. One important confounding aspect is that the time-point chosen for analysis was at 6hpi. This represented the overall peak of neutrophil inflammation, but given the biological variability in the neutrophil counts, it was possible that in some fish, this time-point would coincide with an established inflammatory resolution phase, resulting in more similarity with the controls. One way to reduce this overlap in future would be to choose an earlier time-point for analysis. Another explanation for the Control3 overlap was the possibility that inadvertent sub-clinical injury, not physically observable, may have occurred to the control larva during its free-swimming growth phase to 2dpf since fish were kept in standardised conditions of 60 fish per Petri. It would only be possible to minimise this by performing more repetitions.

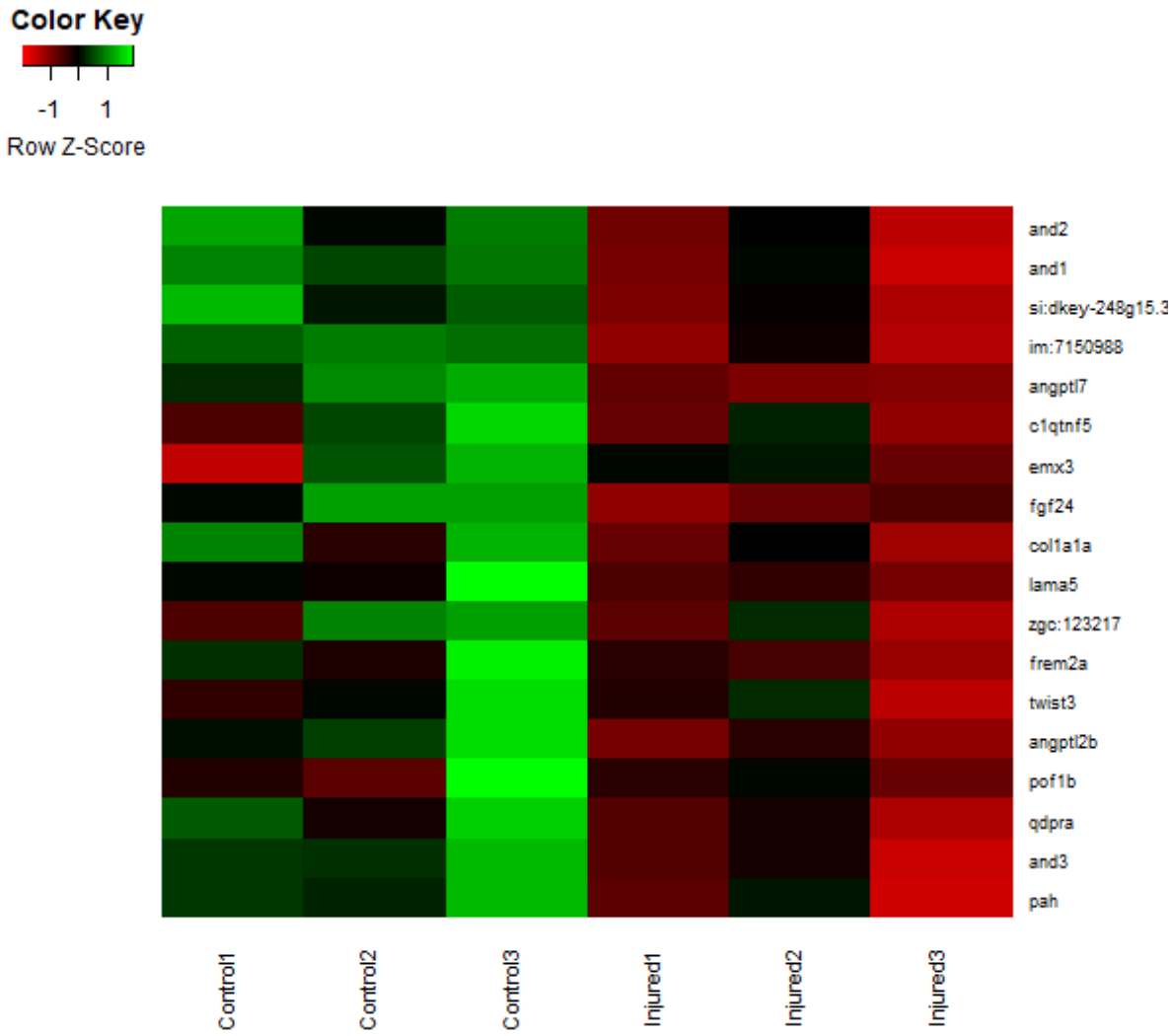

Figure 4-24: Heatmap of up-regulated control genes. Up-regulated (green) genes in the controls were generally down-regulated (red) in injured samples. Number of genes limited to those with ranking of fold-change >1.6. Heatmap produced using *heatmap.2* in R, data scaled to rows.

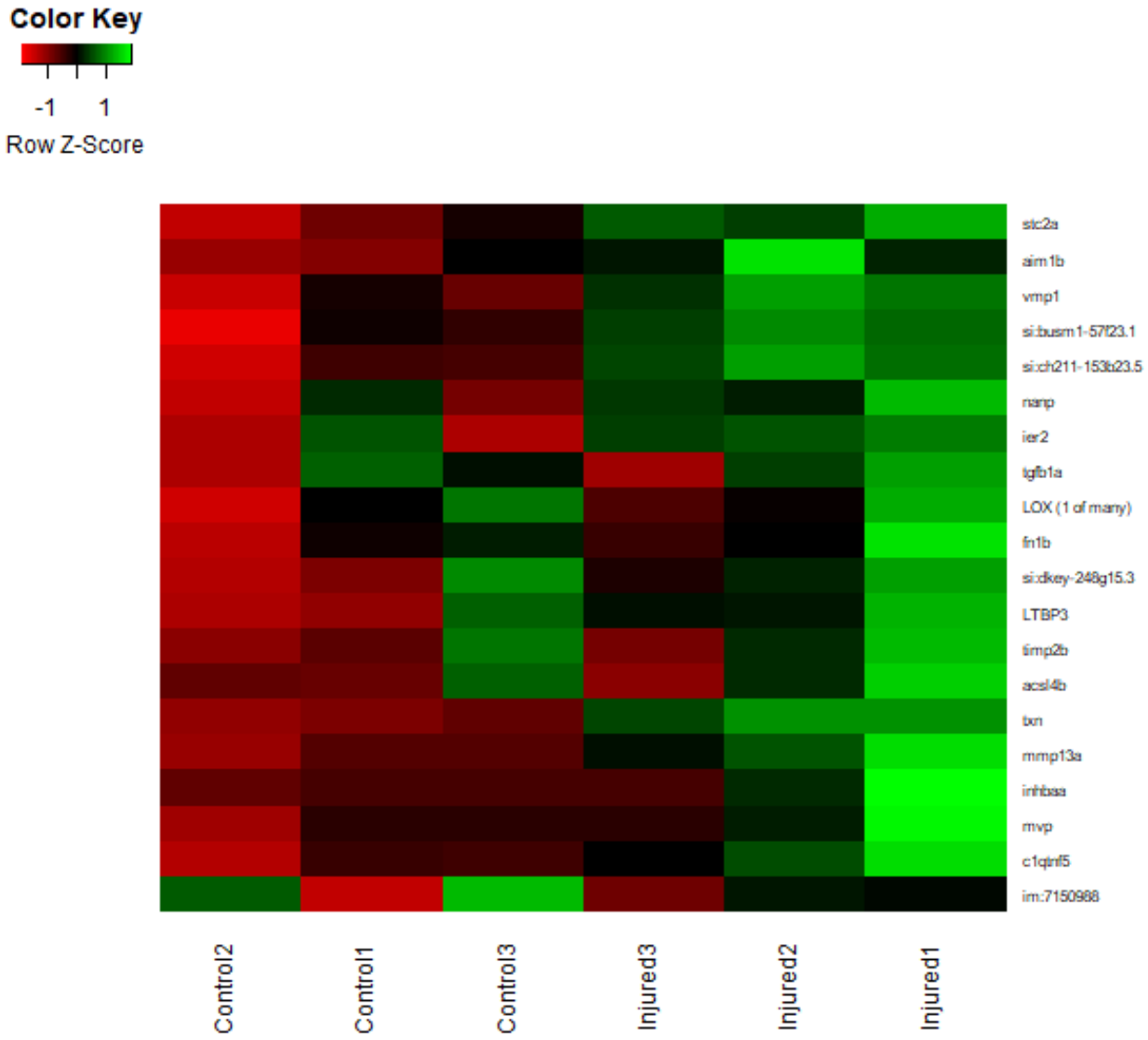

Figure 4-25: Heatmap of up-regulated injured genes. As before, up-regulated (green) genes were generally down-regulated (red) in uninjured control larvae. Number of genes limited to those with ranking of foldchange >1.6. Heatmap produced using *heatmap.2* in R, data scaled to rows.

Figure 4-26: Gene overlap between samples plotted with FunRich. Analysis was performed using the open-source application FunRich **(Pathan *et al.*, 2015)**. **A.** Venn diagram showing the total number of genes in each sample mapped to the Grcz10 zebrafish genome in each circle. Majority of the genes show overlap in each group. **B**. Venn diagram of all the samples compared against each other showing the true number of shared genes as well as the percentage that represents of all the genes mapped for that sample. Control3 shows a marginally higher than average degree of overlap with the injured group.

4.2.13 **Functional enrichment analysis showed differential expression of cellular component genes**

Given the variations and caveats above, each fish was then analysed separately to see if a more informative functional analysis could be obtained given. Analysis of differences in cellular component was performed using FunRich (Pathan *et al.*, 2015). Five components were chosen for interrogation: SNARE complex (involved in organelle and vesicle membrane fusion, (Blair and Flaumenhaft, 2009)), mediator complex (a universal regulator of transcription by interaction with RNA polymerase II (Casamassimi and Napoli, 2007)), ubiquitin ligase complex (involved in cell proliferation and differentiation (Krek, 1998)), receptor complex (proteins that undergo combination with a messenger to effect a change in cell function), and stress fibre (actin filaments involved in wound healing (Gabbiani *et al.*, 1972)). Fold-change increase in expression of the receptor complex was significant for each of the three injured fish, but not in two out of the three control fish. Control3, which was more similar to the injured group as seen in the Venn diagram previously, did show a significant increase in receptor complex as well. The increase in receptor complex in injury would fit with previous work showing its up-regulation in association with up-regulated immune cell infiltration in cancer tissues (Xu, Jin and Qin, 2020).

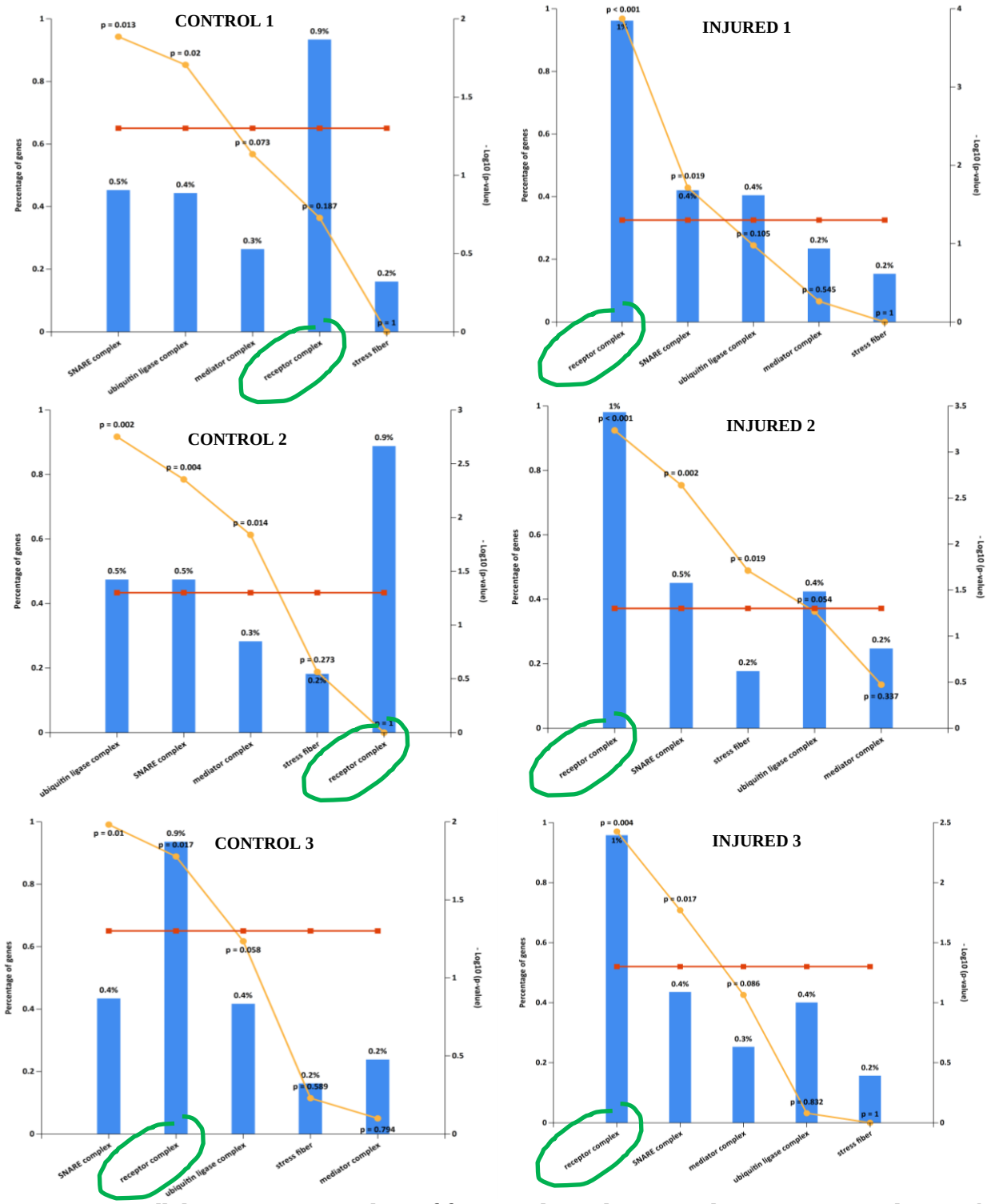

Figure 4-27: Cellular component analysis of functional enrichment analysis using FunRich. In each graph, bars show percentage of genes involved in each component, yellow lines show the statistical significance of Fold-increase, and red lines show the cut-off of p=0.05**.** Receptor complex highlighted with green circle, controls shown in the left column and injured samples in the right column.

4.3 **Discussion and further work**

Each of the three SPMs (LXA4, RvD2, RvE1) was selected to be representative of the parent precursor fatty acid (AA, DHA, EPA), and also because each acts via distinctive receptors. RvD1 was therefore not selected as it acts via the ALX/FPR2 receptor (Recchiuti *et al.*, 2014), similar to LXA4. A homologous *FPR2* receptor could not be found in the zebrafish by genome blasting so the closest match, *fpr1*, was investigated. All receptors were expressed from 1dpf onwards in the zebrafish. Although the *in situ* hybridisation of *fpr1* appeared to demonstrate expression in the kidney region which was absent in the sense controls, in humans this receptor is not highly expressed in the renal system, but is expressed even in the quiescent neutrophil with up-regulated expression in inflammatory states (Dorward *et al.*, 2015). It is possible that the *in situ* expression could be related to the kidney as it is an early site of haematopoiesis in zebrafish (Willett *et al.*, 1999), but in the absence of discrete staining it would be difficult to draw any definitive conclusions regarding expression of *fpr1* in 2dpf zebrafish larvae based on these results alone. Conversely, the expression of *gpr18* in zebrafish larvae appeared to be discrete and located mainly within the region of the CHT in 2dpf larvae. This staining did not increase at the wounding sites at any time. Other studies have shown these receptors to be within zebrafish thrombocytes (Nikhil, 2013), unlike their location in phagocytes in the human (Chiang *et al.*, 2015). The *in situ* staining would fit this known zebrafish expression. Finally, *cmklr1*, the RvE1 receptor, demonstrated localised increased expression at the site of tailfin injury from 6hpi onwards. This finding concurs with earlier neutrophil quantification results, showing that RvE1 does indeed affect its action later in the inflammatory cycle.

The work with transient receptor over-expression alone did not show significant effects on inflammatory responses, and this could be because of either a limited endogenous production of ligands, or exceptionally robust receptor recycling maintaining a low steady state of receptors available for ligand attachment. Evidence exists to support both these suppositions (Koenig and Michael, 1997; Arita *et al.*, 2006), especially since an over-abundance of endogenous SPMs could result in a poor initial inflammatory response to an insult, which in turn could be just as damaging in terms of host defence as an overly robust inflammatory response resulting in a cytokine storm (Darby and Melgar, 2014). Efficient receptor cycling is the other possibility in this model given the similar responses to exogenous application of SPMs compared with the

earlier experiments using unmanipulated larvae. Although transient receptor over-expression allowed rapid analysis, one drawback was that without a fusion fluorescent reporter, true protein expression could not be known with certainty. The CRISPR-Cas9 system has eased genetic manipulation considerably, and although the final phenotype still could be expected to reflect influences beyond that of the intended genetic changed, such as variable site integration, copy number, transgenic mosaicism, as well as epigenetic effects, (Anderson *et al.*, 2015; Zhang *et al.*, 2015), this method could be considered for future investigation.

Transcriptomics involving spatial examination of RNA expression is still in its infancy, but even now shows some promise in defining new areas of investigation. The model was developed here to allow examination of the inflammatory landscape to an injury, but revealed challenges in aligning a continuous dataset, as the subsequent analysis could be significantly changed even if sections were offset by a single slice. Therefore extensive validation was performed to ensure that results matched known end points, for example, the expression of *cldn15la* was confirmed to be confined to the intestinal region, and the expression of *mpx* matched against visual data obtained from imaging fluorescent larvae just prior to freezing. Very minor discrepancies were seen in the matching of fluorescence and *mpx* expression, but technical limitations such as the time between imaging and freezing and the dynamic state of live samples meant that further optimisation of technique would be difficult. Nonetheless, interesting patterns of gene expression was still demonstrated. One example was the expression of *cyr61l1,* an acute phase protein, which was specific to injured samples especially at the wound edge and could be used in addition to *col1a1a* in determining the injured edge for future analyses. Another example was the expression of *alpi.1*, which was increased in the tailfin, an unexpected finding given its extra-intestinal location despite the presence of other alkaline phosphatase isozymes in the zebrafish. Although this finding was unanticipated, this extra-intestinal location of *alpi.1* has been previously seen on *in situ* staining (Thisse and Thisse, 2004). The role of *alpi.1* in this setting remains an area for further investigation.

The RNA libraries were then interrogated ontologically using known tools for microarray and single cell expression analysis. Ontological assessment further confirmed the biological processes up-regulated in the control and injured groups were those expected to be involved in

growth and organ (tailfin) differentiation. This was matched by up-regulation of systems involved in response to stimuli in the injured group. The up-regulated genes in injury involved those involved in immune responses and catabolism, such as the *mmp* family. Further heatmap analysis revealed more genes of interest, such as the *twist3* and GAPR-1 family genes. However, close scrutiny showed considerable overlap between some of the samples. This overlap was highlighted on individual sample functional enrichment analysis of cell components. Significant up-regulation of receptor complex components was found in all injured samples but not in control samples, apart from one. This was the Control sample seen on the Venn diagram to a higher overlap with the injured group compared to the other controls. Two reasons were identified, but only one of which would be amenable to positive action. If control fish had inadvertently been injured, either during imaging (although in this case fish were minimally handled during pre-freezing imaging to avoid introducing artefact), or simply during the free-swimming period of maintenance, this is not easily detected even under microscopy. It is possible however that the inflammatory process was not significantly differentiated from the controls because resolution may have begun in some samples by 6hpi. This difference could be maximised by using an earlier time point for analysis in future.

There remain many challenges in the interpretation of TomoSeq gene expression data generated by Next-Generation Sequencing (NGS) to map out an 'inflammatory landscape' to injury. Due to the biological variation inherent in *in vivo* and whole organism studies (as compared to cell culture) some responses are likely to idiosyncratic and possibly diverse across cell types. Challenges lie in detecting true physiological responses from possible silent mutations causing a range of compensatory mechanisms. Certainly, the generic minimum recommended number of samples per group for RNA sequencing is three (Conesa *et al.*, 2016) but prohibitive costs remain for generation of data, and the ability to generate spatial as well as temporal patterns of expression to capture a 3D inflammatory landscape, requires substantial capital. Nevertheless, even spatial examination alone at a single time-point could reveal new areas of investigation, and there is no doubt that the possibility of examining inflammation in many dimensions could add to our understanding enabling fine-tuned modulation of this process in future.

4.4 **Summary of important findings**

In concordance with the biological responses to exogenous SPM supplementation found previously, the homologous SPM receptors were demonstrated by RT-PCR to be expressed from 1 to 5dpf in zebrafish larvae. Only expression of the RvE1 receptor, *cmklr1*, was up-regulated at tailfin wound sites from 6hpi onwards, whereas *gpr18* appeared to be expressed predominantly within the CHT at this stage of zebrafish development. Transient over-expression of the receptors, apart from *gpr18* in 2dpf larvae did not significantly alter either regeneration or the inflammatory phases in tailfin injury, compared to SPM supplementation alone in the previous chapter. Tomographic RNA sequencing (TomoSeq) was shown to be feasible with zebrafish larvae, allowing comparison and correlation with stages of injury, as demonstrated by the matching of *mpx* expression with visible fluorescence, and validated against known patterns of gene expressions such as *cldn15la*. Comparisons between single larvae as well as across all three samples in each group was possible and revealed lists of highly expressed genes within the group, some of which are known to be strongly involved in wound regeneration, and others whose functions are yet to be determined. This tool holds promise for future development.

Chapter 5: *Enterococcus faecalis* intestinal colonisation in the zebrafish and its effect on inflammation

5.1 The importance of organ specificity, colonisation and *E. faecalis* in inflammation

The investigation of host immune responses to early intestinal colonisation or an acute intestinal injury has its challenges, particularly in this internal, and therefore 'hidden', organ, as real-time visualisation often requires a degree of non-physiological manipulation. Often, the skin or another more superficial mucosal surface is used as a substitute in examining epithelial responses to insults or treatment, but it cannot be denied that the intestinal tract is unique, not only in its physiological environment, but also in its microbial milieu. Indeed, eliminating the variety of intestinal microbiota at the early stages of life has important consequences for the subsequent immune responses in an organism (Gorjifard and Goldszmid, 2016), such as a reduction in the thickness of the colonic mucous layer and associated intestinal anti-microbial proteins (Karlsson *et al.*, 2008; Petersson *et al.*, 2011), as well as in collagen content in healing intestinal wounds of rats (Mastboom, Hendriks and de Boer, 1989). Zebrafish models of intestinal colonisation have revealed a number of insights (Rawls *et al.*, 2006; Rendueles *et al.*, 2012; Toh *et al.*, 2013; Russo *et al.*, 2015; Stones *et al.*, 2017), although they remain fewer in number compared with rodent models. There are substantial similarities in the gastrointestinal system of zebrafish and higher mammals in terms of anatomy (Cheng *et al.*, 2016), microbiome (Rawls *et al.*, 2006) and mucosal immunity (Zhang *et al.*, 2010), making this an ideal model system. Importantly, larval transparency allows live imaging of the host immune cell responses to the intestinal presence of bacteria, injury or drug treatments without need for intestinal exteriorisation. Similar to rodents, germ-free (GF) zebrafish also display phenotypic differences such as epithelial abnormalities, and these GF zebrafish do not survive to adulthood (Rawls, Samuel and Gordon, 2004). Therefore, to avert these difficulties and avoid any possible perturbation of the development of the immune system that may arise from even transient GF conditions, the possibility of a zebrafish model of colonisation with *Enterococcus faecalis* under conventional (non-GF) conditions was explored. *E. faecalis* is an important bacteria in humans, because although it comprises only up to 1% of the species found within the intestinal tract (Sghir *et al.*, 2000), it is one of the most common pathogens isolated from surgical wounds

(Giacometti *et al.*, 2000), and can cause serious nosocomial infections such as endocarditis and urinary tract infections, that are increasingly challenging to treat due to its multiple intrinsic antibiotic resistances (Guzman Prieto *et al.*, 2016). Interestingly, there is an increased predominance of *Enterococcus* within the intestinal microbiome of the elderly (Matsumoto *et al.*, 2011), and this is of clinical relevance in an ageing population. Furthermore, it has been shown that not only can *E. faecalis* slow healing of wounds (Kian *et al.*, 2017), in the intestine it can disrupt the process altogether leading to ALs (Shogan *et al.*, 2015). Wound healing also requires timely resolution of inflammation, SPMs have been shown to drive inflammation resolution without impacting the efficacy of bacterial clearance in a variety of models (Buckley, Gilroy and Serhan, 2014), but no studies have investigated the effect of exogenous supplementation of these SPMs in a localised intestinal injury in the presence of *E. faecalis* colonisation. It was hypothesised that it would be possible to obtain reliable intestinal colonisation by *E. faecalis* in conventional (non-GF) zebrafish, and that the presence of *E. faecalis* would differentially modulate the host innate immune response to SPMs in the setting of an acute intestinal injury.

5.2 **Results**

5.2.1 **Following microgavage, *E. faecalis* persisted in an anatomically distinct region of the zebrafish GIT**

Microbial characterisation of adult zebrafish done previously have shown that the principal phyla dominating the teleost intestine are similar to humans, namely *Proteobacteria* and *Firmicutes*, but in zebrafish, the only representative from the phylum *Firmicutes* was the *Bacilli* class (Lan and Love, 2012). Not only is *E. faecalis* not normally present in the teleost intestine, but all other colonisation studies have previously been performed in germ free (GF) or specific-pathogen-free experimental subjects. Therefore it was unknown if *E. faecalis* could persist within the intestinal tract of larvae raised under conventional (non-GF) conditions. Under these conditions, the developing zebrafish intestine rapidly accumulates a microbiome from the immersion media when the larval mouth achieves patency at 72 hours post fertilisation (hpf) (Stephens *et al.*, 2015). This process was therefore allowed to proceed conventionally for a further 24 hours following oral patency, and only larvae that had an inflated air sac as an indicator of sufficient oral intake to optimise natural colonisation, were selected. Fluorescently

labelled *E. faecalis (*OG1RF-*mCherry*) was then introduced via microgavage directly into the intestinal bulb, or via immersion in swimming media, after larval anal patency at 96 hpf. Anal patency was vital to ensure that bacterial persistence was not simply due to a lack of avenues for bacterial exit. With these methods, the youngest age at which colonisation studies could be performed was 4dpf, and at this age, there appeared to be a threshold of exposure for OG1RF, below which, colonisation, as defined by visible midgut fluorescence and growth of colonies on culture plates, did not reliably occur. This was a single dose of 10^5 CFU for microgavage and 10^6 CFU/ml for overnight immersion (Figure 5-1A). On average, persisting bacteria were approximately 10^4 CFU/larvae, although there was some biological variation, possibly due to the presence of other colonisers (Figure 5-1B). The density of 10^4 CFU is within the density range of normal gut microbiota in 6dpf larvae in published data (Rawls *et al.*, 2007). To standardise the amount of bacteria that passed through the intestinal tract of each zebrafish larvae, avoid any extra-intestinal effects that might occur from prolonged bacterial immersion and allow investigation of host response from the early stages of intestinal exposure to bacteria, subsequent characterisation experiments were performed with microgavage of 10^5 CFU of bacteria. Twelve hours after microgavage, the fluorescent *E. faecalis* invariably persisted only within the midgut (region labelled M in Figure 5-2).

5.2.2 The *E. faecalis* OG1RF-Δ*epaX* mutant had impaired colonisation of the zebrafish intestinal tract

To confirm that this persistence of *E. faecalis* was indeed colonisation, an OG1RF derivative with a mutation in *epaX* was tested. The *epaX* gene is located downstream of the *epaA-epaR* locus encoding the core enterococcal polysaccharide antigen (Epa) (Figure 5-3), that has been proposed to contribute to the decoration of the Epa backbone, and is required for intestinal colonisation in mice (Rigottier-Gois *et al.*, 2015) In contrast to wild-type *E. faecalis*, the *epaX-mCherry* mutant could not be detected as fluorescence within the midgut twelve hours after microgavage (Figure 5-4A). Complementation of *EpaX* rescued the mutant and restored intestinal colonisation (Figure 5-4B-C), demonstrated as the return of visible midgut fluorescence. This suggested that *EpaX* was essential for successful zebrafish colonisation, similar to mice. Absence of visible fluorescence however did not exclude low level persistence of *E. faecalis*, as demonstrated by recovered colonies after culture (Figure 5-4D).

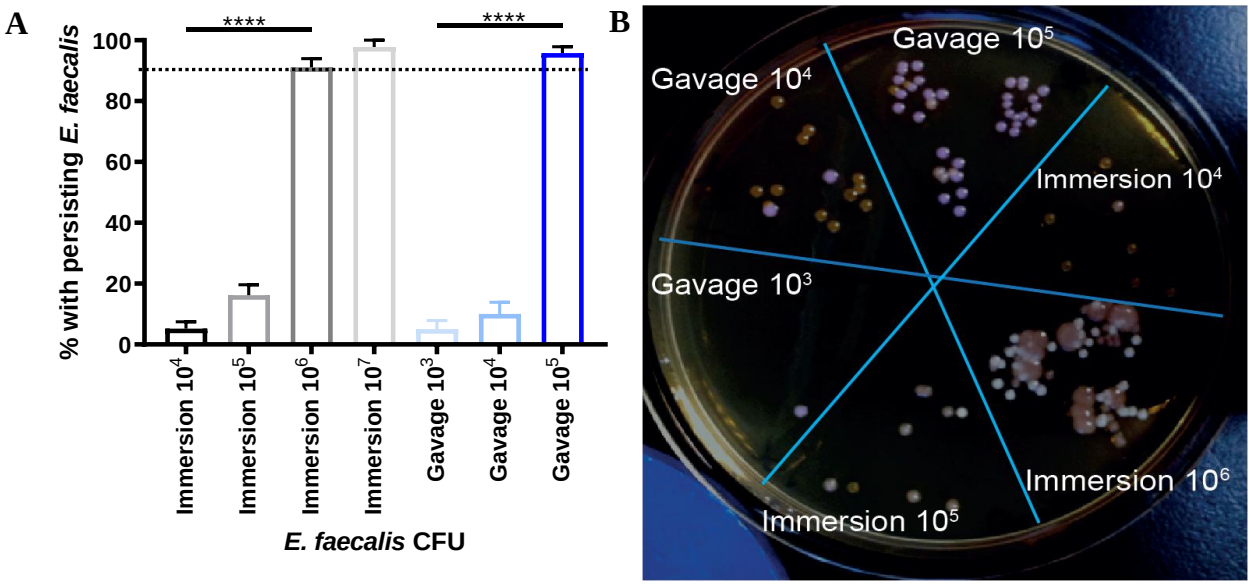

Figure 5-1: Intestinal colonisation by *E. faecalis* in 4dpf zebrafish larvae. A. Percentage of larvae with persisting *E. faecalis* defined as visible fluorescence under stereomicroscopy within the midgut of the zebrafish larval intestine (N=45/group in three independent repeats), comparison with one way ANOVA with Sidak's multiple comparison correction. The dotted line represents 90% colonisation rate, taken as the minimum to allow consistent interpretation of results in further experiments. **B**. Serial dilution (1:1000 final concentration) of macerated larva plated on BHI plate and grown at 37˚C overnight. Each segment represents a single zebrafish larva with three separate spots of 10µL, of which the average readings were quantified. The image has been contrast enhanced +20% to allow visualisation of other bacterial colonies that are non-fluorescent (white) but still growing on the non-selective BHI plate as a demonstration of the presence of other members of the microbiome apart from the microgavaged bacteria of interest. Representative BHI plate, N=6 in three independent repeats.

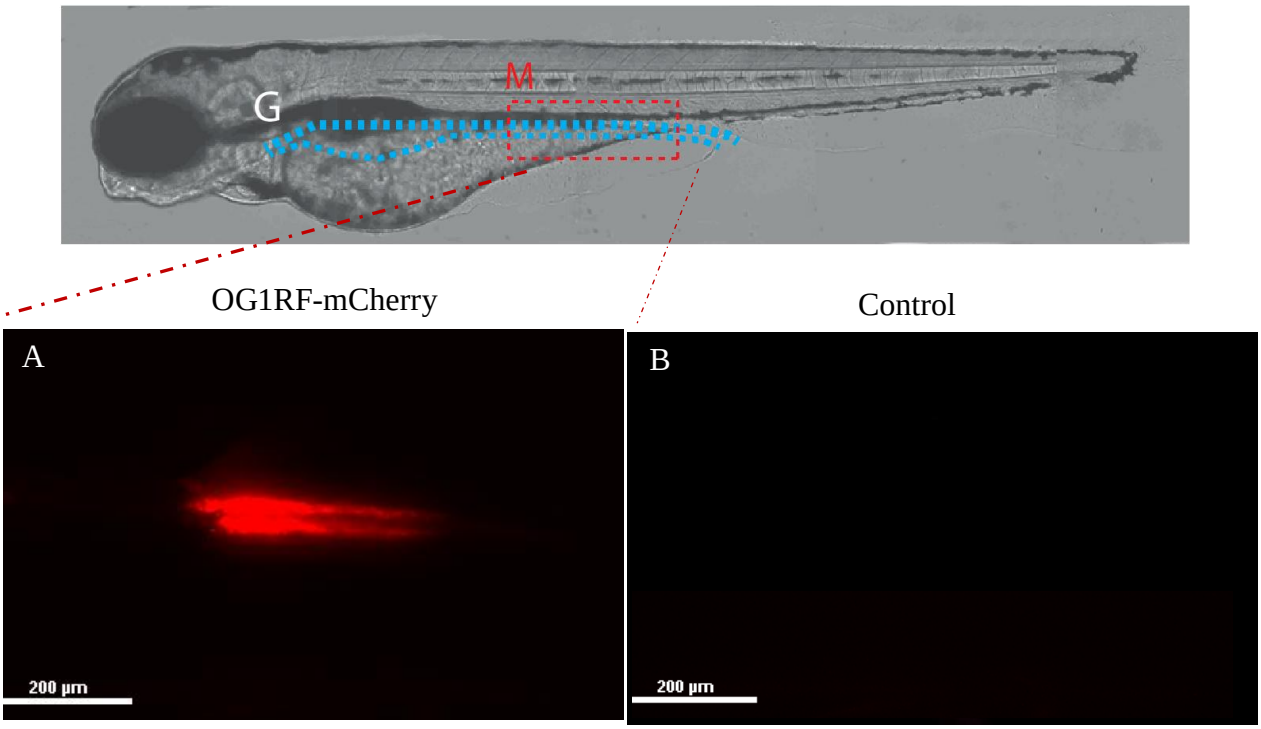

Figure 5-2: *E. faecalis* colonisation of zebrafish intestinal tract. Images obtained with a Nikon Eclipse TE2000-U at 4X objective of wildtype zebrafish larva at approximately 3dpf. Composite image stitched with NIS Elements AR® with midgut (M) boxed in red and gastrointestinal tract **(G)** outlined in blue. All subsequent images in this chapter are of region M, oriented in a similar fashion. **A.** Conventionally raised 4dpf zebrafish larvae were microgavaged with 10^5 CFU E. faecalis and imaged at 20X after 12 hours of free swimming. **B**. Control larvae showing absence of fluorescence in the identical region under identical conditions.

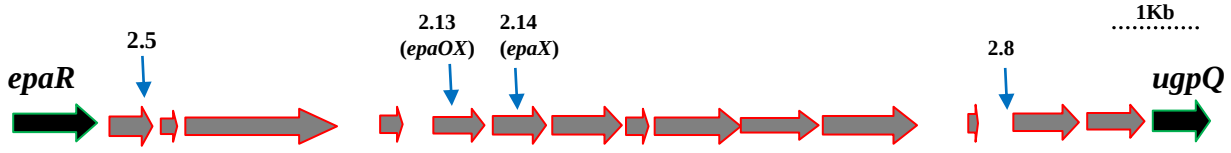

Figure 5-3: Location of *epaX* mutations. Mutation points of region upstream of *epaR* in OG1RF, modified from **(Smith *et al.*, 2019)**. Mutants 2.5, 2.8, 2.14 (*epaX*) and 2.13 (*epaOX*) were a generous gift from the Mesnage Laboratory, University of Sheffield, and tested for intestinal colonisation potential.

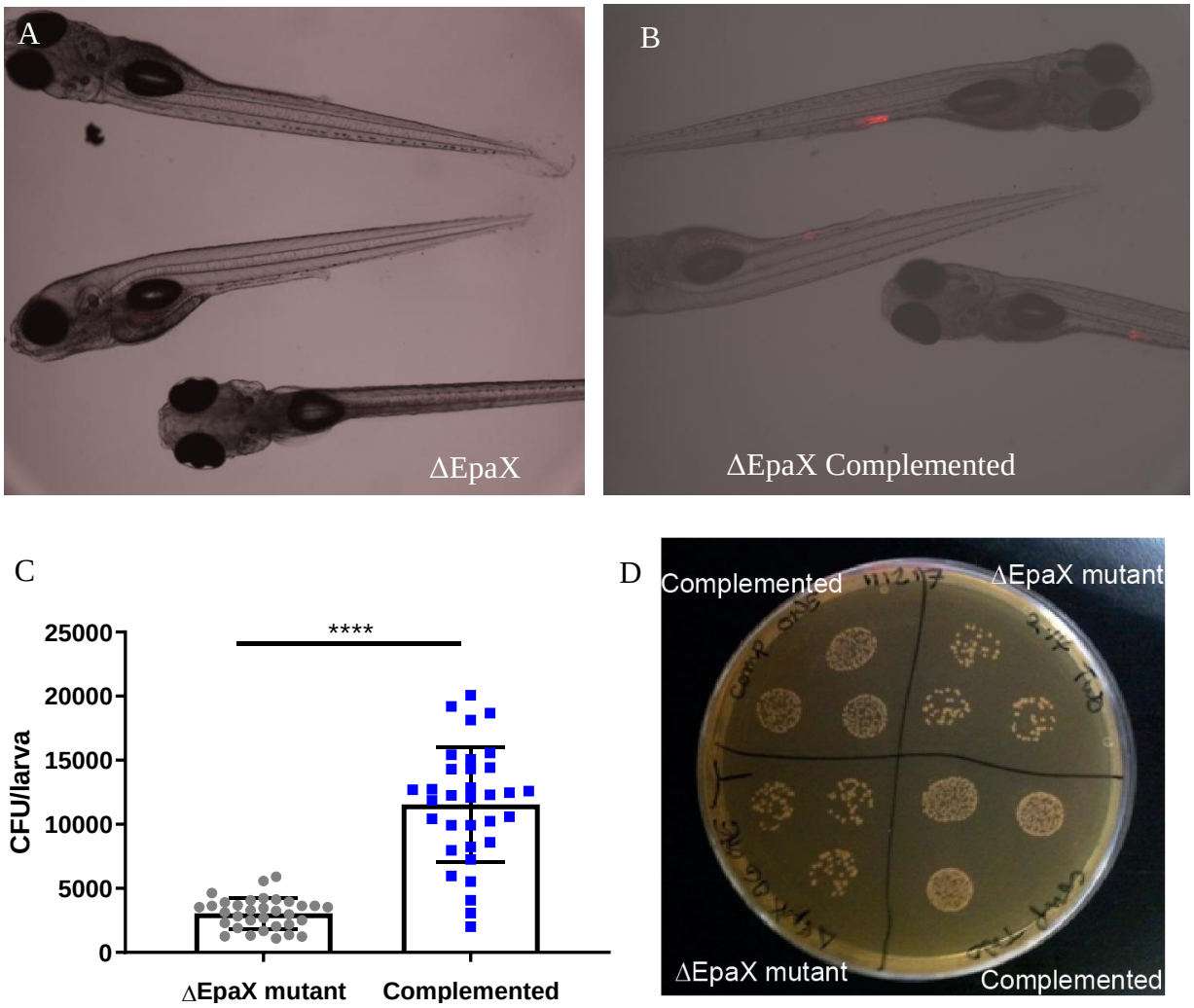

Figure 5-4: *EpaX* is required for *E. faecalis* colonisation of the zebrafish intestine. A. The Δ*EpaX*-mCherry mutant was microgavaged into 4dpf wildtype larvae and imaged 24 hours later at 2X magnification using a Nikon Eclipse TE2000-U. Gain of the mCherry channel doubled to enable pickup of fainter fluorescence. **B**. The *ΔEpaX*-mCherry-complemented strain was microgavaged into 4dpf wildtype larvae and imaged 24 hours later at 2X magnification using a Nikon Eclipse TE2000-U under similar conditions, but without doubling of the mCherry channel gain. Representative images are shown of merged brightfield and fluorescent channels. N=45/group in three independent repeats. **C.** Graph shows CFU/larva for the Δ*EpaX* mutant and rescued complemented strains. Each symbol in the graph represents the average of three CFU readings for a single larva. N=33/group in three independent repeats, comparison with t-test, error bars show SD. **D.** Representative BHI-tetracycline plate showing the difference in CFU/larva between the *ΔEpaX* mutant and rescued (*ΔEpaX*-complemented) strains. Each quadrant represents a single larva with three 10µl 1:1000 dilutions per larva.

5.2.3 **The parental background strain of the Δ*EpaX* mutant did not affect colonisation potential**

The *EpaX* mutants were made in the *E. faecalis OPDV* strain, a strain containing four mutations (Δ*oatA*, Δ*pgdA*, Δ*dltA*, and Δ*sigV*). Although these four mutations do not affect the polysaccharide of interest, growth studies were undertaken to determine if there was any significant growth defect resulting from these mutations, which might be impacting upon the colonisation differences seen. Quantifying OD_{600} hourly for 9 hours of growth under optimal conditions, confirmed a slight growth defect seen in the Δ*EpaX* mutant but this was also seen in the complemented strain (Figure 5-5). Since zebrafish intestinal colonisation was restored in the complemented strain, this growth defect was unlikely to be the cause of the colonisation defect. Interestingly, the *OPDV* strain alone demonstrated enhanced growth compared to wildtype (WT) OG1RF. The *OPDV* strain is from a parental JH2-2 background which has been paradoxically shown to be non-virulent in the zebrafish in its pure parental strain compared to OG1RF (Prajsnar *et al.*, 2013), but equally virulent to OG1RF when the *OPDV* mutation and *Epa* mutations are present (Smith *et al.*, 2019). Both these papers however infected zebrafish larvae at 1dpf, at a time when neutrophils are not yet seen (Le Guyader *et al.*, 2008b), and therefore it is difficult to draw definitive conclusions regarding the true effects on survival with a fully functioning innate system.

In addition to the Δ*EpaX* mutant (mutant 2.14), three other mutants in the region of this locus were tested, numbered mutants 2.5, 2.8 and 2.13 (Figure 5-3) to reduce the chances of the previous findings being a spurious epistatic result. All of these mutants visibly colonised the mid-intestine of larvae after 12 hours, and confirmed that only the Δ*EpaX* mutant was associated with a defect in colonisation (Figure 5-6A) as demonstrated by a significant decrease in CFU recovered from each larvae (Figure 5-6B). This reinforces the hypothesis that *EpaX* plays a specific role in colonisation, similar to rodent studies (Rigottier-Gois *et al.*, 2015), and further confirms that the *OPDV* background itself was not implicated in the colonisation potential of *E. faecalis*, but rather only the specific *EpaX* defect alone.

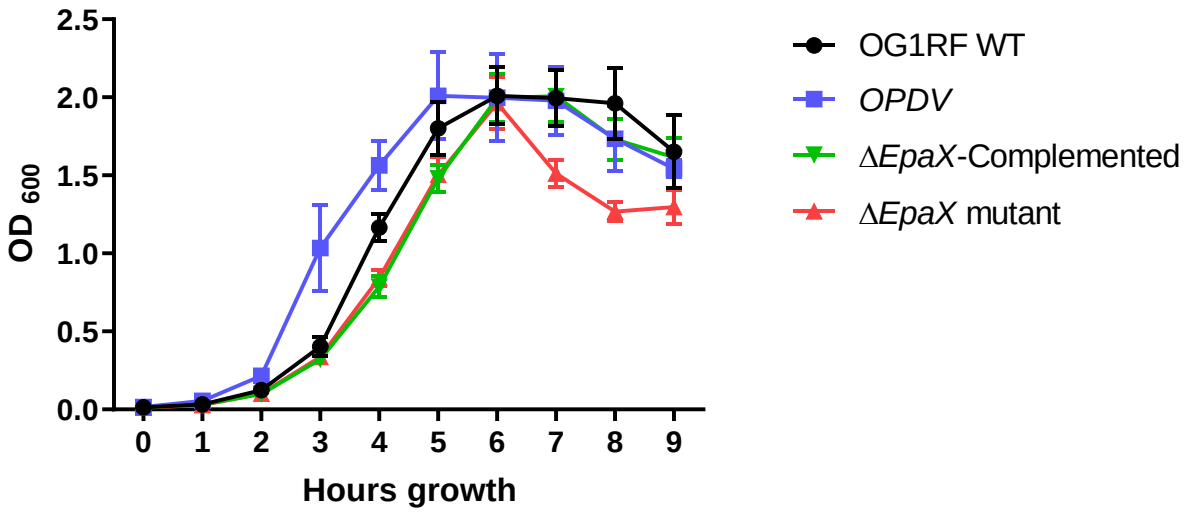

Figure 5-5: Growth curves over 9 hours for OG1RF WT and *OPDV* Δ*EpaX* mutants. Each *E. faecalis* strain was grown at 37˚C with agitation, in a conical flask in 50 mL of BHI with or without antibiotics to select for the relevant plasmid. At each hour, 1 mL from each flask was withdrawn under aseptic conditions and absorbance OD_{600} measured. Error bars show SD, N=3 in three independent repeats.

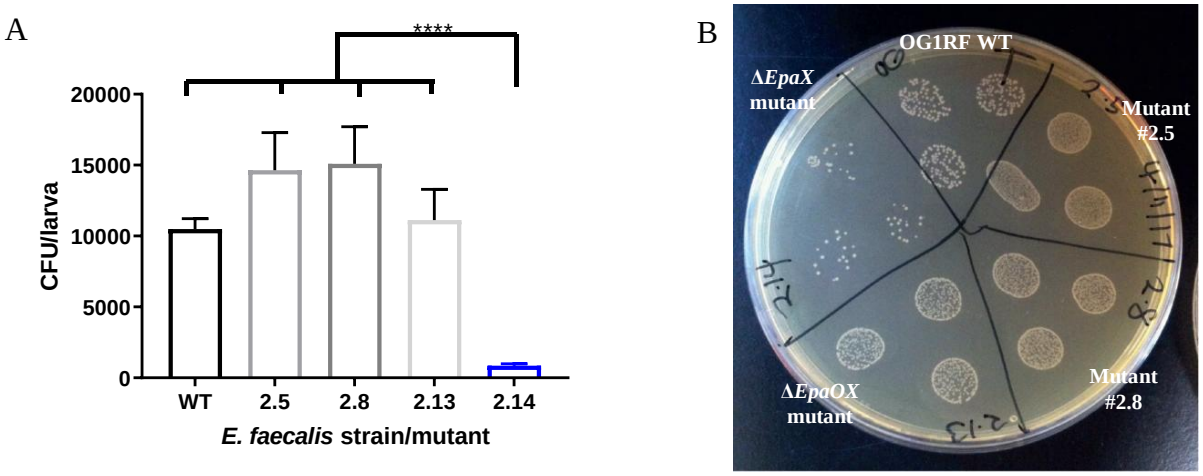

Figure 5-6: The effect of *E. faecalis* mutations on intestinal colonisation. A. Graph of *E. faecalis* CFU recovered from each larvae for the OG1RF wildtype and mutant strains. N=30/group in three independent repeats, comparison with one-way ANOVA, error bars show SD, ****$p<0.0001$. **B**. Representative BHI-tetracycline plate of 1:1000 dilution triplicate CFU plating of mutant strains when grown overnight on selective BHI plates at 37˚C. Each quadrant representing a single larva, average of three spots taken as a single CFU count to be plotted).

5.2.4 **Persisting *E. faecalis* did not induce an increase in physiological inflammatory markers**

Further characterisation of the colonisation model was performed by analysing the zebrafish equivalent of several human markers of intestinal inflammation, for example, a thickened intestinal wall, increased frequency of stools, increased mucous secretion, or rectal bleeding. First, thickness of the zebrafish intestinal wall was measured at the mid-region of the intestinal tract, the area of colonisation. A significant increase in intestinal thickness was seen (Control mean +/- SEM: 27.87µm +/- 0.52, OG1RF: 29.86µm +/- 0.68, p=0.021, t-test, Figure 5-7A). Nonetheless, at this stage of zebrafish development, accelerated maturation could be an alternate explanation rather than an inflammatory response, especially since the increase appeared uniform throughout the GIT, rather than a localised swelling. Next, changes in intestinal motility were investigated. Bacterial sensors are expressed in the intestine, and when highly-stimulated can cause intestinal hypermotility (Caputi *et al.*, 2017). Peristaltic contractions over six minutes were quantified as previously described (Rawls, Samuel and Gordon, 2004), and no significant increase in intestinal motility in response to *E. faecalis* colonisation was demonstrated (Control mean +/- SEM: 7.50 +/- 0.45. OG1RF: 8.27 +/- 0.34, t-test, p=0.1861, Figure 5-7B) . An increase in mucin production and goblet cell number is also often a feature of human intestinal inflammation, and this was assessed next. A positive control was used by using dextran sulphate sodium salts (DSS) 0.5% (w/v) as previously described (Oehlers *et al.*, 2012). This resulted in intraluminal mucin seen only in the DSS group (Figure 5-7C), and often obscured the individual dots of Alcian blue and therefore accurate quantification could not be performed in this group. Quantification of numbers of mucin-containing cells between controls and OG1RF groups revealed no significant differences (Control mean +/- SEM: 98.53 +/- 5.20, OG1RF: 88.62 +/- 4.15, p=0.1394, t-test, Figure 5-7D). Finally, rectal bleeding does not feature strongly in teleosts, but other studies have shown that microbes in close association with, or invading, an epithelial surface can induce host cell death (Ashida *et al.*, 2011). This was investigated using acridine orange staining (Figure 5-8A) and the positive control with 50 µM Glafenine as described (Goldsmith *et al.*, 2013). Persisting *E. faecalis* induced no detectable increase in cell death (Control mean +/- SEM: 0.029% +/- 0.029, OG1RF: 0.030% +/- 0.030, Glafenine: 0.95 +/- 0.032, p>0.9999, Kruskal-Wallis with Dunn's correction, Figure 5-8B).

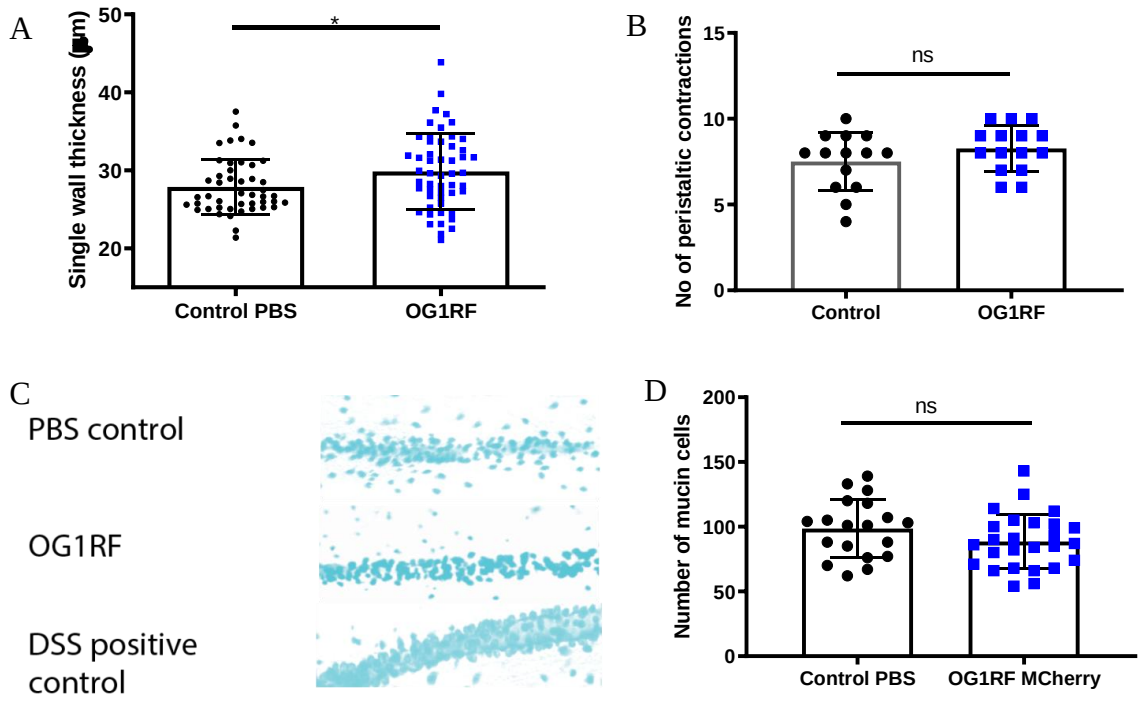

Figure 5-7: Physiological inflammatory markers were not increased in *E. faecalis* colonisation. A. Thickness of intestinal wall measured at mid-point of segment III (region of colonisation) of the larval GIT. Control groups were microgavaged with PBS, and treatment groups with 10^5 CFU of OG1RF-mCherry. Three separate measurements were obtained for each fish, and the mean used for analysis. N=48/group in four independent repeats, error bars show SD, comparison with t-test, *$p<0.05$. **B**. Number of organised peristaltic contractions in the GIT. Live zebrafish larvae microgavaged with PBS or 10^5 CFU OG1RF-mCherry, lightly anaesthetised with Tricaine for live bright field time-lapse imaging for 6 min using a Nikon Eclipse TE2000-U microscope. Quantification was performed blinded using these time-lapse images at a later time. N=15/group in three independent repeats, comparison with t-test, ns=non-significant, error bars show SD. **C**. Alcian blue staining on larvae microgavaged with PBS, OG1RF, or DSS 0.5% (w/v) as a positive control. Representative images (background subtracted) of the mid and distal intestinal tract of larvae are shown. **D**. Graph comparing number of mucin cells quantified in segment III of larvae. N=18/group, in three independent repeats. Comparison with t-test, ns=non-significant, error bars show SD.

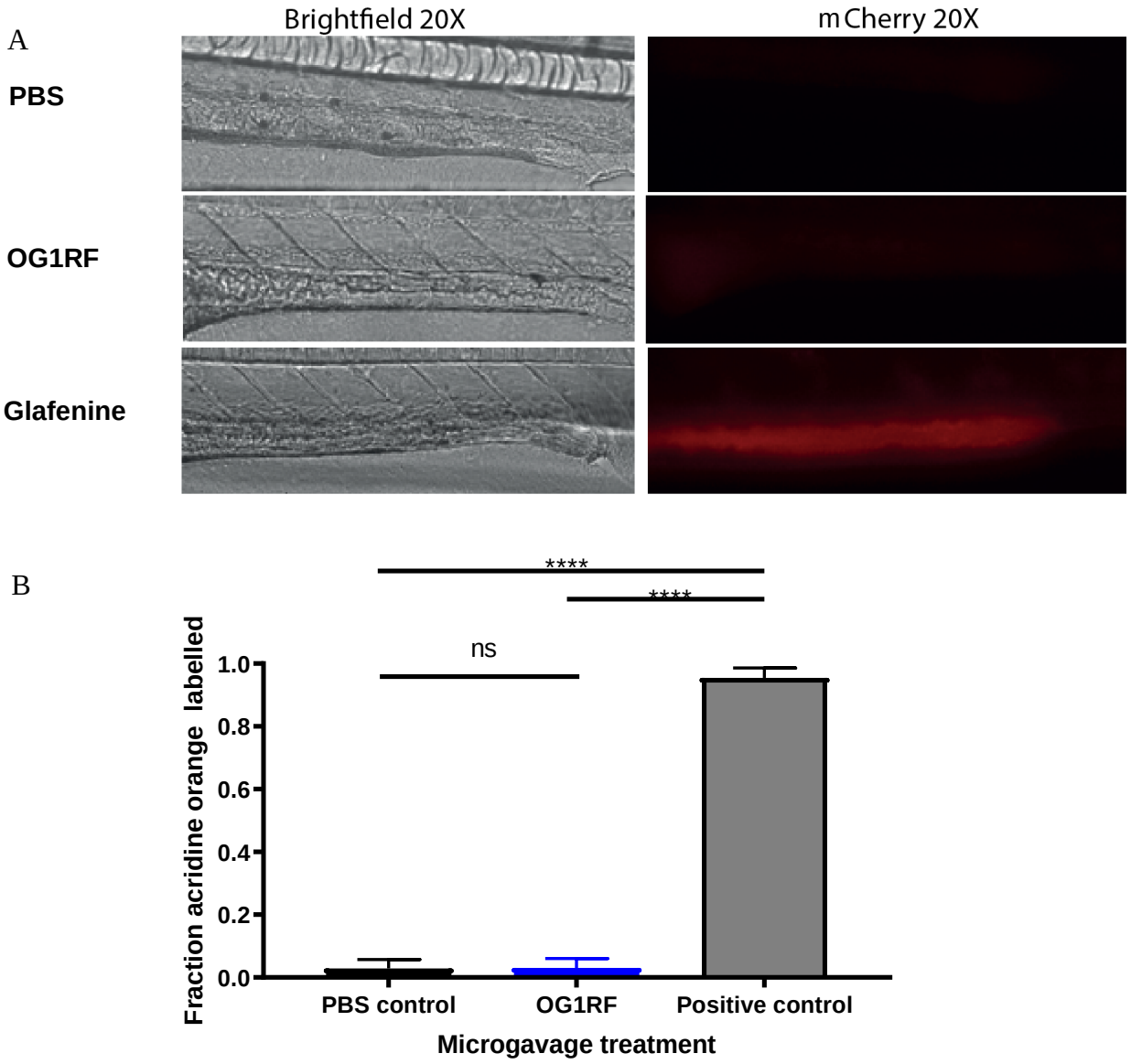

Figure 5-8: Acridine orange staining for cell death as a marker of intestinal inflammation. Larvae were immersed in 1 µg/mL of acridine orange for 30 min, and then rinsed three times in E3 without methylene blue to remove excess dye, prior to immobilisation for imaging. Positive controls were obtained by immersion in glafenine (50 µm) for 6 h prior to acridine orange staining. **A**. Representative images of acridine orange of live larvae immobilised in 0.8% agarose and imaged with a 20X objective, are shown. **B**. Graph showing fraction of larvae demonstrating intestinal fluorescence when visualised with acridine orange filters compared to the positive control of 50 µM glafenine. N=33/group in three independent repeats, comparison with Kruskal-Wallis with Dunn's multiple comparison correction, ns=non-significant, ****p<0.0001, error bars show SD.

5.2.5 *E. faecalis* colonisation increased NFκB expression along the GIT

Next, the host response to persisting *E. faecalis* within the intestine was examined. Nuclear factor-kappa B (NFκB) is a key signalling molecule in inflammatory pathways, and it has been shown that bacteria can utilise the NFκB pathway as a pro-survival method by up-regulating its expression (Kanther *et al.*, 2011). Using the *Tg(6xHsa.NFKB:eGFP)sh235* reporter line, the intensity of fluorescence in the colonised intestine was measured for 12 hours. A significant increase in the NFκB reporter signalling in response to *E. faecalis* colonisation was observed (Overall control mean +/- SEM: 35.17A.U. +/- 2.71, OG1RF: 61.65A.U. +/- 2.56, $p<0.0001$, linear regression, Figure 5-9A and B) in keeping with published data.

5.2.6 *E. faecalis* in an uninjured GIT did not incite a cellular inflammatory response

The neutrophilic response to *E. faecalis* colonisation was then investigated, because up-regulation of NFκB can lead to activation of the pro-inflammatory cascade including release of IL-8 and other neutrophil chemoattractants (Yu *et al.*, 2003). Zebrafish do possess an orthologous gene for IL-8 (*cxcl8*) which is expressed on leukocytes, as well as orthologous genes for its receptors *cxcr1* and *cxcr2*, and this signalling pathway has been shown to be conserved in zebrafish and active in the GIT (Oehlers *et al.*, 2010, p. 8). At 12 hours post colonisation, live imaging of the transgenic line *TgBAC(mpx:GFP)i114*, with or without *E. faecalis* colonisation (Figure 5-10A), demonstrated no difference in neutrophil numbers recruited to the intestinal region (Control mean +/- SEM: 16.02 +/- 0.71, OG1RF: 16.07 +/- 0.72, $p=0.9993$, one-way ANOVA), in contrast to the positive control with DSS (DSS mean +/- SEM: 19.75 +/- 0.91, $p=0.0071$, one-way ANOVA, Figure 5-10B) performed as previously described (Oehlers *et al.*, 2016). Time-lapse imaging was further undertaken for 12 hours to determine if neutrophil numbers were raised at any point, but no difference was seen (Overall control mean: 13.41, OG1RF: 13.34, $p=0.9625$, repeated-measures two-way ANOVA, Figure 5-10C). There was a gradual increase in neutrophil numbers in both groups over time which would be expected given the expected larval maturation and growth over the duration of the time lapse.

A

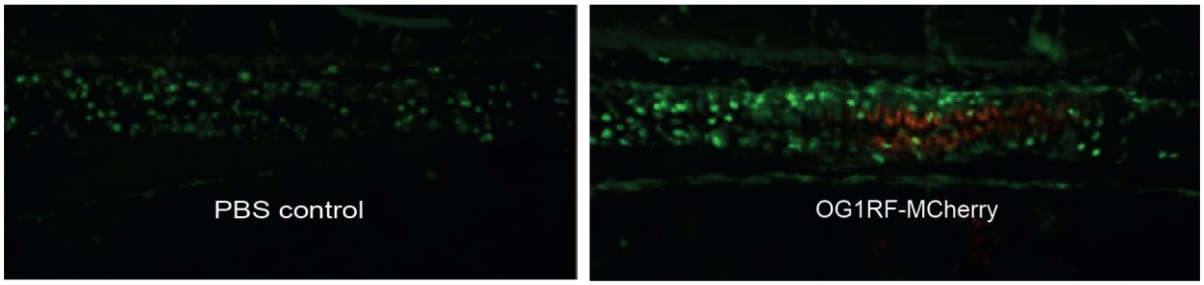

B

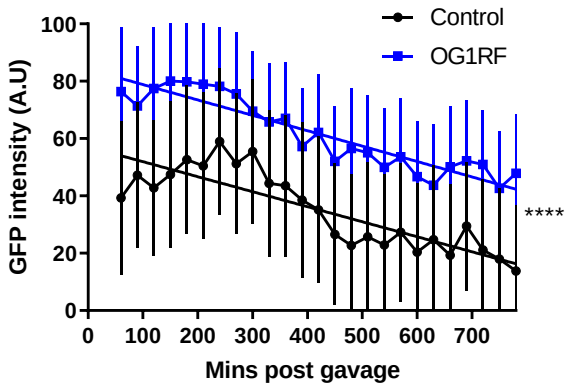

Figure 5-9: NFκB was up-regulated upon colonisation with *E. faecalis*. A. Representative images taken 12 hours post-gavage showing a Maximum intensity projection of the merged GFP and mCherry fluorescent channels at 30X objective using a Nikon Eclipse TE2000-U microscope. No image enhancements were performed, and identical settings were used for laser power, brightness, contrast and exposure times. Colonisation was demonstrated by mCherry fluorescence along the intestinal epithelial surface. The absence of luminal mCherry fluorescence indicated that excess bacteria have been expelled by the time of imaging, and intensity changes would be mainly due to surface colonising bacteria. Imaging was only started at 60 min post-gavage to allow a period of recovery in which excess bacteria could be expelled from the intestinal tract to avoid accumulation at the anal opening once larvae were embedded in agarose, and thus avoid the possibility of a spurious increase from such a situation. **B.** Graph of intensity over time for intestinal region, with background correction only to avoid any bias from differences resulting from the initial 60 minute washout period. Comparison with linear regression, ****$p<0.0001$, N=30/group in four independent repeats, error bars show SEM.

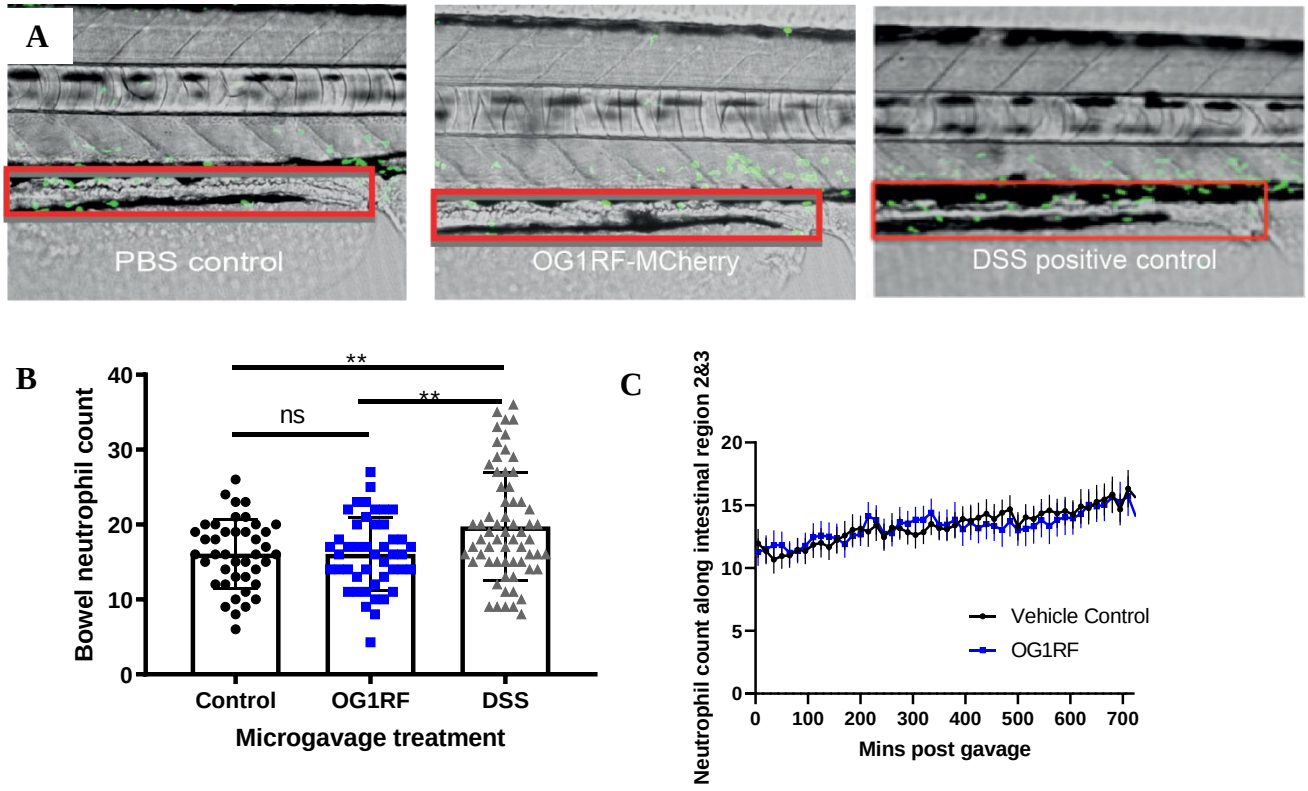

Figure 5-10: Neutrophilic responses in region 2&3 of the zebrafish intestinal tract to PBS, *E. faecalis* or DSS 0.5% (w/v). A. Representative images of sections of 4dpf *TgBAC(mpx:GFP)i114* larvae showing region of neutrophil counts boxed in red taken using a 20X objective Nikon Eclipse TE2000-U microscope, with merged GFP and brightfield channels. Individual neutrophils are seen as green dots. **B**. Graph shows neutrophil counts in section 2 and 3 of the larval intestine at 12 hours post gavage (hpg). Comparison with one-way ANOVA, ns=non-significant, $**p<0.001$, error bars show SD, N=42/group in three independent repeats. **C**. Time lapse performed for 12 hpg to determine if neutrophil counts were raised over controls at any point. N=21/group in three independent repeats, comparison with repeated-measures two-way ANOVA, error bars show SEM.

5.2.7 **In contrast to *E. faecalis*, *S. aureus* SA113 incited a neutrophil response in the uninjured intestine**

In order to demonstrate that the lack of neutrophilic response was specific to *E. faecalis*, a different bacterium, *S. aureus* SA113 was microgavaged. In contrast to *Enterococcus*, *S. aureus* is only found within the human GIT in 20% of the general population (Acton *et al.*, 2009) and is not always a benign commensal (Sollid *et al.*, 2014). The strain SA113 was chosen as it is known to successfully colonise mice (Misawa *et al.*, 2015). With SA113 in zebrafish, colonisation was seen in the same anatomical location as *Enterococcus*, but in addition, a robust neutrophil response was seen attending to the intestinal tract in the uninjured larva (Control mean +/- SEM: 22.19 +/- 0.16, SA113: 27.93 +/- 0.11, $p<0.0001$, linear regression, Figure 5-11A). Despite the increased numbers, neutrophil movement in terms of path length (Control mean +/- SEM: 129.8 +/- 3.69, SA113: 129.3 +/- 4.36, $p=0.9259$, t-test, Figure 5-11B), straightness of travel (Control mean +/- SEM: 0.31 +/- 0.005, SA113: 0.30 +/- 0.005, $p=0.1224$, t-test, Figure 5-11C) and speed (Control mean +/- SEM: 0.035 +/- 0.001, SA113: 0.035 +/- 0.001, $p=0.9757$, t-test, Figure 5-11D), were not altered.

5.2.8 **Colonisation with *E. faecalis* reduced the number of macrophages patrolling the intestinal region**

Next, the macrophage response was investigated. Performing similar colonisation experiments in a fluorescently labelled macrophage line, *Tg(mpeg1:NLS-Clover)*, showed that the number of macrophages in the region of the uninjured intestine was reduced in the presence of *E. faecalis* colonisation (Control Ymax: 55.62, OG1RF Ymax: 51.21, $p<0.0001$, Poisson regression, Figure 5-12A). In addition, the speed of travel of macrophages was significantly increased (Control mean +/- SEM: 0.030 +/- 0.0005, OG1RF: 0.033 +/- 0.0008, $p=0.0041$, t-test, Figure 5-12C). There were no changes in path length (Control mean +/- SEM: 113.8 +/- 3.03, OG1RF: 120.7 +/- 3.41, $p=0.1377$, t-test, Figure 5-12D), time (Control mean +/- SEM: 13.56 +/- 0.18, OG1RF: 13.22 +/- 0.18, $p=0.2010$, t-test, Figure 5-12E) or straightness of travel of macrophages (Control mean +/- SEM: 0.27 +/- 0.005, OG1RF: 0.27 +/- 0.007, $p=0.9897$, t-test, Figure 5-12F) .

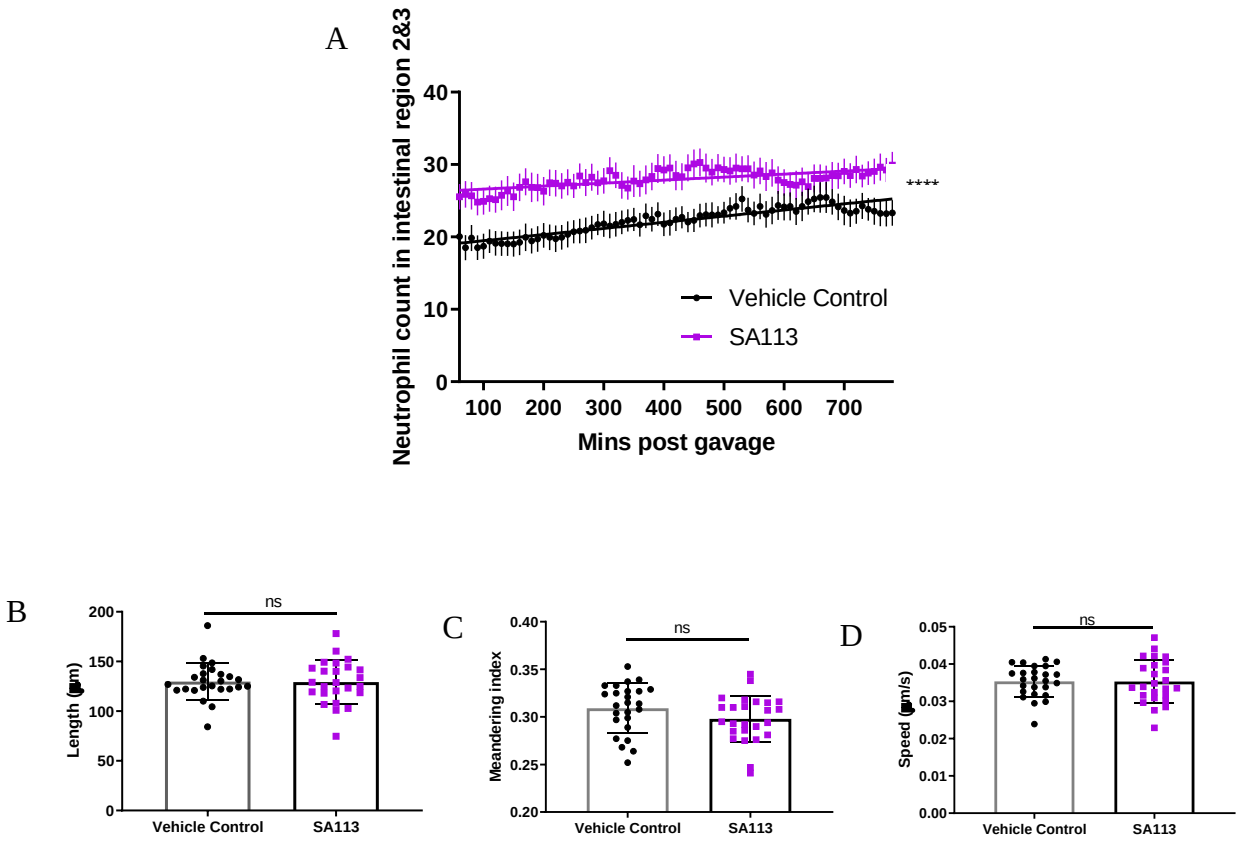

Figure 5-11: Neutrophilic response to SA113 microgavage in the zebrafish larval GIT. 4dpf *TgBAC(mpx:GFP)i114* larvae were microgavaged with either 10^5 CFU of SA113 or PBS control. A 60min recovery period in clean E3 prior to agarose immobilisation was introduced to allow elimination of any excess microgavaged bacteria. Imaging was performed with an inverted Olympus microscope and Yokagawa CXU spinning disk interfaced with Perkin Elmer Volocity® 6.3 software. **A**. Graph of neutrophil numbers versus time. N=24/group in three independent repeats, error bars show SEM, comparison with linear regression, ****$p<0.0001$. Further analysis of neutrophil movement was then made of the tracked cells in terms of **B**. Length, **C**. Meandering index (or straightness of travel), and **D**. Speed of movement. N=24/group in three independent repeats, comparison with t-test, ns=non-significant, error bars show SD.

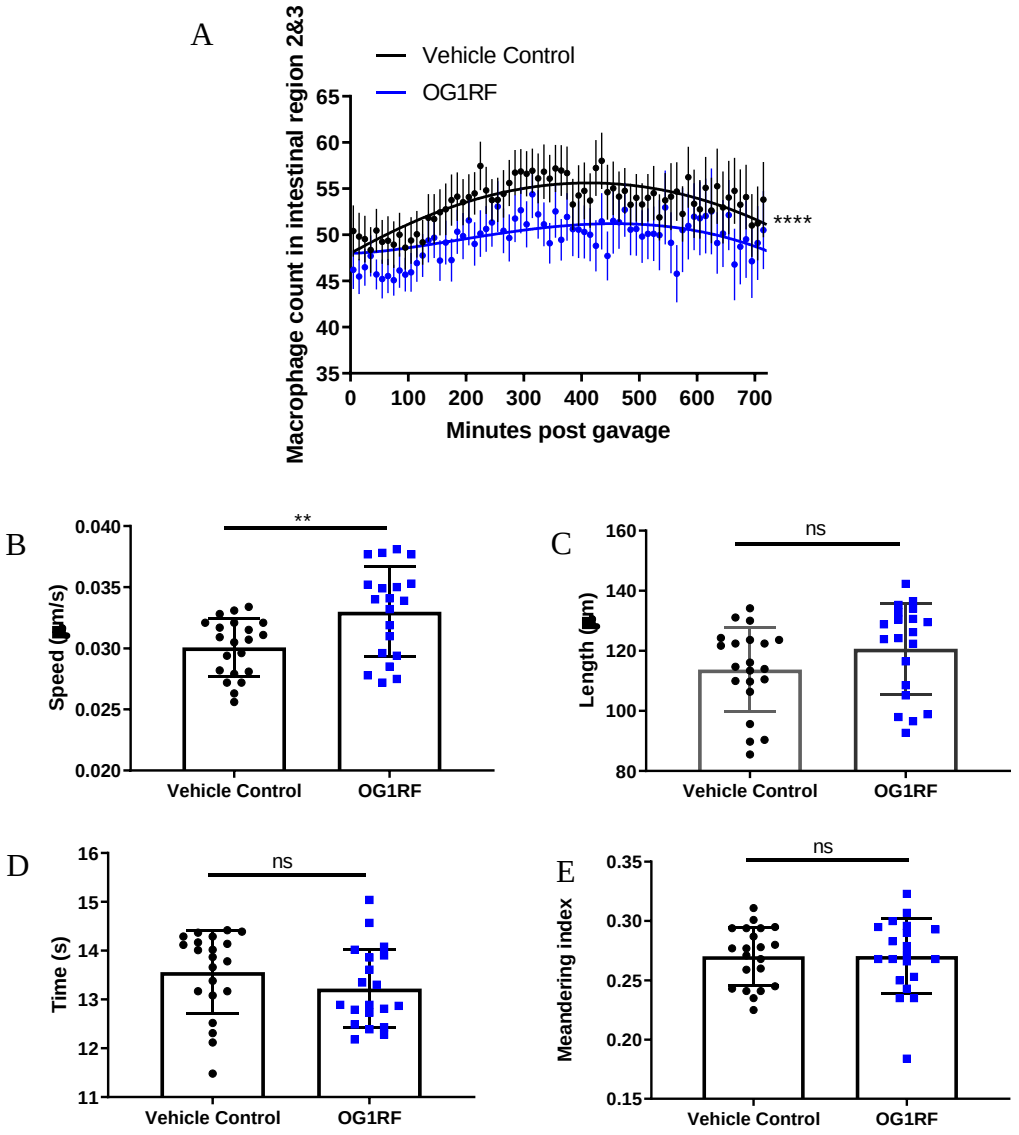

Figure 5-12: Macrophage response to *E. faecalis* colonisation in the uninjured intestine. 4dpf *Tg(mpeg1:NLS-eGFP)sh436* larvae were microgavaged with OG1RF or vehicle control, recovered for 60 minutes then imaged for 12 h using an inverted Olympus microscope and Yokagawa CXU spinning disk interfaced with Perkin Elmer Volocity® 6.3 software. **A**. Graph of number of macrophages in region 2&3 of zebrafish larvae against time. Curve fitted with Beta Growth and Decline model, comparison of Ymax with Poisson regression, ****p<0.0001, N=21/group in three independent repeats. Error bars show SEM. Parameters of macrophage movement were analysed in terms of **B**. speed, **C**. path length, **D**. time of travel, or **E.** meandering index. For each: N=21/group in three independent repeats, comparison with t-test, ns=non-significant, **p<0.01 Error bars show SD.

5.2.9 **Generation of a new transgenic zebrafish *TgBAC(Cldn15la:Col1a2-eGFP)***

The midgut of the zebrafish larvae possesses the equivalent of human intestinal M-cells, which are thought to sample luminal contents by endocytosis (Rombout and van den Berg, 1985). In order to determine the precise anatomical location of colonising *E. faecalis*, a fluorescent line that would outline the intestinal cells was needed, but in addition, a collagen specific reporter line would allow visualisation of intestinal tube healing occurring following intestinal trauma. A new fluorescent gut line was therefore generated, *TgBAC(Cldn15la:Col1a2-eGFP)sh546*, which would express the fusion protein Col1a2-eGFP (Morris *et al.*, 2018) driven by the intestinal specific *Claudin 15-like-a* (*Cldn15la*) promoter on chromosome 2 (Alvers *et al.*, 2014). To enable maximum visualisation of the intestinal tract in the adult fish, the Casper background was utilised. BACs that overlapped the *Cldn15la* (ENSDARG00000016081) site were selected using the zebrafish genome assembly GRCz10, aligned with the CHORI-211 BAC library (Bussmann and Schulte-Merker, 2011), and these were CHORI-211-135K10 and CHORI-211-170H3 (Figure 5-13A). Attempts with CHORI-211-135K10 were unsuccessful and indeed, this BAC has since been removed from the NCBI library as shown by a recent search (Figure 5-13B). Creation of a target construct using CHORI-211-170-H3 was successful, and thus this was used for final targeting of the *Col1a2-eGFP* construct. Successful incorporation and expression of the BAC was demonstrated (Figure 5-13C) in 3dpf larvae. Successive generations were raised to a stable F2 expression.

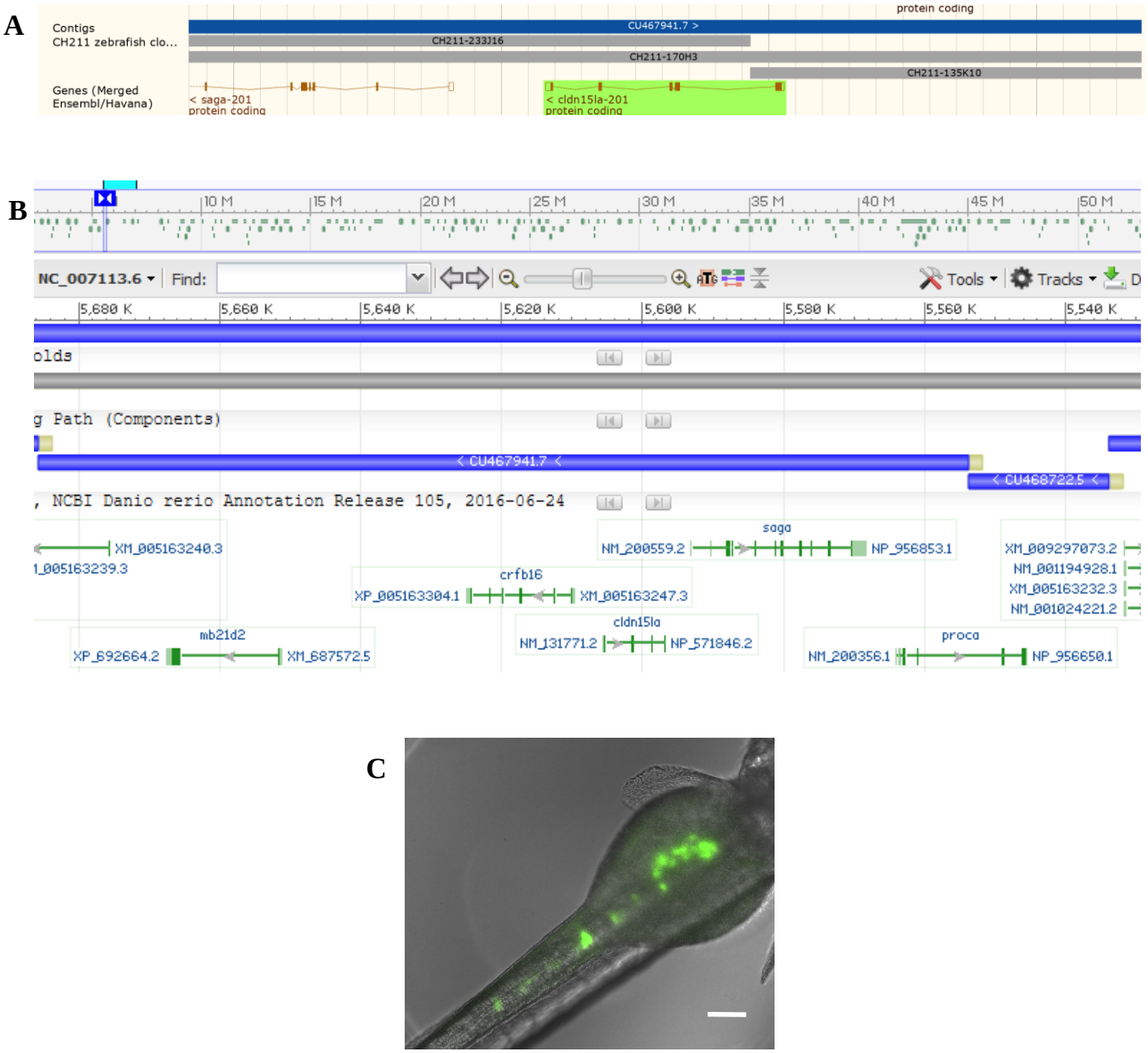

Figure 5-13: Generation of *TgBAC(Cldn15la:Col1a2-eGFP)sh546*. A. Snapshot of original alignment of *cldn15la* on Chromosome 2 (using GRCz10) with the overlapping BAC: CH211-170H3 (chosen) and CH211-135K10. **B**. Subsequent update snapshot of *cldn15la* still using GRCz10, with updated overlapping BAC: CH211-170H3 now renamed CU467941.7 with ruler at the top of the image. **C.** Representative image of successful integration of BAC following iTol2 injections at the single cell stage seen as fluorescence only within the GIT, at 3dpf. White scale bar indicates 50 µm.

5.2.10 **Collagen was expressed within the basement membrane only from 15dpf onwards when infolding of the intestinal tract begins**

The timing of collagen expression within the intestinal tract has thus far not been investigated. The premise of the fusion protein was that, being on a single fibril of the tri-fibrillar final collagen product, it would allow incorporation without structural interference from the attached eGFP molecule. As eGFP expression was driven exogenously by *Cldn15la*, a tight junction protein expressed from 3dpf onwards, knowing when endogenous collagen production occurs in zebrafish larvae would be advantageous to visualise healing. It had not been possible to distinguish intestinal specific collagen 1 from the same collagen within the skin from the TomoSeq data in the previous chapter. Therefore alternative histochemical methods were used. Picrosirius staining was performed on three wildtype zebrafish daily from 1dpf till 30dpf. Whole mount staining was done in younger fish, and the intestine dissected out in older fish, or frozen sections performed to allow differentiation from the skin. From studies in the rat intestine (Komuro, 1988), it was expected that a birefringent lattice appearance as seen in Figure 5-14A&B, would be seen. Surprisingly, no collagen was expressed within the intestinal tract for the first week post fertilisation (Figure 5-14C). In a single fish (of three) at 9dpf, some birefringence was seen in the basement membrane of the anterior intestinal bulb (Figure 5-14D), but none in the distal intestine. It is possible that extracellular matrix (ECM) formation within the anterior intestinal tract differs from that of the mid and distal GIT, as was suggested by differential collagen loss between the stomach and the rest of the GIT in rats after a 30 day space flight (Atiakshin *et al.*, 2019). In the hindgut, birefringence was not demonstrated up to and including 12dpf (Figure 5-14E). Birefringence was only demonstrated in the entire GIT in all three larvae on 13dpf, when the intestinal tract begins to lengthen and fold (Figure 5-15A). After 13dpf, birefringence was reliably demonstrated throughout the intestinal tract. Representative images are shown of 20dpf (Figure 5-15B), 22dpf (Figure 5-15C), and 25dpf larvae (Figure 5-16A). Although there was a suggestion of regular arrangements of collagen fibres in all these images, these appeared to be quite widely spaced (26dpf in Figure 5-15B). A much closer lattice pattern is seen in the gallbladder (27dpf in Figure 5-15C), and again this is of interest as the collagen content of the teleost biliary system has not previously been described.

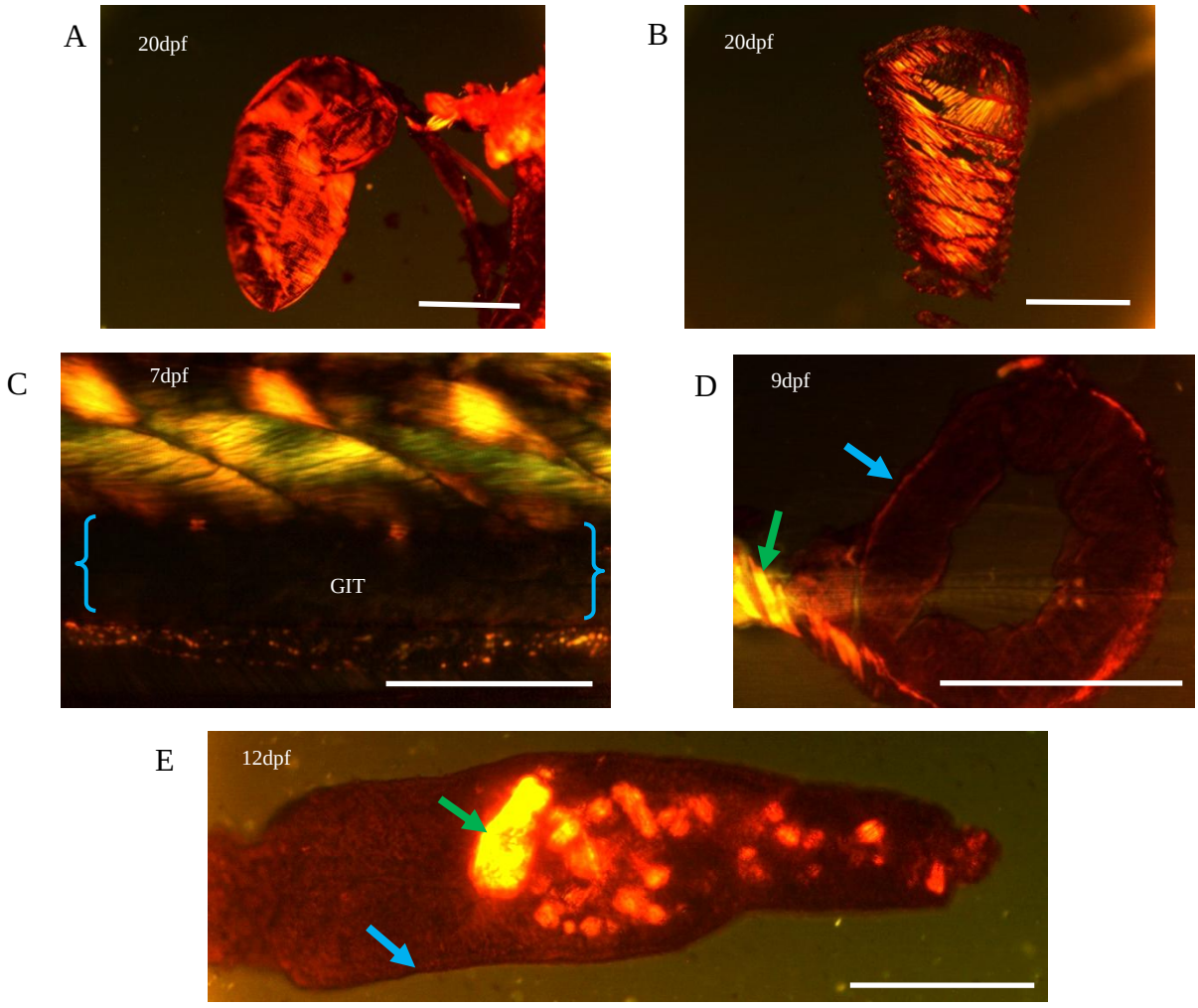

Figure 5-14: Picrosirius staining in 7-12dpf zebrafish. Imaging was performed with polarising lenses on a MZ12.5stereomicroscope (Leica) interfaced with a SPOT Insight Colour camera, and SPOT Advanced digital image capture software (Diagnostic Instruments). **A**. A 20dpf zebrafish, dissected air sac at 5X magnification showing lattice pattern that was expected of collagen deposition. **B**. Longitudinal frozen section of 20dpf zebrafish skin showing the parallel arrangement of collagen fibres. Both these confirm that, if similar collagen arrangements were present in the GIT, the picrosirius experimental protocol, as well as microscopy settings, would be able to demonstrate this sufficiently. **C**. 7dpf zebrafish larvae showing lack of birefringence in the intestinal tract (area bracketed in blue). **D**. Transverse section of 9dpf zebrafish in the region of the anterior intestinal bulb (blue arrow) showing faint birefringence compared to skin (green arrow) in the basement membrane, at 40X magnification. Only one of three fish examined demonstrated this. **E**. 12dpf dissected distal intestine showing a lack of birefringence in the intestinal wall (blue arrow). Birefringence was demonstrated within the lumen from ingested Artemia (green arrow) as the larvae were not kept fasted for this procedure. White Scale bars: 50 µm.

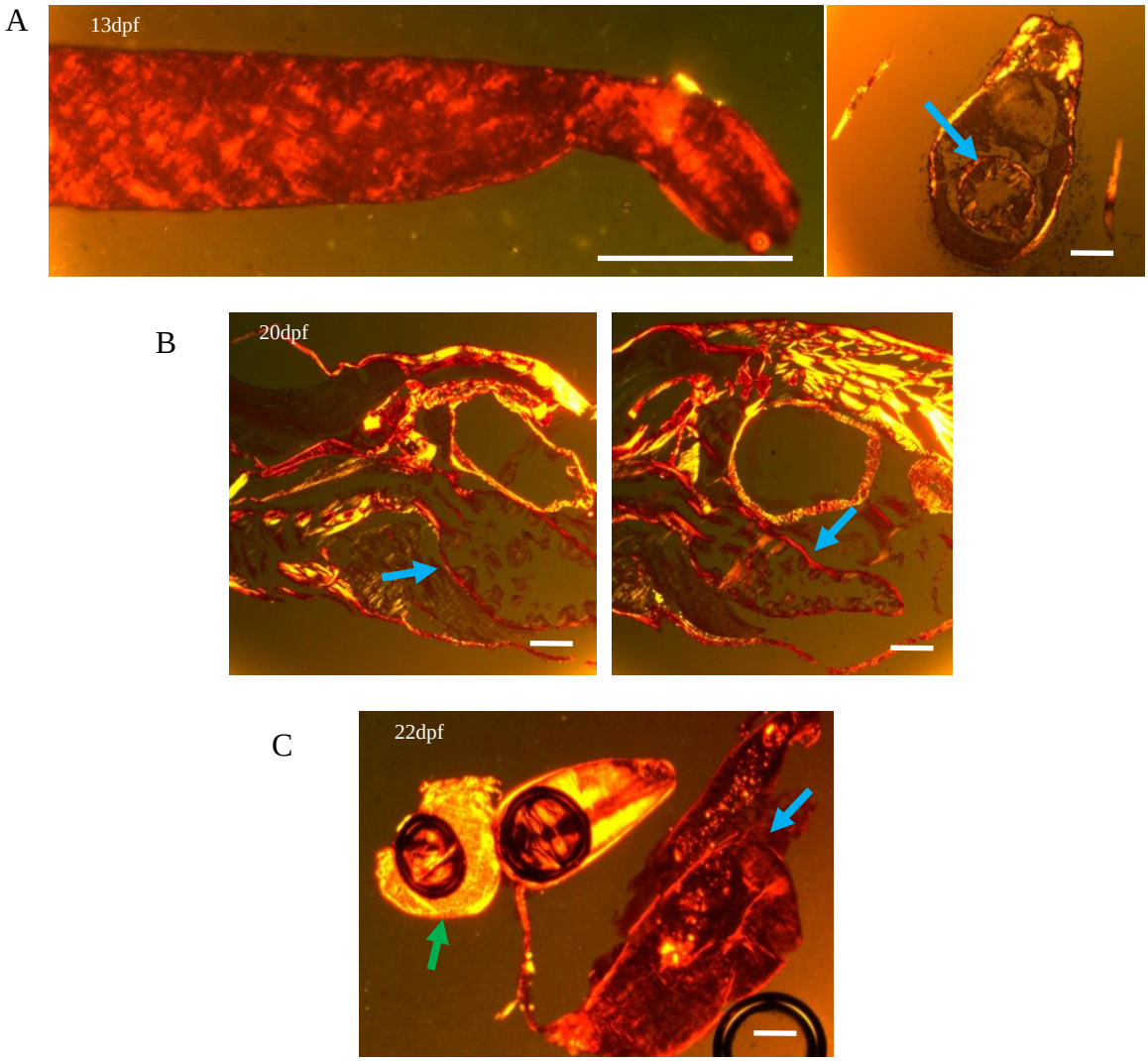

Figure 5-15: Picrosirius staining in 13-22dpf zebrafish. Imaging performed as before. **A**. Picrosirius staining of 13dpf larva. Left image showing a longitudinal section of dissected GIT at 20X magnification, and right image showing a transverse section in situ at 5X magnification (intestinal wall indicated with blue arrow). Ends of pectoral fins seen bilaterally unconnected to the body as this is at the level of the mid-intestine in transverse section. **B**. Sequential longitudinal frozen sections of 20dpf larvae, demonstrating birefringence within the wall of the anterior GIT (blue arrows). **C**. Dissected intestine and air sacs (green arrow) from a 22dpf zebrafish demonstrating birefringence in both organs, as well as the folded nature of the GIT (blue arrow) at this age. White Scale bars: 50 µm.

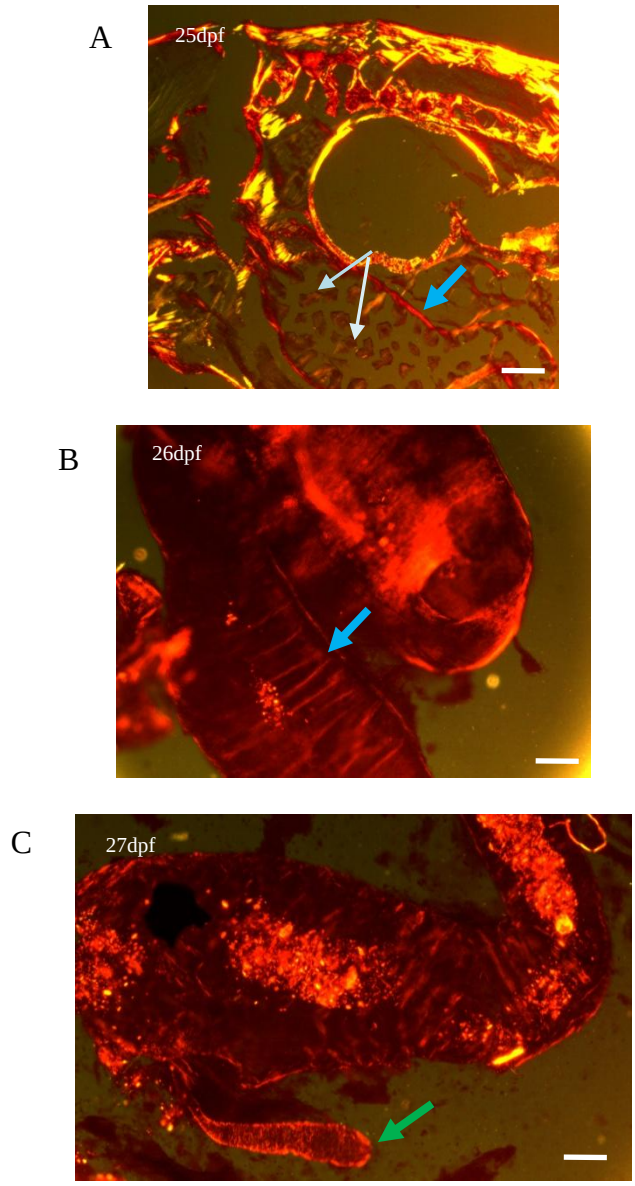

Figure 5-16: Picrosirius staining of 25-27dpf zebrafish. A. 25dpf at 5X magnification, anterior bulb of GIT (blue arrow), including rugae of the bulb (light blue arrow). **B**. 26dpf intestinal tube at 30X magnification. **C**. Dissected GIT of 27dpf zebrafish at 5X magnification. Again, Artemia within the lumen showed strong birefringence. Gallbladder attached (green arrow). White Scale bars: 50 µm.

5.2.11 **Colonising *E. faecalis* was closely association with the intestinal villi**

As the transgenic was driven by an exogenous promoter, *cldn15la*, the gut tube fluoresced from 3dpf enabling use of this line as a generic Gut-GFP transgenic, even though, from the picrosirius staining above, endogenous collagen did not appear to be produced at this time. At older ages of the zebrafish, live imaging of the intestinal tract has inherent complexities due to the frequent peristaltic movement causing artefact during any lengthy image acquisition. Cessation of intestinal peristalsis required for clear image comparison or image reconstruction could be obtained by 1 mM of glucagon within the embedding agarose without appreciable effect on survival. With light sheet microscopy and image mapping with fluorescent beads, 3D reconstruction using FIJI the intestinal tube could be isolated and reconstructed in a whole fish giving detailed intestinal morphology (Figure 5-17A). Utilising this transgenic as a generic Gut-GFP at with OG1RF colonisation at 4dpf, live imaging was performed with rapid image capture without the use of antiperistaltic agents, and z-slices demonstrated that the colonising bacteria were not free flowing within the lumen (Figure 5-17B). However, it was not possible to determine if the bacteria were intra- or extracellular due to the anatomic configuration of the intestinal crypts on the single longitudinal slice. Therefore 3D reconstruction was performed and this suggested, but could not confirm, that the bacterial clumps were extracellular (Figure 5-17C).

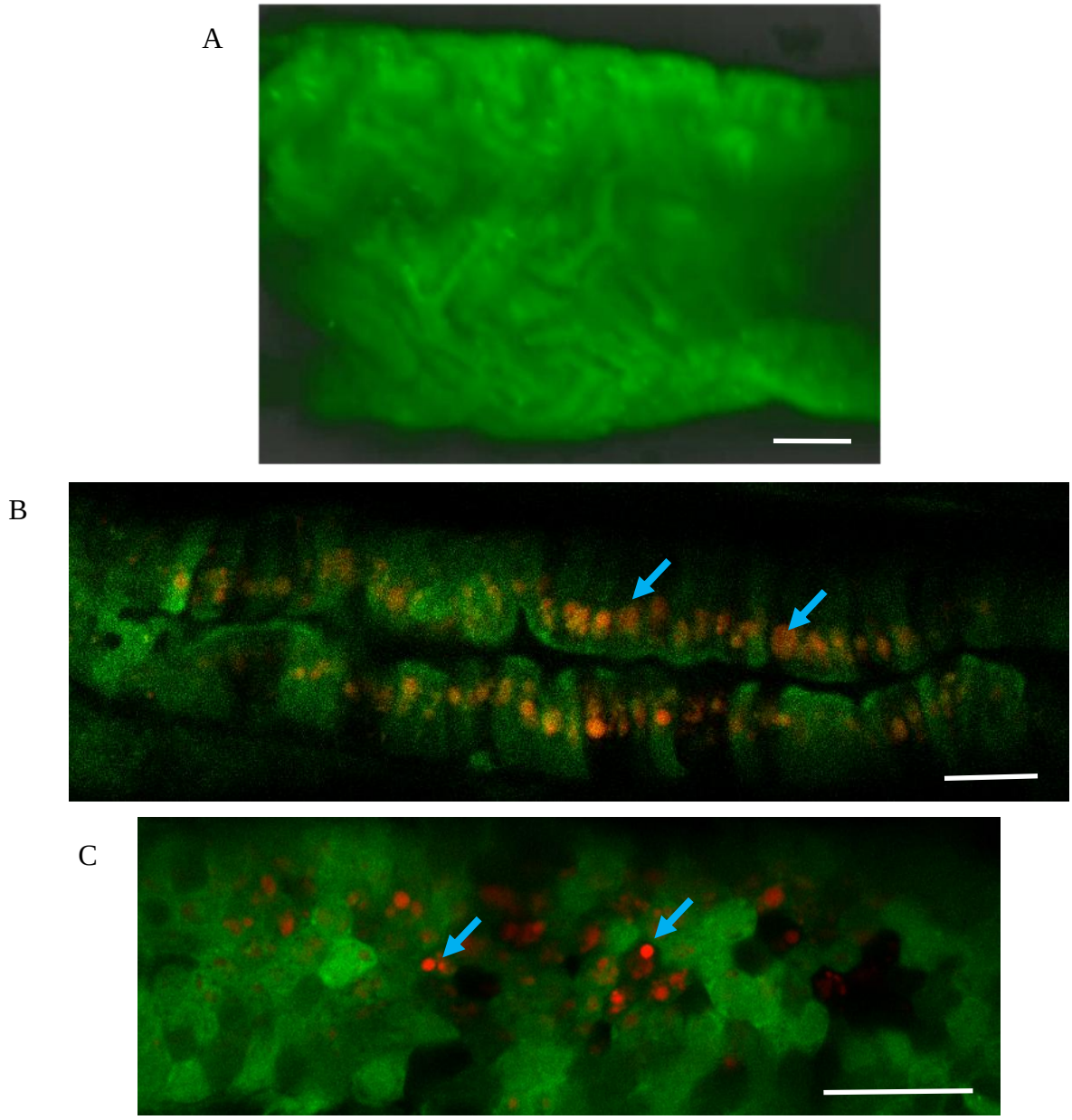

Figure 5-17: Live imaging of *TgBAC(Cldn15la:Col1a2-eGFP)*. A. 14dpf larva imaged using a light sheet Leica TCS SP8 DLS to demonstrate feasibility of isolating the green fluorescence of intestinal epithelial cells with a 10X objective, deconvolution and reconstruction using FIJI. **B**. An *E. faecalis* colonised 5dpf *TgBAC(Cldn15la:Col1a2-eGFP)* larva was imaged using 40X magnification and a Ziess LSM880 AiryScan Confocal for a rapid image capture without the use of anti-peristaltic agents. OG1RF-mCherry clumps indicated by blue arrows. **C**. An *E. faecalis* colonised 5dpf *TgBAC(Cldn15la:Col1a2-eGFP)* larva. Reconstruction of a z-stack (with antiperistaltic agent) using images from the Ziess LSM880 AiryScan Confocal, showed clumps of *E. faecalis* indicated by blue arrows. White Scale bars: 50 µm.

5.2.12 **Colonising *E. faecalis* were viable and not invading intracellularly**

Additional investigations were required to confirm the hypothesis that colonising *E. faecalis* did not invade intra-cellularly, so transmission electron microscopy (TEM) was performed. 100 ultrathin slices from three different larvae were obtained and examined using a FEI Tecnai Transmission Electron Microscope. Live *E. faecalis* were seen closely associated to the intestinal villi (Figure 5-18A), viability was confirmed by the preservation of the ultrastructure of the bacterium (Figure 5-18B&C). It appeared that the close association of *E. faecalis* with the villi was an active process, with the host playing a large role as accidental cessation of circulation through an overdose of anaesthesia during live imaging was observed to result in the discrete clumps disappearing into a smear within a short space of time. This was indirectly suggested by TEM images showing a number of *E. faecalis* within the intestinal lumen, but not closely associated with villi (Figure 5-18D&E). This could be artefactual due to the long TEM preservation process dislodging the bacteria, but the ultrastructure of *E. faecalis* in these cases were preserved suggesting that their viability was intact at the time of fixation. Regions 2&3 of the zebrafish larval intestine are a site of active endocytosis and even though many endocytosed bodies were seen (purple arrows in Figure 5-18F&G), these were considerably larger than *E. faecalis* and no cells contained inclusions with the distinctive septum formation of viable *E. faecalis* (Ran, He and Liang, 2013). This lack of cellular invasion is consistent with the non-pathogenic nature of *E. faecalis* as commensals within the human gastrointestinal tract. Demonstration of the ultrastructure of *E. faecalis* was important for confirmation since other species were also seen intraluminally (Figure 5-19A&B). Several other features of interest were noted. A leukocyte with a multi-segmented nucleus was seen transmigrating at the epithelial border (Figure 5-19C), and collections of lysosomes (Moe, Rostgaard and Behnke, 1965) were seen in the proximal intestine (Figure 5-19D). Anatomically, the proximal intestine was confirmed by the scarcity of mucin secreting Goblet cells which are more prominent only distally within the GIT. The lysosome collections correspond with the digestive capacity of this region of the intestine.

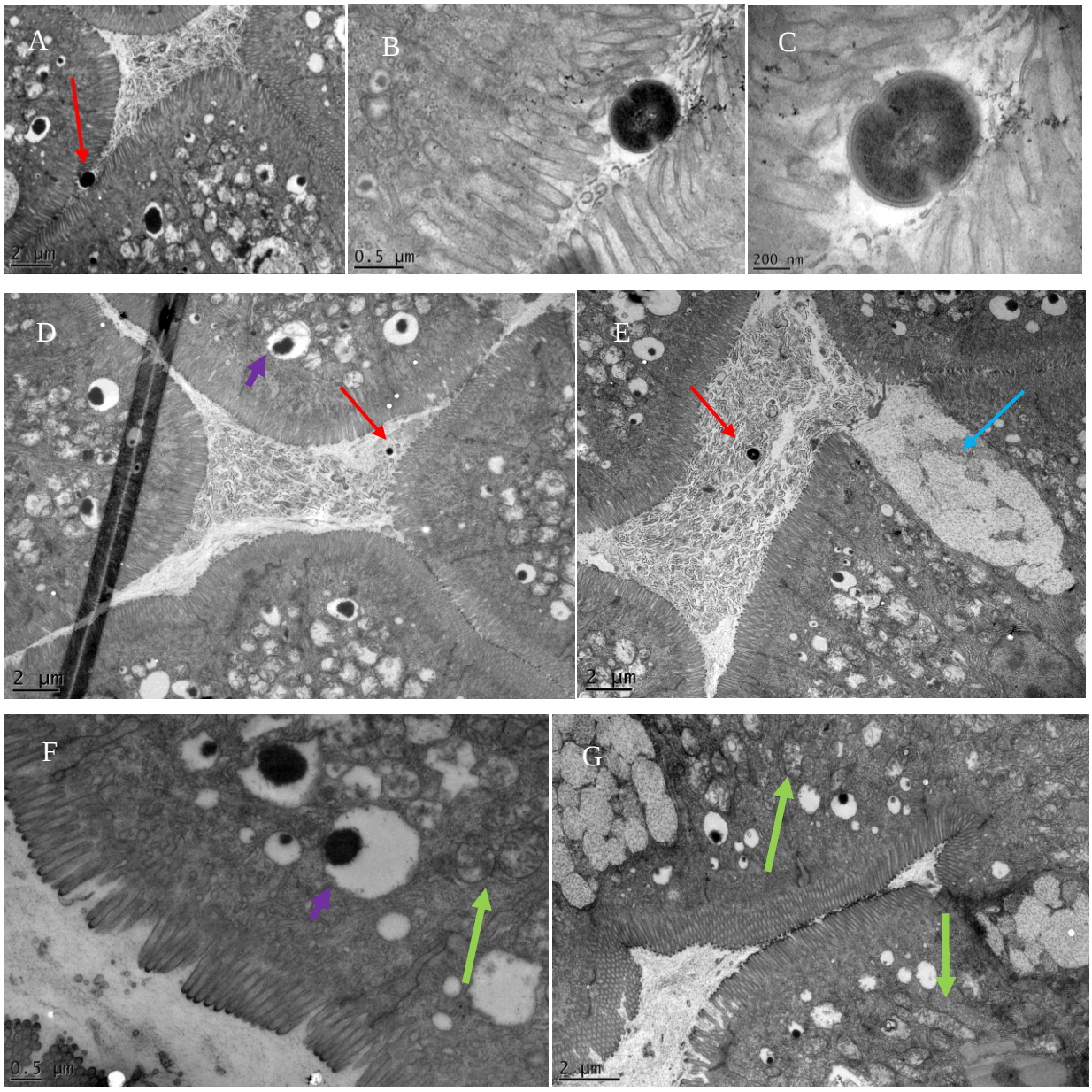

Figure 5-18: TEM images of transverse sections of *E. faecalis* colonised 5dpf zebrafish. A. Extracellular and intraluminal *E. faecalis* (red arrow). **B & C**. Higher magnification demonstrating the distinctive morphology of a viable *E. faecalis*. **D**. *E. faecalis* demonstrated intraluminally (red arrow) but not in close association to villi. **E.** Goblet cells (blue arrow) secreting mucin indicating mid to distal intestinal region, corresponding to the anatomical region of colonisation. F & G. Abundant mitochondria (green arrow) in regions of inclusion bodies (purple arrow).

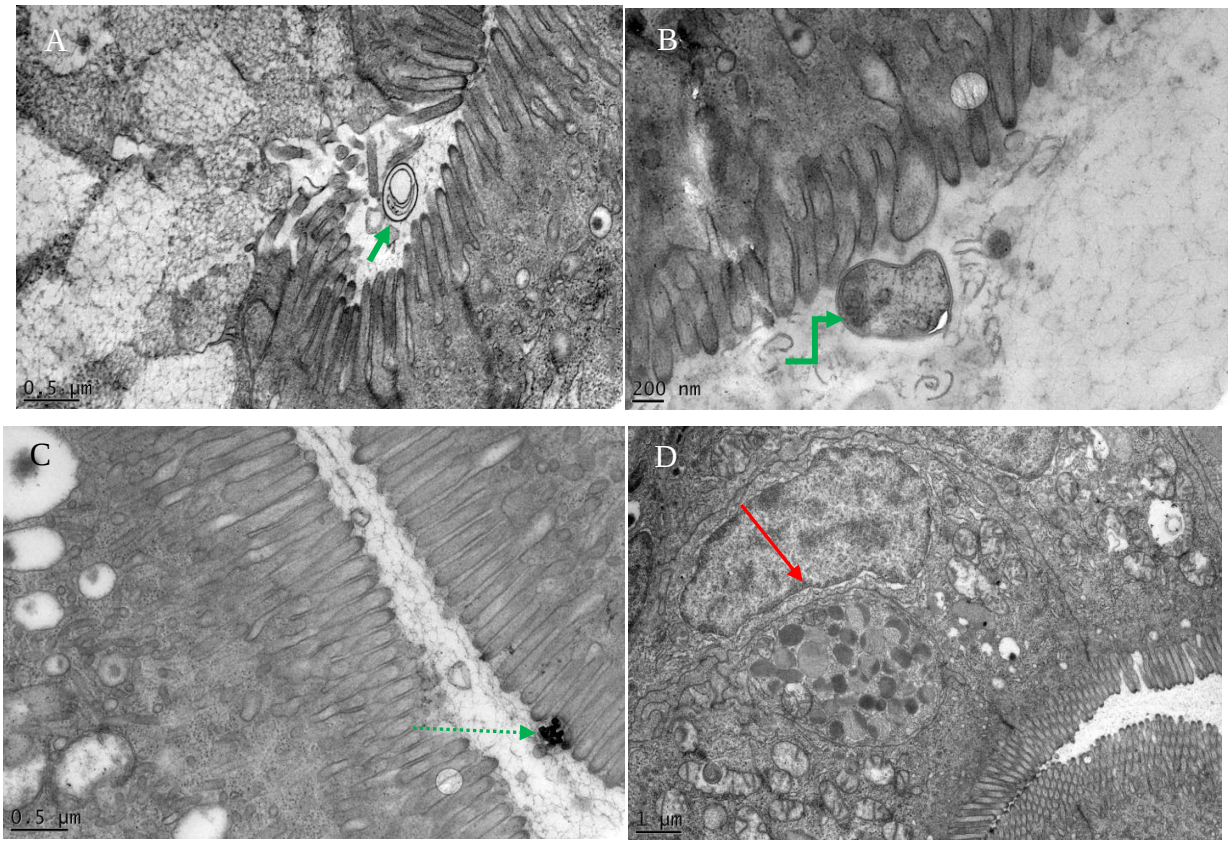

Figure 5-19: TEM images of transverse sections of *E. faecalis* colonised 5dpf zebrafish. Other intraluminal structures were seen and could represent **A**. parasitic ova (green arrow) or **B**. protozoa (green arrow). **C**. Leukocyte with a multi-segmented nucleus (red arrow) seen at the intestinal epithelial border. **D**. Lysosomes (red arrow) indicating region in the proximal intestine with the absence of goblet cells which are present in the distal intestine.

5.2.13 **In the presence of an acute intestinal injury, *E. faecalis* increased neutrophil infiltration**

Rodent studies have shown a 500X increase in *E. faecalis* in the region of the intestinal wounds following a surgical procedure (Shogan *et al.*, 2014), and it was hypothesised that prior colonisation with these bacteria would evoke a more robust inflammatory response to an injury. In the earlier experiments of an uninjured intestine, neutrophil numbers were unchanged by the presence of *E. faecalis* (Figure 5-10). A puncture wound was therefore introduced in the distal intestine, remote from the site of colonisation so as not to cause physical disruption to colonising bacteria. Live imaging immediately following injury showed that the presence of *E. faecalis* in this setting showed an increase in neutrophil number at the intestinal wound (Control Ymax: 21.52, OG1RF: 23.26, $p<0.0001$, Poisson regression, curve fitting using beta growth and decline model, Figure 5-20A). Neutrophils patrolling the wounded area were occasionally seen to contain phagocytosed bacteria (Figure 5-20B), but the presence of *E. faecalis* did not otherwise change other parameters of neutrophil movement such as straightness of travel (Control mean +/- SEM: 0.29 +/- 0.00055, OG1RF: 0.28 +/- 0.0039, $p=0.1312$, t-test, Figure 5-20C), path length (Control mean +/- SEM: 133.9 +/- 2.92, OG1RF: 135.47 +/- 2.69, $p=0.7112$, t-test, Figure 5-20D), speed (Control mean +/- SEM: 0.040 +/- 0.00060, OG1RF: 0.040 +/- 0.00058, $p=0.6557$, t-test, Figure 5-20E) or travel time (Control mean +/- SEM: 12.43 +/- 0.14, OG1RF: 12.62 +/- 0.16, $p=0.3941$, t-test, Figure 5-20F).

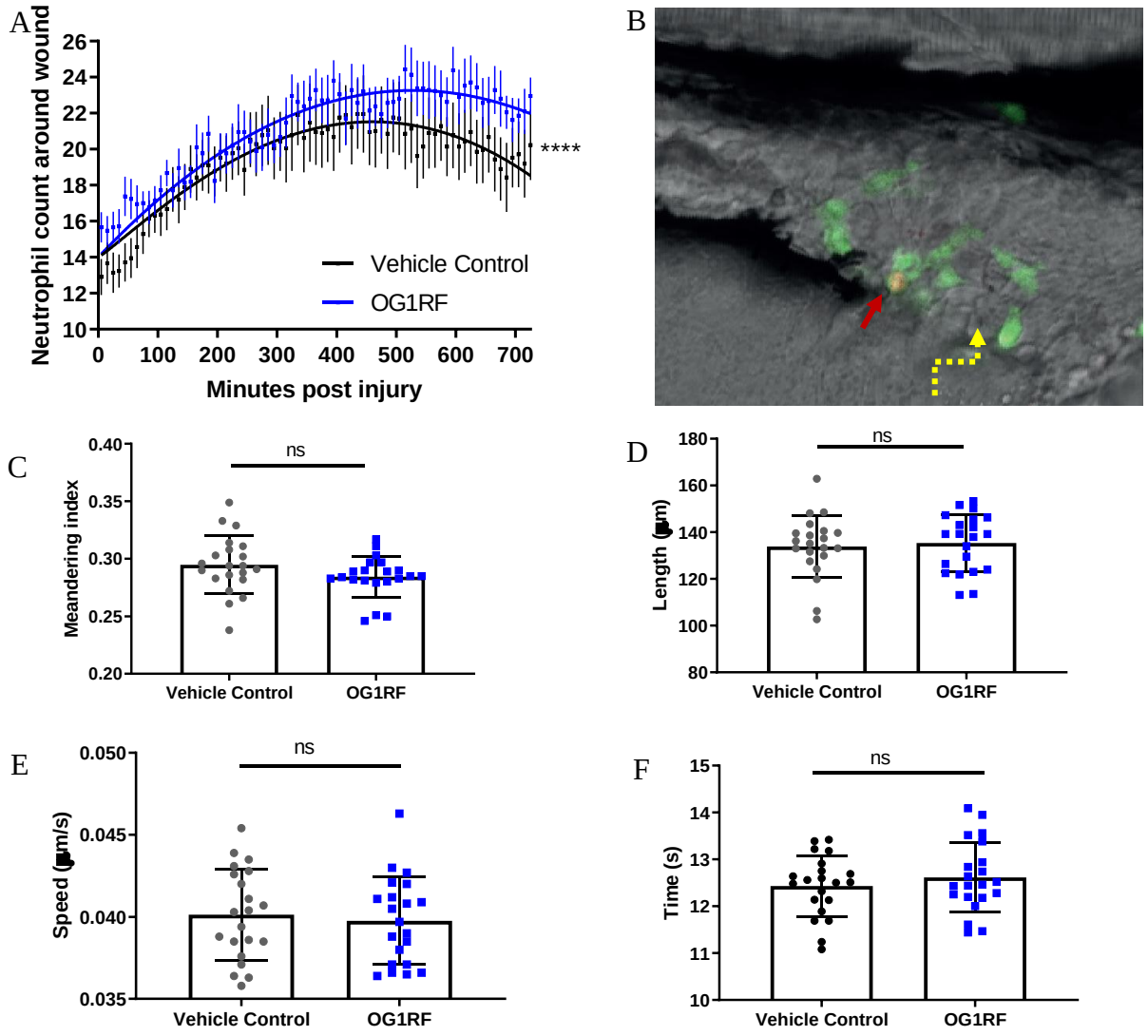

Figure 5-20: Neutrophil responses to an acute intestinal injury in the presence of *E. faecalis* colonisation. 4dpf *Tg(mpx:GFP)*i114 were imaged with an inverted Olympus microscope and Yokagawa CXU spinning disk interfaced with Perkin Elmer Volocity® 6.3 software. **A**. Time course of neutrophil response to the site of injury in the presence of *E. faecalis*. N=21/group in three independent repeats. Comparison of with Poisson regression, ****$p<0.0001$, error bars show SEM. **B**. Image of puncture wound (yellow dotted arrow) taken with 40X objective with the Ziess LSM880 AiryScan Confocal microscope interfaced with Zen Black software. A neutrophil engorged with phagocytosed OG1RF-mCherry bacteria (red arrow) was demonstrated. Characteristics of neutrophil movement were analysed in terms of (**C)** meandering index, (**D)** Path length, (**E)** speed, and (**F)** time. In each: N=21/group in three independent repeats, comparison with unpaired t-test, ns=non-significant. Error bars show SD.

5.2.14 **RvE1 and RvD2, but not LXA4 reduced peak neutrophil numbers at an intestinal injury in the presence of *E. faecalis***

SPMs previously differentially modulated neutrophil responses to an intestinal injury without colonisation. It was hypothesised that the presence of *E. faecalis* would alter these responses. When injury was performed in the presence of *E. faecalis*, LXA4 now no longer affected peak neutrophil counts (Control+OG1RF Ymax: 24.21, LXA4+OG1RF Ymax: 24.48, p=0.1202, Poisson regression, curves fitted with beta growth and decline model, Figure 5-21A). RvD2 appeared to reduce the peak neutrophil numbers (Control+OG1RF Ymax: 21.72, RvD2+OG1RF Ymax: 20.80, p=0.0002, Poisson regression, Figure 5-21C). Where previously neutrophil counts were increased, now in the presence of *E. faecalis*, RvE1 significantly reduced neutrophil numbers (Control+OG1RF Ymax: 25.51, RvE1+OG1RF Ymax: 23.08, p<0.0001, Poisson regression, Figure 5-21C).

Although neutrophil numbers were not reduced by LXA4, neutrophil speed (Control mean +/- SEM: 0.039 +/- 0.0006, LXA4: 0.042 +/- 0.0006, p=0.0071, t-test, Figure 5-22A) and path length (Control mean +/- SEM: 137.8 +/- 2.28, LXA4: 148.6 +/- 2.76, p=0.0039, t-test, Figure 5-22B) were increased, and straightness of travel decreased (Control mean +/- SEM: 0.31 +/- 0.007, LXA4: 0.29 +/- 0.006, p=0.0187, t-test, Figure 5-22C). None of the neutrophil parameters in terms of speed (Control mean +/- SEM: 0.042 +/- 0.001, RvD2: 0.041 +/- 0.001, p=0.7860, t-test), path length (Control mean +/- SEM: 145.3 +/- 3.71, RvD2: 147.8 +/- 3.40, p=0.6275, t-test), or straightness of travel (Control mean +/- SEM: 0.29 +/- 0.05, RvD2: 0.28 +/- 0.007, p=0.1357, t-test) were changed by RvD2. RvE1 did not change speed (Control mean +/- SEM: 0.033 +/- 0.001, RvE1: 0.033 +/- 0.001, p=0.9925, t-test) or path length (Control mean +/- SEM: 122.3 +/- 3.21, RvE1: 124.9 +/- 4.05, p=0.6233, t-test) but increased straightness of travel (Control mean +/- SEM: 0.29 +/- 0.002, RvE1: 0.27 +/- 0.004, p=0.0095, t-test).

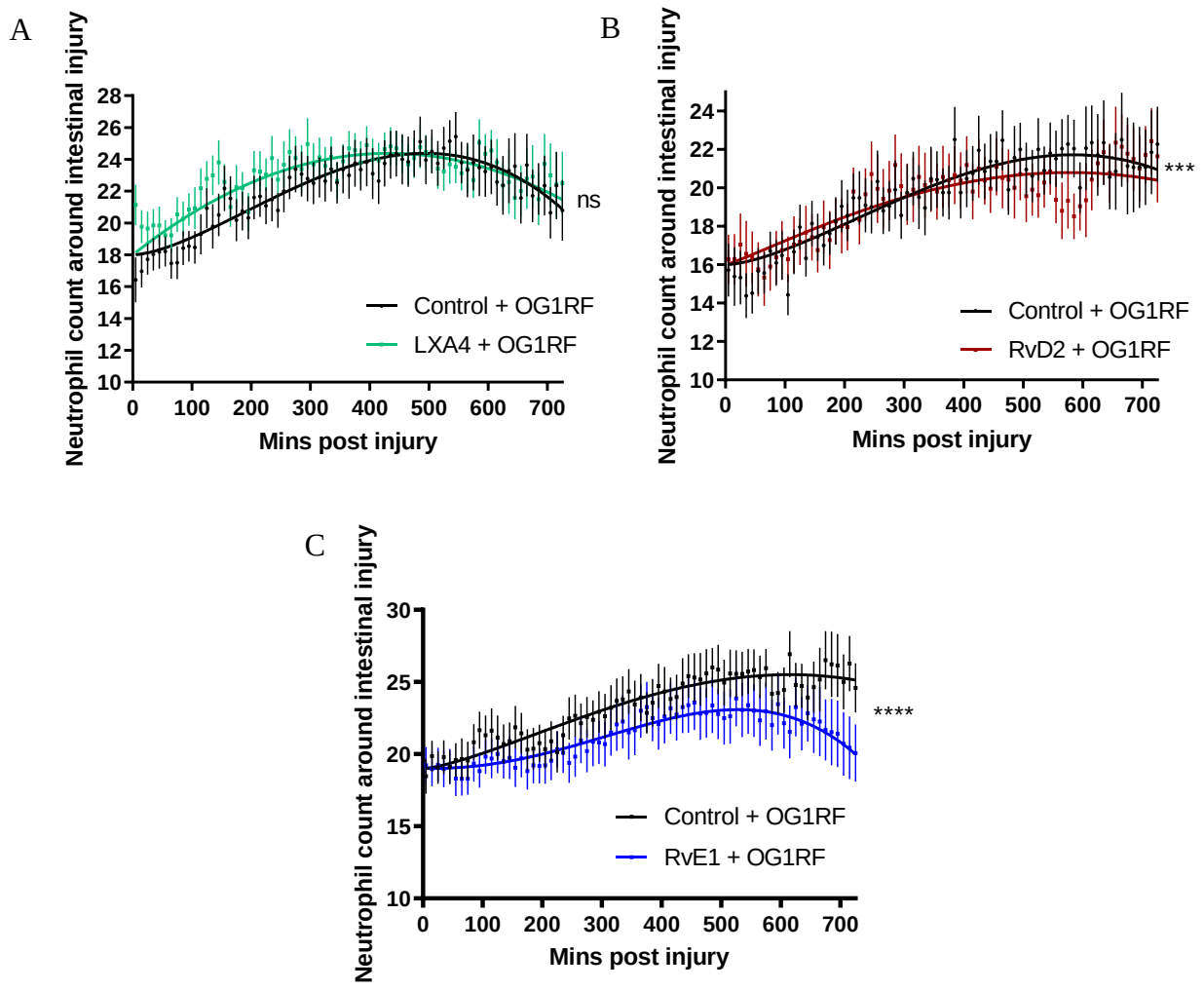

Figure 5-21: Neutrophil responses to an acute intestinal injury in the presence of *E. faecalis* colonisation with treatment with SPM treatment. 4dpf *Tg(mpx:GFP)i114* larvae were imaged with an inverted Olympus microscope and Yokagawa CXU spinning disk interfaced with Perkin Elmer Volocity® 6.3 software. Neutrophils were quantified around the ROI in the distal intestine, for 12h after injury and treatment with SPM or vehicle control A. LXA4. N=28/group in three independent repeats. B. RvD2. N=21/group in three independent repeats. C. RvE1. N=28/group in three independent repeats. In each: curves fitted with the Beta Growth and Decline model, comparison of Ymax with Poisson regression, ns=non-significant, ***p<0.001, ****p<0.0001, error bars show SEM.

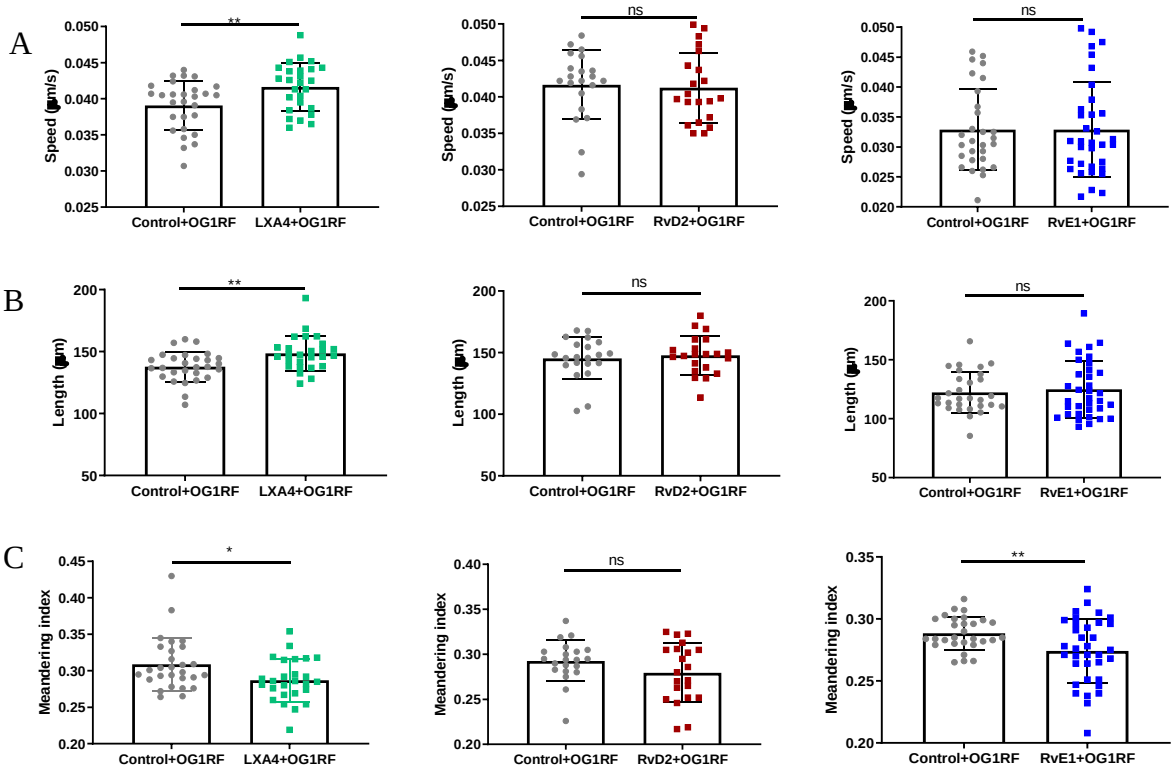

Figure 5-22:Parameters of neutrophil movement around an intestinal injury in the presence of *E. faecalis* with or without SPM treatment. Tracked neutrophils attending to the intestinal wound in the presence of OG1RF, and SPM (LXA4, RvD2 or RvE1) from before were analysed in Volocity® 6.3 software in terms of **A**. Speed, **B**. Path length, and **C**. Meandering index (straightness of travel) For LXA4, N=24/group in three independent repeats. For RvD2, N=21/group in three independent repeats. For RvE1, N=28/group in three independent repeats. In each: error bars show SD, comparison with t-test, ns=non-significant, *p<0.05, **p<0.01.

5.2.15 SPMs differentially affected peak macrophage numbers attending an intestinal wound in the presence of *E. faecalis*

In an intestinal wound in the presence of E. faecalis, LXA4 did not alter peak macrophage numbers (Control+OG1RF Ymax: 36.76, LXA4+OG1rf Ymax: 36.44, p=0.2029, Poisson regression, curves fitted with Beta Growth and Decline model, Figure 5-23A). RvD2 lowered the peak macrophage numbers (Control+OG1RF Ymax: 36.38, RvD2+OG1RF Ymax: 37.01, p=0.0178, Poisson regression, Figure 5-23B). RvE1 appeared to significantly increase the macrophage numbers (Control+OG1RF Ymax: 55.64, RvE1+OG1RF Ymax: 62.04, p<0.0001, Poisson regression, Figure 5-23C), however it must be noted that this was obtained from only a single experiment (N=7) due to a long spell of equipment failure. Nonetheless, parameters of macrophage movement were still analysed in all three SPMs, and were mostly unchanged by SPM treatment. Specifically, macrophage speed was unaffected by LXA4 (Control mean +/- SEM: 0.035 +/- 0.0008, LXA4: 0.035 +/- 0.0007, p=0.9063, t-test, Figure 5-24A), RvD2 (Control mean +/- SEM: 0.035 +/- 0.0007, RvD2: 0.035 +/- 0.0010, p=0.7483, t-test), or RvE1 (Control mean +/- SEM: 0.038 +/- 0.0015, RvE1: 0.040 +/- 0.0012, p=0.3278, t-test). Similarly, path length of macrophages was not affected by LXA4 (Control mean +/- SEM: 137.3 +/- 3.3, LXA4: 136.2 +/- 3.1, p=0.8059, t-test, Figure 5-24B), RvD2 (Control mean +/- SEM: 132.3 +/- 3.5, RvD2: 130.2 +/- 4.3, p=0.7154, t-test), or RvE1 (Control mean +/- SEM: 147.8 +/- 3.9, RvE1: 158.0 +/- 4.1, p=0.0964, t-test). Straightness of macrophage travel was unchanged in LXA4 (Control mean +/- SEM: 0.30 +/- 0.005, LXA4: 0.30 +/- 0.005, p=0.8273, t-test, Figure 5-24C) and RvD2 (Control mean +/- SEM: 0.31 +/- 0.006, RvD2: 0.30 +/- 0.007, p=0.7027, t-test), but RvE1 appeared to decrease straightness of travel (Control mean +/- SEM: 0.32 +/- 0.008, RvE1: 0.29 +/- 0.006, p=0.0274, t-test). This final finding was again obtained from a single experiment (N=7).

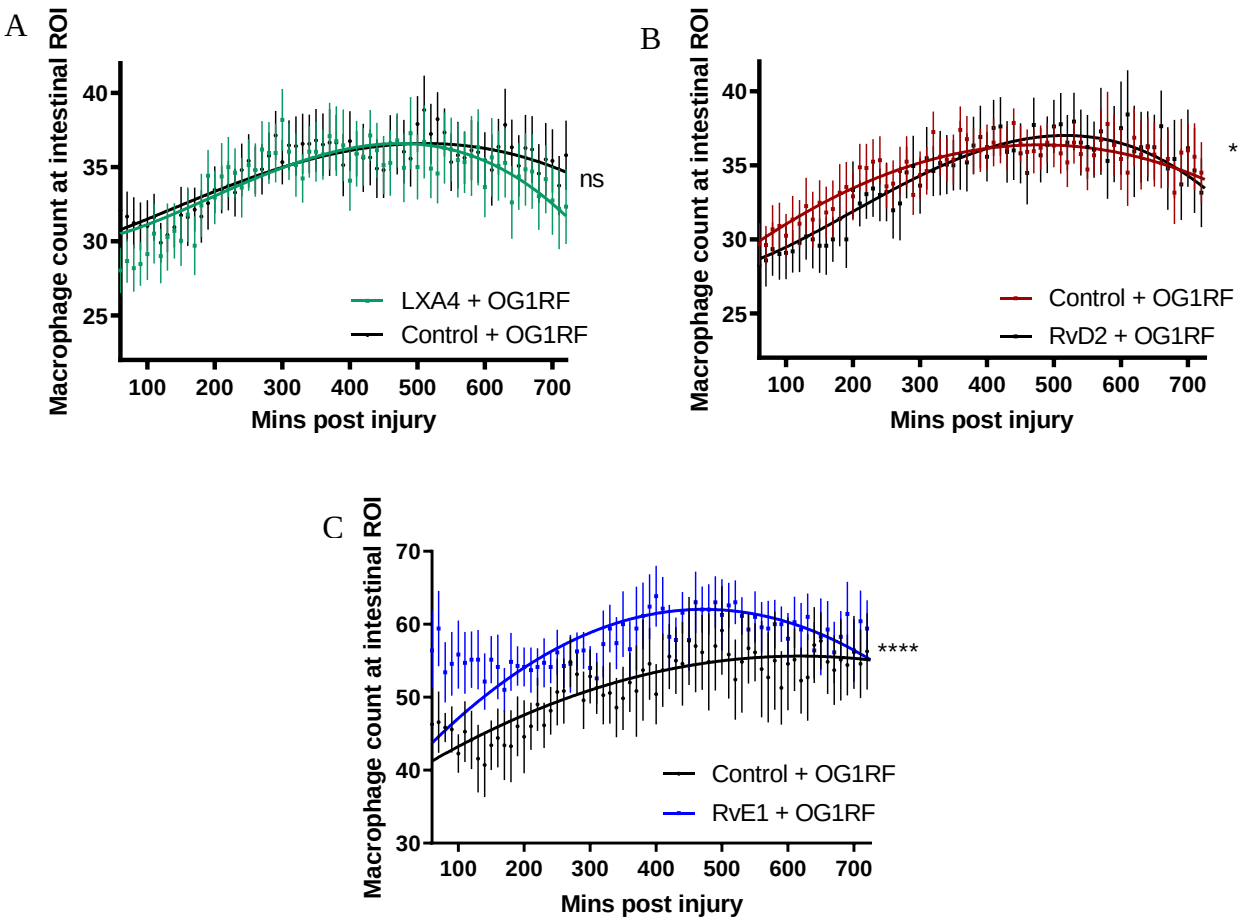

Figure 5-23: Macrophage responses to an acute intestinal injury in the presence of *E. faecalis* colonisation with treatment with SPM treatment. 4dpf *Tg(mpeg1:NLS-Clover)* larvae were imaged with an inverted Olympus microscope and Yokagawa CXU spinning disk interfaced with Perkin Elmer Volocity® 6.3 software. Macrophages were quantified around the ROI in the distal intestine, for 12h after injury and treatment with SPM or vehicle control but imaging was started an hour later than for neutrophils since these cells often have a delayed arrival. **A**. LXA4. N=21/group in three independent repeats. **B**. RvD2. N=21/group in three independent repeats. **C**. RvE1. N=7/group in a single experiment. In each: curves fitted with the Beta Growth and Decline model, comparison of Ymax with Poisson regression, ns=non-significant, *p<0.05, ****p<0.0001, error bars show SEM.

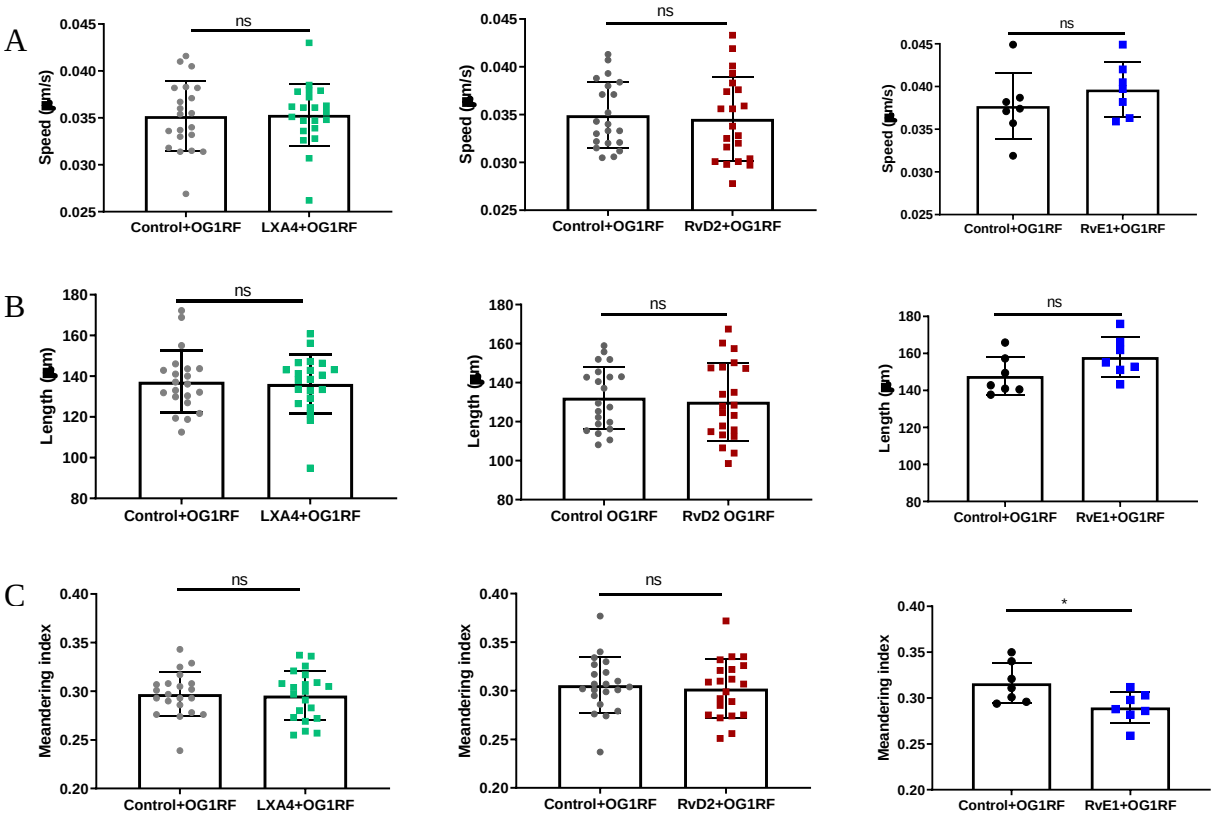

Figure 5-24: Parameters of macrophage movement around an intestinal injury in the presence of *E. faecalis* with or without SPM treatment. Tracked neutrophils attending to the intestinal wound in the presence of OG1RF, and SPM (LXA4, RvD2 or RvE1) from before were analysed in Volocity® 6.3 software in terms of A. Speed, B. Path length, and C. Meandering index (straightness of travel) For LXA4, N=21/group in three independent repeats. For RvD2, N=21/group in three independent repeats. For RvE1, N=7/group in a single experiment. In each: error bars show SD, comparison with t-test, ns=non-significant, *p<0.05.

5.3 **Discussion and future work**

The acute inflammatory response to intestinal injury has always been challenging to observe *in vivo*, since this organ is hidden within a body cavity, and efforts to exteriorise it for observation may impact upon physiological parameters. The zebrafish solves this difficulty by being transparent in the larval stage, whilst having a robust and comparable immune response to injury. This makes visualisation of the initial stages of inflammation in the intestine easily done without need of substantial manipulation. This model was therefore developed to visualise the *in vivo* responses to a mechanical intestinal injury in the presence of a clinically important bacteria, *Enterococcus faecalis*, and investigate how its presence might modulate the host inflammatory response to treatment with SPMs in this complex mucosal surface, distinct from skin.

In an effort to circumvent the unintended and often unavoidable effect that GF conditions can have on the development, priming and maintenance of the immune system and many other physiological parameters such as metabolic, cardiovascular and even growth rates of the organism (Smith, McCoy and Macpherson, 2007), the zebrafish model here was developed under conventional (non-GF) conditions. The model was performed over much shorter periods (days versus weeks) compared to rodent models, but even at this early unprotected stage demonstrated similar requirements for successful colonisation by *E. faecalis* to that of the mammalian intestine, namely, the *epaX* locus. It has been well described that the existing microbiome can influence the ability of a particular strain of bacteria to colonise (Lee *et al.*, 2013) and therefore, in characterising this colonisation model using the OG1RF Δ*EpaX* mutant, numerous larvae were tested on multiple occasions over a period of months, using different generations fish and raised in different mixtures of tank water, to expand possible variations in the core background microbiome. These differences did result in some variation in the actual CFU/larvae obtained but the trend of decreased colonisation by the mutant remained significant throughout.

The spatial distribution of persisting bacteria within the mid-intestine was quite distinctive but previous sequencing methods have shown that of the two dominant phyla within the adult zebrafish, *Proteobacteria* show an increasing abundance toward the caudal region, whereas *Firmicutes*, the phylum to which *E. faecalis* belongs, show the opposite trend (Roeselers *et al.*,

2011). The pattern obtained here in the larval model however does match the pattern of colonisation found with *E. coli* (belonging to the *Proteobacteria* phylum) in gnotobiotic larvae (Barber, Fleming and Mulvey, 2016). It is possible that due to the early stages of development, the adult distribution is yet to be established.

E. faecalis in humans is a widespread and common commensal and does not display pathogenic effects under normal conditions. This model appeared to confirm a similar pattern with zebrafish in that, although an increased NFκB expression was seen, consistent with the trend of published data (Kanther *et al.*, 2011), this did not translate to a higher neutrophil count, consistent with the trend in mammals (Barnett *et al.*, 2016), nor an increase in physiological parameters of inflammation such as mucin cell abundance, peristaltic contractions or cell death. This was further confirmed by the lack of cellular invasion of live *E. faecalis* on both fluorescent microscopy and TEM imaging.

Despite its non-invasive characteristic, *E. faecalis* has been implicated in the breakdown of wounds within the GIT (Shogan *et al.*, 2015). In investigating the early innate immune response to a mechanical injury of the intestinal tract in the presence of this bacteria, it was important to avoid a chemical disruption with TNBS or DSS previously described (Oehlers *et al.*, 2016), as this could have unknown consequences on the balance of intestinal microbiota, so the model of mechanical intestinal injury in zebrafish larvae developed earlier was utilised. Using this model, the expected increase in neutrophil numbers at the intestinal wound site with the additional presence of *E. faecalis* was demonstrated.

Different responses to medical treatment can sometimes be due to differences in microbiome composition (Vétizou *et al.*, 2016; Ananthakrishnan *et al.*, 2017), and it was hypothesised that the additional presence of *E. faecalis* would alter neutrophil responses to treatment with pro-resolving compounds (SPMs). Indeed, the effects of SPMs on the innate immune response to an acute wound were altered in the presence of an *E. faecalis* within the zebrafish larval intestine. *In vitro* cell studies have demonstrated that neutrophils had increased random movement on exposure to LXA4 and RvD2 (Norling *et al.*, 2016) due to blunting of neutrophil responses to the chemoattractant IL-8, and certainly this reached significance in our colonised wounding

model with LXA4 and RvE1 treatment. But in addition, although LXA4 did not alter the overall number of neutrophils attending to the wound site in the presence of *E. faecalis*, neutrophils travelled for longer distances and significantly faster. IL-8 remains an important chemoattractant up to the basal epithelium but the intestine possesses another inflammatory pathway, that of the eicosanoid hepoxilin A3 (HXA3), as an essential last step in driving intestinal inflammation, and which is activated by a variety of bacterial species (Szabady and McCormick, 2013). It had been suggested that LXA4, in binding to GPCRs (Fierro *et al.*, 2003), would be a sufficient functional stop signal in the case of HXA3 mediated migration, but given the preserved numbers of neutrophils in the *E. faecalis* model of injury, it is suggestive that, in the zebrafish at least, whilst LXA4 may act to reduce travel along the chemoattractant gradient for some neutrophils (shown by an increase in random movement), there remains another, possibly the HXA3, pathway attracting more neutrophils to maintain the inflammatory barrier in the presence of bacteria. Hepoxilins have yet to be investigated in the zebrafish. However, it is known that hepoxilin synthase is intrinsic to 12(S)-lipoxygenase which zebrafish are known to express, and indeed, expression of this lipoxygenase in the embryo was seen on early intestinal cells (Haas *et al.*, 2011). It is also of interest that RvE1 is able, in the presence of *E. faecalis*, to significantly reduce the numbers of infiltrating neutrophils. RvE1 has been shown to be a partial antagonist of the leukotriene B4 (LTB4) receptor, BLT1, on leukocytes (Arita *et al.*, 2007). Since neutrophil-derived LTB4 has been observed to play an important role in amplifying the neutrophilic responses to HXA3 *in vitro* (Pazos *et al.*, 2015), it is possible that RvE1 acting on the BLT1 receptor could antagonise this effect to a degree, thus managing to be the sole SPM to achieve a significant reduction in neutrophil infiltration in this case.

Modulating the innate immune responses is anticipated to ultimately influence wound healing, and it would have been ideal to be able to demonstrate this directly. However, live imaging of real time of healing within the intestinal tract is complex, not only due to the deeper location within the body affecting image resolution, but also because of artefactual difficulties in image comparison due to the peristaltic movement of the intestine. The *TgBAC(Cldn15la:Col1a2-eGFP)sh546* transgenic line was developed in the transparent Casper background to allow *in situ* imaging of the intestine in which the laying down of new collagen following an injury could

be observed directly in real time. Regretfully, there was insufficient time during the PhD to fully capitalise on this, and this area remains an area for future investigation.

5.4 **Summary of important findings**

The intestinal microbiome is instrumental in the maturation of the immune system. But models of gut colonisation, through necessity, have always been performed using germ-free or specific-pathogen-free animals. Using conventionally raised zebrafish larvae, intestinal colonisation with *E. faecalis* was successfully demonstrated for the first time, and shown not to induce an inflammatory response, as evidenced by the stable physiological markers and unchanged neutrophil numbers. It was further demonstrated that *E. faecalis ΔEpaX* had impaired colonisation in this model, thus recapitulating rodent studies. Further investigation of the actions of SPMs in this model showed that the presence of *E. faecalis* caused differential responses of the innate immune system, with only RvE1 significantly reducing peak neutrophil numbers to a wound, highlighting the importance of the microenvironment in outcome of treatment. Finally, further investigation of collagen expression in the developing teleost GIT showed that histochemical demonstration of birefringence could only be obtained from 13dpf, and a new transgenic zebrafish line *TgBAC(Cldn15la:Col1a2-eGFP)sh546* was developed, which would hopefully enable direct visualisation of intestinal wound healing in future investigations.

Chapter 6: Investigation of the mechanism of action of intestinal alkaline phosphatase (iAP) in the zebrafish

6.1 Introduction to iAP and its importance in immunology

The intestinal microbiome is closely intertwined with host immunity, not just in shaping the maturation of the immune system (Macpherson, Geuking and McCoy, 2005; Mazmanian *et al.*, 2005), but also in intestinal healing (Krezalek and Alverdy, 2018). But this interaction is complex and not yet fully understood. Many molecules previously thought to function only as digestive enzymes have been shown to also play additional roles in immune modulation and host defence (Ghosh *et al.*, 2002). One such interesting enzyme is intestinal alkaline phosphatase (iAP), originally shown to be involved with fat absorption (Narisawa *et al.*, 2003), but which has more recently been shown to be up-regulated on intestinal colonisation (Bates *et al.*, 2006). It is the most recently discovered of the four isozymes (placental, intestinal, germ cell and liver/bone/kidney) of alkaline phosphatase (ALP), and has been attracting increasing attention for over a decade due to its ability to modulate bacterial virulence by detoxifying lipopolysaccharide (LPS) within the intestine (Bates *et al.*, 2007), thus rendering harmless the bacterial toxin that stimulates the cytokine cascade and inflammatory response (Peters, Masereeuw and Pickkers, 2014a). Many of the beneficial effects that have been observed on administration of iAP, for example in clinical trials showing improvement of kidney function in sepsis (Pickkers *et al.*, 2012), recovery from cardiac surgery (Kats *et al.*, 2009), clinical improvements in ulcerative colitis (Tuin *et al.*, 2009b), and the intestinal microbiome-moderating effects (Kaliannan *et al.*, 2013; Malo *et al.*, 2014) have been attributed to this LPS-dephosphorylating property alone. ALP is present in both eukaryotes and prokaryotes, and is expressed in almost all organs of the body (McComb, Bowers and Posen, 1979). Each of the four isozymes has a distinct anatomical expression within the human body, a distinction also seen in other mammals and in fish (Faccioli *et al.*, 2016). iAP is unique in being the only isozyme that is expressed primarily within the intestine, and that has a different conformation from the other three (Chappelet-tordo *et al.*, 1974) which allows it to evade inhibition by Levamisole but is itself inhibited by L-phenylalanine. In addition, a peculiarity of iAP compared to other intestinal enzymes, is that bidirectional secretion of this enzyme occurs upon stimulation, with release of iAP mostly into the intestinal lumen, but also into the blood stream

(Alpers, Eliakim and DeSchryver-Kecskemeti, 1990). This bidirectional secretion appears to be an active process, making it an effective early indicator of ischaemic bowel in a clinical setting (Rosato *et al.*, 1971) because its decline within serum mirrors a decline in vascular supply to the gastrointestinal tract (GIT). Although less than 5% of the total enzyme is released into the blood stream, this remains an intriguing characteristic since no other digestive enzyme appears to possess this same property. Furthermore, *alpi.1* was shown to be expressed extra-intestinally in the developing zebrafish larva, but its role in this setting is as yet unknown. It was therefore hypothesised that iAP could possess a distinct and direct anti-inflammatory role, that its function was not restricted to the presence of Gram negative bacteria, and indeed could exert anti-inflammatory effect even in the absence of any bacteria. This was tested using *E. faecalis* as a Gram positive representative, and sterile tailfin wounding models in zebrafish.

6.2 **Results**

6.2.1 **Persisting *E. faecalis* increased localised expression of iAP**

Expression of iAP has previously been shown to be up regulated upon normal intestinal colonisation, and its role in this setting was thought to be specifically related to LPS detoxification (Bates *et al.*, 2007). It was hypothesised that if iAP had a role distinct from its effects on LPS in Gram negative bacteria, then intestinal colonisation with Gram positive bacteria, which do not express LPS (Wexler and Oppenheim, 1979), would still induce an increase in iAP. *E. faecalis* (OG1RF-mCherry), was used for this purpose, together with a whole mount *in situ* protocol developed to allow spatio-temporal visualisation of expression of endogenous ALP in zebrafish larvae (Figure 6-1). 24 hours after colonisation with *E. faecalis* in 5dpf zebrafish larvae, a localised increase in iAP expression in the colonised region of intestine was demonstrated on staining, which was absent in controls (Figure 6-2A). Inhibition of the non-intestinal ALP isoforms with 50 µM Levamisole (Figure 6-2B), and conversely, inhibition of iAP with 50 µM L-phenylalanine (Figure 6-2C), confirmed that the differential expression seen was indeed specifically that of iAP. Comparing reciprocal intensity in the intestinal region, as described for histological specimens (Nguyen *et al.*, 2013), a significant increase in iAP expression was demonstrated (Control mean+/-SEM: 67.30A.U. +/-0.84, OG1RF: 74.13A.U. +/- 1.22, $p<0.0001$, t-test, Figure 6-2D).

Figure 6-1: Ventral view of 5.2dpf zebrafish larvae demonstrating *in situ* expression of endogenous alkaline phosphatase. BCIP/NBT staining performed immediately following PFA fixation and stopped when staining within the GIT was first observed (green arrow), usually within 20 min. This specimen was prepared without inhibitors and therefore kidney expression (blue arrows) was also demonstrated within this staining period. Representative image shown, N=21 in three independent repeats.

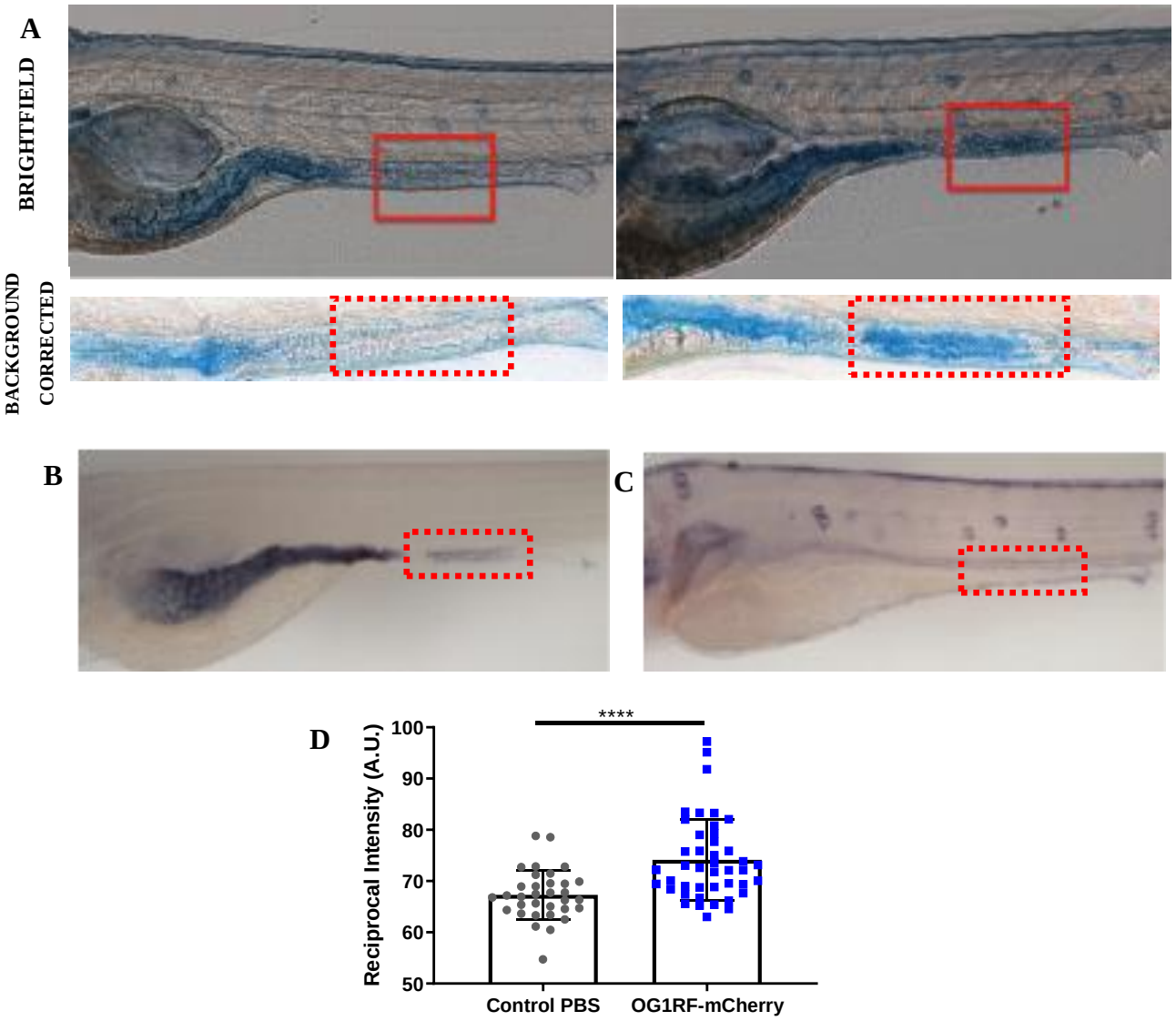

Figure 6-2: Staining of endogenous ALP using NBT/BCIP. A. Staining of ALP with segment III of the GIT in 5dpf zebrafish larvae, 24 hpi, marked in a red box. This area of difference corresponded with the area of bacterial persistence seen previously. Imaging was performed using a transmitted light microscope to allow fluorescence channel imaging to confirm the presence of colonisation. **B.** Treatment with Levamisole (50µM) was used as a control to block non-intestinal isoforms of ALP. **C**. Treatment with L-phenylalanine (50µM) was used as a second control to block only iAP. In B and C, staining was allowed to proceed for an hour and imaging was performed using a using Nikon AZ100 microscope with an automated stage (Prior Scientific) interfaced with NIS-Elements Extended Depth of Focus software (Nikon). **D**. Graph of reciprocal intensity calculated after rolling ball background subtraction in Image J. N=42/group in three independent repeats, comparison with t-test, ****p<0.0001, error bars show SD.

6.2.2 **iAP expression was up-regulated following distal intestinal injury**

Bacteria are able to sense their local environment and increase virulence in the presence of signs of host stress for example in an intestinal injury (Howard *et al.*, 2017). Because the presence of both Gram positive and Gram negative bacteria appeared to induce the expression of iAP, the introduction of an intestinal injury to zebrafish maintained under non-sterile conditions could allow the ingress of bacteria at the injury site and therefore was hypothesised to be able to cause an increase in the local expression of iAP at the site of injury as a protective mechanism. This was tested by performing a puncture wound in 4dpf wildtype larvae (nacre) followed by rapid fixing 6hpi and immediate staining as before. Surprisingly, at 6hpi although there was some increase locally at the site of injury, almost all larvae demonstrated a significant increase in iAP expression in the foregut (Figure 6-3A), whereas minimal increase was noted in either the foregut or the site of injury in the somite injury controls (Figure 6-3B). Comparing reciprocal intensity in the intestinal region as before confirmed a significant increase in iAP expression (Control mean +/- SEM: 51.25A.U. +/- 4.78, Intestinal injury: 107.4A.U. +/- 6.64, $p<0.0001$, t-test, Figure 6-3C).

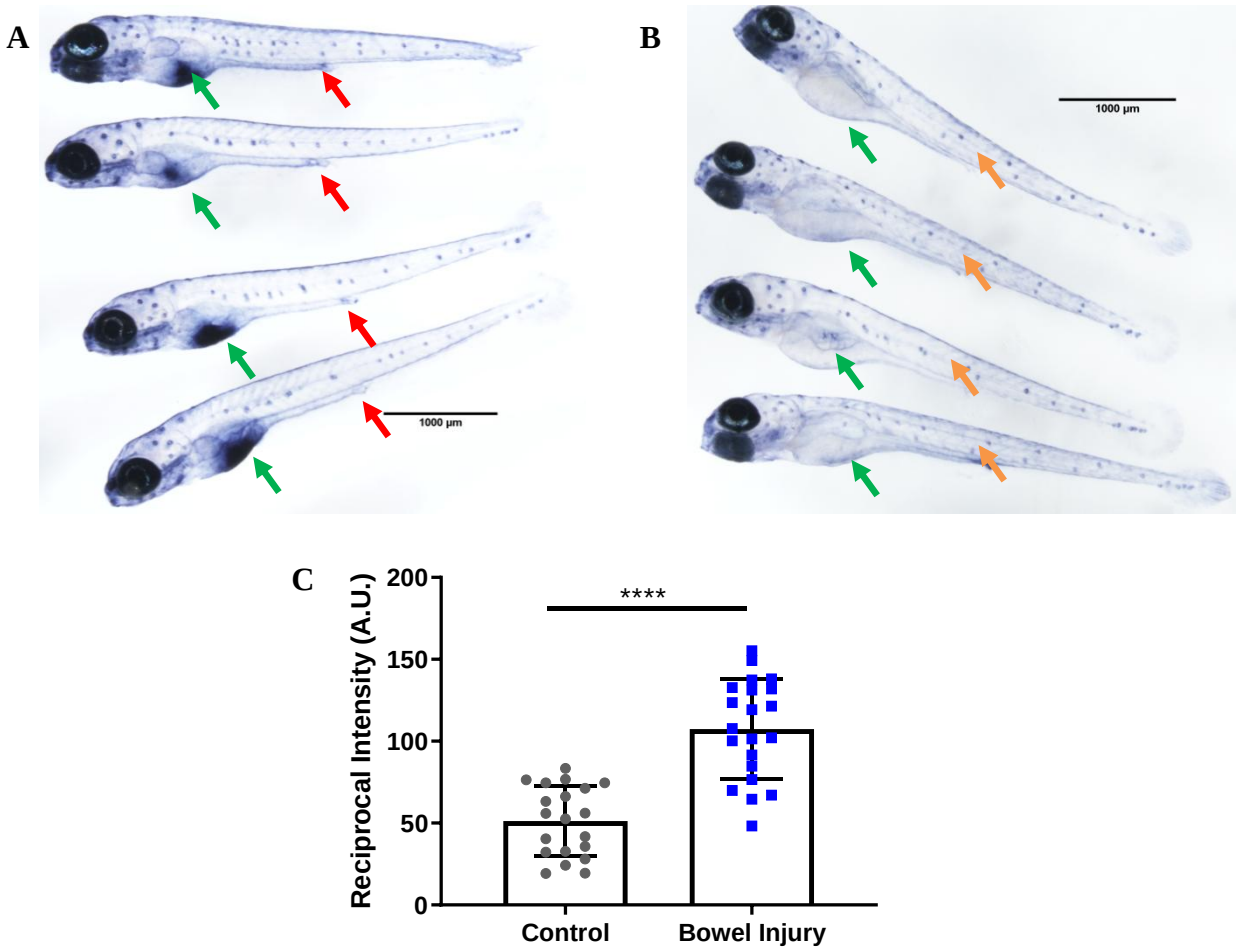

Figure 6-3: Increase in ALP expression in proximal gut 6hpi. A. Representative larvae with distal intestinal puncture wound indicated by red arrows, anterior intestinal bulb indicated by green arrows. **B**. Control larvae which underwent a somite injury at the level of the cloaca (indicated by orange arrows) but no intestinal injury, anterior intestinal bulb indicated again by green arrows. **C**. Reciprocal intensity calculated as before, N=21/group in three independent repeats, comparison with t-test, ****p<0.0001, error bars show SD.

6.2.3 **iAP decreased neutrophil numbers attending to an intestinal wound site, even in the presence of *E. faecalis***

The effect of supplementing additional iAP on the neutrophil response to an injury was then tested in the uncolonised GIT. 4dpf *TgBAC(mpx:GFP)i114* were injured and then microgavaged with iAP and imaged immediately. Treatment with iAP in an uncolonised intestinal injury significantly decreased the peak neutrophil numbers attending the wound (Control Ymax: 41.70, iAP Ymax: 34.67, $p<0.0001$, Poisson regression, Figure 6-4A). Analysis of parameters of neutrophil movement however revealed no differences in speed (Control mean +/- SEM: 0.040 +/- 0.0007, iAP: 0.039 +/- 0.0008, $p=0.6212$, t-test, Figure 6-5A), meandering index (Control mean +/- SEM: 0.302 +/- 0.005, iAP: 0.302 +/- 0.028, $p=0.9432$, t-test, Figure 6-5B), travel time (Control mean +/- SEM: 12.98 +/- 0.22, iAP: 13.10 +/- 0.22, $p=0.7049$, t-test, Figure 6-5C) or path length (Control mean +/- SEM: 142.0 +/- 2.72, iAP: 141.5 +/- 2.88, $p=0.9025$, t-test, Figure 6-5D). Next, the *E. faecalis* colonised model was tested to see if any differences in the response to treatment with iAP could be obtained. 4dpf *E. faecalis* colonised *TgBAC(mpx:GFP)i114* were injured and then microgavaged with iAP and imaged immediately. Treatment with iAP again significantly decreased the peak neutrophil numbers attending to the intestinal wound (Control+OG1RF Ymax: 38.16, iAP+OG1RF Ymax: 36.14, $p<0.0001$, Poisson regression, Figure 6-4B). This time however, the curves diverged less, and this could be due to the endogenous production of iAP that was shown to occur previously, thus blunting the effect of additional exogenous iAP treatment. Again, no effects were seen on parameters of neutrophil movement such as speed (Control+OG1RF mean +/- SEM: 0.03950 +/- 0.0007580, iAP+OG1RF: 0.04089 +/- 0.0008276, $p=0.2235$, t-test, Figure 6-5E), meandering index (Control+OG1RF mean +/- SEM: 0.2902 +/- 0.003023, iAP+OG1RF: 0.2876 +/- 0.002907, $p=0.5386$, t-test, Figure 6-5F), time (Control+OG1RF mean +/- SEM: 13.11 +/- 0.1189, iAP+OG1RF: 13.02 +/-0.1338, $p=0.6279$, t-test, Figure 6-5G), or path length (Control+OG1RF mean +/- SEM:.142.0 +/- 2.524, iAP+OG1RF: 145.7 +/- 2.346, $p=0.2813$, t-test, Figure 6-5H).

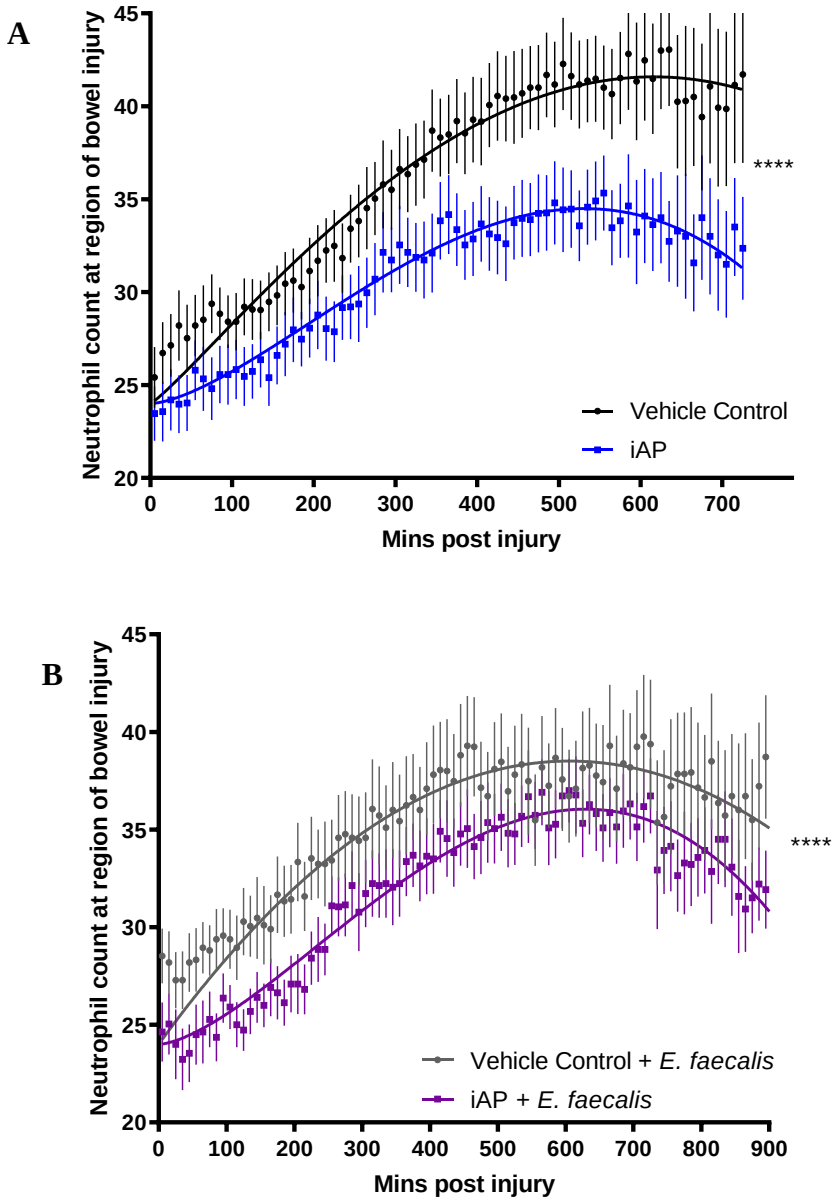

Figure 6-4: Neutrophil numbers in the region of intestinal injury following microgavage with vehicle control or iAP, with or without *E. faecalis*. 4dpf *TgBAC(mpx:GFP)i114* were used with microgavage of iAP or vehicle control immediately post-injury and time-lapse on the inverted Olympus microscope with Yokagawa CXU spinning disk and Volocity ® 6.3. **A.** Uncolonised intestinal injury. N=28/group in three independent repeats. **B**. *E. faecalis* colonised intestinal injury. N=21/group in three independent repeats. In each: Curve fitting with Beta Growth and Decline model, Ymax comparison with Poisson regression, ****$p<0.0001$, error bars show SEM.

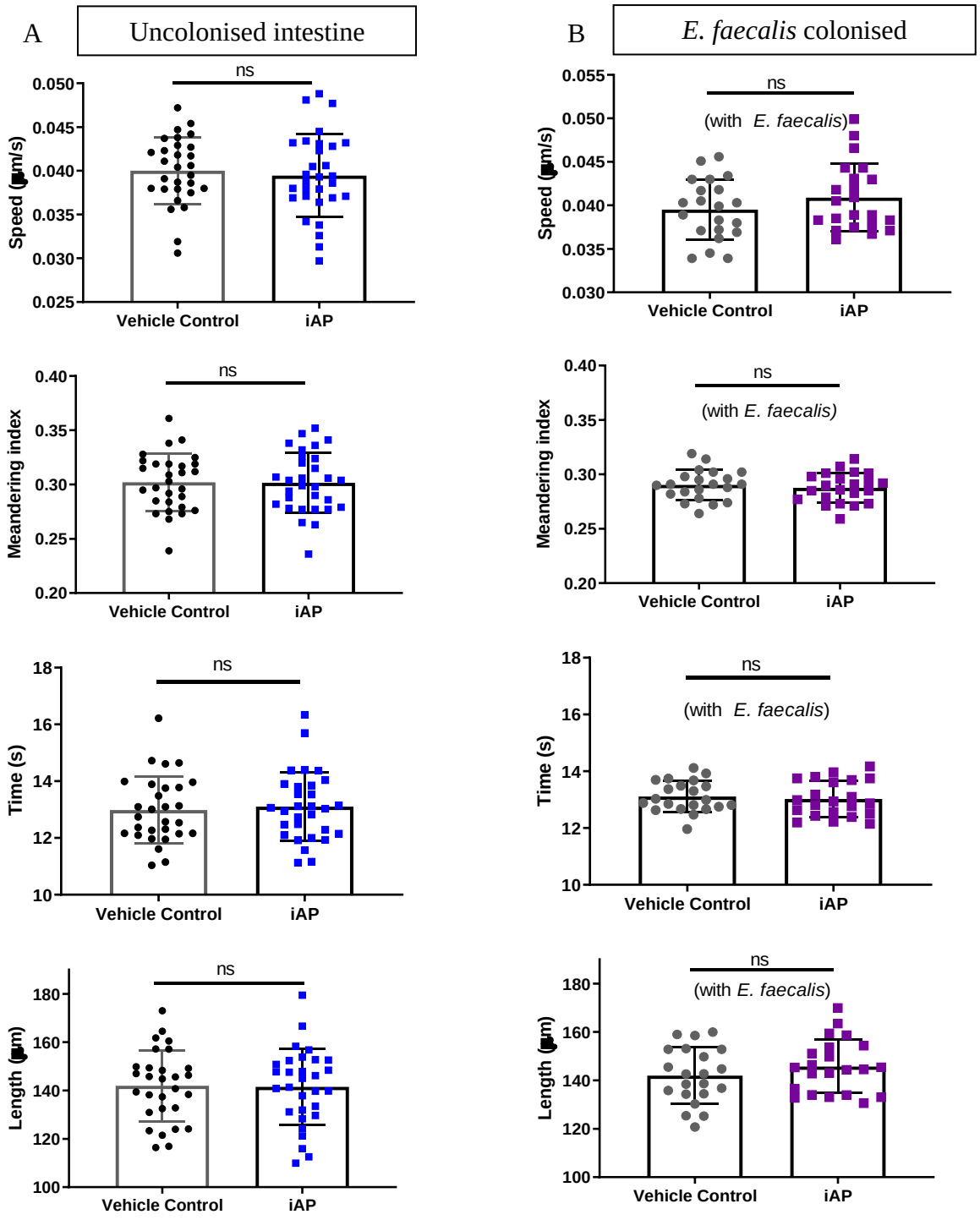

Figure 6-5: Parameters of neutrophil movement after intestinal injury in uncolonised or E. faecalis colonised *TgBAC(mpx:GFP)i114*. Parameters of tracked neutrophils were analysed using Volocity ® 6.3 in terms of speed, meandering index, travel time and path length. **A**. Uncolonised injured intestine. N=28/group in three independent repeats. **B**. *E. faecalis* colonised injured intestine. N=21/group in three independent repeats. In each: comparison with t-test, ns=non-significant, error bars show SD.

6.2.4 **iAP decreased macrophage numbers attending to an intestinal injury**

Given the effect of iAP on neutrophils responding to an intestinal wound, the macrophage response was interrogated as before. Conventionally raised zebrafish larvae of *Tg(mpeg1:NLS-Clover)* at 4dpf underwent an intestinal injury followed by immediate microgavage with iAP or vehicle control and time-lapse imaging performed until 12hpi. Imaging was only started at 1hpi as macrophages are known to arrive at the wound site later than neutrophils. The number of macrophages attending to the area of intestinal injury, was lower at all time points in the iAP treatment group (Control Ymax: 52.32, iAP Ymax: 50.03, $p<0.0001$, Poisson regression) comparison of line elevation with linear regression, Figure 6-6A). Indeed, the pattern of the macrophage response was reminiscent of the effect of RvE1 following an intestinal injury (Figure 3-20C). Analysis of the parameters of macrophage movement following iAP treatment revealed no differences in macrophage speed (Control mean +/- SEM: 0.0359 +/- 0.0008, iAP: 0.0340 +/- 0.0357, $p=0.0971$, t-test, Figure 6-6B), straightness of travel (Control mean +/- SEM: 0.326 +/- 0.007, iAP: 0.328 +/- 0.008, $p=0.9071$, t-test, Figure 6-6C), or travel time (Control mean +/- SEM: 14.19 +/- 0.19, iAP: 13.85 +/- 0.19, $p=0.2201$, t-test, Figure 6-6D). The path length of macrophages however was shorter in the iAP group (Control mean +/- SEM: 141.3 +/- 3.19, iAP: 131.0 +/- 3.13, $p=0.0265$, t-test, Figure 6-6E).

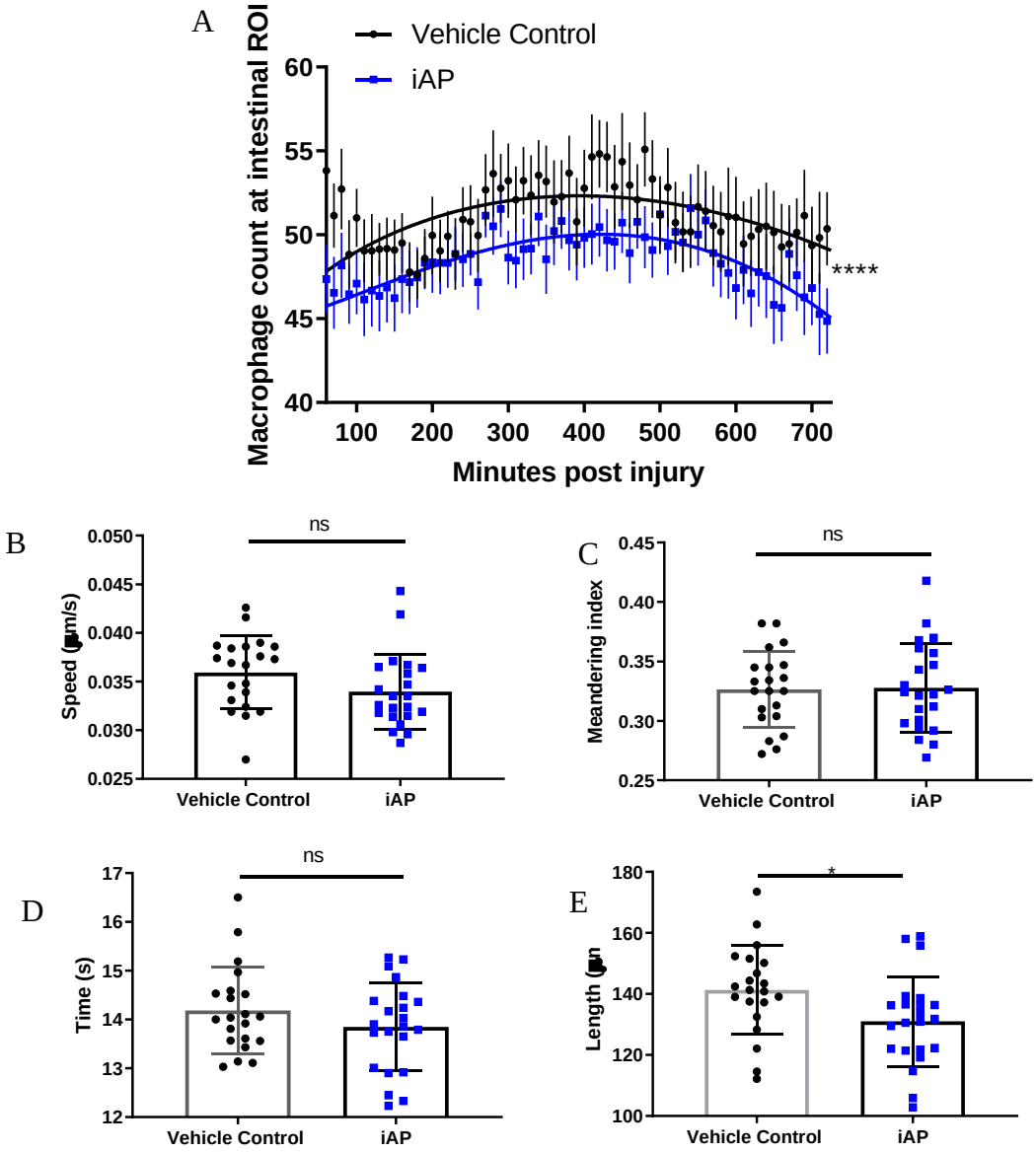

Figure 6-6: Effects of iAP on macrophage response to intestinal wound. 4dpf *Tg(mpeg1: NLS-Clover)* larvae underwent intestinal injury and immediate microgavage with iAP or vehicle control. Imaging was performed using an inverted Olympus microscope with Yokagawa CXU spinning disk and Volocity ® 6.3. **A**. Graph of macrophage numbers attending to the intestinal ROI over time. N=22/group in three independent repeats, curves plotted with Beta Growth and Decline model, Ymax comparison with Poisson regression, ****p<0.0001, error bars show SEM. Further analysis was then made between the vehicle control and iAP for the following parameters of movement of reverse migrated neutrophils: **B.** Speed, **C.** Meandering index (or directness of travel) where a number closer to 1 indicates a straighter path, **D.** Travel time, and E. Path length. In each: N=21/group in three independent repeats, comparison with t-test, ns=non-significant, *p<0.05, error bars show SD.

6.2.5 **iAP reduced neutrophil recruitment and accelerated inflammation resolution in a sterile tailfin injury**

To confirm that the anti-inflammatory effects of iAP persist in the absence of bacteria, a sterile tailfin injury model was used. 2dpf *TgBAC(mpx:GFP)i114* larvae were injured under strict aseptic conditions and treated with iAP or control, and neutrophils quantified in the usual manner. Immediate treatment with iAP reduced the number of neutrophils at the tailfin at 6hpi (Control mean +/- SEM: 27.39 +/- 0.74, iAP: 22.12 +/- 0.71, $p<0.0001$, t-test, Figure 6-7A), and this anti-inflammatory effect persisted even when quantified at 12hpi (Control mean +/- SEM: 18.69 +/- 0.73, iAP: 14.19 +/- 0.69, $p<0.0001$, t-test, Figure 6-7B), but was no longer significant at 24hpi (Control mean +/- SEM: 11.05 +/-0.51, iAP: 10.65 +/-0.56, $p=0.6053$, t-test, Figure 6-7C). Delayed (5.5hpi) iAP treatment accelerated inflammation resolution at 12hpi (Control mean +/- SEM: 15.71 +/- 0.99, iAP: 11.86 +/- 0.66, $p=0.0051$, t-test, Figure 6-8A), with a still significant effect at 24hpi (Control mean +/- SEM: 9.40 +/- 0.70, iAP: 7.75 +/- 0.45, $p=0.0459$, t-test, Figure 6-8B).

6.2.6 **iAP increased the rate of arrival of macrophages but decreased peak macrophage numbers in a sterile tailfin injury**

Next, investigation was extended to determine macrophage responses to iAP treatment in the sterile tailfin wound. 2dpf *Tg(mpeg1:NLS-Clover)* larvae, handled aseptically at all times, underwent a tailfin injury and IV treatment with iAP or vehicle control given immediately post injury. At the site of sterile tailfin injury, iAP caused a subtle but accelerated increase in macrophage numbers up till 6hpi, at which time macrophage numbers began to plateau, ending with a lower peak at 12hpi (Control Ymax: 28.82, iAP Ymax: 27.50, Control gradient: 0.006, iAP gradient: 0.007, $p<0.0001$, Poisson regression, curves fitted with Logistic Growth model, Figure 6-9A). This effect again matches the tailfin pattern seen with RvE1 treatment in Chapter 1 (Figure 3-13C). Treatment with iAP in the tailfin did not change macrophage speed (Control mean +/- SEM: 0.0315 +/- 0.0005, iAP: 0.0308 +/- 0.0005, $p=0.3161$, t-test, Figure 6-9B), meandering index (Control mean +/- SEM: 0.348 +/- 0.007, iAP: 0.352 +/- 0.008, $p=0.7287$, t-test, Figure 6-9C), travel time (Control mean +/- SEM: 16.11 +/- 0.18, iAP: 16.36 +/- 0.23, $p=0.3807$, t-test, Figure 6-9D), or path length (Control mean +/- SEM:47.03 +/- 1.37, iAP: 47.30+/- 1.53, $p=0.8926$, t-test, Figure 6-9E).

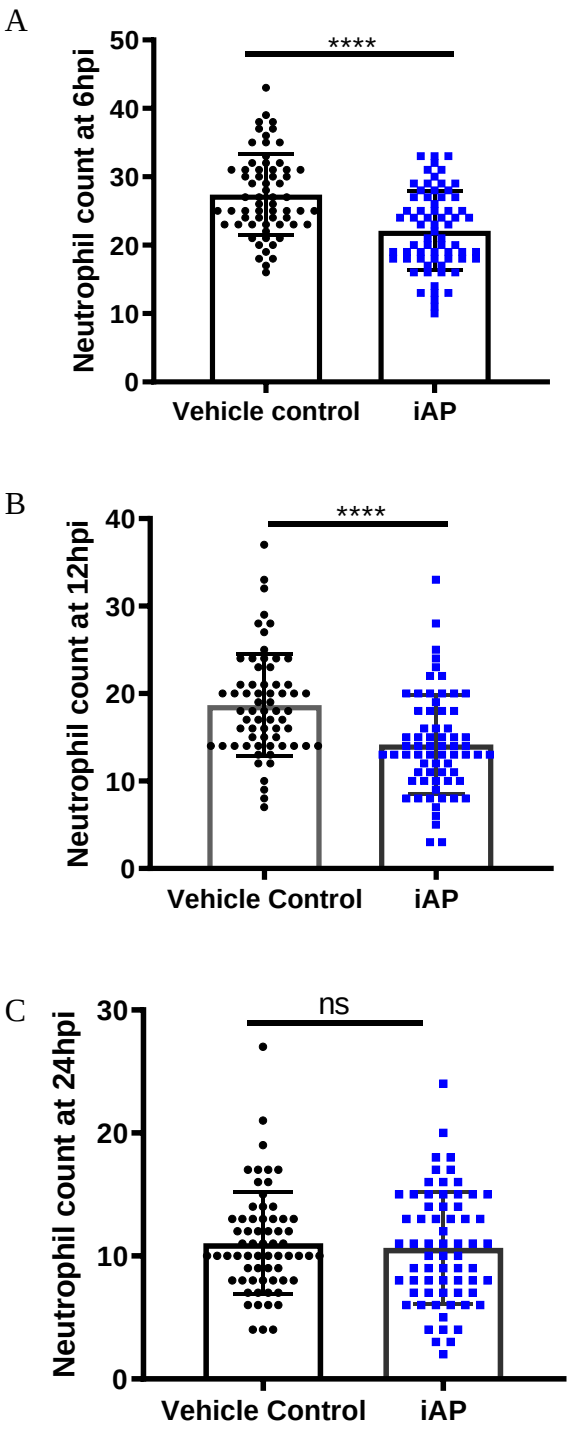

Figure 6-7: Immediate iAP treatment following sterile tailfin injury. 2dpf *TgBAC(mpx:GFP)i114* larvae raised under sterile conditions and injured under strict aseptic methods were treated at 0hpi with iAP or vehicle control. Neutrophils were quantified at **A.** 6hpi, **B.** 12hpi or **C.** 24hpi. Comparison with t-test, ns=non-significant, ****$p<0.0001$, N=60/group for each time point in four independent repeats. Four repeats was performed because of new batch of iAP used for the last two repeats.

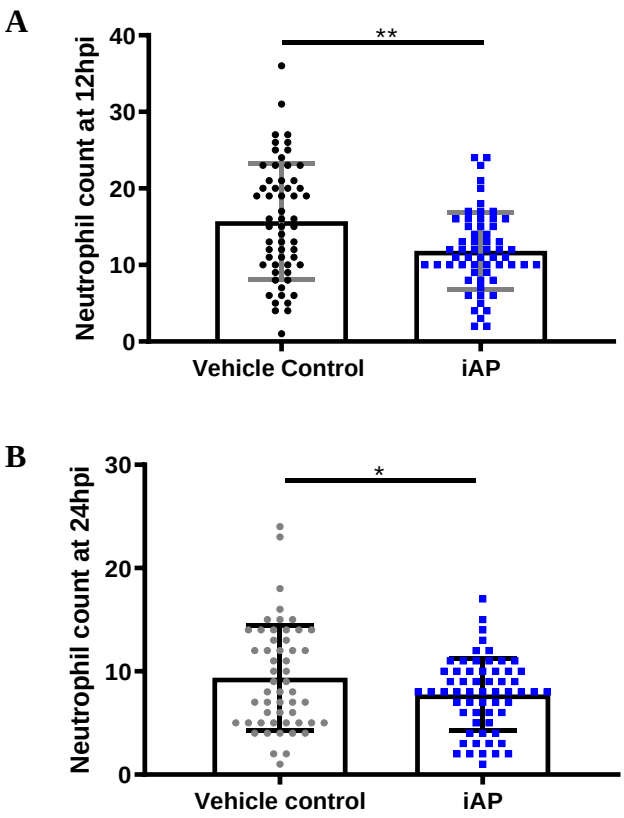

Figure 6-8: Delayed (5.5hpi) iAP treatment following sterile tailfin injury. 2dpf *TgBAC(mpx:GFP)i114* larvae raised under sterile conditions and injured under strict aseptic methods were treated at 5.5hpi with iAP or vehicle control. Neutrophils were quantified at **A**. 12hpi or **B**. 24hpi. In each: N=54/group, in three independent repeats, comparison with t-test, *p<0.05, **p<0.01, error bars show SD.

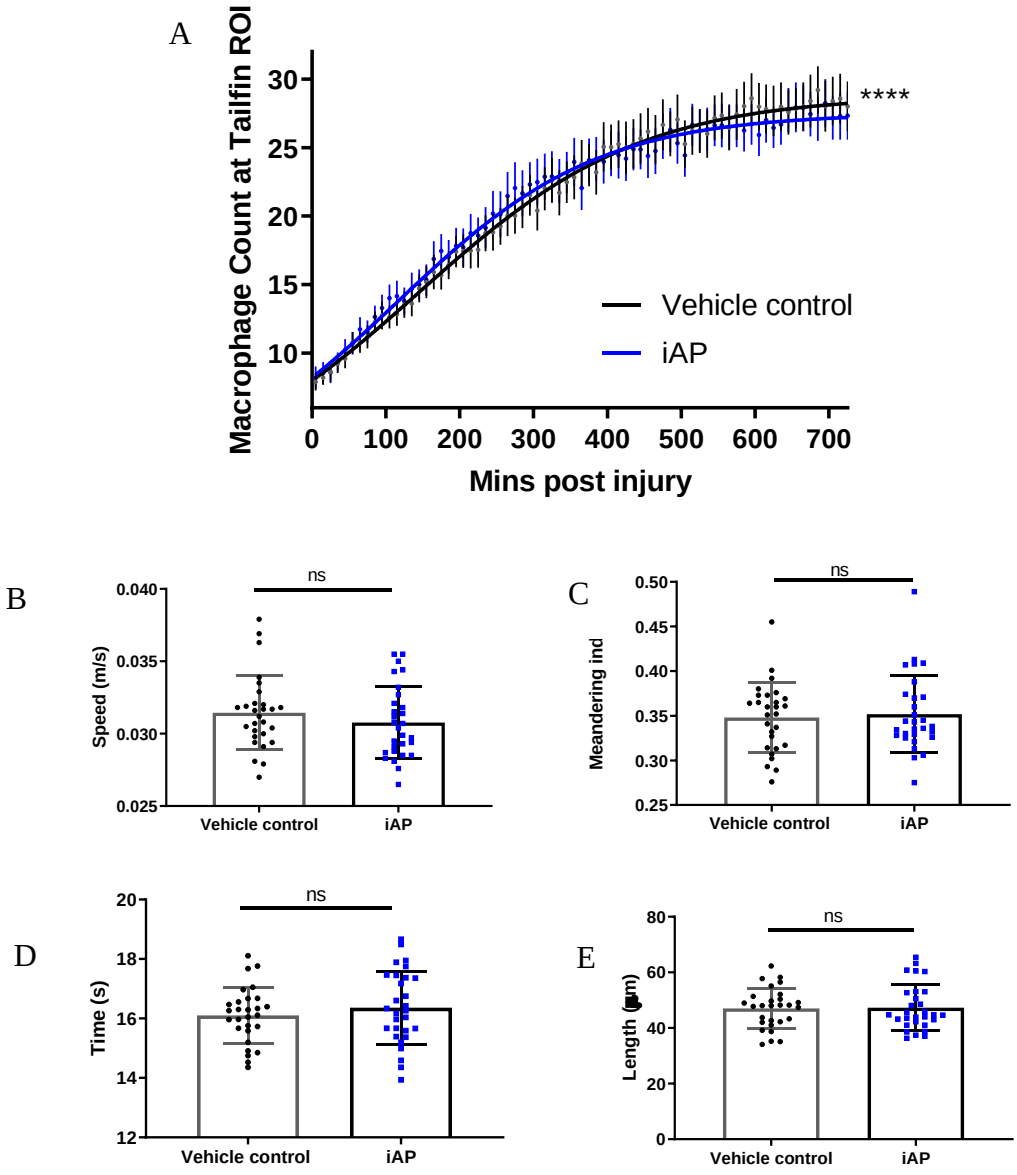

Figure 6-9: Effects of iAP on macrophage response to a sterile tailfin injury. 2dpf *Tg(mpeg1:NLS-Clover)* zebrafish larvae were injured aseptically and treated immediately with iAP or vehicle control. Imaging was performed on an inverted Olympus microscope with Yokagawa CXU spinning disk and Volocity ® 6.3. **A**. Graph of macrophage counts in the region of tailfin injury over time. Curve fitted with Logistic Growth model, Ymax and k comparison with Poisson regression, ****p<0.0001, N=21/group in three separate repeats. Further analysis was then made between the vehicle control and iAP for the following parameters of movement of macrophages: **B**. Speed, **C**. Meandering index (or directness of travel) where a number closer to 1 indicates a straighter path, **D.** Travel time, and **E**. Path length. In each: N=21/group in three independent repeats, comparison with t-test, ns=non-significant, error bars show SD.

6.2.7 **iAP did not increase rate of tailfin regeneration at 24hpi**

An acceleration of inflammation resolution would be thought to accelerate wound healing. Therefore it was hypothesised that the iAP would promote tailfin healing in zebrafish larvae. Tailfin regeneration studies were performed as before, but no significant increase in tailfin length was seen at 24hpi (Control mean +/- SEM: 44.62% +/- 4.64, iAP: 46.58% +/- 6.25, p=0.6094, Mann-Whitney test, Figure 6-10).

6.2.8 **iAP did not improve survival in severe *S. aureus* bacteraemia**

iAP has previously been shown to have a role in preventing sepsis-associated sequelae as a result of its LPS dephosphorylating activity (Peters, Masereeuw and Pickkers, 2014b; Pettengill *et al.*, 2017). To investigate whether the anti-inflammatory effect of iAP could play a larger role in enhancing survival in severe sepsis, a severe bacteraemia with a Gram positive bacteria (*S. aureus* SH1000) was used to obtain 80% mortality. No significant improvement in survival could be demonstrated with iAP treatment (p=0.2153, Mantel-Cox, Figure 6-11).

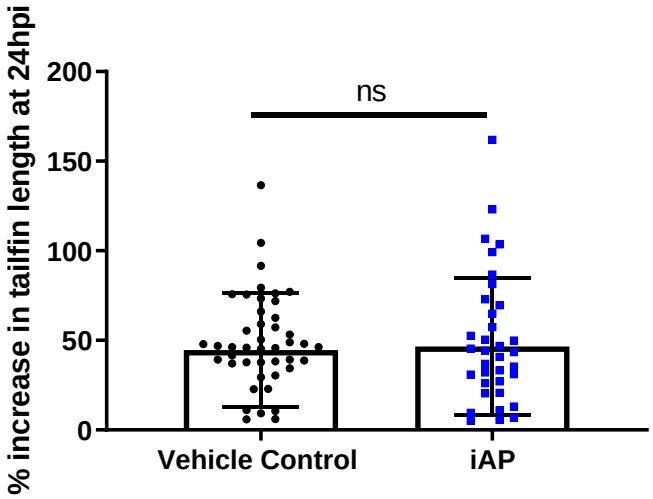

Figure 6-10: Effect of iAP on tailfin regeneration. 2dpf wildtype zebrafish larvae underwent tailfin amputation. Following tailfin injury, larvae were recovered for an hour before imaging to avoid skewing results due to the initial wound contraction, and then treated with intravascular injection of iAP or vehicle control. After 24 hours, larvae were re-imaged and % increase in tailfin length calculated. N=36/group in three independent repeats, comparison with Mann-Whitney test, ns=non-significant, error bars show SD.

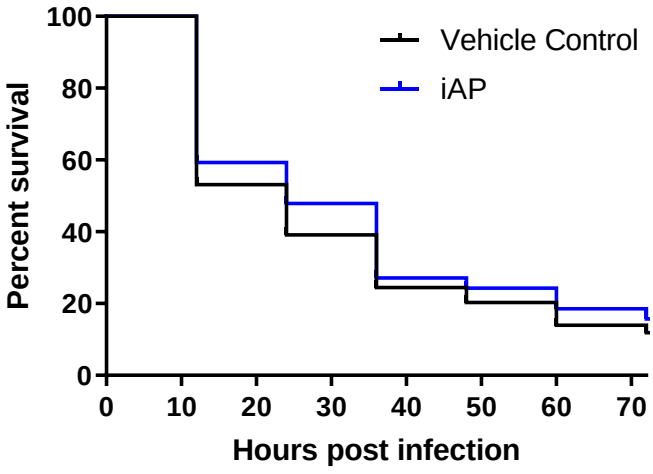

Figure 6-11: Effects of iAP on survival in a severe *S. aureus* bacteraemia. 2dpf wild-type larvae were infected intravascularly with 7500CFU SH1000 and survival monitored till 5.2dpf. Comparison with Mantel-Cox test, ns=non-significant, N=72/group in three independent repeats.

6.2.9 **iAP effects on neutrophil recruitment were abrogated when either a generic adenosine receptor antagonist, or adenosine deaminase, were administered**

Because the anti-inflammatory effects of iAP was demonstrated even in a sterile wound, and persisted even when administration was performed at the height of neutrophilic infiltration, it was hypothesised that iAP mainly exerted its anti-inflammatory effects, not via endotoxin neutralisation, but via adenosine, since ATP and ADP are abundant in wounds, and ALP is a non-selective dephosphorylator. Initial investigation was performed using caffeine, a known generic adenosine receptor antagonist. Sterile tailfin injury and immediate IV treatment was performed as before but with additional treatment with 1 μM caffeine in the larvae media. Treatment with caffeine abolished the anti-inflammatory effects of iAP in the sterile tailfin injury when neutrophil counts were performed at 6hpi (Control mean +/- SEM: 23.51 +/- 1.11, Control with Caffeine: 22.20 +/- 1.14, iAP: 19.13 +/- 0.94, iAP with Caffeine: 24.33 +/- 1.26, p=0.0052, one-way ANOVA, Figure 6-12A). Addition of caffeine did not significantly alter neutrophil numbers as demonstrated by the lack of difference between counts in the control groups (p=0.8462, one-way ANOVA). To further confirm the hypothesis that adenosine was the effector molecule mediating the anti-inflammatory effects of iAP, exogenous adenosine deaminase (ADA 1U in 3ml per 15 larvae) was administered, to effectively remove adenosine, and neutrophils at the site of injury were quantified as before. Once again, the anti-inflammatory effects of iAP on neutrophils were abrogated in the presence of exogenous ADA (Control mean +/- SEM: 30.23 +/- 1.27, Control with ADA: 28.49 +/- 1.03, iAP: 23.23 +/- 0.89, iAP with ADA: 27.52 +/- 1.08, p=0.0234, one way ANOVA, Figure 6-12B). As before, treatment with ADA did not significantly affect baseline neutrophil numbers as evidenced by the lack of difference between counts in the control groups (p=0.6697, one-way ANOVA).

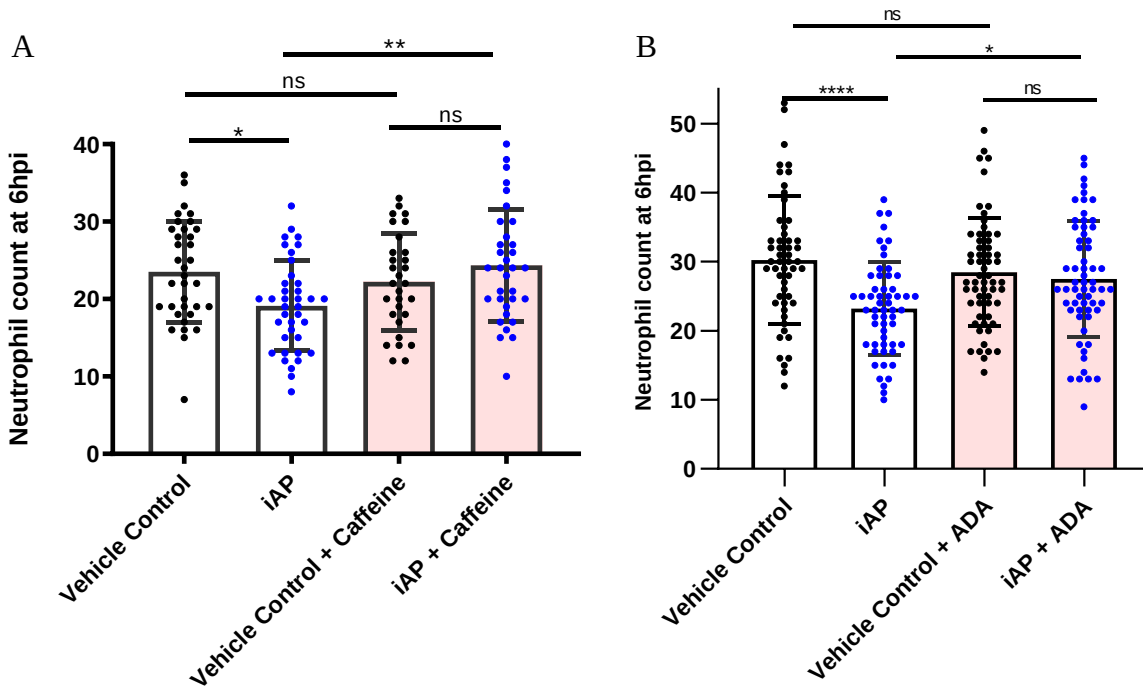

Figure 6-12: Anti-inflammatory effects of iAP were abolished by caffeine, a non-selective adenosine receptor inhibitor, as well as adenosine deaminase. A. Sterile tailfin injury was performed with immediate IV treatment with iAP or vehicle control, and immersion in 1 µM Caffeine in larval media. Neutrophil numbers were quantified at 6hpi. N=21/group in three independent repeats. **B**. Sterile tailfin injury with immediate IV treatment as before and adenosine deaminase (ADA) in larval media. N=60/group in four independent repeats. For each graph: Comparison with one-way ANOVA, ns=non-significant, *p<0.05, **p<0.01,****p<0.0001, error bars show SD.

6.2.10 iAP exerted its neutrophilic anti-inflammatory effects via adenosine A2b receptors, but not A1 or A2a receptors

Zebrafish larvae possess all the adenosine receptors similar to mammals (Boehmler *et al.*, 2009), and investigation was extended to determine if there was a specific receptor through which iAP exerts its maximal effects. The sterile tailfin injury model with IV treatment was again utilised for this purpose, with neutrophil counts performed at 6hpi in each case. Treating the zebrafish larvae with a selective inhibitor for the A1 receptors, DPCPX (1 µM), did not inhibit the anti-inflammatory effects of iAP (Control mean +/- SEM: 28.22 +/- 1.32, iAP: 18.62 +/- 1.05, Control with DPCPX: 23.64 +/- 26.12, iAP with DPCPX: 18.30 +/- 0.78, p=0.0102, one-way ANOVA, Figure 6-13A). It should be noted that treatment with DPCPX alone did cause a significant decrease in neutrophil counts in the control groups (p=0.0225, one-way ANOVA). Treatment with an A2a receptor inhibitor, ZM241385 (1 µM), similarly did not inhibit the anti-inflammatory action of iAP (Control mean +/- SEM: 28.22 +/- 1.32, iAP: 18.62 +/- 1.05, Control with ZM241385: 26.79 +/- 1.73, iAP with ZM241385: 20.54 +/- 1.24, p=0.0104, one-way ANOVA, Figure 6-13B). Treatment with ZM241385 did not affect neutrophil numbers as demonstrated by the similarities of counts between control groups (p=0.9082, one-way ANOVA). Treatment with the A2b receptor inhibitor, MRS1754 (10 nM), at a concentration previously known to work well with zebrafish (Rampon *et al.*, 2014), completely abolished the anti-inflammatory response to iAP in the sterile tailfin wound, strongly suggesting that iAP acted primarily via A2b receptors to bring about its neutrophilic anti-inflammatory effects (Control mean +/- SEM: 31.80 +/- 1.13, iAP: 24.89 +/- 0.85, Control with MRS1754: 34.21 +/- 1.20, iAP with MRS1754: 34.57 +/- 1.06, P<0.0001, one-way ANOVA, Figure 6-13C). Treatment with MRS1754 alone did not affect neutrophil numbers (p=0.3770, one-way ANOVA).

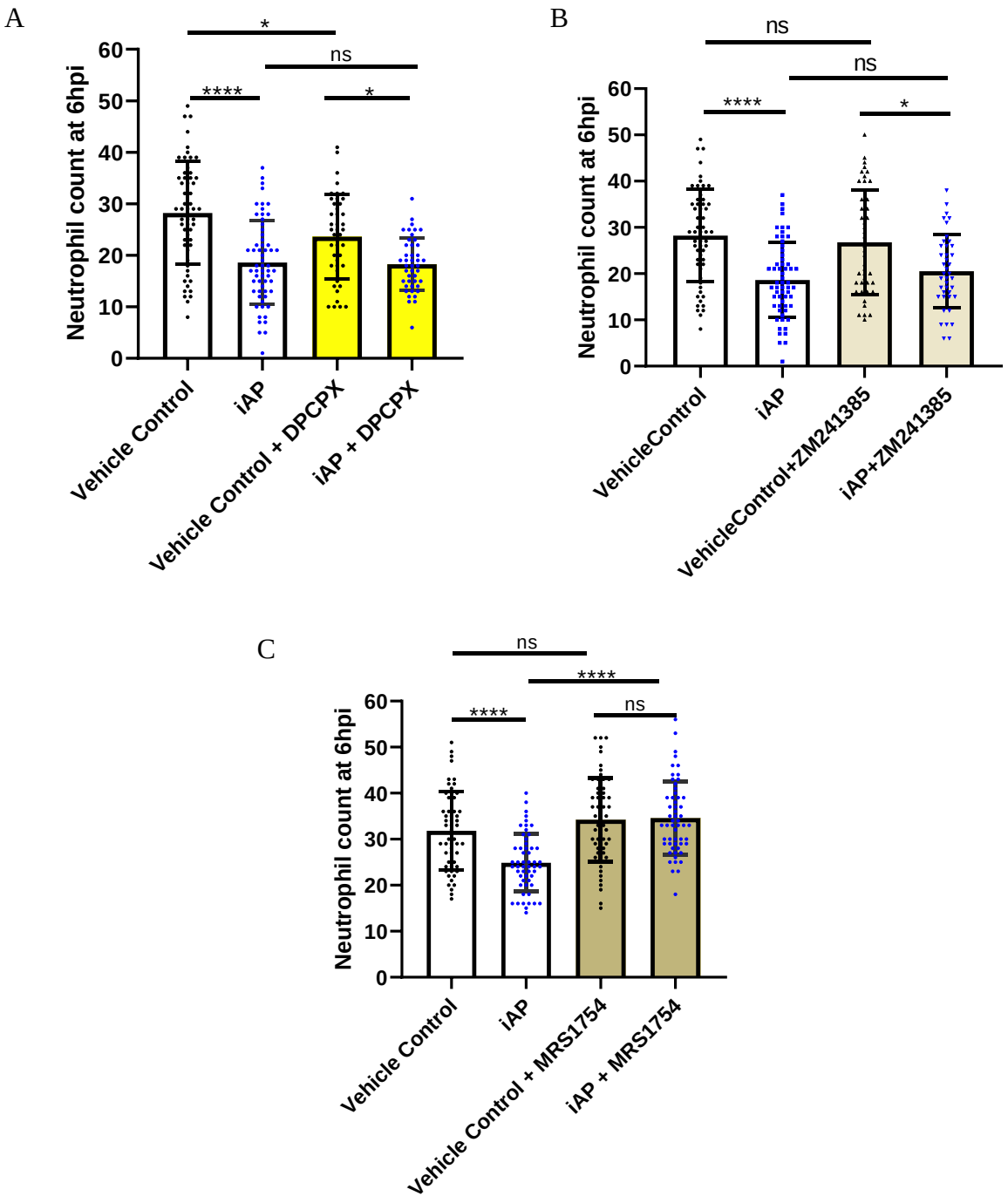

Figure 6-13: Specific adenosine receptor inhibition in sterile tailfin injury in 2dpf *TgBAC(mpx:GFP)i114* larvae. A. DPCPX, a selective A1 receptor antagonist was given in larval media after injury and IV treatment, and neutrophil counts performed at 6hpi. **B**. ZM241385, a selective A2a receptor antagonist was administered in a similar fashion. **C**. MRS1754, a selective A2b receptor antagonist was administered in a similar fashion. Comparisons with one-way ANOVA with Sidak's correction, N>30/group in three independent repeats, ns=non-significant, *p<0.05, ****p<0.0001.

6.2.11 **iAP reduced NFκB expression following tailfin injury**

Adenosine is a potent inhibitor of NFκB (Minguet *et al.,* 2005). Therefore, it was hypothesised that a corresponding reduction in NFκB expression would be seen with iAP treatment. Using the *Tg(6xHsa.NFKB:eGFP)sh235* zebrafish reporter line, sterile tailfin injury with immediate treatment of iAP or vehicle control. An uninjured control group was included, but imaging software memory capacity limited inclusion of this group to 12 hours. Nonetheless, this was sufficient to demonstrate that GFP bleaching did not occur under the settings used and that increase in GFP signalling did not occur without an injury in the tailfin. Treatment with iAP did indeed result in a significant decrease in NFκB expression with an increasing difference over time compared with controls (Control slope +/- SE: 0.12 +/- 0.004, iAP slope: 0.10 +/- 0.003, $p<0.0001$, slope comparison with linear regression, Figure 6-14).

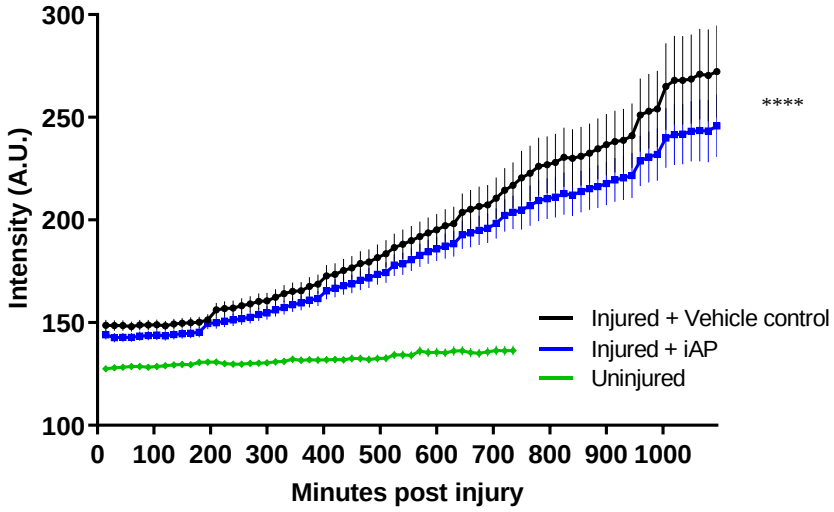

Figure 6-14: NFκB expression following tailfin injury and treatment with iAP or vehicle control. 2dpf *Tg(6xHsa.NFKB:eGFP)sh235* underwent tailfin transection and immediate IV treatment with iAP or vehicle control, together with a second uninjured control group. A 20h time-lapse was started as soon as possible after injury on a Nikon Eclipse TE2000-U microscope interfaced with NIS Elements AR. Intensity of GFP fluorescence was quantified after background correction. Graph of intensity over time. N=24/group in three independent repeats, ****$p<0.0001$, linear regression, error bars show SEM.

6.3 **Discussion and further work**

For many decades since iAP was first discovered, this enzyme was thought of as simply another digestive enzyme. Its role was relegated primarily to the absorption of fatty acids, and its expression pattern, mainly within the absorptive region of the small intestine in both teleosts and mammals, appeared to confirm this impression (Young *et al.*, 1981). However, recent years have uncovered another facet to this interesting enzyme, the ability of iAP to neutralise endotoxins by dephosphorylating the lipid-A moiety of LPS (Beumer *et al.*, 2003; Vaishnava and Hooper, 2007). Several human clinical trials have already shown benefit in various scenarios of inflammatory dysregulation, for example post-cardiopulmonary bypass, but here again its effects were explained by the described control of endotoxins produced by inevitable bacterial translocation during possible periods of peri-operative hypoxia (Kats *et al.*, 2009). No publications thus far have investigated the properties of iAP as a direct anti-inflammatory mediator conferring benefit in the above scenarios.

The first suggestion of LPS-independent activity here was the increase in endogenous iAP upon colonisation with *E. faecalis*, a Gram positive bacteria, that does not express LPS. This increase in expression was not entirely unexpected since the colonisation model did not utilise germ-free conditions, and therefore it was possible that colonisation of *E. faecalis* enabled other symbiotic but unlabelled bacteria to co-habit and also stimulate an increase in iAP expression. However this localised increase in the mid-intestine was absent from larvae raised under similar conditions but without additional microgavage of *E. faecalis*. Investigation was extended to determine if a local injury to the distal intestine could also produce a similar effect, and although no significant increase in iAP around the distal intestinal injury site could be demonstrated, a significant increase in iAP expression in the anterior intestinal tract was seen. It is known that iAP secretion occurs mainly in the proximal gastrointestinal tract, even in lower mammals, with minimal secretion in the distal tract (Lev and Griffiths, 1982; Wada *et al.*, 2001). Therefore it is possible that the injury did indeed induce an increase in intestinal production of iAP, but this was seen at its major site of expression proximally, while the puncture injury was insufficiently severe for detection of accumulated signal under those conditions.

Within the intestinal tract, as would be expected, administration of intraluminal iAP reduced the neutrophilic response to an acute injury, even in the presence of a bacterial colonisation. It is unknown if teleosts also have bidirectional iAP secretion into the intravascular system since previous histochemical studies have only shown iAP to be localised to the intestinal tract (Faccioli *et al.*, 2016). This does not detract from the zebrafish model system however, and may actually make this a cleaner system to analyse the effects of iAP on a sterile wound. In a sterile tailfin injury, iAP administered intravascularly exerted neutrophilic anti-inflammatory effects. The largest neutrophilic anti-inflammatory effects were obtained when treatment was given immediately following injury and neutrophils quantified at the peak of neutrophil recruitment at 6hpi which persisted at 12hpi. Unlike the exacting temporal effects of SPMs, iAP continued to effect a significant decrease in neutrophil numbers even when given late in the inflammatory process.

It is of interest that the macrophage effects both in the tailfin and in the intestinal injury models closely mirror the effects brought about by RvE1. Although RvE1 is thought to exert its actions via specific GPCRs, it has been linked to iAP production within the intestinal tract (Campbell *et al.*, 2010) through mechanisms which are not entirely clear as yet. Certainly, in examining the effect of SPMs in an *E. faecalis* colonised model, only RvE1 reduced neutrophil numbers in a significant manner, similar to iAP treatment alone.

It is of interest that iAP is shown for the first time to positively affect the inflammatory process likely via the production of adenosine, since blocking adenosine receptors with caffeine, and removing adenosine via adenosine deaminase, both abrogated the effects of iAP. Adenosine acts via several adenosine receptors and affects all types of immune cells in different ways. The action of adenosine is complex, depending on concentration and receptor availability. In neutrophils, low adenosine concentrations result in an inflammatory response via the A1 receptors, whereas high concentrations act on anti-inflammatory A2a/A2b receptors to inhibit neutrophil oxidative burst and trafficking (Barletta, Ley and Mehrad, 2012). Zebrafish have 33 purinergic receptor genes and the adenosine receptors A1, A2a and A2b, which are conserved and present in all vertebrates. In addition, zebrafish have an A3 receptor involved in olfactory sensing and expressed solely in the olfactory region (Wakisaka *et al.*, 2017), and therefore

excluded from these investigations. Using receptor specific inhibitors, iAP was demonstrated to mainly exert its neutrophilic anti-inflammatory effects, in a sterile wound, via the A2b receptor. This action via the A2b receptor is of interest because iAP has been shown to be beneficial in the treatment of inflammatory bowel disease in humans (Lukas *et al.*, 2010), and two other treatments that have long been used successfully in the treatment of the same, methotrexate and sulfasalazine, have also been shown to work via this pathway to produce their anti-inflammatory effects (Cronstein, Naime and Ostad, 1993; Gadangi *et al.*, 1996).

In the zebrafish tailfin regeneration model, no increase in tailfin length could be demonstrated. This could be because the model was limited to 24hpi, and although adenosine has previously been shown to enhance wound healing (Montesinos *et al.*, 2002), published results suggest that adenosine begins to affect a difference from the second day onwards in adult zebrafish tailfin injuries (Rampon *et al.*, 2014). The half-life of adenosine is also quite short, and repeated doses of iAP may have been needed in order to demonstrate an increase in regeneration. This was not performed here as the primary goal was to determine if the immediate neutrophil anti-inflammatory effect led to enhanced regeneration rather than a direct effect on regeneration itself. This remains an area of intrigue for further investigation in future.

Adenosine is a key molecule in many opposing pathways where an excess can provoke prolonged inflammation and pathological fibrosis (Blackburn *et al.*, 2000; Chunn *et al.*, 2006), but its presence is required for vascular growth, epithelial protection and inflammation control (Adair, 2005; Csóka *et al.*, 2010; Aherne *et al.*, 2015). Targeting the adenosine pathway directing via kinases and inhibitors has been fraught with difficulty due to the intricacies of its interactions and opposing actions (Chen, Eltzschig and Fredholm, 2013; Faas, Sáez and de Vos, 2017). Perhaps iAP holds the key. Its actions as a non-specific dephosphorylator are well known, removing inflammatory molecules such as ATP and LPS (Beumer *et al.*, 2003), but an additional advantage, shown in the experiments here, is that its actions are also not limited to specific time-points during the inflammatory process like SPMs. This would ease translation into clinical practice. A further benefit that is lesser known, is that iAP also comes with an inbuilt ‘stop signal’, where it is self-inhibited by the abundance of phosphate it creates (Shirazi, Beechey and Butterworth, 1981) . It may be that, like so many other complex systems in nature,

the complexity is the consequence of an exceedingly simple, and therefore more easily malleable, mechanism. Perhaps the quote often credited to Isaac Newton, “Nature is pleased with simplicity”, still has a place in the increasingly complicated biological knowledge of today.

6.4 **Summary of important findings**

Previously assigned mainly to digestive roles, the intestinal isoform of ALP, iAP, also has direct anti-inflammatory actions in sterile wounds distinct from any antibacterial effects, and that these anti-inflammatory processes are also active within the GIT. Endogenous iAP was increased in response to colonisation with a Gram positive bacteria (*E. faecalis*), and to an acute intestinal injury. Intraluminal supplementation of iAP decreased the number of neutrophils attending to an intestinal wound without altering neutrophil behaviour. In addition, intravascular supplementation of iAP to zebrafish larvae with a tailfin injury, given both immediately after injury and also later (5hpi), reduced the number of neutrophils responding to wound site, maximally at 6hpi and 12hpi, but also at 24hpi. Administration of caffeine (1 μM), a generic adenosine receptor antagonist abolished this effect of iAP giving the first evidence that iAP likely exerts its actions via adenosine receptors. Treatment with adenosine deaminase also abolished the neutrophil anti-inflammatory effect, further confirming this hypothesis. A specific A1 receptor antagonist (DPCPX) and a specific A2a receptor antagonist (ZM241385) did not abolish neutrophil anti-inflammatory effects of iAP. However, with MRS1754, a specific A2b receptor antagonist, the neutrophilic anti-inflammatory effects of iAP were completely abolished. In conclusion, iAP has direct neutrophilic anti-inflammatory actions, acting via A2b receptors in a sterile wound.

Chapter 7: Intestinal alkaline phosphatase and intestinal wound healing in the mouse

7.1 The clinical burden of wound healing and the relevance of iAP

Optimal wound healing has long been the concern of surgeons, but increasingly so in modern times. In dealing with wounds sustained outside the surgical theatres and perhaps in battlefields, the early surgeons' role in decontamination, debridement and realignment, was often only an adjunct the body's natural capacity for healing, with healing equally likely to fail regardless of assistance. However, now, many more wounds are inflicted by surgeons themselves, and not uncommonly in a completely asymptomatic patient who may have had an early cancer detected through public health screening programmes. As such, failure to heal, or even an unusually slow-to-heal wound, has substantial consequences, not only impacting on quality of life and distribution of healthcare resources, but also possibly on the continuation of life itself. Healing is a finely balanced cascade of intertwined pathways, and attempting to modulate these can lead to conflicting results. For example, it is established that excessive inflammation leads to disease, but suppressing it can also disrupt the healing process (Cahill *et al.*, 2004). Therefore there exists a sweet spot of inflammation which is optimal for wound healing and this is likely to be specific to the anatomical location of the wound (Turabelidze *et al.*, 2014), and perhaps even genetic makeup (Dimitriou, 2013; Tipton *et al.*, 2020). In the intestine, many molecules could promote wound healing, individually or in concert, and isolating the most important one, if it exists, is fraught with difficulty given the potential for microorganisms to further influence the healing process through secreted microbial products or an increase in virulence in response to environmental modulation.

Intestinal alkaline phosphatase (iAP) has been shown in the previous chapter to have an independent anti-inflammatory role, and is produced endogenously in the GIT in most species that have been investigated, from fish to rodents and larger mammals (Bitar and Reinhold, 1972). The ubiquitous presence of iAP across species is of little surprise given the role in digestion that iAP was purported to hold. Because iAP is present naturally within the GIT, further augmentation may not bring with it the detrimental effects seen in exogenously manipulating the intestinal inflammatory response such as with the use of protein kinase

inhibitors (Lodish, 2013; De Vries *et al.*, 2017). The full range of effects of iAP has yet to be fully investigated, but iAP is thought to act solely by dephosphorylating substrates, in particular LPS. The models used to investigate the action of iAP on LPS range from cell culture, murine, porcine and even humans and mainly involve intravascular iAP treatment (Beumer *et al.*, 2003; Richter *et al.*, 2012). Nonetheless, the beneficial effects of treatment with iAP in the LPS setting are indisputable, and reproducible in iAP-knockout mice undergoing ischaemic-reperfusion injuries (Goldberg *et al.*, 2008).Thus far the intestinal effects of iAP given intraluminally has only been investigated in chemical models of intestinal inflammation in the rat and mouse (Ramasamy *et al.*, 2011; Lee *et al.*, 2014), as well as topically in porcine jejunal explants (Melo *et al.*, 2016). No link as yet has been made between iAP and wound healing but it has been noted that the granulation tissue of burn wounds in rats contain high levels of AP although its role is unknown (Price, Dubois and Gilbert, 1979). Thus, it was hypothesised that exogenous supplementation of iAP may aid anastomotic healing. Treatment with iAP was tested in a standard and leaking anastomosis to determine if differential responses could be elicited.

7.2 **Results**

7.2.1 **Voluntary ingestion of Nutella as a mode of treatment delivery was feasible**

It was first necessary to establish the most suitable mode of treatment delivery. Previous publications suggested that voluntary ingestion of buprenorphine in mice in Nutella at a dose of 0.2 mg/g of mouse could be successful (Jacobsen *et al.*, 2011). However, it was unknown if British-bred mice would reliably do the same without significant prior training especially since older publications suggested mice preferred grain or seed based products over chocolate powder and sugar (Rowe, Bradfield and Redfern, 1974). Therefore a pilot taste test was performed on mice kept for handling practice within the facility. Two groups of mice were tested, six month old male C57BL/6J and 9 month old male BALB/c mice. The first item actually tasted was recorded. Cream cheese and condensed milk rated top in both strains (Figure 7-1A&B), but whilst the C57BL/6J strain most frequently tasted the condensed milk first, they often settled down to prolonged eating of the cream cheese thus facilitating image capture (Figure 7-1C&D). Both the spontaneous top choices of the mice were milk-based products, and could contain traces of iAP therefore the third option, Nutella, being a nut based product, was chosen as the vehicle of choice for delivery of treatment. Oral administration in food was preferred over

gavage as the optimal stress-free treatment method. In addition, in intestinal transit studies, gavaged contrast was eliminated within 6 to 7 hours (Padmanabhan *et al.*, 2013), whereas spontaneous ingestion allowed storage within the fore stomach of mice, which then maintained a steady state supply into the intestine, a mechanism unique to mice and rats (Gärtner, 2002), giving a theoretical constant supply of treatment or vehicle control. 5 µL (100U) of iAP (Invitrogen) or an equal amount of buffer was ingested readily, and completely, by the mice. This dose was chosen based on previous publications showing benefit, and therefore evidence of being bioactive at this dose, in alcoholic steato-hepatitis (Hamarneh *et al.*, 2017), as well as chronic colitis in IL10-/10- mice (Lee *et al.*, 2014). In addition, a small pilot study of six mice was performed in preparation to these experiments, using this dose, and which suggested physiological improvements.

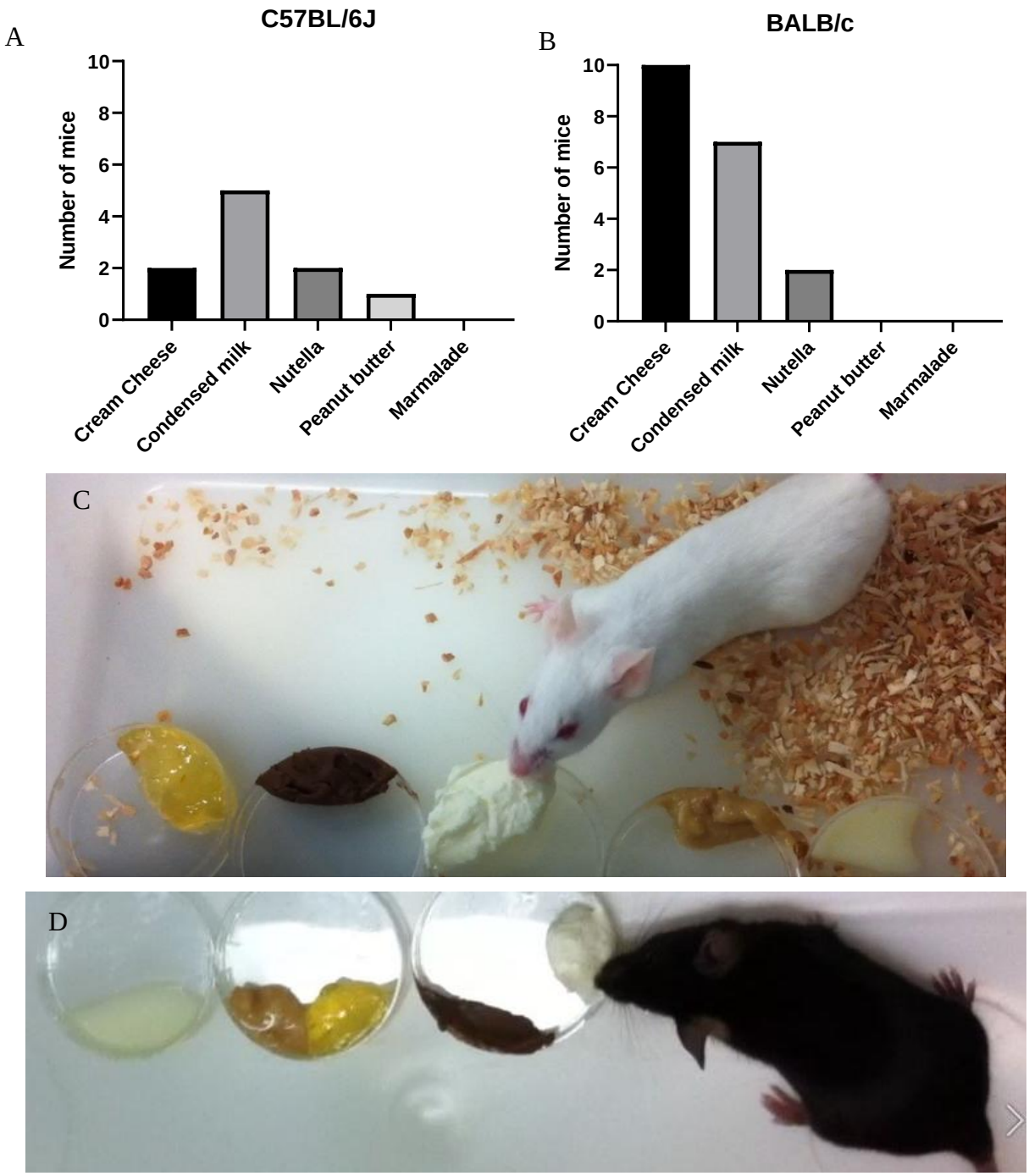

Figure 7-1: Mouse taste test. Test mice were used from two different strains to determine the spontaneous taste preferences of British bred mice. **A.** Graph of first preference in C57BL/6J. N=10. **B.** Graph of first preference in BALB/c. N=20. No statistical tests were performed as this was a single exploratory experiment **C.** BALB/c 9 month old male mice were introduced into a clean box containing Petri dishes with marmalade, Nutella, cream cheese, peanut butter and condensed milk. **D.** C57BL/6J 6 month old male mice were similarly tested. The first sample tasted was recorded.

7.2.2 **A proximal colonic anastomosis was the choice for investigation**

Next, the optimal site of anastomosis was determined. There is some evidence in humans that leaks are more common in the distal colon compared with anastomoses performed in the proximal colon (McDermott *et al.*, 2015), but it is as yet unclear if this is because well vascularised small bowel is anastomosed to colon in proximal resections, whereas in distal colonic resections, colon to colon anastomoses are performed. In experimental mice, both proximal and distal procedures were technically similar (Figure 7-2A&B) and both involved a colon to colon anastomosis. However, the proximal anastomotic model (Figure 7-2C) was chosen because, given the robustness of rodents models requiring severe measures to be taken to ensure experimental leakage (Boersema *et al.*, 2016), the liquidity of stool in the proximal colon compared to the distal colon could allow leaks that would otherwise be subclinical, to manifest clinically. Furthermore the caecal region has high levels of microbial colonisation and shows the greatest immune activation in response to pathogens (O'Hara and Shanahan, 2006; Arrieta and Finlay, 2012), and distances between the proximal and distal regions are small (Figure 7-2D), comprising <20% of total intestinal length (Casteleyn *et al.*, 2010).

7.2.3 **iAP did not significantly alter the post-operative activity index of mice in the standard model**

Five days prior to the operative procedure, mice were weighed twice daily to acclimatise them to handling, and to allow an average weight to be obtained as weight gain was still ongoing at the age of six weeks. Forty eight hours prior to the operative day, Nutella was introduced at a maximum of 4mg per mouse. The ingestion time was much quicker compared to that previously published (Jacobsen *et al.*, 2011), with ingestion complete within 10s of offering the treat. Without exception, all the mice eagerly consumed the Nutella, licking the Petri dish completely clean, and often hopefully turning it over to lick the opposite side (Figure 7-3A), and this continued unchanged in the post-operative period. No mouse hesitated to consume the Nutella, together with the vehicle control or iAP in its entirety, in the standard model. Although all experiments were conducted blinded until analysis was complete, differences between groups could be observed from the night of the operation (Figure 7-3B) with the iAP group repeatedly appearing more active and seemingly without any obvious discomfort as seen by the unimpeded inverted climbing. There were no clinically relevant anastomotic leaks in the standard model.

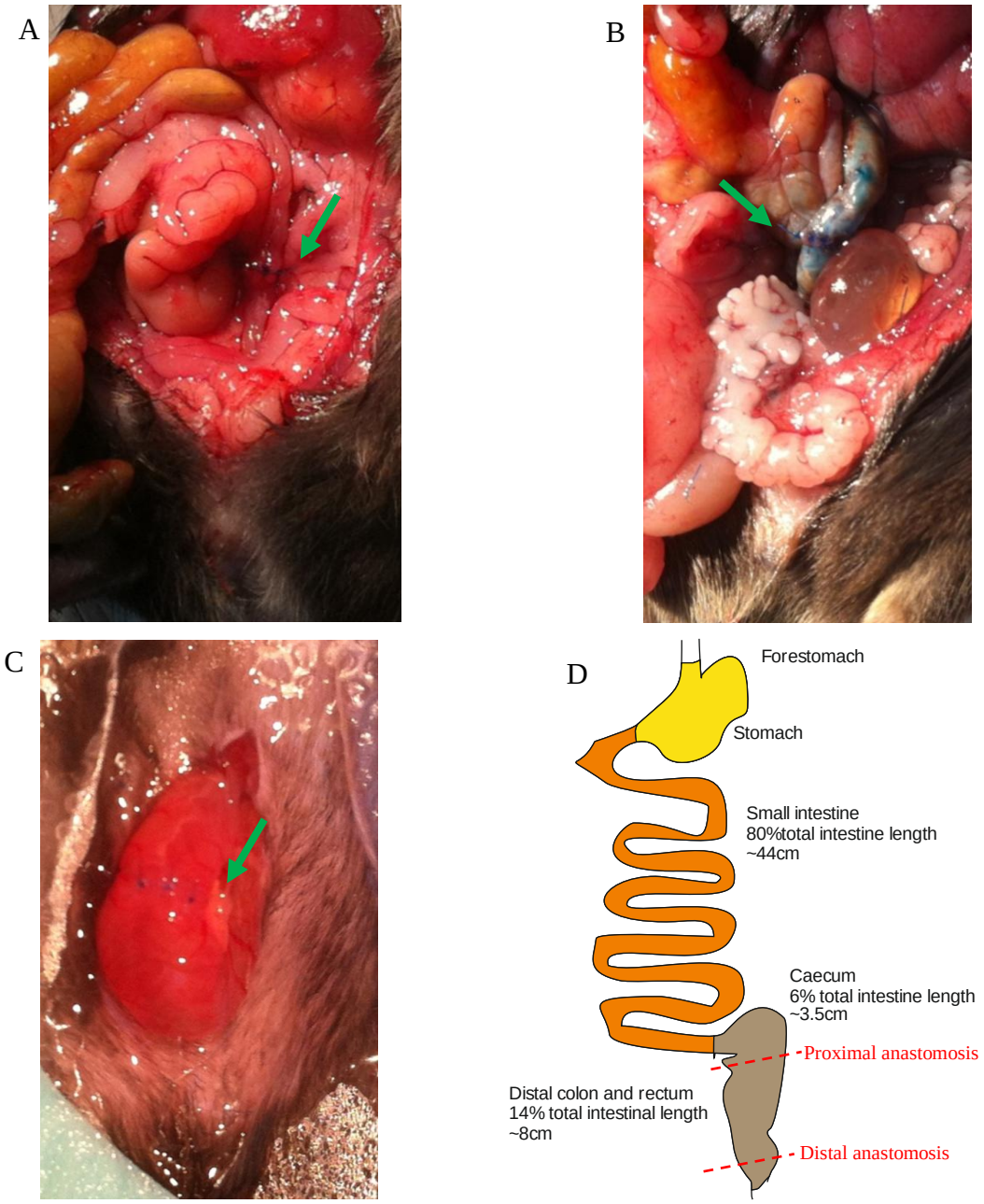

Figure 7-2: Colonic anastomosis in a male mouse. A. A distal anastomosis was feasible and technically similar to its proximal counterpart (green arrow). **B.** After completion, it was equally water-tight when tested with intraluminal methylene blue, but stool is solid during transit at this region and therefore the need for a water-tight seal debatable. **C.** An example of a completed standard proximal anastomosis (green arrow) in an anaesthetised mouse, with 2.5X zoom on a Nikon digital camera. **D.** Schematic showing relative lengths of intestine and locations of proximal and distal anastomoses.

A

B

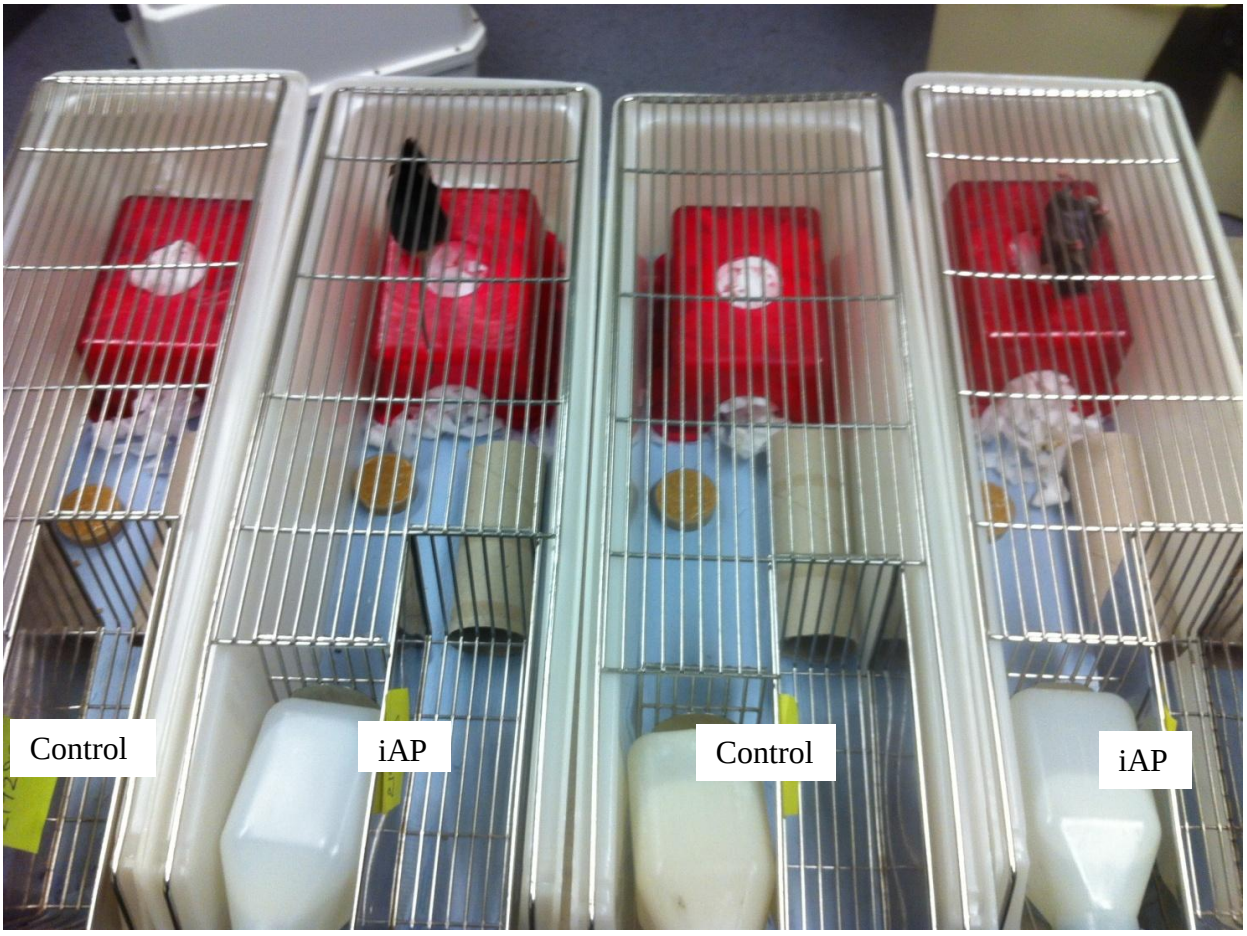

Figure 7-3: Mice approximately 6 hours post-operative. A. Mice completely consumed the Nutella with the included iAP or vehicle control even in the immediate post-operative period. **B**. Differences between the groups could be observed early. Representative image showing a fairly typical finding of mouse activity on the night after their operation. In this image, mice seen climbing were in the iAP treatment group. Mice which were tucked in their houses and not visible in the image, were in the control group. Treatment was blinded until all analysis was completed, and images were then matched to treatment groups.

In order to quantify and compare the original observation of diverging liveliness between groups post-operatively, tracking analysis was performed of a daily 2 minute video recording of each mouse in a recording box. Drawing any strong conclusions from these data however required careful consideration. Mice have differing personalities which influences readiness to explore when presented with new environments (Forkosh *et al.*, 2019), and these differences were apparent during these time lapse captures because of the lack of an incentive to keep moving, unlike the water maze methods (Weitzner *et al.*, 2015), and moments of immobility could simply occur when the mouse may be sniffing the surroundings or looking for escape routes (Figure 7-4A) rather than an actual disinclination to move. In attempt to reduce personality differences to novelty, the mice were acclimatised to time in the recording box three days prior to the day of operation. Even so, the mice continued to exhibit significant variability even in the same mouse, with a propensity for stillness on one day (Figure 7-4B), to running wildly the next (Figure 7-4C). However, on average, movement roughly resembled that of Figure 7-4D, and there were no significant differences between treatment groups in starting (pre-operative) measurements (Control mean +/- SEM: 4.69cm/s +/- 0.15, iAP: 4.81cm/s +/- 0.16, adjusted p=0.811, t-test with Holm-Sidak's multiple comparison correction). It can be seen that there was also a 'practice effect' with mice becoming much bolder and quicker towards the end indicated by the upward trend of the lines in the graph (Figure 7-4E). Despite all these challenges, it was hypothesised that some difference might be expected with the mice who were marginally less well exhibiting a slightly lower activity index. There certainly appeared to be a trend in this direction with differences in the curves of the graph (Figure 7-4E), but these were still not statistically significant despite maximal divergence on post-operative day two (Control mean +/- SEM: 4.16cm/s +/- 0.17, iAP: 4.55cm/s +/- 0.20, adjusted p=0.435, t-test with Holm-Sidak's multiple comparison correction) or day three (Control mean +/- SEM: 4.61cm/s +/- 0.2, iAP: 5.18cm/s +/- 0.18, adjusted p=0.247, t-test with Holm-Sidak's multiple comparison correction, Figure 7-4E). This remained the case for post-operative day four (Control mean +/- SEM: 4.80cm/s +/- 0.22, iAP: 5.44cm/s +/- 0.23, adjusted p=0.293, t-test with Holm-Sidak's multiple comparison correction), day five (Control mean +/- SEM: 5.04cm/s +/- 0.29, iAP: 5.77cn/s +/- 0.23, adjusted p=0.293), day six (Control mean +/- SEM: 5.77cm/s +/- 0.25, iAP: 6.16cm/s +/- 0.23, adjusted p=0.58) and day seven (Control mean +/- SEM: 6.06cm/s +/- 0.25, iAP: 5.94cm/s +/- .026, adjusted p=0.811).

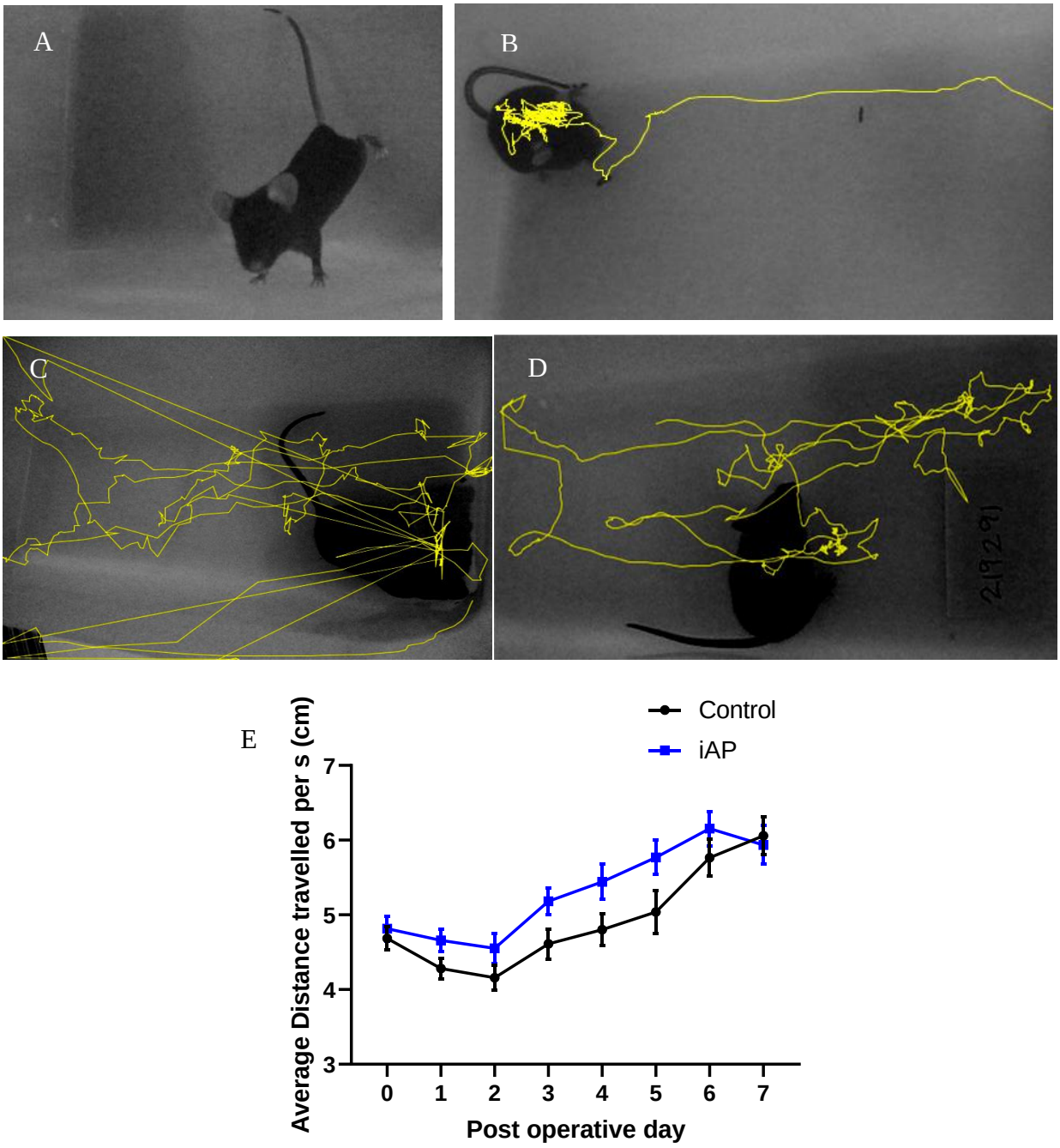

Figure 7-4: Tracking analysis of mouse movement. A. A stationary phase was often spent looking for escape routes in the open top box. **B.** Even after the acclimatisation period, some mice would on one day hardly move, and the next day **(C)** run rapidly from end to end. **D.** An example of an average tracking trace for most mice. **E.** Graph showing the average distance travelled per second on each post-operative day. N=35/ group, error bars show SEM. Comparison with multiple t-tests and Holm-Sidak's correction for multiple comparisons.

7.2.4 iAP significantly accelerated the return of normal bowel function post-operatively in the standard model

The return of normal bowel function was measured by the return to baseline stool (faecal) production in a day. Preliminary stool measurements demonstrated that the actual number of stool pellets passed during a 24 hour period was very variable due to differences in stool size but the weight of faecal matter produced was much more consistent. Therefore 24 hour stool collection was performed and faecal matter weighed after drying in the controlled humidity mouse room for 12 hours (Figure 7-5A). Pre-operatively, there were no differences between the groups in terms of stool production (Control mean +/- SEM: 0.72g +/- 0.02, iAP 0.73g +/- 0.02, adjusted p=0.9002, t-test with Holm-Sidak's correction for multiple comparison, Figure 7-5B). Stool weight fell immediately post-operatively in both groups (Control mean +/- SEM: 0.16g +/- 0.01, iAP: 0.19g +/- 0.01, adjusted p=0.1566, t-test with Holm-Sidak's correction), in keeping with a reduced food intake in the recovery period, as well as a degree of ileus that might be expected following external bowel manipulation. From the second post-operative day the iAP group showed a greater increase in stool weights although this difference did not reach significance (Control mean +/- SEM: 0.26g +/- 0.02, iAP: 0.37g +/- 0.04, adjusted p=0.1380, t-test with Holm-Sidak's correction). However, this trend reached significance on day three (Control mean +/- SEM: 0.38g +/- 0.02, iAP: 0.57g +/- 0.04, adjusted p=0.0006, t-test with Holm-Sidak's correction), day four (Control mean +/- SEM: 0.5g +/- 0.03, iAP: 0.72g +/- 0.04, adjusted p=0.0006, t-test with Holm-Sidak's correction), and day five (Control mean +/- SEM: 0.62g +/- 0.05, iAP: 0.87g +/- 0.05, adjusted p=0.0038, t-test with Holm-Sidak's correction). By day six, stool production was reaching a plateau in both groups (Control mean +/- SEM: 0.84g +/- 0.05, iAP: 0.92g +/- 0.07, adjusted p= 0.6964, t-test with Holm-Sidak's correction). Stool production on day 7 was equal in both groups (Control mean +/- SEM: 0.93g +/- 0.05, iAP: 0.96g +/- 0.06, adjusted p=0.9002, t-test with Holm-Sidak's correction).

A

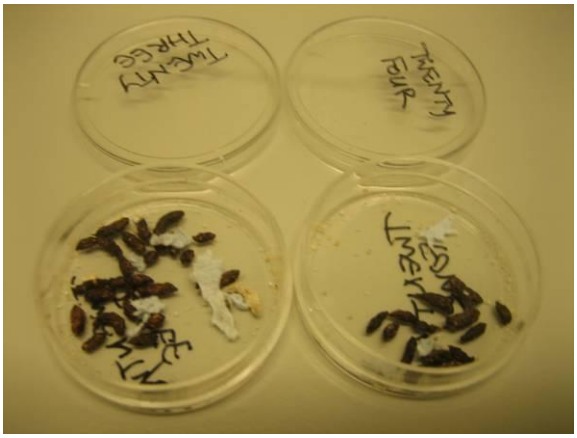

B

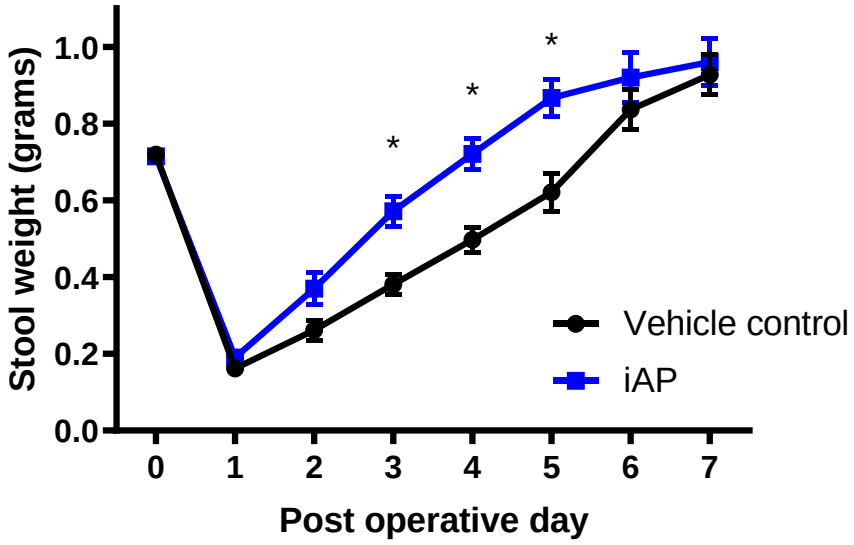

Figure 7-5: Twenty four hour stool collection and weights in the standard anastomosis model. A. A representative picture of the 24 hour stool collection on the second postoperative day in control (right Petri) and iAP (left Petri) groups. **B.** Graph showing the weights of a 24 hour stool collection on each post-operative day. N=35/group, *p<0.05, t-tests with Holm-Sidak's multiple comparison correction, error bars show SEM.

7.2.5 **iAP significantly increased post-operative weight gain in a standard model**

An accelerated return of bowel function to baseline post-operatively would be expected to be reflected in concurrent accelerated weight gain post-operatively. There were no differences in body weight between the groups at the start of the experiment (Control mean +/- SEM: 107.26 +/- 0.78, iAP: 107.11 +/- 0.78, adjusted p=0.8947, t-test with Holm-Sidak's correction for multiple comparisons, Figure 7-6). In keeping with what would be expected from the stool weights, the first post-operative day also did not show any differences (Control mean +/- SEM: 98.31 +/- 0.62, iAP: 98.72 +/- 0.55, adjusted p=0.8587, t-test with Holm-Sidak's correction). Statistically significant increases in the iAP group compared to the control groups were seen starting from 2.5 days post-operative (Control mean +/- SEM: 94.72g +/- 0.63, iAP: 97.64g +/- 0.79, adjusted p=0.0420, t-test with Holm-Sidak's correction). This difference in weight gain was most significant on post-operative day 3.5 (Control mean +/- SEM: 94.47g +/- 0.75, iAP: 98.46g +/- 0.68, adjusted p=0.00695, t-test with Holm-Sidak's correction). The statistical significance in weight difference persisted on day 4 (Control mean +/- SEM: 96.37g +/- 0.89, iAP: 100.46g +/- 0.80, adjusted p=0.0135, t-test with Holm-Sidak's correction), and day 5 (Control mean +/- SEM: 98.16g +/- 1.07, iAP: 102.82g +/- 0.86, adjusted p=0.0140, t-test with Holm-Sidak's correction). Although the weights of the iAP group remained higher than the control group on day 7, this was no longer statistically significant (Control mean +/- SEM: 103.62g +/- 1.03, iAP: 106.98g +/- 1.15, adjusted p=0.1501, t-test with Holm-Sidak's correction).

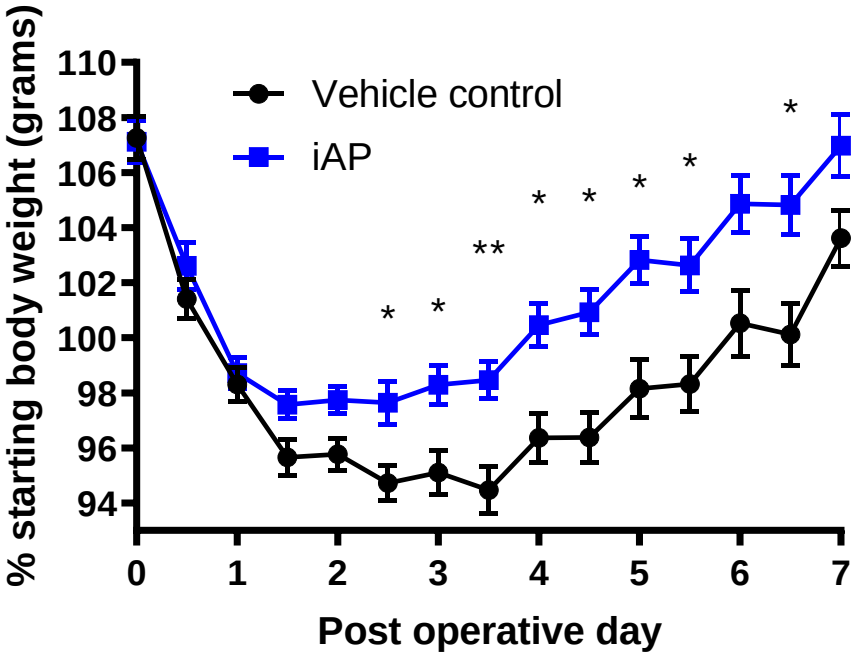

Figure 7-6: Percentage body weight on each post-operative day in the standard anastomosis model. The average body weight of each mouse in the five days preceding the day of surgery was calculated and used as the baseline from which to calculate percentage body weight. N=35/group, t-test with Holm-Sidak's multiple comparison correction, * $p<0.05$, ** $p<0.01$, error bars show SEM.

7.2.6 **iAP significantly increased anastomotic bursting pressure (ABP) on day three in the standard model**

The gold standard of testing the strength of an anastomosis is to determine anastomotic bursting pressure (ABP) (Ravitch 1981, Bosmans 2015). Based upon the return to baseline of stool weight, anastomotic healing was assumed to be complete on day seven. On day three, the ABP was significantly higher in the iAP group (Control mean +/- SEM: 29.34mmHg +/- 4.75, iAP: 52.30mmHg +/- 7.61, p=0.0270, Mann-Whitney test, Figure 7-7A). This increase was no longer significant by the seventh post-operative day (Control mean +/- SEM: 103.10 mmHg +/- 12.31, iAP: 130.70 mmHg +/- 15.82, p=0.1622, Mann-Whitney test, Figure 7-7B). Although the distribution was anticipated to be Gaussian, this was not the case and could be due to the change of manometer to a newer model part-way through the experimental sets, therefore non-parametric analyses were used.

7.2.7 **iAP increased anastomotic hydroxyproline content on day three in the standard model**

Given the increased anastomotic bursting pressure on the third post-operative day, hydroxyproline quantity was hypothesised to be similarly higher. Hydroxyproline content is an indicator of collagen content which contributes toward a stronger, and better-healed anastomosis (Martens and Hendriks, 1991). iAP treatment led to significantly more hydroxyproline in the anastomosis on the third post-operative day (Control mean +/- SEM: 1.38µg/mg +/- 0.56, iAP: 1.68 µg/mg +/- 0.48, p=0.0223, t-test, Figure 7-8A). By the seventh post-operative day however, this difference was no longer significant (Control mean +/- SEM: 2.42 µg/mg +/- 1.06; iAP: 2.74 µg/mg +/- 1.14, p=0.2006, t-test, Figure 7-8B). The lack of persistence of an increased collagen content is of importance and beneficial, because in the motile system of the GIT, excessive collagen deposition leads to fibrosis, impairing distensibility of the lumen, and is the pathological process behind strictures in inflammatory bowel diseases. An attempt was made to visualise the collagen pattern within the anastomosis, and to this end, picrosirius staining was performed. Observation of 20 paired random anastomotic sections revealed equally organised deposition of collagen in all sections (Figure 7-9). Quantification of the birefringence was not attempted because these sections represented only a very small area of the anastomosis (4 µm slice) and therefore results would not be an accurate generalisation.

A

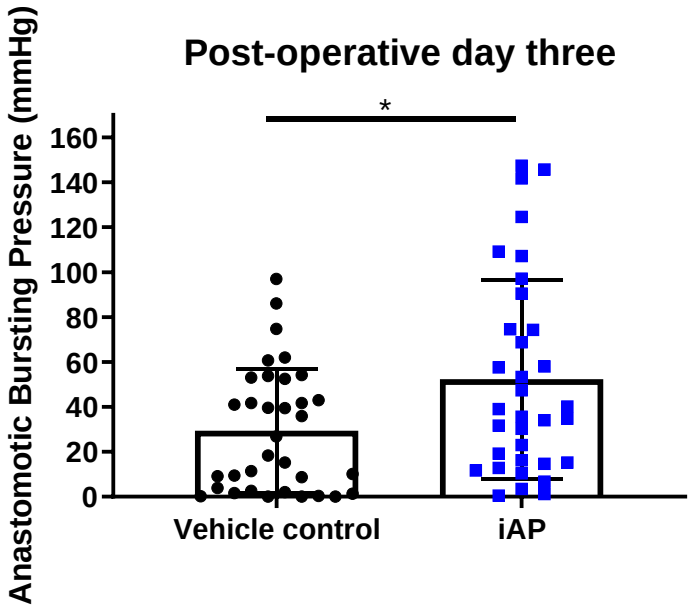

B

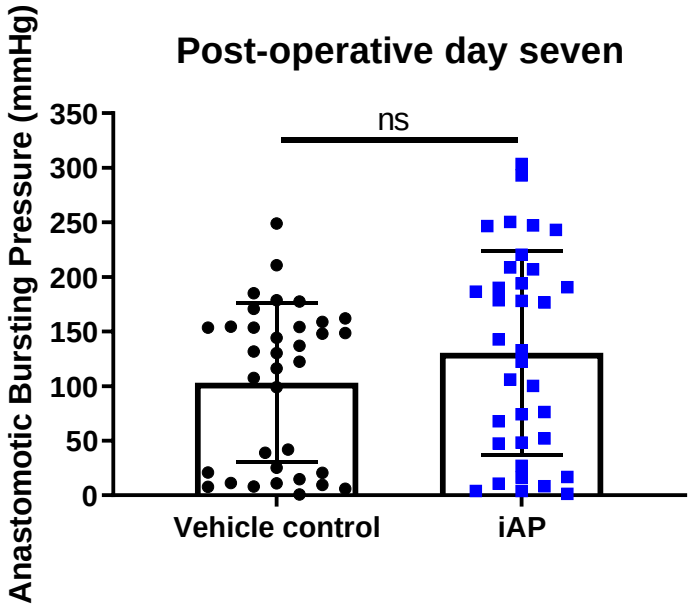

Figure 7-7: Anastomotic bursting pressure (ABP) in the standard anastomosis model. A. ABP measured in mice on the third post-operative day. N=34/group (measurement technical failure in one mouse in the iAP group, and one mouse fewer in the control group due to culling for congenital hydrocephalus), comparison with Mann-Whitney test, *p<0.05, error bars show SD. **B.** ABP measured in mice on the seventh post-operative day. N=35/group, comparison with Mann-Whitney test, ns=non-significant, error bars show SD.

A

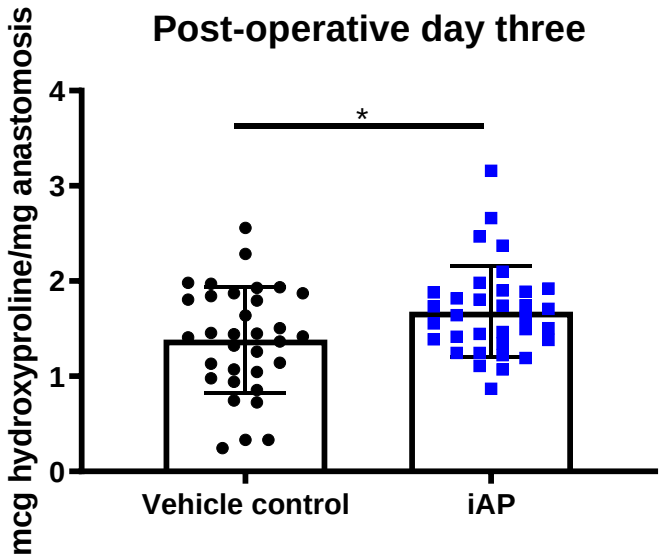

B

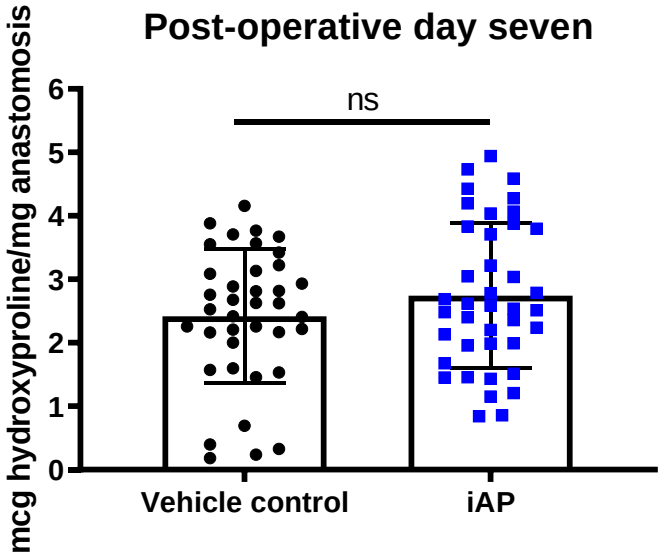

Figure 7-8: Anastomotic hydroxyproline content in the standard anastomosis on the third and seventh post-operative days. A. Third post-operative day hydroxyproline content in a standard anastomosis model. N=34/group in five independent repeats. Comparison with unpaired t-test, ns=non-significant, *$p< 0.05$, error bars show SD. **B**. Seventh post-operative day hydroxyproline content in a standard anastomosis model. N=35/group in five independent repeats. Comparison with unpaired t-test, ns=non-significant, *$p< 0.05$, error bars show SD.

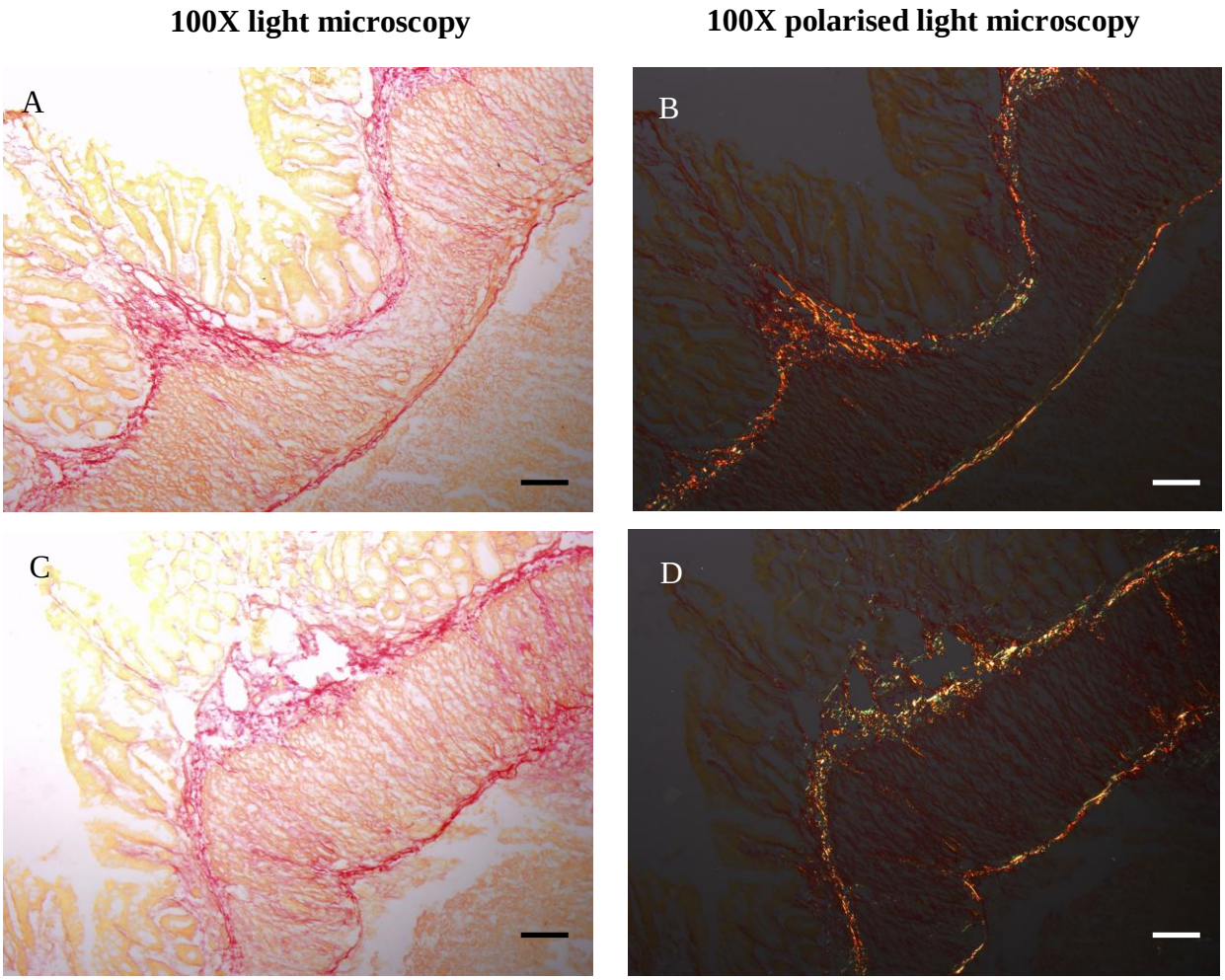

Figure 7-9: Picrosirius staining to investigate collagen architecture in the healed anastomosis. A. 4µm frozen section slice of intestinal anastomosis in a control group mouse visualised at 100X light microscopy imaged with a colour camera. **B.** The same section of anastomosis visualised with polarised light microscopy to demonstrate birefringence of collagen fibrils. **C.** 4 µm frozen section slice of the intestinal anastomosis in the iAP treatment group visualised at 100X light microscopy imaged with a colour camera. **D.** The same section in (C) visualised under polarised light. Black or white scale bars indicate 100 µm.

7.2.8 iAP did not affect hydroxyproline content in the skin wound in the standard model

Many medications are delivered orally to exert a systemic effect; therefore investigation was extended to the healing of the skin wound. It was hypothesised that the oral iAP may enhance laparotomy healing as well. However, there were no significant differences between the groups on day three (Control mean +/- SEM: 20.09µg/mg +/- 1.42, iAP: 19.42 µg/mg +/- 1.17, p=0.7167, t-test, Figure 7-10A). Skin healing was exceedingly good with wounds almost imperceptible by day seven in both groups of mice (Figure 7-10B). Again, no significant differences in wound hydroxyproline content could be demonstrated on day seven (Control mean +/- SEM: 16.44 µg/mg +/- 1.44, iAP: 16.48 µg/mg +/- 1.40, p=0.9836, t-test, Figure 7-10C). Picrosirius staining was performed as before and 20 random pairs analysed. Again, no disorganised collagen deposition was observed in either treatment groups (Figure 7-11A &B).

7.2.9 iAP did not significantly alter spleen weights in the standard model

Hyposplenism has been linked with increased complications of colitis (Ryan *et al.*, 1978), and a spleen-dependent immunomodulatory pathway has previously been shown to improve colitis (Ji *et al.*, 2014; Grandi *et al.*, 2017). Given this possible role of the spleen, it was hypothesised that spleen weights could differ as a result of splenic augmentation following surgery and iAP treatment. However, no differences between groups were observed on both the third (Control mean +/- SEM: 0.069g +/- 0.03, iAP: 0.070g +/- 0.02, p=0.8536, unpaired t-test, Figure 7-12A) and the seventh post-operative days (Control mean +/- SEM: 0.075g +/- 0.02, iAP: 0.079g +/- 0.02, p=0.6051, unpaired t-test, Figure 7-12B).

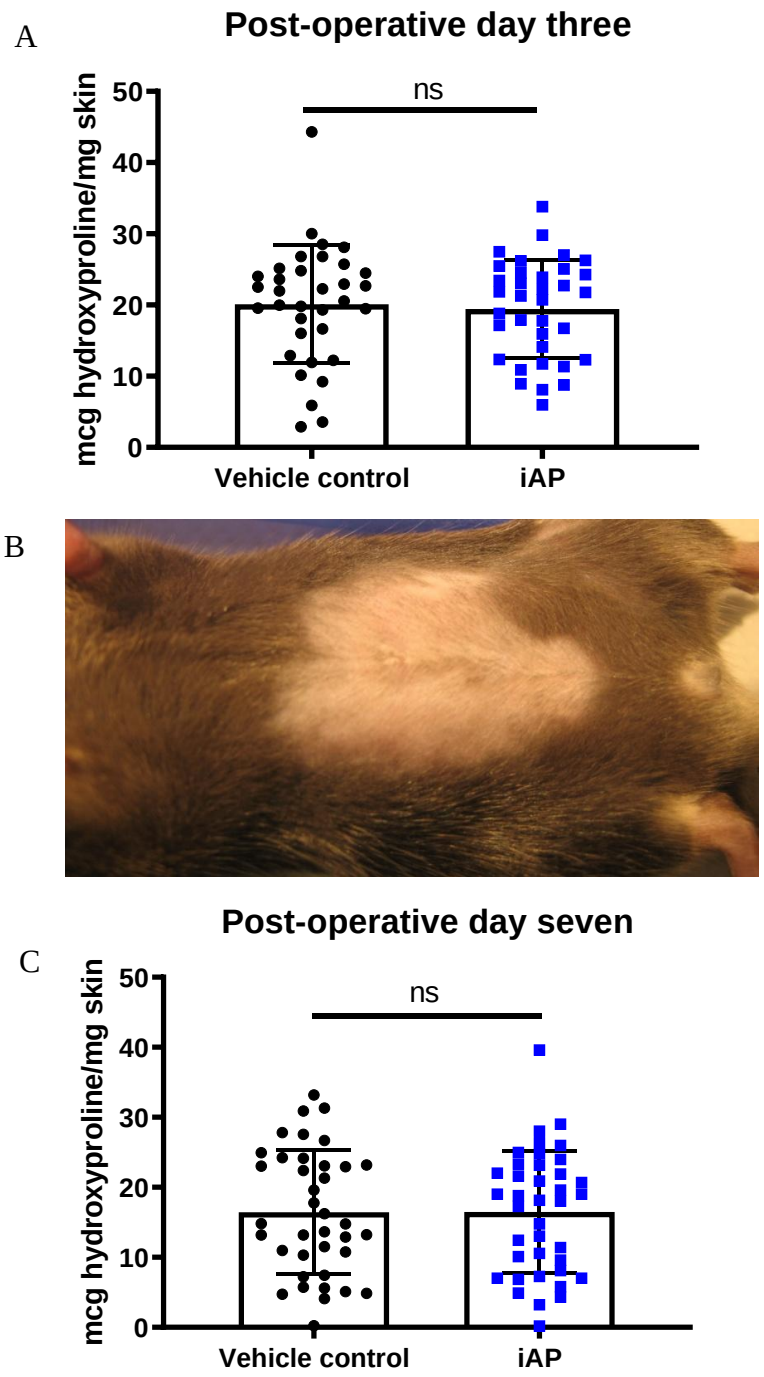

Figure 7-10: Hydroxyproline content in healing skin laparotomy wound in the standard anastomosis model. A. Graph of hydroxyproline content per mg of laparotomy skin wound on the third post-operative day. N=34/group, t-test, ns=non-significant, error bars show SD. **B.** Representative image of the laparotomy skin wound on day seven. **C.** Graph of hydroxyproline in the skin wound on day seven. N=35/group, comparison with t-test, ns=non-significant, error bars show SD.

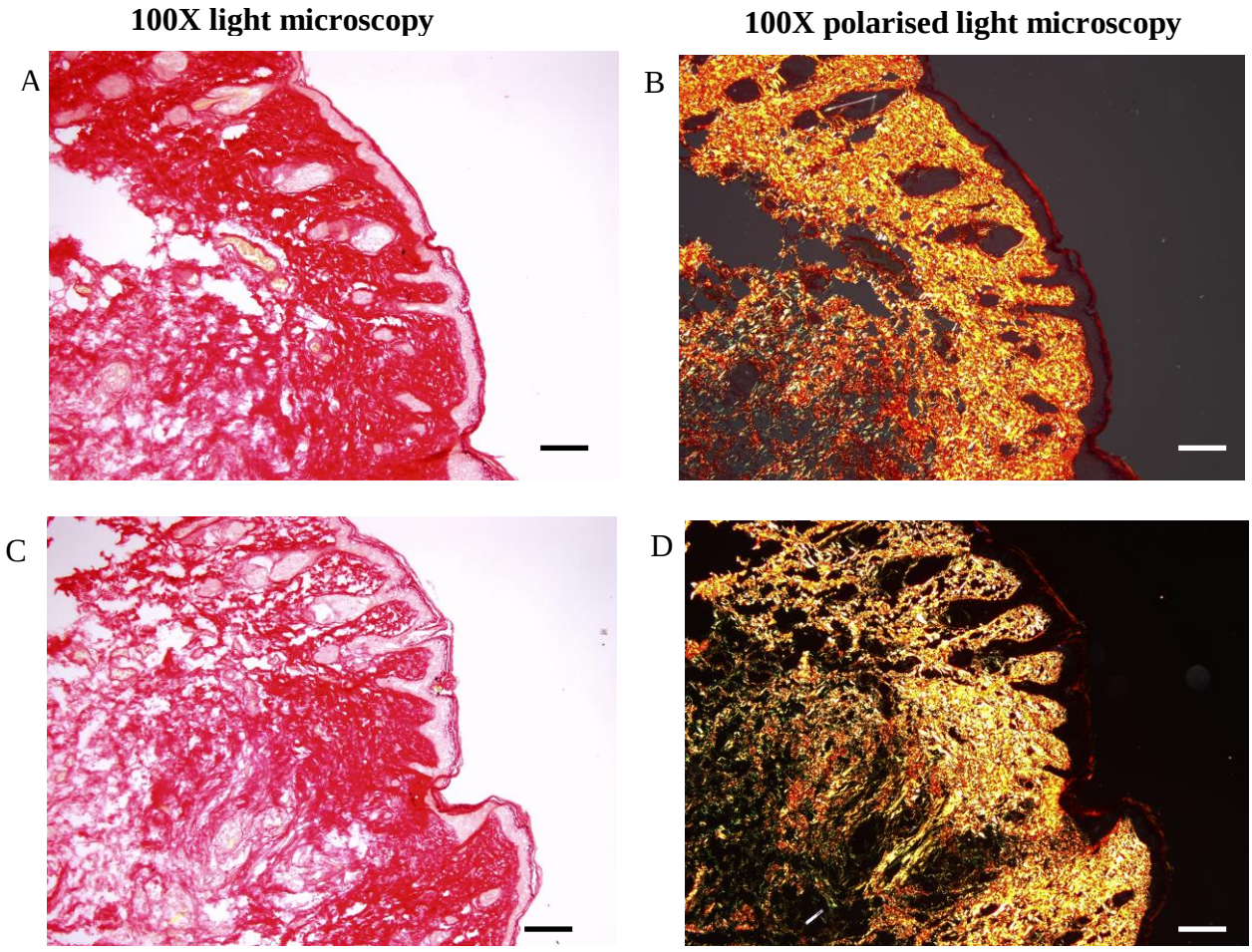

Figure 7-11: Picrosirius red staining of laparotomy skin wound. A. 4µm frozen section slice through the area of the midline skin wound of a mouse in the control group, visualised under light microscopy with 100X magnification. **B.** Polarised light microscopy of the same region in (A) to visualise birefringence. **C.** 4 µm frozen slice in the iAP treatment group visualised under light microscopy with 100X magnification. **D.** The same region as (C) visualised under polarised light. Black or white scale bars indicate 100 µm.

A

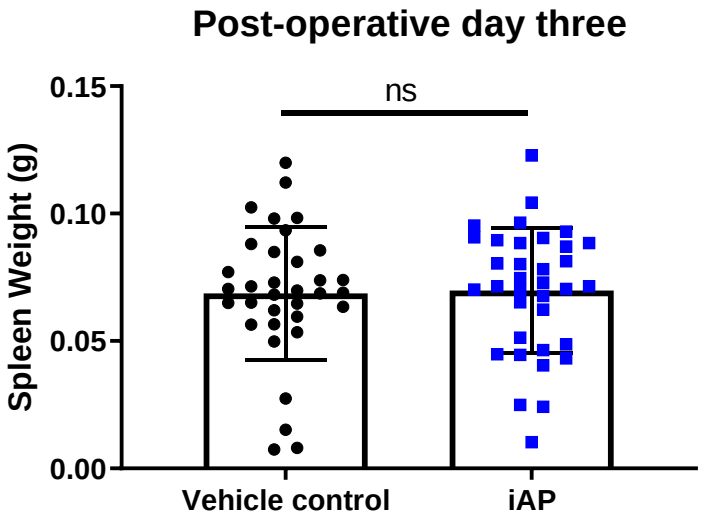

B

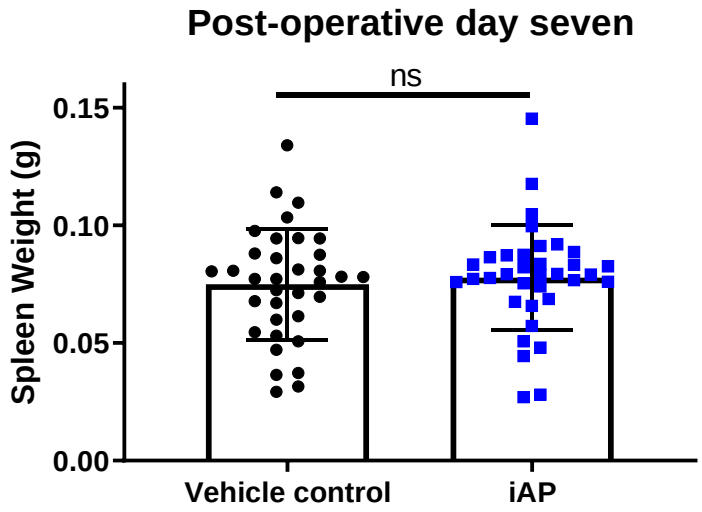

Figure 7-12: Spleen weights in the standard anastomosis model. A. Spleens were weighed immediately following cervical dislocation on the third post-operative day. N=34/group in five independent repeats, comparison with t-test, ns=non-significant, error bars show SD. **B.** Spleens were weighed immediately following cervical dislocation on the seventh post-operative day. N=35/group in five independent repeats, ns=non-significant, comparison with unpaired t-test, error bars show SD.

7.2.10 **iAP did not affect the diversity of faecal bacteria in the standard model**

iAP has been purported to increase the diversity of bacteria within the intestinal tract (Malo *et al.*, 2014) and extended cultures on BHI agar have previously resulted in good reads for microbiome sequencing (Lau *et al.*, 2016). Plate culture was therefore used to see if there were visual differences in the diversity of growing bacteria as a baseline study. Because of the possible variability of microenvironment between plates, treatment pairs were plated together with three replicates from the proximal and distal anastomotic regions in the iAP treatment group on one side, and three replicates similarly from the control group on the other. Comparison was made only between the number of different morphological species seen after overnight growth (Figure 7-13A-C), and longer (72h) growth was undertaken if there was ambiguity. With samples collected on day three, no association was found between number of bacterial morphologies seen and treatment (p=0.9618, Freeman-Halton extension of Fisher's exact test, calculated in http://vassarstats.net/, Figure 7-13A&B) or on day seven (p=0.5181, Freeman-Halton extension of Fisher's exact test, Figure 7-13C).

7.2.11 **iAP did not affect the diversity of faecal fungi in the standard model**

Fungal presence can disrupt wound healing (Kalan *et al.*, 2016b), therefore to investigate fungal growth, Sabouraud Dextrose gel plates were similarly plated with replicate samples of faeces from the anastomotic region. A maximum of two different morphologies were observed and often no growth occurred even after seven days, and this could be due to limitations of culture conditions or the agar nutrients. Nonetheless, no association was noted between number of fungal morphologies and treatment on day three (p=0.7475, Freeman-Halton extension of Fisher's exact test, Figure 7-14A&D), or on day seven (p=0.7262, Freeman-Halton extension of Fisher's exact test, Figure 7-14E).

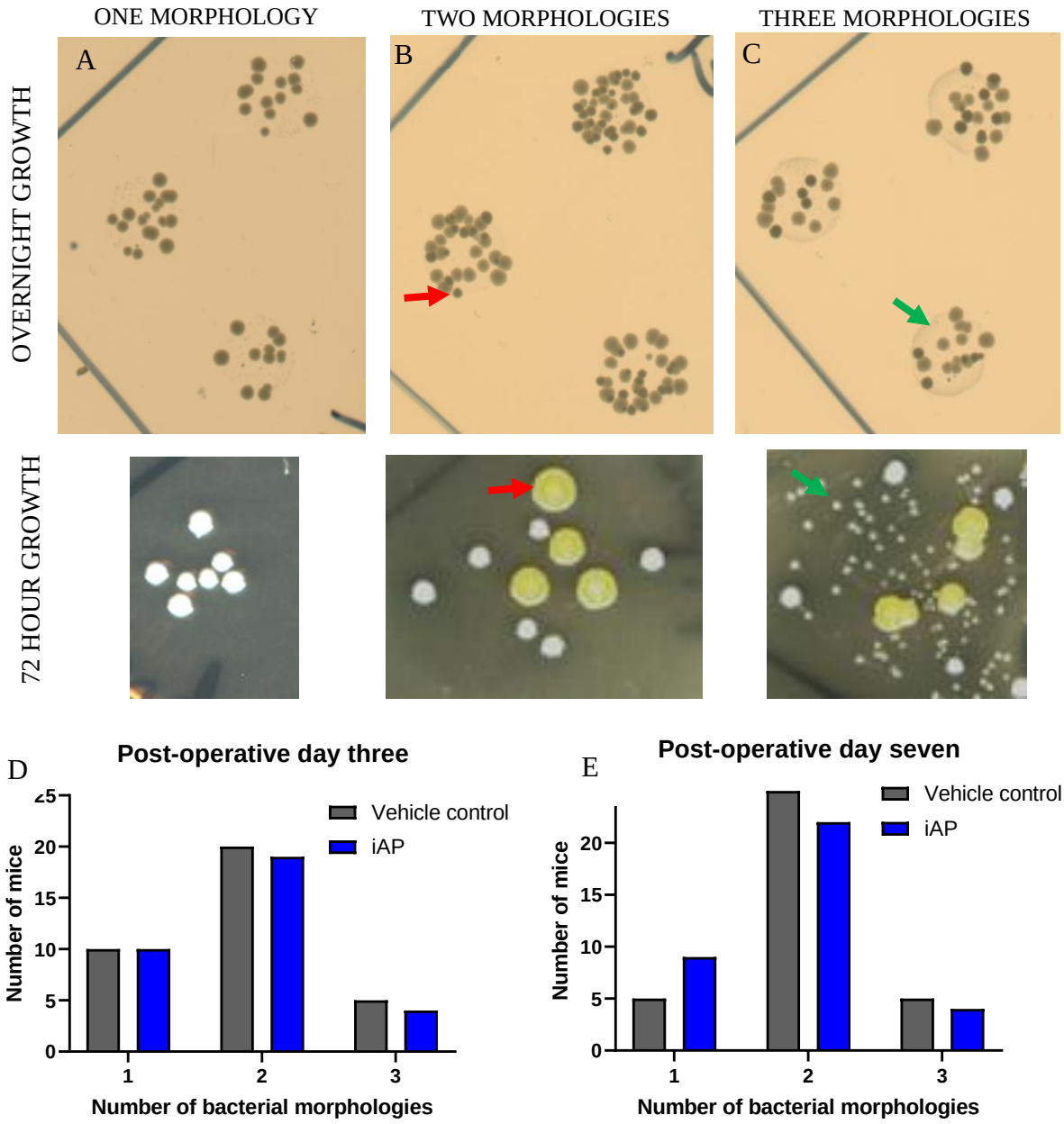

Figure 7-13: Bacterial morphologies isolated from stool in the region of the anastomosis in the standard model. Representative examples of BHI plates after overnight growth at 37˚C. Images below show overgrowth after 72hours. **A.** Single morphology. **B.** Two morphologies. The second morphology is indicated by the red arrow. **C.** Three morphologies. The third morphology is indicated by the green arrow. **D.** Graph showing the number of mice with stool containing each number of morphologies on day three. N=35/group. Freeman-Halton extension of Fisher's exact test. **E.** Graph showing the number of mice with stool containing each number of bacterial morphologies on day seven. N=35/group, Freeman-Halton extension of Fisher's exact test.

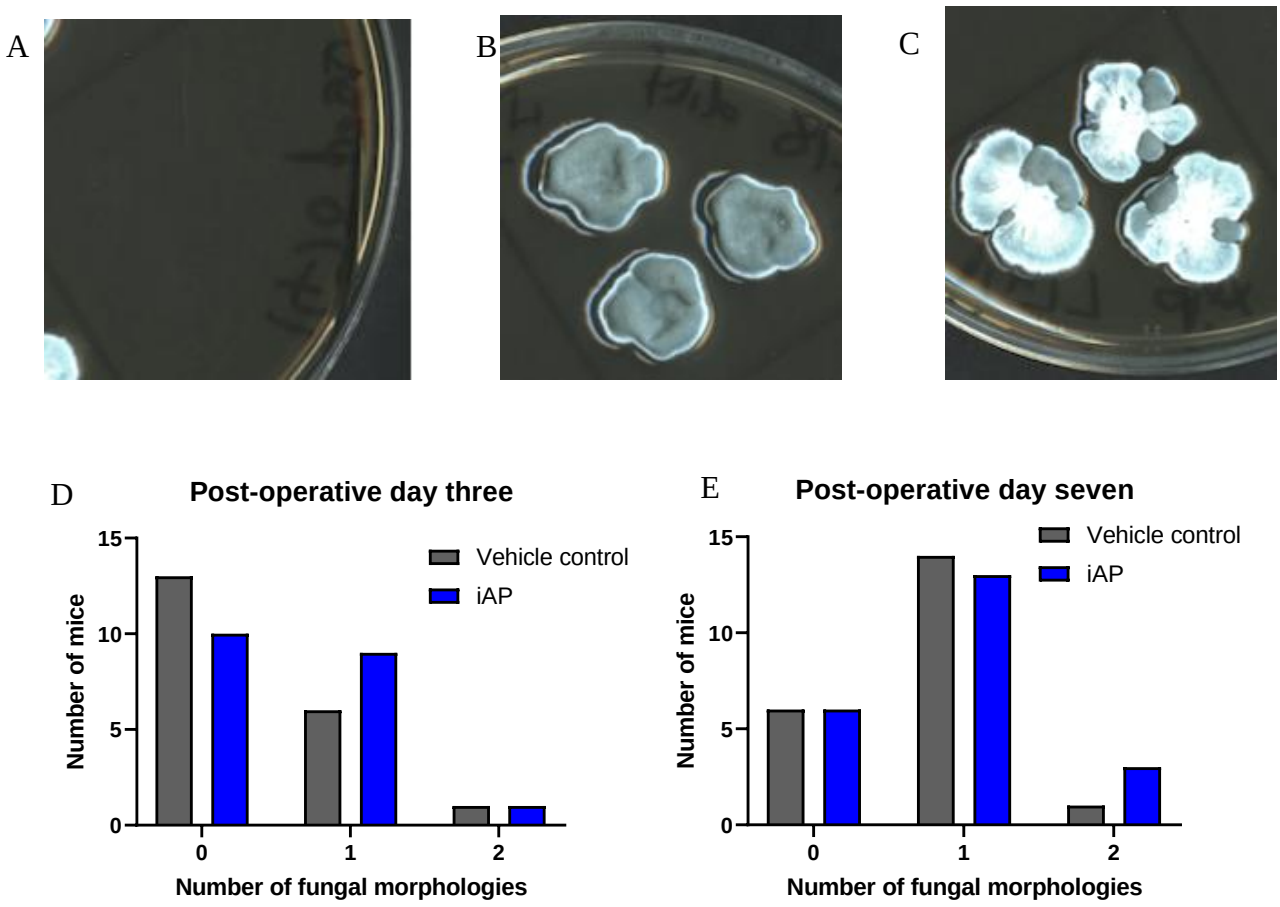

Figure 7-14: Fungi cultured from stool in the region of the anastomosis. Three 10µl samples from each stool specimen was cultured in pairs on Sabouraud Dextrose agar plates at 28˚C, inspected after 72 hours, and imaged after seven days. **A.** Example of plate with no growth. **B.** Example of a single morphology. **C.** Example of a double morphology. **D.** Graph of number of mice with fungal cultures on day three. N=21/group, Freeman-Halton extension of Fisher's exact test, fewer numbers due to lack of media for immediate culture. **E.** Graph of number of mice with fungal cultures on day seven. N=21/group, Freeman-Halton extension of Fisher's exact test, fewer numbers due to lack of media for immediate culture. Delayed culture was not performed to avoid skewing of results from either loss of species, or spurious contamination from storage.

7.2.12 **iAP did not affect faecal cellulolytic activity in the standard model**

Short chain fatty acids (SCFAs) are thought to have a beneficial effect on anastomotic healing (Aguilar-Nascimento *et al.*, 1995; Rolandelli, Buckmire and Bernstein, 1997). Detection of SCFAs is usually performed using chromatography or by mass spectrometry (Dobrowolska−Iwanek *et al.*, 2016; Zhang, Wang and Zhu, 2019) especially if detecting differences in samples in small murine samples, but due to the number of other investigations already being performed on the faecal material, an alternative method was used. SCFAs are derived from breakdown of cellulose from microbial cellulase. Therefore, the breakdown of CMC was used as a marker of the cellulase activity, and thus a surrogate marker of SCFA availability, in stool taken from the region of the anastomosis and this was quantified by measuring the area of lucency after staining with iodine (Figure 7-15A). No differences were seen either on day three (Control mean +/- SEM: 23.95 mm^2 +/- 2.44, iAP: 27.30 mm^2 +/- 2.77, p=0.3663, unpaired t-test, Figure 7-15B) or day seven (Control mean +/- SEM: 32.27 mm^2 +/- 2.45, iAP: 30.56 mm^2 +/- 2.15, p=0.6008, unpaired t-test, Figure 7-15C).

7.2.13 **iAP did not affect faecal proteolytic activity in the standard model**

Proteolytic activity in bacteria have been linked to microbial invasiveness, for example Gelatinase E in *E. faecalis* is a known virulent factor (Sava, Heikens and Huebner, 2010; Maharshak *et al.*, 2015), and there is evidence that proteolytic activity in the region of the anastomosis may contribute to the risk of a leak (Shogan *et al.*, 2015). Therefore the degree of proteolytic activity in bacteria cultured from stool in the anastomotic region was assessed by observing digestion using milk-BHI agar plates. The assay performed here was performed on whole faecal culture. This is because many biosynthetic gene clusters become activated in co-culture rather than under standard laboratory single culture (Bertrand *et al.*, 2014), and this would therefore give the most relevant picture of overall proteolytic activity in the anastomotic region. Proteolytic activity was graded as zero when no digestion was seen (Figure 7-16A), one when only one sample showed digestion (Figure 7-16B), and two when both samples showed digestion (Figure 7-16C). There were no significant associations between proteolytic activity and treatment groups either on day three (p=0.9253, Freeman-Halton extension of Fisher's exact test, Figure 7-16D) or day seven (p=0.9236, Freeman-Halton extension of Fisher's exact test, Figure 7-16E) of the standard model.

A

B

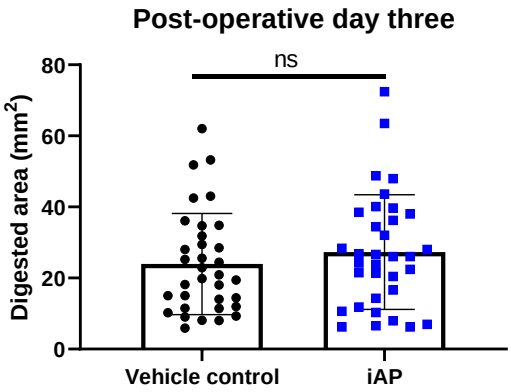

C

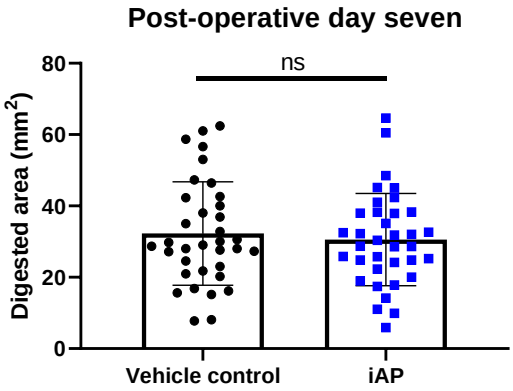

Figure 7-15: Cellulolytic activity in stool from the region of the anastomosis in the standard model. **A.** CMC agar plates were incubated at 37˚C overnight and stained with iodine to delineate digested area before being imaged. A representative stained digested plate shown. **B.** Graph of digested area for each treatment group on post-operative day three of the standard model. N=34/group, comparison with unpaired t-test, ns=non-significant, error bars show SD. **C.** Graph of digested area for each treatment group on post-operative day seven of the standard model. N=35/group, comparison with unpaired t-test, ns=non-significant, error bars show SD.

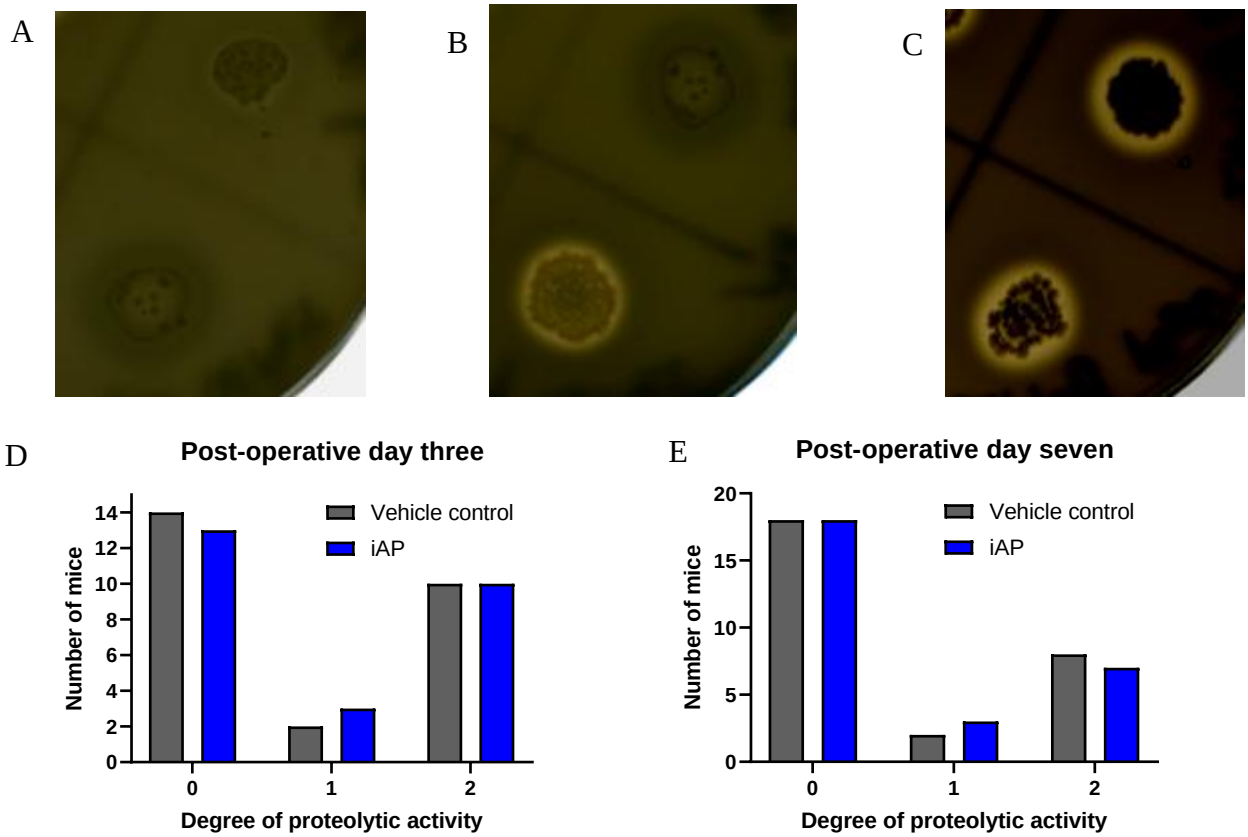

Figure 7-16: Proteolytic activity in the stool from the region of the anastomosis in the standard model. Two separate 10µl samples of faecal matter from the region of the anastomosis were spotted onto BHI agar plates containing 15% sterile milk. Plates were cultured at 37˚C overnight and then imaged to enable visualisation of the lucent areas. **A.** Example of zero protease activity as no lucent regions were seen around either areas of bacterial growth. **B.** Example of one degree of protease activity where one of the two samples demonstrated surrounding lucency. **C.** Example of two degrees of protease activity where both samples displayed surrounding lucency. **D.** Graph showing the number of mice in each group of protease activity on day three. N=26/group, Freeman-Halton extension of Fisher's exact test. **E.** Graph showing number of mice in each group of protease activity on day seven. N=28/group, Freeman-Halton extension of Fisher's exact test.

7.2.14 iAP did not affect anastomotic MMP2 or MMP9 activity in the standard model

MMP2 and MMP9 levels in tissues have both been shown to be altered in states of cancer or delayed healing (Loffek, Schilling and Franzke, 2011). Nonetheless, the complete absence of MMP is detrimental to healing (Caley, Martins and O'Toole, 2015). Therefore it was of interest to determine if there were differences in the expression and activation of MMPs in anastomotic and skin wound samples. No differences in the anastomotic levels of anastomotic MMP2 on day three (Control mean +/- SEM: 0.37A.U. +/- 0.05, 0.38 A.U. +/- 0.05, p=0.9417, Mann-Whitney test, Figure 7-17A), or on day seven (Control mean +/- SEM: 0.55 A.U. +/- 0.04, iAP: 0.43 A.U. +/- 0.04, p=0.0567, Mann-Whitney test, Figure 7-17B). For MMP9 at the anastomotic site, again no differences were seen day three (Control mean +/- SEM: 0.61 A.U. +/- 0.05, 0.58 A.U. +/- 0.05, p=0.6762, Mann-Whitney test, Figure 7-17C), or day seven (Control mean +/- SEM: 0.60 A.U. +/- 0.05, iAP: 0.51 A.U. +/- 0.04, p=0.1196, Mann-Whitney test, Figure 7-17D). To ensure that MMP activity was not due to unequal amounts of starting sample, total protein was determined prior to experimentation via standardised spectrometry, and in addition, simultaneous parallel Western Blotting was performed to confirm that an equal concentration of protein was indeed being loaded. This revealed a small degree of variation (Figure 7-17E), but as long as the paired samples were grossly equivalent (Figure 7-17F), this was accepted. The zymogram samples were not normalised to the Western blot since this could lead to the introduction of additional errors because they were run on parallel but different gels.

7.2.15 iAP did not affect skin MMP2 or MMP9 activity in the standard model

It was hypothesised that given the similarities in skin collagen content, no differences would be seen. Indeed, no differences in skin MMP2 were seen either on day three (Control mean +/- SEM: 0.55 A.U. +/- 0.05, iAP: 0.57 A.U. +/- 0.05, p=0.7316, Mann-Whitney test**,** Figure 7-18A) or day seven (Control mean +/- SEM: 0.59 A.U. +/- 0.04, iAP: 0.62 A.U. +/- 0.05, p=0.6536, Mann-Whitney test, Figure 7-18B). This was also the case for MMP9, with no skin differences on days three (Control mean +/- SEM: 0.34 A.U. +/- 0.05, iAP: 0.44 A.U. +/- 0.06, p=0.4521, Mann-Whitney test, Figure 7-18C) or seven (Control mean +/- SEM: 0.12 A.U. +/- 0.03, iAP: 0.19 A.U. +/- 0.05, p=0.9596, Mann-Whitney test, Figure 7-18D).

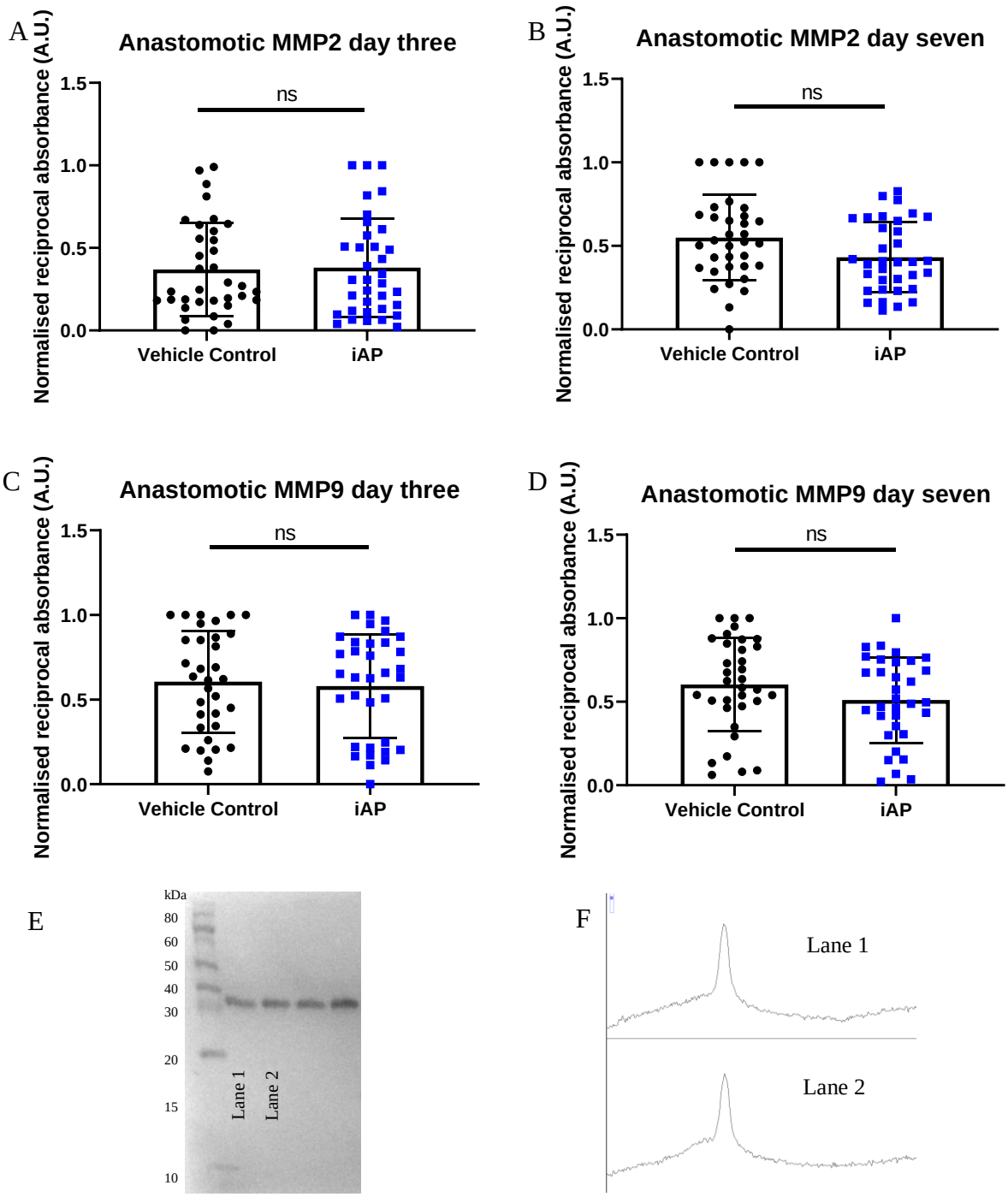

Figure 7-17: Anastomotic MMP2 and MMP 9 on post-operative day three and seven in the standard model. A. Anastomotic MMP2 on day three. **B.** Anastomotic MMP2 on day seven. **C.** Anastomotic MMP9 on day three. **D**. Anastomotic MMP9 on day seven. In each N=35/group, comparison with Mann-Whitney test, ns=non-significant, error bars show SD. **E.** Example image of a parallel Western Blot of GAPDH (size ~37kDa), a different mouse sample in each lane. **F.** Image J density plot showing roughly equivalent peaks of each lane. Both lanes show GAPDH expression of the samples in E.

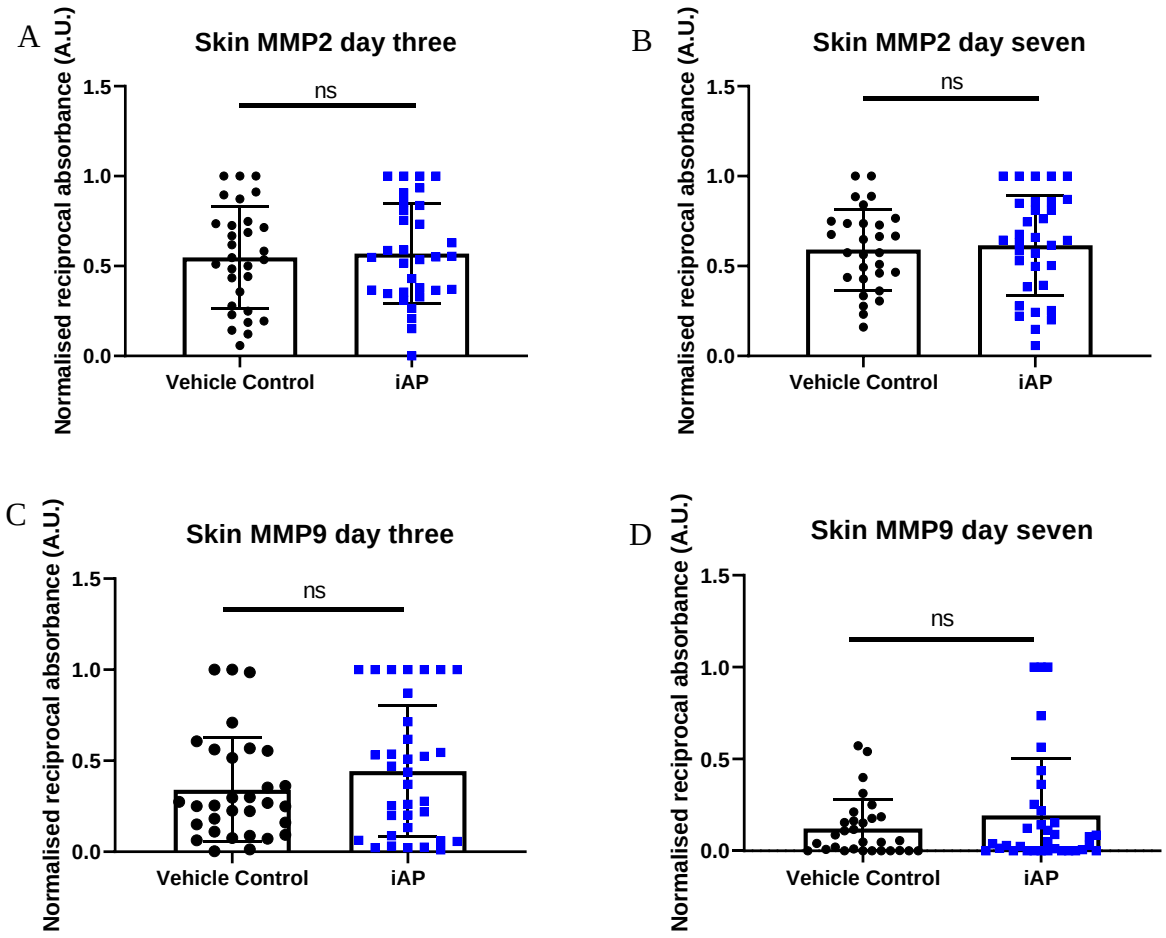

Figure 7-18: MMP2 and MMP9 activity within the skin wound in the standard anastomosis model. Zymograms were run and each gel imaged under identical exposure times using BioRad imager. These images were then exported and analysed with ImageJ. Gel lanes were plotted. Each gel was normalised to the largest value in the single gel. In each gel, samples were paired such that a control sample was always run together with a treatment sample to enable relative comparison. **A.** Skin MMP2 on day three. N=34/group, comparison with Mann-Whitney test, ns=non-significant, error bars show SD **B.** Skin MMP2 on day seven. **C.** Skin MMP9 on day three. **D.** Skin MMP9 on day seven. N=35/group, comparison with Mann-Whitney test, ns= non-significant, error bars show SD.

7.2.16 **iAP significantly increased the activity of anastomotic DISP on day seven in the standard model**

Interestingly, there was an additional enzymatic activity demonstrated in the region <50kD MW in the zymogram gels. Such activity had not been previously published and these regions of activity were not seen in skin, but were specific for the intestinal regions. Enzymatic activity in this region could be due to several enzymes. The MEROPS database (Rawlings, Barrett and Bateman, 2012) lists 14 super families of proteases, and therefore in attempt to streamline identification of the protease of interest, the band was extracted and mass spectrometry performed. The top five mass spectrometry matches included the cysteine protease ATG4B, and the serine protease, Distal Intestinal Serine Protease (DISP or PRSS30) (Table 7-1). To distinguish between these two, it was necessary to see if the zymogram band was the result of a protease of the serine or cysteine family. E64 is an irreversible and highly specific inhibitor of cysteine proteases that does not inhibit serine proteases apart from trypsin (Hanada *et al.*, 1978). Therefore this was first tested by running a parallel second zymogram together with incubation with 10 µM E64 (Sigma Aldrich) in the developing buffer. E64 did not result in abolishment of the digested bands, indicating that this was not a cysteine protease (Figure 7-19A & B). An additional parallel third zymogram was run (in order to ensure similar gel running and enzymatic digestion conditions), and was incubated with and 100 µM leupeptin. Leupeptin inhibits both cysteine and serine proteases (Maeda *et al.*, 1971), however since the activity was completely abolished by leupeptin, but not E64, this suggested the activity to be that of a serine protease (Figure 7-19C). For final confirmation, mass spectrometry was repeated with a segment cut in the same MW region but that did not contain a digested band, and DISP was no longer identified. DISP activity was not significantly different on day three (Control mean +/- SEM: 0.29 A.U. +/- 0.05, iAP: 0.33 A.U. +/- 0.06, p=0.7538, Mann-Whitney test, Figure 7-19D), but was significantly elevated with iAP on day seven (Control mean +/- SEM: 0.35 A.U. +/- 0.05, iAP: 0.54 A.U. +/- 0.05, p=0.0092, Mann-Whitney test, Figure 7-19E).

Table 7-1: Top five mass spectrometry matches according to iBAQ score

Protein Names	Gene names	Mol. weight [kDa]	iBAQ
26S protease regulatory subunit 8	Psmc5	38.751	1E+06
26S protease regulatory subunit 7	Psmc2	52.866	646280
Cysteine protease ATG4B	Atg4b	44.403	348670
CAAX prenyl protease 1 homolog	Zmpste24	54.734	315630
Serine protease 30	Prss30	33.707	205060
26S protease regulatory subunit 6B	Psmc4	43.549	22753

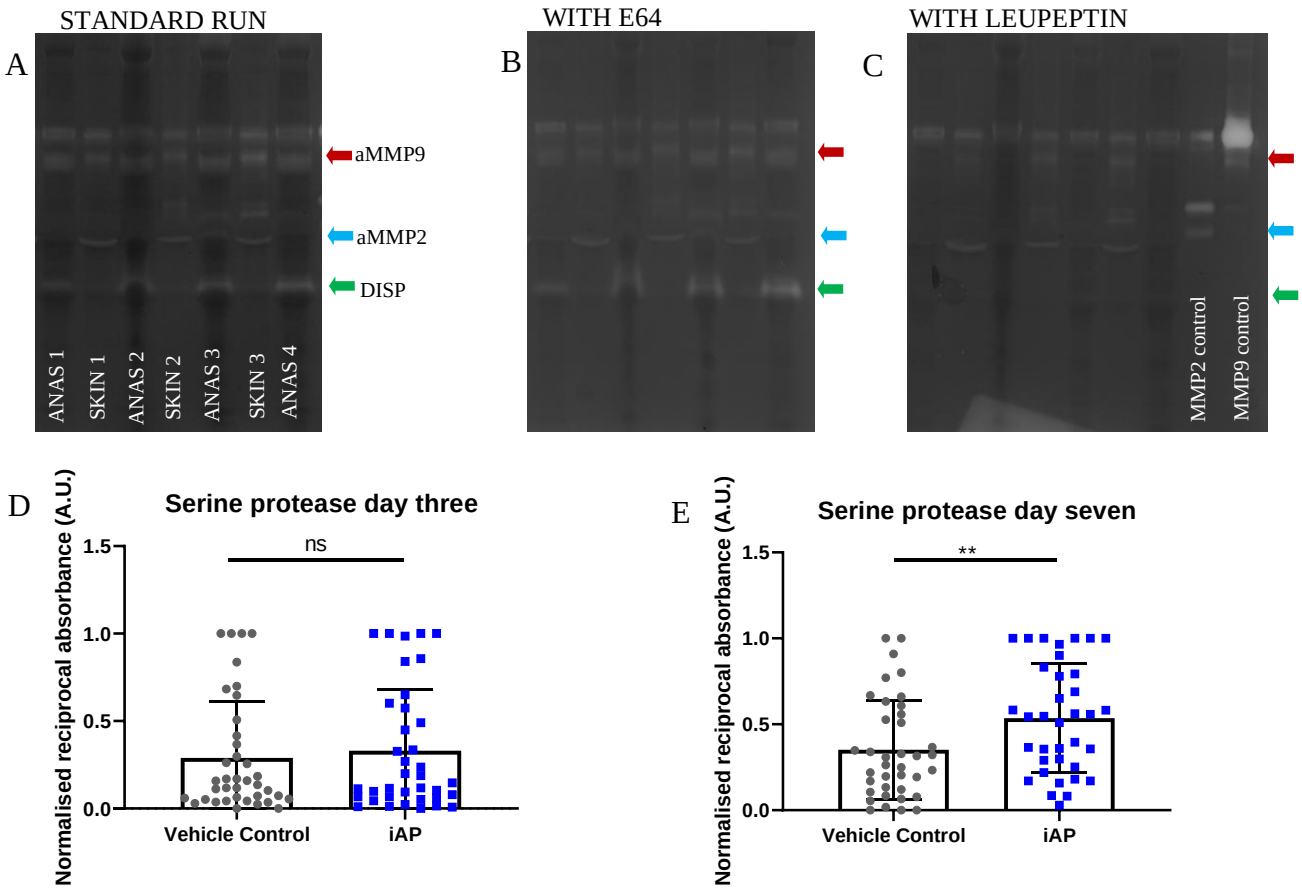

Figure 7-19: An anastomotic serine protease, later identified as DISP, on days three and seven. A. Zymogram with standard digestion showing the bands of activated MMP9 (red arrow), activated MMP2 (blue arrow), and DISP (green arrow). **B.** Parallel zymogram samples run with 10 µM E64 with bands persisting. **C.** Parallel zymogram samples run with 100 µM Leupeptin showing absence of DISP (green arrow). **D.** DISP on day three. **E.** DISP on day seven. In each case N=35/group, comparison with Mann-Whitney test, ns=non-significant, $^{**}p < 0.01$, error bars show SD.

7.2.17 **No ALs occurred in the iAP group in the leaking model**

Although beneficial effects of iAP were seen in the standard anastomosis model, it remained possible that similar benefits may not follow should the environment of the intestine be rendered more hostile by an overdrive in bacterial activity since suppression of the inflammatory response can result in a susceptibility to infection (Kobayashi 2005, Mashimoto 2006). Therefore, a leaking model was used as the next level of investigation. This consisted of an insufficient anastomosis where non-watertight joins are fashioned through the use of a reduced number of stitches. As the anastomoses were located in the proximal colon, faecal contents in this region are liquid, and would leak out more easily if healing was inadequate. Of note, leaks became clinically apparent on the morning of day 2, evidenced by a reluctance to consume Nutella, low Wellness Scores and high Murine Sepsis Scores, and these mice were immediately euthanised. This day two presentation lends strength to the assumption of a failure of healing, rather than a technical failure which would be evident in the immediate, rather than delayed, post-operative period. As all leaks occurred before day three, the total numbers of mice in both post-operative groups were combined giving a leak rate in the control group of 7.14%. There were no leaks in the iAP-treated group. This rate, although comparable with rates quoted in human clinical settings, was insufficient to provide statistical significance linking iAP with decreased leaks when assessed with Fisher's conditional test (p=0.2410, Fishers exact test, Figure 7-20A). Using the lesser known, but more powerful Barnard's unconditional test however (Barnard, 1945), this difference was significant with p=0.046 (calculated using R programming). This experimental model was concluded after three independent repeats as it was powered to detect differences in hydroxyproline content of the anastomosis rather than differences in leaks. However, it was possible that the low number of leaks could be attributable to an unconscious adaptation in technique by the surgeon, as seen by the decreasing severity of leaks in each, with the first leak seen as generalised peritonitis from free faecal contents (Figure 7-20B), the second as a less extensive pelvic collection (Figure 7-20C), and the final leak as a localised collection only in the immediate vicinity of the anastomosis (Figure 7-20D).

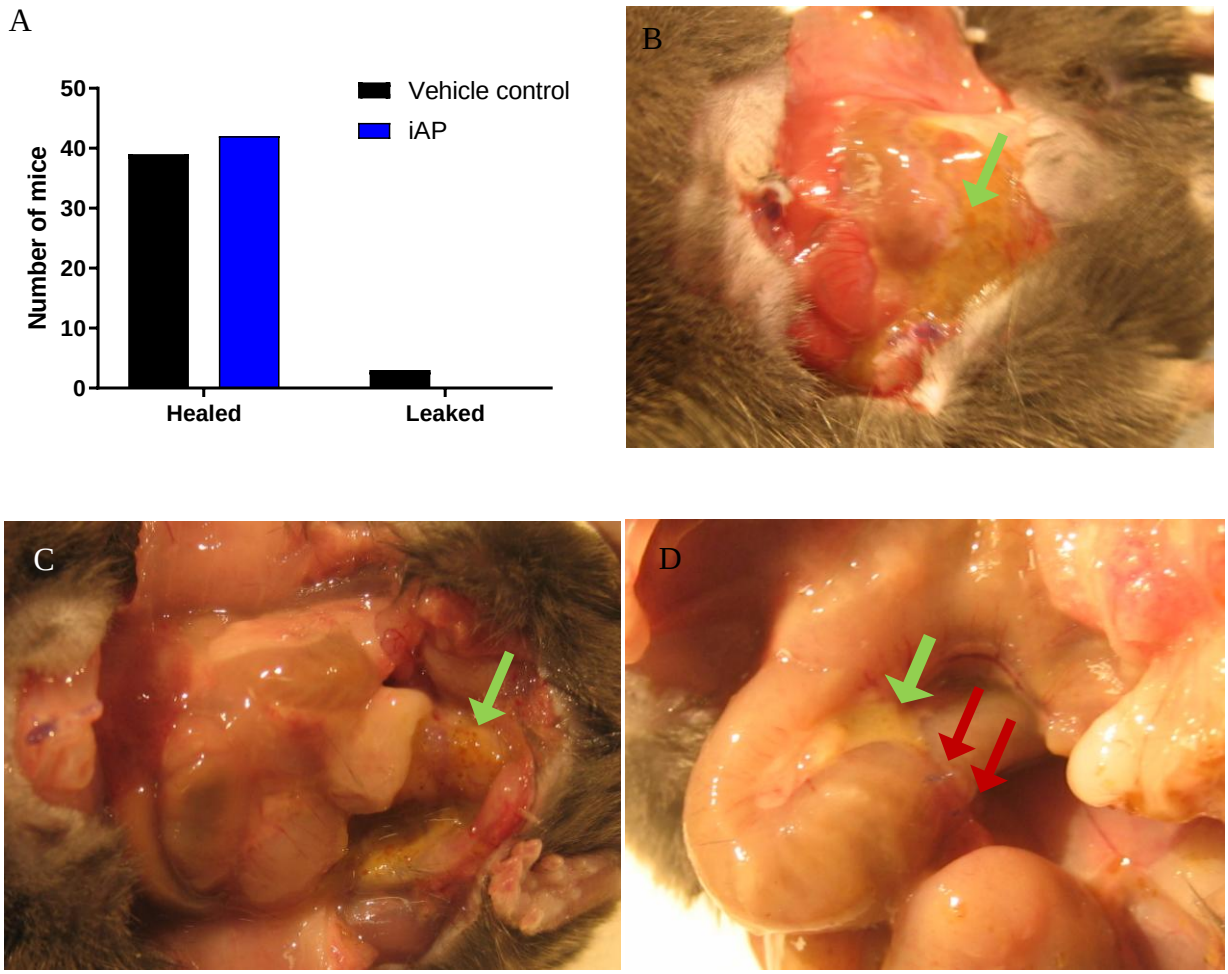

Figure 7-20: Anastomotic leaks in the leaking model. A. Graph showing the number of mice with anastomoses that either healed or leaked in each treatment group. N=42/group in three independent repeats, comparison with Fishers exact test. **B.** Generalised free faecal contents (green arrow) visible immediately on peeling back the skin of the abdominal wall. **C.** Localised pelvic faecal contamination (green arrow) whilst the upper abdomen remains clean. **D.** Localised free intestinal contents (green arrow) only in the region of the anastomosis (sutures indicated by red arrows).

7.2.18 **iAP significantly increased the activity index in the leaking model**

The activity index was calculated for the groups in the leaking anastomosis model as before. This time, there appeared to be a significant increase in the activity of the iAP group on the second post-operative day (Control mean +/- SEM: 4.48cm/s +/- 0.28, iAP: 5.51 cm/s +/- 0.24, adjusted p=0.03716, t-test with Holm-Sidak's correction, Figure 7-21). There were no differences to the starting (pre-operative) activity index in either group (Control mean +/- SEM: 5.29 cm/s +/- 0.27, iAP: 5.24 cm/s +/- 0.24, adjusted p=0.8932, t-test with Holm-Sidak's correction). Although the iAP index was always higher post-operatively, this did not reach significance on day one (Control mean +/- SEM: 4.71 cm/s +/- 0.22, iAP 5.38 cm/s +/- 0.23, adjusted p=0.3296, t-test with Holm-Sidak's correction), day three (Control mean +/- SEM: 5.48 cm/s +/- 0.21, iAP: 6.14 cm/s +/- 0.24, adjusted p=0.3333, t-test with Holm-Sidak's correction), day four (Control mean +/- SEM: 5.87 cm/s +/- 0.35, iAP: 6.71 cm/s +/- 0.47, adjusted p=0.3388, t-test with Holm-Sidak's correction), day five (Control mean +/- SEM: 6.12 cm/s +/- 0.33, iAP: 6.71 cm/s +/- 0.43, adjusted p=0.5768, t-test with Holm-Sidak's correction) day six (Control mean +/- SEM: 6.53 cm/s +/- 0.29, iAP: 7.56 cm/s +/- 0.46, adjusted p=0.2653, t-test with Holm-Sidak's correction), or day seven (Control mean +/- SEM: 6.59 cm/s +/- 0.37, iAP: 7.17 cm/s +/- 0.36, adjusted p=0.5768, t-test with Holm-Sidak's correction).

7.2.19 **iAP accelerated the return of normal bowel movements in the leaking model**

iAP again accelerated the return of normal bowel movements in the leaking model as evidenced by a more rapid return to baseline of 24 hour stool weight. There were no differences in starting stool weights (Control mean +/- SEM: 0.72g +/- 0.03, iAP: 0.76g +/- 0.03, adjusted p= 0.7125, t-test with Holm-Sidak's correction, Figure 7-22) or on post-operative day one (Control mean +/- SEM: 0.18g +/- 0.02, iAP: 0.31g +/- 0.02, adjusted p=0.1762, t-test with Holm-Sidak's correction). The trend in increased stool weights however became significant on day two (Control mean +/- SEM: 0.28g +/- 0.03, iAP: 0.51g +/- 0.05, adjusted p=0.0032, t-test with Holm-Sidak's correction), day three (Control mean +/- SEM: 0.48g +/- 0.03, iAP: 0.72g +/- 0.06, adjusted p=0.0027, t-test with Holm-Sidak's correction) and day four (Control mean +/- SEM: 0.62g +/- 0.05, iAP: 0.84g +/- 0.09, adjusted p=0.0112, t-test with Holm-Sidak's correction). There was no significant difference by day seven (Control mean +/- SEM: 0.91g +/- 0.06, iAP: 0.97g +/- 0.05, adjusted p=0.7125, t-test with Holm-Sidak's correction).

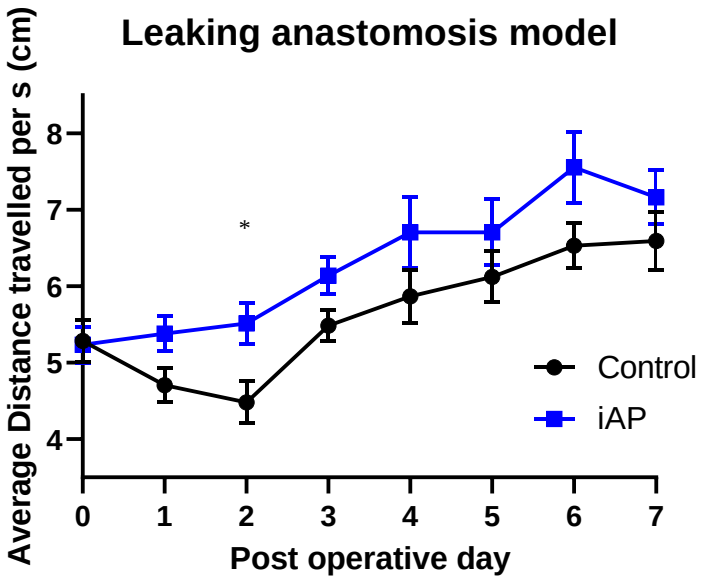

Figure 7-21: Leaking model activity index. Activity index was calculated in the same was as for the standard anastomosis. N=21/group, comparison with t-test with Holm-Sidak's correction for multiple comparisons, * $p<0.05$, error bars show SEM.

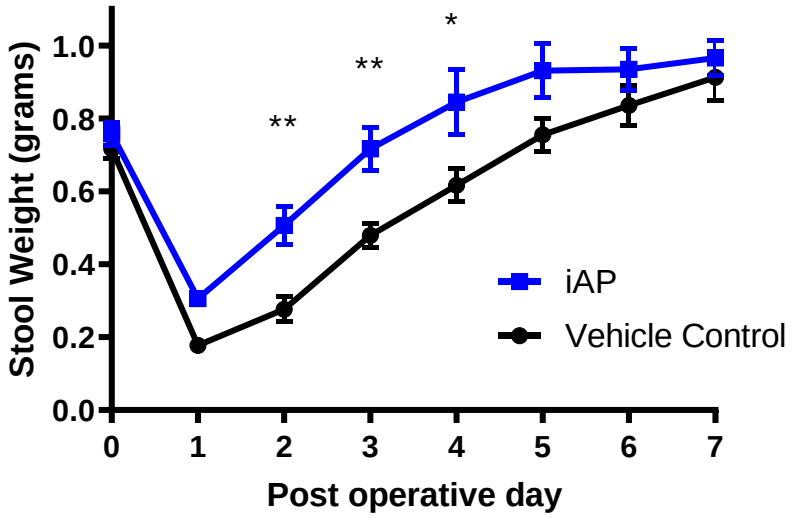

Figure 7-22: Measurement of 24hour Stool weight (grams) in the leaking model. For each treatment group, N=21/group, comparison with multiple t-tests with Holm-Sidak's correction for multiple comparisons, * $p<0.05$, ** $p<0.01$, error bars show SEM.

7.2.20 **iAP accelerated post-operative weight gain in the leaking model**

iAP again significantly increase post-operative weight gain even in the leaking anastomosis model, particularly on day two (Control mean +/- SEM: 94.32g +/- 0.58, iAP: 97.39g +/- 0.58, adjusted p=0.00427, t-test with Holm-Sidak's multiple comparison correction, Figure 7-23), and day three (Control mean +/- SEM: 95.49g +/- 0.75, iAP: 98.62g +/- 0.75, adjusted p=0.0450, t-test with Holm-Sidak's correction). There were no significant differences in starting weight (Control mean +/- SEM: 104.44g +/- 0.43, iAP: 105.25g +/- 0.36, adjusted p=0.4824, t-test with Holm-Sidak's correction) or on and day four (Control mean +/- SEM: 98.36g +/- 1.11, iAP: 101.73g +/- 1.05, adjusted p=0.2634, t-test with Holm-Sidak's correction), day five (Control mean +/- SEM: 100.19g +/- 1.15, iAP: 103.66g +/- 1.13, adjusted p=0.2634, t-test with Holm-Sidak's correction), day six (Control mean +/- SEM: 102.28g +/- 1.11, iAP: 106.2g +/- 1.58, adjusted p=0.2634, t-test with Holm-Sidak's correction) or day seven (Control mean +/- SEM: 105.64g +/- 1.40, iAP: 107.41g +/- 0.95, adjusted p=0.4824, t-test with Holm-Sidak's correction).

7.2.21 **iAP significantly increased ABP on day three in the leaking model**

ABP was significantly increased on day three in the leaking anastomosis model (Control mean +/- SEM: 47.37mmHg +/- 11.13, iAP: 104.1 mmHg +/- 10.23, p=0.0007, t-test, Figure 7-24). This difference was not significant on day seven (Control mean +/- SEM: 188.6 mmHg +/- 8.87, iAP: 192.6 mmHg +/- 7.31, p=0.7322, t-test).

7.2.22 **iAP significantly increased anastomotic hydroxyproline content on day three in the leaking model**

As before, a significant increase in anastomotic hydroxyproline content was seen on day three (Control mean +/- SEM: 1.85µg/mg +/- 0.12, iAP: 2.34 µg/mg +/- 0.20, p=0.038, t-test, Figure 7-25A). On the seventh post-operative day again this difference was no longer significant (Control mean +/- SEM: 3.59 µg/mg +/- 0.44, iAP: 3.11 µg/mg +/- 0.34, p=0.3977, t-test, Figure 7-25B).

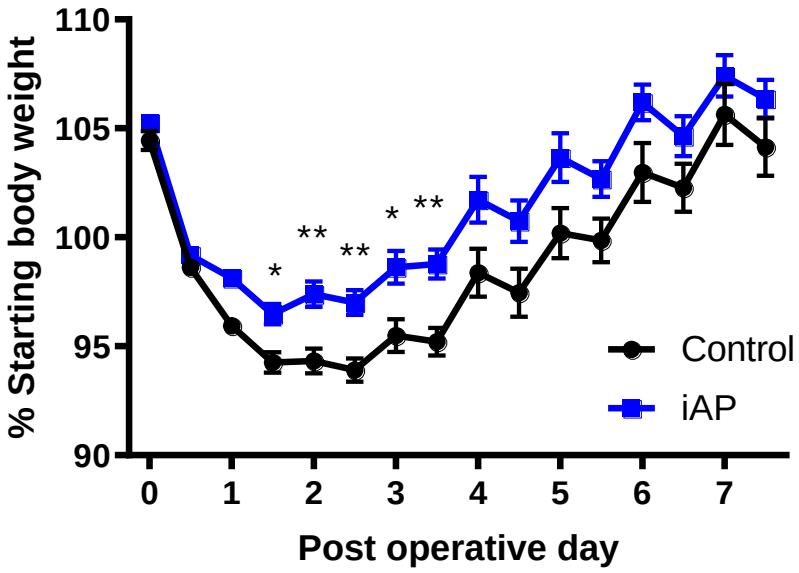

Figure 7-23: Percentage body weight against time for the leaking model. Mice were weighed twice daily. N=21/group in three independent repeats, comparison with t-test and Holm-Sidak's correction for multiple comparisons, * $p<0.05$, ** $p<0.01$, error bars show SEM.

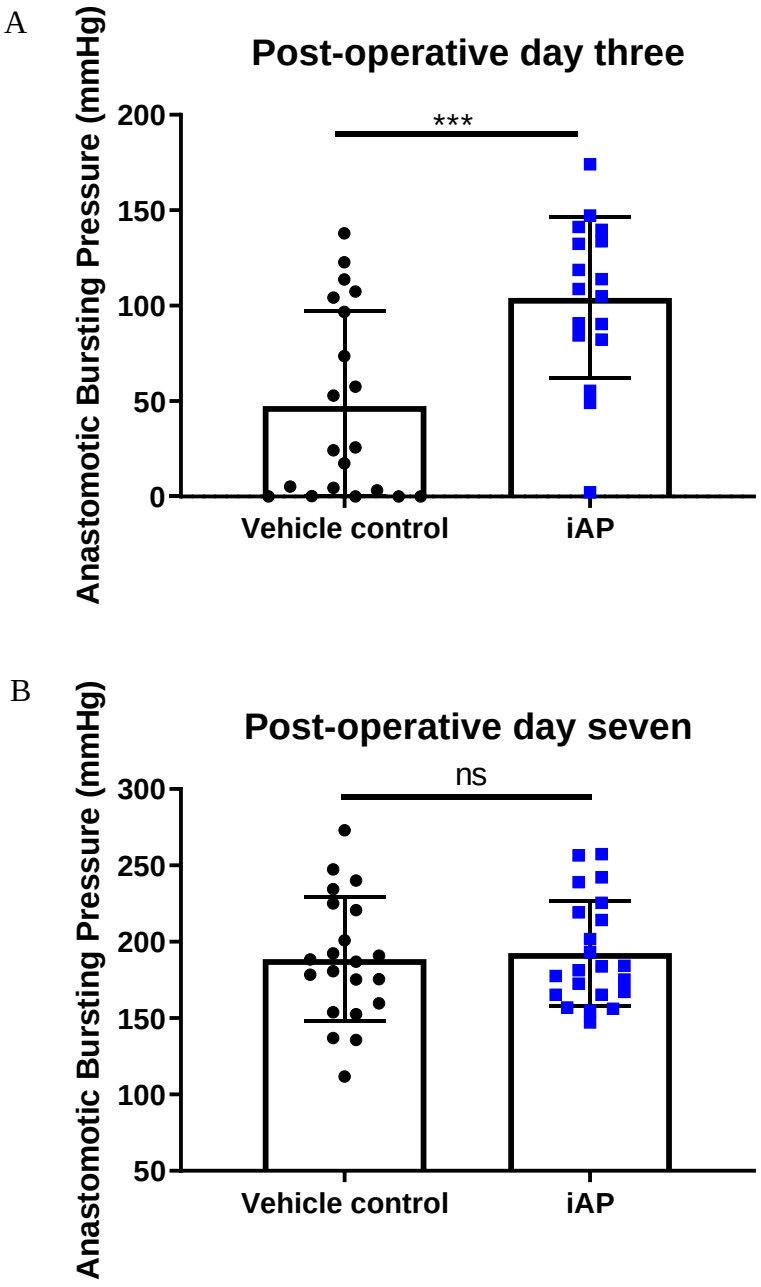

Figure 7-24: Anastomotic bursting pressure in the leaking anastomosis model on the third and seventh post-operative days. A. Graph showing the ABP on day three. N=20/group (2 leaks in the control group) in three independent repeats, t-test, ***$p < 0.005$, error bars show SD. B. Graph showing ABP on day seven. N=22 in the iAP group but 21 in the control group (due to leak with major anastomotic disconnection) in three independent repeats, comparison with t-test, ns=non-significant, error bars show SD.

A

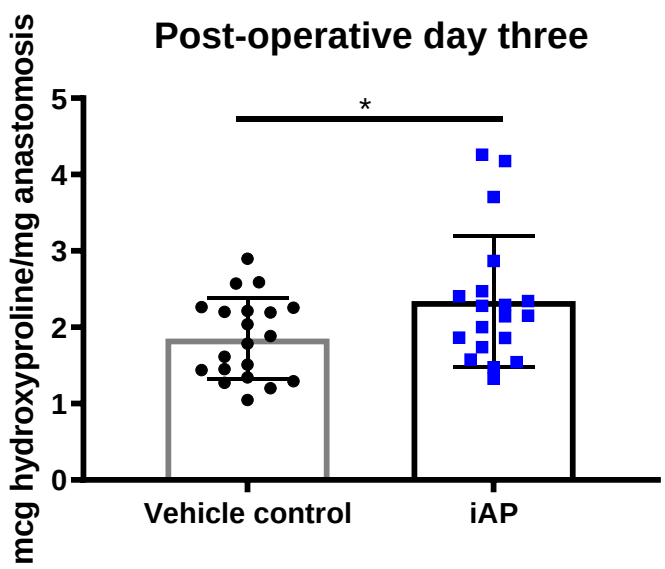

B

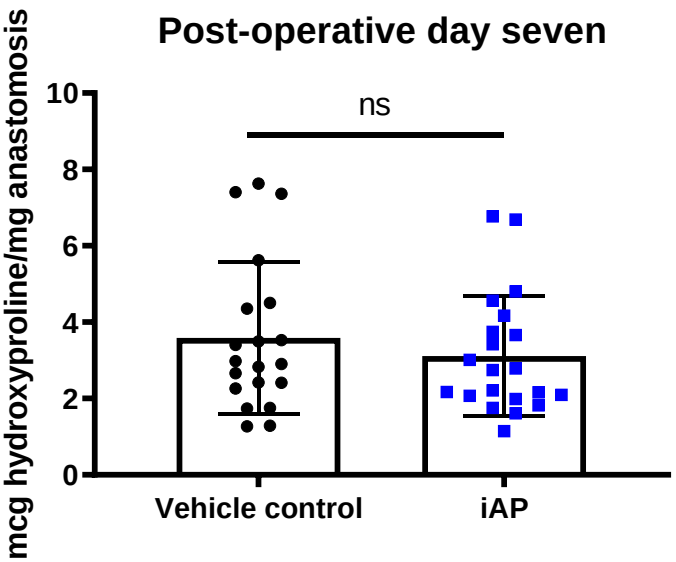

Figure 7-25: Hydroxyproline content in the anastomoses of the leaking model on the third and seventh post-operative days. A. Graph showing hydroxyproline content in each anastomosis on day three. N=20/group in three independent repeats, comparison with unpaired t-test, *$p<0.05$, error bars show SD. B. Graph showing hydroxyproline content in each anastomosis on day seven. N=21/group in three independent repeats, comparison with t-test, ns=non-significant, error bars show SD.

7.2.23 **iAP did not affect spleen weights in the leaking model**

Similar to the standard model, iAP did not affect spleen weights either on the third (Control mean +/- SEM: 0.0858g +/- 0.006, iAP 0.0856g +/- 0.003, p=0.9711, t-test, Figure 7-26A) or the seventh post-operative day (Control mean +/- SEM: 0.0899g +/- 0.005, iAP: 0.0855g +/- 0.004, p=0.5033, t-test, Figure 7-26B).

7.2.24 **iAP did not affect diversity of faecal bacteria in the leaking model**

Once again, even in the leaking model, bacterial diversity appeared similar in both groups, with no significant association between the number of bacterial morphologies seen and treatment on the third (p=0.8606, Freeman-Halton extension of Fisher's exact test, Figure 7-27A) or the seventh post-operative day (p=0.7646, Freeman-Halton extension of Fisher's exact test, Figure 7-27B).

A

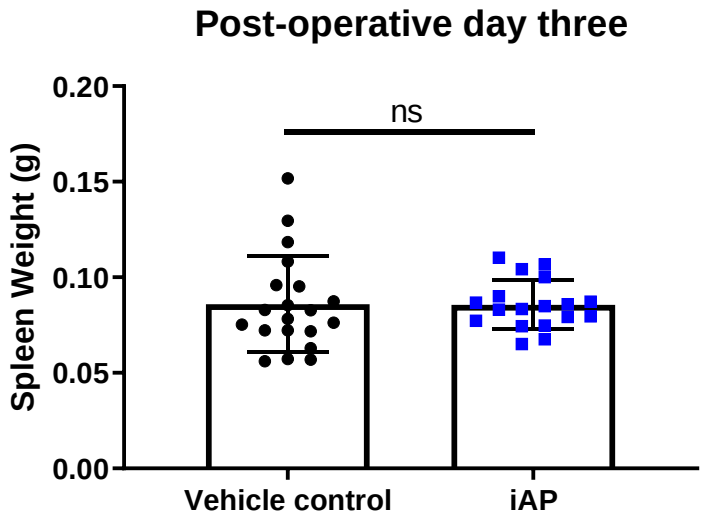

B

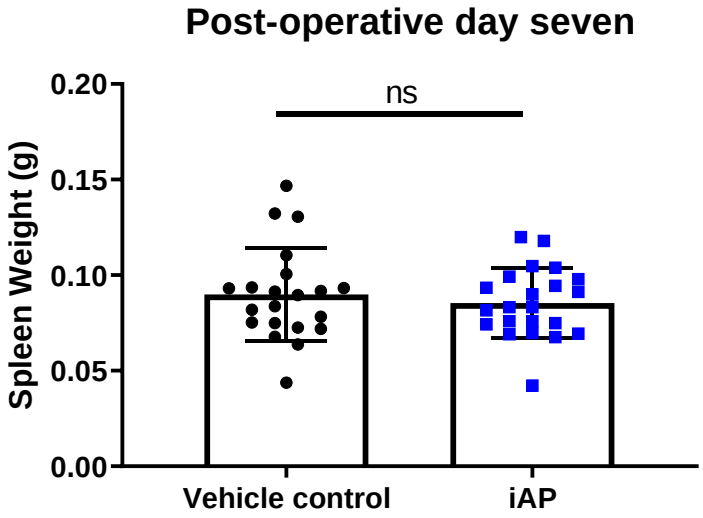

Figure 7-26: Spleen weights on post-operative day three and seven in the leaking model. A. Graph showing splenic weights for each treatment group on day three. B. Graph showing splenic weights for each treatment group on day seven. In each case, N=21/group in three independent repeats, comparison with t-test, ns=non-significant, error bars show SD.

A

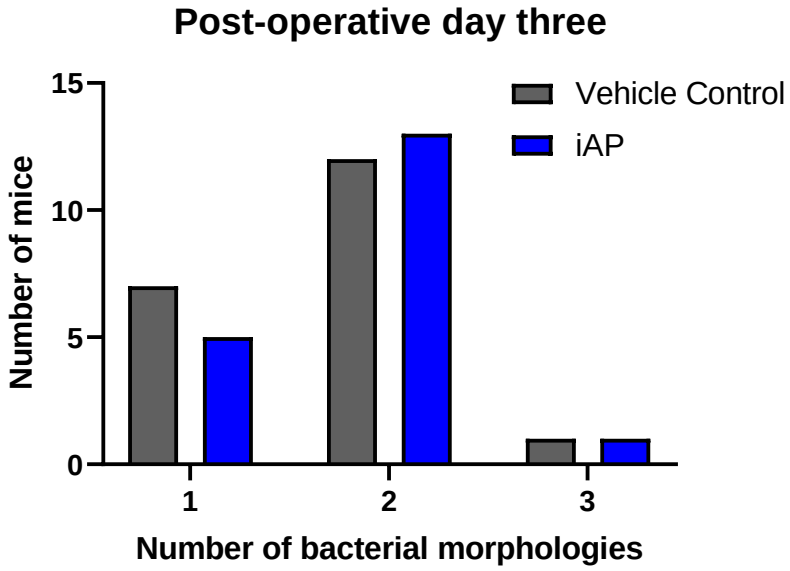

B

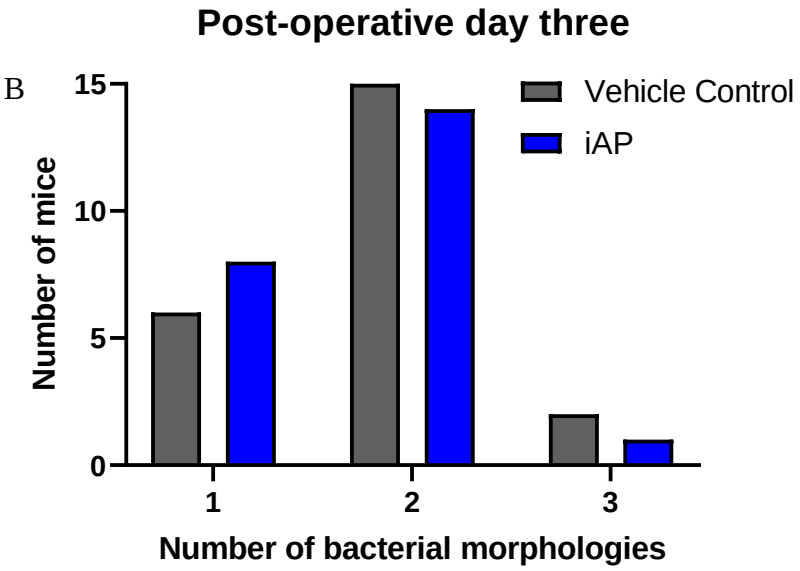

Figure 7-27: Growth of faecal bacteria from the region of the anastomosis in the leaking model on the third and seventh post-operative day. A. Graph showing the bacterial diversity in stool grown on BHI at 37C on the third post-operative day. N=21/treatment group, Fisher's exact test. **B.** Graph showing the bacteria diversity in stool around the region of the anastomosis on the seventh post-operative day. N=21/treatment group, Freeman-Halton extension of Fisher's exact test. For each mouse, three separate replicates were grown and all three always showed the same bacterial morphology.

7.2.25 **iAP did not affect diversity of faecal fungi in the leaking model**

On day three, no association was noted between treatment groups and degree of fungal diversity grown on culture (p=0.5577, Freeman-Halton extension of Fisher's exact test, Figure 7-28A). Similar results were found on day seven, with no association between fungal growth and treatment (p=0.3063, Freeman-Halton extension of Fisher's exact test, Figure 7-28B). Fungal colony morphologies on the plates were very similar to those seen in the standard group. Although no formal identification of these fungi was made, several features were suggestive of identity, for example the samples on the left in Figure 7-28C were an olive green with a yellow posterior (matching left in Figure 7-28D) and could be *Penicillium citrinum* or *Aspergillus flavus* whereas the samples on the right are multicolour with a reddish brown posterior and likely to be *Aspergillus versicolor* (St-Germain and Summerbell, 2003). In either case, these possible fungal species were consistent with fungi previously isolated in mice (Qiu *et al.*, 2015).

7.2.26 **iAP did not affect faecal cellulolytic activity in the leaking model**

Similar to the standard model, cellulase activity was not significantly different in either groups on day three (Control mean +/- SEM: 36.0mm^2 +/- 3.4, iAP: 32.9 mm^2 +/- 2.8, p=0.4828, t-test, Figure 7-29) or day seven (Control mean +/- SEM: 40.0 mm^2 +/- 5.8, iAP: 33.6 mm^2 +/- 3.2, p=0.3408, t-test).

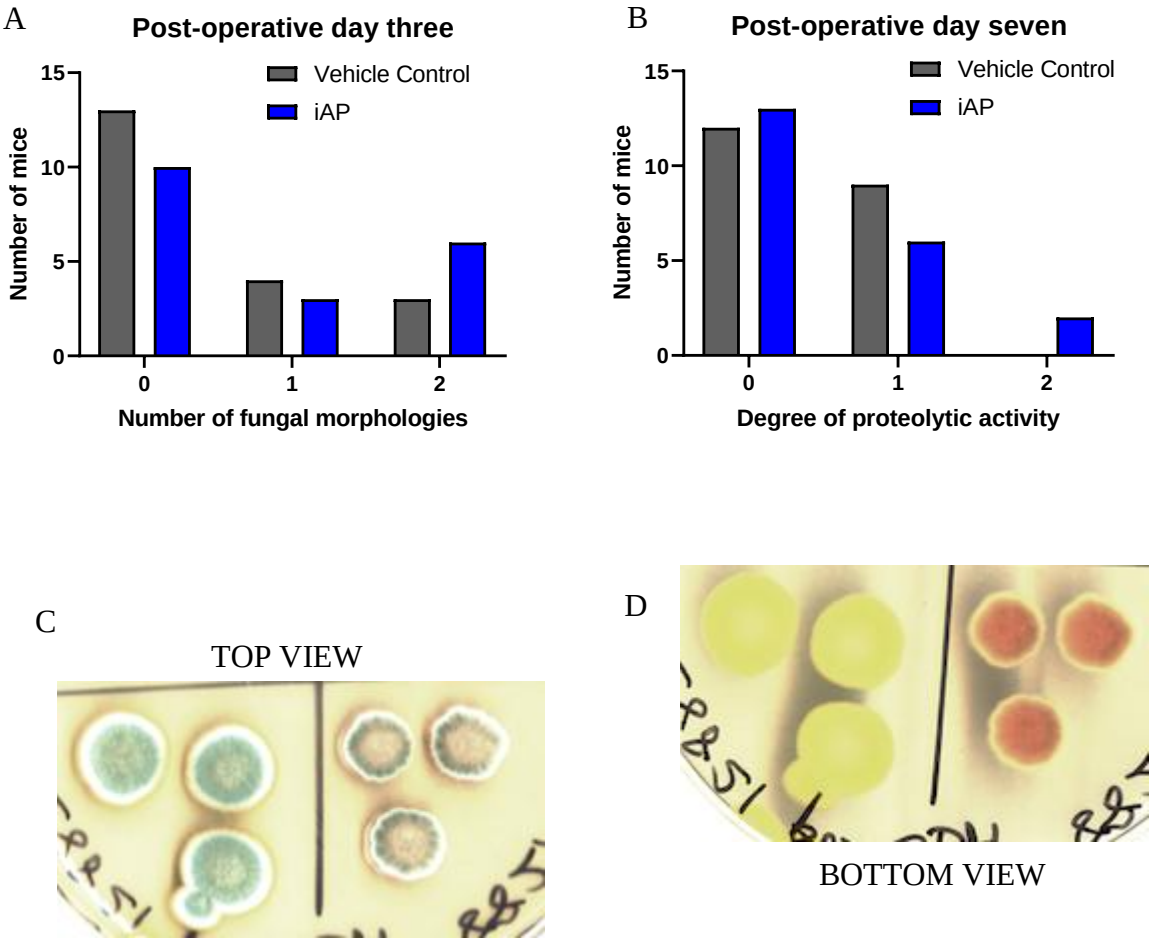

Figure 7-28: Fungal growth morphology cultivated from stool taken from the region of the anastomosis in the leaking model on post-operative days three and seven. A. Graph of fungal morphologies on day three. N=20/group, Freeman-Halton extension of Fisher's exact test. **B.** Graph of fungal morphologies on day seven. N=21/group, Freeman-Halton extension of Fisher's exact test. **C.** Top view of fungal culture plate**. D.** Bottom view of fungal culture. Three 10 µl replicates were cultured from each faecal sample and all three grew identical fungi in each case.

A

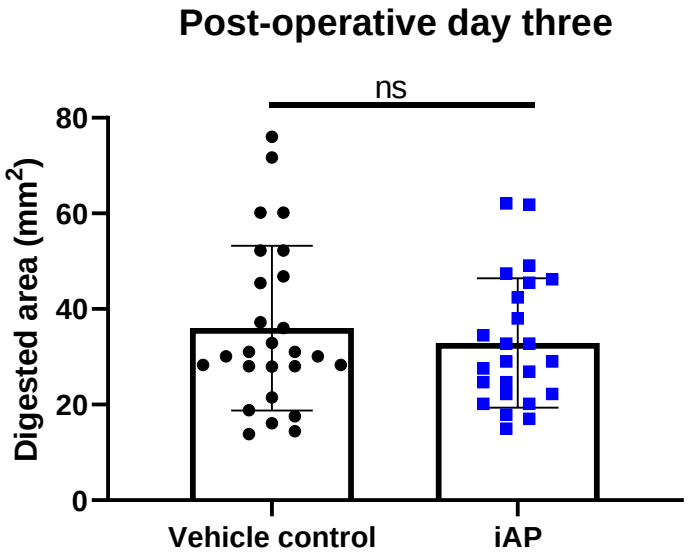

B

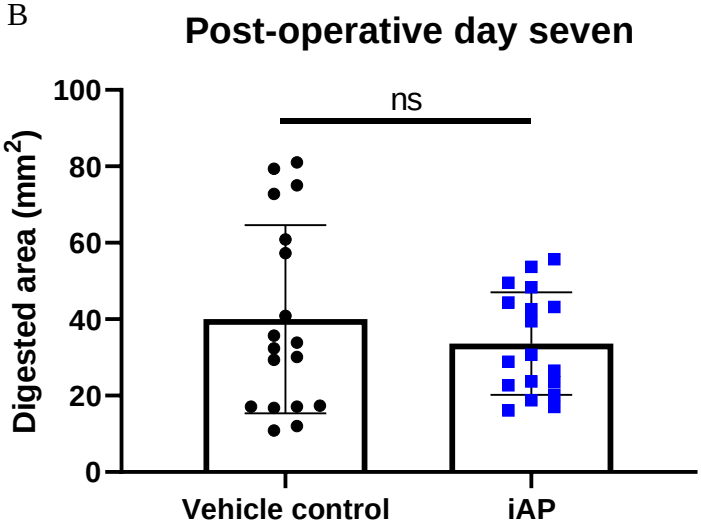

Figure 7-29: Cellulolytic activity assessed using digestion of CMC agar plates on the third and seventh post-operative day in the leaking model. A. Graph showing area of digestion (lucent area) for each treatment group on day three. N=21/group, t-test, ns=non-significant, error bars show SD**. B.** Graph showing area of digestion for each treatment group on day seven. In each, N=18/group (several plates were lost), comparison with unpaired t-test, ns=non-significant, error bars show SD.

7.2.27 **iAP decreased faecal proteolytic activity on day three in the leaking model**

Despite having no differences in the bacterial morphological diversity, in the iAP treatment group, the faecal proteolytic activity showed a decreasing trend when tested on the third day, and this association was significant (p=0.004166, Freeman-Halton extension of Fisher's exact test, Figure 7-30A). There was no association between degree of faecal proteolytic activity and treatment on day seven (p=0.6051, Freeman-Halton extension of Fisher's exact test, Figure 7-30B). Given this difference on day three, an attempt was made to visualise and quantify any leukocytic response at the anastomotic site from histological sections. Haematoxylin and eosin staining of the anastomosis sites of both groups showed normal architecture. However, efforts to quantify leukocytic responses by histological staining proved much more complicated than expected as it was not possible to ensure an equivalent slice of the anastomosis was obtained each time (Figure 7-31) together with the problem of generalising the very small examined area to the entire anastomosis. Furthermore, anastomotic leaks occur at localised areas of weakness, rather than the entire anastomotic circumference being involved, therefore quantification was not attempted as it would not have given an accurate representative picture of the overall anastomotic inflammatory state.

A

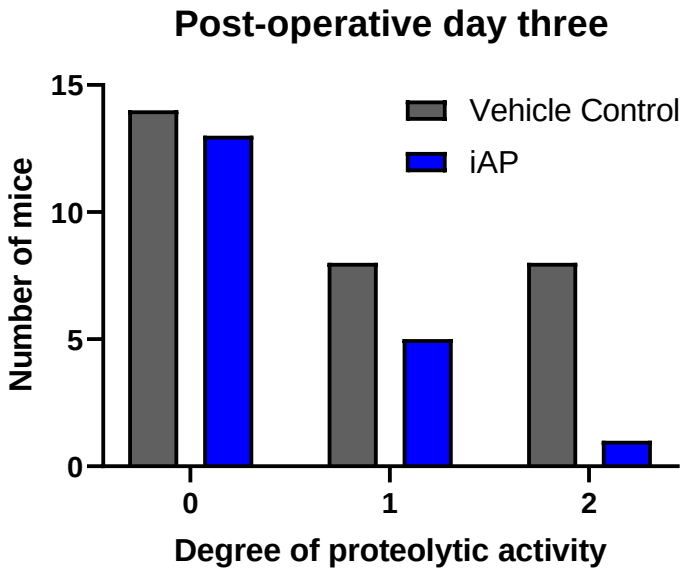

B

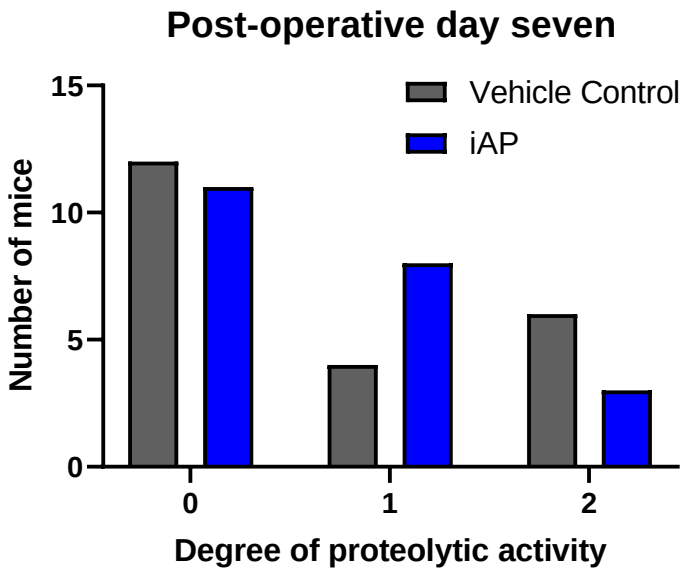

Figure 7-30: Proteolytic activity in the faecal matter from the anastomotic region on the third and seventh post-operative day in the leaking model. A. Graph showing proteolytic activity on day three. N=20/group, Freeman-Halton extension of Fisher's exact test. **B.** Graph showing proteolytic activity on day seven. N=21/group. Freeman-Halton extension of Fisher's exact test.

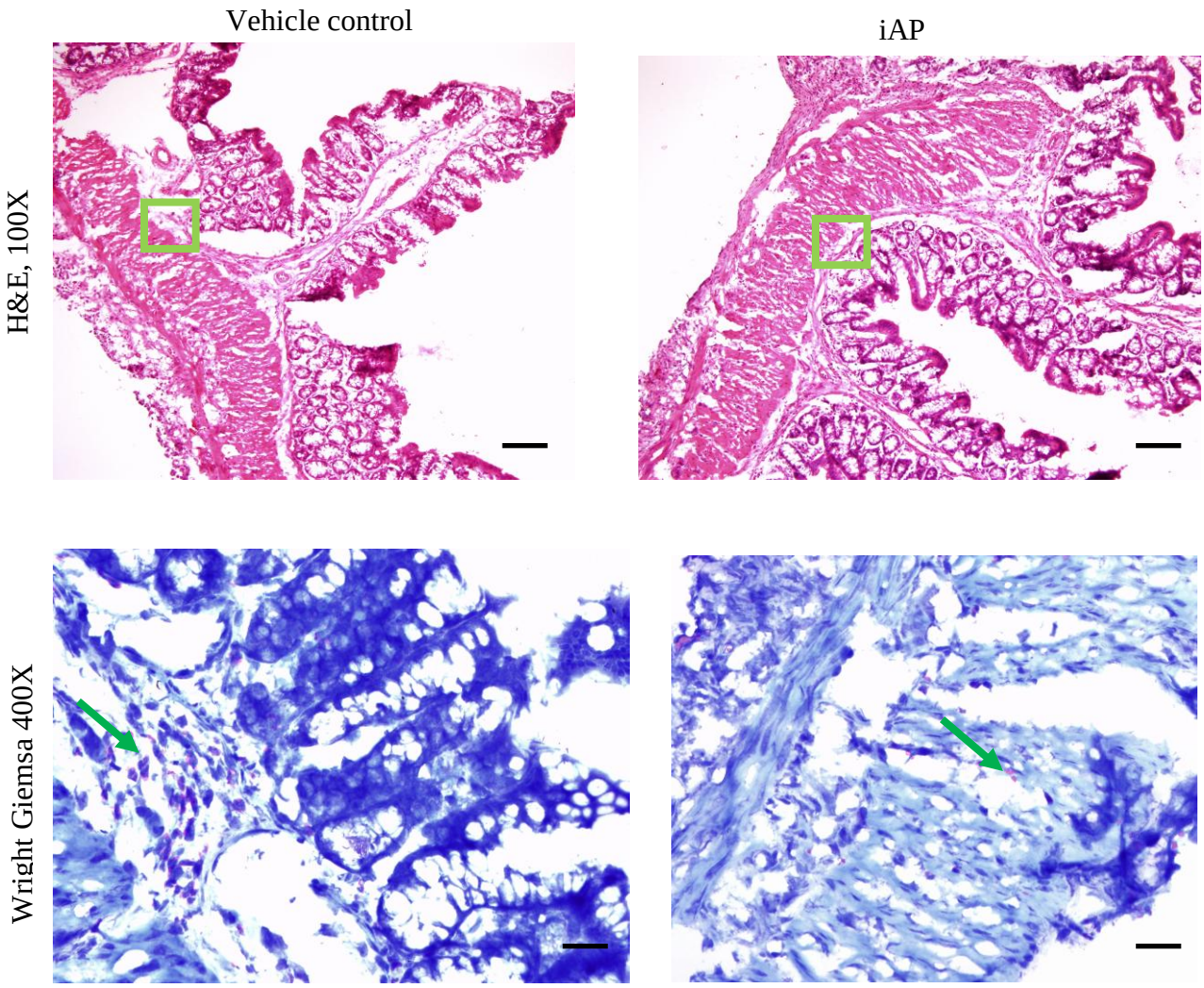

Figure 7-31: Frozen sections of the anastomotic region stained with haematoxylin and eosin (H&E) and Wright Giemsa (WG) on day three in the leaking model. Consecutive 4 µm sections were taken and stained to observed for completeness of healing and presence of leukocytes. Some thawing artefact is seen on the left. H&E sections were imaged at 100X, and WG imaged at 400X centred on the region boxed in green. Leukocytes shown with green arrows. Black scale bars indicate 100 µm.

7.2.28 **iAP did not affect anastomotic MMP2 or MMP9 activity in the leaking model**

In the leaking model, no significant differences were seen in MMP2 at day three (Control mean +/- SEM: 0.43A.U. +/- 0.05, iAP: 0.54 A.U. +/- 0.06, p=0.2798, Mann-Whitney test, Figure 7-32A), or day seven (Control mean +/- SEM: 0.67 A.U. +/- 0.05, iAP: 0.58 A.U. +/- 0.06, p=0.2592, Mann-Whitney test, Figure 7-32B). Anastomotic MMP9 similarly did not differ on day three (Control mean +/- SEM: 0.61 A.U. +/- 0.06, iAP: 0.72 A.U. +/- 0.06, p=0.1942, Mann-Whitney test, Figure 7-32C) or day seven (Control mean +/- SEM: 0.55 A.U. +/- 0.06, iAP: 0.51 A.U. +/- 0.06, p=0.7273, Mann-Whitney test, Figure 7-32D).

7.2.29 **iAP did not affect skin MMP2 or MMP 9 activity in the leaking model**

Skin MMP2 on day three was unaffected by iAP treatment (Control mean +/- SEM: 0.68 A.U. +/- 0.06, iAP: 0.68 A.U. +/- 0.05, p=0.7728, Mann-Whitney test, Figure 7-33A). This remained the case for skin MMP2 on day seven (Control mean +/- SEM: 0.63 A.U. +/- 0.03, iAP: 0.63 A.U. +/- 0.06, p=0.6566, Mann-Whitney test, Figure 7-33B). No differences were seen either in skin MMP9 on day three (Control mean +/- SEM: 0.56 A.U. +/- 0.08, iAP: 0.47 A.U. +/- 0.07, p=0.4261, Mann-Whitney test, Figure 7-33C) or on day seven (Control mean +/- SEM: 0.18 A.U. +/- 0.05, iAP: 0.15 A.U. +/- 0.05, p=0.4608, Mann-Whitney test, Figure 7-33D).

7.2.30 **iAP did not increase DISP activity in the leaking model**

Surprisingly, unlike the standard anastomosis model, the day seven levels of DISP did not appear to be significantly different from the controls (Control mean +/- SEM: 0.49 A.U. +/- 0.07, iAP: 0.38 A.U. +/- 0.07, p=0.1631, Mann-Whitney test, Figure 7-34A). The was a trend toward increased expression on day three but this did not reach statistical significance (Control mean +/- SEM: 0.25 A.U. +/- 0.06, iAP: 0.39 A.U. +/- 0.08, p=0.2267, Mann-Whitney test, Figure 7-34B). It is possible that the peak expression of DISP occurred at a post-operative time not captured by the experimental protocol, as group divergence and re-attainment of starting stool and body weights were achieved at earlier time points in the leaking model compared to the standard model.

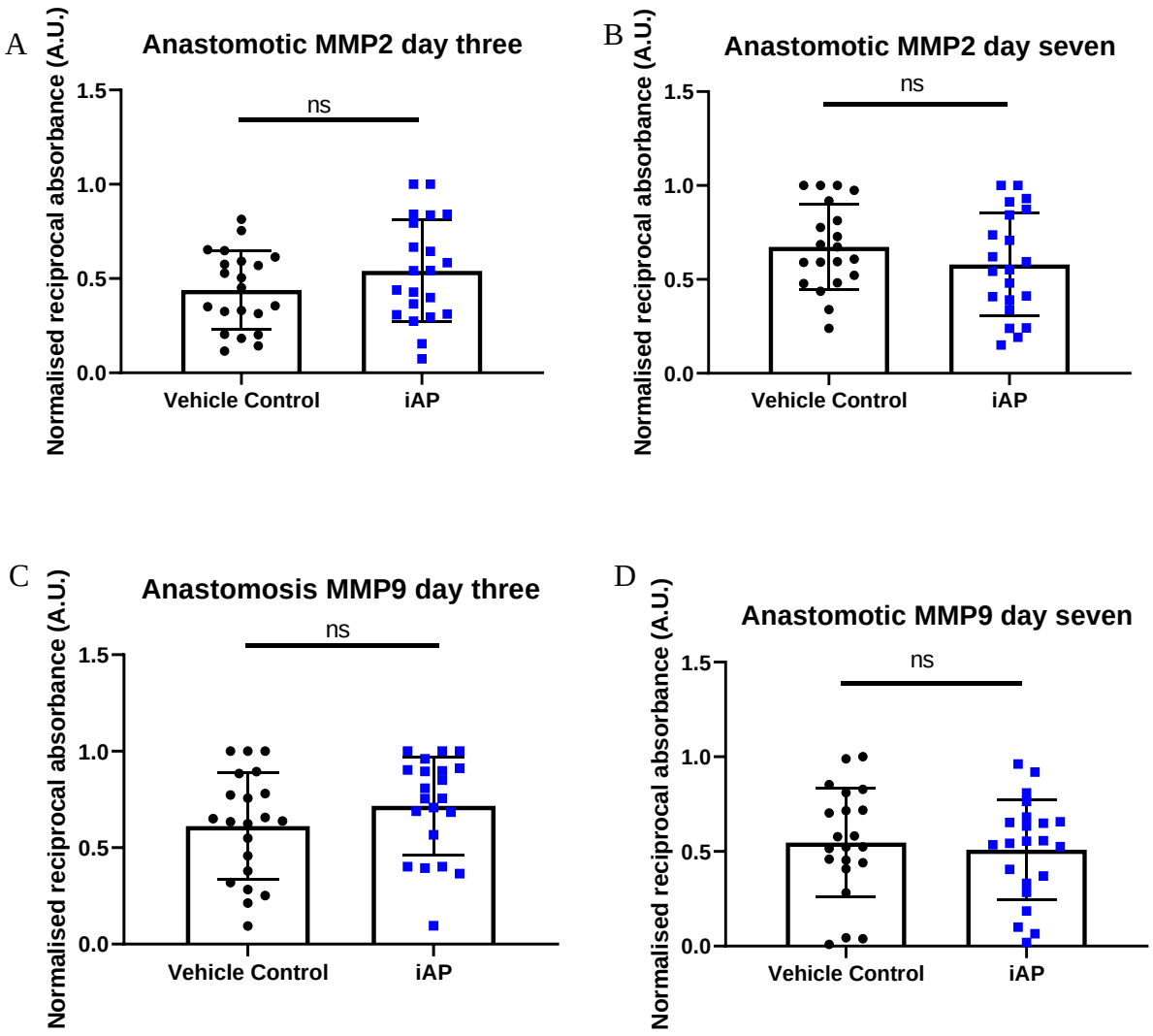

Figure 7-32: MMP2 and MMP9 expression at the anastomosis on day three and seven in the leaking model. A. Anastomotic MMP9 on day three. **B.** Anastomotic MMP9 on day seven. **C.** Anastomotic MMP9 on day three. **D.** Anastomotic MMP9 on day seven. In each case: N=21/group, comparison with Mann-Whitney test, ns=non-significant, error bars show SD.

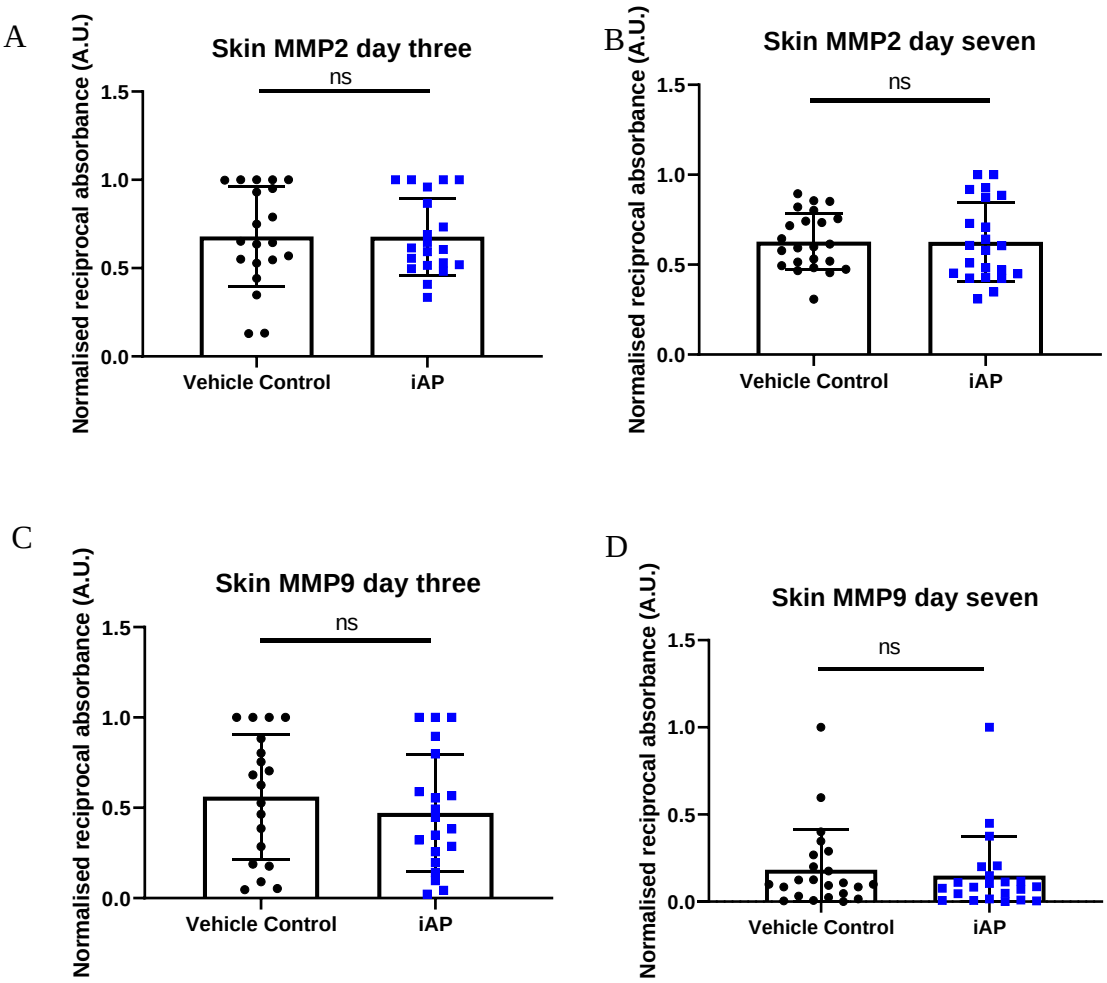

Figure 7-33: Evaluation of MMP2 and MMP9 expression in the skin laparotomy wound on day three and seven in the leaking anastomosis model. A. Skin MMP2 on day three. **B.** Skin MMP2 on day seven. **C.** Skin MMP9 on day three. **D.** Skin MMP9 on day seven. In each case, N=21/group, comparison with Mann-Whitney test, ns=non-significant, error bars show SD.

A

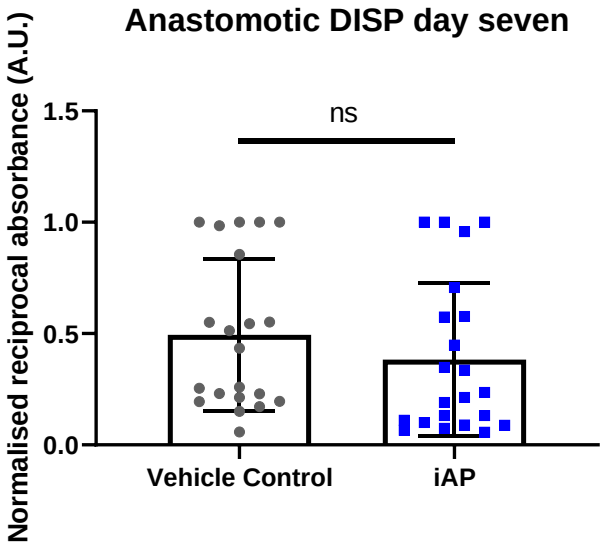

B

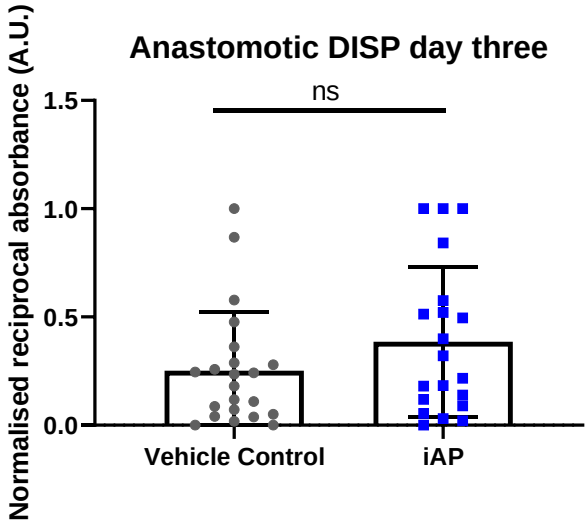

Figure 7-34: Distal intestinal serine protease (DISP) on day three and seven of the leaking model. **A**. DISP on day three. **B.** DISP on day seven. In each case N=21/group, comparison with Mann-Whitney test, ns=non-significant, error bars show SD.

7.3 **Discussion and future work**

Investigating compounds that may be beneficial to wound healing can be less straightforward in an organ such as the GIT, with its multitude of compounding variables, such as the ever-changing microbial balance. The burgeoning field of microbiomics has increasingly shown that small changes in the composition of the intestinal tract microbial diversity can impact experimental reproducibility, and even direct experimental outcomes (Leystra and Clapper, 2019; Vlasova *et al.*, 2019). Nevertheless, animal experimentation remains a cornerstone for investigating potential beneficial compounds and the pathways that may be involved in intestinal healing since nuances that may become significant clinically in humans, can be lost in simpler *in vitro* systems (Pearce *et al.*, 2018; Kim, Koo and Knoblich, 2020). Whilst simpler *in vivo* models such as teleosts have their place in enabling visualisation of selected mechanistic insights, intestinal healing models have been validated mainly in terrestrial animals, with mouse models as one of the recommended standards in an international consensus (Bosmans *et al.*, 2016). Regrettably, uptake of mouse models has been slower than larger animals, and, at the time of writing, was not currently performed in the UK.

Experiments in this study were performed using exclusively male mice. This was for two reasons. Firstly, clinically, male humans undergoing colorectal surgery are more likely to develop an anastomotic leak compared to females (Lipska *et al.*, 2006; Krarup *et al.*, 2013), which, although often attributed to a more difficult anatomical presentation, separate studies have also shown to be an independent risk factor (McDermott *et al.*, 2015; Sánchez-Guillén *et al.*, 2019). Secondly, specific to mice, collagen levels are known to be generally lower in male mice (Kjaer *et al.*, 2018). Thus it was hypothesised that if differences were shown in male mice, this would also likely be the case, if not even more obviously so, in female mice.

In determining the optimal mode of treatment delivery, minimisation of stress as well as reproducibility was important, since both can impact on outcomes in unpredictable ways (Mandillo *et al.*, 2008; Pankevich and Bale, 2008; Sorge *et al.*, 2014). Therefore, a gentler method of providing treatment instead of gavage was prioritised. Previous research had shown that Dutch mice would consume Nutella, and it was fortunate that the liking for Nutella was

universal even in British mice, even though previous publications suggested this may not be the case in all strains (Tordoff, Downing and Voznesenskaya, 2014).

Clinical parameters are early indicators of generic well-being and good surrogate markers for internal healing, thus avoiding the need to sacrifice mice on every single post-operative day to determine healing. Although these clinical parameters have are yet to be validated as exhaustively for anastomotic healing as for models of colitis (Chartier *et al.*, 2020), they remain a useful indicator, and were consistently improved by iAP in these experiments. In both anastomotic models, mice treated with iAP demonstrated an accelerated return to baseline body and stool weights. In the standard model, although the activity levels did not reach statistical significance in the iAP group, there were many confounding factors that persisted despite task familiarisation and optimisation of non-aversive handling methods (Gouveia and Hurst, 2017), and this included unavoidable movement of other personnel in the vicinity of the testing area which could have led to increased variability in mouse behaviour. In the leaking model however, this did achieve significance, and could be due to the more severe nature of the insult. Although mice are thought to mask pain for survival like all other prey animals (Mayer, 2007), significant differences in behaviour can still be observed following ill health (Painsipp *et al.*, 2011).

Testing for anastomotic healing via bursting pressure has been considered the gold standard by international consensus (Bosmans *et al.*, 2016), and yet, due to variations in technique and equipment, comparison of actual values across studies at different sites is not possible. It remains valuable however, and combined with the increase in hydroxyproline content, confirms the more rapid anastomotic healing induced by exogenous iAP, concordant with the improvement in general clinical markers above.

Recent years have uncovered another facet to iAP, the antibacterial effects brought about by dephosphorylation. Here the picture becomes increasingly complex. APs are preserved evolutionarily and are present even among bacteria. So not only can the actions of AP be antibacterial by dephosphorylating LPS (Bates *et al.*, 2007), but they also can be pro-bacterial, by providing a source of phosphate required for bacterial proliferation. This is important since

lack of inorganic phosphate creates a micro-environment of stress to the bacteria (Santos-Beneit, 2015), and causes increasing invasiveness via quorum sensing pathways, as has been demonstrated in *Pseudomonas* (Romanowski *et al.*, 2011; Meng, Ahator and Zhang, 2020), a colonising pathogen in humans which has separately been shown to have a role in anastomotic leaks (Wu, 2005; Olivas *et al.*, 2012). In fact, so essential is phosphate to the preservation of bacterial benevolence, that oral supplementation of phosphate has been demonstrated to prevent anastomotic leaks It had been assumed up till now that iAP exerted its beneficial actions on increasing the diversity of the microbiome by removal of growth-inhibiting triphosphate nucleotide molecules (Malo *et al.*, 2014). But it may be instead that a phosphate-replete environment is more important for bacterial benevolence. This was suggested by the results of the faecal proteolytic activity experiments, a surrogate for specific collagenase activity, which, despite the similarities in bacterial diversity, showed a decreased in the iAP treated group on day three in the leaking model.

The methods in this chapter to assess bacterial diversity were limited to those growing on BHI under the prescribed conditions, and would be subject to confounding effects of inhibition or robustness of species under these specifications. However, no differences in bacterial diversity were noted using the methods described. Quite apart from bacterial diversity, the abundance of SCFAs have also demonstrated benefits in anastomotic healing (Bosmans *et al.*, 2017). Since cellulose degradation by resident bacteria is the precursor to production of SCFAs, the cellulolytic activity of microorganisms present in faecal matter was also assessed as an alternative to mass spectrometry. Again, although the same limitations to culture exist, it remains a good preliminary investigation as to the possibilities underlying improvements seen in the iAP group. This again showed no differences between groups. Fungi are often isolated in clinical leaks (Althuwaini *et al.*, 2018) but its significance as a causative agent of ALs has not been clearly defined, since, the presence of fungal colonisation has been shown to have beneficial effects of minimising inflammation (Paterson, Oh and Underhill, 2017) and even to be beneficial in wound healing (Gressler *et al.*, 2019). Nevertheless, the fungal species identified from observed plate morphology appeared to concur with published fungal species abundance in murine stool (Qiu *et al.*, 2015), and did not differ between groups.

Overall therefore, using these methods, with the methodological limitations in mind, the actions of iAP appear independent of SCFA abundance and bacterial or fungal diversity, and may exert its influence on healing via other pathways which are yet to be delineated. In retrospect, it would have been ideal to have been able to also test MPO levels in the region of the anastomosis using enzyme purification methods (Xia and Zweier, 1997) rather than attempt histological quantification, however, in this experimental setup, there was insufficient tissue to dedicate to histology, MMP, and collagen analysis without compromising on the validity of the conclusions. This remains another area of more directed studies in future.

Unabated MMP activity has been implicated in ALs (Shogan *et al.*, 2015), purported to be an indicator of disease activity in IBD (O'Sullivan, Gilmer and Medina, 2015), and thought to play a role in regulation of bactericidal proteins on the mucosa (Polistena *et al.*, 2011). Therefore it was of interest to see if the activity levels of these MMPs were changed by iAP treatment. Anastomotic MMP9 and MMP2 activity showed no significant differences with treatment in either model, or on either day. But, a distal intestinal serine protease (DISP), was noted for the first time to have gelatinase activity, and this was significantly elevated activity in the iAP group on the seventh day. This was unexpected since most clinical indicators, as well as biochemical evaluation of collagen content and ABP, were no different between groups on the seventh day. At present, the function of DISP remains unknown, and it boasts mention in only two publications (Shaw-Smith *et al.*, 2000; Wong *et al.*, 2004) since its description two decades ago. It has no known enzymatically active human homologues, but has an orthologue in rats (Wong *et al.*, 2004). Disappointingly, this novel DISP increase did not achieve significance at either day three or seven in the leaking model, although it is possible that the timing of analysis did not match its time of maximal expression, as comparison of the clinical parameters between models indicated that return to physiological baseline occurred earlier in the leaking model compared to the standard model. But in addition, the low rate of leaks obtained here could have contributed to the lack of statistical significance in some of the results. Although the leaking model was performed as published (Pommergaard, 2014), the expected 40% rate of anastomotic leaks was not reached despite deliberate attempts to offset any possible subconscious correction of technical deficits. It has been noted that rodents have a surprising resilience against anastomotic leaks despite deliberate and severe intent, and even significant anastomotic ischaemia did not

result in leaks (Pommergaard *et al.*, 2015; Bosmans *et al.*, 2017). This is in contrast to ischaemic anastomoses in dogs (who do not express DISP) where an average of 80% leak rate was obtained (McLachlin and Denton, 1973). Could DISP indeed be the missing link of this resistance to leakage? It is an area full of intrigue, and remains the remit of very exciting future research.

7.4 **Summary of important findings**

iAP is an evolutionarily conserved enzyme and its distribution specifically within the intestine suggests roles that could additionally include enhancement of mucosal barrier function, microbial modulation, and epithelial healing. The mouse anastomotic experiments here have demonstrated that iAP accelerated anastomotic healing and post-operative recovery in mice, demonstrated by faster post-operative weight gain recovery and return of bowel function in both standard and severe models, and higher activity index in the more severe model. The anastomoses were also demonstrably stronger with a significantly higher bursting pressure on post-operative day three. Hydroxyproline content was likewise significantly increased at day three and matched controls on day seven, again suggesting benefit in accelerating anastomotic wound healing without the consequence of pathologically increased fibrosis which could result in strictures. No changes in faecal microbial or fungal diversity were demonstrated in either model, but a novel increase in the activity of a DISP with iAP treatment was observed on day seven of the standard model. Significantly, in the leaking model, supplementation with iAP resulted in no anastomotic leaks. In conclusion, this chapter has demonstrated that with regard to anastomotic healing and prevention of leaks, iAP shows great promise for translation to clinical practice.

Chapter 8: Conclusion and future work

As surgical procedures within the abdomen reach greater numbers, not only because colorectal cancer is the third most common cancer in Europe (Ferlay *et al.*, 2018), but also because an increasing range of innovations allow surgeons to perform operative interventions previously thought to be too heroic, the medical world is entering an era of heightened expectation of good outcomes. Although anastomotic leaks (ALs) represent a relatively small proportion of the complications that could occur, it remains a serious one with possible fatal outcomes. No single cause and effect theory has been able to predict this outcome, or deliver the promise of ameliorating ALs completely, and this has led to mitigating methods of surgery, such as creating temporary diverting stomas (Montedori *et al.*, 2010) to reduce the life-threatening consequences of an AL. But these in turn necessitate further future procedures to reverse the stoma and restore final intestinal continuity, and is associated with not insignificant morbidity, because the reversed stoma can likewise leak. Therefore the search continues for a solution to this knotty problem.

There is very little doubt that persisting inflammation or infection retards healing. This much appears clear. However, there is also evidence that TLR4 and MyD88 signalling pathways evoked by host-pathogen interactions, are necessary for optimal tissue repair in intestinal wounds (Fukata *et al.*, 2006), that preserving the period of time that neutrophils are present at wounds is beneficial for healing in the elderly (Nishio *et al.*, 2008), and that IL-10 (an anti-inflammatory agent) deficient mice actually exhibited enhanced epithelial healing (Eming *et al.*, 2007). Therefore this thesis put forward the hypothesis that simply accelerating, not abolishing, the inflammatory response and its conclusion would preserve the necessary inflammatory mechanisms required for healing, while shortening the opportunity for any microbes in proximity to increase their virulence and invasiveness, and would result in an overall accelerated wound healing.

The role of lipid signalling in disease is undisputed (Wymann and Schneiter, 2008), and recently discovered SPMs, derivatives of PUFAs, appeared promising for simultaneously accelerating inflammation resolution as well as enhancing host defence. The actions of selected SPMs were

investigated in the teleost model and broadly confirmed the anti-inflammatory mechanism of SPMs, although there were differing effects on host-defence to systemic infection. Bearing in mind the caveat of the early developmental stage of the zebrafish, the results validated the teleost model for investigation of SPMs despite the theoretical difference in fish body composition of fatty acids. Further validation of the teleost model was achieved with demonstration of the SPM receptor expression in zebrafish. This was followed by development and validation of a new technique, TomoSeq, to investigate the spatial inflammasome expression to a sterile injury in zebrafish. This, interestingly, showed zebrafish *alpi.1* to be expressed outside the intestinal tract in 2dpf zebrafish, matching the expression seen with *in situ* hybridisation performed by other groups (Thisse *et al*, 2004). The function of *alpi.1* expression at this stage of development has yet to be investigated and the fact that it is expressed even in the presence of other isoforms of ALP, is a curiosity in itself. It is interesting to note however that a similar expression is seen with the vitamin D receptor (VDR), another immuno-active molecule where expression is seen in different tissues in the embryo compared to the adult in humans (Haussler *et al.*, 2013).

Further examination of iAP using zebrafish showed definitively for the first time that this enzyme has independent anti-inflammatory actions in a sterile wound, and that it exerted its anti-inflammatory effect via adenosine A2b receptors. This appears similar to the way sulfasalazine exerts its effects in IBD (Gadangi *et al.*, 1996), with A2b receptors being the main adenosine receptor in the human colon (Strohmeier *et al.*, 1995), which is up-regulated in inflammation (Kolachala *et al.*, 2005). In the zebrafish, expression of iAP was also shown to be up-regulated in intestinal injury, and, in addition, to be uniquely expressed locally in the region of *E. faecalis* colonisation. The zebrafish was further validated as a model for study of colonisation and used to investigate the possible effects of SPMs on injury in the presence of bacteria in the intestine. Introducing bacterial presence into a site-specific injury model was important since intestinal tight junctions have been shown to be disrupted due to bacterial proximity rather than inflammation (Guttman *et al.*, 2006), and disruption of bacterial biofilm formation (Banerjee *et al.*, 2015) was likely the factor promoting rapidly healing cutaneous wounds through treatment with a low voltage AC current (Long *et al.*, 2018). As expected, the presence of colonising *E. faecalis* did increase the inflammatory response and only RvE1 in this

case continued to enhance inflammation resolution. Regrettably there was insufficient time to test the effects of iAP in this setting and this remains for future investigation.

But, microbial imbalance alone appears insufficient to cause the chronic inflammation in IBD (Gophna *et al.*, 2006), nor does accelerating inflammation resolution alone appear sufficient to drive wound healing since most SPMs and iAP alone did not improve sterile tailfin regeneration. Furthermore, healing appears to also be differentially affected in complex systems, with strong environmental influences. This was seen in studies where olive oil (rich in MUFAs), but not fish oil (rich in PUFAs - SPM precursors), was seen to improve cutaneous wound healing in stressed mice (Rosa *et al.*, 2014), whereas both oils improved healing in non-stressed mammals. This could, of course, be due to the combination of compounds found in olive oil (and not fish oil) exerting effects through diverse pathways since secoiridoids were the major source of its anti-inflammatory effects (Fernández del Río *et al.*, 2016; Borzì *et al.*, 2018), polyphenols its antibacterial effects (Medina *et al.*, 2007) and squalene its wound healing effects (Sánchez-Quesada *et al.*, 2018; Karimi *et al.*, 2019).

The actions of individual SPMs also appear receptor- and temporal-specific in the inflammation cascade. In this respect, iAP has an advantage. It brings about its actions not just by diminishing inflammatory mediators through dephosphorylation of Lipid A of LPS (Bates *et al.*, 2007) and reducing NTP (Malo *et al.*, 2014), but also by directly affecting inflammation via adenosine receptors, and likely directly modulating bacteria via provision of inorganic phosphate. Although bacteria possess their own ALP, mammalian ALP is 20 to 30-fold more active than their corresponding bacterial enzymes despite amino acid similarities, due specifically to a change to histidine at positions 153 and 328 (Murphy and Kantrowitz, 1994). Finally, although not investigated here, it is possible that under the correct organ-specific circumstances, iAP can also accelerate wound healing via the adenosine pathway (Feoktistov, Biaggioni and Cronstein, 2009). All these remain areas for confirmation with further directed studies. Nonetheless, iAP demonstrably accelerated anastomotic healing in the standard, as well as severe, murine models. Very few interventions to date have been able to demonstrate such conclusive improvement for anastomotic healing in all parameters as iAP did in these studies (Merad *et al.*, 1998; Slieker *et*

al., 2013; Wiggins *et al.*, 2015), and thus this shows great promise for rapid translation into clinical practice.

However, complicating the picture in clinical settings is that attempts to augment a pathway thought to improve healing could have the complication of assisting tumour growth or spread, and conversely, the necessity of chemotherapy to reduce the risks of tumour spread following cancer surgery could compromise wound integrity even years after the intestinal component should have healed (Bège *et al.*, 2009; Ganapathi *et al.*, 2012; Nakamura *et al.*, 2016). Translating bench science to the bedside in wound healing would always need to bear this cancer aspect in mind, and potentially, investigation into the effects of iAP in a cancer model would be warranted.

But perhaps in this respect, comparative physiology may hold some insights. Mice bred to old age do not show an excess of GIT tumours, and colonic tumours are in fact quite rare. Further testing this observation, even mice fed the much maligned 'unhealthy Western diet' also did not show an excess of GIT cancers (Hill, 1931). Spontaneous tumours of the digestive tract in rats and mice were between 1-2% and none involved the colon in the 360 rats and 254 mice observed (Prejean *et al.*, 1973). Could DISP, which is only expressed in the rodent colon, and not found in humans, be the reason for this? Interestingly an orthologue of DISP is also possessed by *Trichinella*, and this worm has been shown to reduce inflammation in colitis (Motomura *et al.*, 2009) as well as suppress clinical inflammation in murine encephalitis (Kuijk *et al.*, 2012). Helminth therapy underwent a brief period of interest as a potential treatment therapy for IBD (Aranzamendi, Sofronic-Milosavljevic and Pinelli, 2013) as a consequence of the hygiene theory of disease (Fleming, 2013; Garg, Croft and Bager, 2014), but has not been widely used clinically, possibly because of reduced patient acceptance. It is interesting that DISP in the murine model was increased on the seventh day and it is possible that its role lies in modulating the adaptive immune system. It has been shown that ADA inhibition with pentostatin, a purine anti-metabolite, increased T_{reg} numbers and decreased pro-inflammatory cytokine production (Brown *et al.*, 2008) and perhaps DISP may have a similar role to play. Nonetheless the details of DISP activation, its substrates, and the pathways involved remain unknown and interesting areas for investigation in future.

In conclusion, it appears that the most effective strategies for enhancing healing in an organ like the intestine would involve therapies that directly affect both inflammation and microbial benevolence, and iAP fulfils this criteria. It is possible that the most effective therapies in future could lie in appropriating insights from comparative studies and moving forward with concurrent tripartite considerations of inflammation, microbial balance and genetics.

References

Acton, D. S. *et al.* (2009) 'Intestinal carriage of Staphylococcus aureus: How does its frequency compare with that of nasal carriage and what is its clinical impact?', *European Journal of Clinical Microbiology and Infectious Diseases*, 28(2), pp. 115–127. doi: 10.1007/s10096-008-0602-7.

Adair, T. H. (2005) 'Growth regulation of the vascular system: an emerging role for adenosine', *American Journal of Physiology-Regulatory, Integrative and Comparative Physiology*, 289(2), pp. R283–R296. doi: 10.1152/ajpregu.00840.2004.

Adel, S. *et al.* (2014) 'Phosphorylation mimicking mutations of ALOX5 orthologs of different vertebrates do not alter reaction specificities of the enzymes', *Biochimica et Biophysica Acta (BBA) - Molecular and Cell Biology of Lipids*, 1841(10), pp. 1460–1466. doi: 10.1016/j.bbalip.2014.07.005.

Aguilar-Nascimento, J. E. *et al.* (1995) 'Enhanced intra-anastomotic healing by operative lavage with nutrient solutions in experimental left-sided colonic obstruction', *British Journal of Surgery*, 82(4), pp. 461–464. doi: 10.1002/bjs.1800820410.

Aharony, D. (1986) 'Kinetic Mechanism of Guinea Pig Neutrophil 5-Lipoxygenase', *J Biol Chem*, 261(25), pp. 11512–11519.

Aherne, C. M. *et al.* (2015) 'Epithelial-specific A2B adenosine receptor signaling protects the colonic epithelial barrier during acute colitis.', *Mucosal immunology*, 8(6), pp. 1324–1338. doi: 10.1038/mi.2015.22.

Alam, A. *et al.* (2016) 'The microenvironment of injured murine gut elicits a local pro-restitutive microbiota', *Nature Microbiology*, 1(2), p. 15021. doi: 10.1038/nmicrobiol.2015.21.

Albenberg, L. *et al.* (2014) 'Correlation between intraluminal oxygen gradient and radial partitioning of intestinal microbiota in humans and mice', *Gastroenterology*, 147(5), pp. 1055–1063. doi: 10.1053/j.gastro.2014.07.020.Correlation.

Allais, L. *et al.* (2016) 'Chronic cigarette smoke exposure induces microbial and inflammatory shifts and mucin changes in the murine gut', *Environmental Microbiology*, 18(5), pp. 1352–1363. doi: 10.1111/1462-2920.12934.

Alpers, D. H., Eliakim, R. and DeSchryver-Kecskemeti, K. (1990) 'Secretion of hepatic and intestinal alkaline phosphatases: Similarities and differences', *Clinica Chimica Acta*, 186(2), pp. 211–223. doi: 10.1016/0009-8981(90)90039-U.

Althuwaini, S. *et al.* (2018) 'Identification of Bacterial and Fungal Pathogens in Patients with Post-Laparoscopic Sleeve Gastrectomy Leakage', *Obesity Surgery*, 28(12), pp. 3965–3968. doi: 10.1007/s11695-018-3442-2.

Alvarez-Curto, E. and Milligan, G. (2016) ‘Metabolism meets immunity: The role of free fatty acid receptors in the immune system’, *Biochemical Pharmacology*, 114, pp. 3–13. doi: 10.1016/j.bcp.2016.03.017.

Alvers, A. L. *et al.* (2014) ‘Single continuous lumen formation in the zebrafish gut is mediated by smoothened-dependent tissue remodeling.’, *Development*, 141(5), pp. 1110–9. doi: 10.1242/dev.100313.

Ananthakrishnan, A. N. *et al.* (2017) ‘Gut Microbiome Function Predicts Response to Anti-integrin Biologic Therapy in Inflammatory Bowel Diseases’, *Cell Host and Microbe*, 21(5), pp. 603-610.e3. doi: 10.1016/j.chom.2017.04.010.

Anderson, E. M. *et al.* (2015) ‘Systematic analysis of CRISPR–Cas9 mismatch tolerance reveals low levels of off-target activity’, *Journal of Biotechnology*, 211, pp. 56–65. doi: 10.1016/j.jbiotec.2015.06.427.

Anderson, H. W. (1917) ‘Yeast-like fungi of the human intestinal tract’, *Journal of Infectious Diseases*, 21(4), pp. 341–385.

Aranzamendi, C., Sofronic-Milosavljevic, L. and Pinelli, E. (2013) ‘Helminths: Immunoregulation and Inflammatory Diseases—Which Side Are *Trichinella* spp. and *Toxocara* spp. on?’, *Journal of Parasitology Research*, 2013, pp. 1–11. doi: 10.1155/2013/329438.

Arita, M. *et al.* (2006) ‘Metabolic Inactivation of Resolvin E1 and Stabilization of Its Anti-inflammatory Actions’, *Journal of Biological Chemistry*, 281(32), pp. 22847–22854. doi: 10.1074/jbc.M603766200.

Arita, M. *et al.* (2007) ‘Resolvin E1 Selectively Interacts with Leukotriene B $_4$ Receptor BLT1 and ChemR23 to Regulate Inflammation’, *The Journal of Immunology*, 178(6), pp. 3912–3917. doi: 10.4049/jimmunol.178.6.3912.

Arrieta, M.-C. and Finlay, B. B. (2012) ‘The Commensal Microbiota Drives Immune Homeostasis’, *Frontiers in Immunology*, 3. doi: 10.3389/fimmu.2012.00033.

Arwert, E. N., Hoste, E. and Watt, F. M. (2012) ‘Epithelial stem cells, wound healing and cancer’, *Nature Reviews Cancer*, 12(3), pp. 170–180. doi: 10.1038/nrc3217.

Ashida, H. *et al.* (2011) ‘Cell death and infection: A double-edged sword for host and pathogen survival’, *Journal of Cell Biology*, 195(6), pp. 931–942. doi: 10.1083/jcb.201108081.

Atiakshin, D. A. *et al.* (2019) ‘[Extracellular matrix collagen fiber structures of the gastrointestinal connective tissues in mice after a 30 day orbital flight]’, *Voprosy Pitaniia.*, 88(1), pp. 26–40. doi: 10.24411/0042-8833-2019-10003.

Attard, J. A. P. *et al.* (2005) ‘The effects of systemic hypoxia on colon anastomotic healing: An animal model’, *Diseases of the Colon and Rectum*, 48(7), pp. 1460–1470. doi: 10.1007/s10350-005-0047-3.

Avdesh, A. *et al.* (2012) 'Regular care and maintenance of a zebrafish (Danio rerio) laboratory: an introduction.', *Journal of visualized experiments : JoVE*, (69), p. e4196. doi: 10.3791/4196.

Ayten, R. *et al.* (2008) 'The effects of intraperitoneal sildenafil administration on healing of left colonic anastomoses and intra-abdominal adhesion formation in the presence of intra-abdominal infection', *Diseases of the Colon and Rectum*, 51(12), pp. 1837–1841. doi: 10.1007/s10350-008-9398-x.

Azevedo, A. S. *et al.* (2011) 'The regenerative capacity of the zebrafish caudal fin is not affected by repeated amputations', *PLoS ONE*, 6(7), pp. 1–8. doi: 10.1371/journal.pone.0022820.

Aziz, M. *et al.* (2013) 'Current trends in inflammatory and immunomodulatory mediators in sepsis.', *Journal of leukocyte biology*, 93(3), pp. 329–42. doi: 10.1189/jlb.0912437.

Bachmann, R. *et al.* (2017) 'Novel insight into the role of microbiota in colorectal surgery', *Gut*, 66, pp. 738–749. doi: 10.1136/gutjnl-2016-312569.

Baker, N. *et al.* (2009) 'Lipoxin A4: anti-inflammatory and anti-angiogenic impact on endothelial cells.', *Journal of immunology (Baltimore, Md. : 1950)*, 182(6), pp. 3819–26. doi: 10.4049/jimmunol.0803175.

Bakker, N. *et al.* (2015) 'Risk of anastomotic leakage with nonsteroidal anti-inflammatory drugs within an enhanced recovery program', *Journal of Gastrointestinal Surgery*, (November 2014), pp. 776–782. doi: 10.1007/s11605-015-3010-1.

Baldwin, A. S., Hill, C. and Carolina, N. (1996) 'THE NF- κB AND IκB PROTEINS : New Discoveries and Insights', *Ann Rev Immunologyy*, 14(1), pp. 649–683.

Banerjee, J. *et al.* (2015) 'Silver-Zinc Redox-Coupled Electroceutical Wound Dressing Disrupts Bacterial Biofilm', *PLOS ONE*. Edited by M. Wu, 10(3), p. e0119531. doi: 10.1371/journal.pone.0119531.

Bannenberg, G. L. *et al.* (2005) 'Molecular circuits of resolution: formation and actions of resolvins and protectins.', *Journal of immunology (Baltimore, Md. : 1950)*, 174(7), pp. 4345–4355. doi: 10.4049/jimmunol.174.7.4345.

Barber, A. E., Fleming, B. A. and Mulvey, M. A. (2016) 'Similarly Lethal Strains of Extraintestinal Pathogenic Escherichia coli Trigger Markedly Diverse Host Responses in a Zebrafish Model of Sepsis', *mSphere*, 1(2), pp. 1–19. doi: 10.1128/mSphere.00062-16.Editor.

Barletta, K. E., Ley, K. and Mehrad, B. (2012) 'Regulation of neutrophil function by adenosine', *Arteriosclerosis, Thrombosis, and Vascular Biology*, 32(4), pp. 856–864. doi: 10.1161/ATVBAHA.111.226845.

Barnard, G. A. (1945) 'A new test for 2X2 tables', *Nature*, 3954, p. 77.

Barnett, M. P. G. *et al.* (2016) 'Inoculation with enterococci does not affect colon inflammation in the multi-drug resistance 1a-deficient mouse model of IBD', *BMC Gastroenterology*, pp. 10–16. doi: 10.1186/s12876-016-0447-y.

Barski, D. *et al.* (2017) 'Human Amniotic Membrane Is Not Suitable for the Grafting of Colon Lesions and Prevention of Adhesions in a Xenograft Rat Model', *Surgical Innovation*, p. 155335061770982. doi: 10.1177/1553350617709828.

Bates, J. M. *et al.* (2006) 'Distinct signals from the microbiota promote different aspects of zebrafish gut differentiation', *Developmental Biology*, 297(2), pp. 374–386. doi: 10.1016/j.ydbio.2006.05.006.

Bates, J. M. *et al.* (2007) 'Intestinal Alkaline Phosphatase Detoxifies Lipopolysaccharide and Prevents Inflammation in Zebrafish in Response to the Gut Microbiota', *Cell Host & Microbe*, 2(6), pp. 371–382. doi: 10.1016/j.chom.2007.10.010.

Batzer, M. A. and Jorde, L. B. (2007) 'Genetic Similarities Within and Between Human Populations', 359(May), pp. 351–359. doi: 10.1534/genetics.106.067355.

Bège, T. *et al.* (2009) 'Bevacizumab-Related Surgical Site Complication Despite Primary Tumor Resection in Colorectal Cancer Patients', *Annals of Surgical Oncology*, 16(4), pp. 856–860. doi: 10.1245/s10434-008-0279-2.

Benard, E. L. *et al.* (2012) 'Infection of Zebrafish Embryos with Intracellular Bacterial Pathogens', *Journal of Visualized Experiments*, (61), pp. 1–9. doi: 10.3791/3781.

Bercik, P., Collins, S. M. and Verdu, E. F. (2012) 'Microbes and the gut-brain axis', *Neurogastroenterology and Motility*, 24(5), pp. 405–413. doi: 10.1111/j.1365-2982.2012.01906.x.

Berglund, E. *et al.* (2018) 'Spatial maps of prostate cancer transcriptomes reveal an unexplored landscape of heterogeneity', *Nature Communications*, 9(1), p. 2419. doi: 10.1038/s41467-018-04724-5.

Bertrand, S. *et al.* (2014) 'Metabolite induction via microorganism co-culture: A potential way to enhance chemical diversity for drug discovery', *Biotechnology Advances*, 32(6), pp. 1180–1204. doi: 10.1016/j.biotechadv.2014.03.001.

Beumer, C. *et al.* (2003) 'Calf Intestinal Alkaline Phosphatase, a Novel Therapeutic Drug for Lipopolysaccharide (LPS)-Mediated Diseases, Attenuates LPS Toxicity in Mice and Piglets', *Journal of Pharmacology and Experimental Therapeutics*, 307(2), pp. 737–744. doi: 10.1124/jpet.103.056606.

Bitar, K. and Reinhold, J. G. (1972) 'Phytase and alkaline phosphatase activities in intestinal mucosae of rat, chicken, calf, and man', *Biochimica et Biophysica Acta (BBA) - Enzymology*, 268(2), pp. 442–452. doi: 10.1016/0005-2744(72)90340-3.

Blackburn, M. R. *et al.* (2000) 'Metabolic Consequences of Adenosine Deaminase Deficiency in Mice Are Associated with Defects in Alveogenesis, Pulmonary Inflammation, and Airway Obstruction', *The Journal of Experimental Medicine*, 192(2), pp. 159–170. doi: 10.1084/jem.192.2.159.

Blair, P. and Flaumenhaft, R. (2009) 'Platelet α-granules: Basic biology and clinical correlates', *Blood Reviews*, 23(4), pp. 177–189. doi: 10.1016/j.blre.2009.04.001.

Bocan, T. M. A. *et al.* (1998) 'A specific 15-lipoxygenase inhibitor limits the progression and monocyte-macrophage enrichment of hypercholesterolemia-induced atherosclerosis in the rabbit', *Atherosclerosis*, 136(2), pp. 203–216. doi: 10.1016/S0021-9150(97)00204-9.

Boehmler, W. *et al.* (2009) 'Identification of zebrafish A2 adenosine receptors and expression in developing embryos', *Gene Expression Patterns*, 9(3), pp. 144–151. doi: 10.1016/j.gep.2008.11.006.

Boersema, G. S. A. *et al.* (2016) 'Hyperbaric oxygen therapy improves colorectal anastomotic healing', *International Journal of Colorectal Disease*, 31(5), pp. 1031–1038. doi: 10.1007/s00384-016-2573-y.

Bohlen, H. G. and Lash, J. M. (1995) 'Resting oxygenation of rat and rabbit intestine: arteriolar and capillary contributions', *American Journal of Physiology-Heart and Circulatory Physiology*, 269(4), pp. H1342–H1348. doi: 10.1152/ajpheart.1995.269.4.H1342.

Boldock, E. *et al.* (2018) 'Human skin commensals augment Staphylococcus aureus pathogenesis', *Nature Microbiology*, 3(8), pp. 881–890. doi: 10.1038/s41564-018-0198-3.

Borregaard, N. and Herlin, T. (1982) 'Energy Metabolism of Human Neutrophils during Phagocytosis', *Journal of Clinical Investigation*, 70(3), pp. 550–557. doi: 10.1172/JCI110647.

Borzì, A. *et al.* (2018) 'Olive Oil Effects on Colorectal Cancer', *Nutrients*, 11(1), p. 32. doi: 10.3390/nu11010032.

Bosmans, J. W. A. M. *et al.* (2016) 'International consensus statement regarding the use of animal models for research on anastomoses in the lower gastrointestinal tract', *International Journal of Colorectal Disease*, 31(5), pp. 1021–1030. doi: 10.1007/s00384-016-2550-5.

Bosmans, J. W. A. M. *et al.* (2017) 'Functional mucous layer and healing of proximal colonic anastomoses in an experimental model: Mucus and colonic anastomotic leakage', *British Journal of Surgery*, 104(5), pp. 619–630. doi: 10.1002/bjs.10456.

De Bosscher, K., Vanden Berghe, W. and Haegeman, G. (2000) 'Mechanisms of anti-inflammatory action and of immunosuppression by glucocorticoids: Negative interference of activated glucocorticoid receptor with transcription factors', *Journal of Neuroimmunology*, 109(1), pp. 16–22. doi: 10.1016/S0165-5728(00)00297-6.

Boyle, N. *et al.* (2000) 'Intraoperative Assessment of Colonic Perfusion Using Scanning Laser Doppler Flowmetry During Colonic Resection', *J Am Coll Surg*, 191(5), p. 7.

Bradford, Y. M. *et al.* (2017) 'Zebrafish Models of Human Disease: Gaining Insight into Human Disease at ZFIN', *ILAR Journal*, 58(1), pp. 4–16. doi: 10.1093/ilar/ilw040.

Brazil, J. C. *et al.* (2010) 'Neutrophil migration across intestinal epithelium: evidence for a role of CD44 in regulating detachment of migrating cells from the luminal surface.', *Journal of immunology (Baltimore, Md. : 1950)*, 185(11), pp. 7026–36. doi: 10.4049/jimmunol.1001293.

Brink, C. *et al.* (2003) 'International Union of Pharmacology XXXVII. Nomenclature for Leukotriene and Lipoxin Receptors', *Pharmacological Reviews*, 55(1), pp. 195–227. doi: 10.1124/pr.55.1.8.

Brinkmann, V. *et al.* (2004) 'Neutrophil extracellular traps kill bacteria.', *Science*, 303(5663), pp. 1532–1535. doi: 10.1126/science.1092385.

Brown, J. B. *et al.* (2008) 'Therapeutic benefit of pentostatin in severe IL-10−/− Colitis':, *Inflammatory Bowel Diseases*, 14(7), pp. 880–887. doi: 10.1002/ibd.20410.

de Bruin, E. C. *et al.* (2014) 'Spatial and temporal diversity in genomic instability processes defines lung cancer evolution', *Science*, 346(6206), pp. 251–256. doi: 10.1126/science.1253462.

Bryan, N. S., Tribble, G. and Angelov, N. (2017) 'Oral Microbiome and Nitric Oxide: the Missing Link in the Management of Blood Pressure.', *Current hypertension reports*, 19(4), p. 33. doi: 10.1007/s11906-017-0725-2.

Buckley, C. D., Gilroy, D. W. and Serhan, C. N. (2014) 'Proresolving Lipid Mediators and Mechanisms in the Resolution of Acute Inflammation', *Immunity*, 40(3), pp. 315–327. doi: 10.1016/j.immuni.2014.02.009.

Bussmann, J. and Schulte-Merker, S. (2011) 'Rapid BAC selection for tol2-mediated transgenesis in zebrafish', *Development*, 138(19), pp. 4327–4332. doi: 10.1242/dev.068080.

Byrne, C. *et al.* (2015) 'Predicting Risk of Anastomotic Leak in Patients Undergoing Neo-adjuvant Radiotherapy and Low Anterior Resection for Rectal Cancer', *Journal of Gastrointestinal & Digestive System*, 05(01). doi: 10.4172/2161-069X.1000255.

Cahill, R. A. *et al.* (2004) 'Effects of a selective cyclo-oxygenase 2 inhibitor on colonic anastomotic and skin wound integrity', *British Journal of Surgery*, 91(12), pp. 1613–1618. doi: 10.1002/bjs.4722.

Cakir, T. *et al.* (2015) 'Increased collagen maturity with sildenafil citrate: Experimental high risk colonic anastomosis model', *International Journal of Surgery*, 13, pp. 152–156. doi: 10.1016/j.ijsu.2014.11.042.

Caley, M. P., Martins, V. L. C. and O'Toole, E. A. (2015) 'Metalloproteinases and Wound Healing', *Advances in Wound Care*, 4(4), pp. 225–234. doi: 10.1089/wound.2014.0581.

Campbell, E. L. *et al.* (2007) 'Resolvin E1 promotes mucosal surface clearance of neutrophils: a new paradigm for inflammatory resolution.', *The FASEB journal : official publication of the*

Federation of American Societies for Experimental Biology, 21(12), pp. 3162–3170. doi: 10.1096/fj.07-8473com.

Campbell, E. L. *et al.* (2010) 'Resolvin E1-induced intestinal alkaline phosphatase promotes resolution of inflammation through LPS detoxification', *Proceedings of the National Academy of Sciences*, 107(32), pp. 14298–14303. doi: 10.1073/pnas.0914730107.

Campbell, S. C. *et al.* (2016) 'The effect of diet and exercise on intestinal integrity and microbial diversity in mice', *PLoS ONE*, 11(3), pp. 1–17. doi: 10.1371/journal.pone.0150502.

Capra, V. *et al.* (2015) 'Transcellular biosynthesis of eicosanoid lipid mediators', *Biochimica et Biophysica Acta - Molecular and Cell Biology of Lipids*, 1851(4), pp. 377–382. doi: 10.1016/j.bbalip.2014.09.002.

Caputi, V. *et al.* (2017) 'Toll-like receptor 4 modulates small intestine neuromuscular function through nitrergic and purinergic pathways', *Frontiers in Pharmacology*, 8(JUN), pp. 1–15. doi: 10.3389/fphar.2017.00350.

Carding, S. R., Davis, N. and Hoyles, L. (2017) 'Review article: the human intestinal virome in health and disease', *Alimentary Pharmacology & Therapeutics*, (April), pp. 1–16. doi: 10.1111/apt.14280.

Carlberg, K. *et al.* (2019) 'Exploring inflammatory signatures in arthritic joint biopsies with Spatial Transcriptomics', *Scientific Reports*, 9(1), p. 18975. doi: 10.1038/s41598-019-55441-y.

Casamassimi, A. and Napoli, C. (2007) 'Mediator complexes and eukaryotic transcription regulation: An overview', *Biochimie*, 89(12), pp. 1439–1446. doi: 10.1016/j.biochi.2007.08.002.

Casteleyn, C. *et al.* (2010) 'Surface area assessment of the murine intestinal tract as a prerequisite for oral dose translation from mouse to man', *Laboratory Animals*, 44(3), pp. 176–183. doi: 10.1258/la.2009.009112.

Castro-alcaraz, S. *et al.* (2018) 'NF- κ B Regulation in Human Neutrophils by Nuclear I κ B α : Correlation to Apoptosis'. doi: 10.4049/jimmunol.169.7.3947.

Cha, Y. I. and DuBois, R. N. (2007) 'NSAIDs and cancer prevention: targets downstream of COX-2.', *Annual review of medicine*, 58, pp. 239–252. doi: 10.1146/annurev.med.57.121304.131253.

Chang, T. N. and Keshishian, H. (1996) 'Laser Ablation of *Drosophila* Embryonic Motoneurons Causes Ectopic Innervation of Target Muscle Fibers', *The Journal of Neuroscience*, 16(18), pp. 5715–5726. doi: 10.1523/JNEUROSCI.16-18-05715.1996.

Chappelet-tordo, D. *et al.* (1974) 'Intestinal Alkaline Phosphatase . Catalytic Properties and Half of the Sites Reactivity', 13(9). doi: 10.1021/bi00706a002.

Chartier, L. C. *et al.* (2020) 'Affective state determination in a mouse model of colitis-associated colorectal cancer', *PLOS ONE*. Edited by M. Body-Malapel, 15(1), p. e0228413. doi: 10.1371/journal.pone.0228413.

Chen, J.-F., Eltzschig, H. K. and Fredholm, B. B. (2013) 'Adenosine receptors as drug targets — what are the challenges?', *Nature Reviews Drug Discovery*, 12(4), pp. 265–286. doi: 10.1038/nrd3955.

Chen, Y. C. *et al.* (2012) 'Zebrafish Agr2 is required for terminal differentiation of intestinal goblet cells', *PLoS ONE*, 7(4), pp. 1–10. doi: 10.1371/journal.pone.0034408.

Cheng, D. *et al.* (2016) 'Ultrastructural Mapping of the Zebrafish Gastrointestinal System as a Basis for Experimental Drug Studies', *BioMed Research International*, 2016, pp. 12–14. doi: 10.1155/2016/8758460.

Chiang, N. *et al.* (2012) 'Infection regulates pro-resolving mediators that lower antibiotic requirements.', *Nature*, 484(7395), pp. 524–8. doi: 10.1038/nature11042.

Chiang, N. *et al.* (2015) 'Identification of resolvin D2 receptor mediating resolution of infections and organ protection.', *The Journal of experimental medicine*, 212(8), pp. 1203–1217. doi: 10.1084/jem.20150225.

Chiang, N. *et al.* (2017) 'Novel Resolvin D2 Receptor Axis in Infectious Inflammation', *The Journal of Immunology*, 198(2), pp. 842–851. doi: 10.4049/jimmunol.1601650.

Chiang, N. and Serhan, C. N. (2017) 'Structural elucidation and physiologic functions of specialized pro-resolving mediators and their receptors', *Molecular Aspects of Medicine*, 58, pp. 114–129. doi: 10.1016/j.mam.2017.03.005.

Chunn, J. L. *et al.* (2006) 'Partially adenosine deaminase-deficient mice develop pulmonary fibrosis in association with adenosine elevations', *American Journal of Physiology-Lung Cellular and Molecular Physiology*, 290(3), pp. L579–L587. doi: 10.1152/ajplung.00258.2005.

Claesson, M. J. *et al.* (2011) 'Composition, variability, and temporal stability of the intestinal microbiota of the elderly', *Proceedings of the National Academy of Sciences of the United States of America*, 108(Suppl. 1), pp. 4586–4591. doi: 10.1073/pnas.1000097107.

Clarke, R. (1988) *The molecular and cellular biology of wound repair*. Springer (U.S.).

Clevers, H. (2004) 'At the crossroads of inflammation and cancer', *Cell*, 118(6), pp. 671–674. doi: 10.1016/j.cell.2004.09.005.

Cocchiaro, J. L. and Rawls, J. F. (2013) 'Microgavage of Zebrafish Larvae', *Journal of Visualized Experiments*, (72), pp. 1–12. doi: 10.3791/4434.

Cohn, I. and Rives, J. D. (1956) 'Protection of colonic anastomoses with antibiotics.', *Annals of surgery*, 144(4), pp. 738–52.

Colgan, S. P. and Taylor, C. T. (2010) 'Hypoxia: an alarm signal during intestinal inflammation', *Nature Publishing Group*, 7(5), pp. 281–287. doi: 10.1038/nrgastro.2010.39.

Conesa, A. *et al.* (2016) 'A survey of best practices for RNA-seq data analysis', *Genome Biology*, 17(1), p. 13. doi: 10.1186/s13059-016-0881-8.

Cox, J. and Mann, M. (2008) 'MaxQuant enables high peptide identification rates, individualized p.p.b.-range mass accuracies and proteome-wide protein quantification.', *Nature biotechnology*, 26(12), pp. 1367–72. doi: 10.1038/nbt.1511.

Craig, M. P. *et al.* (2012) 'An Optimized Method for Delivering Flow Tracer Particles to Intravital Fluid Environments in the Developing Zebrafish', *Zebrafish*, 9(3), pp. 108–119. doi: 10.1089/zeb.2012.0740.

Cronstein, B. N., Naime, D. and Ostad, E. (1993) 'The Antiinflammatory Mechanism of Methotrexate', *J. Clin. Invest*, 92(6), pp. 2675–2682. doi: 10.1016/S0889-857X(05)70358-6.

Csóka, B. *et al.* (2010) 'A $_{2B}$ Adenosine Receptors Protect against Sepsis-Induced Mortality by Dampening Excessive Inflammation', *The Journal of Immunology*, 185(1), pp. 542–550. doi: 10.4049/jimmunol.0901295.

Cummins, E. P. and Crean, D. (2016) 'Hypoxia and inflammatory bowel disease.', *Microbes and infection*, 19(September), pp. 1–12. doi: 10.1016/j.micinf.2016.09.004.

Dalli, J. and Serhan, C. (2016) 'Macrophage Proresolving Mediators-the When and Where.', *Microbiology spectrum*, 4(3), pp. 37–54. doi: 10.1128/microbiolspec.MCHD-0001-2014.

Darby, T. and Melgar, S. (2014) 'Cytokine & Growth Factor Reviews The complex role of inflammasomes in the pathogenesis of Inflammatory Bowel Diseases – Lessons learned from experimental models', 25, pp. 715–730. doi: 10.1016/j.cytogfr.2014.04.003.

Daseke, M. J. *et al.* (2019) 'Neutrophil proteome shifts over the myocardial infarction time continuum', *Basic Research in Cardiology*, 114(5), p. 37. doi: 10.1007/s00395-019-0746-x.

Datta, K., Biswal, S. S. and Kehrer, J. P. (1999) 'The 5-lipoxygenase-activating protein (FLAP) inhibitor, MK886, induces apoptosis independently of FLAP', *Biochemical Journal*, 340(2), p. 371. doi: 10.1042/0264-6021:3400371.

Davenport, E. R. (2016) 'Elucidating the role of the host genome in shaping microbiome composition', *Gut Microbes*, 7(2), pp. 178–184. doi: 10.1080/19490976.2016.1155022.

Davis, J. M. *et al.* (2002) 'Real-Time Visualization of Mycobacterium-Macrophage Interactions Leading to Initiation of Granuloma Formation in Zebrafish Embryos', *Immunity*, 17(6), pp. 693–702. doi: 10.1016/S1074-7613(02)00475-2.

De Vries, L. C. S. *et al.* (2017) 'The Future of Janus Kinase Inhibitors in Inflammatory Bowel Disease', *Journal of Crohn's and Colitis*, 11(7), pp. 885–893. doi: 10.1093/ecco-jcc/jjx003.

Degett, T. H., Andersen, H. S. and Gögenur, I. (2016) 'Indocyanine green fluorescence angiography for intraoperative assessment of gastrointestinal anastomotic perfusion: a systematic review of clinical trials', *Langenbeck's Archives of Surgery*, 401(6), pp. 767–775. doi: 10.1007/s00423-016-1400-9.

Delvaeye, M. and Conway, E. M. (2019) 'Coagulation and innate immune responses : can we view them separately ?', 114(12), pp. 2367–2375. doi: 10.1182/blood-2009-05-199208.

Dennis, E. A. and Norris, P. C. (2015) 'Eicosanoid storm in infection and inflammation.', *Nature reviews. Immunology*, 15(8), pp. 511–23. doi: 10.1038/nri3859.

Devalaraja, R. M. *et al.* (2000) 'Delayed wound healing in CXCR2 knockout mice.', *The Journal of investigative dermatology*, 115(2), pp. 234–44. doi: 10.1046/j.1523-1747.2000.00034.x.

Dimitriou, R. (2013) 'The genetic profile of bone repair', *Clinical cases in mineral and bone metabolism*. doi: 10.11138/ccmbm/2013.10.1.019.

Dixon, G. *et al.* (2012) 'A Method for the *In Vivo* Measurement of Zebrafish Tissue Neutrophil Lifespan', *ISRN Hematology*, 2012, pp. 1–6. doi: 10.5402/2012/915868.

Dobrowolska−Iwanek, J. *et al.* (2016) 'Procedure optimization for extracting short-chain fatty acids from human faeces', *Journal of Pharmaceutical and Biomedical Analysis*, 124, pp. 337–340. doi: 10.1016/j.jpba.2016.02.042.

Dona, M. *et al.* (2008) 'Resolvin El, an EPA-derived mediator in whole blood, selectively counterregulates leukocytes and platelets', *Blood*, 112(3), pp. 848–855. doi: 10.1182/blood-2007-11-122598.

Dorward, D. A. *et al.* (2015) 'The Role of Formylated Peptides and Formyl Peptide Receptor 1 in Governing Neutrophil Function during Acute Inflammation', *The American Journal of Pathology*, 185(5), pp. 1172–1184. doi: 10.1016/j.ajpath.2015.01.020.

Dovi, J. V, He, L. and Dipietro, L. a (2003) 'Accelerated wound closure in neutrophil-depleted mice Abstract : The infiltration of neutrophils into in- jured tissue is known to protect wounds from in- repair process . To investigate the role of neutro-', *Journal of Leukocyte Biology*, 73, pp. 448–455. doi: 10.1189/jlb.0802406.http.

Dunny, G. M., Brown, B. L. and Clewell, D. B. (1978) 'Induced cell aggregation and mating in Streptococcus faecalis: evidence for a bacterial sex pheromone.', *Proceedings of the National Academy of Sciences*, 75(7), pp. 3479–3483. doi: 10.1073/pnas.75.7.3479.

Dupont, A. *et al.* (2014) 'Antimicrobial peptides and the enteric mucus layer act in concert to protect the intestinal mucosa', *Gut Microbes*, 5(6), pp. 761–765. doi: 10.4161/19490976.2014.972238.

Dvorak, H. F. (1986) 'Tumors: Wounds That Do Not Heal', *New England Journal of Medicine*, 315, pp. 1650–1986. doi: 10.1158/2326-6066.CIR-14-0209.

Eden, E. *et al.* (2009) 'GOrilla: a tool for discovery and visualization of enriched GO terms in ranked gene lists', *BMC Bioinformatics*, 10(1), p. 48. doi: 10.1186/1471-2105-10-48.

Ellett, F. *et al.* (2011) 'Mpeg1 Promoter Transgenes Direct Macrophage-Lineage Expression in Zebrafish', *Blood*, 117(4), pp. e49–e56. doi: 10.1182/blood-2010-10-314120.

Ellett, F. *et al.* (2015) 'Defining the phenotype of neutrophils following reverse migration in zebrafish', *Journal of Leukocyte Biology*, 98(December), pp. 1–7. doi: 10.1189/jlb.3MA0315-105R.

Eming, S. a *et al.* (2007) 'Accelerated wound closure in mice deficient for interleukin-10.', *The American journal of pathology*, 170(1), pp. 188–202. doi: 10.2353/ajpath.2007.060370.

Erb, L., Hyman, N. H. and Osler, T. (2014) 'Abnormal vital signs are common after bowel resection and do not predict anastomotic leak', *Journal of the American College of Surgeons*, 218(6), pp. 1195–1199. doi: 10.1016/j.jamcollsurg.2013.12.059.

Eurostats (2017) *Eurostats: Number of colectomies performed per country. http://ec.europa.eu/eurostat/data/database (accessed 2 May 2017)*. Available at: http://ec.europa.eu/eurostat/data/database (Accessed: 4 May 2017).

Faas, M. M., Sáez, T. and de Vos, P. (2017) 'Extracellular ATP and adenosine: The Yin and Yang in immune responses?', *Molecular Aspects of Medicine*, 55, pp. 9–19. doi: 10.1016/j.mam.2017.01.002.

Faccioli, C. K. *et al.* (2016) 'Acid and alkaline phosphatase localization in the digestive tract mucosa of the Hemisorubim platyrhynchos', *Acta Histochemica*, 118(7), pp. 722–728. doi: 10.1016/j.acthis.2016.08.001.

Fan, P. *et al.* (2019) 'Host genetic effects upon the early gut microbiota in a bovine model with graduated spectrum of genetic variation', *The ISME Journal*. doi: 10.1038/s41396-019-0529-2.

Fenton, J. I. *et al.* (2013) 'Immunomodulation by dietary long chain omega-3 fatty acids and the potential for adverse health outcomes', *Prostaglandins Leukotrienes and Essential Fatty Acids*, 89(6), pp. 379–390. doi: 10.1016/j.plefa.2013.09.011.

Feoktistov, I., Biaggioni, I. and Cronstein, B. N. (2009) 'Adenosine Receptors in Wound Healing, Fibrosis and Angiogenesis', in Wilson, C. N. and Mustafa, S. J. (eds) *Adenosine Receptors in Health and Disease*. Berlin, Heidelberg: Springer Berlin Heidelberg, pp. 383–397. doi: 10.1007/978-3-540-89615-9_13.

Ferlay, J. *et al.* (2018) 'Cancer incidence and mortality patterns in Europe: Estimates for 40 countries and 25 major cancers in 2018', *European Journal of Cancer*, 103, pp. 356–387. doi: 10.1016/j.ejca.2018.07.005.

Fernández del Río, L. *et al.* (2016) 'Olive Oil and the Hallmarks of Aging', *Molecules*, 21(2), p. 163. doi: 10.3390/molecules21020163.

Fierro, I. M. *et al.* (2003) 'Lipoxin A4 and aspirin-triggered 15-epi-lipoxin A4 inhibit human neutrophil migration: comparisons between synthetic 15 epimers in chemotaxis and transmigration with microvessel endothelial cells and epithelial cells.', *Journal of immunology (Baltimore, Md. : 1950)*, 170(5), pp. 2688–2694. doi: 10.4049/jimmunol.170.5.2688.

Finckbeiner, S. *et al.* (2011) 'Transient knockdown and overexpression reveal a developmental role for the zebrafish enosf1b gene', *Cell & Bioscience*, 1(1), p. 32. doi: 10.1186/2045-3701-1-32.

Fleming, J. O. (2013) 'Helminth therapy and multiple sclerosis', *International Journal for Parasitology*, 43(3–4), pp. 259–274. doi: 10.1016/j.ijpara.2012.10.025.

Forkosh, O. *et al.* (2019) 'Identity domains capture individual differences from across the behavioral repertoire', *Nature Neuroscience*, 22(12), pp. 2023–2028. doi: 10.1038/s41593-019-0516-y.

Francescone, R., Hou, V. and Grivennikov, S. I. (2014) 'Microbiome, Inflammation, and Cancer', *The Cancer Journal*, 20(3), pp. 181–189. doi: 10.1097/PPO.0000000000000048.

Fredman, G. and Serhan, C. N. (2011) 'Specialized proresolving mediator targets for RvE1 and RvD1 in peripheral blood and mechanisms of resolution', *Biochemical Journal*, 437(2), pp. 185–197. doi: 10.1042/BJ20110327.

Fukata, M. *et al.* (2006) 'COX-2 is regulated by TLR4 signaling and is important for proliferation and apoptosis in response to intestinal mucosal injury', *Gastroenterology*, 131(3), pp. 862–877.

Gabbiani, G. *et al.* (1972) 'Granulation tissue as a contractile organ: a study of structure and function', *Journal of Experimental Medicine*, 135, pp. 719–733.

Gadangi, P. *et al.* (1996) 'The anti-inflammatory mechanism of sulfasalazine is related to adenosine release at inflamed sites', *Journal of immunology*, 156(5), pp. 1937–1941. doi: 10.4049/jimmunol.164.2.1013.

Ganapathi, A. M. *et al.* (2012) 'Bevacizumab-Associated Fistula Formation in Postoperative Colorectal Cancer Patients', *Journal of the American College of Surgeons*, 214(4), pp. 582–588. doi: 10.1016/j.jamcollsurg.2011.12.030.

Garg, S. K., Croft, A. M. and Bager, P. (2014) 'Helminth therapy (worms) for induction of remission in inflammatory bowel disease', *Cochrane Database of Systematic Reviews*. Edited by Cochrane IBD Group. doi: 10.1002/14651858.CD009400.pub2.

Garsin, D. A. and Lorenz, M. C. (2013) 'Candida albicans and Enterococcus faecalis in the gut: Synergy in commensalism?', *Gut Microbes*, 4(5), pp. 409–415. doi: 10.4161/gmic.26040.

Gärtner, K. (2002) 'The forestomach of rats and mice, an effective device supporting digestive metabolism in muridae (review)', *Journal of Experimental Animal Science*, 42(1), pp. 1–20. doi: 10.1016/S0939-8600(02)80002-5.

Ghosh, D. *et al.* (2002) 'Paneth cell trypsin is the processing enzyme for human defensin-5', *Nature Immunology*, 3(6), pp. 583–590. doi: 10.1038/ni797.

Giacometti, A. *et al.* (2000) 'Epidemiology and Microbiology of Surgical Wound Infections', 38(2), pp. 918–922.

Gilbert, N. C. (2020) 'Structural and mechanistic insights into 5-lipoxygenase inhibition by natural products', *Nature Chemical Biology*, 16, p. 13.

Gitelman, I. (2007) 'Evolution of the vertebrate twist family and synfunctionalization: a mechanism for differential gene loss through merging of expression domains', *Molecular Biology and Evolution*, 24(9), pp. 1912–1925. doi: 10.1093/molbev/msm120.

Glover, L. E., Lee, J. S. and Colgan, S. P. (2016) 'Oxygen metabolism and barrier regulation in the intestinal mucosa.', *The Journal of clinical investigation*, 126(10), pp. 3680–3688. doi: 10.1172/JCI84429.

Godson, C. *et al.* (2000) 'lipoxins rapidly stimulate nonphlogistic phagocytosis of apoptotic neutrophils by monocyte-derived macrophages.', *Journal of immunology (Baltimore, Md. : 1950)*, 164(4), pp. 1663–1667. doi: 10.4049/jimmunol.164.4.1663.

Goldberg, R. F. *et al.* (2008) 'Intestinal alkaline phosphatase is a gut mucosal defense factor maintained by enteral nutrition', *Proceedings of the National Academy of Sciences*, 105(9), pp. 3551–3556. doi: 10.1073/pnas.0712140105.

Goldsmith, J. R. *et al.* (2013) 'Glafenine-induced intestinal injury in zebrafish is ameliorated by μ-opioid signaling via enhancement of Atf6-dependent cellular stress responses.', *Disease models & mechanisms*, 6(1), pp. 146–59. doi: 10.1242/dmm.009852.

Goodrich, J. K. *et al.* (2014) 'Human Genetics Shape the Gut Microbiome', *Cell*, 159(4), pp. 789–799. doi: 10.1016/j.cell.2014.09.053.

Gophna, U. *et al.* (2006) 'Differences between Tissue-Associated Intestinal Microfloras of Patients with Crohn's Disease and Ulcerative Colitis', *Journal of Clinical Microbiology*, 44(11), pp. 4136–4141. doi: 10.1128/JCM.01004-06.

Gorjifard, S. and Goldszmid, R. S. (2016) 'Microbiota--myeloid cell crosstalk beyond the gut', *Journal of Leukocyte Biology*, 100(November), pp. 1–16. doi: 10.1189/jlb.3RI0516-222R.

Gouveia, K. and Hurst, J. L. (2017) 'Optimising reliability of mouse performance in behavioural testing: the major role of non-aversive handling', *Scientific Reports*, 7(1), p. 44999. doi: 10.1038/srep44999.

Grandi, A. *et al.* (2017) 'α7 Nicotinic Agonist AR-R17779 Protects Mice against 2,4,6-Trinitrobenzene Sulfonic Acid-Induced Colitis in a Spleen-Dependent Way', *Frontiers in Pharmacology*, 8, p. 809. doi: 10.3389/fphar.2017.00809.

Graney, M. J. and Graney, C. M. (1980) ‘Colorectal surgery from antiquity to the modern era.’, *Diseases of the colon and rectum*, 23(6), pp. 432–441.

Gressler, M. *et al.* (2019) ‘Definition of the Anti-inflammatory Oligosaccharides Derived From the Galactosaminogalactan (GAG) From Aspergillus fumigatus’, *Frontiers in Cellular and Infection Microbiology*, 9, p. 365. doi: 10.3389/fcimb.2019.00365.

Grivennikov, S. I., Greten, F. R. and Karin, M. (2010) ‘Immunity, Inflammation, and Cancer’, *Cell*, 140(6), pp. 883–899. doi: 10.1016/j.cell.2010.01.025.

Gronert, B. K. *et al.* (1998) ‘Identification of a human enterocyte lipoxin a4 receptor that is regulated by IL13 and IFNg and inhibits TNFa induced IL8 release’, *J Exp Med*, 187(8), pp. 1285–1294.

Gronert, K. (2005) ‘Lipoxins in the eye and their role in wound healing’, *Prostaglandins Leukotrienes and Essential Fatty Acids*, 73(3–4), pp. 221–229. doi: 10.1016/j.plefa.2005.05.009.

Grzegorski, S. J. *et al.* (2014) ‘Natural variability of Kozak sequences correlates with function in a zebrafish model’, *PLoS ONE*, 9(9). doi: 10.1371/journal.pone.0108475.

Guida, F. *et al.* (2017) ‘Antibiotic-induced microbiota perturbation causes gut endocannabinoidome changes, hippocampal neuroglial reorganization and depression in mice’, *Brain, Behavior, and Immunity*. doi: 10.1016/j.bbi.2017.09.001.

Guimarães, F. R. *et al.* (2018) ‘The inhibition of 5-Lipoxygenase (5-LO) products leukotriene B4 (LTB 4) and cysteinyl leukotrienes (cysLTs) modulates the inflammatory response and improves cutaneous wound healing’, *Clinical Immunology*, 190, pp. 74–83. doi: 10.1016/j.clim.2017.08.022.

Gulyás, M. *et al.* (2016) ‘AnimalTracker : An ImageJ-Based Tracking API to Create a Customized Behaviour Analyser Program’, *Neuroinformatics*, pp. 479–481. doi: 10.1007/s12021-016-9303-z.

Guo, S. and DiPietro, L. A. (2010) ‘Factors Affecting Wound Healing’, *Journal of Dental Research*, 89(3), pp. 219–229. doi: 10.1177/0022034509359125.

Gury-benari, M. *et al.* (2016) ‘The Spectrum and Regulatory Landscape of Intestinal Innate Lymphoid Cells Are Shaped by the Article The Spectrum and Regulatory Landscape of Intestinal Innate Lymphoid Cells Are Shaped by the Microbiome’, pp. 1231–1246. doi: 10.1016/j.cell.2016.07.043.

Guttman, J. A. *et al.* (2006) ‘Evidence that Tight Junctions Are Disrupted Due to Intimate Bacterial Contact and Not Inflammation during Attaching and Effacing Pathogen Infection In Vivo’, *Infection and Immunity*, 74(11), pp. 6075–6084. doi: 10.1128/IAI.00721-06.

Le Guyader, D. *et al.* (2008a) ‘Origins and unconventional behavior of neutrophils in developing zebrafisLe Guyader, Dorothée, Michael J Redd, Emma Colucci-Guyon, Emi Murayama, Karima Kissa, Valérie Briolat, Elodie Mordelet, Agustin Zapata, Hiroto Shinomiya,

and Philippe Herbomel. 2007.', *Blood*, 111(1), p. 132 LP – 141. doi: 10.1182/2007-06-095398.An.

Guzman Prieto, A. M. *et al.* (2016) 'Global emergence and dissemination of enterococci as nosocomial pathogens: Attack of the clones?', *Frontiers in Microbiology*, 7(MAY), pp. 1–15. doi: 10.3389/fmicb.2016.00788.

Haas, U. *et al.* (2011) 'Targeted knockdown of a structurally atypical zebrafish 12S lipoxygenase leads to severe impairment of embryonic dvelopmet', *PNAS*, 108(51), pp. 20479–20484. doi: 10.1073/pnas.

Haeggström, J. Z. (2018) 'Leukotriene biosynthetic enzymes as therapeutic targets', *Journal of Clinical Investigation*, 128(7), pp. 2680–2690. doi: 10.1172/JCI97945.

Haffter, P. *et al.* (1996) 'The identification of genes with unique and essential functions in the development of the zebrafish, Danio rerio', *Development*, 123, pp. 1–36.

Hall, A. B., Tolonen, A. C. and Xavier, R. J. (2017) 'Human genetic variation and the gut microbiome in disease', *Nature Publishing Group*, 18(11), pp. 690–699. doi: 10.1038/nrg.2017.63.

Hallback, D. A. *et al.* (1978) 'Evidence for the existence of a countercurrent exchanger in the small intestine in man', *Gastroenterology.*, 74(4), pp. 683–690.

Hamarneh, S. R. *et al.* (2017) 'Intestinal Alkaline Phosphatase Attenuates Alcohol-Induced Hepatosteatosis in Mice', *Digestive Diseases and Sciences*, 62(8), pp. 2021–2034. doi: 10.1007/s10620-017-4576-0.

Hamza, B. *et al.* (2014) 'Retrotaxis of human neutrophils during mechanical confinement inside microfluidic channels.', *Integrative biology : quantitative biosciences from nano to macro*, 6(2), pp. 175–83. doi: 10.1039/c3ib40175h.

Hanada, K. *et al.* (1978) 'Isolation and Characterization of E–64, a New Thiol Protease Inhibitor', *Agricultural and Biological Chemistry*, 42(3), pp. 523–528. doi: 10.1080/00021369.1978.10863014.

Harvie, E. A. and Huttenlocher, A. (2015) 'Non-invasive Imaging of the Innate Immune Response in a Zebrafish Larval Model of Streptococcus iniae Infection Video Link', *J. Vis. Exp.*, (9810), pp. 527883791–52788. doi: 10.3791/52788.

Hasturk, H. *et al.* (2007) 'Resolvin E1 regulates inflammation at the cellular and tissue level and restores tissue homeostasis in vivo.', *Journal of immunology (Baltimore, Md. : 1950)*, 179(10), pp. 7021–7029. doi: 10.4049/jimmunol.179.10.7021.

Haussler, M. R. *et al.* (2013) 'Molecular Mechanisms of Vitamin D Action', *Calcified Tissue International*, 92(2), pp. 77–98. doi: 10.1007/s00223-012-9619-0.

He, F. (2011) 'Laemmli-SDS-PAGE', *Bio-protocol*, 101, p. e80. doi: 10.21769/BioProtoc.80.

Heckel, E. *et al.* (2015) 'Oscillatory Flow Modulates Mechanosensitive klf2a Expression through trpv4 and trpp2 during Heart Valve Development', *Current Biology*, 25(10), pp. 1354–1361. doi: 10.1016/j.cub.2015.03.038.

Herrera, B. S. *et al.* (2015) 'LXA4 actions direct fibroblast function and wound closure', *Biochemical and Biophysical Research Communications*, 464(4), pp. 1072–1077. doi: 10.1016/j.bbrc.2015.07.076.

Hill, L. (1931) 'Spontaneous tumours in mice - influence of diet and age', *Lancet (London, England)*, pp. 966–969.

Hill-burns, E. M. *et al.* (2017) 'Parkinson ' s Disease and Parkinson ' s Disease Medications Have Distinct Signatures of the Gut Microbiome', 00(00), pp. 1–11. doi: 10.1002/mds.26942.

Hoffman, M. *et al.* (2015) 'Cutaneous wound healing is impaired in hemophilia B', *Blood*, 108(9), pp. 3053–3061. doi: 10.1182/blood-2006-05-020495.Supported.

Holmes, G. R. *et al.* (2012) 'Drift-diffusion analysis of neutrophil migration during inflammation resolution in a zebrafish model', *Advances in Hematology*, 2012. doi: 10.1155/2012/792163.

Holte, K. *et al.* (2009) 'Cyclo-oxygenase 2 inhibitors and the risk of anastomotic leakage after fast-track colonic surgery', *British Journal of Surgery*, 96(6), pp. 650–654. doi: 10.1002/bjs.6598.

Horsburgh, M. J. *et al.* (2002) 'SigmaB Modulates Virulence Determinant Expression and Stress Resistance: Characterization of a Functional rsbU Strain Derived from Staphylococcus aureus 8325-4', *Journal of Bacteriology*, 184, p. 11.

Howard, B. M. *et al.* (2017) 'Characterizing the gut microbiome in trauma: significant changes in microbial diversity occur early after severe injury', *Trauma Surgery & Acute Care Open*, 2(1), p. e000108. doi: 10.1136/tsaco-2017-000108.

Howe, K. *et al.* (2013) 'The zebrafish reference genome sequence and its relationship to the human genome.', *Nature*, 496(7446), pp. 498–503. doi: 10.1038/nature12111.

Iliev, I. D. *et al.* (2012) 'Interactions Between Commensal Fungi and the C-Type Lectin Receptor Dectin-1 Influence Colitis', *Science*, 336(6086), pp. 1314–1317. doi: 10.1126/science.1221789.

Irkorucu, O. and Comert, M. (2009) 'Effects of Sildenafil Citrate on Ischemic Colonic Anastomotic Healing in Rats: Its Relationship Between Nitric Oxide and Oxidative Stress', *World Journal of Surgery*, 33(1), pp. 160–160. doi: 10.1007/s00268-008-9767-6.

Jackson, M. A. *et al.* (2016) 'Signatures of early frailty in the gut microbiota', *Genome Medicine*, 8(1), p. 8. doi: 10.1186/s13073-016-0262-7.

Jacobsen, K. *et al.* (2011) 'Voluntary ingestion of buprenorphine in mice', *Animal Welfare*, pp. 591–596.

Jafari, M. D. *et al.* (2015) 'Perfusion assessment in laparoscopic left-sided/anterior resection (PILLAR II): A multi-institutional study', *Journal of the American College of Surgeons*, 220(1), pp. 82-92.e1. doi: 10.1016/j.jamcollsurg.2014.09.015.

Jalanka-Tuovinen, J. *et al.* (2011) 'Intestinal microbiota in healthy adults: Temporal analysis reveals individual and common core and relation to intestinal symptoms', *PLoS ONE*, 6(7). doi: 10.1371/journal.pone.0023035.

Ji, H. *et al.* (2014) 'Central cholinergic activation of a vagus nerve-to-spleen circuit alleviates experimental colitis', *Mucosal Immunology*, 7(2), pp. 335–347. doi: 10.1038/mi.2013.52.

Jiang, D. *et al.* (2016) 'Suppression of Neutrophil-Mediated Tissue Damage-A Novel Skill of Mesenchymal Stem Cells: MSCs Suppress Neutrophil-Mediated Tissue Damage', *Stem Cells*, 34(9), pp. 2393–2406. doi: 10.1002/stem.2417.

Joshi, Y. B. and Praticò, D. (2015) 'The 5-lipoxygenase pathway: oxidative and inflammatory contributions to Alzhiemer's disease phenotype', *Frontiers in Cellular Neuroscience*, 8. doi: 10.3389/fncel.2014.00436.

Jowett (1994) 'Wholemount in situ hybridizations on zebrafish embryos using a mixture of digoxigenin and fluorescein labelled probes', *Technical Bullet*, 10(3), pp. 73–74.

Junker, J. P. *et al.* (2014) 'Genome-wide RNA Tomography in the Zebrafish Embryo', *Cell*, 159(3), pp. 662–675. doi: 10.1016/j.cell.2014.09.038.

Kalan, L. *et al.* (2016a) 'Redefining the chronic-wound microbiome: Fungal communities are prevalent, dynamic, and associated with delayed healing', *mBio*, 7(5), pp. 1–12. doi: 10.1128/mBio.01058-16.

Kalan, L. *et al.* (2016b) 'Redefining the Chronic-Wound Microbiome: Fungal Communities Are Prevalent, Dynamic, and Associated with Delayed Healing', *mBio*, 7(5), pp. e01058-16, /mbio/7/5/e01058-16.atom. doi: 10.1128/mBio.01058-16.

Kalff, J. C. *et al.* (1999) 'Biphasic response to gut manipulation and temporal correlation of cellular infiltrates and muscle dysfunction in rat', *Surgery*, 126(3), pp. 498–509. doi: 10.1016/S0039-6060(99)70091-7.

Kaliannan, K. *et al.* (2013) 'Intestinal alkaline phosphatase prevents metabolic syndrome in mice', *Proceedings of the National Academy of Sciences*, 110(17), pp. 7003–7008. doi: 10.1073/pnas.1220180110.

Kang, T. *et al.* (2001) 'Subcellular Distribution and Cytokine- and Chemokine-regulated Secretion of Leukolysin/MT6-MMP/MMP-25 in Neutrophils', *Journal of Biological Chemistry*, 276(24), pp. 21960–21968. doi: 10.1074/jbc.M007997200.

Kanther, M. *et al.* (2011) 'Microbial Colonization Induces Dynamic Temporal and Spatial Patterns of NF-κB Activation in the Zebrafish Digestive Tract', *Gastroenterology*, 141(1), pp. 197–207. doi: 10.1053/j.gastro.2011.03.042.

Kanther, M. and Rawls, J. F. (2010) 'Host–microbe interactions in the developing zebrafish', *Current Opinion in Immunology*, 22(1), pp. 10–19. doi: 10.1016/j.coi.2010.01.006.

Karimi, Z. *et al.* (2019) 'Impact of olive oil and honey on healing of diabetic foot: a randomized controlled trial', *Clinical, Cosmetic and Investigational Dermatology*, Volume 12, pp. 347–354. doi: 10.2147/CCID.S198577.

Karliczek, A. *et al.* (2009) 'Surgeons lack predictive accuracy for anastomotic leakage in gastrointestinal surgery', *International Journal of Colorectal Disease*, 24(5), pp. 569–576. doi: 10.1007/s00384-009-0658-6.

Karlsson, J. *et al.* (2008) 'Regional variations in Paneth cell antimicrobial peptide expression along the mouse intestinal tract', *BMC Immunology*, 9, pp. 1–11. doi: 10.1186/1471-2172-9-37.

Karra, R. *et al.* (2015) 'Myocardial NF- κ B activation is essential for zebrafish heart regeneration', 112(43), pp. 13255–13260. doi: 10.1073/pnas.1511209112.

Kats, S. *et al.* (2009) 'Anti-inflammatory effects of alkaline phosphatase in coronary artery bypass surgery with cardiopulmonary bypass', *Recent Pat Inflamm Allergy Drug Discov*, 3(3), pp. 214–220. doi: IADD-01 [pii].

El Kebir, D. *et al.* (2009) '15-epi-lipoxin A4 inhibits myeloperoxidase signaling and enhances resolution of acute lung injury', *American Journal of Respiratory and Critical Care Medicine*, 180(4), pp. 311–319. doi: 10.1164/rccm.200810-1601OC.

El Kebir, D. and Filep, J. G. (2010) 'Role of neutrophil apoptosis in the resolution of inflammation.', *TheScientificWorldJournal*, 10, pp. 1731–1748. doi: 10.1100/tsw.2010.169.

El Kebir, D., Gjorstrup, P. and Filep, J. G. (2012) 'Resolvin E1 promotes phagocytosis-induced neutrophil apoptosis and accelerates resolution of pulmonary inflammation.', *Proceedings of the National Academy of Sciences of the United States of America*, 109(37), pp. 14983–8. doi: 10.1073/pnas.1206641109.

Kernbauer, E. *et al.* (2015) 'Gastrointestinal dissemination and transmission of Staphylococcus aureus following bacteremia', *Infection and Immunity*, 83(1), pp. 372–378. doi: 10.1128/IAI.02272-14.

Kian, K. *et al.* (2017) 'Enterococcus faecalis Modulates Immune Activation and Slows Healing During Wound Infection', 216. doi: 10.1093/infdis/jix541.

Kim, D. *et al.* (2017) 'Optimizing methods and dodging pitfalls in microbiome research', *Microbiome*, 5(1), p. 52. doi: 10.1186/s40168-017-0267-5.

Kim, J., Koo, B.-K. and Knoblich, J. A. (2020) 'Human organoids: model systems for human biology and medicine', *Nature Reviews Molecular Cell Biology*. doi: 10.1038/s41580-020-0259-3.

Kimelman, D. *et al.* (2017) 'Regulation of posterior body and epidermal morphogenesis in zebrafish by localized Yap1 and Wwtr1', *eLife*, 6, p. e31065. doi: 10.7554/eLife.31065.

Kingham, T. P. and Pachter, H. L. (2009) 'Colonic Anastomotic Leak: Risk Factors, Diagnosis, and Treatment', *Journal of the American College of Surgeons*, 208(2), pp. 269–278. doi: 10.1016/j.jamcollsurg.2008.10.015.

Kinross, J. *et al.* (2017) 'A prospective analysis of mucosal microbiome-metabonome interactions in colorectal cancer using a combined MAS 1HNMR and metataxonomic strategy', *Scientific Reports*, 7(1), p. 8979. doi: 10.1038/s41598-017-08150-3.

Kivirikko, K. I. and Liesmaa, M. (1959) 'A colorimetric method for determination of hydroxyproline in tissue hydrolysates', *Scandinavian Journal of Clinical and Laboratory Investigation*, 11(2), pp. 128–133. doi: 10.3109/00365515909060420.

Kjaer, M. *et al.* (2018) 'The effect of gender on early colonic anastomotic wound healing', *International Journal of Colorectal Disease*, 33(9), pp. 1269–1276. doi: 10.1007/s00384-018-3089-4.

Koenig, A. and Michael, J. (1997) 'Endocytosis and recycling of G protein-coupled receptors', *Trends in Pharmacological Sciences*, 18(August), pp. 276–286.

Koh, W.-P. *et al.* (2004) 'Interaction between cyclooxygenase-2 gene polymorphism and dietary n-6 polyunsaturated fatty acids on colon cancer risk: the Singapore Chinese Health Study.', *British journal of cancer*, 90(9), pp. 1760–4. doi: 10.1038/sj.bjc.6601797.

Kolachala, V. *et al.* (2005) 'TNF-α upregulates adenosine 2b (A2b) receptor expression and signaling in intestinal epithelial cells: a basis for A2bR overexpression in colitis', *Cellular and Molecular Life Sciences*, 62(22), pp. 2647–2657. doi: 10.1007/s00018-005-5328-4.

Kolaczkowska, E. and Kubes, P. (2013) 'Neutrophil recruitment and function in health and inflammation', *Nature reviews. Immunology*, 13(3), pp. 159–75. doi: 10.1038/nri3399.

Komen, N. *et al.* (2009) 'Colorectal Anastomotic Leakage : A New Experimental Model', *Journal of Surgical Research*, 155(1), pp. 7–12. doi: 10.1016/j.jss.2008.08.019.

Komuro, T. (1988) 'a n d Tissue The lattice arrangement of the collagen fibres in the submucosa of the rat small intestine : scanning electron microscopy', pp. 117–121.

König, D. *et al.* (2017) 'Dynamics of actinotrichia regeneration in the adult zebrafish fin', *Developmental Biology*, (July). doi: 10.1016/j.ydbio.2017.07.024.

Kozak, M. (1986) 'Point mutations define a sequence flanking the AUG initiator codon that modulates translation by eukaryotic ribosomes', *Cell*, 44(2), pp. 283–292. doi: 10.1016/0092-8674(86)90762-2.

Krarup, P.-M. *et al.* (2013) 'Expression and inhibition of matrix metalloproteinase (MMP)-8, MMP-9 and MMP-12 in early colonic anastomotic repair', *International Journal of Colorectal Disease*, 28(8), pp. 1151–1159. doi: 10.1007/s00384-013-1697-6.

Krek, W. (1998) 'Proteolysis and the G1-S transition - the SCF connection', *Current Opinion in Genetics & Development*, 8, pp. 26–42.

Krezalek, M. A. *et al.* (2016) 'The intestinal microbiome and surgical disease', *Current Problems in Surgery*, 53(6), pp. 257–293. doi: 10.1067/j.cpsurg.2016.06.001.

Krezalek, M. A. and Alverdy, J. C. (2018) 'The influence of intestinal microbiome on wound healing and infection', *Seminars in Colon and Rectal Surgery*, 29(1), pp. 17–20. doi: 10.1053/j.scrs.2017.09.004.

Kuhn, H. *et al.* (2018) 'The evolutionary hypothesis of reaction specificity of mammalian ALOX15 orthologs', *Progress in Lipid Research*, 72, pp. 55–74. doi: 10.1016/j.plipres.2018.09.002.

Kuhn, H., Banthiya, S. and van Leyen, K. (2015) 'Mammalian lipoxygenases and their biological relevance', *Biochimica et Biophysica Acta (BBA) - Molecular and Cell Biology of Lipids*, 1851(4), pp. 308–330. doi: 10.1016/j.bbalip.2014.10.002.

Kuhn, K. A. *et al.* (2014) 'IL-6 stimulates intestinal epithelial proliferation and repair after injury', *PLoS ONE*, 9(12), pp. 1–18. doi: 10.1371/journal.pone.0114195.

Kuijk, L. M. *et al.* (2012) 'Soluble helminth products suppress clinical signs in murine experimental autoimmune encephalomyelitis and differentially modulate human dendritic cell activation', *Molecular Immunology*, 51(2), pp. 210–218. doi: 10.1016/j.molimm.2012.03.020.

Kurihara, T. *et al.* (2013) 'Resolvin D2 restores neutrophil directionality and improves survival after burns', *FASEB Journal*, 27(6), pp. 2270–2281. doi: 10.1096/fj.12-219519.

Kusano, C. and Ferrari, B. (2015) 'The biology of nuclear factor kappa beta (NFkB) in health and pathology', *Journal of Arts*, (August 2011), pp. 2231–4172.

Kyritsis, N. *et al.* (2012) 'Acute inflammation initiates the regenerative response in the adult zebrafish brain.', *Science (New York, N.Y.)*, 338, pp. 1353–6. doi: 10.1126/science.1228773.

Lalonde, R. L. *et al.* (2016) 'Differential actinodin1 regulation in zebrafish and mouse appendages', *Developmental Biology*, 417(1), pp. 91–103. doi: 10.1016/j.ydbio.2016.05.019.

Lampa, M. *et al.* (2013) 'Clopidogrel Pharmacokinetics and Pharmacodynamics Vary Widely Despite Exclusion or Noncompliance , Diet , Smoking , Co-Medications (Including Proton

Pump Inhibitors), and Pre-Existent Variability in Platelet Function', 61(8). doi: 10.1016/j.jacc.2012.11.040.

Lan, C.-C. and Love, D. R. (2012) 'Molecular Characterisation of Bacterial Community Structure along the Intestinal Tract of Zebrafish (Danio rerio): A Pilot Study.', *ISRN microbiology*, 2012, p. 590385. doi: 10.5402/2012/590385.

Lander, E. S. (2015) 'Perspective The Heroes of CRISPR', *Cell*, 164(1–2), pp. 18–28. doi: 10.1016/j.cell.2015.12.041.

Lands, B., Bibus, D. and Stark, K. D. (2016) 'Dynamic interactions of n-3 and n-6 fatty acid nutrients', *Prostaglandins Leukotrienes and Essential Fatty Acids*, (January), pp. 0–1. doi: 10.1016/j.plefa.2017.01.012.

Lau, J. T. *et al.* (2016) 'Capturing the diversity of the human gut microbiota through culture-enriched molecular profiling', *Genome Medicine*, 8(1), p. 72. doi: 10.1186/s13073-016-0327-7.

Lau, L. F. (2011) 'CCN1/CYR61: the very model of a modern matricellular protein', *Cellular and Molecular Life Sciences*, 68(19), pp. 3149–3163. doi: 10.1007/s00018-011-0778-3.

Le Guyader, D. *et al.* (2008b) 'Origins and unconventional behavior of neutrophils in developing zebrafish', *Blood*, 111(1), pp. 132–141. doi: 10.1182/blood-2007-06-095398.

Leavitt, T. *et al.* (2016) 'Scarless wound healing: finding the right cells and signals', *Cell and Tissue Research*. doi: 10.1007/s00441-016-2424-8.

Lee, C. *et al.* (2014) 'The effect of intestinal alkaline phosphatase on intestinal epithelial cells, macrophages and chronic colitis in mice', *Life Sciences*, 100(2), pp. 118–124. doi: 10.1016/j.lfs.2014.02.003.

Lee, E.-C. *et al.* (2001) 'A Highly Efficient Escherichia coli-Based Chromosome Engineering System Adapted for Recombinogenic Targeting and Subcloning of BAC DNA', *Genomics*, 73(1), pp. 56–65. doi: 10.1006/geno.2000.6451.

Lee, J. A., Chico, T. J. A. and Renshaw, S. A. (2018) 'The triune of intestinal microbiome, genetics and inflammatory status and its impact on the healing of lower gastrointestinal anastomoses', *The FEBS Journal*, 285(7), pp. 1212–1225. doi: 10.1111/febs.14346.

Lee, J. K. and Mishra, N. (2014) 'Predicting anastomotic leak: Can we?', *Seminars in Colon and Rectal Surgery*, 25(2), pp. 74–78. doi: 10.1053/j.scrs.2014.04.003.

Lee, J. S. *et al.* (2006) 'Klf2 Is an Essential Regulator of Vascular Hemodynamic Forces In Vivo', *Developmental Cell*, 11(6), pp. 845–857. doi: 10.1016/j.devcel.2006.09.006.

Lee, S. M. *et al.* (2013) 'Bacterial colonization factors control specificity and stability of the gut microbiota', *Nature*, 501(7467), pp. 426–429. doi: 10.1038/nature12447.

Lev, R. and Griffiths, W. C. (1982) 'Colonic and small intestinal alkaline phosphatase. A histochemical and biochemical study.', *Gastroenterology*, 82(6), pp. 1427–35.

Levy, B. D. *et al.* (2001) 'Lipid mediator class switching during acute inflammation: Signals in resolution', *Nature Immunology*, 2(7), pp. 612–619. doi: 10.1038/89759.

Leystra, A. A. and Clapper, M. L. (2019) 'Gut Microbiota Influences Experimental Outcomes in Mouse Models of Colorectal Cancer', *Genes*, 10(11), p. 900. doi: 10.3390/genes10110900.

Li, Q.-Q. *et al.* (2018) '12/15 lipoxygenase: A crucial enzyme in diverse types of cell death', *Neurochemistry International*, 118, pp. 34–41. doi: 10.1016/j.neuint.2018.04.002.

Li, Y. *et al.* (2016) 'A Functional Genomics Approach to Understand Variation in Cytokine Production in Humans', *Cell*, 167(4), pp. 1099-1110.e14. doi: 10.1016/j.cell.2016.10.017.

Liguori, G. *et al.* (2016) 'Fungal dysbiosis in mucosa-associated microbiota of Crohn's disease patients', *Journal of Crohn's and Colitis*, 10(3), pp. 296–305. doi: 10.1093/ecco-jcc/jjv209.

Lipska, M. A. *et al.* (2006) 'Anastomotic Leakage after Lower Gastrointestinal Anastomosis: Men are at a Higher Risk', *ANZ Journal of Surgery*, 76(7), pp. 579–585. doi: 10.1111/j.1445-2197.2006.03780.x.

Lister, J. A. *et al.* (1999) 'nacre encodes a zebrafish microphthalmia-related protein that regulates neural-crest-derived pigement cell fate', *Development*, 128, pp. 3757–3787.

Livanos, A. E. *et al.* (2016) 'Antibiotic-mediated gut microbiome perturbation accelerates development of type 1 diabetes in mice', *Nature Microbiology*, 1(August), p. 16140. doi: 10.1038/nmicrobiol.2016.140.

Lodish, M. B. (2013) 'Kinase Inhibitors: Adverse Effects Related to the Endocrine System', *The Journal of Clinical Endocrinology & Metabolism*, 98(4), pp. 1333–1342. doi: 10.1210/jc.2012-4085.

Loffek, S., Schilling, O. and Franzke, C.-W. (2011) 'Biological role of matrix metalloproteinases: a critical balance', *European Respiratory Journal*, 38(1), pp. 191–208. doi: 10.1183/09031936.00146510.

Long, Y. *et al.* (2018) 'Effective Wound Healing Enabled by Discrete Alternative Electric Fields from Wearable Nanogenerators', *ACS Nano*, 12(12), pp. 12533–12540. doi: 10.1021/acsnano.8b07038.

Lopez, C. A. and Skaar, E. P. (2017) 'Crossed Wires: Interspecies Interference Blocks Pathogen Colonization', *Cell Host and Microbe*, 22(6), pp. 721–723. doi: 10.1016/j.chom.2017.11.016.

Lopez, J. and Grinspan, A. (2016) 'Fecal microbiota transplantation for inflammatory bowel disease', *Gastroenterology & hepatology*, 12(6), pp. 374–379.

Louis, N. A. *et al.* (2006) 'Selective induction of mucin-3 by hypoxia in intestinal epithelia', *Journal of Cellular Biochemistry*, 99(6), pp. 1616–1627. doi: 10.1002/jcb.20947.

Luci, D. *et al.* (2010) 'Discovery of ML355, a Potent and Selective Inhibitor of Human 12-Lipoxygenase', (Md), pp. 1–13.

Lukas, M. *et al.* (2010) 'Exogenous alkaline phosphatase for the treatment of patients with moderate to severe ulcerative colitis', *Inflammatory Bowel Diseases*, 16(7), pp. 1180–1186. doi: 10.1002/ibd.21161.

Macpherson, A. J., Geuking, M. B. and McCoy, K. D. (2005) 'Immune responses that adapt the intestinal mucosa to commensal intestinal bacteria', *Immunology*, 115(2), pp. 153–162. doi: 10.1111/j.1365-2567.2005.02159.x.

Maderna, P. *et al.* (2010) 'FPR2/ALX receptor expression and internalization are critical for lipoxin A_4 and annexin-derived peptide-stimulated phagocytosis', *The FASEB Journal*, 24(11), pp. 4240–4249. doi: 10.1096/fj.10-159913.

Maeda, K. *et al.* (1971) 'The structure and activity of leupeptins and related analogs', *The Journal of Antibiotics*, 24(6), pp. 402–404. doi: 10.7164/antibiotics.24.402.

Magalhaes, A. C., Dunn, H. and Ferguson, S. S. (2012) 'Regulation of GPCR activity, trafficking and localization by GPCR-interacting proteins: Regulation of G-protein-coupled receptor activity', *British Journal of Pharmacology*, 165(6), pp. 1717–1736. doi: 10.1111/j.1476-5381.2011.01552.x.

Maharshak, N. *et al.* (2015) 'Enterococcus faecalis Gelatinase Mediates Intestinal Permeability via Protease-Activated Receptor 2', *Infection and Immunity*. Edited by S. R. Blanke, 83(7), pp. 2762–2770. doi: 10.1128/IAI.00425-15.

Maier, T. J. *et al.* (2008) 'Celecoxib inhibits 5-lipoxygenase', *Biochemical Pharmacology*, 76(7), pp. 862–872. doi: 10.1016/j.bcp.2008.07.009.

Malo, M. S. *et al.* (2014) 'Intestinal alkaline phosphatase promotes gut bacterial growth by reducing the concentration of luminal nucleotide triphosphates', *American Journal of Physiology-Gastrointestinal and Liver Physiology*, 306(10), pp. G826–G838. doi: 10.1152/ajpgi.00357.2013.

Mandillo, S. *et al.* (2008) 'Reliability, robustness, and reproducibility in mouse behavioral phenotyping: a cross-laboratory study', *Physiological Genomics*, 34(3), pp. 243–255. doi: 10.1152/physiolgenomics.90207.2008.

Mangino, M. J. *et al.* (2006) 'Lipoxin biosynthesis in inflammatory bowel disease', *Prostaglandins and Other Lipid Mediators*, 79(1–2), pp. 84–92. doi: 10.1016/j.prostaglandins.2005.10.004.

Mangoni, M. L., McDermott, A. M. and Zasloff, M. (2016) 'Antimicrobial peptides and wound healing: biological and therapeutic considerations', *Experimental Dermatology*, 25(3), pp. 167–173. doi: 10.1111/exd.12929.

Mani, N., Tobin, P. and Jayaswal, R. K. (1993) 'Isolation and characterization of autolysis-defective mutants of Staphylococcus aureus created by Tn917-lacZ mutagenesis', *Journal of Bacteriology*, 175(5), pp. 1493–1499. doi: 10.1128/jb.175.5.1493-1499.1993.

Manieri, N. A. *et al.* (2012) 'Igf2bp1 is required for full induction of Ptgs2 mRNA in colonic mesenchymal stem cells in mice', *Gastroenterology*, 143(1), pp. 110–121. doi: 10.1053/j.gastro.2012.03.037.Igf2bp1.

Marks, E. *et al.* (2017) 'Regulation of IL-12p40 by HIF controls Th1/Th17 responses to prevent mucosal inflammation', *Mucosal Immunology*, (January), pp. 1–13. doi: 10.1038/mi.2016.135.

Martel-Pelletier, J. (2003) 'Therapeutic role of dual inhibitors of 5-LOX and COX, selective and non-selective non-steroidal anti-inflammatory drugs', *Annals of the Rheumatic Diseases*, 62(6), pp. 501–509. doi: 10.1136/ard.62.6.501.

Martens, M. F. and Hendriks, T. (1991) 'Postoperative changes in collagen synthesis in intestinal anastomoses of the rat: differences between small and large bowel.', *Gut*, 32(12), pp. 1482–1487. doi: 10.1136/gut.32.12.1482.

Martin, P. *et al.* (2003) 'Wound healing in the PU.1 Null Mouse - Tissue repair is not dependent on inflammatory Cells', *Current Biology*, 13, pp. 1122–1128. doi: 10.1016/S.

Mastboom, W. J. B., Hendriks, T. and de Boer, H. H. M. (1989) 'Collagen changes around intestinal anastomoses in germ-free rats', *British Journal of Surgery*, 76(8), pp. 797–801. doi: 10.1002/bjs.1800760811.

Matrone, G. *et al.* (2013) 'Laser-targeted ablation of the zebrafish embryonic ventricle: A novel model of cardiac injury and repair', *International Journal of Cardiology*, 168(4), pp. 3913–3919. doi: 10.1016/j.ijcard.2013.06.063.

Matsumoto, M. *et al.* (2011) 'Longevity in mice is promoted by probiotic-induced suppression of colonic senescence dependent on upregulation of gut bacterial polyamine production', *PLoS ONE*, 6(8). doi: 10.1371/journal.pone.0023652.

Mayer, J. (2007) 'Use of behavior analysis to recognize pain in small mammals', *Lab Animal*, 36(6), pp. 43–48. doi: 10.1038/laban0607-43.

Mazmanian, S. K. *et al.* (2005) 'An immunomodulatory molecule of symbiotic bacteria directs maturation of the host immune system', *Cell*, 122(1), pp. 107–118. doi: 10.1016/j.cell.2005.05.007.

Mazmanian, S. K., Round, J. L. and Kasper, D. L. (2008) 'A microbial symbiosis factor prevents intestinal inflammatory disease', *Nature*, 453(7195), pp. 620–625. doi: 10.1038/nature07008.

McComb, R., Bowers, G. and Posen, S. (1979) *Alkaline Phosphatase*. Plenum Press, New York, USA.

McDermott, F. D. *et al.* (2015) 'Systematic review of preoperative, intraoperative and postoperative risk factors for colorectal anastomotic leaks', *British Journal of Surgery*, 102(5), pp. 462–479. doi: 10.1002/bjs.9697.

McLachlin, A. D. and Denton, D. W. (1973) 'Omental protection of intestinal anastomoses', *The American Journal of Surgery*, 125(1), pp. 134–140. doi: 10.1016/0002-9610(73)90018-4.

Medina, E. *et al.* (2007) 'Antimicrobial Activity of Olive Oil, Vinegar, and Various Beverages against Foodborne Pathogens', *Journal of Food Protection*, 70(5), pp. 1194–1199. doi: 10.4315/0362-028X-70.5.1194.

Melo, A. D. B. *et al.* (2016) 'Intestinal alkaline phosphatase and sodium butyrate may be beneficial in attenuating LPS-induced intestinal inflammation', *Genetics and Molecular Research*, 15(4). doi: 10.4238/gmr15048875.

Meng, X., Ahator, S. D. and Zhang, L.-H. (2020) 'Molecular Mechanisms of Phosphate Stress Activation of *Pseudomonas aeruginosa* Quorum Sensing Systems', *mSphere*. Edited by C. D. Ellermeier, 5(2), pp. e00119-20, /msphere/5/2/mSphere119-20.atom. doi: 10.1128/mSphere.00119-20.

Mente, B. B. *et al.* (1996) 'Influence of Pulsed Electromagnetic Fields on Healing of Experimental Colonic Anastomosis', *Dis Colon and Rectum*, (39), pp. 1031–1038.

Merad, F. *et al.* (1998) 'Omentoplasty in the Prevention of Anastomotic Leakage After Colonic or Rectal Resection: A Prospective Randomized Study in 712 Patients', *Annals of Surgery*, 227(2), pp. 179–186. doi: 10.1097/00000658-199802000-00005.

Mestre, J. R. *et al.* (2001) 'Redundancy in the Signaling Pathways and Promoter Elements Regulating Cyclooxygenase-2 Gene Expression in Endotoxin-treated Macrophage/Monocytic Cells', *Journal of Biological Chemistry*, 276(6), pp. 3977–3982. doi: 10.1074/jbc.M005077200.

Migeotte, I., Communi, D. and Parmentier, M. (2006) 'Formyl peptide receptors: A promiscuous subfamily of G protein-coupled receptors controlling immune responses', *Cytokine & Growth Factor Reviews*, 17(6), pp. 501–519. doi: 10.1016/j.cytogfr.2006.09.009.

Minguet, S. *et al.* (2005) 'Adenosine and cAMP are potent inhibitors of the NF-?B pathway downstream of immunoreceptors', *European Journal of Immunology*, 35(1), pp. 31–41. doi: 10.1002/eji.200425524.

Misawa, Y. *et al.* (2015) 'Staphylococcus aureus Colonization of the Mouse Gastrointestinal Tract Is Modulated by Wall Teichoic Acid, Capsule, and Surface Proteins', *PLoS Pathogens*, 11(7), pp. 1–21. doi: 10.1371/journal.ppat.1005061.

Mizoguchi, A. (2012) 'Healing of intestinal inflammation by IL-22':, *Inflammatory Bowel Diseases*, 18(9), pp. 1777–1784. doi: 10.1002/ibd.22929.

Moe, H., Rostgaard, J. and Behnke, O. (1965) 'On the Morphology and Origin of Virgin Lysosomes in the Intestinal Epithelium of the Rat 1', 403, pp. 396–403.

Moghadamyeghaneh, Z. *et al.* (2016) 'Risk factors for prolonged ileus following colon surgery', *Surgical Endoscopy and Other Interventional Techniques*, 30(2), pp. 603–609. doi: 10.1007/s00464-015-4247-1.

Montedori, A. *et al.* (2010) 'Covering ileo- or colostomy in anterior resection for rectal carcinoma', *Cochrane Database of Systematic Reviews*. Edited by Cochrane Colorectal Cancer Group. doi: 10.1002/14651858.CD006878.pub2.

Montesinos, M. C. *et al.* (2002) 'Adenosine promotes wound healing and mediates angiogenesis in response to tissue injury via occupancy of A2Areceptors', *American Journal of Pathology*, 160(6), pp. 2009–2018. doi: 10.1016/S0002-9440(10)61151-0.

Morris, J. L. *et al.* (2018) 'Live imaging of collagen deposition during skin development and repair in a collagen I – GFP fusion transgenic zebra fish line', *Developmental Biology*, 441(1), pp. 4–11. doi: 10.1016/j.ydbio.2018.06.001.

Moslemi, S. *et al.* (2016) 'Effect of human amniotic membrane on prevention of colorectal anastomosis leakage in cases with neoadjuvant radiotherapy: An experimental animal study', *Iranian Journal of Medical Sciences*, 41(6), pp. 501–506.

Motomura, Y. *et al.* (2009) 'Helminth antigen-based strategy to ameliorate inflammation in an experimental model of colitis', *Clinical & Experimental Immunology*, 155(1), pp. 88–95. doi: 10.1111/j.1365-2249.2008.03805.x.

Mungo, B. *et al.* (2017) 'The Impact of Operative Approach on Postoperative Complications Following Colectomy for Colon Caner', *World Journal of Surgery*. doi: 10.1007/s00268-017-4001-z.

Muniz, L. R., Knosp, C. and Yeretssian, G. (2012) 'Intestinal antimicrobial peptides during homeostasis, infection, and disease', *Frontiers in Immunology*, 3. doi: 10.3389/fimmu.2012.00310.

Murall, C. L., Abbate, J. L. and Touzel, M. P. (2017) *Invasions of Host-Associated Microbiome Networks*. 1st edn, *Networks of Invasion: Empirical Evidence and Case Studies*. 1st edn. Elsevier Ltd. doi: 10.1016/bs.aecr.2016.11.002.

Murphy, J. E. and Kantrowitz, E. R. (1994) 'Why are mammalian alkaline phosphatases much more active than bacterial alkaline phosphatases?', *Molecular Microbiology*, 12(3), pp. 351–357. doi: 10.1111/j.1365-2958.1994.tb01024.x.

Na, Y. R. *et al.* (2015) 'Consistent inhibition of cyclooxygenase drives macrophages towards the inflammatory phenotype', *PLoS ONE*, 10(2), pp. 1–13. doi: 10.1371/journal.pone.0118203.

Nakamura, H. *et al.* (2016) 'The effects of bevacizumab on intestinal anastomotic healing in rabbits', *Surgery Today*, 46(12), pp. 1456–1463. doi: 10.1007/s00595-016-1342-4.

Nakano, T. *et al.* (2009) 'Role of lysophosphatidylcholine in brush-border intestinal alkaline phosphatase release and restoration', *American Journal of Physiology-Gastrointestinal and Liver Physiology*, 297(1), pp. G207–G214. doi: 10.1152/ajpgi.90590.2008.

Narisawa, S. *et al.* (2003) 'Accelerated Fat Absorption in Intestinal Alkaline Phosphatase Knockout Mice', *Molecular and Cellular Biology*, 23(21), pp. 7525–7530. doi: 10.1128/MCB.23.21.7525-7530.2003.

Newell, M. *et al.* (2017) 'A Critical Review on the Effect of Docosahexaenoic Acid (DHA) on Cancer Cell Cycle Progression', *International Journal of Molecular Sciences*, 18(8), p. 1784. doi: 10.3390/ijms18081784.

Nguyen, D. H. *et al.* (2013) 'Quantifying chromogen intensity in immunohistochemistry via reciprical intensity', *Cancer InCytes*, 2(1). doi: 10.1038/protex.2013.097.

Nikhil, V. (2013) *Expression of G-Protein coupled receptors in young and mature thrombocytes and knockdown of gpr18 in zebrafish (M Sc . Dissertation)*.

Niki, D., Katsu, K. and Yokouchi, Y. (2009) 'Ontogeny of angiopoietin-like protein 1, 2, 3, 4, 5, and 7 genes during chick embryonic development: Expression patterns of chick Angptls', *Development, Growth & Differentiation*, 51(9), pp. 821–832. doi: 10.1111/j.1440-169X.2009.01145.x.

Nishio, N. *et al.* (2008) 'Neutrophil depletion delays wound repair in aged mice', *Age*, 30(1), pp. 11–19. doi: 10.1007/s11357-007-9043-y.

Nordentoft, T. *et al.* (2015) 'Fibrin Glue Does Not Improve Healing of Gastrointestinal Anastomoses : A Systematic Review', *Eu J Surg Research*, 54, pp. 1–13. doi: 10.1159/000366418.

Norling, L. V. *et al.* (2012) 'Resolvin D1 limits polymorphonuclear leukocyte recruitment to inflammatory loci: Receptor-dependent actions', *Arteriosclerosis, Thrombosis, and Vascular Biology*, 32(8), pp. 1970–1978. doi: 10.1161/ATVBAHA.112.249508.

Norling, L. V. *et al.* (2016) 'Proresolving and cartilage-protective actions of resolvin D1 in inflammatory arthritis', *JCI Insight*, 1(5), pp. 1–17. doi: 10.1172/jci.insight.85922.

Norris, P. C., Libreros, S. and Serhan, C. N. (2019) 'Resolution metabolomes activated by hypoxic environment', 4.

Novak, S. *et al.* (2016) 'Anti-Inflammatory Effects of Hyperbaric Oxygenation during DSS-Induced Colitis in BALB/c Mice Include Changes in Gene Expression of HIF-1a, Proinflammatory Cytokines, and Antioxidative Enzymes', *Mediators of Inflammation*, ID 7141430, p. 19. doi: 10.1155/2016/7141430.

Nursal, T. Z. *et al.* (2006) 'Effects of a static magnetic field on wound healing: results in experimental rat colon anastomoses', *American Journal of Surgery*, 192(1), pp. 76–81. doi: 10.1016/j.amjsurg.2006.01.024.

Oehlers, S. H. *et al.* (2012) 'Retinoic acid suppresses intestinal mucus production and exacerbates experimental enterocolitis', *Disease Models & Mechanisms*, 5(4), pp. 457–467. doi: 10.1242/dmm.009365.

Oehlers, S. H. *et al.* (2016) 'A whole animal chemical screen approach to identify modifiers of intestinal neutrophilic inflammation', *The FEBS Journal*. doi: 10.1111/febs.13976.

Oehlers, S. H. B. *et al.* (2010) 'Expression of zebrafish cxcl8 (interleukin-8) and its receptors during development and in response to immune stimulation', *Developmental & Comparative Immunology*, 34(3), pp. 352–359. doi: 10.1016/j.dci.2009.11.007.

Ogilvie, L. A. and Jones, B. V. (2015) 'The human gut virome: A multifaceted majority', *Frontiers in Microbiology*, 6(SEP), pp. 1–12. doi: 10.3389/fmicb.2015.00918.

O'Hara, A. M. and Shanahan, F. (2006) 'The gut flora as a forgotten organ', *EMBO reports*, 7(7), pp. 688–693. doi: 10.1038/sj.embor.7400731.

Ohigashi, S. *et al.* (2013) 'Significant Changes in the Intestinal Environment After Surgery in Patients with Colorectal Cancer', *Journal of Gastrointestinal Surgery*, 17(9), pp. 1657–1664. doi: 10.1007/s11605-013-2270-x.

Ohlemacher, S. I. *et al.* (2017) 'Enterobacteria secrete an inhibitor of Pseudomonas virulence during clinical bacteriuria', *The Journal of Clinical Investigation*, 127(11), pp. 1–13. doi: 10.1172/JCI92464.

Okada, M. (1994) 'The influence of intestinal flora on wound healing in mice', *Surgery Today*, 24(4), pp. 347–355. doi: 10.1007/BF02348566.

Okada, M. *et al.* (1999) 'Experimental study of the influence of intestinal flora on the healing of intestinal anastomoses.', *The British journal of surgery*, 86(7), pp. 961–965. doi: 10.1046/j.1365-2168.1999.01161.x.

Olivas, A. D. *et al.* (2012) 'Intestinal Tissues Induce an SNP Mutation in Pseudomonas aeruginosa That Enhances Its Virulence: Possible Role in Anastomotic Leak', *PLoS ONE*, 7(8). doi: 10.1371/journal.pone.0044326.

de Oliveira, S., Rosowski, E. E. and Huttenlocher, A. (2016) 'Neutrophil migration in infection and wound repair: going forward in reverse', *Nature Reviews Immunology*, 16(6), pp. 378–391. doi: 10.1038/nri.2016.49.

Ongaro, A. *et al.* (2012) 'Electromagnetic fields (EMFs) and adenosine receptors modulate prostaglandin E 2 and cytokine release in human osteoarthritic synovial fibroblasts', *Journal of Cellular Physiology*, 227(6), pp. 2461–2469. doi: 10.1002/jcp.22981.

O'Sullivan, S., Gilmer, J. F. and Medina, C. (2015) 'Matrix Metalloproteinases in Inflammatory Bowel Disease: An Update', *Mediators of Inflammation*, 2015, pp. 1–19. doi: 10.1155/2015/964131.

Padmanabhan, P. *et al.* (2013) 'Gastrointestinal transit measurements in mice with 99mTc-DTPA-labeled activated charcoal using NanoSPECT-CT', *EJNMMI Research*, 3(1), p. 60. doi: 10.1186/2191-219X-3-60.

Painsipp, E. *et al.* (2011) 'Sex-dependent control of murine emotional-affective behaviour in health and colitis by peptide YY and neuropeptide Y: Emotional behaviour, colitis and peptide YY', *British Journal of Pharmacology*, 163(6), pp. 1302–1314. doi: 10.1111/j.1476-5381.2011.01326.x.

Pankevich, D. E. and Bale, T. L. (2008) 'Stress and Sex Influences on Food-seeking Behaviors', *Obesity*, 16(7), pp. 1539–1544. doi: 10.1038/oby.2008.221.

Pantelis, D. *et al.* (2010) 'The effect of sealing with a fixed combination of collagen matrix-bound coagulation factors on the healing of colonic anastomoses in experimental high-risk mice models', *Langenbeck's Archives of Surgery*, 395(8), pp. 1039–1048. doi: 10.1007/s00423-010-0703-5.

Paschoal, V. A. *et al.* (2013) 'Eicosapentaenoic (EPA) and docosahexaenoic (DHA) acid differentially modulate rat neutrophil function in vitro', *Lipids*, 48(2), pp. 93–103. doi: 10.1007/s11745-012-3726-6.

Paterson, M. J., Oh, S. and Underhill, D. M. (2017) 'Host–microbe interactions: commensal fungi in the gut', *Current Opinion in Microbiology*, 40, pp. 131–137. doi: 10.1016/j.mib.2017.11.012.

Pathan, M. *et al.* (2015) 'FunRich: An open access standalone functional enrichment and interaction network analysis tool', *Proteomics*, 15(15), pp. 2597–2601. doi: 10.1002/pmic.201400515.

Pazos, M. A. *et al.* (2015) 'Distinct Cellular Sources of Hepoxilin A 3 and Leukotriene B 4 Are Used To Coordinate Bacterial-Induced Neutrophil Transepithelial Migration', *The Journal of Immunology*, 194(3), pp. 1304–1315. doi: 10.4049/jimmunol.1402489.

Pearce, S. C. *et al.* (2018) 'Intestinal in vitro and ex vivo Models to Study Host-Microbiome Interactions and Acute Stressors', *Frontiers in Physiology*, 9, p. 1584. doi: 10.3389/fphys.2018.01584.

Pei, W. and Burgess, S. M. (2019) 'Microinjection in Zebrafish for Genome Editing and Functional Studies', in Liu, C. and Du, Y. (eds) *Microinjection*, pp. 459–474. doi: 10.1007/978-1-4939-8831-0_26.

Pesce, M. *et al.* (2013) 'Extremely low frequency electromagnetic field and wound healing: Implication of cytokines as biological mediators', *European Cytokine Network*, 24(1), pp. 1–10. doi: 10.1684/ecn.2013.0332.

Peters, E., Masereeuw, R. and Pickkers, P. (2014a) 'The potential of alkaline phosphatase as a treatment for sepsis-associated acute kidney injury', *Nephron - Clinical Practice*, 127(1–4), pp. 144–148. doi: 10.1159/000363256.

Peters, E., Masereeuw, R. and Pickkers, P. (2014b) 'The Potential of Alkaline Phosphatase as a Treatment for Sepsis-Associated Acute Kidney Injury', *Nephron Clinical Practice*, 127(1–4), pp. 144–148. doi: 10.1159/000363256.

Petersson, J. *et al.* (2011) 'Importance and regulation of the colonic mucus barrier in a mouse model of colitis.', *American journal of physiology. Gastrointestinal and liver physiology*, 300(2), pp. G327–G333. doi: 10.1152/ajpgi.00422.2010.

Pettengill, M. *et al.* (2017) 'Human alkaline phosphatase dephosphorylates microbial products and is elevated in preterm neonates with a history of late-onset sepsis', *PLoS ONE*, 12(4), pp. 1–12. doi: 10.1371/journal.pone.0175936.

Pettitt, T. R., Rowley, A. F. and Secombes, C. J. (1989) 'Lipoxins are major lipoxygenase products of rainbow trout macrophages', *FEBS Letters*, 259(1), pp. 168–170. doi: 10.1016/0014-5793(89)81520-0.

Phan, H.-E. *et al.* (2019) 'Differential actinodin1 regulation in embryonic development and adult fin regeneration in Danio rerio', *PLOS ONE*. Edited by M. Schubert, 14(5), p. e0216370. doi: 10.1371/journal.pone.0216370.

Piazzi, G. *et al.* (2014) 'Eicosapentaenoic acid free fatty acid prevents and suppresses colonic neoplasia in colitis-associated colorectal cancer acting on Notch signaling and gut microbiota', *International Journal of Cancer*, 135(9), pp. 2004–2013. doi: 10.1002/ijc.28853.

Pickkers, P. *et al.* (2012) 'Alkaline phosphatase for treatment of sepsis- induced acute kidney injury : a prospective randomized double-blind placebo-controlled trial', *Critical Care*, 16(1), p. R14. doi: 10.1186/cc11159.

Pierce, G. F. (2001) 'Inflammation in nonhealing diabetic wounds: the space-time continuum does matter.', *The American journal of pathology*, 159(2), pp. 399–403. doi: 10.1016/S0002-9440(10)61709-9.

Pillai, P. S. *et al.* (2012) 'Chemical mediators of inflammation and resolution in post-operative abdominal aortic aneurysm patients', *Inflammation*, 35(1), pp. 98–113. doi: 10.1007/s10753-011-9294-8.

Polacek, M. A. and Close, A. S. (1963) 'The effect of antibiotic bowel preparation and peritoneal irrigation on the duration of post-operative ileus', *Am.J Surg.*, 105(June), pp. 768–770.

Polistena, A. *et al.* (2011) 'Matrilysin Expression Related to Radiation and Microflora Changes in Murine Bowel', *Journal of Surgical Research*, 167(2), pp. e137–e143. doi: 10.1016/j.jss.2010.12.031.

Pommergaard, H. *et al.* (2015) 'Impaired Blood Supply in the Colonic Anastomosis in Mice Compromises Healing', *Int Surg*, 100, pp. 70–76. doi: 10.9738/INTSURG-D-13-00191.1.

Pommergaard, H.-C. (2014) ‘Experimental evaluation of clinical colon anastomotic leakage.’, *Danish medical journal*, 61(3), p. B4821.

Poole, E. M. *et al.* (2007) ‘Genetic variability in prostaglandin synthesis, fish intake and risk of colorectal polyps’, *Carcinogenesis*, 28(6), pp. 1259–1263. doi: 10.1093/carcin/bgm026.

Poth, E. J. (1982) ‘Historical development of intestinal antisepsis.’, *World journal of surgery*, 6(2), pp. 153–159. doi: 10.1007/BF01654682.

Prajsnar, T. K. *et al.* (2008) ‘A novel vertebrate model of Staphylococcus aureus infection reveals phagocyte-dependent resistance of zebrafish to non-host specialized pathogens’, *Cellular Microbiology*, 10(11), pp. 2312–2325. doi: 10.1111/j.1462-5822.2008.01213.x.

Prajsnar, T. K. *et al.* (2013) ‘Zebrafish as a novel vertebrate model to dissect enterococcal pathogenesis’, *Infection and Immunity*, 81(11), pp. 4271–4279. doi: 10.1128/IAI.00976-13.

Prat, C. *et al.* (2009) ‘A homolog of formyl peptide receptor-like 1 (FPRL1) inhibitor from Staphylococcus aureus (FPRL1 inhibitory protein) that inhibits FPRL1 and FPR.’, *Journal of immunology (Baltimore, Md. : 1950)*, 183(10), pp. 6569–6578. doi: 10.4049/jimmunol.0801523.

Prejean, J. D. *et al.* (1973) ‘Spontaneous Tumors in Sprague-Dawley Rats and Swiss Mice’, *Cancer Research*, 33, pp. 268–2272.

Price, G. H., Dubois, J. and Gilbert, C. S. (1979) ‘Alkaline phosphatase in the healing burn wound of the rat’, *Journal of Surgical Research*, 27(5), pp. 312–317. doi: 10.1016/0022-4804(79)90145-8.

Pull, S. L. *et al.* (2005) ‘Activated macrophages are an adaptive element of the colonic epithelial progenitor niche necessary for regenerative responses to injury.’, *Proceedings of the National Academy of Sciences of the United States of America*, 102(1), pp. 99–104. doi: 10.1073/pnas.0405979102.

Qiu, X. *et al.* (2015) ‘Changes in the composition of intestinal fungi and their role in mice with dextran sulfate sodium-induced colitis’, *Scientific Reports*, 5(1), p. 10416. doi: 10.1038/srep10416.

Rainuzzo, J. R., Reitan, K. J. I. and Jorgensen, L. (1992) ‘Comparative study on thefatty acid and lipid composition of four marine fish larvae’, *Comp Biochem Physiol*, 103B(1), pp. 21–26.

Raju, D. P. *et al.* (2015) ‘Efficacy and safety of low-dose celecoxib in reducing post-operative paralytic ileus after major abdominal surgery’, *ANZ Journal of Surgery*, 85(12), pp. 946–950. doi: 10.1111/ans.12475.

Ramasamy, S. *et al.* (2011) ‘Intestinal alkaline phosphatase has beneficial effects in mouse models of chronic colitis’:, *Inflammatory Bowel Diseases*, 17(2), pp. 532–542. doi: 10.1002/ibd.21377.

Rampon, C. *et al.* (2014) 'Adenosine enhances progenitor cell recruitment and nerve growth via its A2B receptor during adult fin regeneration', pp. 595–602. doi: 10.1007/s11302-014-9420-9.

Ramsey, M. M. *et al.* (2016) 'Staphylococcus aureus Shifts toward commensalism in response to corynebacterium species', *Frontiers in Microbiology*, 7(AUG), pp. 1–15. doi: 10.3389/fmicb.2016.01230.

Ran, S., He, Z. and Liang, J. (2013) 'Survival of Enterococcus faecalis during alkaline stress: Changes in morphology, ultrastructure, physiochemical properties of the cell wall and specific gene transcripts', *Archives of Oral Biology*, 58(11), pp. 1667–1676. doi: 10.1016/j.archoralbio.2013.08.013.

Rana, S. and Baranski, T. J. (2010) 'Third Extracellular Loop (EC3)-N Terminus Interaction Is Important for Seven-transmembrane Domain Receptor Function: Implications for an activation microswitch region', *Journal of Biological Chemistry*, 285(41), pp. 31472–31483. doi: 10.1074/jbc.M110.129213.

Rather, L. J. (1971) 'Disturbance of function (functio laesa): the legendary fifth cardinal sign of inflammation, added by Galen to the four cardinal signs of Celsus.', *Bulletin of the New York Academy of Medicine*, 47(3), pp. 303–22.

Rawlings, N. D., Barrett, A. J. and Bateman, A. (2012) 'MEROPS: the database of proteolytic enzymes, their substrates and inhibitors', *Nucleic Acids Research*, 40(D1), pp. D343–D350. doi: 10.1093/nar/gkr987.

Rawls, J. F. *et al.* (2006) 'Reciprocal Gut Microbiota Transplants from Zebrafish and Mice to Germ-free Recipients Reveal Host Habitat Selection', *Cell*, 127(2), pp. 423–433. doi: 10.1016/j.cell.2006.08.043.

Rawls, J. F. *et al.* (2007) 'In vivo imaging and genetic analysis link bacterial motility and symbiosis in the zebrafish gut', *Proceedings of the National Academy of Sciences of the United States of America*, 104(18), pp. 7622–7627. doi: 10.1073/pnas.0702386104.

Rawls, J. F., Samuel, B. S. and Gordon, J. I. (2004) 'Gnotobiotic zebrafish reveal evolutionarily conserved responses to the gut microbiota', *Proc Natl Acad Sci U S A*, 101(13), pp. 4596–4601. doi: 10.1073/pnas.0400706101.

Recchiuti, A. *et al.* (2014) 'Immunoresolving actions of oral resolvin D1 include selective regulation of the transcription machinery in resolution-phase mouse macrophages', *The FASEB Journal*, 28(7), pp. 3090–3102. doi: 10.1096/fj.13-248393.

Reisinger, K. W. *et al.* (2017) 'Cyclooxygenase-2 Is Essential for Colorectal Anastomotic Healing', *Annals of Surgery*, 265(3), pp. 547–554. doi: 10.1097/SLA.0000000000001744.

Rendueles, O. *et al.* (2012) 'A new zebrafish model of oro-intestinal pathogen colonization reveals a key role for adhesion in protection by probiotic bacteria', *PLoS Pathogens*, 8(7), p. 12. doi: 10.1371/journal.ppat.1002815.

Renshaw, S. A. *et al.* (2006) 'A transgenic zebrafish model of neutrophilic inflammation', *Blood*, 108(13), pp. 3976–3978. doi: 10.1182/blood-2006-05-024075.

Reunanen, J. *et al.* (2015) 'Akkermansia muciniphila adheres to enterocytes and strengthens the integrity of the epithelial cell layer', *Applied and Environmental Microbiology*, 81(11), pp. 3655–3662. doi: 10.1128/AEM.04050-14.

Richter, J. M. *et al.* (2012) 'LPS-binding Protein Enables Intestinal Epithelial Restitution Despite LPS Exposure':, *Journal of Pediatric Gastroenterology and Nutrition*, 54(5), pp. 639–644. doi: 10.1097/MPG.0b013e31823a895a.

Rigottier-Gois, L. *et al.* (2015) 'The surface rhamnopolysaccharide epa of enterococcus faecalis is a key determinant of intestinal colonization', *Journal of Infectious Diseases*, 211(1), pp. 62–71. doi: 10.1093/infdis/jiu402.

Robinson, A. *et al.* (2008) 'Mucosal Protection by Hypoxia-Inducible Factor Prolyl Hydroxylase Inhibition', *Gastroenterology*, 134(1), pp. 145–155. doi: 10.1053/j.gastro.2007.09.033.

Roeselers, G. *et al.* (2011) 'Evidence for a core gut microbiota in the zebrafish.', *The ISME journal*, 5(10), pp. 1595–608. doi: 10.1038/ismej.2011.38.

Rohlke, F. and Stollman, N. (2012) 'Fecal microbiota transplantation in relapsing Clostridium difficile infection', pp. 403–420. doi: 10.1177/1756283X12453637.

Rolandelli, R. H., Buckmire, M. A. and Bernstein, K. A. (1997) 'Intravenous butyrate and healing of colonic anastomoses in the rat':, *Diseases of the Colon & Rectum*, 40(1), pp. 67–70. doi: 10.1007/BF02055684.

Romanowski, K. *et al.* (2011) 'Prevention of siderophore- mediated gut-derived sepsis due to P. aeruginosa can be achieved without iron provision by maintaining local phosphate abundance: role of pH', *BMC Microbiology*, 11(1), p. 212. doi: 10.1186/1471-2180-11-212.

Rombout, J. H. W. M. and van den Berg, A. A. (1985) 'Uptake and transport of ferritin in the epithelium of carp (Cyprinus Carpio L.) and the possible immunological implications', *Cell Biology International Reports*, 9(6), p. 516. doi: 10.1016/0309-1651(85)90003-7.

Rosa, A. dos S. *et al.* (2014) 'Supplementation with olive oil, but not fish oil, improves cutaneous wound healing in stressed mice: Olive and fish oils and chronic stress', *Wound Repair and Regeneration*, 22(4), pp. 537–547. doi: 10.1111/wrr.12191.

Rosato, F. E. *et al.* (1971) 'Changes in intestinal alkaline phosphatase in bowel ischemia', *Am J Surg*, 121(3), pp. 289–292. doi: 0002-9610(71)90206-6 [pii].

Rosen, J. N., Sweeney, M. F. and Mably, J. D. (2009) 'Microinjection of Zebrafish Embryos to Analyze Gene Function', *Journal of Visualized Experiments*, (25), pp. 1–5. doi: 10.3791/1115.

Rowe, F. P., Bradfield, A. and Redfern, R. (1974) ‘Food preferences of wild house-mice (*Mus musculus* L.)’, *Journal of Hygiene*, 73(3), pp. 473–478. doi: 10.1017/S0022172400042819.

Ruiz, V. E. *et al.* (2017) ‘A single early-in-life macrolide course has lasting effects on murine microbial network topology and immunity’, *Nature Communications*, 8(1), p. 518. doi: 10.1038/s41467-017-00531-6.

Russo, P. *et al.* (2015) ‘Zebrafish gut colonization by mCherry-labelled lactic acid bacteria’, *Applied Microbiology and Biotechnology*, 99(8), pp. 3479–3490. doi: 10.1007/s00253-014-6351-x.

Ryan, F. P. *et al.* (1978) ‘Hyposplenism in inflammatory bowel disease’, *Gut*, 19, pp. 50–55.

Salamaga, B. *et al.* (2017) ‘Bacterial size matters: Multiple mechanisms controlling septum cleavage and diplococcus formation are critical for the virulence of the opportunistic pathogen Enterococcus faecalis’, *PLOS Pathogens*. Edited by D. S. Schneider, 13(7), p. e1006526. doi: 10.1371/journal.ppat.1006526.

Sánchez-Guillén, L. *et al.* (2019) ‘Risk factors for leak, complications and mortality after ileocolic anastomosis: comparison of two anastomotic techniques’, *The Annals of The Royal College of Surgeons of England*, 101(8), pp. 571–578. doi: 10.1308/rcsann.2019.0098.

Sánchez-Quesada, C. *et al.* (2018) ‘Squalene Stimulates a Key Innate Immune Cell to Foster Wound Healing and Tissue Repair’, *Evidence-Based Complementary and Alternative Medicine*, 2018, pp. 1–9. doi: 10.1155/2018/9473094.

Santos-Beneit, F. (2015) ‘The Pho regulon: a huge regulatory network in bacteria’, *Frontiers in Microbiology*, 6. doi: 10.3389/fmicb.2015.00402.

Sava, I. G., Heikens, E. and Huebner, J. (2010) ‘Pathogenesis and immunity in enterococcal infections’, *Clinical Microbiology and Infection*, 16(6), pp. 533–540. doi: 10.1111/j.1469-0691.2010.03213.x.

Schardey, H. M. *et al.* (2017) ‘Are gut bacteria associated with the development of anastomotic leaks?’, *Coloproctology*, (January), pp. 94–100. doi: 10.1007/s00053-016-0136-x.

Schiff, A. *et al.* (2016) ‘Estimated rate of post-operative anastomotic leak following colorectal surgery: A systematic review’, *J Surgery and Surgical Research*, 2(1), pp. 60–69. doi: 10.17352/2455-2968.0000.

Schindelin, J. *et al.* (2012) ‘Fiji: an open-source platform for biological-image analysis’, *Nature Methods*, 9(7), pp. 676–682. doi: 10.1038/nmeth.2019.

Schouten, S. B. *et al.* (2014) ‘Is microvessel density correlated with anastomotic leakage after low anterior resection?’, *Hepato-gastroenterology*, 61(129), pp. 90–3. doi: 10.5754/hge12817.

Schwarz, N. T. *et al.* (2001) 'Prostanoid production via COX-2 as a causative mechanism of rodent postoperative ileus', *Gastroenterology*, 121(6), pp. 1354–1371. doi: 10.1053/gast.2001.29605.

Segal, A. W. and Loewi, G. (1976) 'Neutrophil Dysfunction in Crohn'S Disease', *The Lancet*, 308(7979), pp. 219–221. doi: 10.1016/S0140-6736(76)91024-2.

Seki, H. *et al.* (2011) 'The antiinflammatory and proresolving mediator resolvin E1 protects mice from bacterial pneumonia and acute lung injury', 184(2), pp. 836–843. doi: 10.4049/jimmunol.0901809.The.

Senol, M. *et al.* (2013) 'The Effect of Fibrin Glue on the Intensity of Colonic Anastomosis in the Presence and Absence of Peritonitis: An Experimental Randomized Controlled Trial on', *ISRN surgery*, 2013, p. 521413. doi: 10.1155/2013/521413.

Serhan, C. N. (2007) 'Resolution Phase of Inflammation: Novel Endogenous Anti-Inflammatory and Proresolving Lipid Mediators and Pathways', *Annual Review of Immunology*, 25(1), pp. 101–137. doi: 10.1146/annurev.immunol.25.022106.141647.

Serhan, C. N. *et al.* (2009) 'Maresins: novel macrophage mediators with potent antiinflammatory and proresolving actions.', *The Journal of experimental medicine*, 206(1), pp. 15–23. doi: 10.1084/jem.20081880.

Serhan, C. N. (2017) 'Discovery of specialized pro-resolving mediators marks the dawn of resolution physiology and pharmacology', *Molecular Aspects of Medicine*, 58, pp. 1–11. doi: 10.1016/j.mam.2017.03.001.

Serrano, R. L. *et al.* (2004) 'Structural Analysis of the Human Golgi-associated Plant Pathogenesis Related Protein GAPR-1 Implicates Dimerization as a Regulatory Mechanism', *Journal of Molecular Biology*, 339(1), pp. 173–183. doi: 10.1016/j.jmb.2004.03.015.

Sghir, A. *et al.* (2000) 'Quantification of Bacterial Groups within Human Fecal Flora by Oligonucleotide Probe Hybridization Quantification of Bacterial Groups within Human Fecal Flora by Oligonucleotide Probe Hybridization', *Applied and Environmental Microbiology*, 66(5), pp. 2263–2266. doi: 10.1128/AEM.66.5.2263-2266.2000.Updated.

Shakhsheer, B. A. *et al.* (2017) 'Lack of evidence for tissue hypoxia as a contributing factor in anastomotic leak following colon anastomosis and segmental devascularization in rats', *International Journal of Colorectal Disease*, 32(4), pp. 539–547. doi: 10.1007/s00384-016-2737-9.

Shaw-Smith, C. J. *et al.* (2000) 'Characterisation of a novel murine intestinal serine protease, DISP', *Biochimica et Biophysica Acta (BBA) - Gene Structure and Expression*, 1490(1–2), pp. 131–136. doi: 10.1016/S0167-4781(99)00226-2.

Shen, L.-J. *et al.* (2013) 'Using modified whole-mount in situ hybridization to study mpo expression in zebrafish', *Experimental and Therapeutic Medicine*, 5(4), pp. 1043–1047. doi: 10.3892/etm.2013.947.

Shifrin, D. A. *et al.* (2012) 'Enterocyte microvillus-derived vesicles detoxify bacterial products and regulate epithelial-microbial interactions', *Current Biology*, 22(7), pp. 627–631. doi: 10.1016/j.cub.2012.02.022.

Shirazi, S. P., Beechey, R. B. and Butterworth, P. J. (1981) 'Potent inhibition of membrane-bound rat intestinal alkaline phosphatase by a new series of phosphate analogues', *Biochemical Journal*, 194(3), pp. 797–802. doi: 10.1042/bj1940797.

Shogan, B. D. *et al.* (2013) 'Do We Really Know Why Colorectal Anastomoses Leak?', *Journal of Gastrointestinal Surgery*, 17(9), pp. 1698–1707. doi: 10.1007/s11605-013-2227-0.

Shogan, B. D. *et al.* (2014) 'Intestinal anastomotic injury alters spatially defined microbiome composition and function', *Microbiome*, 2(1), p. 35. doi: 10.1186/2049-2618-2-35.

Shogan, B. D. *et al.* (2015) 'Collagen degradation and MMP9 activation by Enterococcus faecalis contribute to intestinal anastomotic leak.', *Science translational medicine*, 7(286), p. 286ra68. doi: 10.1126/scitranslmed.3010658.

Shrum, B. *et al.* (2014) 'A robust scoring system to evaluate sepsis severity in an animal model', *BMC Research Notes*, 7(1), p. 233. doi: 10.1186/1756-0500-7-233.

Silverman, M. A., Konnikova, L. and Gerber, J. S. (2017) 'Impact of Antibiotics on Necrotizing Enterocolitis and Antibiotic-Associated Diarrhea', *Gastroenterology Clinics of North America*, 46(1), pp. 61–76. doi: 10.1016/j.gtc.2016.09.010.

Simpson, D. M. and Ross, R. (1972) 'The neutrophilic leukocyte in wound repair a study with antineutrophil serum.', *Journal of Clinical Investigation*, 51(8), pp. 2009–2023. doi: 10.1172/JCI107007.

Singh, R. K. *et al.* (2017) 'Influence of diet on the gut microbiome and implications for human health', *Journal of Translational Medicine*, 15(1), p. 73. doi: 10.1186/s12967-017-1175-y.

Slieker, J. C. *et al.* (2013) 'Prevention of leakage by sealing colon anastomosis: experimental study in a mouse model', *Journal of Surgical Research*, 184(2), pp. 819–824. doi: 10.1016/j.jss.2013.04.015.

Smith, K., McCoy, K. D. and Macpherson, A. J. (2007) 'Use of axenic animals in studying the adaptation of mammals to their commensal intestinal microbiota', *Seminars in Immunology*, 19(2), pp. 59–69. doi: 10.1016/j.smim.2006.10.002.

Smith, R. E. *et al.* (2019) 'Decoration of the enterococcal polysaccharide antigen EPA is essential for virulence, cell surface charge and interaction with effectors of the innate immune system', *PLOS Pathogens*. Edited by P. M. Sullam, 15(5), p. e1007730. doi: 10.1371/journal.ppat.1007730.

Smythies, L. E. *et al.* (2005) 'Human intestinal macrophages display profound inflammatory anergy despite avid phagocytic and bacteriocidal activity', *Journal of Clinical Investigation*, 115(1), pp. 66–75. doi: 10.1172/JCI200519229.

Sokol, H. *et al.* (2008) 'Faecalibacterium prausnitzii is an anti-inflammatory commensal bacterium identified by gut microbiota analysis of Crohn disease patients', *Proceedings of the National Academy of Sciences*, 105(43), pp. 16731–16736. doi: 10.1073/pnas.0804812105.

Sollid, J. U. E. *et al.* (2014) 'Staphylococcus aureus: Determinants of human carriage', *Infection, Genetics and Evolution*, 21, pp. 531–541. doi: 10.1016/j.meegid.2013.03.020.

Sordi, R. *et al.* (2013) 'Dual role of lipoxin A4 in pneumosepsis pathogenesis', *International Immunopharmacology*, 17(2), pp. 283–292. doi: 10.1016/j.intimp.2013.06.010.

Sorge, R. E. *et al.* (2014) 'Olfactory exposure to males, including men, causes stress and related analgesia in rodents', *Nature Methods*, 11(6), pp. 629–632. doi: 10.1038/nmeth.2935.

Souza, D. G. *et al.* (2004) 'The Essential Role of the Intestinal Microbiota in Facilitating Acute Inflammatory Responses', *The Journal of Immunology*, 173(6), pp. 4137–4146. doi: 10.4049/jimmunol.173.6.4137.

Souza, P. R. and Norling, L. V (2015) 'Implications for eicosapentaenoic acid- and docosahexaenoic acid-derived resolvins as therapeutics for arthritis.', *European journal of pharmacology*, pp. 1–9. doi: 10.1016/j.ejphar.2015.05.072.

Stephens, Z. W. *et al.* (2015) 'The composition of the zebrafish intestinal microbial community varies across development.', *The ISME journal*, 10(3), pp. 1–11. doi: 10.1038/ismej.2015.140.

St-Germain, G. and Summerbell, R. (2003) *Identifying filamentous fungi: a clinical laboratory handbook*. Belmont, Star publishing.

Stones, D. *et al.* (2017) 'Zebrafish (Danio rerio) as a vertebrate model host to study colonisation, pathogenesis and transmission of foodborne Escherichia coli 0157', *mSphere*, 2(5), pp. 1–15.

Strohmeier, G. *et al.* (1995) 'The A2b adenosine receptor mediates cAMP responses to adenosine receptor agonists in human intestinal epithelia', *J Biol Chem*, 270(5), pp. 2387–2394.

Sun, L. *et al.* (2015) 'Claudin multigene family in channel catfish and their expression profiles in response to bacterial infection and hypoxia as revealed by meta-analysis of RNA-Seq datasets', *Comparative Biochemistry and Physiology - Part D: Genomics and Proteomics*, 13, pp. 60–69. doi: 10.1016/j.cbd.2015.01.002.

Sunkara, T. *et al.* (2018) 'Fecal microbiota transplant – a new frontier in inflammatory bowel disease', *Journal of Inflammation Research*, Volume 11, pp. 321–328. doi: 10.2147/JIR.S176190.

Szabady, R. L. and McCormick, B. A. (2013) 'Control of neutrophil inflammation at mucosal surfaces by secreted epithelial products', *Frontiers in Immunology*, 4(JUL), pp. 1–6. doi: 10.3389/fimmu.2013.00220.

Szpaderska, A., Zuckerman, J. and Dipietro, L. A. (2003) 'Differential injury responses in Oral Mucosal and Cutaneous Wounds', *J Dent Res*, 82(8), pp. 621–626. doi: 10.1177/154405910308200810.

Sztal, T. *et al.* (2011) 'Characterization of the laminin gene family and evolution in zebrafish', *Developmental Dynamics*, 240(2), pp. 422–431. doi: 10.1002/dvdy.22537.

Tabola, R. *et al.* (2017) 'A systematic analysis of controlled clinical trials using the NiTi CAR™ compression ring in colorectal anastomoses', *Techniques in Coloproctology*, 21(3), pp. 177–184. doi: 10.1007/s10151-017-1583-2.

Tauzin, S. *et al.* (2014) 'Redox and Src family kinase signaling control leukocyte wound attraction and neutrophil reverse migration', *The Journal of Cell Biology*, 207(5), pp. 589–598. doi: 10.1083/jcb.201408090.

Telem, D. A. *et al.* (2010) 'Risk Factors for Anastomotic Leak Following Colorectal Surgery A Case-Control Study', *Arch Surg.*, 145(4), pp. 371–376. doi: 10.1001/archsurg.2010.40.

The, F. O. *et al.* (2007) 'Intestinal handling-induced mast cell activation and inflammation in human postoperative ileus', *Gut*, 57(1), pp. 33–40. doi: 10.1136/gut.2007.120238.

Theriot, C. M. *et al.* (2014) 'Antibiotic-induced shifts in the mouse gut microbiome and metabolome increase susceptibility to Clostridium difficile infection', *Nature Communications*, 5. doi: 10.1038/ncomms4114.

Thisse, B. and Thisse, C. (2004) *Fast Release Clones: A high throughput expression analysis*, *ZFIN Direct Data Submission*. Available at: https://zfin.org/ZDB-PUB-040907-1 (Accessed: 28 July 2020).

Thornton, F. J. and Barbul, A. (1997) 'Healing in the gastrointestinal tract', *Surgical Clinics of North America*, 77(3), pp. 549–574. doi: 10.1016/S0039-6109(05)70568-5.

Ticinesi, A. *et al.* (2017) 'Gut microbiota composition is associated with polypharmacy in elderly hospitalized patients', *Scientific Reports*, 7(1), p. 11102. doi: 10.1038/s41598-017-10734-y.

Tipton, C. D. *et al.* (2020) 'Patient genetics is linked to chronic wound microbiome composition and healing', *PLOS Pathogens*. Edited by M. C. Wolfgang, 16(6), p. e1008511. doi: 10.1371/journal.ppat.1008511.

Tipton, J. and Dingman, R. (1966) 'Some aspects of wound healing in germfree animals', *Plastic and Reconstructive Surgery*, 38(6), pp. 499–506.

Titos, E. *et al.* (2011) 'Resolvin D1 and Its Precursor Docosahexaenoic Acid Promote Resolution of Adipose Tissue Inflammation by Eliciting Macrophage Polarization toward an M2-Like Phenotype', *Journal of Immunology*, 187(10), pp. 5408–5418. doi: 10.4049/jimmunol.1100225.

Tobin, D. M. *et al.* (2010) 'The lta4h locus modulates susceptibility to mycobacterial infection in zebrafish and humans', *Cell*, 140(5), pp. 717–730. doi: 10.1016/j.cell.2010.02.013.The.

Tobin, D. M. *et al.* (2012) 'Host genotype-specific therapies can optimize the inflammatory response to mycobacterial infections', *Cell*, 148(3), pp. 434–446. doi: 10.1016/j.cell.2011.12.023.

Toh, M. C. *et al.* (2013) 'Colonizing the embryonic zebrafish gut with anaerobic bacteria derived from the human gastrointestinal tract.', *Zebrafish*, 10(2), pp. 194–8. doi: 10.1089/zeb.2012.0814.

Tordoff, M. G., Downing, A. and Voznesenskaya, A. (2014) 'Macronutrient selection by seven inbred mouse strains and three taste-related knockout strains', *Physiology & Behavior*, 135, pp. 49–54. doi: 10.1016/j.physbeh.2014.05.039.

Torraca, V. *et al.* (2014) 'Macrophage-pathogen interactions in infectious diseases: new therapeutic insights from the zebrafish host model', *Disease Models & Mechanisms*, 7(7), pp. 785–797. doi: 10.1242/dmm.015594.

Trencheva, K. *et al.* (2012) 'Identifying Important Predictors for Anastomotic Leak After Colon and Rectal Resection', *Annals of Surgery*, p. 1. doi: 10.1097/SLA.0b013e318262a6cd.

Tuin, A. *et al.* (2009a) 'Role of alkaline phosphatase in colitis in man and rats', *Gut*, 58(3), pp. 379–387. doi: 10.1136/gut.2007.128868.

Tuin, A. *et al.* (2009b) 'Role of alkaline phosphatase in colitis in man and rats', *Gut*, 58(3), pp. 379–387. doi: 10.1136/gut.2007.128868.

Turabelidze, A. *et al.* (2014) 'Intrinsic Differences between Oral and Skin Keratinocytes', *PLoS ONE*. Edited by A. T. Slominski, 9(9), p. e101480. doi: 10.1371/journal.pone.0101480.

Vaishnava, S. and Hooper, L. V. (2007) 'Alkaline Phosphatase: Keeping the Peace at the Gut Epithelial Surface', *Cell Host and Microbe*, 2(6), pp. 365–367. doi: 10.1016/j.chom.2007.11.004.

Vétizou, M. *et al.* (2016) 'HHS Public Access', 350(6264), pp. 1079–1084. doi: 10.1126/science.aad1329.Anticancer.

Vignali, A. *et al.* (2000) 'Altered microperfusion at the rectal stump is predictive for rectal anastomotic leak.', *Diseases of the colon and rectum*, 43(1), pp. 76–82. doi: 10.1007/BF02237248.

Vlachopoulos, C. *et al.* (2015) 'Acute effect of sildenafil on inflammatory markers/mediators in patients with vasculogenic erectile dysfunction', *International Journal of Cardiology*, 182(C), pp. 98–101. doi: 10.1016/j.ijcard.2014.12.072.

Vlasova, A. N. *et al.* (2019) 'How the gut microbiome regulates host immune responses to viral vaccines', *Current Opinion in Virology*, 37, pp. 16–25. doi: 10.1016/j.coviro.2019.05.001.

Wada, H. *et al.* (2001) 'Distribution and properties of rat intestinal alkaline phosphatase isoenzymes.', *Experimental animals / Japanese Association for Laboratory Animal Science*, 50(2), pp. 153–8.

Wakisaka, N. *et al.* (2017) 'An Adenosine Receptor for Olfaction in Fish', *Current Biology*, 27(10), pp. 1437-1447.e4. doi: 10.1016/j.cub.2017.04.014.

Wallace, K. N. *et al.* (2005) 'Intestinal growth and differentiation in zebrafish', *Mechanisms of Development*, 122(2), pp. 157–173. doi: 10.1016/j.mod.2004.10.009.

Wang, J. *et al.* (2017) 'Visualizing the function and fate of neutrophils in sterile injury and repair', *Science*, 358(6359), pp. 111–116. doi: 10.1126/science.aam9690.

Wang, X. *et al.* (2014) 'Inhibitors of neutrophil recruitment identified using transgenic zebrafish to screen a natural product library.', *Disease models & mechanisms*, 7(1), pp. 163–9. doi: 10.1242/dmm.012047.

Wang, X. *et al.* (2017) 'Macrophage Cyclooxygenase-2 Protects Against Development of Diabetic Nephropathy', *Diabetes*, 66(2), pp. 494–504. doi: 10.2337/db16-0773.

Warusavitarne, J. and Phillips, R. K. S. (2007) 'Hemorrhoids Throughout History-A Historical Perspective', *Seminars in Colon and Rectal Surgery*, 18(3), pp. 140–146. doi: 10.1053/j.scrs.2007.07.002.

Weigand, M. (1996) 'Composition , accumulation and utilization of yolk lipids in teleost fish', *Reviews in Fish biology and fFsheries*, 6, pp. 259–286.

Weitzner, D. S. *et al.* (2015) 'Morris Water Maze Test: Optimization for Mouse Strain and Testing Environment', *Journal of Visualized Experiments*, (100), p. 52706. doi: 10.3791/52706.

Westerfield, M. (2007) *The Zebrafi sh Book: A Guide for the Laboratory Use of Zebrafish (Danio rerio)*. University of Oregon Press.

Wexler, H. and Oppenheim, J. D. (1979) 'Isolation , Characterization , and Biological Properties of an Endotoxin-Like Material from the Gram-Positive Organism Listeria monocytogenes', 23(3), pp. 845–857.

White, R. M. *et al.* (2008) 'Transparent Adult Zebrafish as a Tool for In Vivo Transplantation Analysis', *Cell Stem Cell*, 2(2), pp. 183–189. doi: 10.1016/j.stem.2007.11.002.

Wiggins, T. *et al.* (2015) 'Anastomotic reinforcement with omentoplasty following gastrointestinal anastomosis: A systematic review and meta-analysis', *Surgical Oncology*, 24(3), pp. 181–186. doi: 10.1016/j.suronc.2015.06.011.

Wilfinger, W. W., Mackey, K. and Chomczynski, P. (1997) 'Effect of pH and Ionic Strength on the Spectrophotometric Assessment of Nucleic Acid Purity', *BioTechniques*, 22(3), pp. 474–481. doi: 10.2144/97223st01.

Willenborg, S. and Eming, S. A. (2018) 'Cellular networks in wound healing', *Science*, 362(6417), pp. 891–892. doi: 10.1126/science.aav5542.

Willett, C. E. *et al.* (1999) 'Early hematopoiesis and developing lymphoid organs in the zebrafish', *Dev Dyn*, 214, pp. 323–336.

Wong, G. W. *et al.* (2004) 'Mouse Chromosome 17A3.3 Contains 13 Genes That Encode Functional Tryptic-like Serine Proteases with Distinct Tissue and Cell Expression Patterns', *Journal of Biological Chemistry*, 279(4), pp. 2438–2452. doi: 10.1074/jbc.M308209200.

Wu, L. (2005) 'Recognition of Host Immune Activation by Pseudomonas aeruginosa', *Science*, 309(5735), pp. 774–777. doi: 10.1126/science.1112422.

Wu, Z., Freek, D. and Lange, J. (2014) 'Do normal clinical signs and laboratory tests exclude anastomotic leakage?', *Journal of the American College of Surgeons*, 219(1), p. 164. doi: 10.1016/j.jamcollsurg.2014.03.044.

Wymann, M. P. and Schneiter, R. (2008) 'Lipid signalling in disease', *Nature Reviews Molecular Cell Biology*, 9(2), pp. 162–176. doi: 10.1038/nrm2335.

Xia, Y. and Zweier, J. L. (1997) 'Measurement of Myeloperoxidase in Leukocyte-Containing Tissues', *Analytical Biochemistry*, 245(1), pp. 93–96. doi: 10.1006/abio.1996.9940.

Xu, L., Jin, Y. and Qin, X. (2020) 'Comprehensive analysis of significant genes and immune cell infiltration in HPV-related head and neck squamous cell carcinoma', *International Immunopharmacology*, 87, p. 106844. doi: 10.1016/j.intimp.2020.106844.

Yeo, G. H. *et al.* (2009) 'Phylogenetic and evolutionary relationships and developmental expression patterns of the zebrafish twist gene family', *Development Genes and Evolution*, 219(6), pp. 289–300. doi: 10.1007/s00427-009-0290-z.

Yesildag, E., Muñiz, R. M. and Buyukunal, S. N. C. (2010) 'How did the surgeons treat neonates with imperforate anus in the eighteenth century?', *Pediatric Surgery International*, 26(12), pp. 1149–1158. doi: 10.1007/s00383-010-2672-8.

Young, G. P. *et al.* (1981) 'Effect of fat feeding on intestinal alkaline phosphatase activity in tissue and serum', *American Journal of Physiology-Gastrointestinal and Liver Physiology*, 241(6), pp. G461–G468.

Yu, Y. *et al.* (2003) 'TLR5-mediated activation of p38 MAPK regulates epithelial IL-8 expression via posttranscriptional mechanism.', *American journal of physiology. Gastrointestinal and liver physiology*, 285(2), pp. G282-90. doi: 10.1152/ajpgi.00503.2002.

Zarini, S. *et al.* (2014) 'Lysophospholipid acyltransferases and eicosanoid biosynthesis in zebrafish myeloid cells', *Prostaglandins and Other Lipid Mediators*, 113–115, pp. 52–61. doi: 10.1016/j.prostaglandins.2014.08.003.

Zhang, S., Wang, H. and Zhu, M.-J. (2019) ‘A sensitive GC/MS detection method for analyzing microbial metabolites short chain fatty acids in fecal and serum samples’, *Talanta*, 196, pp. 249–254. doi: 10.1016/j.talanta.2018.12.049.

Zhang, X.-H. *et al.* (2015) ‘Off-target Effects in CRISPR/Cas9-mediated Genome Engineering’, *Molecular Therapy - Nucleic Acids*, 4, p. e264. doi: 10.1038/mtna.2015.37.

Zhang, Y. A. *et al.* (2010) ‘IgT, a primitive immunoglobulin class specialized in mucosal immunity’, *Nature Immunology*, 11(9), pp. 827–835. doi: 10.1038/ni.1913.

Zhao, W. M. *et al.* (2016) ‘Branches of the NF- κ B signaling pathway regulate proliferation of oval cells in rat liver regeneration’, 15(1).

Zheng, L., Kelly, C. J. and Colgan, S. P. (2015) ‘Physiologic hypoxia and oxygen homeostasis in the healthy intestine. A Review in the Theme: Cellular Responses to Hypoxia.’, *American journal of physiology. Cell physiology*, 309(6), pp. C350-60. doi: 10.1152/ajpcell.00191.2015.

Zmora, N. *et al.* (2018) ‘Personalized Gut Mucosal Colonization Resistance to Empiric Probiotics Is Associated with Unique Host and Microbiome Features’, *Cell*, 174(6), pp. 1388-1405.e21. doi: 10.1016/j.cell.2018.08.041.

Appendix 1: TomoSeq numbered primer sequences in 5’ to 3’ direction

#	Primer sequence
1	CGATTGAGGCCGGTAATACGACTCACTATAGGGGTTCAGAGTTCTACAGTCCGACGATCCATCACGC NNNNTTTTTTTTTTTTTTTTTTTTTTTV
2	CGATTGAGGCCGGTAATACGACTCACTATAGGGGTTCAGAGTTCTACAGTCCGACGATCGTCGTCGC NNNNTTTTTTTTTTTTTTTTTTTTTTTV
3	CGATTGAGGCCGGTAATACGACTCACTATAGGGGTTCAGAGTTCTACAGTCCGACGATCACGACCG CNNNNTTTTTTTTTTTTTTTTTTTTTTV
4	CGATTGAGGCCGGTAATACGACTCACTATAGGGGTTCAGAGTTCTACAGTCCGACGATCTGATGCGC NNNNTTTTTTTTTTTTTTTTTTTTTTTV
5	CGATTGAGGCCGGTAATACGACTCACTATAGGGGTTCAGAGTTCTACAGTCCGACGATCCATCAATC NNNNTTTTTTTTTTTTTTTTTTTTTTTV
6	CGATTGAGGCCGGTAATACGACTCACTATAGGGGTTCAGAGTTCTACAGTCCGACGATCGTCGTATC NNNNTTTTTTTTTTTTTTTTTTTTTTTV
7	CGATTGAGGCCGGTAATACGACTCACTATAGGGGTTCAGAGTTCTACAGTCCGACGATCACGACAT CNNNNTTTTTTTTTTTTTTTTTTTTTTV
8	CGATTGAGGCCGGTAATACGACTCACTATAGGGGTTCAGAGTTCTACAGTCCGACGATCTGATGATC NNNNTTTTTTTTTTTTTTTTTTTTTTTV
9	CGATTGAGGCCGGTAATACGACTCACTATAGGGGTTCAGAGTTCTACAGTCCGACGATCCATCATCC NNNNTTTTTTTTTTTTTTTTTTTTTTTV
10	CGATTGAGGCCGGTAATACGACTCACTATAGGGGTTCAGAGTTCTACAGTCCGACGATCGTCGTTCC NNNNTTTTTTTTTTTTTTTTTTTTTTTV
11	CGATTGAGGCCGGTAATACGACTCACTATAGGGGTTCAGAGTTCTACAGTCCGACGATCACGACTCC NNNNTTTTTTTTTTTTTTTTTTTTTTTV
12	CGATTGAGGCCGGTAATACGACTCACTATAGGGGTTCAGAGTTCTACAGTCCGACGATCTGATGTCC NNNNTTTTTTTTTTTTTTTTTTTTTTTV
13	CGATTGAGGCCGGTAATACGACTCACTATAGGGGTTCAGAGTTCTACAGTCCGACGATCCATCAGA ANNNNTTTTTTTTTTTTTTTTTTTTTTV
14	CGATTGAGGCCGGTAATACGACTCACTATAGGGGTTCAGAGTTCTACAGTCCGACGATCGTCGTGA ANNNNTTTTTTTTTTTTTTTTTTTTTTV
15	CGATTGAGGCCGGTAATACGACTCACTATAGGGGTTCAGAGTTCTACAGTCCGACGATCACGACGA ANNNNTTTTTTTTTTTTTTTTTTTTTTV
16	CGATTGAGGCCGGTAATACGACTCACTATAGGGGTTCAGAGTTCTACAGTCCGACGATCTGATGGA ANNNNTTTTTTTTTTTTTTTTTTTTTTV
17	CGATTGAGGCCGGTAATACGACTCACTATAGGGGTTCAGAGTTCTACAGTCCGACGATCTCACACGC NNNNTTTTTTTTTTTTTTTTTTTTTTTV
18	CGATTGAGGCCGGTAATACGACTCACTATAGGGGTTCAGAGTTCTACAGTCCGACGATCCGTGTCGC NNNNTTTTTTTTTTTTTTTTTTTTTTTV
19	CGATTGAGGCCGGTAATACGACTCACTATAGGGGTTCAGAGTTCTACAGTCCGACGATCGACACCG CNNNNTTTTTTTTTTTTTTTTTTTTTTV
20	CGATTGAGGCCGGTAATACGACTCACTATAGGGGTTCAGAGTTCTACAGTCCGACGATCATGTGCGC NNNNTTTTTTTTTTTTTTTTTTTTTTTV
21	CGATTGAGGCCGGTAATACGACTCACTATAGGGGTTCAGAGTTCTACAGTCCGACGATCTCACATCA NNNNTTTTTTTTTTTTTTTTTTTTTTTV
22	CGATTGAGGCCGGTAATACGACTCACTATAGGGGTTCAGAGTTCTACAGTCCGACGATCCGTGTTCA NNNNTTTTTTTTTTTTTTTTTTTTTTTV
23	CGATTGAGGCCGGTAATACGACTCACTATAGGGGTTCAGAGTTCTACAGTCCGACGATCGACACTC ANNNNTTTTTTTTTTTTTTTTTTTTTTV
24	CGATTGAGGCCGGTAATACGACTCACTATAGGGGTTCAGAGTTCTACAGTCCGACGATCATGTGTCA NNNNTTTTTTTTTTTTTTTTTTTTTTTV
25	CGATTGAGGCCGGTAATACGACTCACTATAGGGGTTCAGAGTTCTACAGTCCGACGATCTCACAGA GNNNNTTTTTTTTTTTTTTTTTTTTTTV
26	CGATTGAGGCCGGTAATACGACTCACTATAGGGGTTCAGAGTTCTACAGTCCGACGATCCGTGTGA

	GNNNNTTTTTTTTTTTTTTTTTTTTTTV
27	CGATTGAGGCCGGTAATACGACTCACTATAGGGGTTCAGAGTTCTACAGTCCGACGATCGACACGA GNNNNTTTTTTTTTTTTTTTTTTTTTTV
28	CGATTGAGGCCGGTAATACGACTCACTATAGGGGTTCAGAGTTCTACAGTCCGACGATCATGTGGA GNNNNTTTTTTTTTTTTTTTTTTTTTTV
29	CGATTGAGGCCGGTAATACGACTCACTATAGGGGTTCAGAGTTCTACAGTCCGACGATCCTAACCGC NNNNTTTTTTTTTTTTTTTTTTTTTTV
30	CGATTGAGGCCGGTAATACGACTCACTATAGGGGTTCAGAGTTCTACAGTCCGACGATCGCTTGCGC NNNNTTTTTTTTTTTTTTTTTTTTTTV
31	CGATTGAGGCCGGTAATACGACTCACTATAGGGGTTCAGAGTTCTACAGTCCGACGATCAGCCACG CNNNNTTTTTTTTTTTTTTTTTTTTTTV
32	CGATTGAGGCCGGTAATACGACTCACTATAGGGGTTCAGAGTTCTACAGTCCGACGATCTAGGTCGC NNNNTTTTTTTTTTTTTTTTTTTTTTV
33	CGATTGAGGCCGGTAATACGACTCACTATAGGGGTTCAGAGTTCTACAGTCCGACGATCCTAACTCA NNNNTTTTTTTTTTTTTTTTTTTTTTV
34	CGATTGAGGCCGGTAATACGACTCACTATAGGGGTTCAGAGTTCTACAGTCCGACGATCGCTTGTCA NNNNTTTTTTTTTTTTTTTTTTTTTTV
35	CGATTGAGGCCGGTAATACGACTCACTATAGGGGTTCAGAGTTCTACAGTCCGACGATCAGCCATC ANNNNTTTTTTTTTTTTTTTTTTTTTTV
36	CGATTGAGGCCGGTAATACGACTCACTATAGGGGTTCAGAGTTCTACAGTCCGACGATCTAGGTTCA NNNNTTTTTTTTTTTTTTTTTTTTTTV
37	CGATTGAGGCCGGTAATACGACTCACTATAGGGGTTCAGAGTTCTACAGTCCGACGATCCTAACGA GNNNNTTTTTTTTTTTTTTTTTTTTTTV
38	CGATTGAGGCCGGTAATACGACTCACTATAGGGGTTCAGAGTTCTACAGTCCGACGATCGCTTGGA GNNNNTTTTTTTTTTTTTTTTTTTTTTV
39	CGATTGAGGCCGGTAATACGACTCACTATAGGGGTTCAGAGTTCTACAGTCCGACGATCAGCCAGA GNNNNTTTTTTTTTTTTTTTTTTTTTTV
40	CGATTGAGGCCGGTAATACGACTCACTATAGGGGTTCAGAGTTCTACAGTCCGACGATCTAGGTGA GNNNNTTTTTTTTTTTTTTTTTTTTTTV
41	CGATTGAGGCCGGTAATACGACTCACTATAGGGGTTCAGAGTTCTACAGTCCGACGATCGAATCCG ANNNNTTTTTTTTTTTTTTTTTTTTTTV
42	CGATTGAGGCCGGTAATACGACTCACTATAGGGGTTCAGAGTTCTACAGTCCGACGATCATTCGCGA NNNNTTTTTTTTTTTTTTTTTTTTTTV
43	CGATTGAGGCCGGTAATACGACTCACTATAGGGGTTCAGAGTTCTACAGTCCGACGATCTCCGACG ANNNNTTTTTTTTTTTTTTTTTTTTTTV
44	CGATTGAGGCCGGTAATACGACTCACTATAGGGGTTCAGAGTTCTACAGTCCGACGATCCGGATCG ANNNNTTTTTTTTTTTTTTTTTTTTTTV
45	CGATTGAGGCCGGTAATACGACTCACTATAGGGGTTCAGAGTTCTACAGTCCGACGATCGAATCATC NNNNTTTTTTTTTTTTTTTTTTTTTTV
46	CGATTGAGGCCGGTAATACGACTCACTATAGGGGTTCAGAGTTCTACAGTCCGACGATCATTCGATC NNNNTTTTTTTTTTTTTTTTTTTTTTV
47	CGATTGAGGCCGGTAATACGACTCACTATAGGGGTTCAGAGTTCTACAGTCCGACGATCTCCGAATC NNNNTTTTTTTTTTTTTTTTTTTTTTV
48	CGATTGAGGCCGGTAATACGACTCACTATAGGGGTTCAGAGTTCTACAGTCCGACGATCCGGATATC NNNNTTTTTTTTTTTTTTTTTTTTTTV
49	CGATTGAGGCCGGTAATACGACTCACTATAGGGGTTCAGAGTTCTACAGTCCGACGATCGAATCTCG NNNNTTTTTTTTTTTTTTTTTTTTTTV
50	CGATTGAGGCCGGTAATACGACTCACTATAGGGGTTCAGAGTTCTACAGTCCGACGATCATTCGTCG NNNNTTTTTTTTTTTTTTTTTTTTTTV
51	CGATTGAGGCCGGTAATACGACTCACTATAGGGGTTCAGAGTTCTACAGTCCGACGATCTCCGATCG NNNNTTTTTTTTTTTTTTTTTTTTTTV
52	CGATTGAGGCCGGTAATACGACTCACTATAGGGGTTCAGAGTTCTACAGTCCGACGATCCGGATTCG NNNNTTTTTTTTTTTTTTTTTTTTTTV
53	CGATTGAGGCCGGTAATACGACTCACTATAGGGGTTCAGAGTTCTACAGTCCGACGATCGAATCGA TNNNNTTTTTTTTTTTTTTTTTTTTTTV

54	CGATTGAGGCCGGTAATACGACTCACTATAGGGGTTCAGAGTTCTACAGTCCGACGATCATTCGGAT NNNNTTTTTTTTTTTTTTTTTTTTTTV
55	CGATTGAGGCCGGTAATACGACTCACTATAGGGGTTCAGAGTTCTACAGTCCGACGATCTCCGAGAT NNNNTTTTTTTTTTTTTTTTTTTTTTV
56	CGATTGAGGCCGGTAATACGACTCACTATAGGGGTTCAGAGTTCTACAGTCCGACGATCCGGATGA TNNNNTTTTTTTTTTTTTTTTTTTTTTV
57	CGATTGAGGCCGGTAATACGACTCACTATAGGGGTTCAGAGTTCTACAGTCCGACGATCAGCGTCG ANNNNTTTTTTTTTTTTTTTTTTTTTTV
58	CGATTGAGGCCGGTAATACGACTCACTATAGGGGTTCAGAGTTCTACAGTCCGACGATCTAGACCG ANNNNTTTTTTTTTTTTTTTTTTTTTTV
59	CGATTGAGGCCGGTAATACGACTCACTATAGGGGTTCAGAGTTCTACAGTCCGACGATCCTATGCGA NNNNTTTTTTTTTTTTTTTTTTTTTTV
60	CGATTGAGGCCGGTAATACGACTCACTATAGGGGTTCAGAGTTCTACAGTCCGACGATCGCTCACG ANNNNTTTTTTTTTTTTTTTTTTTTTTV
61	CGATTGAGGCCGGTAATACGACTCACTATAGGGGTTCAGAGTTCTACAGTCCGACGATCAGCGTATC NNNNTTTTTTTTTTTTTTTTTTTTTTV
62	CGATTGAGGCCGGTAATACGACTCACTATAGGGGTTCAGAGTTCTACAGTCCGACGATCTAGACATC NNNNTTTTTTTTTTTTTTTTTTTTTTV
63	CGATTGAGGCCGGTAATACGACTCACTATAGGGGTTCAGAGTTCTACAGTCCGACGATCCTATGATC NNNNTTTTTTTTTTTTTTTTTTTTTTV
64	CGATTGAGGCCGGTAATACGACTCACTATAGGGGTTCAGAGTTCTACAGTCCGACGATCGCTCAATC NNNNTTTTTTTTTTTTTTTTTTTTTTV
65	CGATTGAGGCCGGTAATACGACTCACTATAGGGGTTCAGAGTTCTACAGTCCGACGATCAGCGTTCG NNNNTTTTTTTTTTTTTTTTTTTTTTV
66	CGATTGAGGCCGGTAATACGACTCACTATAGGGGTTCAGAGTTCTACAGTCCGACGATCTAGACTCG NNNNTTTTTTTTTTTTTTTTTTTTTTV
67	CGATTGAGGCCGGTAATACGACTCACTATAGGGGTTCAGAGTTCTACAGTCCGACGATCCTATGTCG NNNNTTTTTTTTTTTTTTTTTTTTTTV
68	CGATTGAGGCCGGTAATACGACTCACTATAGGGGTTCAGAGTTCTACAGTCCGACGATCGCTCATCG NNNNTTTTTTTTTTTTTTTTTTTTTTV
69	CGATTGAGGCCGGTAATACGACTCACTATAGGGGTTCAGAGTTCTACAGTCCGACGATCAGCGTGA TNNNNTTTTTTTTTTTTTTTTTTTTTTV
70	CGATTGAGGCCGGTAATACGACTCACTATAGGGGTTCAGAGTTCTACAGTCCGACGATCTAGACGA TNNNNTTTTTTTTTTTTTTTTTTTTTTV
71	CGATTGAGGCCGGTAATACGACTCACTATAGGGGTTCAGAGTTCTACAGTCCGACGATCCTATGGAT NNNNTTTTTTTTTTTTTTTTTTTTTTV
72	CGATTGAGGCCGGTAATACGACTCACTATAGGGGTTCAGAGTTCTACAGTCCGACGATCGCTCAGAT NNNNTTTTTTTTTTTTTTTTTTTTTTV
73	CGATTGAGGCCGGTAATACGACTCACTATAGGGGTTCAGAGTTCTACAGTCCGACGATCACTGACG ANNNNTTTTTTTTTTTTTTTTTTTTTTV
74	CGATTGAGGCCGGTAATACGACTCACTATAGGGGTTCAGAGTTCTACAGTCCGACGATCTGCATCGA NNNNTTTTTTTTTTTTTTTTTTTTTTV
75	CGATTGAGGCCGGTAATACGACTCACTATAGGGGTTCAGAGTTCTACAGTCCGACGATCCAGTCCG ANNNNTTTTTTTTTTTTTTTTTTTTTTV
76	CGATTGAGGCCGGTAATACGACTCACTATAGGGGTTCAGAGTTCTACAGTCCGACGATCGTACGCG ANNNNTTTTTTTTTTTTTTTTTTTTTTV
77	CGATTGAGGCCGGTAATACGACTCACTATAGGGGTTCAGAGTTCTACAGTCCGACGATCACTGAATC NNNNTTTTTTTTTTTTTTTTTTTTTTV
78	CGATTGAGGCCGGTAATACGACTCACTATAGGGGTTCAGAGTTCTACAGTCCGACGATCTGCATATC NNNNTTTTTTTTTTTTTTTTTTTTTTV
79	CGATTGAGGCCGGTAATACGACTCACTATAGGGGTTCAGAGTTCTACAGTCCGACGATCCAGTCATC NNNNTTTTTTTTTTTTTTTTTTTTTTV
80	CGATTGAGGCCGGTAATACGACTCACTATAGGGGTTCAGAGTTCTACAGTCCGACGATCGTACGATC NNNNTTTTTTTTTTTTTTTTTTTTTTV
81	CGATTGAGGCCGGTAATACGACTCACTATAGGGGTTCAGAGTTCTACAGTCCGACGATCACTGATCG

	NNNNTTTTTTTTTTTTTTTTTTTTTTV
82	CGATTGAGGCCGGTAATACGACTCACTATAGGGGTTCAGAGTTCTACAGTCCGACGATCTGCATTCG NNNNTTTTTTTTTTTTTTTTTTTTTTV
83	CGATTGAGGCCGGTAATACGACTCACTATAGGGGTTCAGAGTTCTACAGTCCGACGATCCAGTCTCG NNNNTTTTTTTTTTTTTTTTTTTTTTV
84	CGATTGAGGCCGGTAATACGACTCACTATAGGGGTTCAGAGTTCTACAGTCCGACGATCGTACGTCG NNNNTTTTTTTTTTTTTTTTTTTTTTV
85	CGATTGAGGCCGGTAATACGACTCACTATAGGGGTTCAGAGTTCTACAGTCCGACGATCACTGAGA TNNNNTTTTTTTTTTTTTTTTTTTTTTV
86	CGATTGAGGCCGGTAATACGACTCACTATAGGGGTTCAGAGTTCTACAGTCCGACGATCTGCATGAT NNNNTTTTTTTTTTTTTTTTTTTTTTV
87	CGATTGAGGCCGGTAATACGACTCACTATAGGGGTTCAGAGTTCTACAGTCCGACGATCCAGTCGAT NNNNTTTTTTTTTTTTTTTTTTTTTTV
88	CGATTGAGGCCGGTAATACGACTCACTATAGGGGTTCAGAGTTCTACAGTCCGACGATCGTACGGA TNNNNTTTTTTTTTTTTTTTTTTTTTTV
89	CGATTGAGGCCGGTAATACGACTCACTATAGGGGTTCAGAGTTCTACAGTCCGACGATCTGTACCGA NNNNTTTTTTTTTTTTTTTTTTTTTTV
90	CGATTGAGGCCGGTAATACGACTCACTATAGGGGTTCAGAGTTCTACAGTCCGACGATCCACTGCG ANNNNTTTTTTTTTTTTTTTTTTTTTTV
91	CGATTGAGGCCGGTAATACGACTCACTATAGGGGTTCAGAGTTCTACAGTCCGACGATCGTGCACG ANNNNTTTTTTTTTTTTTTTTTTTTTTV
92	CGATTGAGGCCGGTAATACGACTCACTATAGGGGTTCAGAGTTCTACAGTCCGACGATCACAGTCG ANNNNTTTTTTTTTTTTTTTTTTTTTTV
93	CGATTGAGGCCGGTAATACGACTCACTATAGGGGTTCAGAGTTCTACAGTCCGACGATCTGTACATC NNNNTTTTTTTTTTTTTTTTTTTTTTV
94	CGATTGAGGCCGGTAATACGACTCACTATAGGGGTTCAGAGTTCTACAGTCCGACGATCCACTGATC NNNNTTTTTTTTTTTTTTTTTTTTTTV
95	CGATTGAGGCCGGTAATACGACTCACTATAGGGGTTCAGAGTTCTACAGTCCGACGATCGTGCAATC NNNNTTTTTTTTTTTTTTTTTTTTTTV
96	CGATTGAGGCCGGTAATACGACTCACTATAGGGGTTCAGAGTTCTACAGTCCGACGATCACAGTATC NNNNTTTTTTTTTTTTTTTTTTTTTTV